Technical Report
TR-21-03
December 2022

Post-closure safety for the final repository for spent nuclear fuel at Forsmark

Buffer, backfill and closure process report, PSAR version

SVENSK KÄRNBRÄNSLEHANTERING AB

SWEDISH NUCLEAR FUEL
AND WASTE MANAGEMENT CO

Box 3091, SE-169 03 Solna
Phone +46 8 459 84 00
skb.se

ISSN 1404-0344
SKB TR-21-03
ID 1895038
December 2022

Post-closure safety for the final repository for spent nuclear fuel at Forsmark

Buffer, backfill and closure process report, PSAR version

Svensk Kärnbränslehantering AB

This report is published on www.skb.se

Abstract

This report gives an account of processes in buffer, deposition tunnel backfill and the closure important for the long-term evolution of a KBS-3 repository for spent nuclear fuel, and of how they are addressed in the PSAR.

Sammanfattning

Denna rapport beskriver processer i bufferten, återfyllningen i deponeringstunnlarna och förslutningen som är viktiga för den långsiktiga utvecklingen i ett KBS-3 förvar för använt kärnbränsle, och av hur de hanteras i PSAR.

Contents

1 Introduction

1.1 Role of this report in the PSAR

1.1.1 Overall methodology

This report documents processes related to the buffer, backfill and closure identified as relevant to the post-closure safety of a KBS-3 repository. It forms an important part of the PSAR for a final repository at the Forsmark site.[1] The report is an update of the corresponding process report for the safety assessment SR-Site (SKB 2010a). The extent of the update is described in some detail in Section 1.1.5. The detailed assessment methodology, including the role of the process reports in the assessment, is described in Chapter 2 of the **Post-closure safety report**.[2] The following excerpts describe the methodology and clarify the role of this process report in the assessment.

The repository system, broadly defined as the deposited spent nuclear fuel, the engineered barriers surrounding it, the host rock and the biosphere in the proximity of the repository, will evolve over time. Future states of the system will depend on:

- the initial state of the system,
- a number of radiation-related, thermal, hydraulic, mechanical, chemical and biological processes acting within the repository system over time, and
- external influences acting on the system.

A previously established methodology in eleven steps has been applied in the PSAR as summarised in Figure 1-1 and described below.

1. Identification of Features, Events and Processes (FEP processing) (FEP processing).

   This step consists of identifying all the factors that need to be included in the analysis. Experience from earlier safety assessments and KBS-3 specific and international databases of relevant features, events and processes (FEPs) influencing long-term safety are utilised. An SKB FEP database is developed in which the great majority of FEPs are classified as being either initial state FEPs, internal processes or external FEPs. Remaining FEPs are either related to assessment methodology in general or deemed irrelevant for the KBS-3 concept. Based on the results of the FEP processing, an FEP catalogue, containing FEPs to be handled in the safety assessment, has been established. Within the PSAR work, an evaluation was made of the international developments as regards FEPs since the reporting of SR-Site and of review comments on SR-Site. These efforts led to the conclusion that the SR-Site version of the FEP database and the FEP report are adequate also for the PSAR, with a minor modification regarding the canister. See further Chapter 3 of the **Post-closure safety report** and the **FEP report**.

2. Description of the initial state.

   The initial state of the system is described based on the design specifications of the KBS-3 repository, a descriptive model of the repository site and a site-specific layout of the repository. The initial state of the fuel and the engineered components is that immediately after deposition, as summarised in Chapter 5 of the **Post-closure safety report**. The initial state of the geosphere and the biosphere is that of the natural system prior to excavation as described in the site descriptive model supporting the PSAR, see further Chapter 4 of the **Post-closure safety report**.

[1] The present report is published some time before the submission of the PSAR. In case the need for any changes of the contents of this report arises between its publication and the submission of the PSAR, a report of these changes will be provided in the PSAR.

[2] To improve readability, abbreviated names in bold font are used to refer to the PSAR Post-closure safety report and its main references. Full report names are provided in the reference list, and in Table 1-1.

3. Description of external conditions.

   Factors related to external conditions are handled in the categories “climate related issues”, “large-scale geological processes and effects” and “future human actions”. The handling of climate related issues is described in the **Climate report**, whereas the few external, large-scale geosphere processes are addressed in the **Geosphere process report**. The treatment of future human actions is described in the **FHA report**.

4. Compilation of process reports.

   The identification of relevant processes is based on earlier assessments and FEP screening. All identified processes within the system boundary relevant to the long-term evolution of the system are described in dedicated Process reports, i.e. this report, the **Fuel and canister process report** and the **Geosphere process report**. Also short-term geosphere processes/alterations due to repository excavation are included. For each process, its general characteristics, the time frame in which it is important, the other processes to which it is coupled, and how the process is handled in the safety assessment, are documented.

5. Definition of safety functions, function indicators and function indicator criteria.

   This step consists of an account of the safety functions of the system and of how they can be evaluated by means of a set of function indicators that are, in principle, measurable or calculable properties of the system. Criteria for the safety function indicators are provided. The Process reports are important references for this step. A FEP chart is developed, showing how FEPs are related to the function indicators.

6. Compilation of input data.

   Data to be used in the quantification of repository evolution and in dose calculations are selected. The process of selection and the data adopted are reported in a dedicated **Data report**. Also, a template for discussion of input data uncertainties has been developed and applied.

7. Definition and analysis of reference evolution.

   A reference evolution, providing a description of a plausible evolution of the repository system, is defined and analysed. The isolation potential of the system over time is analysed, yielding a description of the general system evolution and an evaluation of the safety function indicators. Each process is handled in accordance with the plans outlined in the process reports. Radiological consequences of potential canister failures are not analysed in this step.

8. Selection of scenarios.

   A set of scenarios for the assessment is selected. A comprehensive main scenario is defined in accordance with SSM’s regulations SSMFS 2008:21. The main scenario is closely related to the reference evolution analysed in step 7. The selection of additional scenarios is focused on the safety functions of the repository, and the safety function indicators defined in step 4 form an important basis for the selection. For each safety function, an assessment is made as to whether any reasonable situation where it is not maintained can be identified. If this is the case, the corresponding scenario is included in the risk evaluation for the repository, with the overall risk determined by a summation over such scenarios. The set of selected scenarios also includes scenarios explicitly mentioned in applicable regulations; e.g., human intrusion scenarios, and scenarios and variants to explore design issues and the roles of various components in the repository.

9. Analysis of scenarios.

   The main scenario is analysed essentially by referring to the reference evolution in step 7, complemented by consequence calculations for potential canister failures in the reference evolution yielding a calculated risk contribution from the main scenario. The additional scenarios are analysed by focusing on the factors potentially leading to situations in which the safety function in question is not maintained. In most cases, these analyses are carried out by comparison with the evolution for the main scenario, meaning that they only encompass aspects of repository evolution for which the scenario in question differs from the main one. If the scenario leads to canister failures, consequence calculations are carried out. If the likelihood of the scenario is non-negligible, a risk contribution is also calculated.

10. Additional analyses.

    In this step, a number of additional analyses, required to complete the safety assessment, are carried out. These comprise:

    - The selection and analysis of Future Human Action (FHA) scenarios, including a brief description of the methodology for the selection.
    - Analyses required to demonstrate optimisation and use of best available technique.
    - Verification that FEPs omitted in earlier parts of the assessment are negligible in light of the completed scenario and risk analysis.
    - A brief account of the time period beyond one million years.
    - Natural analogues

11. Conclusions.

    This step includes integration of the results from the various scenario analyses, development of conclusions regarding safety in relation to acceptance criteria and feedback concerning design, continued site investigations, and the R&D programme.

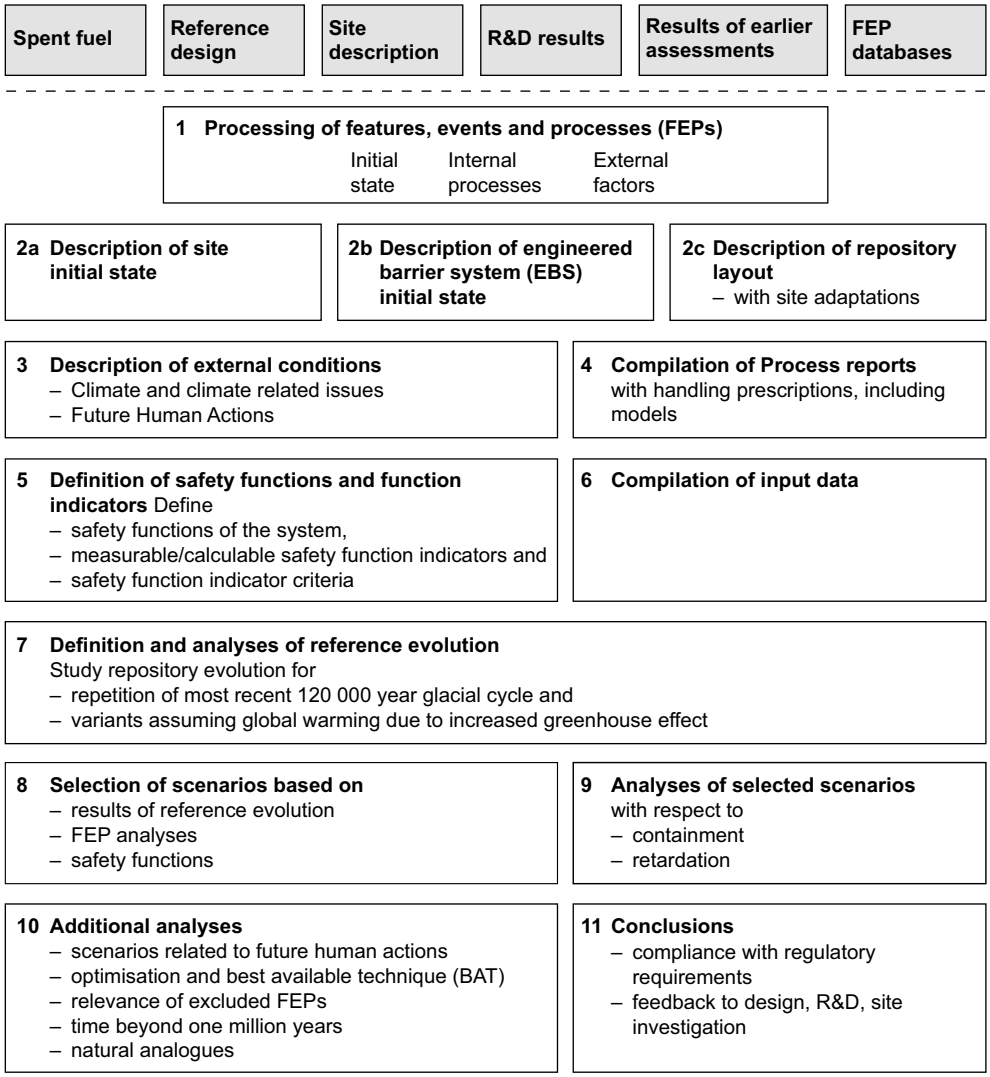

Figure 1-1. *An outline of the eleven main steps of the PSAR. The boxes at the top above the dashed line are inputs to the assessment.*

Table 1-1. Abbreviated report names used in this report and their full references.

Abbreviation used when referenced in this report	Full reference, as given in the reference list
Backfill production report.	**Backfill production report, 2022.** Produktionsrapport Återfyllning. SKBdoc 1525864 ver 4.0, Svensk Kärnbränslehantering AB. (In Swedish.) (Internal document.)
Buffer production report.	**Buffer production report, 2022.** Produktionsrapport Buffert. SKBdoc 1392269 ver 5.0, Svensk Kärnbränslehantering AB. (In Swedish.) (Internal document.)
Canister production report.	**Canister production report, 2022.** Produktionsrapport Kapsel. SKBdoc 1407944 ver 2.0, Svensk Kärnbränslehantering AB. (In Swedish.) (Internal document.)
Climate report.	**Climate report, 2020.** Post-closure safety for the final repository for spent nuclear fuel at Forsmark – Climate and climate related issues, PSAR version. SKB TR-20-12, Svensk Kärnbränslehantering AB.
Closure production report.	**Closure production report, 2022.** Produktionsrapport Förslutning. SKBdoc 1387771 ver 3.0, Svensk Kärnbränslehantering AB. (In Swedish.) (Internal document.)
Data report.	**Data report, 2022.** Post-closure safety for the final repository for spent nuclear fuel at Forsmark – Data report, PSAR version. SKB TR-21-06, Svensk Kärnbränslehantering AB.
Deposition tunnel plug production report.	**Deposition tunnel plug production report, 2022.** Produktions-rapport Valvplugg. SKBdoc 1562518 ver 3.0, Svensk Kärnbränslehantering AB. (In Swedish.) (Internal document.)
FEP report.	**FEP report, 2010.** FEP report for the safety assessment SR-Site. SKB TR-10-45, Svensk Kärnbränslehantering AB.
FHA report.	**FHA report, 2010.** Handling of future human actions in the safety assessment SR-Site. SKB TR-10-53, Svensk Kärnbränslehantering AB.
Fuel and canister process report.	**Fuel and canister process report, 2022.** Post-closure safety for the final repository for spent nuclear fuel at Forsmark – Fuel and canister process report, PSAR version. SKB TR-21-02, Svensk Kärnbränslehantering AB.
Geosphere process report.	**Geosphere process report, 2022.** Post-closure safety for the final repository for spent nuclear fuel at Forsmark – Geosphere process report, PSAR version. SKB TR-21-04, Svensk Kärnbränslehantering AB.
Model summary report.	**Model summary report, 2022.** Post-closure safety for the final repository for spent nuclear fuel at Forsmark – Model summary report, PSAR version. SKB TR-21-05, Svensk Kärnbränslehantering AB.
Post-closure safety report.	**Post-closure safety report, 2022.** Post-closure safety for the final repository for spent nuclear fuel at Forsmark – Main report, PSAR version. SKB TR-21-01, Svensk Kärnbränslehantering AB.
Radionuclide transport report.	**Radionuclide transport report, 2022.** Post-closure safety for the final repository for spent nuclear fuel at Forsmark – Radionuclide transport report, PSAR version. SKB TR-21-07, Svensk Kärnbränslehantering AB.
Spent fuel report.	**Spent fuel report, 2021.** Använt kärnbränsle att hantera i KBS-3-systemet. SKBdoc 1380282 ver 3.0, Svensk Kärnbränslehantering AB. (In Swedish.) (Internal document.)

This **Buffer, backfill and closure process report** is one of the process reports required to complete step 4. The purpose of the process reports is to document the scientific knowledge of the processes to a level required for their adequate treatment in the safety assessment. The documentation is not exhaustive from a scientific point of view, since such a treatment is neither necessary for the purposes of the safety assessment nor possible within the scope of an assessment. However, it must be sufficiently detailed to facilitate, by arguments founded on scientific understanding, the treatment of each process in the safety assessment. The purpose is to determine how to handle each process in the safety assessment at an appropriate degree of detail, and to demonstrate how uncertainties are taken care of, given the suggested handling. The means of handling processes established in this report are used in the analysis of the reference evolution, step 7, and in the analyses of scenarios, step 9.

1.1.2 Identification of processes

The process documentation in this PSAR version of the process report is an update of the descriptions in the SR-Site version of the process report (SKB 2010a) and the FEP processing carried out for the previous analyses. In the current assessment, PSAR, no need to modify the list of relevant processes that were included in the SR-Site version of the process report was identified, with one exception: The process “Gaseous speciation and reactions” has been added to the list of relevant process.

1.1.3 Relation to specific sites

The PSAR builds on site-specific data and site-descriptive models of the Forsmark site, i.e. the location of the repository facility to which the PSAR applies. The result of the quantitative evaluations of the processes in the different scenarios analysed in the PSAR will, in many cases, be dependent on site-specific data. These data are not given here, but in dedicated model studies. In addition, the most essential data for the safety assessment are thoroughly evaluated in the **Data report**, step 6 above.

1.1.4 Intended audience of this report

This report is written by, and for, experts in the relevant scientific fields. It should though be possible for a generalist in the area of long-term safety assessments of geologic nuclear waste repositories to comprehend the contents of the report. The report is an important part of the PSAR, providing a scientifically motivated plan for the handling of fuel and canister processes. It is, furthermore, foreseen that the report will be essential for reviewers scrutinising the handling of buffer and backfill issues in the PSAR.

1.1.5 Extent of update of the SR-Site buffer, backfill and sealing process report

As mentioned above, the present report is an update of the buffer, backill and closure process report for the safety assessment SR-Site (SKB 2010a). The update is based on requests during the review of SR-Site and on additional findings from SKB’s RD&D programme. The introductory Chapter 1 has been updated to reflect the context of the PSAR. The extent of the update of factual information in the remainder of the report, with details for the indidiual processes only for thebuffer section, is described in Table 1-2.

Table 1-2. Update of factual content relative to the SR-Site version of this report.

Section		Update relative to SR-Site version
2.2	Buffer	Updated to reflect the current reference design of the buffer. Only slight changes in the variables and handling of processes.
2.3	Backfill	Updated to reflect the current reference design of the backfill. Only slight changes in the variables and handling of processes.
2.4	Tunnel plug	Minor updates
2.5	Central area	Minor updates
2.6	Top Seal	Minor updates
2.7	Bottom plate	Revised to reflect the new design of the bottom plate
2.8	Borehole seals	Revised to reflect the new design of the borehole seals
3.1.1	Radiation attenuation/heat generation	Only editorial changes.
3.2.1	Heat transport	Updated with new references
3.2.2	Freezing	Minor update, but includes a revision of the performance target
3.3.1	Water transport under unsaturated conditions	Considerable revision to include assessment work after SR-Site
3.3.2	Water transport for saturated conditions	Minor update
3.3.3	Gas transport/dissolution	Minor update
3.3.4	Piping/Erosion	Revision to include assessment work after SR-Site
3.4.1	Swelling/mass redistribution	Considerable revision to include assessment work after SR-Site
3.4.2	Liquefaction	Only editorial changes.
3.5.1	Advective transport of species	Only editorial changes.
3.5.2	Diffusive transport of species	Updated with new references
3.5.3	Sorption (including ion-exchange of major ions)	Updated with new references
3.5.4	Aqueous speciation and reactions	Only editorial changes.
3.5.5	Gaseous speciation and reactions	New process
3.5.6	Alterations of accessory minerals	Updated with new references
3.5.7	Osmosis	Only editorial changes
3.5.8	Montmorillonite transformation	Updated with new references
3.5.9	Iron – bentonite interaction	Updated with new references
3.5.10	Cementation	Only editorial changes
3.5.11	Montmorillonite colloid release	Considerable revision to include assessment work after SR-Site
3.5.12	Colloid transport/filtration	Updated with new references
3.5.13	Radiation-induced transformations	Only editorial changes
3.5.14	Radiolysis of porewater	Only editorial changes
3.5.15	Microbial processes	Revised and updated with new references
3.6.1	Speciation of radionuclides	Only editorial changes
3.6.2	Transport of radionuclides in the water phase	Only editorial changes
3.6.3	Transport of radionuclides in a gas phase	Only editorial changes
Chapters 4–9		Significant revision to shorten the text and to avoid duplications from chapter 3. The handling of process are however in most cases identical to SR-Site.

1.2 Structure for process descriptions

All identified processes are documented using a template, adopted, with minor modifications, from the SR-Site version of the report. The template is described below.

Overview

Under this heading, a general description of current knowledge regarding the process is given.

Dependencies between process and system variables

For each system component, in this case the buffer, backfill, tunnel plugs, central area, top seal, bottom plate in deposition holes and borehole seals, a set of physical variables that defines the state of the system is specified. For each process, a table is presented under this heading with documentation of how the process is influenced by the specified set of physical variables and vice versa, i.e. how the process influences the variables. In addition, the handling of each influence in the PSAR is indicated in the table.

Boundary conditions

The boundary conditions for each process are discussed. These refer to the boundaries of the buffer, backfill, tunnel plugs, central area, top seal, bottom plate in deposition holes and borehole seal systems, respectively. The processes for which boundary conditions need to be described are, in general, related to transport of material or energy across the boundaries.

Model studies/experimental studies

Modelling and experimental studies of the process are summarised. This documentation constitutes the major source of information for many of the processes.

Time perspective

The timescale or timescales over which the process occurs are documented, if such timescales can be defined.

Natural analogues/observations in nature

If relevant, natural analogues and/or observations in nature that contribute to the present understanding of the process are documented under this heading.

Handling in the PSAR

Under this heading, the handling of the process in the PSAR is described. Typically, the process is either

- neglected on the basis of the information under the previous headings, or
- included by means of modelling.

The following aspects need to be covered, although no prescribed format for the documentation is given:

Boundary conditions: The handling of boundary conditions is discussed, especially any spatial and temporally varying chemical and hydraulic conditions.

Influences and coupling to other processes: The handling of the documented influences is discussed, as is coupling to other processes within that part of the system.

The method of treatment for all processes is discussed and where relevant, the models that have been developed for each process are described.

Handling of uncertainties in the PSAR

The handling of different types of uncertainties associated with each process is summarised. The uncertainties regarding a specific process are generally considered in the **Post-closure safety report**. Uncertainties in models and data are normally handled in specific model reports for the the processes in question e.g Åkesson et al. (2010a), Sena et al. (2010a). Uncertainties regarding radinuclide transport are handled in the **Radionuclide transport report**.

Uncertainties in mechanistic understanding: The uncertainty in the general understanding of the process is discussed based on the available scientific literature and with the aim of addressing whether the basic scientific mechanisms governing the process are understood to the level necessary for the suggested handling.

Model simplification uncertainties: In most cases, the quantitative representation of a process will contain simplifications. These may be a significant source of uncertainty in the description of system evolution. These uncertainties are discussed and approaches to addressing them are identified including alternative models or alternative approaches to simplification of a particular conceptual model.

Input data and data uncertainties: The set of input data necessary to quantify the process for the suggested handling is documented. The further treatment of important input data and input data uncertainties is described in a separate report, the **Data report**, to which reference is made if relevant.

References

A list of references used in the process documentation is given at the end of the report. In the SR-Site version of the report (SKB 2010a), each process also had the sub-heading "*Adequacy of the references supporting the handling in SR-Site*". Under that heading, statements were provided concerning the adequacy of the references in a quality assurance perspective, since some references were not qualified according to the requirements in the SR-Site QA plan. Some of those references are used also in the PSAR version, without repeating the qualification statement from the SR-Site assessment. All new references in the PSAR version are qualified according to the SKB management system, as specified in the PSAR QA plan. The mentioned sub-heading is thus obsolete and is not used in the PSAR version.

2 Definition of system components and summary of handling of processes in the PSAR

2.1 Overview

This section defines and describes the system components and gives a summary of their handling in the PSAR. For the purpose of the PSAR the components have been defined as:

- Buffer
- Backfill
- Tunnel plug
- Central area
- Top seal
- Bottom plate
- Bore hole seals

The manufacturing, design and installation process of these components are described in a set of different production reports, all in Swedish, where the **Buffer production report** covers the buffer and the bottom plate, the **Backfill production report** covers the backfill, the **Deposition tunnel plug production report** covers the Tunnel plug and the **Closure production report** covers the Central area, the top seal and the bore hole seals.

2.2 Clays, bentonites, and smectites

Bentonite is a swelling clay that consists of swelling clay minerals (smectites), normally montmorillonite, and various accessory minerals. A clay is defined as a naturally occurring material that is composed primarily of fine-grained minerals, which is generally plastic at appropriate water contents and will harden when dried or fired (Bergaya et al. 2006). A mineral is defined as a naturally occurring (non-manmade) homogeneous solid with a well-defined chemical composition and crystal structure, and is usually formed by inorganic processes (Klein and Hurlbut 1998). Bergaya et al. (2006) listed various characteristics of clay minerals, but no stringent or non-ambiguous definition of a clay mineral is given. Clay minerals are genetically either detrital allogenic minerals (transported residues from parent rock with no genetic relation to their present environment) or newly formed secondary or authigenic minerals formed in the sediment where the mineral was found. Smectites are typically authigenic and are often formed by alteration of volcanic rock or by precipitation in alkaline continental basins (Bergaya et al. 2006). The term bentonite comes from the clay formation at Fort Benton (Montana, USA) and bentonite comes in many colours (Figure 2-1and Figure 2-2) and qualities. Bentonite is often found in layers with more or less of other layers of sediments on top, and hence in the commercial product, minor contributions from the other layers may also appear sporadically together with various contaminations.

Smectites are layered silicates (phyllosilicates) which are structurally and chemically very similar to the macroscopic mineral mica. Although the difference in chemistry is quite small, the difference in some physical properties, such as swelling, is huge. Stacks of smectite sheets are called tactoids, where each layer is randomly rotated on top of one another; this is called ‘turbostratic disorder’.

Figure 2-1. *Different colors of bentonite from Bavaria, Germany.*

Figure 2-2. *Bentonite in Wyoming, U.S.A. Notice how the colour changes in the different parts of the bentonite, which is generally interpreted as being due to differences in the Fe-redox chemistry in the bentonite.*

The smectite layers can be visualized with a transmission electron microscope (Figure 2-3 and Figure 2-4), and although montmorillonite does not form macroscopic layers which can be seen by the eye, rectorite from Fort Sandeman in Pakistan does, and is perhaps the closest one can come to visually observe montmorillonite layers (Figure 2-4). The Fort Sandeman rectorite is an ordered interstratification (super structure) of a swelling clay mineral (montmorillonite/ beidellite) with a non-swelling clay mineral (illite/mica; Kodama 1966). In dry conditions, this material has a basal reflection (distance between each layer) of 24 Å (14 Å smectite + 10 Å illite/mica), and after liquid water has been added, the smectite component swells, whereas the illite/mica component remains unhydrated, giving the rectorite a basal spacing of 29 Å (19 Å smectite and 10 Å illite/mica). Different clay minerals often occur together as interstratified and/or separate phases. An estimation of the amount of illite in illite-smectite interstratified clay can be made by swelling the sample with ethylene glycol (Moore and Reynolds 1997). Some new details about the contribution of water upon ethylene glycol swelling were identified in Svensson and Hansen (2010a).

Clay minerals are divided into 1:1 layer clay minerals with one tetrahedral and one octahedral sheet (e.g. kaolinite and serpentine) and 2:1 layer clay minerals, with one octahedral sheet sandwiched between two tetrahedral sheets (e.g. pyrophyllite, talc, smectite, vermiculite, and illite; Figure 2-5).

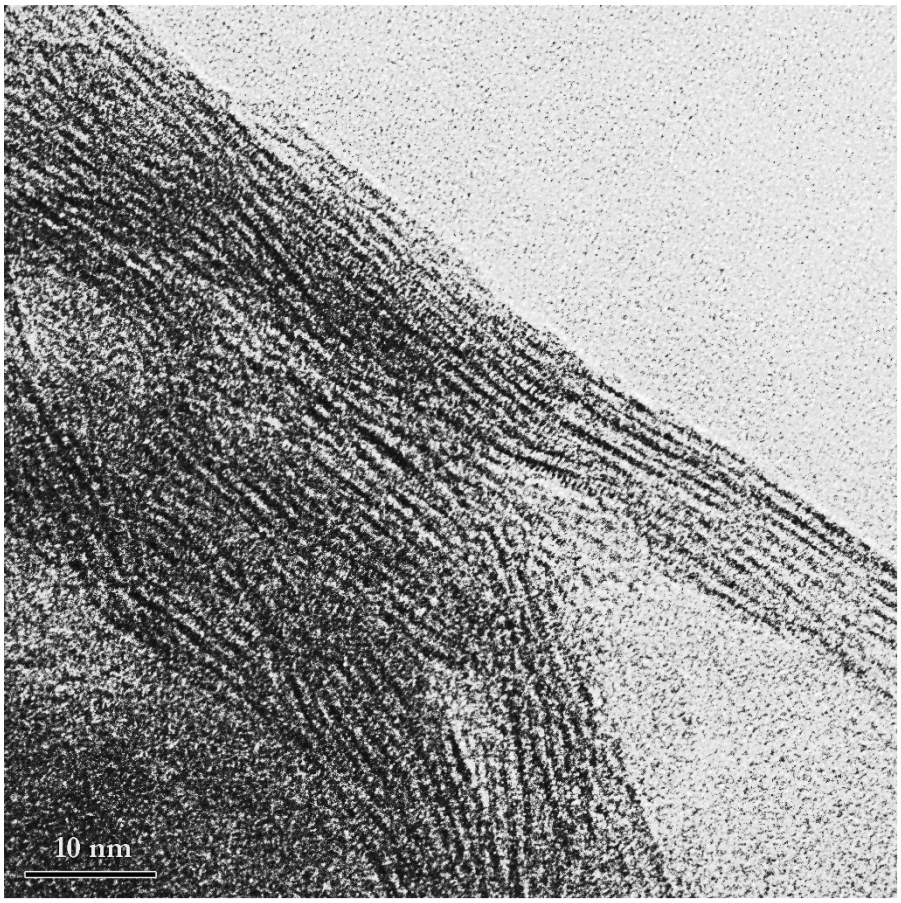

Figure 2-3. *Transmission electron microscopy (TEM) micrograph of Na-montmorillonite (Wyoming) showing a platy texture. The scale bar is 10 nm. Image captured in collaboration with Reine Wallenberg, National Center for High Resolution Electron Microscopy, Lund University.*

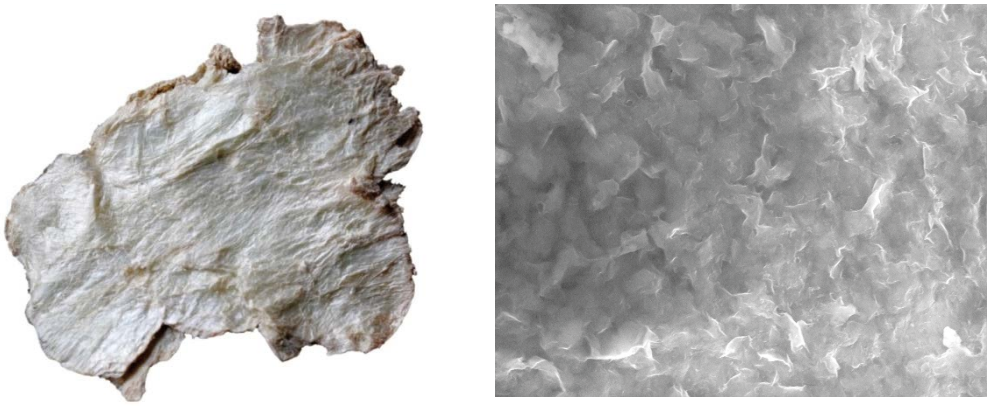

Figure 2-4. *Left: rectorite from Fort Sandeman, Pakistan. Rectorite is an ordered interstratification of swelling and non-swelling clay minerals (specimen size: 47 × 35 mm) and is probably the closest one can come to looking macroscopically at montmorillonite. Right: TEM micrograph of Wyoming montmorillonite (image width ≈ 8 µm) showing its platy and wavy structures. Image captured in collaboration with Reine Wallenberg, National Center for High Resolution Electron Microscopy, Lund University.*

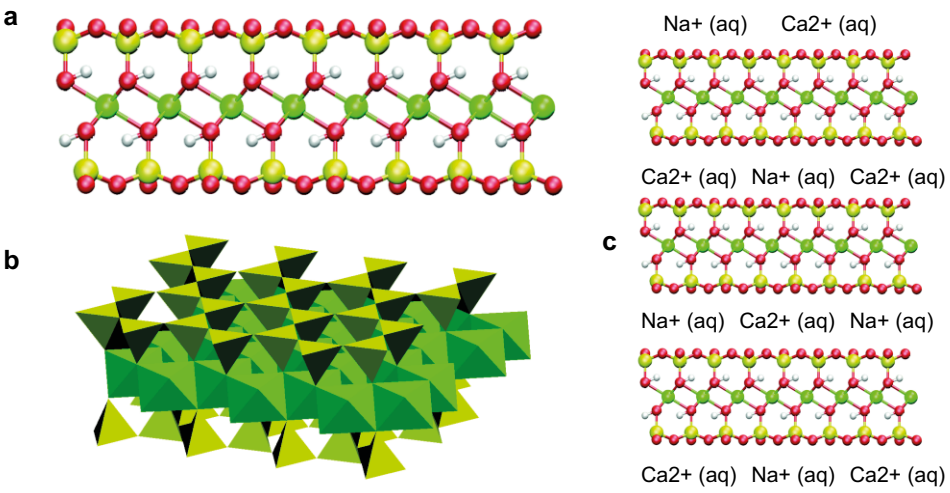

Figure 2-5. *Illustration of the crystal structure of the smectite 2:1 layer. (a) Ball-and-stick representation (green = Al, Mg, Fe; yellow = Si, Al; red = O; white = H). (b) Polyhedral representation. (c) Schematic illustration with interlayer cations in-between the smectite layers. Generated with VMD software by the University of Illinois at Urbana-Champaign, IL, USA.*

In montmorillonite the outer two sheets usually consist of silicon and aluminum (in corner sharing oxygen tetrahedra) and the middle sheet usually contains aluminum, magnesium and iron (in edge sharing oxygen octahedra). Because of isomorphous substitutions in the crystal structure, each 2:1 layer has a negative charge (the most common substitutions are $Al^{3+} \rightarrow Mg^{2+}$ and $Si^{4+} \rightarrow Al^{3+}$). The size of this layer charge is what distinguishes smectites from other phyllosilicate minerals. If the layer charge were larger they would be approaching vermiculites and micas, and if it were absent, they would be pyrophyllite. In order to balance this negative layer charge, positively charged inter-layer cations are situated between each layer (Figure 2-5**c**). The octahedral sheet of the smectite layer can contain three divalent metal ions per half unit cell (*e.g,* Mg^{2+}, Fe^{2+}, Cu^{2+}, Zn^{2+}) and is then called 'trioctahedral', or it can contain two trivalent metal ions (*e.g,*. Al^{3+}, Fe^{3+}, Cr^{3+}) and is then called 'dioctahedral' (Moore and Reynolds 1997). The charge can originate from substitution either in the octahedral layer (*e.g.* dioctahedral montmorillonite and trioctahedral hectorite) or in the tetrahedral layer (*e.g.* dioctahedral beidellite, nontronite and trioctahedral saponite).

An example of a structural formula per unit cell for a sodium saturated Wyoming montmorillonite is:

$Na_{0.65}(Al_{3.1,}\ Mg_{0.49,}\ Fe_{0.38,}\ Ti_{0.01})(Si_{7.89}Al_{0.11})O_{20}(OH)_4$ (Karnland et al. 2006).

Iron may be present as both Fe(II) and Fe(III) in the octahedral layer and is susceptible to redox reactions. If Fe(III) is reduced to Fe(II) this may impact the layer charge and hence some of the properties of the smectite (Stucki et al. 2002). The presence of several clay minerals (interstratified or not), accessory minerals, poorly crystallized or amorphous phases and sometimes also organic substances, can make analysis a challenge, especially if the stability of the sample is also taken into consideration.

2.3 Buffer

2.3.1 Initial state of the buffer

The **Buffer production report** presents the technical design requirements, the reference design of a bentonite buffer, verifying analyses showing that the reference design fulfils the design premises requirements and the production and control procedures selected to achieve the reference design. The report also includes an account of the achieved results from test manufacturing and buffer installation.

The following sections give a summary of the contents of the **Buffer production report** and a specification of the Initial state.

The main function of the buffer is to restrict water flow around the canisters. This is achieved by a low hydraulic conductivity, which makes diffusion the dominant transport mechanism, and a swelling pressure, which makes the buffer self-sealing. The buffer should also keep the canisters in position in the deposition holes, mitigate impact of rock shear movements and maintain its properties for the timescale of the assessment. The buffer should, furthermore, limit microbial activity in the buffer and on the canisters surface and filter colloidal particles. The buffer should not significantly impair the functions of the other barriers.

The water saturation and swelling processes form part of the long-term evolution of the buffer; hence the result of these processes and cannot be inspected at the initial state installation. Based on analyses of these processes, the ability of the buffer, as specified in the reference design, to provide the above functions can be evaluated.

Technical design requirements

To guide the design and production of the buffer, technical design requirements on characteristics that can be inspected and verified in the production are stated (Posiva SKB 2017). The technical design requirements are based on the assessment of the post-closure evolution of the buffer in the repository and available technology and shall be fulfilled at initial state.

- The following shall be determined for the selected buffer material:
  - the maximum dry density yielding a swelling pressure < 10 MPa when determined with a specific specified laboratory test procedure.
  - the minimum dry density yielding a swelling pressure > 3 MPa when determined with a specific specified laboratory test procedure.
  - the minimum dry density yielding a hydraulic conductivity in saturated state < 10^{-12} m/s when determined with a specific specified laboratory test procedure.
  - the maximum dry density yielding an unconfined compressive strength at failure < 4 MPa at a deformation rate of 0.8 %/min when determined with a specific specified laboratory test procedure.
- The buffer volume shall be cylindrical and determined from its cross sectional area in the deposition hole and its height, i.e. the sum of its thickness above and below the canister and the distance between the surface of the canister lid and bottom, minus the canister volume.
- The buffer thickness shall be
  - at least 50 cm below the canister
  - at least 50 cm above the canister
  - at least 30 cm around the canister.
- The installed buffer material mass shall in average in the buffer volume (Figure 5-10) result in
  - a dry density ≥ the lowest required material-specific dry density determined for the specific buffer material.
  - a dry density ≤ the highest allowed dry density determined for the specific buffer material.
- Acceptable contents of impurities:
  - organic carbon should be less than 1 wt-%.
  - sulphide should not exceed 0.5 wt-% of the total mass, corresponding to approximately 1 wt-% of pyrite.
  - total sulphur (including the sulphide) should not exceed 1 wt-%.

Furthermore, the thermal conductivity over the installed buffer shall, given the allowed decay power in the canister, the thermal properties of the canister and the rock and the canister spacing, yield a buffer temperature < 100 °C.

Reference design and production procedures

Reference design

The reference design of the buffer is described by a set of design parameters for which nominal values and acceptable variations are given. The design parameters will be inspected in the production to confirm that the installed buffer conforms to the reference design and to provide an estimate of the actual properties of the buffer at the initial state.

The reference geometry of the buffer in the deposition hole is shown in Figure 2-6. The buffer material is a bentonite clay with a high content of smectites (swelling minerals), mostly montmorillonite, to uphold and maintain the required minimum swelling pressure, maximum hydraulic conductivity and allowed stiffness. In addition, the content of harmful accessory minerals has to be low. The properties of bentonite from different sources differ as is discussed in Svensson et al. (2017a, 2019). The natural variation is handled in the design of the buffer (Luterkort et al. 2017) as some design parameters for buffer blocks and pellets needs to be adapted to the specific bentonite. Therefore, no buffer material is specified reference design.

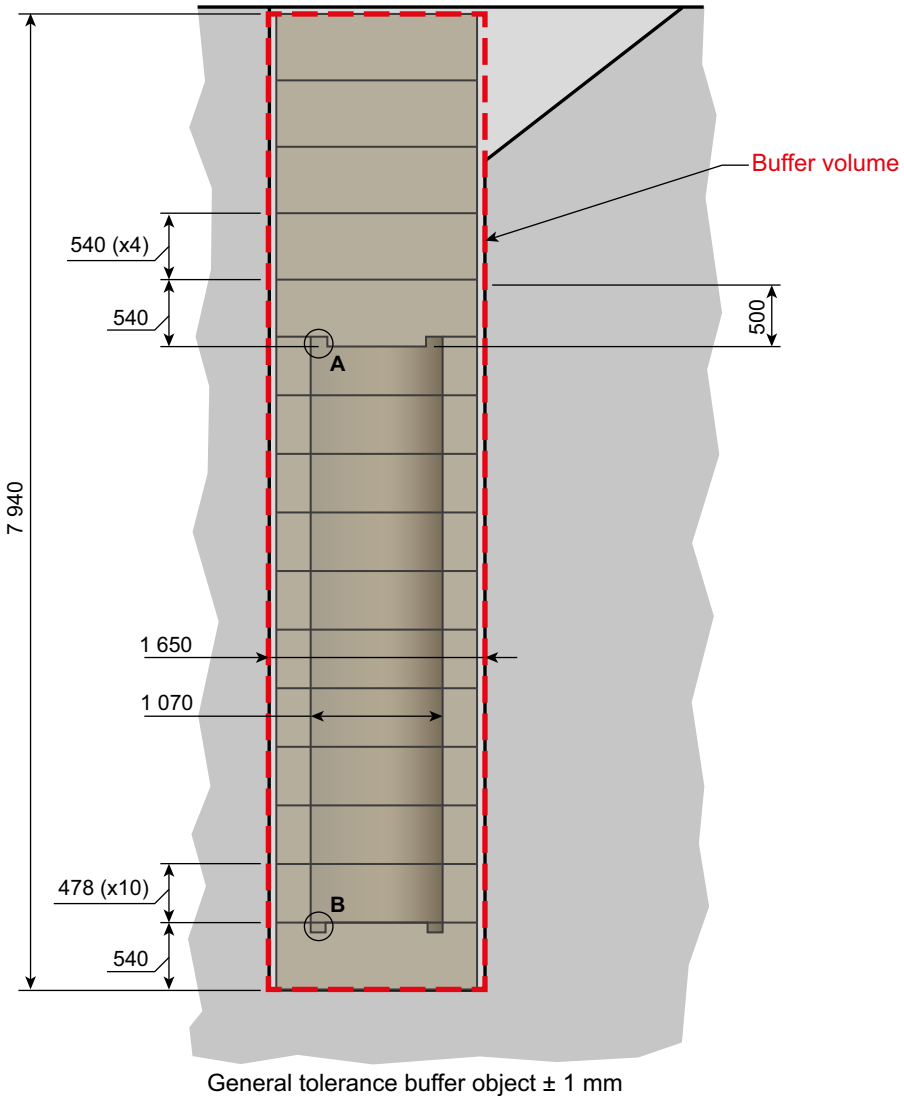

Figure 2-6. *The geometrical configuration of the buffer in the deposition hole (Buffer production report).*

In the PSAR, MX-80, a bentonite from a large deposit that is mined by a large bentonite supplier can be seen as one relevant illustration of a possible bentonite to be used in the repository. For bentonite material that has been investigated by SKB it is the correlation between swelling pressure and dry density that determine the acceptable dry density range. Figure 2-7 shows the relation between swelling pressure and dry density for MX-80 exposed to extreme cases of groundwater composition, deionised water and 1M $CaCl_2$ solutions, respectively. The figure shows that the dry density of a buffer of MX-80 may vary between about 1453–1558 kg/m^3 to fulfil the governing design premises requirement which states that the swelling pressure should be between 3 MPa and 10 MPa.

The density and homogeneity of compacted blocks and pellets will depend on the granule size distribution and water content of the material to be compacted and on the compaction pressure. To achieve high reliability in the production, the granule size distribution and water content must be specified for the selected material.

For the current reference design, the buffer volume is defined by the geometry of the deposition hole up to nominal tunnel floor minus the canister volume. The bevel is not included and the material in the bevel is a part of the backfill. Design premises apply on average for this volume. The bevel is filled with backfill pellets. The centre line of the buffer blocks shall coincide with the centre line of the deposition hole. The gap between the blocks and the rock surface of the deposition hole is filled with bentonite pellets. The buffer thickness around the canister (i.e. the radial distance from the canister surface to the wall of the deposition hole, after saturation, depend on the diameter of the deposition hole and its variation along the hole and on the position of the ring-shaped blocks within it. The buffer thickness will also be affected by the position of the canister within the ring shaped blocks and the diameter of the canister.

The canister lids and bottoms are not flat but contain hollows and edges. These volumes must be filled with bentonite. This is done by specially machined solid blocks.

The buffer takes up additional water after installation and will develop a swelling pressure at the end of the water saturation process. This will lead to an upward expansion of the buffer and a corresponding compaction of the overlying deposition tunnel backfill until an equilibrium is reached. The reference design, in particular the installed mass and installed dry density, has been determined with regard to this swelling process, so that the required swelling pressure, hydraulic conductivity and unconfined compressive strength is obtained also after swelling.

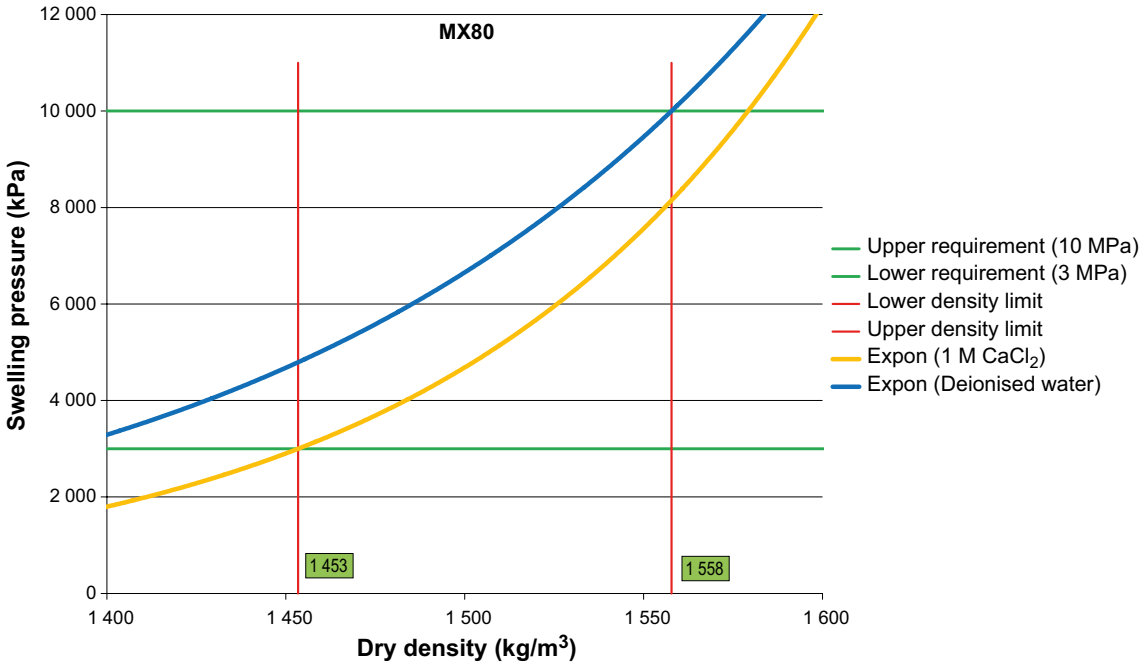

Figure 2-7. *MX-80 swelling pressure vs dry density for deionized waster and 1 mol $CaCl_2$ lines indicates the technical design requirement interval 3–10 MPa and the red lines shows the acceptable dry density (1453–1558 kg/m^3)that has been selected as the target for the reference design (Buffer production report)*

An upward swelling of the buffer is expected to occur due to buffer water up-take, resulting in compression of the backfill. Expansion calculations shows that the buffer reference design fulfils the design requirements also after 175 mm upheave (see the **Buffer production report**). As the expansion process is part of the long-term evolution, it is further accounted for in the **Post-closure safety report**.

After installation of blocks and pellets of MX 80 in a deposition hole with dimensions as specified in Figure 2-6.

A plate of copper attached to bottom buffer block to prevent rapid groundwater uptake in the bottom of the buffer.

Production and installation

The production line for the buffer consists of four main parts:

- Purchase, excavation and delivery.
- Quality control at delivery.
- Manufacturing of blocks and pellets.
- Handling and installation.

Details about the production can be found in the **Buffer production report**.

Bentonite deposits exist at many places around the world and excavation and delivery can be made by alternative companies. The desired material properties will be specified at ordering. Each shipment of bentonite will be accompanied by a protocol from the supplier that describes the actual composition of the delivered material.

The delivered material is inspected as a basis for the acceptance of the delivery. Inspections for the production comprise content of impurities, water content and granule size distribution of the delivered material and measurement of its total weight. Material specific design parameters of importance for the functions of the buffer are the relationship between dry density and hydraulic conductivity, swelling pressure and compressive strength, respectively.

Before compaction, the bentonite is crushed and dried and the granule size distribution and water content is adjusted. The reference method for pressing of blocks is uniaxial compaction. The pressure applied determines the block density and has to be adapted to the specific bentonite material. The compacted blocks are machined to specified dimensions in order to achieve a well-aligned stack of blocks in the deposition hole and the required installed dry density. The weight and dimensions (height, inner and outer diameter) of each block are inspected to check that the density is within the specified range. The reference method to manufacture pellets is to compact the conditioned material to small briquettes. The water content, granule size distribution and setting of press parameters for different materials are based on tests performed during material characterization.

The installation of the buffer is based on the fact that deposition holes, according to specifications, are provided from the underground opening production line. The excavation and inspection of deposition holes is described in the **Underground openings construction report**.[3]

The installation of buffer starts with the lower base block. Then the annular blocks are installed and it is checked that the blocks are placed horizontally and in the correct position. The copper canister is thereafter deposited. Finally the buffer blocks on top of the canister and pellets in the slot between the blocks and the rock are emplaced.

The canister can then be deposited as described in the **Canister production report**.

When the canister has been deposited the four top buffer blocks are installed as well as the buffer pellets. The installed average bulk density is determined based on the total installed buffer mass and the volumes of the deposition hole and the canister. Finally, the top buffer block is installed, which has an appropriate height for the specific deposition hole. The gap around the top block and bevel is

[3] Produktionsrapport Bergutrymmen. Svensk Kärnbränslehantering AB. (In Swedish.) (Internal document.) *In prep*.

filled with backfill pellets. Pellets are filled into the gap by placing a conical hood on top of the last installed bentonite block and pouring the pellets into the deposition hole.

The backfill in the deposition tunnel prevent swelling and expansion (up-lift) of the buffer and the buffer installation sequence needs to be adapted to the inflow of groundwater to the deposition holes. Therefore, buffer and canisters are first installed in relatively dry deposition holes in a deposition tunnel, i.e. where the heaving of the buffer is slow. Deposition holes that are not approved for disposal of canisters are in parallel backfilled with solid buffer blocks and buffer pellets. The deposition holes where the water inflow is approved, but relatively large, are left empty. The installation of buffer and canisters in these deposition holes are done in connection with the installation of the backfill in the deposition tunnel.

Initial state

The initial state of the buffer is the state when the auxiliary equipment used during installation is removed and all buffer components are installed in the deposition hole. Inflow of groundwater to the deposition hole and its impact on the buffer is not accounted for in the initial state.

The properties of the buffer to be designed to conform to the design requirements for post-closure safety are:

- Material composition.
- Installed dry density.
- Buffer geometry.

These properties are to some extent interdependent. The design density, for example, is based on a selected material. In the current report section, the buffer is characterised by a number of variables. Most of the initial state values for these variables are determined by the design properties. This is illustrated in Table 2-1.

Table 2-1. Relation between the designed buffer properties and the variables used in the safety assessment. References to where, or how, initial state values of the variables not related designed buffer properties can be found or derived are also given.

Variable	Buffer property	Initial state values
Water content	Material composition	
Gas content		
Bentonite composition		
Montmorillonite composition		
Porewater composition		
Hydrovariables (pressure and flows)	Material composition Installed density	
Stress state		
Pore geometry	Installed density	
Buffer geometry	Installed dimensions and geometrical configuration	
Radiation intensity	–	Calculated Radiation intensity on canister surface (**Spent fuel report**).
Temperature	–	Calculated
Structural and stray materials	–	Bottom plate and material and dimensions according to the reference design (**Underground openings construction report**,[4] Section 3.2).

[4] Produktionsrapport Bergutrymmen. Svensk Kärnbränslehantering AB. (In Swedish.) (Internal document.) *In prep*.

Material composition

A maximum inventory of certain impurities are specified among the design requirements (see the previous section). Regarding these requirements, it is concluded that the specified limitations on organic carbon, sulphide and sulphur are fulfilled at the initial state. This conclusion is based on the presented analyses of the compositions of MX 80 which is used as an example material and of the handling and inspection procedures outlined in the description of the production of the buffer.

To evaluate the long term performance of the buffer, a more detailed characterization of the material is needed. Important parameters in the description of the materials are:

- Chemical composition.
- Mineralogical composition.
- Grain density.
- Specific surface area.
- Grain size distribution.
- Water content.

In addition to this the clay fraction of the material is characterized by:

- Structural formula including:
  - Layer charge.
  - Charge distribution.
- Cation exchange capacity.
- Original exchangeable cations.

These parameters are further described in the Section 2.3.2 and are defined as the Bentonite composition and the Montmorillonite composition variables.

In natural bentonite, the charge compensating cations are usually a mixture of mono- and divalent ions. The swelling properties are to a large extent dependant on the magnitude and the position of the layer charge, but also on the type of charge compensating cation. The dominating cation is therefore often used to describe the type of bentonite, e.g. sodium bentonite, although the content of other ions may be quite large. High-quality commercial bentonites normally contain over 80 % of montmorillonite, which is expected to give various bentonite products similar sealing properties. However, the other minerals in bentonite may vary substantially within, and especially between, different quarries. Typical accessory minerals are other clays, feldspars, quartz, cristobalite, gypsum, calcite and pyrite. There are quantitative limits for sulphide, total sulphur and organic carbon. The mineralogical composition of the material (MX 80) used for the PSAR is presented in Table 2-2

For the purpose of the calculation of radiation shielding as well as the check on the maximum contents of sulphur and organic carbon it is important to determine the total chemical composition of the bentonite. The mean chemical composition of the bulk material from Table 2-3 expressed as oxides are shown in Table 2-3 for MX-80. The initial conditions of other parameters for bentonite and montmorillonite composition, together with their relevance for the post closure performance, are discussed in Svensson et al. (2017a, 2019).

Water content, gas content and porewater composition

There are no specific design requirements with regard to gas content and porewater composition, but these properties need to be known for the subsequent analysis. In the reference design with MX-80, the initial water content in blocks is selected to be 17 % and 15 % in pellets. Water content is determined by a standard geotechnical method. The original water content in the buffer material is adjusted to facilitate the manufacturing process. All porosity not filled with water contains air. The initial porewater composition may be calculated but not directly measured. The calculated content of installed mass and volume of water and air in a deposition hole is presented in Table 2-4.

Table 2-2. Mineralogy in Wyoming MX-80 batches as determined by XRD/Siroquant. SD(n), n = number of measurements used for calculation of standard deviation (Svensson et al. 2017a, 2019).

	Mineralogy (%)									
MX-80 batch	**Montmorillonite**	**Quartz**	**Anorthite**	**Cristobalite**	**Calcite**	**Albite**	**Pyrite**	**Mica/illite**	**Gypsum**	**Tridymite**
MX80 2015	85.43	4.18	0.00	1.15	0.43	2.03	0.35	4.63	0.85	0.95
SD (4):	0.73	0.38	0.00	0.10	0.10	0.26	0.06	1.52	0.40	0.06
MX80 2012	86.15	4.56	0.37	0.35	0.23	1.41	0.33	5.27	0.49	0.83
SD (10):	1.83	0.81	0.99	0.05	0.14	0.47	0.00	0.74	0.08	0.08
MX80 2006	83.9	2.7	0	2.1	0.2	3.3	0.2	6	0.5	1.1
MX80 2002	83.90	4.23	0.77	1.37	0.17	1.47	0.30	5.73	0.87	1.13
SD (3):	0.85	0.15	0.83	0.12	0.21	0.42	0.00	0.40	0.12	0.06
MX80 1993	82.83	3.13	0.57	1.97	0.17	3.27	0.13	5.70	0.87	1.30
SD (3):	0.83	0.25	0.60	0.12	0.12	0.65	0.06	0.56	0.06	0.00

Table 2-3. Overview of the chemical content in the bentonite batches (Svensson et al. 2017a).

	Chemical composition expressed as oxides (%)											
MX-80 batch	**Na_2O**	**MgO**	**Al_2O_3**	**SiO_2**	**Fe_2O_3**	**P_2O_5**	**SO_3**	**Cl**	**K_2O**	**CaO**	**TiO_2**	**MnO**
MX80 2015	1.87	2.44	22.28	66.09	4.39	0.00	0.58	0.01	0.59	1.54	0.19	0.01
MX80 2012	1.91	2.59	22.42	64.44	4.95	0.02	0.81	0.01	0.72	1.86	0.25	0.02
MX80 2006	1.67	2.52	21.55	66.71	4.35	0.01	0.83	0.01	0.55	1.60	0.18	0.01
MX80 2002	1.56	2.45	21.87	66.64	4.75	0.00	0.46	0.00	0.46	1.66	0.14	0.01
MX80 1993	1.69	2.33	21.32	67.21	4.93	0.01	0.41	0.01	0.52	1.39	0.16	0.01

Table 2-4 Buffer Volume-canister + bevel, installed total mass and volume of buffer material, water and air in a deposition hole + bevel, assuming nominal blocks and pellets and nominal dimensions of the deposition hole including their tolerances.

	Mass (ton)	Volume (m^3)
Full dep hole + Bevel-canister		17.21
Solid Buffer vol + bevel	25.37	9.09
Water Buffer vol + bevel	4.31	4.31
Air Buffer vol + bevel	~ 0	3.81
Total	**29.69**	**17.21**

Installed dry density

The initial state represents the installed buffer blocks and pellets with dry densities given by the manufacturing process. The parameters in the initial state should produce a saturated buffer that lies within the required swelling pressure, hydraulic conductivity and compressive strength after saturation.

The average installed buffer dry density will depend on the density and dimensions of the installed blocks and pellets, i.e. the installed buffer mass, and the volumes of the deposition hole and canister. The impact of the variations of volume of the canister and dimensions of the blocks on the installed buffer density can be neglected. The important parameters are the installed density of the blocks and pellets and the volume of the deposition hole.

A simulation of the adapted buffer reference design (MX-80) including 10 000 deposition holes and nominal data with tolerances on blocks, pellets and deposition holes has been performed. The process is iterated aiming at an average swelling pressure of 10 MPa in the buffer volume. The results are presented in Table 2-5 and Table 2-6. The swelling pressure is within the acceptance interval (3–10 MPa) in the ring section around the canister. The swelling pressure in the block section above the canister will be higher, which is acceptable.

Table 2-5. Results of simulation of variation between deposition holes of average key buffer properties within a hole. Resulting dry densities with standard deviation and 95 % confidence. Corresponding maximum (1M $CaCl_2$ solutions) and minimum (deionised water) swelling pressures are given.

Without heave	Dry density (kg/m^3)	Std dev	Dry density min (kg/m^3)	Dry density max (kg/m^3)	Swelling pressure min, $CaCl_2$ (kPa)	Swelling pressure max, Deion (kPa)
Average deposition hole	1 547.1	3.3	1 540.5	1 553.6	6 906	9 711
Block section	1 584.0	3.7	1 576.8	1 591.3	9 772	12 664
Ring section	1 509.3	4.0	1 501.6	1 517.0	4 756	7 504

Table 2-6. Additional data.

Parameter	Value
Dry mass, pellets	2 120 tonnes
Dry mass, blocks	21 088 tons
Water ratio, pellets	0.15
Water ratio, blocks	0.17

In the **Buffer production report** it is concluded that the methods for producing the buffer will yield installed average densities that fulfil the specification of the reference design.

Geometry

The thickness of the saturated buffer around the canister is determined by the dimensions of the deposition hole, the position of the installed ring-shaped blocks, the position of the canister in the buffer, and the diameter of the canister. The impact of the variation in canister placement and canister diameter on the buffer thickness can be neglected. The actual deposition hole diameter will deviate from the nominal. The thickness of the buffer below and above the canister depends only on the variation in height of the installed, solid buffer blocks.

2.3.2 Definition of buffer variables

Each component in the EBS initial state is described by a specified set of physical variables, selected to allow an adequate description of the long-term evolution of the component in question in the safety assessment.

The buffer is bounded on the inside by an interface with the canister, on the outside by the interface with the rock surface of the deposition hole, at the bottom by an interface with the copper plate at the base of the deposition hole and on the top by its interface with the backfill (the top in Figure 2-6, but not clearly indicated).

The buffer is characterised thermally by its temperature distribution and with respect to radiation by the intensity of the radiation field it is exposed to, mainly γ and neutron radiation.

Hydraulically, the buffer is characterised by its water content, sometimes by gas content (desaturation) and by hydrovariables (pressure and flows), which are mainly of interest in the transient period when the buffer is being saturated with water.

The buffer is characterised mechanically by its stress state.

The chemical state of the buffer is defined by its mineralogy, including the montmorillonite composition, other clay minerals, and any other accessory minerals. The chemical state is also defined by the porewater composition and the occurrence of structural and stray materials in the deposition hole.

The variables are defined in Table 2-7. The values of some of the variables are dependent on the density of the different phases. The following values have been used: density of water (ρ_w) 1 000 kg/m^3 and density of clay solids (ρ_{cs}) 2 780 kg/m^3.

The initial values of the variables, i.e. the values at the time of deposition, are given in the **Post-closure safety report**.

Table 2-7. Definition of buffer variables.

Variable	Definition
Buffer geometry	Geometric dimensions for buffer. An example is description of interfaces (on the inside towards the canister and on the outside towards the geosphere).
Pore geometry	Pore geometry in buffer as a function of time and space. The total porosity, (the fraction of the volume that is not occupied by solid material) is often given.
Radiation intensity	Intensity of α, β, γ and neutron radiation as a function of time and space in buffer.
Temperature	Temperature as a function of time and space in buffer.
Water content	Water content as a function of time and space in buffer.
Gas content	Gas content (including any radionuclides) as a function of time and space in buffer.
Hydrovariables (pressure and flows)	Flows and pressures of water and gas as a function of time and space in buffer.
Stress state	Stress conditions as a function of time and space in buffer.
Bentonite composition	Chemical composition of the bentonite (including any radionuclides) in time and space in buffer, levels of accessory minerals in time and space in buffer.
Montmorillonite composition	The molecular structure of montmorillonite component in the bentonite including the type of charge compensating cations.
Porewater composition	Composition of the porewater (including any radionuclides and dissolved gases) in time and space in the buffer.
Structural and stray materials	Chemical composition and quantity of any stray materials accidentally left in the buffer. At this stage, no structural materials are defined for this component.

2.3.3 Buffer performance and safety

A Safety Function in a KBS-3 repository is defined as function that contributes to isolation from the surface environment, to containment of radionuclides and/or to retention of them, and to retardation of their dispersion into the environment, either directly or indirectly by protecting the barriers in the repository.

In order to quantitatively evaluate safety, it is desirable to relate or express the safety functions to measurable or calculable quantities, often in the form of barrier conditions. This is defined as a safety function indicator (Table 2-8). In order to determine whether a safety function is maintained or not, it is desirable to have quantitative criteria against which the safety function indicators can be evaluated over the time period covered by the safety assessment.

The main safety functions of a KBS-3 repository are to, either directly or indirectly by protecting and preserving the safety functions of the barrier system, isolate the repository and the encapsulated spent nuclear fuel from the surface environment; contain radionuclides and to retain and retard their dispersion into the environment (Posiva SKB 2017). The buffer shall protect and preserve the containment of the radionuclides by limiting the transport and availability of corrodants at the canister surface. Further, to preserve the containment the buffer must be designed with respect to

the mechanical integrity of the canister. If canisters are breached the buffer shall contribute to retain radionuclides and retard their dispersion into the environment. With respect to this the buffer is assigned the safety functions to (Posiva SKB 2017):

- limit advective mass transfer,
- limit microbial activity,
- filter colloids,
- protect the canister from detrimental mechanical loads
  - rock shear load,
  - pressure load,
- resist transformation,
- keep the canister in position,
- retain sufficient mass over life cycle.

The choice of clay containing swelling material as a buffer between the canister and rock is made with respect to its ability to maintain these safety functions.

Clay materials have as an additional feature contributing to retaining radionuclides and retarding their dispersion, the capacity to sorb radionuclides if the containment should be breached. The materials and design of the buffer must be compatible with, and not unduly impair the safety functions of the engineered barriers or the rock. With respect to this, the material used for the buffer must not jeopardise the chemically favourable conditions in the repository. This has resulted in technical design requirements for the content of accessory minerals in the buffer. In addition, so as not to impair the safety functions of the engineered barriers or the rock there are technical design requirements for the gas transport properties of the buffer.

Table 2-8. Summary of the buffer safety functions and safety function indicators with their respective criteria.

Label (Post-closure safety report)	Safety function indicators and criteria	Safety function	Reference
Buff1	Bulk hydraulic conductivity $k^{Buff} < 10^{-12}$ m/s	Limit advective mass transfer to a diffusion dominated process	3.3.2
Buff1	Swelling pressure > 1 MPa	Limit advective mass transfer through sufficient tightness and self-sealing	3.4.1
Buff4	Maximum temperature $T^{Buffer} < 100$ °C pH < 11	Ensure that the buffer will retain its favourable properties in the long term (Resist transformation)	3.5.8
Buff6	Minimum temperature $T^{Buffer} > -6$ °C Swelling pressure < 10 MPa	Protect the canister from detrimental mechanical loads – pressure load	3.2.2 3.4.1
Buff5	Swelling pressure around entire canister > 0.2 MPa	Keep the canister in position	3.4.1
Buff2	Saturated density > 1 850 kg/m^3 (dry density >1 330 kg/m^3)	Limit microbial activity	3.5.15
	Buffer dry density around entire canister > 1 000 kg/m^3	Prevent colloid transport through buffer (filter colloids)	3.5.12
Buff3	Mitigate impact of 5 cm rock shear displacement at a rate of 1 m/s to a load acceptable for the canister	Protect the canister from detrimental mechanical loads – rock shear load	3.4.1
R1	Stable in contact with water with total charge equivalent of cations Σq [Mq+] > 8 ×10^{-3} mol/L	Retain sufficient mass over life cycle	3.5.11

The list in Table 2-8 is not fully consistent. Some safety function indicators relate directly to the properties of the installed buffer, while others relate to environmental parameters that are (almost) independent of the buffer design. The second group refers to temperature and groundwater composition.

2.3.4 Summary of handling of buffer processes in the PSAR

Table 2-9 summarises the handling of buffer processes in the PSAR, as suggested in this report. In the table, the process is either "mapped" to a model by which it is quantified or, alternatively a brief verbal description of how it will be handled is provided. The models are described in the section "handling in safety assessment" for each process where a model is used. More information regarding models can be found in the **Model summary report**. Since the initial evolution, characterised by unsaturated conditions and elevated temperatures, is in many respects different from the long-term, saturated period, the description in the table has been divided accordingly. The duration of the resaturation and thermal periods are not identical. The period with elevated temperatures in the repository near field will persist for around 1 000 years, while the saturation period may range from tens of years in some canister positions to thousands of years in other. In most instances, the handling is identical to the handling in the SR-Site safety assessment. For some processes, the handling has been supplemented with the additional information that was supplied to the Swedish regulator as a part of the review process of SR-Site. For a few processes, new assessments have been performed.

The information in the table can be summarised as follows:

For the initial saturation phase, the peak canister and buffer temperatures and the THM evolution as the buffer saturates need is quantified. Modelling of the thermal evolution of the entire near field is performed with the near field evolution model to evaluate peak canister and buffer temperatures. Coupled THM modelling of the buffer is performed to clearly describe the hydraulic evolution for different hydraulic conditions in the bedrock. The swelling at the end of the saturation phase is addressed the THM model.

Chemical evolution during the thermal phase of elevated and varying temperature in the buffer are addressed by the chemistry model.

Most other processes are not affected to any significant extent by the thermal and unsaturated conditions and are therefore neglected during the early saturation and thermal phases. One typical example would be the process "freezing".

Table 2-9. Process table for the buffer describing how buffer processes are handled in different time frames and for the special case of an earthquake. Green fields denote processes that are neglected or not relevant for the time period of concern. Red fields denote processes that are quantified by modelling in the safety assessment. Orange fields denote processes that are neglected subject to a specified condition.

	Resaturation/ "thermal" period	Long-term after saturation and "thermal" period	Earthquakes	Notes
Intact canister				
Bu1 Radiation attenuation/ heat generation	Neglected since dose rate is too low to be of importance for the buffer	Neglected since dose rate is too low to be of importance for the buffer	Not relevant	
Bu2 Heat transport	System model	System model	Not relevant	
Bu3 Freezing	Neglected, since this requires permafrost conditions	Neglected if buffer temperature > −6 °C. Otherwise bounding consequence calculation	Not relevant	Repository temperature in long term obtained from permafrost depth modelling
Bu4 Water uptake and transport for unsaturated conditions	THM model	Not relevant by definition	Not relevant	

	Resaturation/ "thermal" period	Long-term after saturation and "thermal" period	Earthquakes	Notes
Bu5 Water transport for saturated conditions	Neglected by definition under unsaturated conditions. For saturated conditions the treatment is the same as for "Long-term"	Neglected if hydraulic conductivity < 10^{-12} m/s since diffusion would then dominate	Consider pressure transients	The consequences of a buffer with high hydraulic conductivity are evaluated. Two different cases are studied: • the buffer acts as a porous medium with high conductivity (mass loss) • the buffer is fractured (alteration)
Bu6 Gas transport/ dissolution	Through dissolution/ THM model	(Through dissolution) No gas phase is assumed to be present	(Through dissolution) No gas phase is assumed to be present	
Bu7 Piping/Erosion	Model study	Not relevant, see also Bu18	Not relevant	Loss of buffer mass is calculated
Bu8 Swelling/mass redistribution	THM modelling including interaction buffer/backfill and thermal expansion	Integrated evaluation of erosion, convergence, corrosion products, creep, swelling pressure changes due to ion exchange and salinity, canister sinking	Part of integrated assessment of buffer/canister/rock	Need to also consider deviations in amount of buffer initially deposited
Bu9 Liquefaction	Not relevant in an unsaturated material	Cannot occur	Cannot occur	
Bu10 Advective transport of species	Simplified assumptions of mass transport of dissolved species during saturation	Neglected if hydraulic conductivity < 10^{-12} m/s	Consider pressure transients	See "Water transport for saturated conditions" (Bu5)
Bu11 Diffusive transport transport of species	Chemistry model (thermal, saturated phase; unsaturated phase disregarded)	Chemistry model	Consider altered geometry (diffusion pathways)	Consider varying groundwater compositions The initial thermal gradient is considered
Bu12 Sorption (including ion-exchange)	Chemistry model (thermal, saturated phase; unsaturated phase disregarded)	Chemistry model	Not specifically treated	
Bu13 Alteration of accessory minerals	Chemistry model (thermal, saturated phase; unsaturated phase disregarded)	Chemistry model	Not specifically treated	
Bu14a Aqueous speciation and reactions	Chemistry model (thermal, saturated phase; unsaturated phase disregarded)	Chemistry model	Not specifically treated	
Bu14b Gaseous speciation and reactions	Included as a partial pressure in geochemical modelling Included in corrosion estimates Neglected in THM modelling	Not relevant by definition		
Bu15 Osmosis	Evaluation through comparison with empirical data	Evaluation through comparison with empirical data	Not specifically treated	Handling of long-term intrusion of saline water

	Resaturation/ "thermal" period	Long-term after saturation and "thermal" period	Earthquakes	Notes
Bu16 Montmorillonite transformation	Model calculations (thermal, saturated phase; unsaturated phase disregarded)	Estimate based on evidence from nature	Part of integrated assessment of buffer/canister/rock	
Bu17 Iron-bentonite interaction	Neglected since no iron will be in contact with the bentonite	Only considered for failed canister. Possible loss of buffer efficiency	Only considered for failed canister. Possible loss of buffer efficiency	
Bu18 Montmorillonite colloid release	Neglected if total cation charge is > 8 mM. Otherwise modelled	Neglected if total cation charge is > 8 mM. Otherwise modelled	Not specifically treated	Loss of buffer mass is calculated See also water transport under saturated conditions
Bu19 Radiation-induced transformations	Neglected since dose rate outside canister is too low to have any effect	Neglected since dose rate outside canister is too low to have any effect	Neglected since dose rate outside canister is too low to have any effect	
Bu20 Radiolysis of porewater	Neglected since dose rate outside canister is too low to have any effect	Neglected since dose rate outside canister is too low to have any effect	Neglected since dose rate outside canister is too low to have any effect	
Bu21 Microbial processes	Neglected under unsaturated conditions, in this case the unsaturated part of the buffer, since the extent of aqueous reactions is limited. For saturated conditions the treatment is the same as for "Long-term"	Neglected if buffer density is sufficient. Quantitative estimate of sulphate reduction, limited by supply of microbe nutrients in groundwater	Not specifically treated	
Bu22 Cementation	Discussed together with Process Bu16 "Montmorillonite transformation"	Discussed together with Process Bu16 "Montmorillonite transformation"	Part of integrated assessment of buffer/canister/rock	
Failed canister				
Bu6 Failed canister. Gas transport/dissolution	Quantitative estimate based on empirical data (*no failures are expected this period*)	Quantitative estimate based on empirical data	Quantitative estimate based on empirical data	
Bu19 Failed canister. Radiation-induced transformations	Neglected since dose rate outside canister is too low to have any effect	The effect of α-radiation from nuclides from a failed canister is estimated	The effect of α-radiation from nuclides from a failed canister is estimated	The effect of α-radiation from nuclides is estimated in Section 3.5.13. There, it is concluded that the consequences can be neglected.
Bu23 Colloid transport	Neglected if dry density > 1 000 kg/m^3, otherwise bounding calculation (*no failures are expected this period*)	Neglected if dry density > 1 000 kg/m^3, otherwise bounding calculation	Neglected if dry density > 1 000 kg/m^3, otherwise bounding calculation	
Bu24 Speciation of radionuclides	No failures are expected this period	Assumptions based on empirical data	Assumptions based on empirical data	
Bu25 Transport of radionuclides in water phase	No failures are expected this period	COMP23	COMP23 Reduced diffusion path	
Bu26 Transport of radionuclides in gas phase	No failures are expected this period	Quantitative estimate	Quantitative estimate	

The long-term chemical evolution following the thermal phase is addressed by the chemistry model and and for the varying boundary conditions expected as a result of climate change etc. The model provides a spatially resolved result and involves chemical reactions. Montmorillonite transformation is handled by separate modelling. Erosion due to intrusion of dilute groundwater during glacial conditions must be addressed if the hydrogeochemical analyses imply that ionic strengths below the given criterion (Section 3.5.11) cannot be excluded. Colloidal release is modelled accordingly.

The effects of chemical evolution on key properties such as swelling pressure and hydraulic conductivity will be evaluated using empirical relationships. A number of issues related to mass redistribution in the buffer still need to be evaluated for the long-term evolution.

In the case of a canister failure, the release of gas from the corroding cast iron canister insert will be handled by quantitative estimates based on experimental studies of gas transport through bentonite. Diffusion of radionuclides through the buffer is calculated taking into account radionuclide speciation, necessary for the selection of diffusion and sorption data and estimated on the basis of experimental data. Transport of fuel colloids through the bentonite is neglected if the buffer density exceeds a specified value; otherwise the effect of this process on potential dose consequences is estimated by a bounding calculation case.

2.4 Backfill

2.4.1 Initial state of the backfill in the PSAR

The following is an overview description of the initial state of the backfill, i.e. its state at the time of deposition. A more formal and exhaustive account is given in the **Backfill production report** and in the **Post-closure safety report**. In that description, the specified set of variables describing the backfill is utilised.

When the holes in a deposition tunnel have been filled with canisters and the buffer the tunnel will be backfilled. Before backfilling, all tunnel installations will be removed. In PSAR, the deposition tunnels as well as the transport tunnels and the lower part of the ramp and shaft, extending from 200 m down to the repository is assumed to be filled with backfill material and will be considered as "backfill". The transport tunnels and ramp and shaft are considered as "closure" in the **Backfill production report**.

The backfill concept is based on precompacted blocks of natural swelling clay (not necessarily a bentonite). A bentonite from Ashapura Minechem is used as an example of such a material in the PSAR. This particular material was delivered to SKB in 2012 and the name "Asha 2012" is used as reference.

The backfill is installed as blocks and pellets, pellets as a bottom bed, blocks stacked in the tunnel and the additional space between the stack and the rock is filled with pellets. The reference backfill geometry is presented in Figure 2-8.

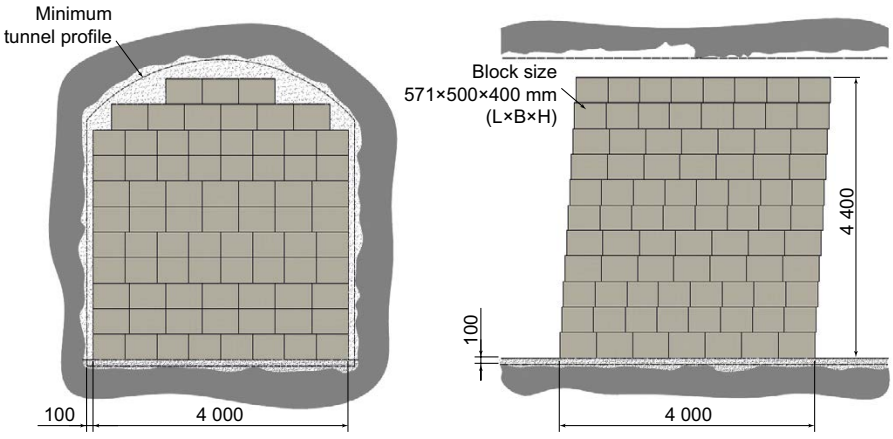

Figure 2-8. *Reference geometry of the installed backfill in a tunnel showing vertical cross sections perpendicular (left) and along (right) the tunnel.*

A technical design requirement for the backfill is an acceptable dry density is one giving a swelling pressure > 1 MPa when determined with a specific laboratory test (Posiva SKB 2017). Figure 2-9 shows the relation between swelling pressure and dry density for Asha 2012.

Design

The reference designs of the blocks and pellets are given in Table 2-10 and the design parameters specifying the installed backfill properties that the components shall have when they are installed are given in Table 2-11.

Pellets around the blocks are needed as a buffering volume to suck up groundwater flow from the surrounding rock that otherwise can erode the bentonite blocks. The acceptable water content in the backfill pellets is designed to contribute to the water storage properties.

The installed dry density of the backfill will depend on the volume of the deposition tunnel and the mass of backfill material installed in the tunnel. The installed density is calculated per tunnel section, defined as the average distance between two deposition holes, i.e. about 6 m. The calculated installed density for the reference design of backfill components according to Table 2-10 and the installed backfill according to Table 2-11, are set out in Table 2-12.

The calculated average dry density in a backfilled tunnel section is reported in the **Backfill production report**. The calculated dry density of Asha 2012 is 1 488 kg/m^3 if the design parameters for the backfill have their nominal values and the excavated tunnel volume including the expected average of 18 % overbreak. At 30 % overbreak, the corresponding calculated average density is 1 437 kg/m^3. At both these values, the interval of acceptance for Asha 2012 on installed dry density is achieved. Even the lowest calculated density that can be obtained with the present design, that is when all design parameters have their lowest accepted value, meets the interval of acceptance.

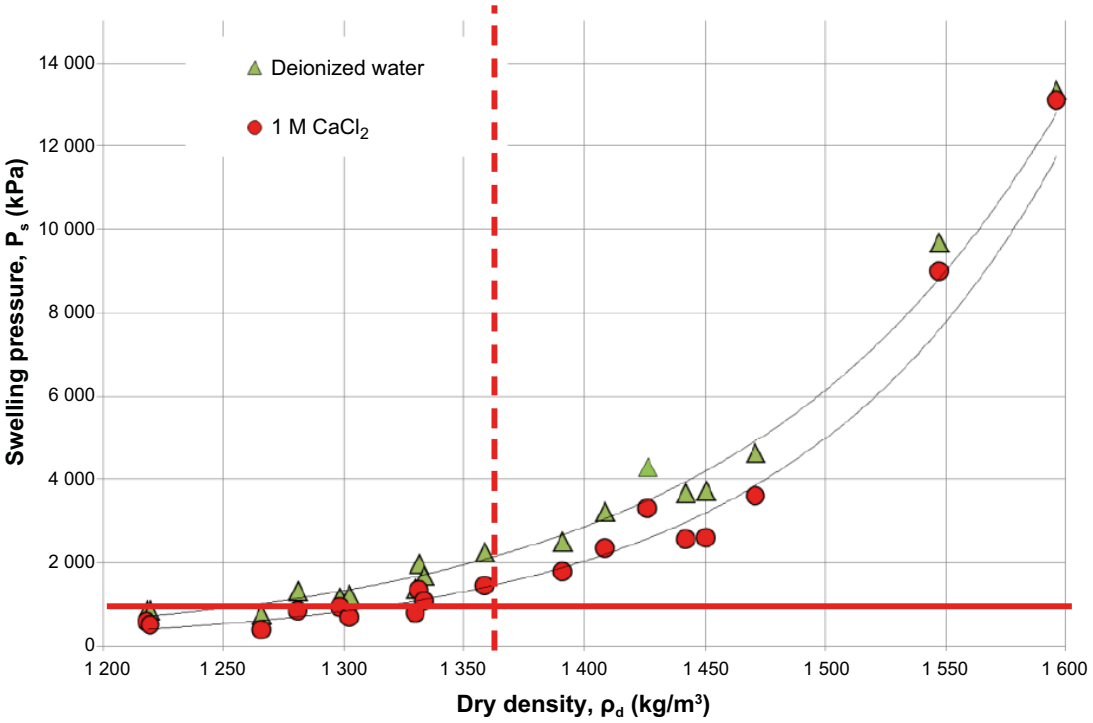

Figure 2-9. *Relation between swelling pressure and dry density for Asha 2012. The red line indicates the Technical Design Requirement of 1 MPa and the dotted red line shows the dry density of 1 361 that has been selected as the target for the adaptive design (Backfill production report).*

Table 2-10. Reference blocks and pellets ready for installation (based on Asha 2012).

Design parameter	Nominal design	Accepted variation
Blocks		
Dry density Asha 2012 (kg/m^3)	1 725	≥ 1 650
Water content (%)	20 (As in the material ready for compaction)	± 1.5 (As in the material ready for compaction)
Dimensions (mm^3)	500 × 571 × 400	± 1 × 1 × 2
Tensile strength (kPa)	-	> 200
Pellets		
Dry density Asha 2012 (kg/m^3)	900	≥ 850
Dimensions (mm^3)	Ø 6 L: 6-22	–
Water content		< 20
Pellet durability		Sufficient to have less than 10 % fine material in the pellets filling

Table 2-11. Reference design of installed backfill (based on Asha 2012).

Design parameter	Nominal design	Accepted variation
Blocks		
Geometry	According to Figure 2-8	The number of blocks must not be changed
Free space between blocks and nominal tunnel profile (mm)	100	≥ 100
Pellet filling in gap between blocks and tunnel walls		
Pellet-filled proportion of free space between block and tunnel wall (%)	94	≥ 90
Percentage of fine material in the installed pellet filling (%)	-	< 10
Pellet bottom bed		
Thickness (above theoretical floor above deposition hole (mm)	100	± 20
Surface roughness (mm)	Perfectly even	± 5
Calculated installed average dry density between deposition holes		
Dry density Asha 2012 (kg/m^3)	1 488	≤ 1 361

[1)] In the reference design buffer blocks are used and the design parameters are the ones specified for solid blocks in the **Buffer production report**, Table 3-4.

[2)] In the reference design the same kind of pellets are used for the bottom bed and the gap between the blocks and tunnel walls. This may be changed.

Table 2-12. Calculated average installed backfill dry density for reference design with Asha 2012.

Design parameter	Value, average overbreak (V_t=136.5 m^3)	Value, highest acceptable overbreak (V_t=150.4 m^3)
Dry density blocks	1 725 kg/m^3	1 725 kg/m^3
Volyme, block stack incl. space between blocks	100.7 m^3	100.7 m^3
Dry density, pellets	980 kg/m^3	980 kg/m^3
Volume, free space between blocks and tunnel profile	30.2 m^3	44.1 m^3
Volume, pellets bottom bed	5.6 m^3	5.6 m^3
Volume, pellets bevel in deposition hole	1.9 m^3	1.9 m^3
Degree of filling, pellets between block stack and rock	94 %	94 %
Degree of filling, pellets bottom bed and bevel	100 %	100 %
Average dry density in tunnel section with one deposition hole.	1 488 kg/m^3	1 437 kg/m^3

The initial state of the backfill is the state when the entire deposition tunnel is backfilled. Inflow of groundwater to the deposition tunnel and its impact on the backfill is not accounted for in the initial state. The presented initial state of the backfill is the outcome of the design parameters that can be expected based on the experience and results from the test production.

The properties of the backfill to be designed to conform to the design requirements for post-closure safety are:

- Material composition.
- Installed density.

In this report (Section 2.4.2), the backfill is characterised by a number of variables. Most of the initial state values for these variables are determined by the design properties. The relation between the variables and the design parameters are basically the same as for the buffer, see Table 2-1.

Material composition

According to the design requirements the backfill material must not contain substances that may cause harmful buffer degradation or canister corrosion. This entails that the backfill material must not be a significant source of sulfide that can corrode the copper canister. Currently, no limits are given as design requirement from the assessment of the post-closure safety.

As a check on the maximum contents of sulphur and organic carbon it is important to determine the total chemical composition of the bentonite. The mean chemical composition of the bulk material expressed as oxides are given in Table 2-13 for Asha 2012. Descriptive statistics on the exchangeable cations are given in Table 2-14.The total carbon content of five samples of Asha 2012 ranges from 0.54 to 0.70 % C. The acid-soluble carbon content is systematically somewhat lower, which suggests that carbon sources other than carbonates may exist. If so, a probable source is organic matter. The remnant carbon content (i.e. total minus acid-soluble carbon) is 0.24 % C at a maximum (Sandén et al. 2014).

Based on the specifications of the example bentonite material (Asha 2012), the impact of the backfill material composition on buffer degradation and canister corrosion is assessed in the PSAR.

Table 2-13. Overview of the chemical composition of the bentonite samples from the batch Asha 2012. Major elements by ICP-AES, S and C by evolved gas (Sandén et al. 2014).

Bentonite	Chemical composition (%)														
	SiO_2	Al_2O_3	Fe_2O_3	MgO	CaO	Na_2O	K_2O	TiO_2	P_2O_5	MnO	Cr_2O_3	LOI	C_{tot}	S_{tot}	CO_2
Asha 2012 mean (N=5)	47.62	18.54	14.50	2.71	3.29	1.64	0.10	1.03	0.11	0.15	0.034	10.0	0.60	0.12	1.61
stdev	0.82	0.87	1.78	0.07	0.30	0.15	0.01	0.02	0.01	0.03	0.004	0.3	0.07	0.05	0.11

Table 2-14. Descriptive statistics on the exchangeable cations in Asha 2012 (Sandén et al. 2014).

Bentonite	Cation	Mean meq/100 g	Std.dev.	Max. value meq/100 g	Min. value meq/100 g
Asha 2012 (N=5)	Ca	30.5	3.67	35	26.0
	Mg	13.4	0.75	15	13
	K	0.5	0.03	0.6	0.5
	Na	46.9	4.21	53	43
	Sum	91	1.7	93	90

Water content, gas content and porewater composition

There are no specific design requirements with regard to gas content and porewater composition, but these properties need to be known for the subsequent analysis of post-closure safety. In the reference design with Asha, the initial water content in blocks is selected to be 20 % and 19 % in pellets. Water content is determined by a standard geotechnical method. All porosity not filled with water contains air. The initial porewater composition may be calculated but not directly measured. The calculated content of installed mass and volume of water and air in a deposition hole is presented in Table 2-15.

Table 2-15. Backfill, installed total mass and volume of backfill material, water and air in a deposition tunnel section (6.0 m), assuming nominal and nominal dimensions of the deposition tunnel, blocks and pellets.

	Mass (tons)				Volume (m^3)			
	Total	Solid	Water	Air	Total	Solid	Water	Air
6 m tunnel	242.19	202.11	40.08	~0	136.24	69.41	40.08	26.75

Installed density

The installed dry density in the backfill shall be > 1 361 kg/m^3 on average between two deposition holes. This limit is valid for the reference material in the PSAR. Another backfill material would most likely have another density limit. The density of the installed backfill blocks and pellets can be found in Table 2-10. The installed blocks and pellets with dry densities given by the manufacturing process shall also fulfil the required properties after saturation.

The average installed backfill dry density will depend on the density and dimensions of the installed blocks and pellets, i.e. the installed buffer mass and the backfill geometry which is dependent on the excavated tunnel volumes. The dimensions of the tunnel and the installed mass will be registered during installation and the average installed dry density calculated to ensure that the properties at initial state fulfil the reference design.

Based on the initial state values of the design parameters of the backfill and the deposition tunnel volumes the installed dry density, mass and porosity to be used in the PSAR have been calculated, the results are presented in Table 2-16. The reference design values are given as comparison.

During operation some backfill material in already completed and plugged deposition tunnels may be lost by piping and erosion. Material may also be lost in the future during the assessment period both during and after saturation of the backfill. Countermeasures related to piping erosion during installation due to water inflow have been taken in the reference design of the pellets surrounding the block pile (see the **Backfill production report**).

Table 2-16. The backfill design parameters at the initial state.

Design parameter	Reference design and initial state	Acceptable tolerances
Dry density of blocks (Asha 2012) (kg/m^3) - Tunnel section	1 725	≥ 1 650
Dry density of pellet filling (kg/m^3) - Bottom bed - Between blocks and rock wall - Bevel in deposition hole	900	≥ 850
Geometry	Nominal: Figure 2-8	
Average dry density in deposition tunnel (Asha 2012)*	1 437*–1 488	≥ 1 361

* Interval is given by variations in the tunnel volume (18 to 30 % overbreak)

2.4.2 Definition of backfill variables

The deposition tunnels are constrained by the rock surrounding the tunnel but also by the buffer in the deposition holes and the plugs at the tunnel ends. In the case of rejected deposition holes (**Backfill production report**), the subsystem is constrained also by the rock around rejected deposition holes.

The transport tunnels are constrained by the surrounding rock as well as tunnel plugs separating them from the deposition tunnels and the central area.

The backfill in the tunnels is characterised thermally by its temperature. Hydraulically it is characterised by its pore geometry, water content, gas content and the hydrovariables (pressure and flow). Mechanically, the backfill is characterised by the stress state. The chemical state is also defined by the porewater composition and the occurrence of structural and stray materials in the deposition tunnel.

The radiation intensity (dose rate) in the backfill has not been calculated, since it is considerably lower than on the outside of the buffer and is therefore of no importance in the safety assessment.

All variables are defined in Table 2-17. The initial values of the variables are given in the **Backfill production report**.

2.4.3 Backfill performance

In order to evaluate the performance of the tunnel backfill, a few so called safety function indicator criteria (performance targets in Posiva SKB (2017) have been established together with criteria these should fulfil over time (Posiva SKB 2017). These criteria are summarised in Table 2-18, referencing sections in this report where the reasoning for these criteria are given.

Table 2-17. Variables for the tunnel backfill.

Variable	Definition
Backfill geometry	Geometric dimensions for backfill. A description of e.g. interfaces towards buffer and towards the geosphere.
Backfill pore geometry	Pore geometry as a function of time and space in backfill. The total porosity, i.e. the fraction of the volume that is not occupied by solid material is often given.
Temperature	Temperature as a function of time and space in deposition tunnels.
Water content	Water content as a function of time and space in deposition tunnels.
Gas content	Gas content (including any radionuclides) as a function of time and space in deposition tunnels.
Hydrovariables (pressure and flows)	Flows and pressures of water and gas as a function of time and space in deposition tunnels.
Stress state	Stress state as a function of time and space in backfill.
Backfill materials – composition and content	Total chemical composition and content of the backfill material (including any radionuclides) in time and space.
Backfill porewater composition	Composition of the porewater (including any radionuclides and dissolved gases) in time and space in backfill.
Structural and stray materials	Chemical composition and quantity of structural materials (rock bolts, filling material in boreholes for grouting, nets etc) and stray materials in deposition tunnels.

Table 2-18. Summary of the Tunnel Backfill safety function indicators and the criteria they should fulfil (Posiva SKB 2017).

Function indicator	Criterion	Rationale	Reference
Bulk hydraulic conductivity	$k^{Backfill} < 10^{-10}$ m/s	Limit advective transport	4.2.2
Swelling pressure	> 0.1 MPa	Ensure homogeneity and avoid preferential pathways	4.3.1

2.4.4 Summary of handling of backfill processes in the PSAR

Table 2-19 summaries the handling of backfill processes in the PSAR, as suggested in this report. In the table, the process is either "mapped" to a model by which it will be quantified or a brief verbal description of how it will be handled is provided. Since the initial evolution, characterised by unsaturated conditions and elevated temperatures is in many respects different from the long-term, saturated phase, the description in the table has been divided accordingly.

The information in the table can be summarised as follows:

- For the initial saturation phase, the saturation and swelling of the backfill in the deposition tunnels and its interaction with the buffer needs to be quantified.
- If hydraulic gradients are present in the early phase, the potential effect of piping and erosion has to be evaluated.
- The temperature increase in the backfill will be moderate and therefore no effects of elevated temperature will be evaluated.

The most important processes in the long-term are physical and chemical processes that could lead to an undesirable change in backfill properties. These include ion-exchange, osmosis, colloid release and montmorillonite transformation.

In the case of a canister failure, radionuclide transport in the backfill will be calculated both in the near- and far field models, including advective and diffusive transport as well as sorption.

Table 2-19. Process table for the backfill describing how backfill processes will be handled in different time frames and in the special cases of earthquakes and failed canisters. (Green fields denote processes that are neglected or irrelevant for the time period of concern. Red fields denote processes that are quantified by modelling in the safety assessment. Orange fields denote processes that are neglected subject to a specified condition.)

	Resaturation/ "thermal" period	Long-term after saturation and "thermal" period	Notes
Intact canister			
BfT1. Heat transport	Simplified assumption	Simplified assumption	
BfT2. Freezing	Neglected, since this requires permafrost conditions	Neglected if backfill temperature > –6 °C. Otherwise discussed	Less severe consequences than for buffer
BfT3. Water uptake and transport for unsaturated conditions	THM model	Not relevant by definition	The pellets are included in the model
BfT4. Water transport for saturated conditions	Neglected under unsaturated conditions, for saturated conditions the treatment is the same as for "Long-term"	Included in geosphere modelling	Evaluate effects on conductivity of chemical evolution and mass redistribution/loss and of possible changes of hydraulic gradients for permafrost and glaciation
BfT5. Gas transport/ dissolution	THM model	(Through dissolution)	The presence of a trapped gas phase is considered in the modelling of the saturation of the backfill (not the case for the buffer)
BfT6. Piping/erosion	Quantitative estimate with an empirical model	Not relevant, see also BfT16	See also water transport for saturated conditions (BfT4)
BfT7. Swelling/Mass redistribution	THM modelling including interaction buffer/backfill and homogenisation in tunnel	Integrated evaluation of erosion, convergence, creep, swelling pressure changes due to ion exchange and salinity and transformation	Need to also consider deviations in amount of buffer and backfill initially deposited and buffer saturating before tunnel backfill
BfT8. Liquefaction	Not relevant	Not relevant	Less severe consequences than for buffer.
BfT9. Advective transport of species	Simplified assumptions of mass transport of dissolved species during saturation	Included in geosphere modelling. Cases without the backfill path will be considered	See "Water transport for saturated conditions"
BfT10. Diffusive transport of species	The early stage is not studied specifically, since the conditions in the backfill will be about the same as for the long-term evolution	Chemistry model	Consider varying groundwater composition
BfT11. Sorption (including ion-exchange)	The early stage is not studied specifically, since the conditions in the backfill will be comparable to those for the long-term evolution	Chemistry model	
BfT12. Alteration of accessory minerals	The effect on inorganic reduction of oxygen is modelled	Chemistry model	
BfT13a. Aqueous speciation and reactions	The early stage is not studied specifically, since the conditions in the backfill will be about the same as for the long-term evolution	Chemistry model	

	Resaturation/ “thermal” period	Long-term after saturation and “thermal” period	Notes
BfT13b. Gaseous speciation and reactions	Included as a partial pressure in geochemical modelling Included in corrosion estimates Neglected in THM modelling	Not relevant by definition	
BfT14. Osmosis	Hydraulic conductivity in THM model chosen so as to handle osmosis	Evaluation through comparison with empirical data	Handling of long-term intrusion of saline water
BfT15. Montmorillonite transformation	Model calculations (thermal, saturated phase; unsaturated phase disregarded)	Model calculations	
BfT16. Colloid release	Neglected if total cation charge is > 8 mM Otherwise modelled	Neglected if total cation charge is > 8 mM Otherwise modelled	Loss of backfill is calculated
BfT17. Radiation-induced transformations	Neglected, since dose rate in backfill is too low to have any effect	Neglected, since dose rate in backfill is too low to have any effect	
BfT18. Microbial processes	Excluded, (the effect on oxygen consumption is not considered)	Mass balance considerations	
Failed canister			
BfT5 Failed can. Gas transport/ dissolution	Neglected, since gas volumes (from buffer) assumed to be too low to reach backfill during this period	Neglected, pessimistically since transport would delay radioactive releases and decrease buffer pressure. The backfill would act as a sink for gas.	Gas release from canister
BfT19. Colloid formation and transport	See geosphere (no failures are expected this period)	See geosphere	Called “colloid transport” for buffer Reference to corresponding geosphere process
BfT20. Speciation of radionuclides	Assumptions based on empirical data (no failures are expected this period)	Assumptions based on empirical data	
BfT21. Transport of radionuclides in water phase	COMP23 (no failures are expected this period)	COMP23	
BfT22. Transport of radionuclides in gas phase	By-passed (no failures are expected this period)	By-passed	

2.4.5 Main tunnels and transport tunnels

To conform to the design premises closure of the main tunnels and transport tunnels at repository level (also called central tunnels in this report) will be based on the same principle as the backfill in deposition tunnels with compacted blocks and pellets but the material and density will be different.

According to current guidelines, the closure in transport tunnels and trunk tunnels should have a similar conceptual design as the backfill in the deposition tunnels (**Backfill production report**). It involves the use of bentonite material in some form to fill in the tunnels. Figure 2-11 shows transport tunnels and main tunnels.

2.4.6 Ramp and shafts

The final repository is linked to the surface via a ramp and three types of shafts; skip shaft, elevator shaft and ventilation shaft. The shaft has circular cross sections. In the closure reference design the ramp and shafts, from level −470 m up to level −370 m, are backfilled with compacted bentonite blocks and pellets in accordance with the current reference design for the backfill in the deposition tunnels. The top part of the ramp and shafts are described in Section 2.7.

2.5 Tunnel plug

2.5.1 Initial state of the tunnel plug

The plugs in the deposition tunnels are especially designed with respect to the properties and function of the buffer and backfill. The plug consists of several parts that in different ways will contribute to maintaining its functions during the curing phase, the sealing phase and the post-closure phase of its lifetime (see the **Deposition tunnel plug production report**). The main purpose of the plug is to keep the backfill in place during the operation of the repository. The plug should also limit the exchange of gas between the deposition tunnel and the main tunnel.

The detailed design of the plug has a water tight seal of highly compacted bentonite and a concrete dome installed into a slot deepened from the excavated tunnel contour with a non-damaging technique so deep that all possible flow paths caused by excavation disturbance are cut off. The backfill, bentonite seal and the concrete dome are separated by different materials. The concrete dome is cast from low-pH concrete without reinforcement but it contains cooling pipes to limit the temperature during curing. The bentonite seal consists of compacted bentonite blocks and pellets (same bentonite as in the buffer).

There are a number of different components that constitute the tunnel plugs (Figure 2-10). These are (counted from inside the tunnel and outwards):

1. Backfill end zone.
2. Porous lightweight concrete beams (LECA® beams) as material separators between backfill end zone in the deposition tunnel and filter.
3. Filter (macadam) with drainage pipe.
4. Geotextile as material separator between filter and sealing layer.
5. Sealing layer of bentonite.
6. Concrete beams and geotextile as a material separator between sealing layer and concrete dome.
7. Concrete dome with cooling pipes and injection pipes.
8. Trench with leakage monitoring.

The materials, dimensions and volumes of the different parts of the deposition tunnel plug are given in Table 2-20.

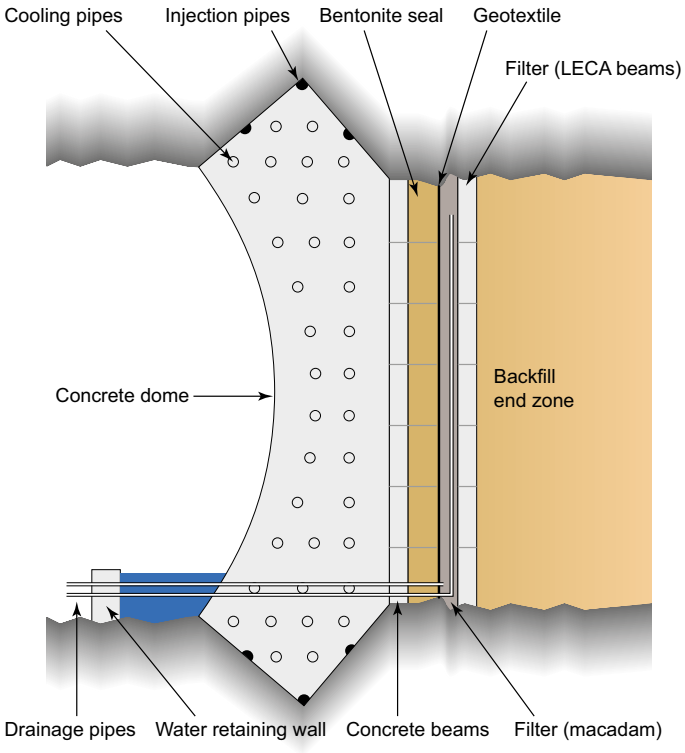

Figure 2-10. *Schematic section of the reference design of the plug (Deposition tunnel plug production report).*

Table 2-20. The main components and design parameters of the installed deposition tunnel plug. (Will be translated).

Component	Design
Concrete dome	
Dimensions	R=3.9 m
Concrete	Low-pH concrete B200 (Vogt et al. 2009).
Cooling system	Steel pipes (or if necessary copper pipes) with internal diameter 25 mm. Prefabricated sub-sections which are assembled together on a load-bearing steel frame in the slot.
Injection pipes	Polyethylene drain hose (diameter approx 50 mm, split in the middle), is attached to the rock surface with geotextile cloth and clamps.
Sealing layer of bentonite	
Thickness	0.5 m
Installed dry density	The installed dry density shall result in a swelling pressure of 2 MPa averaged over the cross-section vs the dome.
Material	Buffer bentonite
Filter	
Thickness	0.3 m
Installed dry density	~1 400 kg/m^3
Material	Washed macadam
Concrete beams and other prefabricated elements	
Concrete beams	Cast with low-pH concrete, reinforced with standard steel.
Leca beams	Cast with low-pH concrete, reinforced with standard steel.
Geotextile	Needle punched felt or fiberglass, ≥1 000 g/m^2
Drainage pipes (material)	Stainless steel
Drainage pipes (dimension)	Diameter 42 mm
Backfill end zone	
Thickness	0.5–1 m
Installed dry density	The installed dry density shall result in a swelling pressure of 2 MPa averaged over the cross-section vs the dome.
Material	Backfill bentonite

Other plugs

Plugs in the repository, other than the deposition tunnel plugs, have different purposes. They separate closed and open underground openings by keeping the closure material in place until the opening on the other side of the plug is filled with closure material. The design of the different types of plugs depends on the properties of the surrounding rock.

The plugs contain no materials that can impair the barrier functions of other barriers and the concrete used for all plugs have the same composition as the concrete in the deposition tunnel plugs.

Only deposition tunnel plugs are treated specifically in the PSAR

Main tunnels and transport tunnels

To conform to the design premises closure of the main tunnels and transport tunnels at repository level will be based on the same principle as the backfill in deposition tunnels with compacted blocks and pellets but the material and density will be different.

According to current guidelines, the closure in transport tunnels and trunk tunnels should have a similar conceptual design as the backfill in the deposition tunnels (**Backfill production report**). It involves the use of bentonite material in some form to fill in the tunnels. Figure 2-11shows transport tunnels and trunk tunnels.

In practice, the requirements on the material composition and the installed density in the main and transport tunnels are relaxed compared to those for the deposition tunnels. For example, there is no need to prevent buffer expansion and the acceptable hydraulic conductivity is higher.

2.5.2 Definition of tunnel plug variables

The tunnel plugs are bounded on the inside by the backfill in the deposition tunnels and on the outside by the backfill in transport tunnels. The plugs are surrounded by the surface of the rock. There will be tunnel plugs separating the transport tunnels from the central area as well.

The tunnel plugs are characterised thermally by their temperature.

No radiation variable is defined for the plugs since the levels of radiation caused by the repository always will remain very low at the positions of the plugs.

Hydraulically, the plugs are characterised by their pore geometry, hydrovariables (pressure and flows), water content, and sometimes by gas content, which are mainly of interest during the period when the plug is being saturated with water.

The plugs are characterised mechanically by their stress state.

The chemical state of the plugs is defined by the composition of the concrete plug, the concrete beams, the bentonite, the drainage and the filter material. The chemical state is also defined by the porewater composition.

The variables are defined in Table 2-21. The initial values of the variables, i.e. the values at the time of deposition, are given in the **Closure production report**.

Table 2-21. Definition of tunnel plug variables.

Variable	Definition
Plug geometry	Geometric dimensions of the plug
Plug pore geometry	Pore geometry as a function of time and space in the components. The porosity (the fraction of the volume that is not occupied by solid material) is often given
Temperature	Temperature as a function of time and space in the plug
Water content	Water content as a function of time and space in the plug
Gas content	Gas content as a function of time and space in the components
Hydrovariables (pressure and flows)	Flows and pressures of water and gas as a function of time and space in the plug
Stress state	Stress conditions as a function of time and space in the plug
Plug materials – composition and content	Composition of the concrete plug, the concrete beams, the bentonite, the drainage and the filter material in space and time
Plug porewater composition	Composition of the porewater in time and space in the plug
Structural and stray materials	(undefined) The structural materials in the plug are already included in the “Plug materials” variable – stray materials are assumed to be of no concern since no long-term performance is expected from the plug

2.5.3 Summary of handling of tunnel plug processes in The PSAR

Table 2-22 summarises the handling of tunnel plug processes in the PSAR, as suggested in the Process Report. In the table, the process is either "mapped" to a model by which it will be quantified or a brief verbal description of how it will be handled is provided. Since the initial evolution, characterised by unsaturated conditions and elevated temperatures is in many respects different from the long-term, saturated phase, the description in the table has been divided accordingly.

Table 2-22. Process table for the tunnel plugs describing how tunnel plug processes are handled in different time frames. Green fields denote processes that are neglected or not relevant for the time period of concern. Red fields denote processes that are quantified by modelling in the safety assessment. Orange fields denote processes that are neglected subject to a specified condition.

	Resaturation/ "thermal" period	Long-term after saturation and "thermal" period	Notes
Intact canister			
Pg1 Heat transport	Temperature as a function of distance from deposition holes is calculated. However, no specific estimate of the temperature in the plugs is done. The temperature in this component will under all circumstances remain relatively low	Temperature as a function of distance from deposition holes is calculated. However, no specific estimate of the temperature in the plugs is done. The temperature in this component will under all circumstances remain relatively low	
Pg2 Freezing	Neglected, since this requires permafrost conditions	Neglected, since there are no long-term performance requirements on the plugs	
Pg3 Water uptake and transport under unsaturated conditions	The plug will be artificially saturated during construction	Not relevant by definition	
Pg4 Water transport under saturated conditions	Assumed to be a part of the tunnel with high hydraulic conductivity	Assumed to be a part of the tunnel with high hydraulic conductivity	
Pg5 Gas transport/ dissolution	The plug will be artificially saturated during construction No gas transport can occur.	Neglected – any effect from the plugs on gas migration would be positive, since they could act as sinks. However, the effect is impossible to quantify	
Pg6 Piping/erosion	The plug is a part in the integrated treatment of piping. However, no assessment of piping in the plug itself is done	Neglected, since piping only occurs during the early part of the repository evolution	
Pg7 Swelling/mass redistribution	The plug will be artificially saturated during.construction	Neglected, since there are no long-term performance requirements on the plugs	
Pg8 Advective transport of species	Assumed to be a part of the tunnel with high hydraulic conductivity	Assumed to be a part of the tunnel with high hydraulic conductivity	
Pg9 Diffusive transport of species	Neglected since advection will dominate	Neglected since advection will dominate	
Pg10 Sorption	Sorption will occur in the plugs, but is pessimistically neglected	Sorption will occur in the plugs, but is pessimistically neglected	
Pg11 Alteration of concrete	Separate modelling of concrete degradation	Separate modelling of concrete degradation	
Pg12 Aqueous speciation and reactions	Separate modelling of concrete degradation	Separate modelling of concrete degradation	
Pg13 Osmosis	Osmotic effects are neglected due to the lack of an osmotic flow in the tunnel	Osmotic effects are neglected due to the lack of an osmotic flow in the tunnel	

	Resaturation/ “thermal” period	Long-term after saturation and “thermal” period	Notes
Pg14 Montmorillonite transformation	Neglected, since there are no long-term performance requirements on the plugs	Neglected, since there are no long-term performance requirements on the plugs	
Pg15 Montmorillonite colloid release	Neglected, since there are no long-term performance requirements on the plugs	Neglected, since there are no long-term performance requirements on the plugs	
Pg16 Microbial processes	Neglected under unsaturated conditions, since the extent of aqueous reactions is limited. For saturated conditions the treatment is the same as for “Long-term”	Microbial effects in tunnel plugs will be included in the description of the geochemistry in the repository	
Failed canister			
Pg5 Failed canister. Gas transport/dissolution	Assumed to be a part of the tunnel with high hydraulic conductivity (no failures expected in this period)	Assumed to be a part of the tunnel with high hydraulic conductivity	
Pg17 Speciation of radionuclides	Assumptions based on empirical data (no failures are expected this period)	Indirectly accounted for through the selection of parameters for radionuclide transport	
Pg18 Transport of radionuclides in water phase	Assumed to be a part of the tunnel with high hydraulic conductivity (no failures are expected this period)	Assumed to be a part of the tunnel with high hydraulic conductivity	

2.6 Central area

2.6.1 Initial state of the central area

The central area is the assembled part of the sub-surface of the KBS-3 repository facility comprising rock cavities for operation, logistics and maintenance. The rock cavities of the central area shall house transfer of canisters, storage and transhipment of rock masses, buffer, backfill and closure material, storage of equipment etc, garages and workshops, spaces for personnel and visitors and spaces for technical systems.

The central area will be filled with crushed rock. The following is an overview description of the initial state of the central area (Figure 2-11). The initial state for this component is defined as the state at the closure of the repository. A more formal and exhaustive account is given in the **Closure production report**. The repository part that is included in this description is the central area at the repository level where the ramp and shafts for transporting material and personnel start.

The total volume of this area is 125 000 m^3. The entire volume is filled with crushed rock from the site. The final density and porosity will be 1 900 kg/m^3 and 27 % (in the compacted rock fill; 100 % in the crown space) respectively. Since crushed rock is a non-swelling material there will be an open gap of about 10 cm in the top of the central area.

The only function of the closure of the cavities in the central area (Figure 2-11), is to occupy the space with no other design premise than to prevent substantial convergence and subsidence of the surrounding rock. With respect to this the reference design is crushed rock that will be placed in horizontal compacted layers. Table 2-23 shows achieved dry density of crushed rock alternatives.

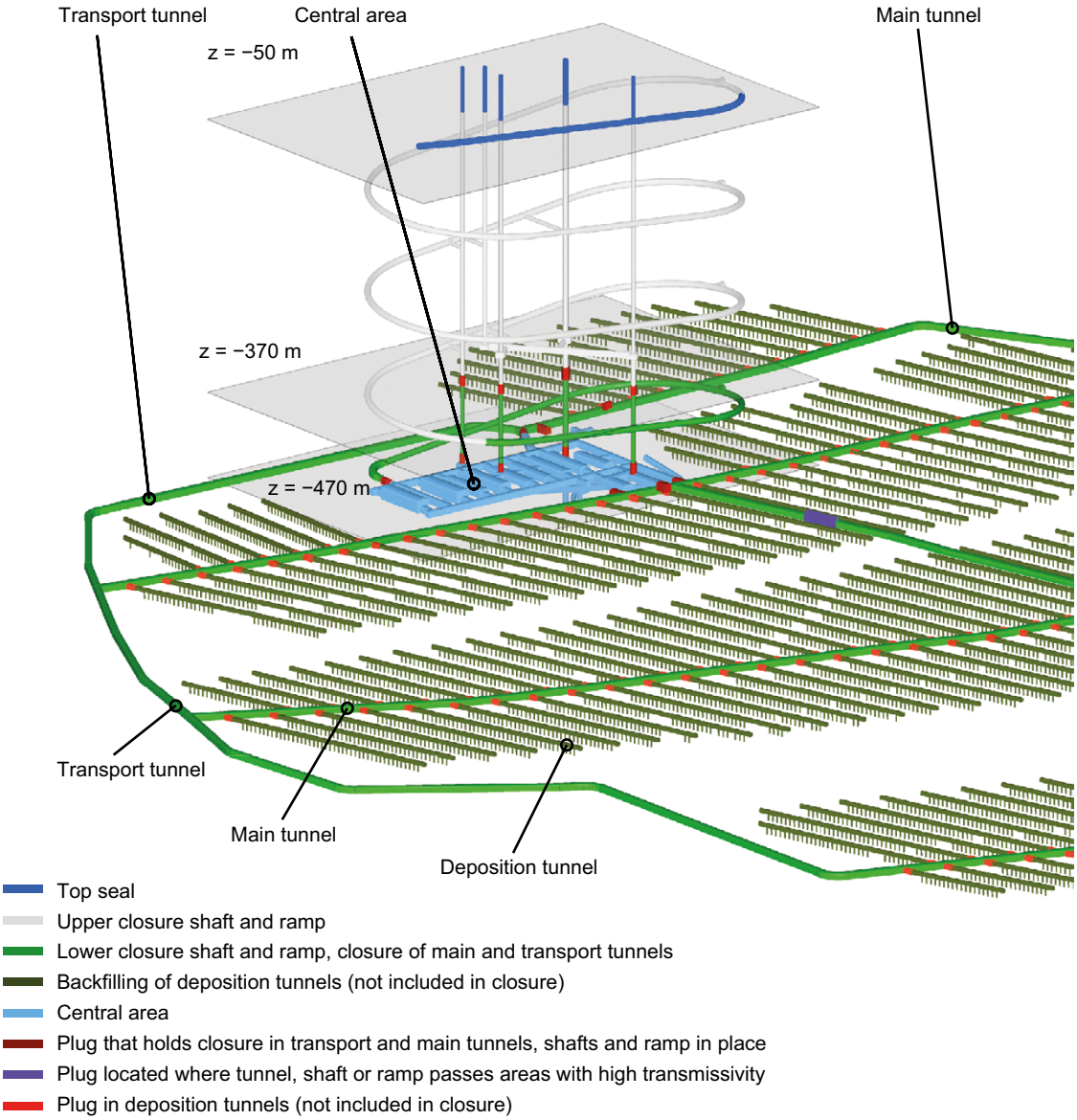

Figure 2-11. *Outline of the reference designs of closure and plugs in the underground openings (Closure production report).*

Table 2-23. Achieved dry densities of filling masses – results from road and dam constructions and backfill experiments at Äspö HRL.

Material	Dry density (kg/m^3)
Horizontael layers (packed with 5-ton vibration roller)	
Raw TBM muck	2 390–2 470
Crushed rock from blasting and TBM muck	2 100–2 300
Road	2 050–2 200
Dam construction (6-ton vibration roller)	2 000
Inclined layers	
Raw TBM muck, no compaction	1 600–2 120
Raw TBM muck, compacted	2 210–2 330
Crushed rock from blasting and TBM muck	2 110–2 210

2.6.2 Definition of central area variables

Each component in the EBS is described by a specified set of physical variables, selected to allow an adequate description of the long-term evolution of the component in question in the safety assessment.

The central area is bounded on one side by the plugs separating the transport tunnels from the central area and on the other side by the plugs separating the backfill in the ramp and shaft from the central area.

The central area is surrounded by the surface of the rock.

The central area is delimited by the variable component geometry, which in this case means actual size of the cavern. It is characterised thermally by its temperature.

No radiation variable is defined for these components since the levels of radiation caused by the repository always will remain very low.

Hydraulically, the central area is characterised by its pore geometry, hydrovariables (pressure and flows), water content, and sometimes by gas content, which are mainly of interest in the phase when the area is being saturated with water.

The central area is characterised mechanically by its stress state.

The chemical state of the central area is defined by the composition of the crushed rock and the structural and stray materials within the component. The chemical state is also defined by the porewater composition.

The variables are defined in Table 2-24. The initial values of the variables, i.e. the values at the time of deposition, are given in the initial state section in the **Post-closure safety report**.

Table 2-24. Definition of central area variables.

Variable	Definition
Central area geometry	Geometric dimensions of the component (**Closure production report**)
Central area pore geometry	Pore geometry as a function of time and space in the component. The porosity (the fraction of the volume that is not occupied by solid material) is often given
Temperature	Temperature as a function of time and space in the component
Water content	Water content as a function of time and space in the component
Gas content	Gas content as a function of time and space in the component
Hydrovariables (pressure and flows)	Flows and pressures of water and gas as a function of time and space in the component
Stress state	Stress conditions as a function of time and space in the component
Central area materials – composition and content	Composition of the crushed rock in time and space in the component (**Closure production report**)
Central area porewater composition	Composition of the porewater in time and space in the component
Structural and stray materials	Composition and quantity of construction, reinforcements and stray materials in the component as a function of time and space. (**Closure production report**)

2.6.3 Summary of handling of central area processes in the PSAR

Table 2-25 summarises the handling of central area processes in the PSAR, as suggested in this Process Report. In the table, the process is either “mapped” to a model by which it will be quantified or associated with a brief verbal description of how it will be handled. Since the initial evolution, characterised by unsaturated conditions and elevated temperatures is in many respects different from the long-term, saturated phase, the description in the table has been divided accordingly.

Table 2-25. Process table for the central area describing how the central area processes are handled in different time frames. Green fields denote processes that are neglected or not relevant for the time period of concern. Red fields denote processes that are quantified by modelling in the safety assessment. Orange fields denote processes that are neglected subject to a specified condition.

	Resaturation/ "thermal" period	Long-term after saturation and "thermal" period	Notes
Intact canister			
CA1 Heat transport	Temperature as a function of distance from deposition holes is calculated. However, no specific estimate of the temperature in the central area is made. The temperature in this component will under all circumstances remain relatively low	Temperature as a function of distance from deposition holes is calculated. However, no specific estimate of the temperature in the area is done. The temperature in this component will under all circumstances remain relatively low	
CA2 Freezing	Neglected, since this requires permafrost conditions	Neglected, due to small impact	
CA3 Water uptake and transport under unsaturated conditions	THM model	Not relevant by definition	
CA4 Water transport under saturated conditions	Assumed to be a part of the repository with high hydraulic conductivity	Assumed to be a part of the repository with high hydraulic conductivity	
CA5 Gas transport/ dissolution	THM model	Neglected, could potentially be a sink for gas	
CA6 Piping/erosion	Piping in the crushed rock cannot be excluded. However, the central area is always assumed to be a part of the repository with high hydraulic conductivity	Piping in the crushed rock cannot be excluded. However, the central area is always assumed to be a part of the repository with high hydraulic conductivity	
CA7 Swelling/mass redistribution	Most mechanical processes can be neglected since the impact and the requirements on the material are low. However, the interaction between plugs and the central area will be treated in the THM-modelling	Neglected, since there are no long-term performance requirements on the central area	
CA8 Liquefaction	Neglected, since impact is low – if the process occurs at all	Neglected, since impact is low – if the process occurs at all	
CA9 Advective transport of species	Assumed to be a part of the repository with high hydraulic conductivity	Assumed to be a part of the repository with high hydraulic conductivity	
CA10 Diffusive transport of species	Neglected since advection will dominate	Neglected since advection will dominate	
CA11 Sorption	Sorption will occur in the central area, but is pessimistically neglected	Sorption will occur in the central area, but is pessimistically neglected	
CA12 Alteration of the central area backfill	Modelling of the geochemical evolution	Modelling of the geochemical evolution	
CA13 Aqueous speciation and reactions	Separate modelling of concrete degradation	Separate modelling of concrete degradation	
CA14 Osmosis	Osmotic effects will be insignificant in the crushed rock material	Osmotic effects will be insignificant in the crushed rock material	
CA15 Alteration of concrete components	Separate modelling of concrete degradation	Separate modelling of concrete degradation	
CA16 Corrosion of steel components	Modelling of the geochemical evolution	Modelling of the geochemical evolution	
CA17 Microbial processes	Neglected under unsaturated conditions, since the extent of aqueous reactions is limited. For saturated conditions the treatment is the same as for "Long-term"	Microbial effects in the central area will be included in the description of the geochemistry in the repository	

	Resaturation/ “thermal” period	Long-term after saturation and “thermal” period	Notes
Failed canister			
CA18 Speciation of radionuclides	Assumptions based on empirical data *(no failures are expected this period)*	Indirectly accounted for through the selection of parameters for radionuclide transport	
CA19 Transport of radionuclides in water phase	Assumed to be a part of the repository with high hydraulic conductivity *(no failures are expected this period)*	Assumed to be a part of the repository with high hydraulic conductivity	

2.7 Top Seal

2.7.1 Initial state of the top seal

In this report the term “Top seal” has been used for both the filling of the ramp and shaft above ~370 m below ground surface as well as for the actual “top seal” which stretches from 50 m below surface to the surface. From the level of −370 m up to the level of −50 m, the ramp and shaft are sealed with crushed rock. The top seal is in the uppermost 50 meters of the shaft and ramp. To conform to the requirement that “closure in the upper part of the ramp, shafts and boreholes shall hinder unintentional intrusion into the repository” the ramp and shafts, from –50 m depth to the zero ground level, is filled with fairly well fitted rock blocks and the crushed rock compacted by its own weight. The sealing the upper part of the ramp and shafts on a repository scale is indicated in Figure 2-11.

2.7.2 Definition of top seal variables

Each component in the EBS is described by a specified set of physical variables, selected to allow an adequate description of the long-term evolution of the component in question in the safety assessment.

The top seal is bounded on one side by the backfill in the lower part of the ramp and shaft and on the other side by the ground surface. The top seal is surrounded by the surface of the host rock.

The top seal, as it is delimited by the variable geometry, is characterised thermally by its temperature.

No radiation variable is defined for this component since the levels of radiation caused by the repository always will remain very low at the locations of the top seals.

Hydraulically, the top seal is characterised by its pore geometry, hydrovariables (pressure and flows), water content, and sometimes by gas content, which are mainly of interest in the phase when the filling is being saturated with water.

The top seal is characterised mechanically by its stress state.

The chemical state of the top seal is defined by the composition of the crushed rock and the structural and stray materials within the component. The chemical state is also defined by the porewater composition.

The variables are defined in Table 2-26. The initial values of the variables, i.e. the values at the time of deposition, are given in the **Closure production report**.

2.7.3 Summary of handling of top seal processes in the PSAR

Table 2-27 summarises the handling of top seal processes in the safety assessment the PSAR, as suggested in the process report. In the table, the process is either “mapped” to a model by which it will be quantified or a brief verbal description of how it will be handled is provided. Since the initial evolution, characterised by unsaturated conditions and elevated temperatures is in many respects different from the long-term, saturated phase, the description in the table has been divided accordingly.

Table 2-26. Definition of top seal variables.

Variable	Definition
Top seal geometry	Geometric dimensions of the component (**Closure production report**).
Top seal pore geometry	Pore geometry as a function of time and space in the components. The porosity (the fraction of the volume that is not occupied by solid material) is often given
Temperature	Temperature as a function of time and space in the component
Water content	Water content as a function of time and space in the component
Gas content	Gas content as a function of time and space in the component
Hydrovariables (pressure and flows)	Flows and pressures of water and gas as a function of time and space in the component
Stress state	Stress conditions as a function of time and space in the component
Top seal materials – composition and content	Composition of the crushed rock in time and space in the component (**Closure production report**)
Top seal porewater composition	Composition of the porewater in time and space in the component
Structural and stray materials	Composition and quantity of construction, reinforcements and stray materials in the component as a function of time and space

Table 2-27. Process table for the top seal describing how top seal processes are handled in different time frames. Green fields denote processes that are neglected or not relevant for the time period of concern. Red fields denote processes that are quantified by modelling in the safety assessment. Orange fields denote processes that are neglected subject to a specified condition.

	Resaturation/ “thermal” period	Long-term after saturation and “thermal” period	Notes
Intact canister			
TS1 Heat transport	Temperature as a function of distance from deposition holes is calculated. However, no specific estimate of the temperature in the top seal is made	Temperature as a function of distance from deposition holes is calculated. However, no specific estimate of the temperature in the top seal is done	
TS2 Freezing	Neglected, since this requires permafrost conditions (probably not entirely true, since the top of the top seal may freeze during winter, see “Long-term”)	The top seal will freeze during permafrost periods. However, the consequences can be neglected due to the high hydraulic conductivity of the material	
TS3 Water uptake and transport under unsaturated conditions	Rough estimate of time to reach saturation	Not relevant by definition	
TS4 Water transport under saturated conditions	Assumed to be a part of the repository with high hydraulic conductivity	Assumed to be a part of the repository with high hydraulic conductivity	
TS5 Gas transport/ dissolution	Rough estimate of time to reach saturation	Neglected – the top seal will have limited effect on gas movement in the repository	
TS6 Piping/erosion	Neglected, since piping cannot occur in the material	Neglected, since piping cannot occur in the material	
TS7 Swelling/mass redistribution	Mechanical processes in the top seal are of no concern for the performance of the repository	Mechanical processes in the top seal are of no concern for the performance of the repository	There will be an interaction between top seal and ramp/ shaft backfill – this is discussed in Section 7.3.1
TS8 Liquefaction	Neglected, cannot occur in this type of material	Neglected, cannot occur in this type of material	

	Resaturation/ “thermal” period	Long-term after saturation and “thermal” period	Notes
TS9 Advective transport of species	Assumed to be a part of the repository with high hydraulic conductivity	Assumed to be a part of the repository with high hydraulic conductivity	
TS10 Diffusive transport of species	Neglected, since advection will dominate	Neglected, since advection will dominate	
TS11 Sorption	Sorption may occur in the top seal, but is pessimistically neglected	Sorption may occur in the top seal, but is pessimistically neglected	
TS12 Alteration of concrete	Neglected, due to the distance chemical processes in this component will have limited impact on the performance of the rest of the repository. The hydraulic conductivity of this component will under all circum-stances be high	Neglected, due to the distance chemical processes in this component will have limited impact on the performance of the rest of the repository. The hydraulic conductivity of this component will under all circumstances be high	
TS13 Aqueous speciation and reactions	Neglected, due to the distance chemical processes in this component will have limited impact on the performance of the rest of the repository	Neglected, due to the distance chemical processes in this component will have limited impact on the performance of the rest of the repository	
TS14 Colloid release	Neglected, will have no effect on the performance	Neglected, will have no effect on the performance	
TS15 Steel corrosion	Neglected, due to the distance chemical processes in this component will have limited impact on the performance of the rest of the repository	Neglected, due to the distance chemical processes in this component will have limited impact on the performance of the rest of the repository	
TS16 Microbial processes	Neglected under unsaturated conditions, since the extent of aqueous reactions is limited. For saturated conditions the treatment is the same as for “Long-term”	No specific treatment of microbial processes in the top seal will be done – is not expected to differ from the rest of the repository	
Failed canister			
TS17 Speciation of radionuclides	Assumptions based on empirical data *(no failures are expected this period)*	Indirectly accounted for through the selection of parameters for radionuclide transport	
TS18 Transport of radionuclides in water phase	Assumed to be a part of the repository with high hydraulic con-ductivity *(No failures are expected this period)*	Assumed to be a part of the repository with high hydraulic conductivity	

2.8 Bottom plate

2.8.1 Initial state of the bottom plate

Bottom plate in deposition holes

The reference method for drilling deposition holes will not accomplish a completely flat bottom in the deposition holes. Therefore, a plate is installed to achieve sufficiently flat bottom as base for the buffer block stack and to prevent groundwater uptake in the bottom bentonite block.

In the reference design the bottom plate consists of a thin copper plate that covers the bottom and the lower part of the mantle surface of the bentonite block, seeFigure 2-12. The bottom plate is attached to the bottom bentonite block prior to installation.

The design of the bottom plate has changed entirely since SR-Site and it could be argued that this component should be left of from the description of components in the report and instead be included as “stray material”

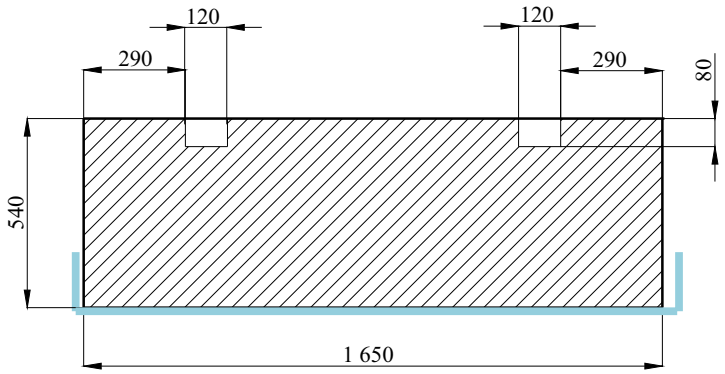

Figure 2-12. *The bottom plate in the deposition hole.*

2.8.2 Definition of bottom plate variables

The bottom plate is bounded on the top by the buffer in the deposition hole and by the bottom and sides of the rock wall.

The bottom plate, as it is delimited by the variable geometry, are characterised thermally by its temperature.

No radiation variable is defined for the bottom plate since the levels of radiation caused by the spent fuel in the canister always will remain low at this location and the radiation will not affect the intended performance of the bottom plate.

Hydraulically, the bottom plate is characterised by its geometry.

The bottom plate is characterised mechanically by its stress state.

The chemical state of the bottom plate is defined by the composition of the copper plate.

The variables are defined in Table 2-28. The initial values of the variables, i.e. the values at the time of deposition, are given in the **Post-closure safety report**.

Table 2-28. Definition of bottom plate variables.

Variable	Definition
Bottom plate geometry	Geometric dimensions of the bottom plate
Bottom plate pore geometry	Pore geometry as a function of time and space in the plate components. Will be zero for an unaltered copper plate
Temperature	Temperature as a function of time and space in the bottom plate
Water content	Water content as a function of time and space in the bottom plate. Will be zero for an unaltered copper plate
Gas content	Gas content as a function of time and space in the bottom plate. Will be zero for an unaltered copper plate
Hydrovariables (pressure and flows)	Flows and pressures of water and gas as a function of time and space in the bottom plate
Stress state	Stress conditions as a function of time and space in the bottom plate
Bottom plate materials – composition and content	Composition of the copper plate
Bottom plate porewater composition	Composition of the porewater in time and space in contact with the bottom plate
Structural and stray materials	(undefined) The structural materials in the bottom plate are already included in the “Bottom plate materials – composition and content” variable – stray materials are assumed to be of no concern since no long-term performance is expected from the bottom plate

2.8.3 Summary of handling of bottom plate processes in the PSAR

Table 2-29 summarises the handling of bottom plate processes in the PSAR, as suggested in the Process Report. In the table, the process is either "mapped" to a model by which it will be quantified or a brief verbal description of how it will be handled is provided. Since the initial evolution, characterised by unsaturated conditions and elevated temperatures is in many respects different from the long-term, saturated phase, the description in the table has been divided accordingly.

Table 2-29. Process table for the bottom plate describing how bottom plate processes are handled in different time frames. Green fields denote processes that are neglected or not relevant for the time period of concern. Red fields denote processes that are quantified by modelling in the safety assessment. Orange fields denote processes that are neglected subject to a specified condition. Some numbers (BP#) are missing in the table and these reflect the processes that have disappeared due to the new design of the bottom plate. The numbers from SR-Site are kept.

	Resaturation/ "thermal" period	Long-term after saturation and "thermal" period	Notes
Intact canister			
BP1 Heat transport	Temperature as a function of distance from deposition holes is calculated. However, no specific estimate of the temperature in the bottom plate is made, since thermal effects on the properties of the bottom plate are disregarded	Temperature as a function of distance from deposition holes is calculated. However, no specific estimate of the temperature in the bottom plate is made since thermal effects on the properties of the bottom plate are disregarded	
BP2 Freezing	Neglected, since this requires permafrost conditions	Of no significance, since no long term performance is expected from the bottom plate. Cannot occur in an intact bottom plate	
BP3 Water uptake and transport under unsaturated conditions	The bottom plate is included in the THM modelling of the saturation of the buffer	Not relevant by definition	
BP6 Piping/erosion	The process does not take place in the bottom plate – but piping in the buffer may be of importance for the interaction with the bottom plate and will be assessed. This is treated in Process BP7	Does not occur	
BP7 Swelling/mass redistribution	Included in THM-modelling	Neglected, of no concern	
BP10 Sorption	Sorption may occur in the bottom plate, but is pessimistically neglected	Sorption may occur in the bottom plate, but is pessimistically neglected	
BP12 Aqueous speciation and reactions	Neglected	Negleted	
BP13 Copper corrosion	Neglected, since no long term performance is required from the copper	Neglected, since no long term performance is required from the copper	
BP14 Microbial processes	Pessimisstical neglected, the copper plate could potentially serve as a sink for sulphide, which could lower canister corrosion	Pessimisstical neglected,, the copper plate could potentially serve as a sink for sulphide, which could lower canister corrosion	
Failed canister			
BP15 Speciation of radionuclides	Assumptions based on empirical data *(no failures are expected this period)*	Irrelevant	
BP16 Transport of radionuclides in water phase	Pessimistically neglected	Pessimistically neglected	

2.9 Borehole seals

2.9.1 Initial state of the borehole seals

A number of more or less vertical investigation or surface-based characterisation boreholes were drilled during the site investigations in order to obtain inter alia data on the properties of the host rock. These boreholes will be sealed no later than at the closure of the final repository. Holes will also be drilled from the repository tunnels during the construction phase, implying that horizontal and upwards directed holes also have to be sealed. Longevity (chemical stability over time) is an essential property of borehole plugs.

Many investigation boreholes have been drilled in the area for the planned Spent Fuel Repository. The variation of borehole types is high, from short boreholes which mainly are drilled through the regolith layers to deep investigation boreholes passing through or close to the planned repository. Due to the large variation of borehole types, it has been decided to perform a classification of all boreholes based on borehole depth, distance to the repository area and on the presence of hydraulic connections between the borehole and the repository area. The work with inventory and classification is ongoing (Sandén et al. 2018).

The boreholes are suggested to be divided into three classes:

- BHC1. Shallow boreholes, 0–75 m, which are assessed to have no hydraulic influence on a repository. This group includes both boreholes going through regolith and through rock and that are not crossing any water bearing fracture zones with hydraulic connections to the repository.
- BHC2. Deep boreholes, 75 to > 1 000 m, located rather far from the repository area, > 400 m. The boreholes are not crossing water bearing fracture zones with hydraulic connections to the repository.
- BHC3. Deep boreholes, 75 to > 1 000 m, located close to the repository area, < 400 m. Also, other boreholes that are hydraulically connected to the repository area should be in this class.

Borehole Class BHC1

Shallow boreholes which are assessed to have no hydraulic influence on a repository. The boreholes in this class are divided into two subgroups:

Type A: Shallow boreholes in regolith.

Type B: Shallow boreholes going in both regolith and rock.

Borehole depth: < 75 m.

Hydraulic influence: The boreholes should not cross any water bearing fracture zones with hydraulic connections to the repository area. If they do, they should be upgraded to BHC3.

Distance from repository: Concerns all boreholes that have been drilled in the disposal area.

The requirements relevant for borehole Class BHC1 are:

- Tightness (hydraulic conductivity). Surface water should not be able to flow via the borehole down to water bearing layers. Different water bearing regolith layers shall not have contact with each other via the sealed borehole. This should be guaranteed by having installed a seal material that is much tighter than the surrounding regolith layers.
- Mechanical. The material should constitute a mechanical support for the borehole walls.
- Post closure safety. No requirements.

To fulfill the requirements these boreholes should be filled with bentonite pellets. The bentonite pellet filling will have a hydraulic conductivity that is much lower than the surrounding regolith layers and it will also constitute a mechanical support for the borehole walls.

The boreholes in this class are divided according to the following, Figure 2-13:

- Borehole Type A. Boreholes that only are going through the regolith layer will be filled with bentonite pellets.
- Borehole Type B. If the borehole also is going into the bedrock (borehole Type B), a concrete plug is installed in the upper part of the rock, before reaching the regolith layer. The plug consists of concrete that is in-situ cast in a borehole section with a diameter larger than the nominal.

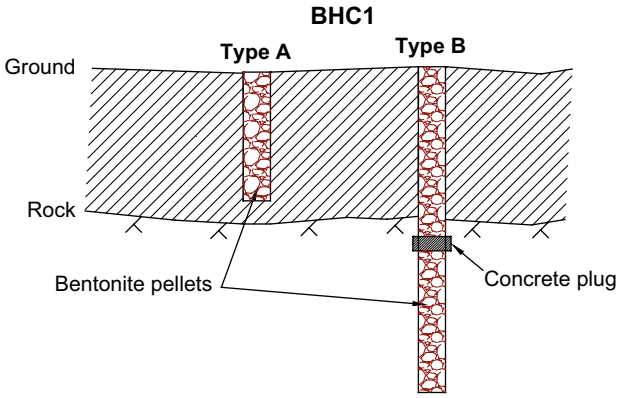

Figure 2-13. *Schematic showing how shallow boreholes are sealed with pellets of bentonite (Sandén et al. 2018).*

A top closure (the uppermost meter of the borehole) will consist of either compacted regolith (same as the surroundings) or with conventional concrete.

Borehole Class BHC2

Boreholes with different depths, 75 to > 1 000 m, located relatively far from the disposal area. Boreholes in this class are assessed to have marginal or no hydraulic impact on the repository. It is recommended to seal these boreholes with a rather simple method.

Borehole depth: 75 to > 1 000 m

Hydraulic influence: The boreholes should not cross any water bearing fracture zones with hydraulic connections to the repository area. If they do, they should be upgraded to BHC3.

Distance from repository: > 400 m

The requirements that are relevant for borehole Class BHC2 are:

- Tightness (hydraulic conductivity).
  1. Regolith layer: Same as for class BHC1
  2. Rock: No requirements on hydraulic tightness for the parts of the borehole that is going through the rock.
- Mechanical. The material should constitute a mechanical support for the borehole walls.
- Post closure safety. No requirements.

The closure of boreholes in this class can be divided in three parts, Figure 2-14:

1. The regolith layers. To fulfill the requirements this section of the borehole should be filled with bentonite pellets. The bentonite pellet filling will have a hydraulic conductivity that is much lower than the surrounding regolith layers and it will also constitute a mechanical support for the borehole walls.
2. Upper part of the borehole section going in rock. A concrete plug is installed in the upper part of the rock, before reaching the regolith layer. The plug consists of concrete that is in-situ cast in a reamed section with larger diameter.
3. Borehole going through rock. Since there are no requirements on the hydraulic tightness for these parts of the boreholes in this class, sand will be used to fill up the volume and give a me-chanical support to the borehole walls.

A top closure (the uppermost meter of the borehole) will consist of either compacted regolith (same as the surroundings) or with conventional concrete.

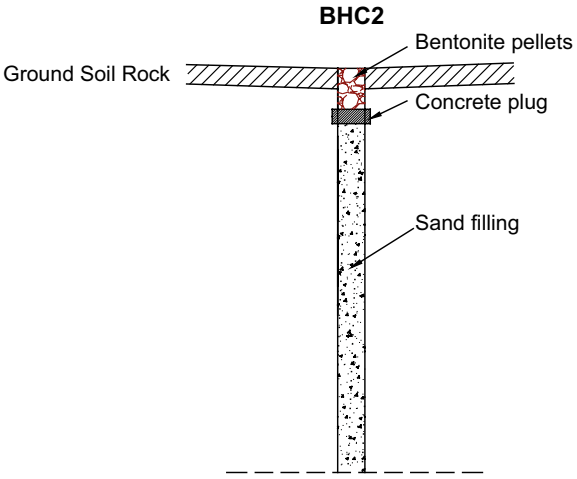

Figure 2-14. *Schematic showing how deep boreholes which are not hydraulic connected to the repository area are sealed (Sandén et al. 2018).*

Borehole Class BHC3

Medium deep and deep boreholes close to the repository area. These boreholes are assessed to have a certain influence on the hydraulic situation on repository depth. Boreholes in this class are recommended to be sealed in an efficient way to prevent axial water flow.

Borehole depth: 75 to > 1 000 m.

Hydraulic influence: All boreholes in the nearfield, < 400 m, with a depth > 75 meters are included in this class.

Distance from repository: < 400 m.

The requirements that are relevant for borehole Class BHC3 are:

- Tightness (hydraulic conductivity).
  1. Regolith layer: Same as for class BHC1.
  2. Rock: The hydraulic conductivity of the sealing should be 10^{-6} m/s or lower.
- Mechanical. The material should constitute a mechanical support for the borehole walls and for the sealing sections that are planned to be installed.
- Post closure safety. The requirements on mechanical stability and hydraulic conductivity should be fulfilled on the life span of the repository.

Boreholes in this class should be sealed with the so-called Sandwich method (Sandén et al. 2018). The closure of boreholes in this class consists of following components (Figure 2-15):

Bentonite pellets. To fulfill the requirements on the part of the borehole that is going through regolith layers, this part should be filled with bentonite pellets. The bentonite pellet filling will have a hydraulic conductivity that is much lower than the surrounding regolith layers and it will also constitute a mechanical support for the borehole walls.

1. Concrete plug (Upper top seal). A concrete plug is installed in the upper part of the rock, before reaching the regolith layer. The plug consists of concrete that is in-situ cast in a reamed borehole section a larger diameter.
2. Sand. The main part of the borehole is filled with sand. The sand is mechanically and chemically stable.
3. Bentonite. Highly compacted bentonite plugs are positioned in selected borehole sections with good rock quality i.e. there are no water bearing fractures present. These sections will after satu-ration have a very low hydraulic conductivity.

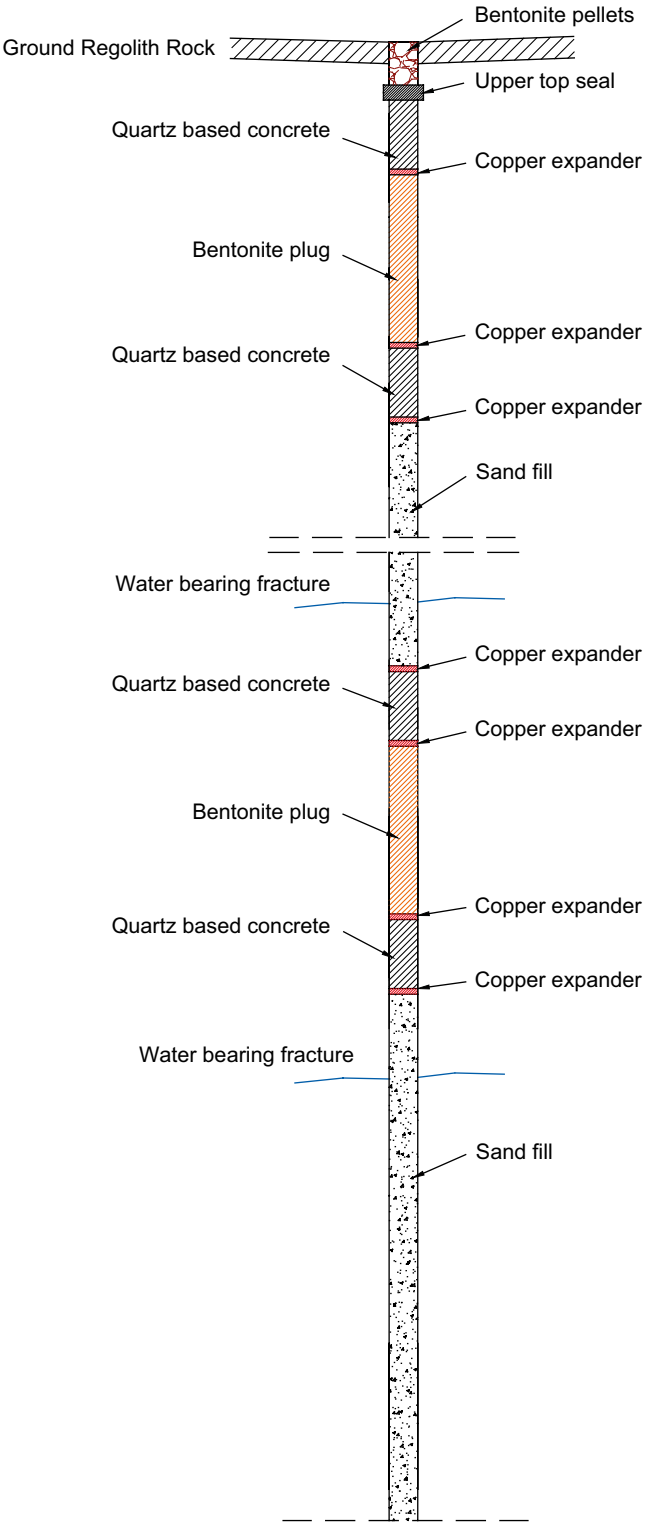

Figure 2-15. *Schematic showing the suggested principle for sealing of deep investigation boreholes, the so called "Sandwich-concept". The design includes dense bentonite plugs positioned in selected borehole sections with good rock quality i.e. there are no water bearing fractures present. Permeable sand is filling up the main part of the borehole. Concrete is positioned in the transition zones between bentonite and sand. Copper expanders are installed to separate different materials (Sandén et al. 2018).*

4. Concrete. Concrete with low cement content will be positioned in the transition zones between bentonite and sand.
5. Copper expanders (bridge plugs). The copper expanders are installed to separate different materials. They facilitate the installation e.g. prevents concrete from flowing into the annular gap between bentonite plugs and rock walls and they will also prevent mixing between different materials in the long term.

A top sealing of a borehole i.e. the uppermost meter of the borehole, will consist of either compacted regolith (if the borehole entrance is in regolith) or of conventional concrete (if the borehole entrance is in rock).

2.9.2 Definition of variables for borehole seals

Each component in the EBS is described by a specified set of physical variables, selected to allow an adequate description of the long-term evolution of the component in question in the safety assessment.

The borehole seals are bounded on one side either by the ground surface or by the tunnel backfill.

The borehole seals are entirely surrounded by the rock.

The borehole seals, as delimited by the variable geometry, are characterised thermally by their temperature.

No radiation variable is defined for this component since the levels of radiation caused by the repository always will remain very low at the locations of the borehole seals.

Hydraulically, the borehole seals are characterised by their pore geometry, hydrovariables (pressure and flows), water content, and sometimes by gas content, which are mainly of interest in the phase when the bentonite in the seals is being saturated with water.

The borehole seals are characterised mechanically by their stress state.

The chemical state of the borehole seals is defined by the composition of the sand, the bentonite, the copper expanders and the concrete mix design. The chemical state is also defined by the porewater composition.

The variables are defined in Table 2-30.The initial values of the variables, i.e. the values at the time of deposition, are not clearly specified at the moment, but the crucial information can be found in Sandén et al. (2018) and in the **Post-closure safety report**.

Table 2-30. Definition of borehole seal variables.

Variable	Definition
Borehole geometry	Geometric dimensions of the components
Pore geometry	Pore geometry as a function of time and space in the component. The porosity (the fraction of the volume that is not occupied by solid material) is often given
Temperature	Temperature as a function of time and space in the components
Water content	Water content as a function of time and space in the components
Gas content	Gas content as a function of time and space in the components
Hydrovariables (pressure and flows)	Flows and pressures of water and gas as a function of time and space in the component
Stress state	Stress conditions as a function of time and space in the component
Sealing materials – composition and content	Composition of the sand, bentonite and the concrete in time and space in the component
Porewater composition	Composition of the porewater in time and space in the component
Structural and stray materials	Composition and quantity of construction, reinforcements and stray materials in the components as a function of time and space. This includes the copper expanders, and the anchor materials

2.9.3 Summary of handling of borehole seal processes in the PSAR

Table 2-31 summarises the handling of borehole seal processes in the PSAR, as suggested in this Process Report. In the table, the process is either "mapped" to a model by which it will be quantified or a brief verbal description of how it will be handled is provided. Since the initial evolution, characterised by unsaturated conditions and elevated temperatures is in many respects different from the long-term, saturated phase, the description in the table has been divided accordingly.

Table 2-31. Process table for the borehole seals describing how borehole seal processes are handled in different time frames. Green fields denote processes that are neglected or not relevant for the time period of concern. Red fields denote processes that are quantified by modelling in the safety assessment. Orange fields denote processes that are neglected subject to a specified condition.

	Resaturation/ "thermal" period	Long-term after saturation and "thermal" period	Notes
Intact canister			
BHS1 Heat transport	Temperature as a function of distance from deposition holes is calculated. However, no specific estimate of the temperature in the borehole seals is made	Temperature as a function of distance from deposition holes is calculated. However, no specific estimate of the temperature in the borehole seals is made	
BHS2 Freezing	A specific assessment of the evolution of the borehole seals during freezing conditions is done. This is done for an older type of bore hole seals.	A specific assessment of the evolution of the borehole seals during permafrost conditions is done This is done for an older type of bore hole seals.	
BHS3 Water uptake and transport under unsaturated conditions	Assessment of the timescale of borehole seal hydration. This is done for an older type of bore hole seals.	Not relevant by definition	
BHS4 Water transport under saturated conditions	Can be neglected as long as the bentonite component remains in place. The case of lost sealing will be assessed in the modelling of the geosphere	Can be neglected as long as the bentonite part remains in place. The case of lost sealing will be assessed in the modelling of the geosphere	
BHS5 Gas transport/ dissolution	No specific assessment of the saturation of the borehole seals will be done. The process is expected to be rather fast since the diameter is small	Neglected – no gas is expected to enter the borehole seals	
BHS6 Piping/erosion	Neglected since the holes are initially water filled and no gradients are expected	Neglected, since piping only occurs during the early part of the repository evolution	
BHS7 Swelling/mass redistribution	Separate modelling of the homogenisation. This is done for an older type of bore hole seals.	Assessment of the consequences of a local loss of bentonite. This is done for an older type of bore hole seals.	
BHS8 Liquefaction	Neglected, based on same arguments as for the buffer	Neglected, based on same arguments as for the buffer	
BHS9 Advective transport of species	Can be neglected as long as the bentonite part remains in place. The case of lost sealing will be assessed in the modelling of the geosphere	Can be neglected as long as the bentonite part remains in place. The case of lost sealing will be assessed in the modelling of the geosphere	
BHS10 Diffusive transport of species	Neglected since diffusive transport in the borehole seals will be very slow	Neglected since diffusive transport in the borehole seals will be very slow	
BHS11 Sorption	Sorption will occur in the borehole seals, but is pessimistically neglected	Sorption will occur in the borehole seals, but is pessimistically neglected	

	Resaturation/ “thermal” period	Long-term after saturation and “thermal” period	Notes
BHS12 Alteration of concrete	Separate modelling of concrete degradation	Separate modelling of concrete degradation	
BHS13 Aqueous speciation and reactions	Separate modelling of concrete degradation	Separate modelling of concrete degradation	
BHS14 Copper corrosion	Neglected for the expanders, since no long term performance is required from the copper there	Neglected for the expanders, since no long term performance is required from the copper there	
BHS15 Alteration of accessory minerals in bentonite	Neglected, since no thermal gradients will exist	No specific assessment – the results from the modelling of the buffer will be used as “analogue”	
BHS16 Osmosis	No specific assessment of the saturation of the bore hole seals will be done. The process is expected to be rather fast since the diameter is small. For post saturation, see “long term”	Evaluation of swelling pressure and hydraulic conductivity of the bentonite part of the seals through comparison with empirical data	
BHS17 Montmorillonite transformation	Neglected, process will not occur on short time scale (see long term)	Estimate based on comparison with natural systems. Separate discussion on the interaction between bentonite and concrete	
BHS18 Montmorillonite colloid release	Neglected if total cation charge is > 8 mM Otherwise discussed	Neglected if total cation charge is > 8 mM Otherwise discussed	
BHS19 Microbial processes	Neglected under unsaturated conditions, since the extent of aqueous reactions is limited. For saturated conditions the treatment is the same as for “Long-term”	No specific treatment of microbial process will be done – is not expected to differ from the rest of the repository	
Failed canister			
BHS21 Speciation of radionuclides	Assumptions based on empirical data *(no failures are expected this period)*	Indirectly accounted for through the selection of parameters for radionuclide transport	
BHS22 Transport of radionuclides in water phase	(No failures are expected this period)	Can be neglected as long as the bentonite part remains in place The case of lost sealing will be assessed in the modelling of the geosphere	

3 Processes in the buffer

3.1 Radiation-related processes

3.1.1 Radiation attenuation/heat generation

Overview

Gamma and neutron radiation from the canister are attenuated in the buffer. The process is described in the **Fuel and canister process report**. The maximum dose outside the canister has been calculated to be less than 500 mGy/h at time of encapsulation. The dose is dominated by Cs-137, which has a half-life of ~ 30 years. The radiation that is not attenuated reaches as far as near-field rock. The main part of the gamma radiation from the spent fuel is shielded by the iron and copper in the canister. Only a minor fraction will reach the buffer.

Radiation is of importance owing to its effect on the chemical processes, principally radiation-induced montmorillonite decomposition and gamma radiolysis of porewater.

Dependencies between process and buffer variables

Table 3-1 summarises how the process influences and is influenced by all buffer variables and how these effects are treated in the PSAR.

Table 3-1. Direct dependences between the process "Radiation attenuation/heat generation" and the defined buffer variables and a short note on the handling in the PSAR.

Variable	Variable influence on process		Process influence on variable	
	Influence present? (Yes/No) Description	Handling of influence? (How/Why not)	Influence present? (Yes/No) Description	Handling of influence? (How/Why not)
Buffer geometry	Yes. Determines mass/ volume available	Included in dose rate calculation	No	
Pore geometry	No		No	
Radiation intensity	Yes. Determines energy deposited	Included in dose rate calculation	Yes. Shielding	Included in dose rate calculation
Temperature	No		Yes. Energy is deposited	Neglected since it is negligible compared to other processes influencing temperature
Water content	Yes. Determines how energy is deposited	Included in dose rate calculation	No	
Gas content	No, but indirectly through water content	See row above	Indirectly through Radiolysis of porewater (3.5.14)	
Hydrovariables (pressure and flows)	No		No	
Stress state	No		No	
Bentonite composition	Yes. Determines how energy is deposited	Included in dose rate calculation	No	
Montmorillonite composition	Yes. Determines how energy is deposited	Included in dose rate calculation	Yes	Negligible, see Radiation-induced transformations (3.5.13)
Porewater composition	Yes. Determines how energy is deposited, but the effect is minor	Neglected, Water density does not vary very much	No	
Structural and stray materials	No		Negligible	Of no concern

The result is a radiation field in the buffer that can lead to radiolysis and that has a marginal impact on the montmorillonite, see further Sections 3.5.13 and 3.5.14.

Attenuation of gamma and neutron radiation will raise the temperature of the buffer, but the effect is negligible compared with other temperature-raising processes.

Boundary conditions

The boundary condition is the radiation intensity to which the buffer is exposed, i.e. the flux leaving the outer surface of the canister.

Model studies/experimental studies

Attenuation of gamma and neutron radiation can be calculated theoretically for an arbitrary material if geometry and composition are known, see e.g. the model studies mentioned for the corresponding process in the canister.

Natural analogues/observations in nature

Not applicable.

Time perspective

The time perspective is determined by the decay properties of the spent fuel. The gamma and neutron radiation are significant over the first 1 000 years. Details of the fuel decay characteristics are provided in the **Fuel and canister process report**.

Handling in the safety assessment the PSAR

Quantification of this process is needed to evaluate the processes 3.5.13 Radiation-induced transformations and 3.5.14 Radiolysis of porewater. The former is shown to be negligible for the relevant radiation intensities. The latter could affect the canister surface, but also this effect is shown to be insignificant, see further Sections 3.5.14 and the relevant canister process (**Fuel and canister process report**). The radiation field outside a canister has been calculated in Lundgren (2004). The calculated dose rate is lower than 500 mGy/h (100–150 mGy/h) at the time of deposition.

Uncertainties

Uncertainties in mechanistic understanding

The understanding of the process is deemed sufficient for the needs of the safety assessment.

Model simplification uncertainties in the PSAR

Not relevant.

Input data and data uncertainties in the PSAR

In general, data for a quantitative description of the process are known with sufficient accuracy for the needs of the safety assessment, considering the small effects of this process on the repository system.

3.2 Thermal processes

3.2.1 Heat transport

Overview

Heat is transported from the canister surface to the buffer, through the buffer and finally from the buffer to the rock both directly and via the tunnel backfill. Initially after deposition there will be gaps between the canister and the buffer and between the buffer and the rock. During this time, heat will be transported by a combination of radiation and conduction across the two gaps and by pure conduction across the bentonite that will be unsaturated. There may be some convection, but because of the low permeability of the bentonite and because of the narrow gaps, this contribution can be ignored. In particular the heat resistance of the gap between canister and bentonite will be high because of the low emissivity of the copper surface and the associated low radiant heat transfer. The heat resistance of the pellet-filled gap between buffer and rock will be lower and will not have such a large impact on the canister temperature as the canister/buffer gap. In addition, the pellet-filled gap will start to close soon after deposition while the canister/buffer gap will remain open longer. However, the blocks could also crack and form thermal bridges which would increase the heat transport over the slot. The efficiency of heat transport through the buffer region is important for the performance of the system, since it affects the maximum buffer temperature for which a design threshold (< 100 °C) has been established.

When the buffer has been water-saturated and has swelled so that all gaps and joints are filled, heat transport will take place by conduction through water-saturated bentonite. The saturation of the buffer takes place in the time period from years to a thousand years, while the peak temperature of the buffer is reached in 5–15 years. Thermal conductivity was measured on material from the FEBEX test (Villar et al. 2018). The result shows that the thermal conductivity was largely unchanged after 18 years in repository conditions.

Shortly after deposition, heat transport through the buffer is largely independent of the buffer heat capacity, and heat conduction in the buffer can be approximately described by the time-independent heat conduction equation:

$$\nabla(\lambda \nabla T) = 0 \qquad (3\text{-}1)$$

The most important parameter is thus the thermal conductivity, λ, of different parts of the system. The thermal conductivity of bentonite is primarily dependent on its density, water saturation and mineral composition. The thermal conductivity of water-saturated MX-80 bentonite that has swelled to its intended density of 2 000 kg/m^3, is about 1.3 W/(m · K) according to laboratory experiments (Svensson et al. 2019).

The thermal conductivity of the pellets-filled gap between the bentonite blocks and the surrounding rock is 0.3–0.4 W/(m · K) (Hökmark et al. 2009). For the hot air filling the canister-bentonite space, the conductivity is about 0.03 W/(m · K), but radiant heat transfer contributes such that the resulting effective conductivity can be set at 0.04 W/(m · K) (Hökmark et al. 2009).

Dependencies between process and buffer variables

Table 3-2 summarises how the process influences and is influenced by all buffer variables and how these effects are treated in PSAR.

Buffer geometry: The resistance to heat transport in the buffer prior to its achieving water saturation is dependent on the distance between the canister and the deposition hole boundary, which entails changes in the temperature of the buffer if the dimensions of the canister hole or the location of the canister in the hole should be altered. After water saturation, however, the variations in geometry that could occur due to block fallout or a poorly centred canister have negligible effects. This is also true of the effects of instantaneous or time-dependent deformations that can alter the geometry of the canister hole. Before water saturation, a poorly centred canister can be of importance for the distribution of gas-filled volumes and therefore for the temperature level and temperature distribution in the buffer. The thermal expansion of the buffer material is insignificant.

Pore geometry: The geometry of the pore system will change slightly because of thermal expansion. The porosity, i.e. the volume fraction taken up by pores, influences the thermal conductivity. In the unsaturated state, i.e. before swelling and homogenization has started to even out porosity differences, the nominal conductivities of perfectly dry bentonite blocks and perfectly dry bentonite pellets differ significantly. In dry Prototype Repository deposition holes the block thermal conductivity was found to be around 1.25 W/(m · K) and the pellet slot conductivity around 0.4 W/(m · K) (Hökmark et al. 2009).

Table 3-2. Direct dependencies between the process "Heat transport" and the defined buffer variables and a short note on the handling in PSAR.

Variable	Variable influence on process		Process influence on variable	
	Influence present? (Yes/No) Description	Handling of influence (How/Why not)	Influence present? (Yes/No) Description	Handling of influence (How/Why not)
Buffer geometry	Yes	Given as data in the thermal calculation	Yes, but insignificant	Ignored
Pore geometry	Yes	Given as data in the thermal calculation	No, but indirectly via temperature	
Radiation intensity	No		No	
Temperature	Yes. In the unsaturated state, thermally driven vaporization/diffusion/ condensation contributes to heat transport	Included in model where appropriate	Yes	Result from the model (in time and space)
Water content	Yes	Given as data in the thermal calculation	Yes	Treated in Water transport under unsaturated conditions (3.3.1)
Gas content	No, but indirectly via water content		No, but indirectly via water content	
Hydrovariables (pressure and flows)	No		No, but indirectly via temperature and insignificant	Ignored
Stress state	No		No	
Bentonite composition	Yes	Given as data in the thermal calculation	No	
Montmorillonite composition	No		No	
Porewater composition	No		No	
Structural and stray materials	Yes. May affect thermal conductivity	Neglected, since to be of any importance to the heat transport, there must be very significant amounts of non-buffer materials	No	

Temperature: The influence of heat transport on the buffer temperature is obvious. If the heat transport is efficient, the temperature in the inner parts of the system will be lower than if there is a high thermal resistance. The temperature in the outer parts, however, is practically independent of the conditions in the interior of the deposition holes. Different models have been proposed for estimating the influence of the temperature on the thermal conductivity of bentonite (Knutsson 1983). The effect of temperature on thermal conductivity is also discussed in Dixon (2019) and the conclusion is that there is a small increase with temperature.. However, the overall effect is small compared to effect of water content and dry density and can be ignored for practical reasons. Under unsaturated conditions, vaporisation, vapour diffusion and condensation contribute to the heat

transport. The contribution is however small and not noticeable other than in the low porosity pellet slot (Kristensson and Hökmark 2010).

Water content: The thermal conductivity of bentonite depends on the degree of saturation S_r experimental results shown under "Model studies/experimental studies" below. The conductivity is about 1.3 W/(m · K) for fully saturated bentonite with a KBS-3 buffer density and about 1.0 W/(m · K) if the degree of saturation is 60 %. The sensitivity to saturation variations is larger if the saturation drops below 50–60 %.

As long as there is heat transport and incomplete saturation, thermal gradients in the buffer may influence the state of saturation, such that the water content of the innermost parts of the buffer decreases temporarily due to moisture relocation to cooler regions further away from the canister. Modelling has been carried out in Luterkort et al. (2017) where the effect of redistribution of water due to thermal gradients has been considered when calculating the maximum temperature of the canister has been calculated. The results are similar to that calculated in Hökmark et al. (2009). This suggests that the assumptions made in Hökmark et al. (2009) regarding thermal conductivity is valid even for dry deposition holes.

Gas content: Heat transport will not affect the gas content. The gas content in itself does not have any influence on the heat transport. If there is a gas phase, the effects of this will be just those of the incomplete saturation.

Hydro variables: Temperature variations will cause insignificant changes to the porewater pressure. During the unsaturated changes there is no or little pressure. During the saturated phase, temperature changes are too slow to impact on the pressure.

Stress state: Different models have been proposed for estimating the influence of increasing pressure on the conductivity of bentonite (Knutsson 1983). They show a slight increase of the thermal conductivity, but the effect is not sufficiently verified to be credited (Börgesson et al. 1994).

Bentonite composition: There is no influence on the composition of the smectite. The presence of accessory minerals may affect the thermal conductivity. To be of any importance, the impurity content must be high and the thermal properties of the impurities significantly different from those of the bentonite. High contents of quartz, for instance, will increase the conductivity.

Montmorillonite composition: Variability of the internal structure of the montmorillonite is unimportant to thermal conductivity.

Structural and stray materials: To be of any importance to the heat transport, there must be very significant amounts of non-buffer materials.

Boundary conditions

There are two boundary conditions:

- The heat flux from the local canister, determined by the output at the time of deposition and by the heat decay characteristics of the waste.
- The temperature at the walls of the deposition hole.

The distribution of the total heat output over the surface of the canister will depend on the way the initial canister-bentonite clearance develops. There is also a dependence on the vertical distribution of the heat generation within the canister, i.e. on the burn-up ratio between the end parts and the mid-parts of the fuel elements. As long as the canister-buffer clearance, or part of that clearance, remains open there will be some redirection of the heat flow towards regions with direct canister-bentonite contact, for instance at the canister base and top. In regions where the clearance is open, part of the flux will be due to heat radiation.

The temperature at the rock wall depends not only on the heat output from the local canister but also on the contribution from other canisters, on the rock's thermal properties and on the repository layout.

Model studies/experimental studies

Model studies. Predictions of the temperature evolution in the near field have been done analytically (Claesson and Probert 1996, Hökmark and Fälth 2003, Hedin 2004) and numerically (Thunvik and Braester 1991, Ageskog and Jansson 1999, Hökmark et al. 2009, Luterkort et al. 2017).

These studies have all generated consistent results. The temperature at the buffer/canister transition reaches a peak after about 5–15 years, depending on layout and rock thermal properties, while the rock wall peak temperature is reached after 30–50 years. If, for example, the canister spacing is 7.5 m, the tunnel spacing 40 m, the canister output at the time of deposition 1 700 W and the effective rock thermal conductivity 2.6 W/(m·K), the maximum temperature increase at the wall of the deposition hole will be 50 °C and about 8 °C higher if the canister spacing is 6.0 m. One of the objectives of these studies has to been to find out how the canister spacing influences the maximum rock wall temperature and to establish layout guidelines that ensure that the peak buffer temperature does not exceed 100 °C for any canister. The duration of the temperature pulse is a few thousand years. After 2 000 years, the maximum excess temperature in the repository is 15–20 °C, again depending on the repository layout and on the rock thermal properties. After 5 000 years, the maximum elevation in temperature from the initial ambient is about 10 °C. The thermal gradients within the buffer are almost zero already after 2 000 years.

Hökmark and Fälth (2003) and Hedin (2004) used results from different near-field thermal analyses as boundary conditions in numerical and analytical calculations of the heat transfer across the bentonite buffer and across the different gaps. The results indicated that the effects of open canister-buffer gaps are more important than possible temporal and spatial variations of the heat transport properties within the buffer.

Experimental studies: Börgesson et al. (1994) measured the thermal conductivity of samples of compacted MX-80 bentonite by use of a transient line source probe. The thermal conductivity of MX-80 have also been measured by Svensson et al. (2019) with a transient plane source sensor. The result between the two different measurements match well which can be seen in Figure 3-1. These results also match results obtained for similar materials, for instance the bentonite tested in the FEBEX experiment (Huertas et al. 2000, Villar et al. 2018).

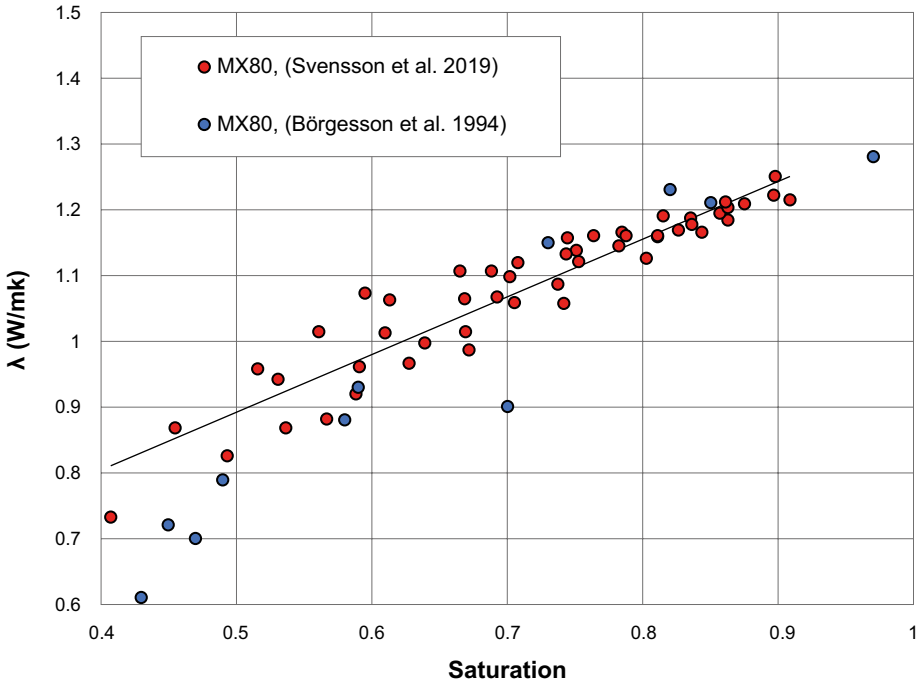

Figure 3-1. *Heat conductivity measures in laboratory as function of saturation. Data taken from Börgesson et al. (1994) and Svensson et al. (2019).*

The Prototype Repository at Äspö HRL includes six full-scale deposition holes in two tunnel sections separated by a concrete plug (Goudarzi et al. 2003a). There are two deposition holes in the outer section and four in the inner one. Inflow measurements performed prior to bentonite emplacement and start of the actual test showed that there are very significant differences between individual holes. The supply of water to the two holes in the outer section is sufficiently low that the inner parts of the bentonite buffer were practically in its initial state of saturation after about 6 months of test operation. The temperature drop across the still open canister/bentonite space in the dry holes was about 19 °C 50 days after test start. In at least one of the holes in the inner section, there are indications, e.g. no measurable temperature drop between canister and bentonite, that the annular space between canister and rock was almost saturated (i.e. the initial gap was closed) about two years after test start.

The effective thermal conductivity λ_{eff} of the buffer in the annular space between canister and rock wall at canister mid-height can be estimated by use of the following expression:

$$\lambda_{eff} = \frac{q_c}{\Delta T} \cdot R_c \cdot \ln \frac{R_2}{R_1} \qquad (3\text{-}2)$$

Here ΔT is the temperature difference between two points at distances R_1 and R_2, respectively, from the heater axis. R_c is the canister radius. The canister surface heat flux q_c at canister mid-height must be estimated from the total power and corrected to account for the non-uniform distribution of the heat output over the canister surface (Hökmark et al. 2009). Applying the expression to the dry hole in the outer tunnel section described above using data reported by Goudarzi et al. (2003a) gives bentonite conductivity values ranging between 1.2 and 1.3 W/(m·K) (Hökmark et al. 2009).

The TBT (Temperature Buffer Test) experiment in Äspö HRL is run under high thermal gradients and with maximum buffer temperatures well above 130 °C (Goudarzi et al. 2008). The buffer material is MX80 bentonite with the same properties (e.g. density and initial saturation) as the Prototype Repository bentonite blocks. The temperatures along a radial scan-line from the cylindrical, 0.6 m diameter heater to the rock wall are monitored by use of numerous, densely positioned, thermocouples. Using Equation 3-2 above, the thermal conductivity, or rather the change in thermal conductivity, along the scan-line is evaluated and used as an indicator of wetting/drying. The conductivity was found to drop by about 50 % in a 0.10–0.15 m wide zone around the heater soon after test start because of drying. Some five years after test start the conductivity has increased and seems to be almost, but not completely, uniformly distributed along the scan-line. This is an effect of water being supplied from the surrounding pressurised sand filter boundary.

Natural analogues/observations in nature

Not applicable.

Time perspective

There are two relevant time perspectives: the water saturation perspective and the heat production perspective. The time it takes to achieve full water saturation is dependent on, inter alia, the pressure conditions in the groundwater in the near field. The process is estimated to take a number of years, see Section 3.3.1. After that, all heat transport takes place by conduction and under well-defined conditions with known thermal conductivities. Before then, heat transport can be influenced by the presence of gaps and joints.

After a few thousand years, the heat production, and thereby the heat transport through the buffer, will have been reduced to a few percent of their original values.

Handling in the PSAR

The integrated thermal evolution of the buffer and rock is modelled with the set of models described in Hökmark et al. (2009, 2010). Aspects of heat transport relevant to the THM evolution of the buffer are treated in Åkesson et al. (2010a).

An important purpose of the modelling is to evaluate the peak buffer temperature that must not exceed 100 °C, taking all relevant uncertainties into consideration. Which is the technical design requirement used for the design of the buffer. These include the possible presence of gaps between canister and buffer and between buffer and rock and data for describing heat transport across these.

The peak buffer temperature will depend not only on the properties of the buffer and the gaps, but also on the repository layout and the rock thermal properties. Therefore, the critical temperature calculations were conducted prior to establishing the layout. These calculations are reported in the Site engineering report (SKB 2009).

Time periods: The modelling will encompass at least 10 000 years, but the critical timescale is that period during which the peak canister temperature is reached, i.e. the first tens of years. For time-scales beyond a few thousand years, it is important to determine if permafrost conditions could lead to freezing of the buffer, see further Section 3.2.2. This is done by a comparison of the rock thermal evolution during permafrost conditions to the buffer freezing temperature, taking the residual power of the canisters into account if relevant.

Boundary conditions: The treatment of heat transfer over the buffer boundaries is described in Hökmark et al. (2009).

Handling of variables influencing the process: The process is coupled to the water saturation process (Section 3.3.1) which is difficult to model in detail, especially the evolution of gaps. Also, the water saturation process is highly dependent on the uncertain hydraulic conditions in the rock around the deposition hole. The peak canister temperature will therefore be determined under the assumption that no additional water is taken up by the buffer after deposition, i.e. time-independent, pessimistically chosen heat conductivity is used. Hereby, the influences of varying hydraulic conditions in the saturating buffer, including porosity variations, are conservatively neglected. The redistribution of moisture as a result of vaporisation and vapour diffusion is accounted for by additional margins. The thermal conductivity of the buffer will also be calculated after taking into consideration the possible influence of accessory minerals and presence of stray materials in the system. The gap between the canister and the buffer will conservatively be assumed to be open until the peak temperature has been reached. The period after the peak temperature do not need considered during the thermal dimensioning of the repository.

Handling of variables influenced by the process: The temperature is explicitly calculated. The water content is handled in process Water transport under unsaturated conditions (3.3.1).

The special cases of failed canister and of earthquakes: Canister failures and earthquakes of a magnitude that could affect the thermal evolution are not expected during the roughly 1 000-year time period in which the buffer temperature evolves significantly. The process is thus not handled for these cases. Should the assumptions regarding significant, early canister failures or earthquakes not be confirmed by the results of the safety assessment, handling of the special cases will be reconsidered.

Uncertainties

Uncertainties in mechanistic understanding

Heat transfer from the hot canisters via the buffer to the near-field rock and backfill is in principle a simple process that can be described with reference to basic laws of physics. The character of the sub-processes that participate in the heat transport is also known and the theoretical modelling of their function is based on well-known physical principles.

Model simplification uncertainties in PSAR

Several modelling simplifications regarding coupling to the hydraulic evolution are described under “Handling in the PSAR” above. The conservative simplifications used in the models are justified since the prime purpose of the modelling is to obtain upper limits on canister and buffer temperatures. Sensitivity analyses will in some cases shed light on the effects of the simplifications.

Input data and data uncertainties in PSAR

Critical input data for the modelling of this process is given in the **Data report**. Critical uncertain input data for use in determining the peak canister temperature include the heat power of the fuel, the thermal conductivity of the partly saturated buffer material and of the host rock. Also, uncertainties of the emissivities of the inner buffer and in particular the outer copper surfaces are decisive in determining the peak canister temperature. All uncertainties associated with peak buffer temperature calculations are presented in Hökmark et al. (2009).

3.2.2 Freezing

Overview

During the evolution of the repository, it will most likely experience glacial cycles with associated periods of permafrost. The ground temperature consequently does vary, not only with depth, but also with time and will at times be below 0 °C.

When water freezes the density decreases and the pressure will increase in a confined system. The pressure increase in a pure water system can be calculated with the Clausius–Clapeyron relation.

Several KBS-3 repository components include bentonite: buffer, tunnel backfill, tunnel plugs and investigation borehole seals. The main function of bentonite is to provide a sealing swelling pressure and low hydraulic conductivity. Bentonite is a swelling material, which makes it rather unique as a soil in the sense that some of its properties are dependent on external conditions. The process of swelling, specifically, only occurs when bentonite is in contact with an external aqueous reservoir, and the concept of swelling pressure can consequently only be defined under such conditions. This means, in particular, that a bentonite component within the KBS-3 repository will be affected by freezing as soon as the groundwater in the surrounding rock freezes even though the component itself may remain unfrozen. The process of freezing bentonite in the following context therefore also includes the temperature range between the freezing point of the aqueous reservoir and the actual freezing point of the bentonite, in order to provide a full description of bentonite as temperature is lowered.

The freezing point of a soil is defined as the temperature where ice start to form in the material. The phase transition between ice and liquid state of the soil porewater is affected by pressure and the presence of solutes in the same manner as bulk water. However, the freezing point is generally depressed in a soil compared to the corresponding bulk solution due to the geometrical constraints of the water in a porous medium. The freezing point of a soil is thus dependent on the stress state, the porewater chemistry, the detailed distribution of the pore volume, the chemical and physical properties of the surfaces of the constituting minerals, and the degree of water saturation.

A further consequence of ice formation taking place in a porous material is that all the porewater will not freeze at one specific temperature. There exists a temperature range below the freezing point where equilibrium exists between ice and water in liquid form. The evidence establishing the existence of a continuous, unfrozen water phase that separates ice from the mineral matrix in porous media such as soils is widely accepted (Anderson 1966, Miller 1963, Nersesova and Tsytovich 1965, Williams 1964). For a frozen soil, it is therefore relevant to partition the total water content into unfrozen water content and ice content.

$$w = w_u + w_i \tag{3-3}$$

The maximum amount of unfrozen water $w_{u,\max}$ naturally decreases with temperature (keeping all other factors constant). $w_{u,\max}$ depends on various other factors among which particle mineral composition, specific surface area of particles, solute concentrations and pressure are the most significant (Anderson and Tice 1972). The influence of pressure and solutes is not unique for soil porewater and is known to be such that the freezing point lowers with increasing pressure and solute concentration.

Numerous studies of the relationship between the (maximum) unfrozen water content and temperature, for different types of soils, have been performed (see e.g. Anderson and Tice 1973, Nersesova and Tsytovich 1965, Andersland and Ladanyi 1994).

It has been concluded (Anderson and Tice 1972) that several of the variables describing a specific soil in turn can be related to the specific surface area S, and that a relation between only $w_{u,\max}$, S, and temperature usually gives a satisfactory description (for constant pressure and solute concentration). By fitting a mathematical expression to empirical data for 10 representative soils (isothermal calorimeter measurements), Anderson and Tice (1972) achieved the following equation relating maximum unfrozen water content to surface area (m^2/g) and θ, the temperature below freezing (°C):

$$\ln w_u = 0.2618 + 0.5519 \ln S - 1.449\, S^{-0,264} \ln \theta \qquad (3\text{-}4)$$

Equation (3-4) can be graphically presented as in Figure 3-2.

Ice will not be present in a soil unless the total water content exceeds $w_{u,\max}$. Hence, Equation (3-4) also gives the freezing point of a soil whose total water amount equals $w_{u,\max}$. Specifically, Equation (3-4) can be used to determine the freezing point of the buffer material.

From Equation (3-4) it is found that a material with a specific surface area of the magnitude 800 m^2/g at a temperature of –5 °C gives a $w_{u,\max}$ of ca 35 %. This value is larger than the total water content of the saturated buffer, which should be ~27 % for the reference density, and from the above it can be concluded that the freezing point of the water- saturated buffer is below –5 °C.

The other factors not taken into account in the present estimation (pressure, solutes) of the buffer freezing point will contribute to an even lower value.

If ice is not present in the system no significant increase in volume and no stress increase will take place and therefore questions related to ice lens formation will be of no relevance in the buffer.

Despite the significant freezing point depression in the buffer, the effect of freezing will influence swelling pressure at temperatures above the actual freezing point. Swelling and swelling pressure are phenomena which depend not only on properties of the bentonite itself but also on properties of the external aqueous reservoir. Hence the bentonite swelling pressure will be affected by freezing as soon as the external reservoir freezes.

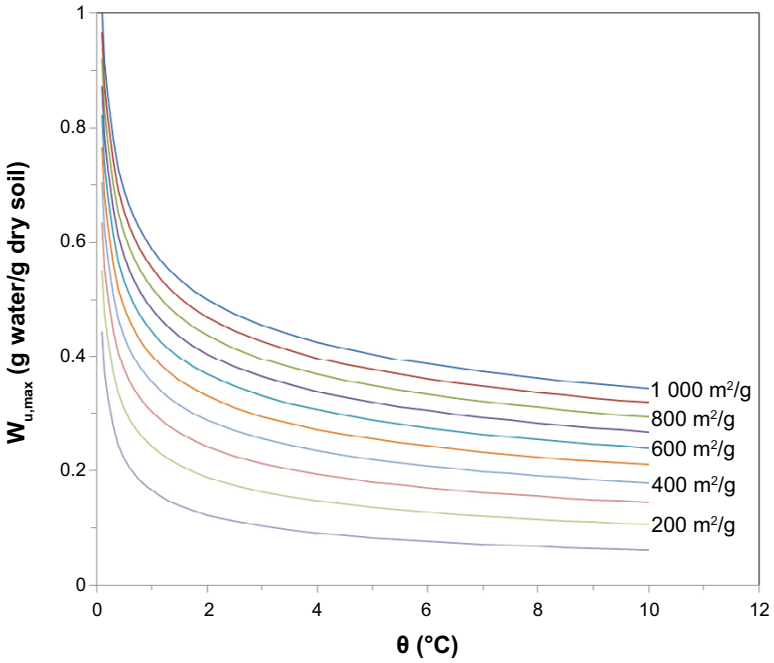

Figure 3-2. *Maximum unfrozen water content as function of θ for various values of specific surface areas. θ denotes the number of degrees (°C) below the freezing point. (After Anderson and Tice 1972).*

It is possible to derive the temperature dependence on swelling pressure of a water saturated swelling clay (Birgersson et al. 2008).

$$P_s(w,T) \approx P_s(w, 0\ °C) - \frac{\Delta s(w)}{v_{c.w.}(w)} \cdot T \qquad (3\text{-}5)$$

where T still denotes temperature below 0 °C, $v_{c.w.}(w)$ is the partial molar volume of porewater, $\Delta s(w)$ is the partial molar entropy difference between water in the clay and water in an external ice phase. For values of water content relevant to buffer conditions, $\Delta s(w)$ is of the same order as the molar entropy difference between ice and liquid bulk water (22 J/°C /mol), and a swelling pressure drop with temperature is expected, of the order of 1 MPa/°C. Note, at the temperature given by

$$T_c \approx \frac{v_{c.w.}(w)}{\Delta s(w)} P_s(w, 0\ °C) \qquad (3\text{-}6)$$

swelling pressure is completely lost. This temperature corresponds to the situation when the possible amount of unfrozen water equals the total water content, i.e. expresses the freezing point depression. Assuming a typical buffer swelling pressure above 0 °C of 7 MPa and a partial molar volume equal to the value for bulk water (18 cm^3/mol) gives $T_c \approx$–6 °C, in good agreement with the Anderson & Tice expression presented in Equation (3-4) and Figure 3-2.

Dependencies between process and buffer variables

Table 3-3 summarises how the process influences and is influenced by all buffer variables and how these effects are treated in PSAR.

Boundary conditions

For the buffer to freeze, meaning that ice starts to form, the water in the surrounding rock must be present as ice. The ability for (water) mass transport across this boundary is therefore very limited.

Model studies/experimental studies

The swelling pressure response of water-saturated samples of the PSAR reference material MX-80 at various water contents has been measured down to temperatures of around –10 °C (Birgersson et al. 2008, 2010). A typical result is presented in Figure 3-3. The pressure drop as described by Equation (3-5) was shown to agree quantitatively with measurements. Also, the existence of a water content dependent temperature where swelling pressure is completely lost (Equation (3-6)) was demonstrated. The processes were shown to be completely reversible during several freezing/thawing cycles. No pressure peaks around 0 °C were observed.

Furthermore, the experiments were successfully explained by thermodynamics and the assumption of a homogeneous bentonite with only one type of nm-wide slit like pores. The behaviour was concluded to be completely analogous to freezing point depression in electrolyte solutions. Detailed measurements using synchrotron X-ray diffraction during freezing-thawing cycles of Na- and Ca- montmorillonite with and without salt in the system showed that the effects of freezing are much smaller with salt, and also much smaller at liquid/solid ratios similar to bentonite buffer compared to more dispersed systems (Svensson and Hansen 2010b, 2013b).

Table 3-3. Direct dependencies between the process “Freezing” and the defined buffer variables and a short note on the handling in PSAR.

Variable	Variable influence on process		Process influence on variable	
	Influence present? (Yes/No) Description	**Handling of influence (How/Why not)**	**Influence present? (Yes/No) Description**	**Handling of influence (How/Why not)**
Buffer geometry	Yes. If extended to regions with very low temperatures	Neglected. Large scale freezing is not expected to occur	Yes. Geometry could change through expansion towards the backfill	Neglected. Large scale freezing is not expected to occur
Pore geometry	Yes	See Equation 3-7, which is the main argument why freezing can be neglected	Yes	Neglected, No increase in pressure is expected
Radiation intensity	No		No	
Temperature	Yes	Included in the assessment	No	
Water content	Yes via freezing point and transport capacity	Included in the assessment	Yes, If freezing takes place redistribution of water	Included in the assessment
Gas content	(Yes)	Indirect through water content	No	
Hydrovariables (pressure and flows)	Yes, freezing induces water transport	Included in the assessment	Yes	Included in the assessment
Stress state	Yes, influences the freezing point to a small degree	Neglected, effect is small	Yes. Swelling pressure affected also before ice formation	Calculated/estimated
Bentonite composition	Yes, via the specific surface area	Included in the assessment	No	
Montmorillonite composition	Yes, via the specific surface area and types of counter ions	Included in the assessment	No	
Porewater composition	Yes, influences the freezing point	Neglected, since variations will be small	No	
Structural and stray materials	Yes (potentially)	Neglected, since no stray materials are expected.	No	

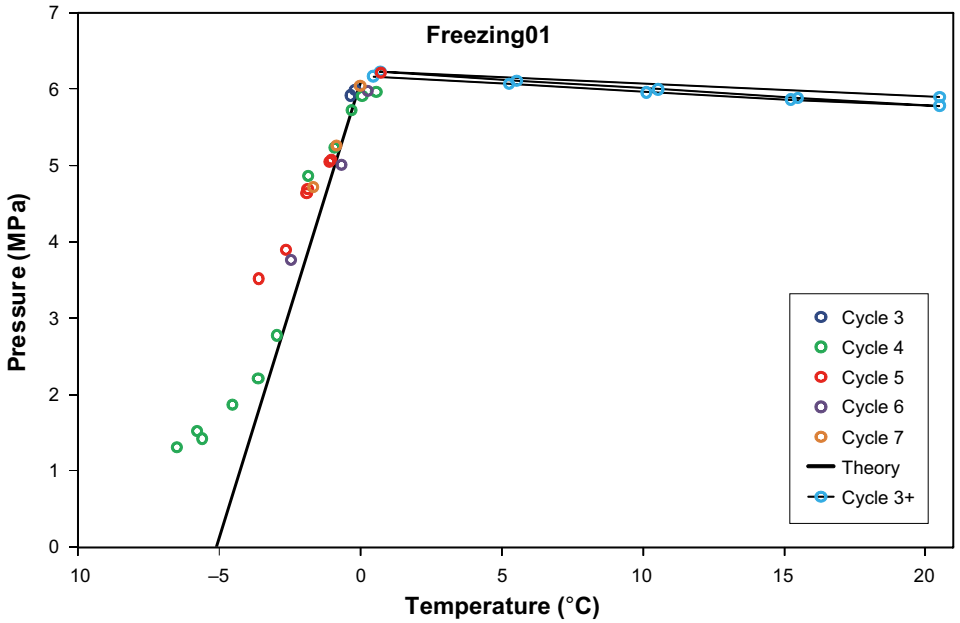

Figure 3-3. *Measured swelling pressures below and above 0 °C of a sample of MX-80 bentonite which exerts a swelling pressure of approximately 6 MPa at 0 °C (Birgersson et al. 2010). Different colors refers to different freezing/thawing cycles. The theoretical prediction below 0 °C (Equation 3-8) is labelled "Theory".*

Schatz and Martikainen (2010) performed a series of experiments using closed, constant-volume cells to evaluate the effect of freezing and thawing on a compacted bentonite buffer. The tests were set up as follows:

- Pre- and post-freezing swelling pressure measurements were performed on fully saturated MX-80 and Deponit CA-N bentonite samples, at dry density values of approximately 1.6 g/cm^3, over five freeze/thaw cycles from room temperature to −18 °C with rapid (instantaneous) temperature exposure.
- Pressure measurements were performed on fully saturated MX-80 bentonite samples, at dry density values of 1.470 and 1.501 g/cm^3, during a temperature run from room temperature to −10 °C with step-change temperature exposure and back from −10 °C to room temperature under continuous temperature change exposure at 0.1 °C/h.
- Pressure measurements were performed on fully saturated MX-80 bentonite samples, encompassing a range of dry density values from 0.940 to 1.534 g/cm^3, during repeated temperature runs from room temperature to −10 °C and back with continuous temperature change exposure at 0.1 °C/h.
- Pressure measurements were performed on a fully saturated Deponit CA-N bentonite sample, at a dry density of 1.484 g/cm^3, during a temperature run from room temperature to −10 °C and back with continuous temperature change exposure at 0.1 °C/h.
- In some cases, hydraulic conductivity measurements were performed before and after freeze/thaw exposure.

In general, exposure to freezing temperatures, down to an average temperature of −10 °C, results in the development of significant internal pressures in compacted bentonite samples, which is attributed to the formation of ice. The relative pressure increase was strong for low density samples, while it was more modest at expected buffer density (a factor of 1.8 to 2.2). The observed pressure increases fall below a pressure limit described by the standard Clapeyron equation. Sample hydraulic conductivities were likely not affected by freezing and thawing exposure. Some loss of swelling pressure was observed during step-change temperature exposure for MX-80 bentonite samples between 0 and −5 °C. This is consistent with the thermodynamic theory describing their behaviour as the partial molar entropy of water in bentonite changes sign at a high enough water ratio (Birgersson et al. 2010).

Schatz and Martikainen (2010) estimate the effect of ice formation on the pressure in the buffer. For a change in state from a solid to a liquid, the latent heat of fusion (L_f) can be used to calculate the pressure effect according to Clausius–Clapeyron:

$$\frac{dP}{dT} = \frac{L_f}{T\Delta V} \tag{3-7}$$

Considering the question of how much pressure is needed to melt ice at a temperature below 0 °C, with L_f = 333.88 J/g and ΔV = −0.0906 cm^3/g (specific volume of water minus that of ice), Equation (3-7) predicts a very large increase in pressure for small changes in temperature below 0 °C, i.e., −13.49 MPa/°C. This value represents the pressure limit for the phase transition at equilibrium, i.e., the pressure required to melt ice at a temperature below its freezing point for a system subjected to equal pressure changes on the ice and water phases. These boundary conditions are applicable to a hydraulically-closed, frozen repository. In a hydraulically-closed, frozen repository, pressure increases due to exposure of the buffer material to temperatures below the freezing point of the porewater can be estimated on the basis of Equation (3-7) as both the ice and water phases become pressurised.

Natural analogues/observations in nature

No specific studies of natural analogues of frozen clays for the purpose of radioactive waste disposal have been made. However, knowledge can probably be achieved by studying permafrost areas.

Time perspective

The process of freezing is relevant during the entire repository lifetime.

Handling in PSAR

The key issue for the freezing process is when the pressure generated from the volume expansion of the ice can be harmful for the canister and the rock. According to Posiva SKB (2017) the performance target for the canister is that it should withstand isostatic load ≤ 50 MPa. The mean crack initiation stress level for the main rock type in Forsmark is 116 MPa and the minimum is 60 MPa SKB (2008). The crack damage stress level is, according to Cai et al. (2004), in between 70 to 90 % of the Unconfined Compressive Strength. This implies that the mean lies between 158 MPa and 203 MPa, with the minimum at 109 MPa. According to Equation (3-7), 50 MPa is generated when ice is cooled by 3.7 °C below the freezing point of water. This pressure would be reached in a deposition hole filled with pure water at −3.7 °C. The presence of bentonite will lower the freezing point of water, thus lower the temperature when the pressure from the ice will be 50 MPa.

The freezing process in a bentonite buffer is studied in Birgersson et al. (2010). The temperature when ice starts to form can be predicted with the empirical approach in Equation (3-4) or the thermodynamic approach in Equation (3-6). They both predict that no ice will be formed in an intact buffer at standard density at a temperature above −5 °C. Using the lowest swelling pressure value for the technical design requirement in Posiva SKB (2017) of 3 MPa, the critical temperature according to Equation (3-6) is −2.5 °C. The most pessimistic value for when freezing causes a pressure above 50 MPa is therefore −2.5–3.7 °C = −6.2 °C. Based on this −6 °C is selected as the performance target for the safety function "Limit pressure on canister and rock – Buffer freezing". In a situation with ice formation in the deposition hole, no hydrostatic pressure and no swelling pressure needs to be considered.

In Posiva SKB (2017) the performance target was defined as the temperature when ice formation starts (−2.5 °C) and the volume expansion of water was not considered.

The swelling pressure drop described above only occurs when the transport paths in the surrounding rock are frozen. Since the buffer is completely recovered at thawing, any deterioration of the sealing properties due to the pressure drop is of no concern for the buffer itself.

Handling of variables influencing the process: The temperature evolution is estimated in the **Climate report**.

Uncertainties

Uncertainties in mechanistic understanding

The freezing of soils is a well-known process. The description of swelling pressure response due to temperature changes is based on robust, fundamental thermodynamic arguments.

The very high pressures predicted by Equation (3-7) is not observed in the experiments performed by Birgersson et al. (2010) and Schatz and Martikainen (2010). The reason for this may be that there is an assumption of equal pressures on the water and the ice. Assuming the liquid water pressure remains constant (e.g., constant groundwater pressure), while the ice pressure is free to vary with temperature, the pressure increase would be significantly less (Schatz and Martikainen 2010).

Model simplification uncertainties for the above handling in PSAR

The reproducibility of the pressure response due to freezing is good. The process can be well described with the equations presented in this section.

Input data and data uncertainties for the above handling in SR-Site

The bentonite freezing point is strongly dependent on density. If a significant loss of material occurs, e.g. due to chemical erosion, a corresponding change in the freezing behaviour is expected.

The precise value of (minimum) temperature is uncertain. If it stays above 0 °C, no phase change at all will occur.

3.3 Hydraulic processes

3.3.1 Water transport under unsaturated conditions

Overview

Motive and sub-processes

The bentonite buffer will be installed as blocks and pellets, and both these materials are water-unsaturated from the start, i.e. a significant part of the voids is air-filled. Groundwater from the surrounding rock will flow to the buffer in the deposition holes, either directly through the rock wall of the deposition holes or via the tunnel, and this inflow will eventually water saturate the bentonite buffer. The process, denoted buffer hydration, is complicated by the heat generation from each canister, which means that water in the buffer will be redistributed from warmer to cooler zones of the buffer.

The motive for analysing water uptake and transport at unsaturated conditions is twofold: i) to assess the time-scale of buffer hydration; and ii) to assess the extent of moisture redistribution under dry conditions.

Since this process is quite extensive and diverse, it is suitable to describe it as four separate sub-processes:

- *Water uptake*, i.e. the transport and filling of pores under isothermal and fairly homogenous conditions.
- *Dehydration/ moisture redistribution*, i.e. the transport of water, under non-isothermal conditions, from warmer to colder zones.
- *Fractured rock/ local water entry*, i.e. the heterogeneous inflow of water from the rock.
- *Water transport in pellets-filled slots*, i.e. the transport and filling of pores under isothermal but heterogeneous conditions.

Description

The main description of this process follows the set of constitutive equations and equilibrium restrictions implemented in the finite element tool Code_Bright (CIMNE 2002). The motive for this is that a large part of the model studies presented in this section was performed using this code. This description is

well-established and has also been implemented in a large set of other codes (Schäfers et al. 2020). The following constitutive equations are used for describing the water transport:

- *Darcy's law*, by which the liquid volumetric flux (q_l) is driven by gradients in liquid pressure (p_l) and by gravity (g).

$$\mathbf{q_l} = -\frac{\mathbf{k} \cdot k_{rl}}{\mu_l}\left[\nabla p_l - \rho_l \cdot \mathbf{g}\right] \tag{3-8}$$

  where k is the intrinsic permeability, k_{rl} is the liquid relative permeability, ρ_l is the liquid density and μ_l is the liquid viscosity. The relative permeability is defined as a function of the degree of saturation (S_r) which generally increases towards the value 1 when S_r increases to 1; usually on the form $k_{rl} = (S_r)^3$. The intrinsic permeability can be defined as a function of the porosity (n), for instance on the form $k = k_0 \cdot \exp[b(n-n_0)]$. The intrinsic permeability (k) is related to the hydraulic conductivity (K) by the relation $K = \rho_l \cdot g \cdot \mu_l^{-1} \cdot k$. Experimental values for K is shown in Figure 3-4 (left).

  It should be noted the p_l can assume large negative values. This should however not be taken literally, but rather as a measure of the chemical potential of the clay water. The quantity p_g-p_l, where p_g is the gas pressure, is referred to as suction (s).

- *Fick's law*, by which the vapor mass flux (i_g^w) is driven by gradients in vapor mass fraction in the gas phase (ω_g^w):

$$\mathbf{i_g^w} = -\left(n\rho_g(1-S_r)D_m^w\right) \cdot \nabla \varpi_g^w \tag{3-9}$$

  where ρ_g is the gas density and D_m^w is the diffusion coefficient of vapor in the gas phase. The latter is calculated as $D_m^w = \tau \times 5.9 \times 10^{-6} \times (273.15+T)^{2.3} \times (p_g)^{-1}$ (m^2/s), where τ is the vapor tortuosity and T is the temperature.

- *Water retention curve,* which is defined as a relation between the degree of saturation and the suction, $S_r(s)$. In general, the suction value decreases toward zero when the degree of saturation increases to unity. The van Genuchten curve is a commonly used form for this. A variant of this function which includes a porosity dependence is also implemented in Code_Bright.

- *Phase densities & viscosities*. The liquid density is defined as a function of the liquid pressure and the temperature (both the *compressibility* and the *thermal expansion coefficient of water* is taken into account). The liquid viscosity is defined as a function of the temperature.

The following equilibrium restrictions are used for water:

- *Kelvin's law,* which describes the relation between the suction and the relative humidity, i.e. $RH = p_v/p_v^{sat}$, where p_v is the vapor pressure and p_v^{sat} is the saturated vapor pressure.

- *The saturated vapor pressure* is defined as a function of the temperature.

Apart from these relations there are other descriptions of major importance:

- *Moisture diffusivity.* The water uptake under isothermal and fairly homogenous conditions can be described as a diffusion process, in which the water transport is driven by gradients in gravimetric water content (w) and which fulfils Fick's second law: $\partial w/\partial t = D \cdot \Delta w$, where D is the moisture diffusivity. This quantity was found to have a value in the order of $3\text{-}4 \times 10^{-10}$ m^2/s for MX-80 with e = 0.7 (SSM 1–4). This parameter can be related to k, k_{rl}, n, μ_l and the derivative of the retention curve (dP_l/dS_r) with the expression: $D = k \cdot k_{rl} \cdot dP_l/dS_r \cdot (n \cdot \mu_l)^{-1}$.

- *The swelling pressure and suction properties* are closely related and can be derived from the chemical potential of the clay water (μ). For water-saturated conditions this can be described as a function of the water content (w) and the *pressure* (P):

$$\mu = \mu_0 + RT \cdot \ln[RH(w)] + v_c \cdot P \tag{3-10}$$

where μ_0 is the chemical potential of a reference state, R is the universal gas constant, T is the absolute temperature, v_c is the molar volume of the clay water, and RH is the relative humidity of the clay at free swelling conditions. This can be rearranged as:

$$-\frac{\mu-\mu_0}{v_0} = -\frac{RT}{v_0}\cdot \ln[RH(w)] - \frac{v_c}{v_0}\cdot P \qquad (3\text{-}11)$$

where v_0 is the molar volume of bulk water. The term on the left-hand side can be identified as *suction* (s), while the first term on the right side is denoted the *clay potential* (Ψ). Assuming that v_0 and v_c are equal, this can simply be expressed as:

$$s = \Psi(w) - P \qquad (3\text{-}12)$$

This means that suction equals $\Psi(w)$ under free swelling condition (P=0) and that the pressure (i.e. the swelling pressure) equals $\Psi(w)$ under confined conditions with free access of water (s=0). It should be noted that the suction corresponds to the RH in an external gas phase (according to Kelvin's law). Correspondingly, it corresponds to the negative value of the external water pressure under confined condition. This means that the clay potential is defined in a similar way as the *effective stress*.

It should also be noted that the clay potential is not only a function of the water content but also of the path of reaching the state (see Figure 3-4, right). When the bentonite takes up water, it follows a path with a relatively high RH (or low swelling pressure) for a certain water content, whereas it follows a path with relatively low RH when it dehydrates. This behavior has been used as a basis for the development of a hysteresis-based material model (Börgesson et al. 2020a).

For unsaturated conditions, the corresponding relation between the water content, pressure and suction has not been investigated. It is however reasonable to assume that Equation (3-12) could be generalized by introducing a factor ($\alpha-1$) on the pressure term, and that α is related to the saturation degree and assumes positive values below 1 (exactly 1 for saturated conditions). The α could then be interpreted as the ratio between the contact area between saturated grains and the total section area. A similar approach was investigated by Åkesson and Hökmark (2007).

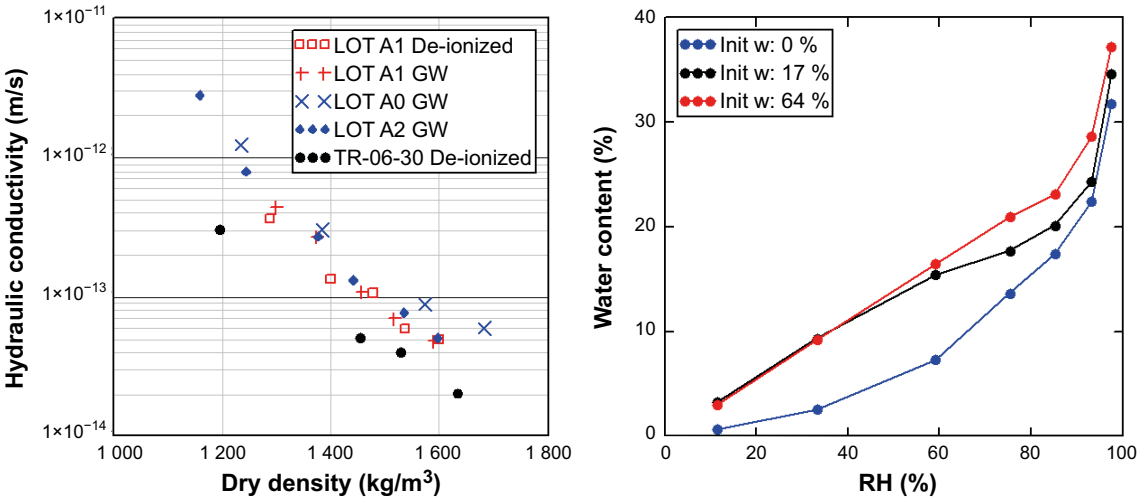

Figure 3-4. *Hydraulic conductivity versus dry density for MX-80 (left): LOT A1 (Karnland et al. 2000), LOT A0 and A2 (Karnland et al. 2009), TR 06-30 (Karnland et al. 2006). Water content versus RH in free swelling water retention measurements for MX-80 (right): initial water content 0 and 64 % (Dueck and Nilsson 2010), 17 % (Dueck 2004).*

The presence of dissolved ions in the clay water will contribute with an additional osmotic pressure term (Π), given by the van't Hoff equation. In addition, a similar expression for suction, osmotic pressure and pressure can be formulated for an external solution, e.g. in a filter or in the rock:

$$\begin{cases} s &= \Psi(w) + \Pi - P \\ s_{ext} &= \Pi_{ext} - P_{ext} \end{cases} \quad (3\text{-}13)$$

If the two systems are in equilibrium ($s=s_{ext}$) and if $P_{ext}=0$, then this will mean that the swelling pressure will be reduced as: $P = \Psi(w) - (\Pi_{ext} - \Pi)$.

The influence of the temperature on the retention properties for free swelling conditions was described by Birgersson et al. (2010) with the following expression:

$$\Psi(w,T) = \Psi(w,T_0) + \frac{\Delta s(w) \cdot \Delta T}{\nu} \quad (3\text{-}14)$$

$\Delta s(w)$ is the difference in partial molar entropy between clay water and bulk water, ν is the molar volume of the bulk water and the temperature difference ΔT was defined as $T-T_0$.

Finally, it can be noted that Karnland et al. (2006) observed that the product of the swelling pressure and the hydraulic conductivity was almost constant over a wide range of densities for several bentonite materials. This therefore indicates that there is a close relationship in the underlying mechanisms of these two properties.

- *Coupled flow phenomena*. Different flow types are driven by their own potential gradients (Mitchell 1993). For example, liquid volumetric flux is driven by gradients in liquid pressure (Darcy's law), while heat flow is driven by temperature gradients (Fourier's law). A *coupled flow* is a flow of one type which is driven by a potential gradient of another type. For instance, a fluid flow driven by a temperature gradient is denoted thermo-osmosis. Such a coupled flow phenomenon is supported by non-equilibrium thermodynamics (de Groot and Mazur 1984) and is one of several coupled flow phenomena which can occur. The hypothetical influence of thermos-osmosis has been analysed by Sánchez et al. (2007) and Zheng and Samper (2008). A similar, although only partly related, topic is the separation of the vapour diffusion in a thermal and an isothermal component, which in turn is driven by gradients in temperature and water content, respectively. Such an expression was derived by Philip and de Vries (1957). It can be mentioned that the buffer hydration calculation that has been performed with the Abaqus FEM tool has used an additional temperature-gradient driven term added to Darcy's law.
- *Natural convection* is a mechanism of heat transfer, involving the motion of a fluid (air in this case), which is the result of density differences, which in turn are caused by the exchange of heat. The potential contribution of this transport process to more pronounced moisture redistribution has been identified as a conceptual uncertainty for the evolution of the re-saturation. In general, it should be possible to model this process by addressing conservation of mass, energy and momentum, together with the thermal expansion of the air and the gas permeability of the porous medium. High gas permeability implies however that the process can be numerically very demanding to analyse together with the slow transport coefficients for water transport.

Dependencies

Table 3-4 summarizes how the process influences and is influenced by all the buffer variables and how these effects are treated in the PSAR.

Influence of water and gas content as well as dry density: The flow coefficient is influenced by the degree of saturation through the relative permeability, Equation (3-8) The hydraulic conductivity is strongly related to the dry density (Figure 3-4, left) and this is considered through the porosity dependence of the intrinsic permeability. The flow potential at unsaturated conditions (suction) is strongly related to the water content, see Equation (3-12).

Influence of hydro-variables: The flow potential at unsaturated conditions (suction) is essentially the negative value of the liquid pressure ($s = p_g - p_l$). Two-phase flow (i.e. including gas transport) must be addressed for temperatures above 100 °C, since this implies that the saturated vapor pressure exceeds 1 bar.

Table 3-4. Direct dependencies between the process "Water uptake and transport under unsaturated conditions" and the defined buffer variables and a short note on the handling in the PSAR.

Variable	Variable influence on process		Process influence on variable	
	Influence present? (Yes/No) Description	**Handling of influence (How/Why not)**	**Influence present? (Yes/No) Description**	**Handling of influence (How/Why not)**
Buffer geometry	Yes, mainly through distance to wet rock	Given as input data in saturation calculation	Yes. Influencing through the swelling of blocks	See swelling/mass redistribution (3.4.1)
Pore geometry	Yes, the pore geometry (density) influences the water and vapour transport rate	Included in material data	Yes, through the degree of water saturation that together with the void ratio determines the pore geometry	Degree of saturation and void ratio are calculated
Radiation intensity	No		No	
Temperature	Yes, through water viscosity and through the hydrovariables in a temperature gradient	Included in the models	Yes, through the influence of degree of saturation and void ratio on the thermal properties	Temperature as a function of time and space is calculated for the resaturation phase. See also Heat transport (3.2.1)
Water content	Yes, decisive for the retention curve	Initial water content is given as input data in saturation calculation. The degree of saturation and the void ratio, which determines the water content, are variables in the model	Yes, changes the water content	Degree of saturation and void ratio are calculated
Gas content	Yes, included in the degree of saturation	Initial gas content is given as input data in saturation calculation. The degree of saturation and the void ratio, which determines the gas content, are variables in the model	Yes, changes the gas content	Degree of saturation and void ratio are calculated
Hydrovariables (pressure and flows)	Yes, main variables in the saturation process	Included variables in the saturation calculation	Yes, changes the hydrovariables	Included variables in the saturation calculation
Stress state	Yes, influences the retention curve.	Included variables in the saturation calculation	Yes, changes the swelling pressure	The pressure and suction are calculated
Bentonite composition	Yes, influence through the retention curve and other properties	Included through input data in the saturation calculation	No, unless via mineral conversion	Not relevant for the saturation period
Montmorillonite composition	Yes, influence through the retention curve and other properties	Included through input data in the saturation calculation	No, unless via mineral conversion	Not relevant for saturation period
Porewater composition	Yes, influences the hydraulic properties	Included through input data in the saturation calculation	Yes, through ion transport in a temperature gradient and from absorbed groundwater	See 3.5.6
Structural and stray materials	Insignificant	Excluded, no stray materials are expected in the buffer	No	

Influence of stress state: The flow potential at unsaturated conditions (suction) is strongly related to the stress state, see Equation (3-12) and the related discussion on unsaturated conditions.

Influence of pore water composition: The flow potential at unsaturated conditions (suction) is related to osmotic pressure of salt solutions in both the clay water and the external water, see Equation (3-13). The hydraulic conductivity is also influenced by the salt concentration and the dominating cation (e.g. see Karnland et al. 2006).

Influence of temperature: The liquid flux is dependent on the liquid viscosity, Equation (3-8), which in turn is dependent on the temperature. Moreover, the diffusion coefficient of vapour diffusion in air, Equation (3-9), is also dependent on the temperature. The saturated vapour pressure is strongly dependent of the temperature. Finally, the flow potential at unsaturated conditions (suction) is related to the temperature according to Equation (3-14).

Influence of bentonite composition: Both the flow coefficient, e.g. the hydraulic conductivity as well as the retention properties are influenced by type of bentonite used, for instance through the montmorillonite content and the dominating cation.

Boundary conditions

The *hydraulic boundary condition* (BC) is of major importance for the water uptake and the hydration of the buffer. This is governed by the hydraulic properties and conditions of the surrounding rock, which determines the rates of inflow, hydraulic pressures, distribution of inflow points and distance to unaffected hydrostatic groundwater pressure. In general, the bentonite hydration is controlled by the bentonite properties if the rock is sufficiently permeable and by the rock properties if the rock is sufficiently impermeable.

In addition, the *thermal BC*, i.e. the heat transport from canister to rock and (backfill), has a major influence on the water transport for conditions with impermeable (dry) rock, since this will cause moisture redistribution from warmer to cooler zones of the bentonite components.

Model studies/experimental studies

This section briefly describes studies performed since 2010 of relevance for this process. The description begins with two modelling tasks included in the SR-Site modelling report. After that follows summaries of different studies related to the four sub-processes: water uptake; dehydration and moisture redistribution; fractured rock/local water entry and; water transport in pellets-filled slots.

Task 3. Assessment of time-scale of buffer-hydration

The time scale to fully water saturate the buffer was analysed within the framework of SR-Site by Åkesson et al. (2010a). Several thermo-hydraulic axis-symmetric 2D finite element models (solved with CODE_BRIGHT) were used for the studies. Responses from models with different hydraulic properties and with or without water bearing features were studied and compared. Three types of geometries were analysed: i) deposition holes intersected by a single fracture at the mid-height of the canister (*CMH-fracture*); ii) deposition holes with no fractures, but where the tunnel just above the deposition hole is intersected by a single fracture (*T-fracture*); iii) deposition holes with no nearby fractures, and no nearby tunnel fractures (*Unfractured rock*). Two different representations of the buffer were analysed since no mechanical processes were addressed: either as fully homogenized from start (*Hom*) or with the initial dry density distributions given by the blocks and pellets at installation (*Init*). The influence of several other properties and conditions were also investigated: permeability and the retention properties of the rock; the permeability of the buffer, the retention properties of the bentonite blocks, and also the influence of initially ventilated tunnels. The results from the calculation are summarized in Figure 3-5. It was found that the time scale to saturate the buffer was in the order of 7–20 years for cases with permeable rock (unfractured rock $K=10^{-10}$ m/s or fractured rock with $K=10^{-11}$ m/s), whereas the time was found to be significantly longer for cases with low-permeable rock. For instance, the time exceeded 150 years for unfractured rock $K=10^{-12}$ m/s. In general, the influence of uncertainties related to the rock (properties and distance to hydraulic boundary) was found to be much larger than for the uncertainties related to the buffer material.

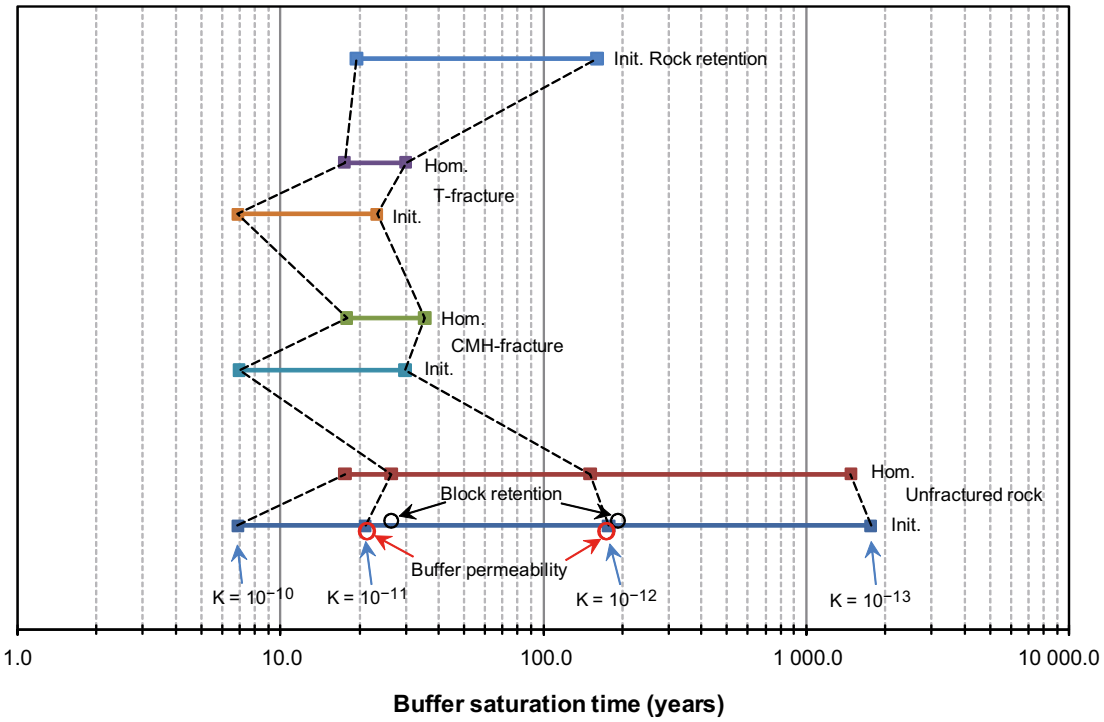

Figure 3-5. *Compilation of the buffer saturation times (Sr ≥ 0.99 in the entire buffer) for different simulations. The text to the right of the lines indicate the representation of the rock: Unfractured rock, CHM-fracture, T-fracture and Rock retention (changed rock water retention curve). For all cases (except rock retention) the buffer was represented with the initial dry density distribution (Init.), and as in a fully homogenized from start (Hom.) as indicated to the right of the corresponding horizontal line. The results obtained using the same rock conductivity, indicated below the bottom line, are connected by hatched lines. The results from changing the Buffer permeability or Block retention are indicated by red or black circles, respectively.*

Task 4. Moisture redistribution under dry rock conditions

An analysis of the moisture redistribution in a dry rock scenario was presented by Åkesson et al. (2010a) within the framework of SR-Site and consisted of two parts.

The first part aimed at providing thermal conductivity distributions for the buffer as input to the thermal dimensioning of the repository presented by Hökmark et al. (2009). A number of thermo-hydraulic axis-symmetric 2D finite element models (solved with CODE_BRIGHT) were used for the studies. The absence of any hydraulic boundary conditions enabled an analysis of the moisture redistribution under completely dry conditions. The main TH process was the diffusion of water vapor, which was the sole means for transferring moisture from hot to cold parts. The modelling work was performed prior to the data qualification for THM modelling of buffer and backfill with in SR-Site (Åkesson et al. 2010b) and differed in a few cases regarding the representation of the bentonite-based components, although this was deemed not to reduce the relevance of the results.

The second part was an analytical investigation of the dehydration of the surrounding rock. This was performed through analysing steady-state liquid pressure profiles resulting from radial inflow into a cylindrical tunnel. Large arrays of parameter values describing the retention properties, the relative permeability, the permeability and the distance to pressure boundary were investigated. Such profiles corresponded to a certain gas-filled pore volume for a given canister spacing which could be compared with the water volume in the installed buffer. The method could identify parameter value combinations with potentially extensive dehydration following from venting of deposition tunnels. For reported retention and relative permeability parameters, however, the analysis showed that the gas-filled pore volume was significantly smaller than the available water volume in the installed buffer.

Water uptake

The *BRIE water-uptake test* was a laboratory test which was performed with bentonite blocks with the same MX-80 bentonite, and with the same dimensions and initial properties as in the BRIE field experiment (see below; Fransson et al. 2017). The objective of the test was to provide data from an experiment with radial water-uptake, which would give a clear-cut description of the hydraulic processes in the bentonite in the field experiment. The tests resulted in three major sets of experimental data: i) evolutions of the cumulative water uptake; ii) evolutions of the relative humidity and stresses; and iii) profiles of degree of saturation and void ratio. The tests results were evaluated through: i) the optimization of two saturation dependent moisture diffusivity functions, which either were based on the water-uptake data (i.e. inflows) or on the water saturation data (measured after dismantling); ii) the adoption of two in-situ retention curves (van Genuchten and square law type), which were based on initial and final data from RH sensors and measured degrees of saturation; and iii) the evaluation of saturation dependent permeability functions from the diffusivity functions and retention curves. These tests resulted in a parameter set which was consistent with the material model previously adopted for MX-80 bentonite (Åkesson et al. 2010b).

The aim of the *SSM 1.4 analysis* (Sellin et al. 2017) was: i) to present the available data concerning hydro-mechanical properties for bentonites other than MX-80; and ii) to evaluate whether these properties can lead to other modelling results than those which were presented in SR-Site. Results from measurements of hydraulic conductivity, swelling pressure, retention properties and from water uptake tests were presented for the following bentonites: Deponit Ca-N, Ibeco RWC BF, Asha, Friedland and Febex. A simple way to estimate the water-uptake capacity for different materials was to evaluate the moisture diffusivity from water uptake tests. The moisture diffusivity could also be evaluated as a function of the saturation degree from the intrinsic permeability, the relative permeability relation, the derivative of the retention curve, a homogenous porosity, and the water viscosity (see the description section above). The consistency between different data sets could in this way be corroborated, at the same time as the material model could be verified from independent measurements. Evaluated moisture diffusivity data was used to make a simple comparison of materials. The reason for this was that the time scale of hydration is basically inversely proportional to the diffusivity (e.g. $t_{febex} \sim t_{mx80} \cdot D_{mx80}/D_{febex}$). Although the variability of the moisture diffusivity was found to be fairly small, it was noted that the lowest values were found for MX-80. This implied that the time-scale of hydration for other materials would be slightly shorter than for MX-80 (the reduction would be approximately 1/2 for Friedland, and 1/3 for the other analysed materials).

The main aim of the *SSM 3.2 analysis* (Sellin et al. 2017) was to analyse how a low inflow rate in single points in a deposition hole will affect the wetting and homogenization of the buffer. This was motivated by the prediction that the deposition holes and tunnels in the Forsmark repository will be very dry with none or a single inflow point in most of the deposition holes. No inhomogeneous wetting was expected if the time to reach saturation exceeds 1 500 years, i.e. the time needed for the expected inflow through the rock matrix to saturate the buffer (Figure 3-5). The time to fill all empty pores in the buffer would be 3 500 and 350 years if the inflow rate was 10^{-6} and 10^{-5} l/min, respectively. The inflow rate through the rock matrix would therefore be somewhere in that interval.

The main analyses were performed with Abaqus as either a hydro-mechanical or a hydraulic problem, and did not include any thermal processes.. The analysis was based on a geometry in which the water inflow was localized to a point at the mid-section of the canister. A constant flow rate or a constant water pressure was used as boundary condition in this point. The flow boundaries were adjusted for increasing pressures so that this did not exceed the hydrostatic pressure. The influence of different assumed relations between the saturation degree and the hydraulic conductivity was investigated. These calculations were however affected by numerical difficulties and in general, these indicated saturation times in the order of 1 500 years, for inflow rates of 10^{-6} as well as for 10^{-4} l/min. A case with constant (atmospheric) boundary pressure resulted in saturation times of 5 000 to 15 000 years. The results of the mechanical simulations of these cases indicated that the inhomogeneity of the buffer caused by the uneven wetting was rather small, although some horizontal displacement of the canister could be expected as well as some local inhomogeneity around the inflow point, and also that there were several uncertainties associated with these simulations.

An alternative analysis of the wetting of the pellets filling was based on: i) a 1D axisymmetric representation of the pellets-filled slot; ii) a solution of the diffusion equation based on an explicit finite-difference method; and iii) a description of the water transport based on theoretical saturation

dependent moisture diffusivity function D(S). This was in turn adopted from an analysis with the aim to quantify the moisture transfer flow coefficients for different dry densities and water contents in general, and for typical pellets properties in particular. The bentonite was regarded as a system of two phases: water-saturated grains and gas-filled voids, in which the moisture was transferred as liquid or as vapour, respectively. Both these fluxes were described as driven by gradients in water content, and moisture diffusivity values for liquid (D_l) as well as vapour (D_v) were quantified in that way. An effective diffusivity value was finally estimated for the bentonite as a whole, and for this the phases were assumed to behave as a composite medium arranged either in series or in parallel. The relative distribution of these phases was assumed to be equal to the fraction of grains and gas-filled voids, respectively. For lower water contents (13–25 %) D_l displayed an increasing trend for increasing water contents, whereas D_v, in contrast, displayed a decreasing trend. The values coincided at the level of 5×10^{-10} m^2/s at a water content of approximately 25 %. For higher water contents, the D_l displayed a maximum of 7×10^{-10} m^2/s at 30–35 % and decreased above that down to 2×10^{-10} m^2/s at 64 %. The D_v, in contrast, displayed a strong decreasing trend and fell below 1×10^{-10} m^2/s at water contents above 35 %. The effective diffusivity for arrangements in series (which was used to adopt a saturation dependent diffusivity function D(S)) was closer to the D_v-values, whereas the corresponding values for parallel arrangements were closer to the D_l-values. Both effective diffusivity functions could be regarded as in fairly good agreement with the empirical data mentioned above. The results from the numerical solution of the 1D axisymmetric representation showed that the time needed to reach 99 % saturation degree was 22 kyears for a case with a constant moisture diffusivity (2×10^{-10} m^2/s) and 91 kyears for the evaluated D(S) function.

Dehydration and moisture redistribution

According to the current plan for the installation sequence of KBS 3V, there will be a time period of up to three months from the installation of the canister and buffer to the backfilling of the tunnel above the deposition hole. This means that the buffer will be subjected to the heat from the canister, and possibly also inflowing groundwater from the rock, during this period when the buffer is not confined from above. This may in turn have different consequences, e.g. dehydration, heaving, swelling and fracturing. Different methods to mitigate such effects have therefore been considered, i.e. a water-proof protection of the buffer blocks, drainage of deposition hole, and immediate filling of the outer slot with pellets. Several large-scale tests have been performed in order to investigate the processes and the effect of different method to mitigate the unwanted effects. In the *Buster projec*t (Johannesson et al. 2014) a test was performed with two 0.5 m high buffer rings with full-scale radial dimensions, with a heater simulating the canister and with a cylindrical steel tank simulating the rock wall in a completely dry deposition hole. Moreover, the outer slot between the blocks and the tank was kept empty, thereby simulating the case with a buffer protection system located close to the rock wall. This procedure resulted in an extensive dehydration of the buffer blocks due to condensation at the simulated rock wall. In the subsequent *BÅT project* (Luterkort et al. 2017, two tests were performed in a full-scale depositions hole (same as in CRT) with a rate of water inflow of approximately 8×10^{-4} l/min. The outer slot was filled with pellets in the first of these tests. In general, this procedure led to a fairly limited dehydration and moisture redistribution and the heaving of the top block was found to be approximately 40 mm. In the second test, a procedure with a buffer protection cover around the upper cylinders was combined with a continuous drainage at the bottom, but the outer slot was kept open. This procedure resulted in: i) fallout of bentonite pieces from the bottom block, ii) significant dehydration of the rings, and iii) fracturing of the top cylinders.

The *"sauna" effect*, in which salt from inflowing groundwater is deposited in or near the bentonite buffer, has been addressed in the Bastu project. Tests with vapor transport through a pellet-filled volume showed that i) water uptake due to condensation dominated these tests; ii) condensation starts in a nucleus which grows successively; and iii) a substantial amount of the vapor was able to flow through the pellets without being absorbed (Birgersson and Goudarzi 2013). It was also shown that a restriction of the swelling had a major impact on the rate of water uptake and thus had a major effect in reducing the loss of vapor. Vapor transport through the inner slot between the buffer rings and the canister was also investigated (Birgersson and Goudarzi 2016). These tests were performed with a heater (Ø 0.1 m), with bentonite blocks (ring-shaped or cylindrical with height 0.1 m and outer Ø 0.3 m) with an approximately 5 mm wide inner slot, and with the entire setup installed in a Plexiglas tube. Different combinations of setups were analysed. The dominating mechanism of water uptake observed in this study was that of localized water condensation: both in the lower ring-shaped blocks

and in the top cylinders. Vapor may therefore be transported quite far before being taken up by the bentonite. Still, the presence of a top blocks can effectively inhibit further vapor transport. As a consequence of localized water condensation, many bentonite rings did crack due to uneven swelling, and in certain cases the cracking was severe which tended to open additional pathways for vapor. In tests where the outer parts of the set-up were sealed with bentonite powder, it was demonstrated that potential vapor loss from these pathways was negligible. Finally, in a summary report (Birgersson and Goudarzi 2017) an evaluation of the possibility of salt accumulation was presented. A critical inflow rate of 10^{-4} L/min was adopted through a theoretical calculation of the accumulated mass of NaCl during a period of 1 000 year, and this inflow rate was related to the capacity to transport vapour, either through the inner open slot or the outer pellets-filled slot. The experimental results strongly suggest that the vapour transport capacity within the KBS-3 buffer is not large enough to support significant amount of salt accumulation.

The main goal of the *SSM 1.1 analysis* (Sellin et al. 2017) was to evaluate the relevance of different conceptual uncertainties for the re-saturation calculations within SR-Site. Three non-standard flow models described in the literature were evaluated: i) threshold gradient in Darcy's law; ii) thermo-osmotic effects, and iii) micro-fabric evolution. Two additional uncertainties were also addressed: i) natural convection in pellets-filled slots, and ii) the temperature dependence of the retention properties. The analysis showed that both the *threshold gradient* and *the thermo-osmosis* (as described in the literature) would lead to a remaining unsaturated void space during non-isothermal conditions. In the case with a *threshold gradient*, the effect would be very small for KBS-3 conditions (with remaining degrees of saturation above 99 %). In the case with *thermo-osmosis* the effect would diminish with decreasing thermal load, and the unsaturated void space would therefore only remain for a few hundred years. The notion of *micro-fabric evolution* has been suggested as an explanation for the slow water uptake observed in a large-scale experiment. This effect has been described as a reduced relative permeability relation, especially close to water-saturation, although it is unclear why the effective conductivity value close to saturation would be orders of magnitude lower than the measured hydraulic conductivity. Still, the slow water uptake observed in the experiment, was in the current analysis evaluated as a low moisture diffusivity value, which seems to coincide with similar values for low density MX-80. This was consistent with a conventional relative permeability relation and with a retention curve derived from the experimental data. The material model adopted for buffer hydration calculations in SR-Site corresponded to a moisture diffusivity of approximately 7×10^{-10} m^2/s. If the SR-Site calculations would have been performed with the lowest empirical diffusivity value ($\sim 2 \times 10^{-10}$ m^2/s) then this would lead to a 3.5 times longer time-scale for buffer-hydration (at wet rock conditions). The potential contribution of *natural convection* to the moisture redistribution was evaluated since vapour diffusion was the only means to transfer moisture from hot to cold parts in the buffer hydration models presented in SR-Site. Two modes of this process were suggested: either through a loop in the outer pellets-filled slot; or through a loop in both the inner and the outer slots, as well as through the joints between the bentonite blocks. The conditions for this process to occur were evaluated by analysing the Nusselt number for a rectangular porous medium. With the available information, it appeared to be more probable to have a sustained natural convection through both the inner and the outer slot, than through solely the outer. An implication of this is that the water retention properties of the bentonite, and the temperature difference between the hot parts close to the canisters and the cold parts in the tunnel ceiling, defines how far the moisture redistribution potentially can proceed. And a completely equilibrated vapour pressure would imply a major dehydration of the buffer. How much further the actual moisture redistribution will proceed in comparison to the case with only vapour diffusion should depend on the flow rates of the natural convection. Experimental data show that the *retention properties display temperature dependence*. The general trend is that RH increases (suction decreases) with increasing temperature. This effect was evaluated with a relation for the chemical potential of the clay water, and with data on the entropy difference between clay water and pure water, Equation (3-14). Such theoretical temperature dependence appeared to be in general agreement with experimental results. The theoretical relation was used to evaluate relations between water content and temperature at zero suction and a specified pressure level, and these relations could in principle constitute saturation profiles for which the hydration stops. However, the resulting difference in water content at the inner and outer radii was found to be very small for temperature intervals typical for KBS-3. Alternative conceptual flow models, and other issues like the influence of the representation of intersecting fractures and of pellets-filled slots, were further analysed by Geier et al. (2018). This research study on the resaturation of bentonite buffer consisted of three parts: hydrological modelling, modelling of resaturation, and coupling

between bentonite and rock. The first part supplied boundary conditions of ground water flow to the second part of coupled THM-modelling. The third part focused on the on modelling of the coupled processes at the interface between the bentonite and the bedrock.

Several *large-scale experiments at Äspö HRL* have contributed to the process understanding. The *Canister Retrieval Test (CRT*) was a full-scale field experiment simulating a deposition hole in a high level radioactive waste repository of KBS-3V design with the main purpose to demonstrate that canister retrieval is technically feasible after full water saturation of the bentonite buffer. This test was carried out from 1999 to 2006. THM modelling of the test was performed within the framework of the task force on engineered barrier systems, where it was given as one of the full-scale experiment assignments (Börgesson et al. 2016). In addition, a model and experimental data concerning CRT was used in SR-Site for which the homogenization process and the remaining heterogeneity after the water uptake process were investigated (Åkesson et al. 2010a). The goal of the *SSM 1.2 analysis* (Sellin et al. 2017) was to perform a comparison of measured and modelled water inflow into the CRT. Based on different data sets from the experiments, and an interpretation of a THM model of the test (described in Åkesson et al. 2010a, Chapter 5) it was concluded that the modelled water uptake seemed to slightly underestimate the actual water uptake, and that there was no indication of any process, which had been disregarded in the model which may have delayed the water saturation rate. The goal of the *SSM 1.3 analysis* (Sellin et al. 2017) was to describe the difference between different models related to CRT (described in Åkesson et al. 2010a, Section 3.4). The "CRT-model" was a THM model and this was compared with two TH models representing the initial dry density distribution and a Homogenized dry density, especially regarding the saturation time. The shortest saturation time was found for the TH CRT Initial model, the longest was found for TH CRT Homogenized, while the saturation time for the THM CRT model was found in between these two TH models.

The *Temperature Buffer Test (TBT)* was a joint project between SKB and ANDRA which aimed at improving the understanding and to model the thermo-hydro-mechanical (THM) behaviour of buffers made of swelling clay exposed to high temperatures (over 100 °C) during the water saturation process (Åkesson 2012). The test was carried out in a KBS-3 deposition hole and was installed during the spring of 2003. Two steel heaters and two buffer arrangements were investigated: the lower heater was surrounded by rings of compacted MX-80 bentonite only, whereas the upper heater was surrounded by a composite barrier, with a sand shield between the heater and the bentonite. The test was dismantled and sampled during the winter of 2009/2010. The final THM modelling task was resumed after the dismantling operation (Åkesson et al. 2012). Three modelling teams presented several model cases for different geometries and different degree of process complexity, and two numerical codes, CODE_BRIGHT and ABAQUS, were used. An assessment of the validity of the material models showed that the material models could satisfactory reproduces some of the experimental results: the thermal evolution; the hydration process around the upper heater; the swelling pressures (i.e. the relation between the void ratio and net mean stress during the final state) and the cable forces. Other aspects were less well reproduced: the dehydration around the lower heater which was generally exaggerated; the early evolution of relative humidity and the occurrence of pore pressures, especially around the lower heater, were generally not reproduced; the calculated von Mises stresses were in some cases significantly lower than the experimental data.

The *Prototype Repository* is a full-scale field experiment at Äspö HRL at a depth of 450 m (Svemar et al. 2016). The experiment aims to simulate conditions that are largely relevant to the Swedish/ Finnish KBS-3V disposal concept for spent nuclear fuel. A 64 m long experimental tunnel contains six deposition holes in which as many full-scale copper canisters surrounded by MX-80 bentonite buffer were installed. The inner section, with four deposition holes, was installed in 2001 and the outer section, with two deposition holes, in 2003. Each section was backfilled with a mixture of bentonite (30 % by weight) and crushed rock (70 % by weight) and finally sealed by reinforced concrete dome plugs. The outer section (23 meter long) was retrieved during 2010/2011, i.e. after about seven years of operation. Semi-blind predictions were carried out by the EBS-TF with the aim of predicting the THM processes taking place in the buffer during saturation and to check the results against recorded sensor readings. Main objectives of the modelling were: i) to predict the condition in the outer section at the opening and retrieval; and ii) to reproduce the THM processes during the operation of the Prototype Repository. See also "Fractured rock/Local water entry".

Fractured rock; Local water entry

The *Bentonite Rock Interaction Experiment (BRIE)* was a field experiment, performed at a depth of 420 m at Äspö HRL, which addressed the hydraulic interaction between compacted bentonite and fractured crystalline rock (Fransson et al. 2017). Two bentonite parcels (denoted Hole 17 and 18) were installed in two Ø300 mm core-drilled test holes in September 2012. The lengths of the parcels were 3.5 and 3.0 m, respectively, and were put together with compacted blocks of MX-80 bentonite (Ø298 mm and height 100 mm) which were threaded on a central tube (Ø40 mm) and confined with steel plates in the bottom and the top. Each parcel was instrumented at two sections with sensors for measurement of relative humidity, total pressure and pore pressure. Monitoring was performed during a period of 419 days for Hole 17 and 515 days for Hole 18. The bentonite parcels were dismantled during the winter of 2013/2014, and were subsequently documented, partitioned, sampled and analysed with respect to water content and density. Photographs of the parcel surfaces displayed traces of the main fractures of interest as well as previously uncharted fractures (especially for Hole 18). These traces were in many cases correlated with measured water content distribution. The results from the water content measurements were consistent with the recorded RH data.

The BRIE experiment was used for a joint modelling task (*Task 8*) of the SKB Task forces on Engineered Barrier Systems (EBS) and on Groundwater Flow and Transport of Solutes (GWFTS). The task definition (Vidstrand et al. 2017) consisted of material properties for bentonite and rock, and data characteristic for the test site, water inflow, deterministic fractures and a discrete fracture network (DFN). One of the contributors to this task (Malmberg and Åkesson 2018) used the same FEM tool (Code_Bright) as was used for the buffer and backfill hydration calculations presented by Åkesson et al. (2010b). However, since it wasn't possible to implement a DFN in this code, the transport properties of the rock around the experimental boreholes had to be handled with a simplified conceptual model in which the rock was treated as a homogeneous material everywhere except in a small cylinder (thickness 0.15 m) around the borehole, where the rock was treated as consisting of low permeability matrix ($k = 10{-}21$ m^2) intersected by fractures. Using updated models, with knowledge about the experimental data on RH evolution and water content distribution and updated fracture geometries, it was possible to achieve an excellent match between modelled and experimental data for borehole 17 and an acceptable match in borehole 18. The hydraulic material model for the bentonite was essentially validated in this task (see water uptake test above). Still, the hysteresis behaviour of the water-retention curve was well known before Task 8, but its importance became clearer during this project. Concerning the material model for the rock, an alternative k_r-relation was evaluated from vapour permeability data for granite samples found in the literature, and this relation was found to imply that the flux through the matrix would be sensitive to the pressure level outside the zone of influence. This could in turn mean that higher matrix permeability values, more consistent with independent conductivity measurements, could potentially be used for Task 8 with good agreement with experimental data. However, since the alternative k_r-relation was essentially discontinuous, it appeared to be very difficult to use in a finite element code. Concerning the conceptual model of the rock, a motivation for the thickness a cylinder of low-permeability was sought through an analysis of the fracture statistics provided in the task description (i.e. fracture intensity and transmissivity), and this suggested that a relevant thickness was closely related to the total fracture intensity.

A similar conceptual model was employed for the TH modelling of the Prototype repository (Malmberg and Kristensson 2014). To represent the hydraulic transport properties of the rock without including a complex fracture network, the host rock was represented by a set of volumes equipped with different conductivities calibrated by comparing simulated and measured inflows to tunnel and deposition holes. A deposition hole in the local models (see below), was embedded in a 1 m thick material with low permeability, which was intersected at different positions by horizontal arcs with 45° angular extension and 0.1 m thick, representing identified local-inflow zones. In order to avoid exceedingly long computation times and numerical instability, the modelling was done in three steps using two types of geometries on different scales: i) large-scale three-dimensional models of the entire experiment with a large volume of host rock, and ii) a local scale three-dimensional model of one deposition hole, with corresponding tunnel backfill and a small part of the host rock. The following models were utilized in the three-step solution strategy: i) A large-scale hydraulic model prior to installation of the experiment, with an empty tunnel and deposition holes, to calibrate the rock material with respect to measured inflow; ii) Large-scale uncoupled thermal and hydraulic models after installation of the

experiment to determine boundary conditions for the local model; and iii) a set of local-scale, coupled thermo-hydraulic models for studying the wetting process in the buffer, from installation to excavation.

The aim of the *SSM 2.0 analysis* (Sellin et al. 2017) was to analyse the distribution of saturation times expected in the Forsmark repository using a combination of 1) fracture data from groundwater models of the site and 2) Code_Bright models of the saturation process of both the deposition-hole buffer and the tunnel backfill. The hydraulic conductivity of the so-called matrix (K_m) was crucial for the distribution of saturation times. The effect for different K_m values could be summarized as:

- High matrix conductivity ($K_m \geq 10^{-11}$ m/s): only a tiny fraction of the deposition holes is saturated through direct fracture flow and none through water entering the deposition hole via the tunnel backfill. All deposition holes will have reached full saturation within approximately 27 years or less.
- Intermediate matrix conductivity ($10^{-12} > K_m \geq 10^{-13}$ m/s): between 10 % and 30 % of the deposition holes are saturated trough fracture flow or via water entering via the tunnel backfill. The remaining deposition holes are saturated primarily via matrix flow, all deposition holes are saturated between approximately 177 and 1 760 years.
- Low matrix conductivity ($10^{-13} > K_m \geq 10^{-14}$ m/s): A significant fraction (30–60 %) of all deposition holes are saturated via fracture flow or by water entering via the tunnel backfill. All deposition holes will have reached full saturation within approximately 22 000 years.
- Extremely low matrix conductivity ($K_m < 10^{-14}$ m/s): If the matrix conductivity would be extremely low almost all deposition holes will be saturated through fracture flow. Deposition holes situated in tunnels where there are no fractures will reach full saturation at a very late time, possibly after 10^6 years.

The aim of the *SSM 1.5 analysis* (Sellin et al. 2017) was to analyse the impact of hydraulically connected deposition holes on the saturation time. Approximately 10 % of all deposition holes will be intersected by fractures according to groundwater models mentioned above. However, since only fractures with inflow rates of $10^{-4} < q_F < 10^{-3}$ L/min is of interest, this fraction falls to 2.6 %. Half (1.3 %) of these deposition holes are intersected by a fracture which intersects at least one additional deposition hole. The effect of such connections is in the most extreme case that the deposition holes in question are saturated via matrix or through tunnel backfill flow, rather than through fracture, and will therefore behave similarly to the majority of the deposition holes (see above).

Water transport in pellets-filled slots

The *SSM 3.2 analysis* (Sellin et al. 2017) also included a conceptual model of the wetting of pellet fillings and the distribution of water at conditions with constant flow rate. The water transport properties in pellet filling are complicated and the water distribution caused by water inflow is difficult to predict, not always repeatable and to some extent random. There is also an influence of pellet type, bentonite type and salt concentration. However, some observed patterns were used to formulate a "model" (although very primitive and uncertain). A successive transition of different wetting patterns could be discerned for different inflow rates:

- At very high inflow rates ($q \geq 0.1$ L/min), the water inflow is faster than the individual pellets can absorb so the free water will fill up the empty pore space and by gravity flow downwards.
- At fairly high inflow rates ($q = 0.01$ L/min), the flow is spread equally in all directions and thus fills the slot circularly with the inflow point as centre and with increasing radius with time.
- At low inflow rates ($q = 0.001$ L/min), the flow seems to move upwards in a rather narrow channel.
- At very low inflow rates ($q = 0.0001$ L/min), an elliptic pattern seems to be formed with a tendency to move upwards and with the major axis directed vertically.
- At extremely low inflow rates ($q \leq 0.00001$ L/min), the water seems to follow a diffusion-like behaviour and spread concentrically as circles.

The model is mainly based on results on the tests made on roller compacted pellets made of MX-80 but may probably also be used for extruded pellets, although the defined flow rate levels appear to be higher for such pellets.

This process has been investigated as a modelling task with the EBS Taskforce. The aim of this task was to investigate the ability of models (existing or new) to simulate water transport at different test conditions. Two subtasks have addressed two test types: A) 1D-tests with water freely available (water uptake tests), and C) 1D-tests with water redistribution in a temperature gradient. Tests were performed with two different pellets materials: extruded Asha NW BFL-L and roller compacted MX-80. The methodology, the equipment, the results and task descriptions for both test types were presented by Åkesson et al. (2020). Different modelling teams have been using different numerical codes for this task, e.g. COMSOL Multiphysics (Eriksson 2019) or Code_Bright (Åkesson 2020a). An evaluation of all contributions was presented by Åkesson (2020b). In general, the used material models included established constitutive relations: i) water retention curves; ii) the Darcy's law for unsaturated liquid transport; and iii) vapour diffusion. Results show that the processes in Test A and C can be described with these relations. A third test type, with constant water inflow rate from point inflow, has also been investigated, but this subtask has not yet been finalized.

Natural analogues/observations in nature

Wetting of bentonite in nature has not been studied and would probably not contribute to the knowledge necessary for the assessment of water uptake in a repository.

Time perspectives

Buffer hydration calculations show that the time to reach full water saturation of the buffer can vary significantly depending above all on the interaction with the surrounding rock. For wet conditions in the host rock, saturation may be reached within 10 years. If there are few fractures and if the rock matrix has a low permeability, then the saturation time may take thousands of years. The time scale for moisture redistribution under dry rock conditions is governed by the temperature evolution, which in turn governed by the heat decay of the spent fuel, and the flow to effect for moisture redistribution. The peak temperature in the buffer is expected to occur 5–15 years after deposition (Hökmark et al. 2009), although the power output will only fall to approximately 30 % of the initial power after 100 years.

Handling in the safety assessment of the PSAR

The water saturation process itself has no direct impact on the safety function of the buffer. It is still important to understand the water saturation process since it defines the state of the barriers in the early evolution of the repository. The *time-scale for the hydration of the buffer* was investigated with:

a. several TH models (Code_Bright) which were analysed for a number of cases with different conditions and assumptions (Åkesson et al. 2010a);

b. through analysing the distribution of saturation times expected in the Forsmark repository by using a combination of fracture data from groundwater models of the site and Code_Bright models of the saturation process of both the deposition-hole buffer and the tunnel backfill (SSM 2.0);

c. through analysing the impact of hydraulically connected deposition holes on the saturation time (SSM 1.5);

d. to present the available data concerning hydro-mechanical properties for bentonites other than MX-80 and to evaluate whether these properties can lead to other modelling results than those which were presented in SR-Site (SSM 1.4);

e. quantify the moisture transfer flow coefficients for different dry densities and water contents, in general, and for typical pellets properties, in particular (SSM 3.2), (Sellin et al. 2017).

Conditions with dry surrounding rock mass may lead to *dehydration/moisture redistribution* in the buffer which potentially can cause an increase of the peak temperature and thus affect the safety function Buff4. This process was investigated with

i. an analytical calculation of the potential dehydration of the surrounding rock, and TH models (Code_Bright) which resulted in water saturation field which was translated into thermal conductivities used for the calculation of the thermal evolution (Åkesson et al. 2010a);

ii. an evaluation of the relevance of different conceptual uncertainties for the re-saturation calculations, i.e. threshold gradient in Darcy's law, thermo-osmotic effects and micro-fabric evolution, as well as two additional uncertainties, i.e. natural convection in pellets-filled slots and the temperature dependence of the retention properties (SSM 1.1);

iii. comparisons of measured and modelled water inflow into the CRT (SSM 1.2) and analysis of the difference between different models related to CRT (SSM 1.3), (Sellin et al. 2017).

It is assumed that the material properties of the buffer will not be adversely affected, by a long water saturation phase to an extent that it would affectthe long-term performance.

Handing of uncertainties in the PSAR

Mechanistic understanding

The processes of water uptake and unsaturated water transport are generally well understood. However, the physical chemical basis for properties like hydraulic conductivity and retention properties is still unclear. Regarding the mechanisms for two-phase flow and relative permeability, there are still a significant lack of mechanistic understanding; especially concerning water transport and convective vapor transport in pellets-filled slots.

Model simplifications

The finite element program Code_Bright has been the main tool for analysing this process, and in general this is highly developed for solving the problems at hand. However, there are few simplifications that should be observed:

- *Water retention curves*. The use of a relation between the degree of saturation and the suction can be a sufficient representation of the water retention properties if the mechanical processes can be neglected. In addition, the porosity dependence implemented in Code_Bright for a variant of the van Genuchten curve may also be able to capture some features when mechanical processes are addressed. However, in order to have a consistent representation of the hydro-mechanical processes, both the retention properties and the mechanical constitutive laws should be based on the relation derived from the chemical potential of the clay water.
- *Chemical interactions* are not included in the code, which means that any potential effects of such interactions cannot be captured. Still, the installed dry density levels of the buffer are sufficiently high to imply that these effects can be safely overlooked.
- *Discrete fracture networks* in the rock cannot be represented in the code, which means that the influence of such networks cannot be directly captured. Still, the findings from the BRIE and Task 8 (Malmberg and Åkesson 2018) suggest that the hydraulic effect of a fracture network can be mimicked with the approach in which the rock can be treated as a homogeneous material except in a small cylinder around the borehole, where the rock is treated as consisting of low-conductivity matrix intersected by fractures.
- *Gas transport* is generally numerically very demanding to analyse together with the slow transport coefficients for water transport. It is therefore effectively impossible to include convective vapour transport in pellets-filled (and open) slots.

Input data and data uncertainties

The most important data uncertainty for the prediction of the time scale of buffer hydration is the hydraulic properties of the rock, especially regarding the fracture network.

The empirical data on hydraulic conductivity of bentonites generally displays a scatter. Furthermore, the expectation is that that this property displays hysteresis behaviour, although this has not been investigated.

3.3.2 Water transport for saturated conditions

Overview

Motivation and sub-processes

Once the bentonite buffer has reached full water saturation its main function is to restrict the water transport through the bentonite. The motive for analysing water transport for saturated conditions is primarily to specify a requirement on the hydraulic conductivity for the buffer material. Advective water transport is a fairly clear-cut process which does not have to be divided in sub-processes.

Description

The most important mechanism under saturated conditions is transport of water in the liquid phase, which is driven by a water pressure gradient. This transport process can be described by Darcy's Law (see Equation (3-8)). A requirement of the hydraulic conductivity for the buffer was described by SKB (2010a):

> "An approximate condition for transport by flow to be more important than diffusive transport is given by: $D_e/\Delta L < K \cdot i$, where D_e = the effective diffusivity, ΔL = the transport length (one-dimensional), K = the hydraulic conductivity and i = the hydraulic gradient. For the stage after restoration of the hydraulic situation in the repository, i can be set equal to 10^{-2} and, for anions $D_e = 10^{-12}$ m^2/s, which for the buffer thickness ΔL=0.35 m requires that K exceeds 3×10^{-10} m/s. This value of K is at least two orders of magnitude higher than the actual conductivity of the buffer. The margin for cations, which have a higher diffusivity, is considerably greater. The conclusion can therefore be made that the only important transport mechanism for both water and dissolved species through the buffer is diffusion…
>
> The requirement to have a hydraulic conductivity that is so low that advection (flow) can be neglected has led to a demand on the hydraulic conductivity of the buffer of
>
> $K < 10^{-12}$ m/s,
>
> which is about 2 orders of magnitude lower than theoretically required for the mass transport process to be diffusion-dominated. Since this demand can only be fulfilled if all initially-present slots or gaps are healed and there is a perfect contact between the buffer and the rock, a requirement for a minimum swelling pressure, σ_s, in the system also exists and is:
>
> $\sigma_s > 1$ MPa
>
> This value is chosen since the hydraulic conductivity is clearly lower than 10^{-12} m/s at that swelling pressure. 1 MPa is also high enough to efficiently fill irregularities on the rock surface in a deposition hole."

Darcy's law describes a linear relation between the hydraulic gradient and the volumetric flux. Two deviations from this can be found in the literature. One is the notion of a threshold gradient beneath which no flow occurs (e.g. Dixon et al. 1999, Hansbo 1960). One is caused by the mechanical coupling, which will lead to a displacement whenever a hydraulic gradient is applied, which in turn means that the apparent hydraulic conductivity will display a decreasing trend for an increasing gradient (Birgersson and Karnland 2015). The latter behaviour is described in Section 2.4.

Dependences

Table 3-5 summarizes how the process influences and is influenced by all the buffer variables and how these effects are treated in the PSAR.

Influence of water and gas content as well as dry density: The hydraulic conductivity is strongly related to the dry density (Figure 3-4, left) and this is taken into account through the porosity dependence of the intrinsic permeability.

Influence of hydro-variables: The flow potential at saturated conditions is the liquid pressure.

Influence of stress state: The bentonite will swell/consolidate if the effective stress is decreased/increased.

Influence of pore water composition: The hydraulic conductivity is influenced by the salt concentration and the dominating cation (e.g. see Karnland et al. 2006).

Influence of temperature: The liquid flux is dependent on the liquid viscosity, Equation (3-8), which in turn is dependent on the temperature.

Influence of bentonite composition: The hydraulic conductivity is influenced by the type of bentonite used, for instance through the montmorillonite content and the dominating cation.

Table 3-5. Direct dependencies between the process "Water transport under saturated conditions" and the defined buffer variables and a short note on the handling in the PSAR.

Variable	Variable influence on process		Process influence on variable	
	Influence present? (Yes/No) Description	Handling of influence (How/Why not)	Influence present? (Yes/No) Description	Handling of influence (How/Why not)
Buffer geometry	Yes, mainly by the flow path	Given as input data. The effect of the geometry, meaning how the buffer expands into other volumes (the backfill) is described in Swelling/mass redistribution (3.4.1)	Yes, during swelling since water flowing into the voids makes the buffer swell if there is space available for swelling	Included in the mechanical model
Pore geometry	Yes, determines the hydraulic conductivity (see text)	Included in the value of the hydraulic conductivity as a function of the density. The pore geometry can be affected by mineral transformation or a change in porewater composition. The effects are discussed in Alteration of accessory minerals (3.5.6) and Osmosis (3.5.7).	Yes, during swelling since water flow into the voids makes the buffer swell if there is space available	Included in the mechanical model
Radiation intensity	No		No	
Temperature	Yes, affects water viscosity. The increase of hydraulic conductivity as a function of temperature is about a factor of 3 between 20 °C and 90 °C	This is neglected in the PSAR because the thermal pulse will be over before any significant radionuclide release may have entered the buffer	Insignificantly. The heat transport due to water transport is very limited	No
Water content	Indirectly through density (pore geometry)		Yes, during swelling since water flow into the voids makes the buffer swell if there is space available	Included in the mechanical model
Gas content	Insignificantly (dissolved gases)	Excluded since it would reduce hydraulic conductivity	No	
Hydrovariables (pressure and flows)	Yes, main variables	Included in the flow model	Yes	Diffusion only for intact buffer. If the hydraulic conductivity once the process is taken into account is below 10^{-12} m/s, and the swelling pressure above 1 MPa, advection will be neglected. If the hydraulic conductivity and/or the swelling pressure do not meet the assigned function indicators, it has to be evaluated if advection could be of importance to the system

Variable	Variable influence on process		Process influence on variable	
	Influence present? (Yes/No) Description	Handling of influence (How/Why not)	Influence present? (Yes/No) Description	Handling of influence (How/Why not)
Stress state	Yes. If the effective stress on the buffer deviates from the swelling pressure the bentonite will change volume and water will flow into or out from it	Included in the mechanical model.	Yes	Included in the mechanical model
Bentonite composition	Yes, determines the hydraulic conductivity (see text)	Included in the model	No	
Montmorillonite composition	Yes, determines the hydraulic conductivity (see text)	Included in the model	No	
Porewater composition	Yes, determines the hydraulic conductivity (see text)	Included in the model	Yes	Replacement of porewater is discussed in 3.5.6
Structural and stray materials	(Insignificant)	Neglected, since no stray materials are expected	No	

Boundary conditions

The *hydraulic BC*, especially the hydraulic gradient, is of major importance for the saturated water transport. This gradient in expected to be very small, once the bentonite fillings have water saturated. However, hydraulic gradients associated with the steep frontal part of a theoretical ice sheet profile during glacial conditions were presented by the **Climate report**, and according to this data the gradient may reach a level of 1.49 m/m.

The *geochemical BC*, i.e. the groundwater composition, is also expected to influence the water transport under saturated conditions through ion exchange and osmotic effects according to (3-9) affecting the hydraulic conductivity, especially at low dry densities (Karnland et al. 2006). The supply of Ca^{2+} ions is determined by the flow conditions in the rock.

Model studies/experimental studies

Within the framework of the *FORGE* project a study was performed with the aim to get a better understanding of the response in bentonite due to external fluid pressurization, in particular due to gas pressurization (Birgersson and Karnland 2015). In addition, a number of experiments with external water pressure differences was performed which were quite similar to the test setup of a hydraulic conductivity test. These tests showed that Darcy's law hold up to an applied water pressure difference of approximately two times the swelling pressure for the dry density in question. These tests also show that the effective hydraulic conductivity decreases slightly with increasing hydraulic gradient. A theory was also presented for steady-state conditions (Birgersson and Karnland 2015), which was based on the empirical observations that: i) the swelling pressure is an exponential function of the porosity; and ii) that the product of the swelling pressure and the hydraulic conductivity is a constant. From this followed that the porosity distribution is a straight line and that the water flux is given by the expression:

$$q = \frac{2 \cdot K^0 \cdot P_s^0}{L} \cdot \mathrm{asinh}\left(\frac{P_w}{2 \cdot P_s^0} \right) \qquad (3\text{-}15)$$

where K_0 and P_s^0 are the hydraulic conductivity and swelling pressure for the average porosity, P_w is the applied water pressure and L is the length of the specimen. Note that the pressures have the unit of meter water column. It was shown that this expression gave good agreement with experimental data for cases in which the applied water pressure was increased to a level 6 times higher than the original swelling pressure (Figure 3-6 right).

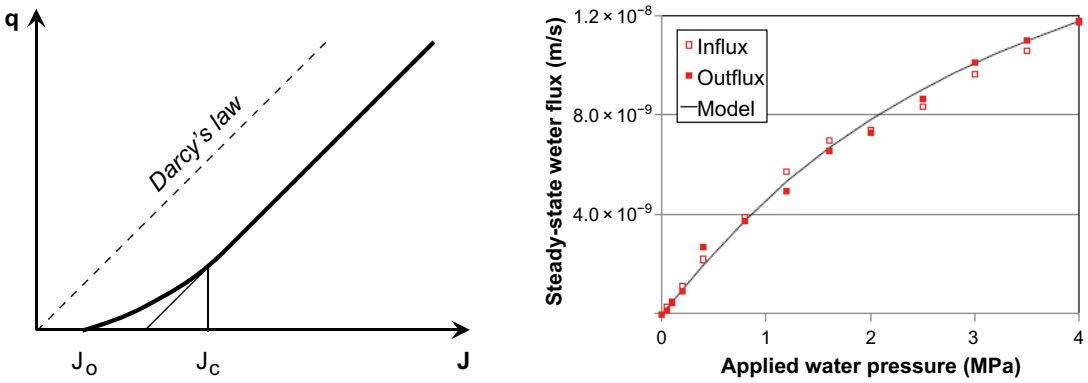

Figure 3-6. *Non-linear relations between the hydraulic gradient and the flux. Due to a threshold gradient (left) and a mechanical coupling (right).*

An analysis regarding *low hydraulic gradients and hydraulic conductivity tests* was performed with the objective to determine the hydraulic conductivity on material from the field experiment Canister Retrieval Test, CRT, using a lower hydraulic gradient than generally used (Dueck et al. 2011a). Both exposed and reference MX-80 samples were analysed. The analysed dry density was 1 500–1 650 kg/m^3, corresponding to swelling pressures 5–13 MPa. The hydraulic gradients used during the tests were 40, 200 and 4 000 m/m which corresponded to water pressure differences of 10 kPa, 50 kPa and 800 kPa, respectively over the samples. A tendency of gradient dependence on the hydraulic conductivity was seen at low hydraulic gradients. The effective hydraulic conductivity increased with a factor of 3–5 when the gradient was decreased from 4 000 to 200 m/m. However, the low accuracy of these measurements makes any conclusions uncertain.

Natural analogs/observations in nature

Water transport in water saturated bentonite has not been studied in nature and would probably not contribute to the knowledge necessary for the assessment of water transport in a repository.

Time perspectives

A time scale of relevance for water transport at saturated conditions can be assessed as the turn-over time of water in the buffer between the rock and the canister. The water volume per unit area in the buffer can be estimated as the product of the thickness (ΔL=0.35 m) and the porosity (n=0.44) of the buffer. The water velocity is given as the product of the hydraulic conductivity (K) and the hydraulic gradient (i). The performance target for limiting the advective mass transfer is set to $K < 10^{-12}$ m/s (Posiva SKB 2017), whereas the hydraulic gradient is expected to reach a level of 0.15–1.5 m/m during glaciation (**Climate report**). Taken together, the turnover time $\Delta L \cdot n/(K \cdot i)$ during such conditions will fall to a level of 3–30 kyrs.

Handling in the safety assessment of the PSAR

The motive for addressing this process is primarily to specify a requirement on the hydraulic conductivity of the buffer material. No special handling was therefore performed.

Handing of uncertainties in the PSAR

Mechanistic understanding

The processes of water transport for saturated conditions are generally well understood. However, the physical chemical basis for properties like hydraulic conductivity and retention properties is still unclear.

Model simplifications

This process has not been analysed through any particular model studies, but the finite element program Code_Bright could very well be used for such simulations. However, Code_Bright has no representation of chemical interaction and discrete fractures.

- *Chemical interactions* are not included in the code, which means that any potential effects of such interactions cannot be captured. Still, the installed dry density levels of the buffer are sufficiently high to imply that these effects can be safely overlooked.
- *Discrete fracture networks* in the rock cannot be represented in the code, which means that the influence of such networks cannot be directly captured. Still, the findings from the BRIE and Task 8 suggest that the hydraulic effect of a fracture network can be mimicked with the approach in which the rock can be treated as a homogeneous material except in a small cylinder around the borehole, where the rock is treated as consisting of low-conductivity matrix intersected by fractures.

Input data and data uncertainties

The empirical data on hydraulic conductivity of bentonites generally displays a scatter. It can also be expected that this property displays hysteresis behaviour, although this has not been investigated.

3.3.3 Gas transport/dissolution

Overview

Transport of gas in the buffer can occur in two phases of the repository's evolution:

- When the repository is sealed, air will be trapped in the buffer. As the buffer becomes saturated with water, the air must escape.
- If a canister should be defective such that water could penetrate through the copper shell, the cast iron insert is expected to corrode, resulting in hydrogen gas formation. If more hydrogen is produced than can be dissolved in the water resident in the canister and surrounding buffer, a separate gas phase will form.

Gas which is trapped in or by the buffer can escape by two principal mechanisms:

- If the production rate is low or the gas quantity small, the gas can be dissolved in the porewater and be removed by diffusion.
- If the production rate is higher or the gas quantity is larger than can be removed via dissolution and diffusive processes, a gas phase will form, the pressure will rise, and a flow path is expected to be formed through the buffer at a critical pressure.

Water saturation phase: Gas flux in conjunction with wetting of the buffer is described in Section 3.3.1. Under these conditions, all gas originally present in the buffer is expected to be dissolved in the buffer's porewater and transported by diffusion.

Gas transport from failed canister before saturation: Before the buffer is saturated, water is only expected to be able to get into a damaged canister via vapour-phase diffusion. Hydrogen production from corrosion will therefore be limited and the gas that is formed is expected to be able to leave the buffer via diffusive transport. The gas transport resistance in an unsaturated buffer is also considerably lower than in a saturated one. Canister damages at this early stage are very unlikely and so this process is considered to be very unlikely.

Gas from defective canister after saturation: After saturation, no gas is expected to be present in the buffer unless there is a penetration defect in the canister and water can get into contact with the cast iron insert. The following section only describes the situation with a breached canister.

Diffusion: Hydrogen gas formed by corrosion of the cast iron insert can dissolve in the porewater and migrate from the canister by diffusion. The maximum transport capacity for different conditions has been estimated by Wikramaratna et al. (1993).

The results of the calculations show that the diffusive transport capacity is considerably lower than the hydrogen gas production from corrosion, if it is assumed that the entire surface of the cast iron insert is accessible for corrosion and the water supply does not limit corrosion. Under such conditions it is probable that a gas phase will be formed inside the canister and that the gas must escape by gas-phase flow.

Gas flow: The following picture of the subsequent course of events is an interpretation of the results of theoretical and experimental studies: At a critical pressure (entry pressure), the buffer is expected to allow the gas to pass through. When the pressure reaches this value, a transport pathway is formed through the buffer and gas is released. After the pathway is formed, two different evolutions are possible:

1. If gas production is maintained, the pressure will fall to a steady-state pressure. When the production ceases the pressure falls, and if the gas production is low enough, the transport pathway is expected to close. This takes place at a so-called "shut-in pressure", which could be dependent on the swelling pressure. At pressures lower than the shut-in pressure, gas migrates solely by diffusion.
2. If the gas production rate is small compared to the permeability of the initial flow path(s), as gas pressure declines, the permeability of the pathways will decline. If gas production is unable to produce sufficient gas to maintain an adequate supply then the aperture of the pathways will decrease (and may well close), potentially resulting in an episodic type response.

The European Commission FORGE (Fate Of Repository GasEs) project was a panEuropean project with links to international radioactive waste management organisations, regulators and academia, specifically designed to tackle some of the key research issues associated with the generation and movement of gases in the context of a repository for the disposal of radioactive waste. The following is summary of results from FORGE concerning gas migration in bentonite barriers (Norris 2015).

In an unsaturated or partially saturated bentonite there is a linear dependence between gas flow rate and pressure gradient, which indicates that two-phase flow, is the dominating transport mechanism. This may also be the case for saturated sand-bentonite mixtures if the sand content is sufficiently high. At a degree of saturation of ~80–90 % or higher the behaviour changes entirely. No flow of gas will take place in the bentonite unless the applied pressure is equal to or higher than the total stress. The only transport mechanism is the omnipresent diffusion of dissolved gas. If the gas pressure reaches a higher value than the pressure in the bentonite a mechanical interaction will occur. This will lead to either:

1. Consolidation of the bentonite, and/or
2. Formation of dilatant pathways

Consolidation means that a gas volume will be formed within the clay that and that the clay is compressed. This increases the clay density closest to the gas volume and the local swelling pressure is increased to balance the gas pressure. There is however a limit to the extent of consolidation. At some critical pressure, pathways will be formed and the gas will become mobile. The pathways are characterized by a strong coupling between total stress (σ), Π (swelling pressure) and pore pressure (Pp), localised changes in σ, Π and Pp, unstable low, exhibiting spatio- temporal evolution, localised outflows during gas breakthrough and no measurable desaturation in any test samples. It is still unclear when consolidation ends and pathway formation starts. In some tests, pathways form when the gas pressure reaches the sample pressure (sum of swelling pressure and pore pressure). An example of this is the full scale Lasgit (Large scale gas injection) test (Cuss et al. 2010). Other tests show pathway formation at an gas injection overpressure at about 20–30 %, while there also are tests where breakthrough occurs at injection pressures 2–3 times higher than the sample pressure. The effect is clearly geometry dependent, but other factors may be involved as well. However, it is clear that classical two-phase flow models cannot correctly represent gas migration in a compacted saturated bentonite. In FORGE, substantial effort has been devoted to the study of gas migration in interfaces. A simple summary of the findings is:

1. Interfaces will, not surprisingly, be the preferred pathway in an unsaturated system.
2. If given the opportunity, gas will generally move along the interface between the clay and another material in a saturated system as well. This does not however seem to affect the transport mechanisms (previous paragraph).

3. In most cases bentonite/bentonite interfaces will seal upon saturation and will not be preferential pathways for gas.
4. It is possible to design experiments where the gas is "forced" to move through the matrix.

In FORGE WP experiments have been performed in a multitude of different setups, boundary conditions, geometries (small and full scale) and materials. Overall, the results from the tests provide a consistent story. This indicates that the knowledge about the processes involved could be upscaled to repository conditions, both in time and in space

The energy that drives gas transport comes from compression of the gas inside the canister and is proportional to the available gas volume. If it is assumed that the volume is a cubic metre and the gas pressure drops from 12 to 9 MPa, 30 MJ will be released when the transport pathway is formed. In a system with confined clay (deposition holes), the gas will presumably be released in a controlled fashion, i.e. it will not entrain the buffer material along with it, but experiments (performed in low density clays) under unconfined conditions, show that gas breakthrough can be a violent process (Donohew et al. 2000).

Available experimental results show that gas can migrate through a highly-compacted buffer without jeopardising the continued function of the engineered barriers. However, no experiment has been conducted with a gas volume equivalent to the volume in the canister cavity (approximately 1 m^3), and it is therefore not completely clear what effect the release of large quantities of gas will have on the performance of the repository. However, this aspect of gas migration can be explored through the ongoing LASGIT project (Cuss et al. 2010) which is a full-scale demonstration test.

Dependencies between process and buffer variables

Table 3-6 summarises how the process influences and is influenced by all buffer variables and how these effects are treated in the PSAR.

Boundary conditions

The essential boundary conditions for this process are the geometries of the conducting features at the buffer interfaces to the canister, the backfill and the rock around the deposition hole, the pressure and volume of gas trapped inside the inner interface (the rate/evolution of these components will also influence the gas migration process), and the material properties of the buffer and host rock. The geometric aspects of these boundaries include the nature of the opening in a defective canister, the number, location and geometry of fractures intersecting the deposition hole and the excavation damaged zones around the deposition hole and in the floor of the deposition tunnel.

Once the gas has reached the excavation-disturbed zone (EDZ) or the near-field rock, the pressure required for it to migrate further is much lower than in the buffer. This will result in an expansion of the gas volume and the displacement of porewater around the deposition hole and gallery opening. It must exceed the sum of the water pressure and the capillary tensions in the fine fractures in the EDZ or in channels in fractures that intersect the deposition holes, which together gives a pressure of 5–10 MPa.

Model studies/experimental studies

Gas dissolution: No specific studies have been conducted for the purpose of studying how gas dissolves in the porewater in the bentonite. However, experience from water saturation tests shows that highly-compacted bentonite normally achieves complete water-saturation and that no trapped gas remains. The mechanistic interpretation is that the suction of the bentonite causes water to enter, which compresses trapped gas (significantly reducing its volume), which is then dissolved in the porewater and this gas is ultimately transported away by diffusion. Gas dissolution essentially follows Henry's law.

Gas transport: A number of gas migration experiments in compacted clays, with different materials, geometries and boundary conditions, have been performed over the last 30 years. Several of these are summarised in Norris (2015).

Table 3-6. Direct dependencies between the process "Gas transport/dissolution" and the defined buffer variables and a short note on the handling in the PSAR.

Variable	Variable influence on process		Process influence on variable	
	Influence present? (Yes/ No) Description	**Handling of influence (How/Why not)**	**Influence present? (Yes/No) Description**	**Handling of influence (How/Why not)**
Buffer geometry	The importance of the buffer volume on gas transport is currently unknown	Assumed to be unimportant	It is important to demonstrate that the gas does NOT influence the buffer geometry	Qualitative assessment
Pore geometry	Is assumed to determine break through pressure – coupled to stress state	See stress state	Fracturing from gas transport	No effect on water transport is assumed
Radiation intensity	No		No	
Temperature	Gas pressure and buffer properties are temperature dependent	Included in the THM modelling of the saturation. For the case of a breached canister this will be neglected since gas transport will take place after the thermal period	No	
Water content	The gas permeability of the bentonite is strongly dependent on the water content	This is considered in the calculation of the saturation process See Section 3.3.1 This will be neglected for a defective canister since in that case gas transport will take place after the saturation phase	The gas may potentially desaturate the clay	Included in the modelling of saturation. This is found to be of limited extent and can be neglected for corrosion gases. A case where contaminated water is pushed out from the canister is assessed within the radionuclilde transport calculations
Gas content	See water content	See water content	The gas may potentially desaturate the clay	The de-saturation effect is assumed to be small based on experimental evidence. Diffusive transport of hydrogen is considered
Hydrovariables (pressure and flows)	Gas pressure (gas generation rate) and hydrostatic pressure determine how and when gas can be transported through the buffer	Gas pressure (gas generation rate) is included in the description of the process	The gas pressure is a coupled component in the total near-field pressure	Maximum pressure is estimated
Stress state	The swelling assumed to determine break through pressure in a saturated clay	The swelling pressure is included in the description of the process in the assessment	The gas pressure is a component in the total near-field pressure	Maximum pressure and pressure evolution estimated
Bentonite composition	Indirect influence through stress state		No	
Montmorillonite composition	Indirect influence through stress state		No	
Porewater composition	Indirect influence through stress state		No	
Structural and stray materials	No		No	

In the case where more gas is generated than what can escape with diffusion a free gas phase will form. Initially, the gas phase will consolidate the clay phase. Experiments have demonstrated, not only that a gas phase does not interact mechanically with water-saturated bentonite when its pressure is below the pressure of the bentonite, but also that mechanical interaction inevitably takes place when the gas pressure exceeds the initial pressure of the clay (Norris 2015). This is clearly illustrated in Figure 3-7, which shows the pressure response of an MX-80 bentonite sample at differently applied gas pressures gradients.

An interesting feature of the test output recorded in Figure 3-7 is that although it clearly demonstrates mechanical influence of the gas on the clay, it does not indicate any additional transport mechanism apart from the ever-present gas diffusion. In contrast, in other tests, gas breakthrough events have been demonstrated to occur for gas pressures at or above the pressure of the clay sample.

Two-phase flow conditions are encountered when gas invades a porous medium as a separate phase. This process is associated with the drainage of interstitial fluid as the non-wetting phase (gas) displaces the wetting phase (pore water). Flow is within the original inter-granular porosity resulting in an iso-volumetric boundary condition. What is meant with regard to bentonite is visco-capillary flow where the properties of the clay capillaries are playing a control on gas displacing water. Based on experimental data from Villar et al. (2012), two-phase flow seems to take place for degrees of saturation lower than about 93 % in compacted bentonite. The experimental work within FORGE clearly demonstrates that no two-phase flow occurs in an initially saturated bentonite (Cuss et al. 2011, Graham et al. 2012).

Lasgit (Cuss et al. 2022) was a full-scale demonstration experiment conducted at a depth of 420 m at the Äspö Hard Rock Laboratory. The experiment started following the closure of the deposition hole on 1st February 2005 and logged data for a total of 5 782 days, finally being decommissioned by mid-February 2021. The main objectives for the Lasgit experiment were fully achieved during this 17-year project, allowing the upscaling of laboratory-derived process understanding to the field scale. The findings provide fundamental information that addresses key questions relating to the treatment of gas in safety assessment and the resulting implications for the evolution of the buffer in the event of a deposition hole containing a defective canister. The main conclusions were: 1) In all tests, regardless of initial gas volume, the movement of gas occurred at a pressure very close to the local total stress; 2) No signs of localised consolidation of the bentonite were observed; 3) The measured peak gas pressures should not lead to any mechanical damage to the buffer or to other barrier components in the repository; 4) Peak gas pressure is linked to the hydraulic permeability of the buffer and the ease at which gas can exit a deposition hole; 5) Gas is transported through a limited number of dilatant pathways. The pathways are expected to be small, in relation to the total volume of the buffer, and temporally variable; 6) No desaturation of the bentonite buffer as a result of gas transport was observed; 7) Over the timescale of the project, pathway closure was only partially successful; 8) The gas pathways are expected to slowly close at a finite “shut-in” pressure; 9) Gas migration through a bentonite will notis highly unlikely to alter the favourable hydromechanical properties of the barrier; 10) The impact of emplaced and long-lived persistent heterogeneities within the bentonite on gas pressure remains unclear.

The results from gas test 1 (GT1) through gast test 6 (GT6) and the full canister test FCT show gas transport processes are scale invariantwhen compared with laboratory experiments and insensitive to the initial upstream gas volume. This may have been expected but had never been tested, beyond laboratory scales, prior to Lasgit. The role of water and the maturity (i.e. state of pore-pressure, hydraulic conductivity, and stress homogenisation of the buffer in the time-frame of the experiment) have been shown to strongly impact gas flow in the buffer. Given the similarities in behaviour between individual tests and those performed in the laboratory, it is reasonable to assume that while peak gas pressures would increase as the buffer continued to mature and reach a state of hydraulic equilibrium, any change would be relatively small, linked to increases in swelling and porewater pressure. The absence of high peak gas pressures such as those sometimes observed during laboratory testing is an important outcome from Lasgit. While gas-induced consolidation may not have been directly observed, the similarities in gas migration behaviour at both scales indicate that it can be further investigated in the laboratory.

These findings are consistent with other recent studies involving argillaceous materials (Ortiz et al. 2002, Angeli et al. 2009, Cuss et al. 2010, Skurtveit et al. 2010, Harrington et al. 2009), as well as earlier studies in bentonite (Pusch et al. 1985, Harrington and Horseman 2003, Horseman et al. 1999).

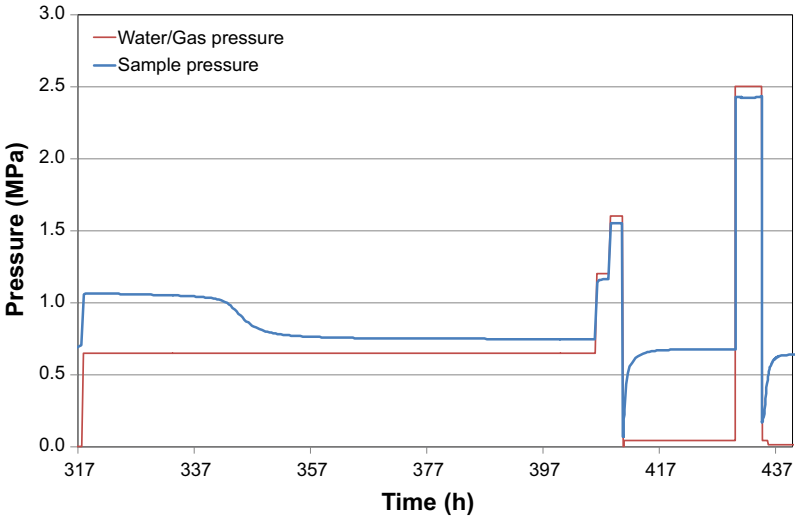

Figure 3-7. *Response of an MX-80 sample which is being pressurized with gas above and below initial swelling pressure. The pressure of the sample is independent of gas pressure when the gas pressure is below the initial swelling pressure (~0.75 MPa), while it is basically equal to the gas pressure at higher injection pressures. Note that water is the pressurizing fluid at the beginning of the displayed pressure evolution (317–340 h) (Norris 2015).*

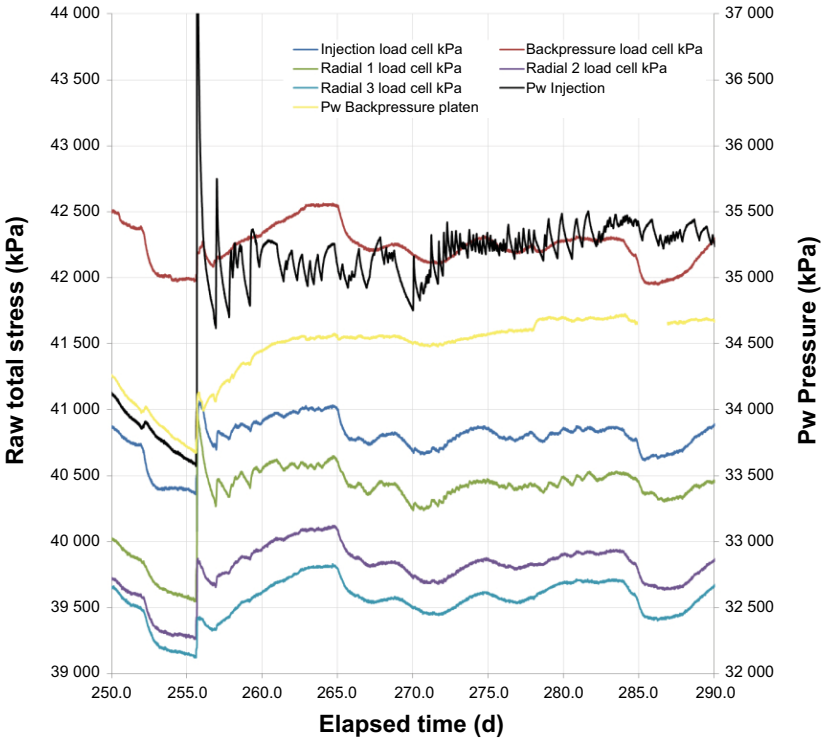

Figure 3-8. *Output of laboratory studies by BGS, showing that under all tested conditions during the project, observations indicate that the primary mode of gas transport is by dilatant pathway formation (Norris 2015).*

Birgersson and Karnland (2015) have tested the gas breakthrough behaviour by lowering the total pressure of the bentonite system by flushing a strong NaCl solution on the outlet side while a constant gas pressure, below the initial pressure of the bentonite, was maintained on the inlet side. The bentonite pressure immediately started to fall after the flushing, and when it became comparable in size to the injection gas pressure a gas breakthrough event occurred). This behaviour was demonstrated in the same sample for different gas injection pressures, giving a clear-cut evidence of the osmotic nature of the system.

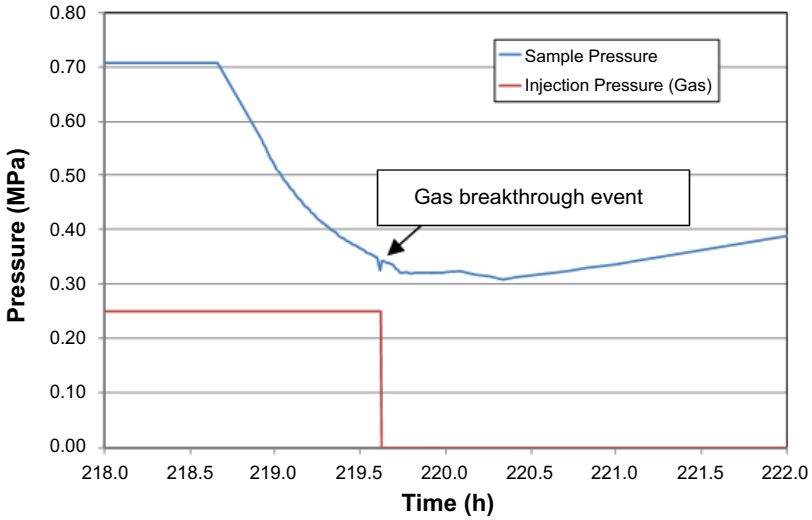

Figure 3-9. *Response of an MX-80 sample which is being flushed by a 3 M NaCl solution at the top filter (at ~218.75 h). The bottom filter is pressurized with air at 0.25 MPa. A breakthrough event occurs when the sample pressure becomes similar to the gas injection pressure (Norris 2015).*

Natural analogues/observations in nature

(Tissot and Pelet 1971) discuss oil and gas movements in clay-shale: "The extraction of oil or gas from a finely structured clay matrix runs contrary to the capillary laws and is in principle impossible. However, the barrier can be broken in one way. The pressure in the fluids that is formed in the pores in the clay increases when kerogen is formed. When this pressure exceeds the mechanical strength of the clay, microchannels will form which are orders of magnitude larger than the natural pores and will thereby allow an oil or gas phase to pass, until the pressure falls below a threshold value and the channels fill again and a new cycle begins." These observations are consistent with the preceding discussions on mechanisms from the gas transport experiments in bentonite.

In the context of gas migration in shallow marine sediments, Judd and Sim (1998) go so far as to declare "Preliminary modelling suggests that, at shallow subsea depths, gas migration will be initiated by fracture failure rather than capillary migration for all sediment types except coarse sands". Clayton and Hay (1992) extend the debate to argillaceous rocks, suggesting that shaly cap-rocks at current depths of burial less than 500 m are always breached by fracturing, the fracture network providing the main route for leakage of liquid and gaseous hydrocarbons across the cap-rock.

Time perspective

Gas transport can occur when water is in contact with the cast iron insert in a damaged or breached (corroded) canister. Unless damaged prior to installation or as the result of some other post-emplacement mechanism, it is unlikely that gas will be generated during the first 10 000 years of the repository lifetime.

Handling in the safety assessment the PSAR

Unsaturated conditions: The gas/air quantity in a deposition hole is approximately six percent of the whole volume at atmospheric pressure. When the hydrostatic pressure has built up, this gas volume will have declined by a factor of 50, at an assumed 5 MPa hydrostatic head. The fate of trapped gas is treated in the modelling of the THM-evolution described in Section 3.3.1.

Saturated conditions: The bentonite buffer is an important barrier in the KBS-3 system. The key purpose of the buffer is to serve as a diffusional barrier between the canister and the groundwater in the rock. An important performance requirement on the buffer material is not to cause any harm to the other barriers. Gas build-up from corrosion of the iron insert could potentially affect the buffer performance in five ways:

1. Permanent pathways in the buffer could form at gas break-through. This could potentially lead to a loss of the diffusional barrier.
2. If the buffer does not let the gas through, the pressure could lead to mechanical damage of the other barriers. The main concern is damage to the near field rock.
3. The gas could de-water the buffer.
4. A gas phase could push water containing radionuclides through the buffer along gas-generated pathways.
5. Some radionuclides may be transported in a gaseous phase.

The process of gas transport within the buffer is neglected except for deposition holes containing a defective canister. For that case, results of model and experimental studies of gas build-up and transport are considered in an integrated assessment of the internal evolution of a damaged canister, including corrosion of the cast iron insert and water transport in the canister. The coupling between gas, porewater pressure and stress within the deposition hole and near field are considered.

Model: No quantitative model describing the consequences of gas generation is available; hence the consequences are estimated based on the experimental evidence mentioned above.

Boundary conditions: Gas is generated inside the canister and will be released to the rock through the buffer. Increased total pressure (and porewater pressure) may occur anywhere in the system.

Handling of variables influencing this process: The global rate of corrosion of the insert determines if the hydrogen gas produced can escape by diffusion or if a separate gas phase will be formed. Therefore, the corrosion rate primarily determines the rate of pressure increase. This pressure may be transferred to the near-field rock and the backfill. It is assumed that the buffer will open and let the gas through at a certain gas pressure. This maximum pressure is dependent on the swelling pressure of the buffer. However, while the swelling pressure (at constant volume) is a very important parameter which should be approximately equal to the minimum pressure at which gas remains mobile in the buffer, the maximum gas pressure is strongly associated with the ease at which gas can escape from the deposition hole, i.e. the number, location and geometry of available sinks. If the gas fails to find a sink, the pressure continues to rise. It is also influenced by the hydrostatic pressure and therefore the effect of a glacial overburden, leading to increased pressures, needs special consideration. The gas pathway in the buffer will stay open as long as the gas production rate is sufficiently high.

The integrated assessment of the internal evolution of a damaged canister will be carried out in the **Post-closure safety report**.

After repository closure, the only direct flammability hazard to man that could arise is from the release of hydrogen at the surface. This has been assessed and found to be extremely unlikely to present any hazard (the calculation was for release into a building (Baker et al. 1997)). The flammability hazard is not analysed in the PSAR.

Uncertainties

Uncertainties in mechanistic understanding

Gas transport: A remaining uncertainty in the understanding of gas transport in the buffer material concerns the number, size and spatial arrangement of the gas-bearing features and the volume (stress-strain) behaviour of the clay during gas injection. As mentioned in the Experiments/Models section above, the gas transport observed through bentonite can be interpreted in a number of different ways.

One critical uncertainty is the break-through pressure, i.e. the pressure when the buffer opens and lets the gas through. This determines the maximum pressure that can be created within the near field of the repository. Another uncertainty is the closure pressure, the pressure at which the pathways in the bentonite close. A further uncertainly relates to the volume of water displaced during gas flow. Potential de-watering of the clay may affect the engineering performance of the buffer.

These uncertainties are considered in the integrated assessment mentioned above.

Model simplification uncertainties in the PSAR

The evolution of the gas pressure and the gas transport in bentonite in the PSAR is still based entirely on values obtained from experimental results. The complexity of the flow processes and the uncertainties regarding the interpretation of the experiments make predictive modelling difficult at this stage (see above). The paucity of laboratory data available for further model development and calibration (both conceptual and numerical) is a major issue in relation to the quantitative treatment of gas in performance assessment.

Input data and data uncertainties in the PSAR

The maximum gas pressure in the near-field is determined by the break-through pressure in the bentonite. In some experiments, this pressure has been found to be above 20 MPa for a bentonite with a swelling pressure of ~ 6 MPa. These high pressures may be an effect of the small experimental specimen, the boundary condions, or possibly of the rate with which the gas pressure was increased Since these high overpressures never have been observed in lager scale tests, they are not considered in the safety assessment. This aspect of the gas migration process is also explored through the Lasgit project and there the maximum pressure was substantially lower (Cuss et al. 2010)

Even with an early failure it would take a very long time to generate a gas pressure. The effect of elevated temperatures on gas pressures can therefore be neglected.

The gas production (corrosion) rate, which determines the timescale of the gas evolution history, is uncertain, as well as the effect of the rate of pressure increase on the process itself.

These data uncertainties are considered in the integrated assessment mentioned above.

3.3.4 Piping/Erosion

Overview

The water-uptake of the bentonite buffer will result in a build-up of a swelling pressure. Once the bentonite buffer has reached full water saturation it will exert a high swelling pressure which will act on the rock surface and restrict the water transport through the bentonite. However, before water saturation has been reached, the bentonite may not be able to prevent inflowing water from the rock due to the high groundwater pressures at repository depth. Such inflows, which may continue through the deposition hole and the deposition tunnel, will lead to the erosion of the buffer.

The motive for analysing piping/erosion is to assess the bentonite mass loss during different flow conditions, especially in pellets-filled slots.

The process can be further divided in three sub-processes, which can be described separately (see Figure 3-10).

- *Piping* is regarded to be a hydraulic process with water transport through channels, which is sustained as long as the pore pressure is equal to the total pressure of the surrounding bentonite. Moreover, the water in the channel is not necessarily in equilibrium with the adjacent clay water.
- *Sealing* (or self-healing) is regarded to be a hydro-mechanical process, which includes the water uptake into the surrounding bentonite, which in turn results in the swelling of the surrounding bentonite.
- The *loss of material* is regarded to be a complex process, which includes the *erosion* of the bentonite into the water phase, as well as the sedimentation and the advective transport of bentonite.

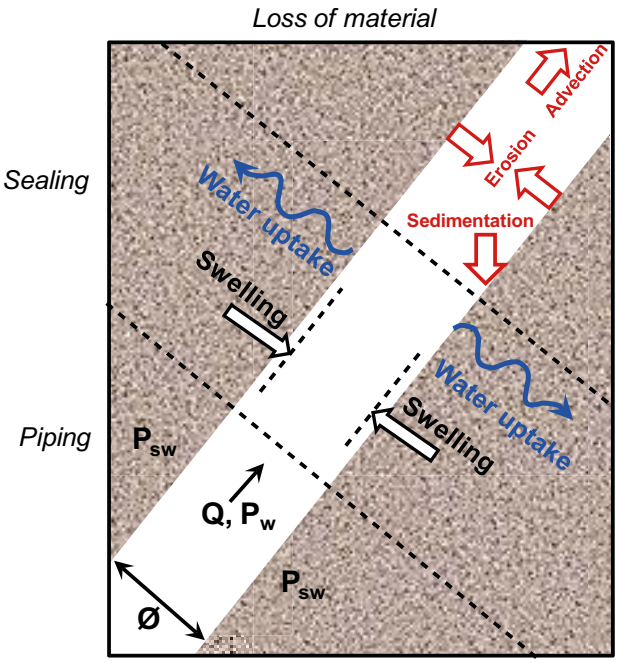

Figure 3-10. *Schematic illustration of piping, sealing and loss of material.*

Description

Loss of material has been analysed in so-called *erosion tests*, in which water is allowed to flow through a pellets-filled slot (or tube) and the bentonite concentration in the effluent is analysed. Several tests with specified salt concentrations, flow rates and slot geometries have been reported (Börgesson and Sandén 2006, Sandén et al. 2008, Sandén and Börgesson 2010, Börgesson et al. 2015). A number of general observations can be made from these tests:

- The main result from an erosion test is the evolution of bentonite concentration in out-flowing water. A quite typical behaviour appears to be that the highest concentrations are found in the beginning of a test, after which the concentrations decrease. This is especially pronounced in solutions dominated by calcium: the initial concentration in vertical tests is typically 0.5–5 g/l, whereas the decrease appears to be approximately one order of magnitude during the first hundreds of litres of out-flowing water (orange and brown symbols in Figure 3-11). In contrast, a pure sodium solution tends to imply fairly low initial bentonite concentration in out-flowing water, which subsequently is fairly constant (red symbols in Figure 3-11).
- A secondary result is the formation of a channel, which can be more or less filled with aggregates. Several parallel channels may appear in the beginning, but the number decreases with time and in the end, there is usually only one remaining channel. The width of this channel increases with time. The formed channels tend to be smooth and stable in the case of pure sodium solutions, whereas channels tend to be wide, grainy, fragile and loose in the case of pure calcium solutions.
- Influence of direction of water flow. The concentration in out-flowing water from horizontal erosion tests is significantly higher than in vertical tests (initially 10s of grams per liter).
- Influence of length. The influence of the length of the pellets filling on the concentration in out-flowing water appears to be weak.
- Influence of flow rate. The influence of the flow rate on the concentration in out-flowing water also appears to by weak; although random fluctuations appear to be more frequent at low flow rates.

An *empirical model* has been derived from erosion tests results, assuming a linear relation in a double logarithmic diagram:

$$m_s = \beta \cdot (m_w)^{\alpha} \qquad (3\text{-}16)$$

where m_s = accumulated mass of eroded bentonite (g); m_w = accumulated mass of eroding water (g); β parameter with values 0.02–2; and α parameter with value 0.65 (see Figure 3-12). The model does not account for the orientation.

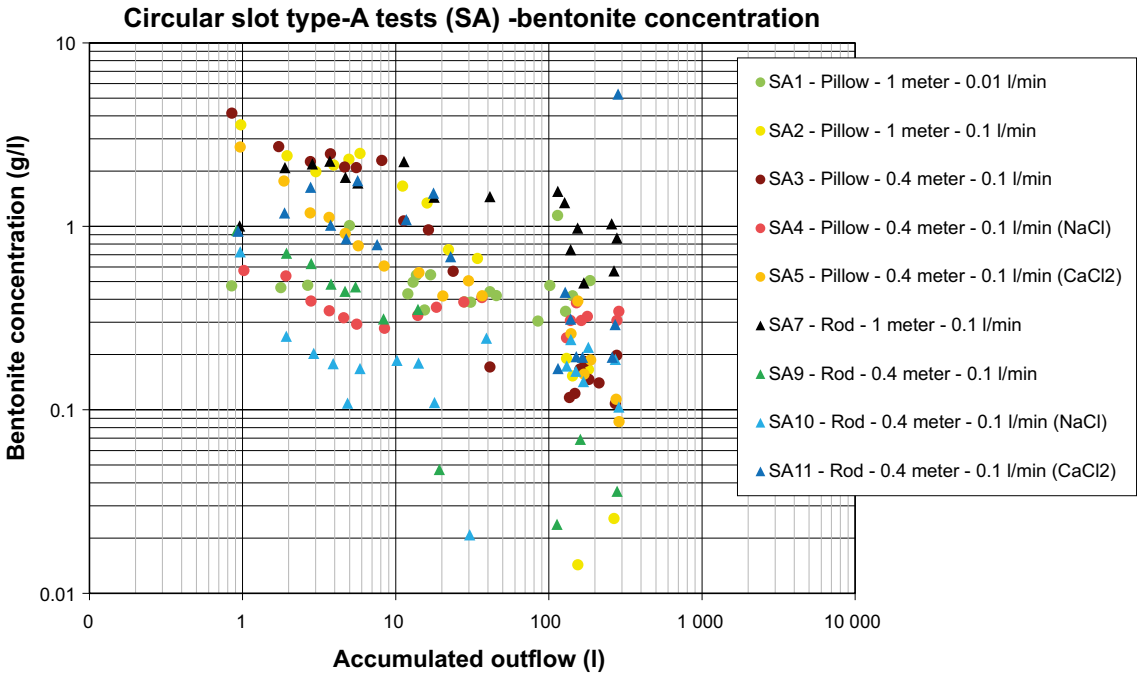

Figure 3-11. *Bentonite concentrations in the outflowing water as a function of accumulated outflow.*

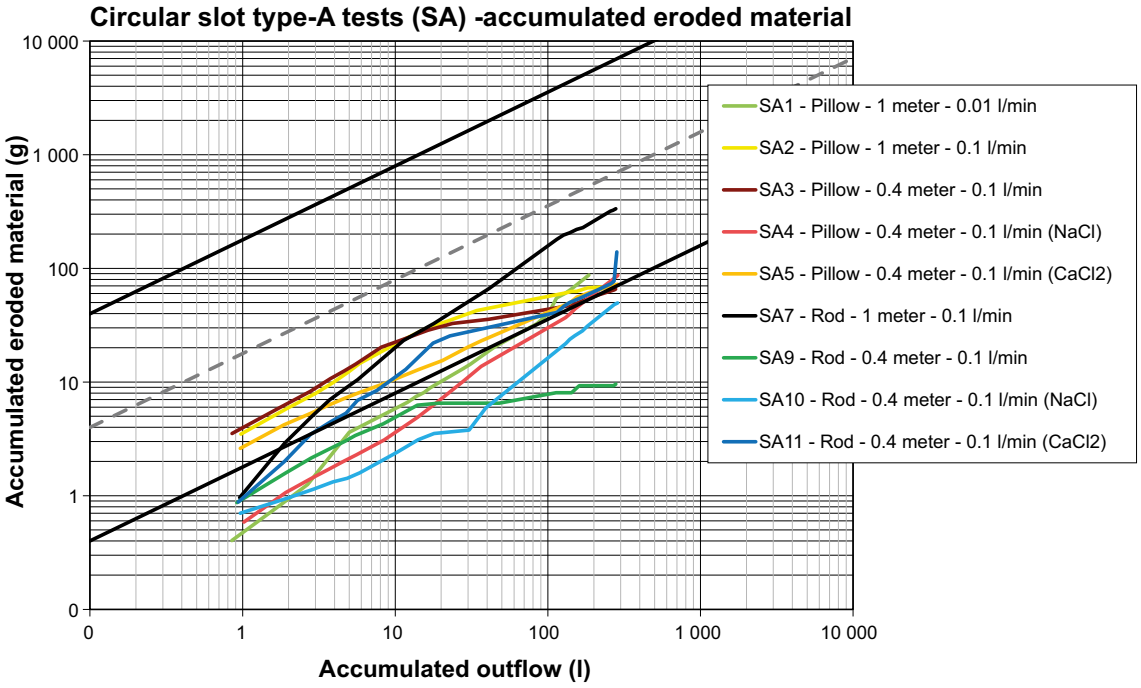

Figure 3-12. *Accumulated eroded material as a function of accumulated outflow. Straight black lines show the empirical model with β = 0.02 (lower) and β = 2.0 (upper). The slope corresponding to α = 0.65.*

Dependences

Table 3-7 summarizes how the process influences and is influenced by all the buffer variables and how these effects are treated in the PSAR.

Influence of water and gas content as well as dry density: The erosion rate and the risk of piping is influenced by the degree of saturation. The risk of piping as well as the possibility to self-heal erosion channels is also influenced by the dry density (through the swelling pressure).

Influence of hydro-variables: The risk of piping is influenced by the pore pressure as well as the flow rate. The relation between the flow rate and the erosion rate is fairly weak.

Influence of stress state: The risk of piping is influenced by the swelling pressure.

Influence of pore water composition: The erosion rate as well as the possibility to self-heal erosion channels is influenced by the chemical composition of the pore water. More specifically, the conversion to Ca^{2+} dominated bentonite leads to a reduction of swelling pressure at lower dry densities, and therefore a reduced ability to self-heal.

Influence of temperature: The influence of the temperature on the erosion rate and the risk of piping is probably low, although no systematic investigations have been performed.

Influence of bentonite composition: Both the possibility to self-heal erosion channels and the risk of piping is probably influenced by the bentonite composition, e.g. the cation composition (through the swelling pressure).

Boundary conditions

The *hydraulic* boundary condition is of major importance for piping and erosion. This is governed by the hydraulic properties and conditions of the surrounding rock, which determines the rates of inflow, hydraulic pressures, distribution of inflow points and distance to unaffected hydrostatic groundwater pressure. The corresponding BC downstream the tunnel plug determines whether there is a hydraulic gradient along the tunnel. The gradient may possibly display heterogeneities, caused by the fractured rock and the backfill, but the overall drawdown will be caused by the open tunnel. The sealing function of the tunnel plug is therefore crucial for limitation of piping and erosion.

The *geochemical* boundary condition, i.e. the groundwater composition, is also expected (through ion exchange) to have an influence on the piping/erosion. The supply of Ca^{2+} ions is determined by the flow conditions in the rock.

Model studies/experimental studies

This section briefly describes studies performed since 2010 of relevance for this process. The description begins with one modelling task included in the SR-Site modelling report. After that follows summaries of different studies performed within the EVA project (see Börgesson et al. 2015).

Task 11. Piping and erosion

Erosion in a deposition hole was analysed within the framework of SR-Site by Åkesson et al. (2010a). The empirical model described above (Equation 3-1) was used to suggest a *total allowable water inflow into a deposition hole*. This was based on an allowable mass loss of 100 kg, (based on an accompanying analysis of homogenization of erosion damages, see Section 4.4 and Task 6). Together with the (conservative) parameter values $\beta=2$ and $\alpha=0.65$, the resulting water volume was found to be 17 m^3 or about 1.4 % of the total volume space available in the tunnel 1 250 m^3, which includes a certain percentage of leakage through the plug. It was however noted that if a lower β-value of 0.2, evaluated from tests with vertical flow, could be confirmed, then this would yield a water volume of 586 m^3.

Table 3-7. Direct dependencies between the process "Piping/erosion" and the defined buffer variables and a short note on the handling in the PSAR.

Variable	Variable influence on process		Process influence on variable	
	Influence present? (Yes/No) Description	**Handling of influence (How/Why not)**	**Influence present? (Yes/No) Description**	**Handling of influence (How/Why not)**
Buffer geometry	Yes, the distance between the bentonite blocks and the rock surface strongly influences the susceptibility to piping, since it affects the time to reach a high swelling pressure	The geometry of the buffer is simplified – only a mass balance is used	Yes, through lost buffer material	Amount of lost buffer is calculated
Pore geometry	Yes, by influence of void size distribution in the pellet gap and indirectly through the stress state	Included in the mass balance estimations	No, but indirect through stress state	
Radiation intensity	No		No	
Temperature	No		No	
Water content	Yes, a change in water content changes the swelling pressure, which influences the piping risk. It also influences the hydraulic conductivity, which influences the swelling rate	Piping will only occur before the buffer is fully saturated and homogenised	Yes. Piping may increase the saturation rate and thus affect the water ratio and degree of saturation since it may distribute the water in a more homogeneous manner via a net of pipes inside the pellets. Erosion will change the final water content	Amount of lost buffer is calculated
Gas content	Yes, the degree of saturation and the porewater pressure in the backfill influences the risk of piping and the erosion rate	Piping will only occur before the buffer is fully saturated and homogenised	No	
Hydrovariables (pressure and flows)	Yes, basic variables	The hydraulic gradient, the water flow and the duration are included in the estimate of piping and erosion	Yes	The pipes are assumed to seal when the hydraulic gradients are restored. An "after piping" hydraulic conductivity based on the loss of mass is estimated
Stress state	Yes, determines if piping occurs	Included in the consequence estimation	Yes	An "after piping" swelling pressure distribution is estimated
Bentonite composition	Yes, the bentonite and montmorillonite composition affects important variables	Included in the consequence estimation made indirectly through stress state	No	
Montmorillonite composition	Yes, the bentonite and montmorillonite composition affects important variables	Included in the consequence estimation made indirectly through stress state	No	
Porewater composition	Yes, the salinity of the water affects many variables that govern susceptibility to piping and erosion, i.e. the swelling pressure, the swelling rate (through hydraulic conductivity) and the erodability	Included in the consequence estimation since the porewater composition will affect the amount of eroded buffer. However, a conservative upper limit is used in the PSAR	No	
Structural and stray materials	No		No	

A slightly different analysis was presented by SKB (2011), which also was based on the empirical model (α=0.65; β=2 and 0.2). As stated above a total volume of about 1 250 m^3 water is expected to flow into the tunnel before it is filled with water and sealed including possible leakage through the plug. In an extreme case, in which all water to the entire tunnel comes from one single deposition hole, the eroding mass of bentonite will be 16.4–164 kg according to the model.

EVA project

The goals of the EVA project (Börgesson et al. 2015) were to understand and develop models for critical processes at an early stage after installation of the buffer and the canister, and to find bases for leakage criteria for the end plug in the deposition tunnel. Several laboratory tests were performed to give information on the piping/erosion process.

Erosion tests in pellets-filled slots were performed with the purpose to investigate the influence of factors such as test geometry (equipment shape and length), water type (salinity and salt type), water flow rate, and pellet types (extruded or compacted). Three different test equipment shapes were used: i) Tube tests (0.1 m diameter); ii) Circular slot tests type A (hollow cylinder with 0.20/0.29 m inner/outer diameter with open upper boundary); and iii) Circular slot tests type B (as type A but with confined upper boundary). The inlets and outlets were located at the bottom and the top of the equipment in all tests. All equipment was made of Plexiglas to allow for continuous photo documentation of the test procedure. The amount of eroded material was determined, and the water pressure was registered for all tests. Finally, some tests were selected for further analyses where ion-exchange processes and grain size distributions were investigated.

Piping tests in pellets-filled cylinders were performed with the purpose to analyse when and how piping is formed and under which conditions piping channels are kept open. Two different test cylinders were used (steel and acrylic plastic). The inner dimensions were 50 mm in diameter and 50 mm in height. The water flow was either axial (for the steel cylinder) or circumferential (for the acrylic plastic). The water pressure and the water flow were either measured or controlled. Tests were performed with different

The overall conclusions from these tests were that piping will take place and the pipe kept open unless: i) There is a stop in the flow for at least 10–15 minutes; ii) The water flow rate is lower than 0.1 mL/min; and iii) The water pressure is lower than 10 kPa. However, the tests also indicated that the low density of the pellet filling means that a water pressure higher than 500–1 000 kPa cannot be resisted, but renewed piping or other destructive processes like gel extrusion or water pocket formation will take place.

The ability to stop piping was analysed with specially designed laboratory tests. The tests were performed in a steel cylinder with inner dimensions: 60 mm in diameter and 120 mm in height. Cylindrical bentonite specimens with 50 mm diameter were placed inside the steel cylinder, thereby forming a slot. Part of the cylinder wall was covered with a filter that was fed with water from the outside. On the opposite side of the cylinder, a water inlet was located at the bottom and an outlet was located at the top. The remaining space of the slot was either left empty or filled with crushed pellets.

In the tests with long testing time the installed dry density was approximately 1 200–1 300 kg/m^3. Only a few tests resulted in such a high flow resistance that the water pressure increased to more than 1 MPa. However, the tightening took place within two days from test start and after breakthrough the flow resistance was rather poor and decreased with time. None of the long-time tests showed any water flow stop that yielded a water pressure higher than 100 kPa after 100 hours when there should have been enough swelling pressure to stop piping.

Self-sealing of erosion channels was analysed with specially designed laboratory tests. The material was mounted in a test device either, by filling the device with bentonite pellets, or by placing a ring of compacted bentonite in the device and by filling the hole within the ring with pellets. Erosion was subsequently achieved by flushing a limited amount of saline water vertically through the specimens. The device was then equipped with filters in top and bottom and the specimens were left with water freely available in order to simulate the self-healing process. Finally, measurements of swelling pressure and hydraulic conductivity were performed, after which the specimens were dismantled, and the water content and density were determined. were performed with different flow rates, eroded dry mass

A small increase in hydraulic conductivity was measured for the tests with ring-shaped specimen filled with pellets. This was however also seen for the reference test without any erosion. Since the test that showed the highest conductivity increase was a test with very little erosion (indicating a scatter problem) and since the only test made on pellets alone showed no influence, the preliminary conclusion was that there was no significant effect of the erosion after self-healing.

A similar study was performed by Johannesson et al. (2010) who tested the self-healing ability by drilling holes in saturated specimens and then let them have access to water again for three weeks. The hydraulic conductivity was measured before drilling of the central hole and then again after three weeks of healing. These tests showed that the self-healing ability was rather poor at dry densities below 1 400 kg/m^3, and especially at a dry density level typical for pellets (~1 000 kg/m^3).

The formation of water and gel-filled pockets and outflow of bentonite gel were observed in the studies of erosion process. Additional test series with the Circular slot tests type B equipment were therefore performed in order to try to better understand the underlying mechanisms behind these processes. These tests were made with lower flow rates than in the erosion tests. These tests aimed at provoking the formation of water- and gel-filled pockets and also the occurrence of gel extrusion. Despite some limitations of the equipment capacity to maintain high water pressures, these processes were observed in many of the tests. The slot type of equipment does not seem to reduce the occurrence of these processes. The conclusion was therefore made that these processes very well may take place in the pellets-filled slots in the deposition holes.

An attempt to develop a *theoretical model* for the loss of material was also made within the EVA project. The water flow was described as flowing through a circular pipe. Basic fluid mechanics could then be used to define the maximum shear stress at the pipe wall as a function of the flow rate and the hydraulic gradient. An empirical relation between shear strength and water content was adopted, which combined with the maximum shear stress function could be used to define the maximum bentonite concentration (C_p^{max}) as a function of the flow rate and the hydraulic gradient. Concentration dependent rates of erosion and sedimentation were subsequently defined. The rate of erosion was assumed to be proportional to the difference between the maximum particle concentration and the current particle concentration (C_p): $k_e \cdot (C_p^{max} - C_p)$ (kg · m^{-3} · s^{-1}). The rate of aggregation was assumed to be proportional to the current particle concentration: $k_a \cdot C_p$ (kg · m^{-3} · s^{-1}). The only two parameters used in the model (k_e and k_a) were introduced for these rates. Finally, a differential equation for the bentonite concentration in a pipe section was derived from a mass balance in which rates for erosion, sedimentation and advection were combined. The model could resemble some typical behaviour for the erosion tests, e.g. the general concentration levels, the formation of large channels filled with aggregates and the weak influence of channel length and flow rate. However, the major concentration reduction found in experiments was not captured, and the influence of different cations could not be explained with this approach.

Natural analogs/observations in nature

Piping and erosion of bentonite in nature has not been studied and would probably not contribute to the knowledge necessary for the assessment of these processes in a repository.

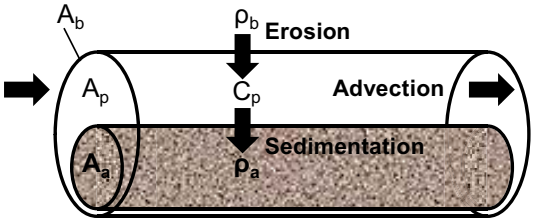

Figure 3-13. *Schematic illustration of mass loss from an eroding pipe.*

Time perspectives

The timeframe, during which piping and erosion potentially can occur, largely coincides with the time period when a drawdown around the deposition tunnel is anticipated. This is, in turn, governed by the operation time for the different stages, among which the one with the longest duration (stage C) is expected to last for approximately 20 years (SKB 2011). It should be noted that this is much shorter than the expected time-scale for the hydration of the backfill, especially for tunnels with low inflow rates.

Handling in the PSAR

The loss of bentonite due to the erosion from inflowing water into a deposition hole may lead to a reduction in buffer density. An empirical model was used to estimate the mass of eroded material (SKB 2011), either based on the total possible water volume that could flow into a tunnel or based on the limit value for acceptance in accordance with the design premise. A judgement was also based on the likelihood of fractures intersecting the tunnel rather than the deposition holes (SKB 2011). An alternative analysis was based on an allowable mass loss from which a total allowable water inflow into one deposition hole was suggested (Åkesson et al. 2010a).

The calculations in SR-Site showed that 100 kg material can be lost by piping and erosion without jeopardising the performance of the buffer. To avoid negative consequences of the process requirements are set on:

- Inflow to the deposition holes
- The backfilling sequence
- The sealing ability of the tunnel plug

The probability for buffer loss in the PSAR is based on SKB (2013). To illustrate the probability for piping and erosion the base case without excavation damaged zone (EDZ) from Joyce et al. (2013) is used. The data needed are:

1. Total inflow to each deposition tunnel. Data are given for 207 tunnels.
2. Total inflow to the deposition holes in the respective deposition tunnels.
3. The inflow to each deposition hole in the respective deposition tunnels.
4. The total void volume in the deposition tunnels. Here a simplified assumption that all tunnels have the same volume is made.
5. The erosion model described earlier in this section: $m_s = \beta \cdot (m_w)^{\alpha}$ (3-16)

Handing of uncertainties in the PSAR

Mechanistic understanding

Even if a significant body of data has been collected regarding erosion rates as well as the risk of piping at different conditions there is still a significant lack of understanding concerning the underlying mechanisms, for instance regarding the mechanisms behind the concentration of suspended particles in the channel water, and regarding the force balance between the water pressure in the channels and the swelling pressure in the surrounding bentonite.

Model simplifications

The influence of the cation composition in the bentonite and in the flowing salt solution is not considered in the empirical model.

The empirical model is used to extrapolate accumulated mass losses for accumulated water volumes. A continuous decreasing concentration level is implicit for the empirical mode and described by α=0.65. However, there is no data to support a decreasing trend for very high accumulated water volumes.

Input data and data uncertainties

Data that has been collected regarding erosion rates as well as the risk of piping displays a significant scatter.

3.4 Mechanical processes

3.4.1 Swelling/mass redistribution

Overview

Motivation and sub-processes

The bentonite buffer will be installed as blocks and pellets. These components differ in terms of bentonite densities. There will therefore be significant density heterogeneity from start with high densities close to the canisters and lower density close to the rock wall of the deposition holes. The bentonite exerts a swelling pressure due to its high affinity for water, and higher densities generally results in higher swelling pressures. This material property therefore tends to reduce the density heterogeneities.

The motive for analysing swelling/mass distribution is threefold: i) to assess the distribution of densities and stresses after the buffer hydration; ii) to assess the mechanical transmission of forces across the buffer during a rock shear; iii) to assess the long-term stability of the buffer, e.g. regarding the remaining heterogeneities.

The process can be further divided and described separately as four sub-processes:

- *Homogenization,* i.e. reduction of heterogeneities caused by: i) the installation due to density differences of different components; ii) the loss of bentonite through erosion; and iii) the disintegration of the concrete in the bottom plate. A related process is the potential occurrence of uneven swelling which may be harmful for the cannister.
- *Rock shear,* i.e. the shearing of the deposition hole during an earthquake, which potentially can cause substantial damage to the canister. The shear strength of the bentonite is a crucial property of the bentonite for this process.
- *Buffer upward swelling,* i.e. the swelling of the buffer up into the deposition tunnel which will lead to a reduction of the density of the buffer in the upper part of the deposition hole.
- *Canister sinking,* i.e. the potential sinking of the canister to the bottom of the deposition hole due to gravity which in turn may lead to the short-circuiting of the buffer.

Description

The description of the mechanical process of bentonite has not reached the same level of refinement as the hydraulic processes. This is probably due to the higher level of complexity of the mechanical processes. It is therefore instructive to begin this section with an overview of the basic hydro-mechanical properties of bentonite:

The swelling pressure and suction properties are basically the same as described for the water uptake (Section 3.3.1) these are derived from the chemical potential of the clay water, and which states a relation between the suction (s), the pressure (P) and the *clay potential* (Ψ). The latter can be described as a function of the water content:

$$s = \Psi(w) - P \qquad (3\text{-}17)$$

although it is probably more correct to describe it as a function of the void ratio (e) or the dry density (ρ_d) at water saturated conditions.

This means that the swelling pressure (p_{swell}) is equal to the clay potential under confined conditions with free access of water. Swelling pressure tests are performed on a compacted, initially unsaturated, specimen in a rigid steel cell, with free access of water through a filter, and by measuring the axial force. The swelling pressure is evaluated as the axial stress after the water-uptake is completed. Oedometer tests are performed on a water saturated specimen in a rigid steel cylinder, which ensures zero lateral strains, with free access of water through a filter, and by subjecting the specimen to stepwise increasing or decreasing axial loads. After each change in load, the specimen is left to equilibrate, i.e. through consolidation or swelling, and for these test conditions the axial and radial stresses as well as the void ratio are quantified.

Two basic characteristics can generally be identified: The swelling pressure is a strictly decreasing function of the void ratio, and results from oedometer tests exhibit a path dependence, so that bentonite undergoing consolidation displays a higher axial stress than a specimen which follows a swelling path (Figure 3-14 left). Correspondingly, the suction is a strictly decreasing function of the water content, and bentonite undergoing a dehydration path displays a higher suction value than a specimen which follows a hydration path (Figure 3-14, right).

According to the current technical design requirements the swelling pressure of the initially installed buffer should fall in the interval 3–10 MPa. The lower limit was selected to limit advective mass transfer, limit microbial activity, and to keep the canister in position. The corresponding upper limit was selected to limit the pressure on the canister (Posiva SKB 2017).

Shear strength. The bentonite has the ability to sustain and to limit different stresses in different directions. The suction value in a water retention test does not display any direction dependence. In an oedometer test however the stresses are general non-isotropic, e.g. the axial stress exceeds the radial stress during consolidation, whereas the relation is the opposite during swelling. Yet, there are limits for how large the difference between the stresses in different directions can be. This is usually quantified on water-saturated bentonite specimen as either an unconfined or a triaxial compression test. The latter type can be performed at either drained or undrained test conditions. The main test result is the von Mises stress at failure. This quantity can be related either to the mean effective stress or the void ratio of the specimen and is also a strictly decreasing function of the void ratio (Figure 3-14 right).

According to the current technical design requirements the unconfined compressive strength at should not exceed 4 MPa at a deformation rate of 0.8 %/min. This limit was selected to mitigate the impact of rock shear on the canister (Posiva SKB 2017).

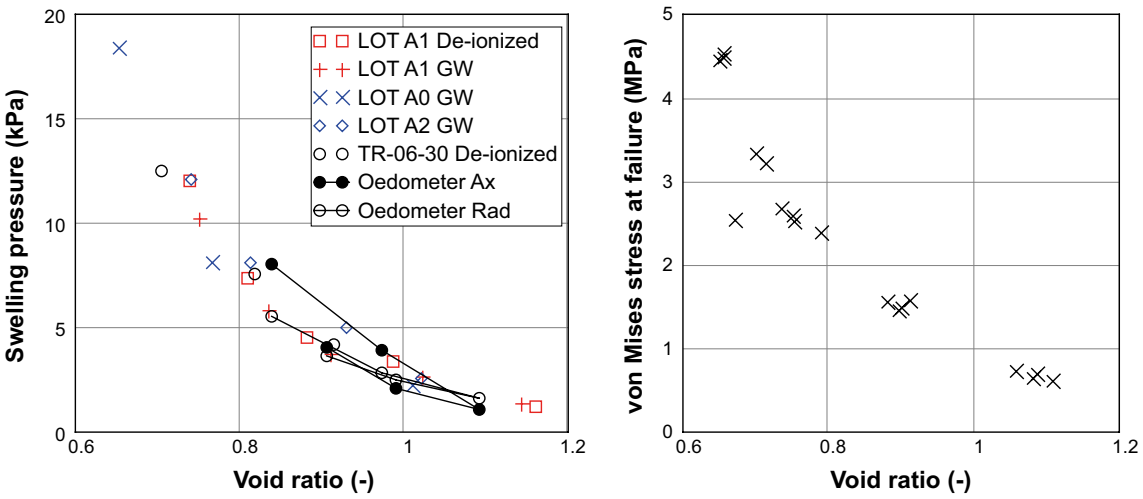

Figure 3-14. *Swelling pressure versus void ratio for MX-80 (left): LOT A1 (Karnland et al. 2000), LOT A0 and A2 (Karnland et al. 2009), TR 06-30 (Karnland et al. 2006), and oedometer data (Börgesson et al. 2015). Uniaxial compression tests data for MX-80 reference sample from Canister retrieval tests (data from Dueck et al. 2011a)*

Thermal expansion. Bentonite block display an expansion when exposed to a temperature increase (Luterkort et al. 2017). Analogous, a confined buffer installation exposed to heating in which there has been a build-up of swelling pressure, displays a drop in swelling pressure if the heating is reduced rapidly. These thermo-mechanical couplings are governed by the thermal expansion of water, α_w, which means the effects of temperature changes on the swelling pressure will diminish once the water pressure (suction) has equilibrated with the surroundings. The corresponding thermal expansion for the bentonite mineral can be regarded as insignificant. Still it should be noted that there can be influence of temperature on the swelling pressure (after equilibration), but this can be described as an entropy effect.

Constitutive models. Numerical models, especially finite element tools, have to be used for performing quantitative analyses of complicated hydro-mechanical problems. These tools utilize defined constitutive models for description of the buffer material.

One of these is the Barcelona Basic Model (BBM) (Alonso et al. 1990), which is implemented in Code_Bright. This is an elasto-plastic model which can be viewed as a generalization of the Modified Cam Clay model for water-unsaturated conditions and with the net mean stress (p´) and suction as independent state variables for representing isotropic stress states. The net mean stress is defined as $-(\sigma_x+\sigma_y+\sigma_z)/3 - p_g$, where stresses ($\sigma$) are negative for compressive stresses and p_g is the gas pressure. Suction is defined as the difference between the gas pressure and the liquid pressure ($s = p_g - p_l$). The strain is composed of three parts: elastic (ε^e), plastic (ε^p) and hydraulic (ε^h). The elastic stress-strain relation is basically governed by three parameters: the κ_i modulus (see Figure 3-15), the Poisson's ratio (ν) and a minimum bulk modulus (K_{min}). Plastic deformations are activated once the yield surface is reached (Figure 3-15, right). This surface is composed of two functions in the s-p´ plane: the tensile strength (p_s) and the pre-consolidation stress (p_0), which both are expressed as functions of suction, and the latter is also a function of the pre-consolidation stress for saturated conditions (p_0^*). These lines are joined with an elliptic function in the q-p´ plane, described with p_s, p_0 and the critical state line parameter (M). The hardening law describes a relation between increments in the plastic volumetric strain and in increments in p_0^* which is governed by the κ_i and λ_0 moduli. Finally, the hydraulic suction strain relation is governed by the κ_s modulus. In the original formulation of BBM, the κ_i and κ_s parameters were regarded as constants. In the TEP (thermo-elastoplastic) constitutive laws of Code_Bright, however, they have been developed as functions. The κ_i is defined as a function of suction, while κ_s is defined as a function of p´, suction and the void ratio. The latter dependence is based on a defined swelling pressure relation, $p_{swell}(e)$ (Åkesson et al. 2010b), and this means that the swelling stops precisely when the net mean stress reaches the swelling pressure for the current void ratio.

Several constitutive laws have been used for hydro-mechanical modelling with the code Abaqus; the Porous Elastic Model, the Moisture swelling, the Drucker-Prager Plasticity model, the Claytech plastic cap model, and a Creep model. The average effective stress ($p = -(\sigma_x+\sigma_y+\sigma_z)/3 - p_l$) is generally used as the governing state variable. For unsaturated conditions this is generalized according to Bishop with the χ-parameter assigned to a value equal to the degree of saturation (S_r).

The Porous Elastic Model is similar to the elastic part of the BBM model and is described by two parameters: the κ_i modulus (seeFigure 3-16) and the Poisson's ratio. The Moisture swelling function represents the swelling of the material for unsaturated conditions and is described with an additional volumetric strain ($M.S. = \ln(1+\varepsilon_v)$) being defined as a function of the degree of saturation. The Drucker-Prager Plasticity model is defined within a zone between a yield surface and a failure surface, and a tabulated yield function describes a relation between the stresses and the plastic strains. The Claytech plastic cap model defines a yield surface and a failure surface according to Figure 3-15, as well as a flow surface and a flow rule. If the average effective stress exceeds the "pre-consolidation pressure" p_b then this will result in non-recoverable plastic volume decrease and an expansion of the cap, i.e. cap hardening, and this behaviour is described with a tabulated relation between p_b and the plastic volumetric strain. Correspondingly, a plastic expansion due to dilation close to the failure envelop will lead to the shrinkage of the cap. Finally, the used Creep model addresses deviatoric creep which describes a relation between the deviatoric creep rate ($\dot{\epsilon}_{cdt}$), the degree of mobilized Mises' strength (Q_r) and time (t). Q_r is defined as the ratio between the actual von Mises stress and the von Mises stress at failure (Figure 3-17).

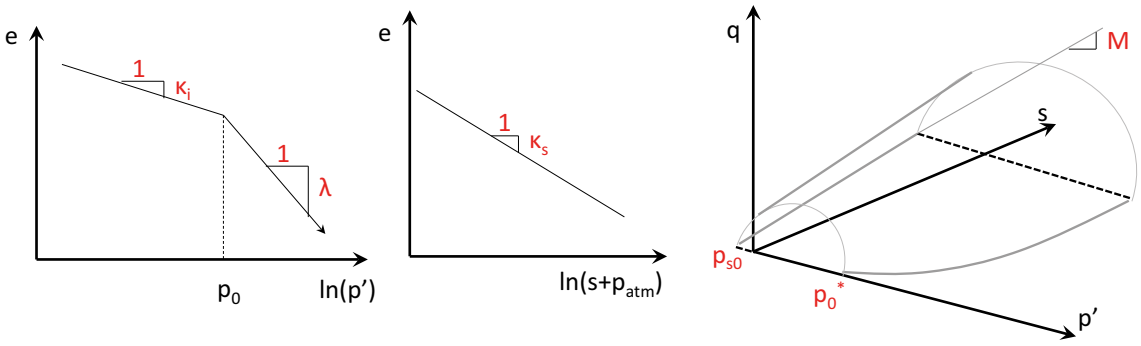

Figure 3-15. *Elements of the BBM used in Code_Bright.*

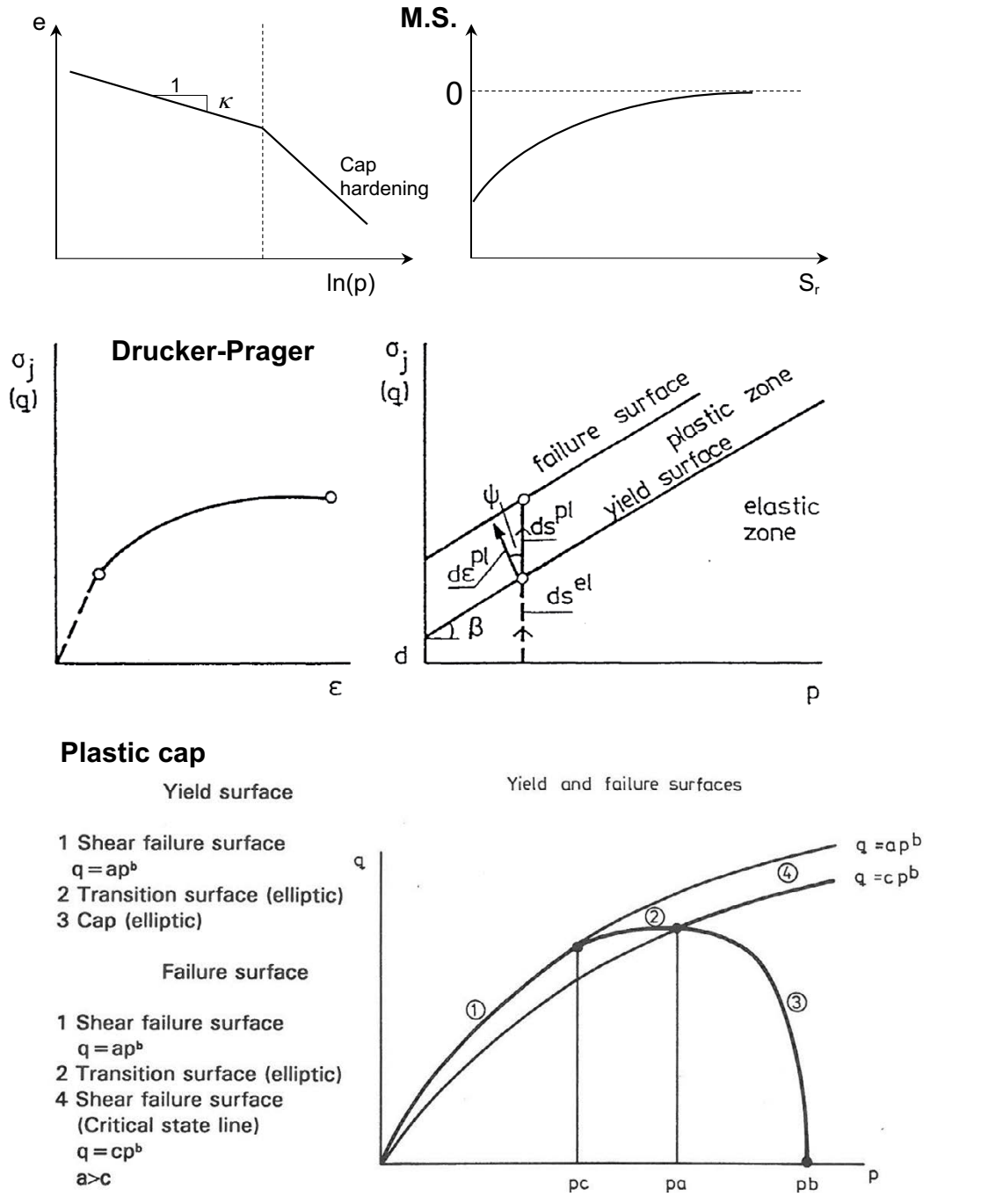

Figure 3-16. *Elements of hydro-mechanical constitutive models used in Abaqus.*

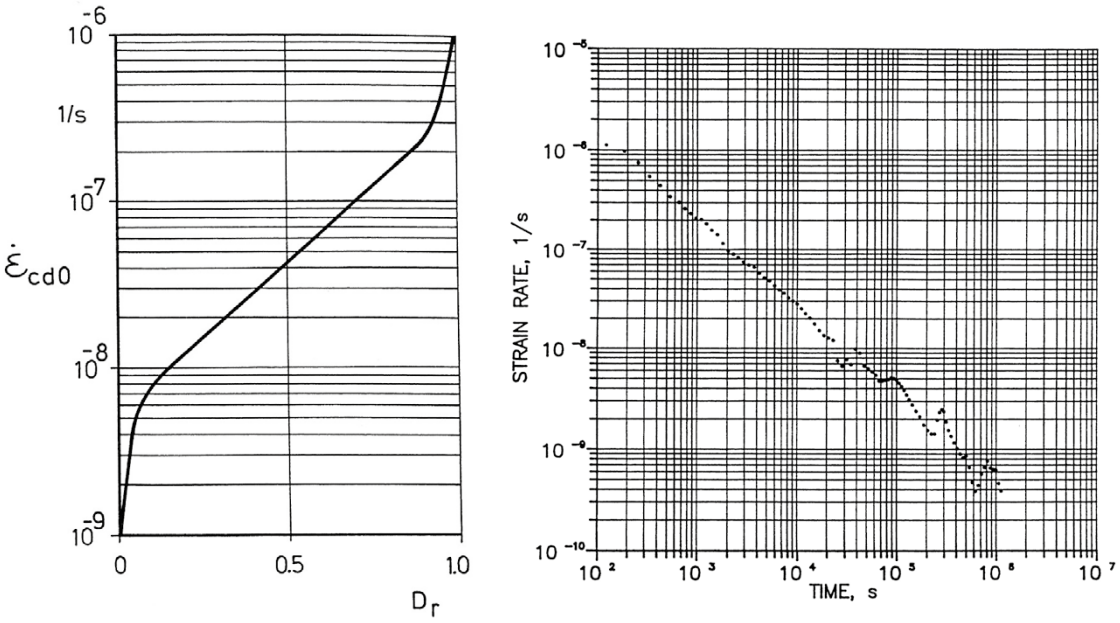

Figure 3-17. *Model relation between degree of mobilized strength and deviatoric strain rate (left). Measured creep rate as a function of time (right).*

Dependences

Table 3-8 summarizes how the process influences and is influenced by all the buffer variables and how these effects are treated in the PSAR.

Influence of water and gas content as well as dry density: The swelling pressure at zero suction, i.e. the clay potential, see Equation (3-17), is influenced by the water content as well as the dry density. The von Mises stress at failure is influenced by the void ratio.

Influence of hydro-variables: The total pressure is equal to the sum of the swelling pressure and the pore pressure. The von Mises stress at failure is independent of the hydro-variables.

Influence of stress state: The stress state is an integral part of the hydro-mechanical processes.

Influence of pore water composition: The swelling pressure is influenced by the external salt solution, see Equation (3-13).The von Mises stress at failure is however not influenced.

Influence of temperature: The swelling pressure is related to the temperature according to Equation (3-14). The influence of the temperature on the von Mises stress at failure appears to be weak, although a tendency of increasing values with increasing temperatures have been observed. However, the strain at failure is generally reduced when specimens have been exposed to increasing temperature.

Influence of bentonite composition: The swelling pressure is influenced by type of bentonite used, for instance through the montmorillonite content and the dominating cation. The von Mises stress at failure is also influenced by the montmorillonite content but not by the dominating cation.

Table 3-8. Direct dependencies between the process "Swelling/mass redistribution" and the defined buffer variables and a short note on the handling in the PSAR.

Variable	Variable influence on process		Process influence on variable	
	Influence present? (Yes/No) Description	**Handling of influence (How/Why not)**	**Influence present? (Yes/No) Description**	**Handling of influence (How/Why not)**
Buffer geometry	Yes. Any phenomenon leading to alterations of the buffer bulk geometry influences swelling	The initial position of the buffer is the starting point of the evaluation	Yes	The buffer geometry after swelling is included in the model
Pore geometry	Yes. Through void ratio and indirectly through stress state	Void ratio is included in the model	Yes. Through void ratio and indirectly through stress state	Void ratio is included in the model
Radiation intensity	No		No	
Temperature	Yes, by thermal expansion and indirectly via the hydro-variables	Excluded from assessment (see below)	(Insignificantly)	
Water content	Yes, decisive variable	Included in THM modelling of unsaturated buffer	Yes	Included in THM modelling of unsaturated buffer
Gas content	Yes, degree of saturation is a model variable	Included in THM modelling of unsaturated buffer	Yes, degree of saturation is a model variable	Included in THM modelling of unsaturated buffer
Hydrovariables (pressure and flows)	Yes, model variables	Included in THM modelling of unsaturated buffer	Yes, model variables	Included in THM modelling of unsaturated buffer
Stress state	Yes, model variable	Included in THM modelling of unsaturated buffer and included in calculation of the mechanical interaction with the canister as well as backfill	Yes, model variable	Included in THM modelling of unsaturated bufferIs and included in calculation of the mechanical interaction with backfill
Bentonite composition	Yes, influences the suction potential and the swelling pressure	The initial composition of the buffer is the starting point of the evaluation	No	
Montmorillonite composition	Yes, influences the suction potential and the swelling pressure	The initial composition of the buffer is the starting point of the evaluation	No	
Porewater composition	Yes, influences the suction potential and the swelling pressure	Included in the model via the suction potential and the swelling pressure etc	No	
Structural and stray materials	Unclear	Not considered with the the PSAR assessment, since no stray materials are expected in the buffer	No	

Boundary conditions

The *mechanical BC* is of major importance for swelling and mass distribution. Both the rock and the canister constitute stiff boundaries. The bentonite may nevertheless slip along these materials although such movements have to overcome the friction between the bentonite and the boundary. A special mechanical BC of the rock is the case with rock shearing.

The *hydraulic BC* is also of importance for swelling/mass distribution. This is governed by the hydraulic properties and conditions of the surrounding rock, which determines the rates of inflow, hydraulic pressures, distribution of inflow points and distance to unaffected hydrostatic groundwater pressure.

The *geochemical BC*, i.e. the groundwater composition, is also expected to have an influence, through ion exchange, on the swelling/mass redistribution processes, through the swelling pressure and suction properties, especially at low dry densities (e.g. Karnland et al. 2006). The supply of Ca^{2+} ions is determined by the flow conditions in the rock.

Model studies/experimental studies

This section briefly describes studies performed since 2010 of relevance for this process. The description begins with seven modelling tasks included in the SR-Site modelling report. After that follows summaries of different studies related to homogenization, uneven swelling and shear strength, respectively.

Task 5. Buffer homogenization

Three different analyses of the natural homogenisation process in the buffer were performed by Åkesson et al. (2010a): i) with an analytical analysis; ii) by studying the process in more detail with the FE code Code_Bright; and iii) by using the code Abaqus for simulating an entire deposition hole.

The *analytical analysis* was performed with an expression describing the swelling pressure (and suction at free swelling) as a function of the void ratio and a reference (i.e. initial) water content, $p(e,w_{ref})$. Two material components (blocks and pellets) were treated as isotropic singular elements, and each described by a void ratio and a reference water content, thereby yielding a swelling pressure (p^b and p^p) for blocks and pellets, respectively. The ratio between the pressures of the pellets and the blocks was defined as a parameter: $\alpha = p^p/p^b$, and from empirical data from triaxial compression test a value of 0.65 could be motivated for a pressure of 7 MPa. Corresponding values of 0.8–0.9 were evaluated from a Code_Bright model of CRT (see below). Two wetting schemes were analysed: serial wetting (w_{ref} for blocks 17 %; w_{ref} for pellets 64 %) and parallel wetting (w_{ref} for blocks 17 %; w_{ref} for pellets 17 %), and relations between the void ratio for blocks and pellets were generated for α-values ranging from 0.7 to 1. An additional relation between the void ratios was based on the volumes of blocks and pellets at installation and with the assumption of constant total volume. The model showed that the wetting scheme had a significant impact on the level of remaining heterogeneity of the buffer system. Also, the difference in total pressure in the block and pellet slot (indicated by the α-value) was found to have a significant effect on the homogenization process.

The *numerical analysis using Code_Bright* was focused on the homogenization process for a buffer ring at canister mid-height using a 1D axisymmetric THM model. The mechanical material model used for this was the thermo-elastoplastic constitutive law which is based on the Barcelona Basic Model (BBM). The geometry of the models included the initial open slot between the canister and the buffer blocks, the buffer blocks themselves and the pellet filled outer slot. The key phenomena investigated with the Code_Bright, was the influence of the slot width on the homogenization and swelling pressure and also the wetting sequence. In the study, the slot width was varied from 3 to 9 cm with the other parameters kept constant. The effect of the wetting sequence was tested by the assumption of either entirely serial or parallel wetting. In the case of serial wetting water uptake comes from the pellet slot, while parallel wetting assumes that both components are swelling simultaneously. The results from the two models have been compared with the results obtained from the Canister Retrieval Test (CRT). Compared with CRT results, pure serial wetting produces more heterogeneity in the void ratio field. The parallel wetting process produces less heterogeneity than the CRT measurements.

The *numerical analysis using Abaqus* was focused on simulating the homogenization processes in CRT by using a full-size 2D axisymmetric model. The mechanical material model used for this consisted of the porous elastic model, the Drucker-Prager plasticity model, and the so-called “moisture swelling” procedure. A comparison of experimental data with model results for a 1D axisymmetric geometry confirmed that the material model of unsaturated bentonite blocks, and the calculation technique used, were relevant for modelling of the homogenisation process, since the agreement between modelled and measured density distribution in the buffer between the canister and the rock after full saturation was very good. The material model and calculation technique were then used to model the homogenisation process in an entire deposition hole with identical initial conditions and boundary conditions to those in CRT. The results gave an expected final density and stress distribution in a deposition hole covered with a backfill which was is compressed about 3 cm. However, there

was no obvious density gradient in the upper part of the buffer, in spite of the upward swelling of 3 cm. This result thus deviated from the results from buffer upwards swelling calculations (see Task 8 below) in which initially completely water-saturated and homogenized conditions was used. This indicated that influence of the wetting history was probably not negligible.

Task 6. Homogenisation after loss of bentonite mass

Buffer homogenisation (i.e. the limitation of the heterogeneities) is crucial for fulfilling the safety functions related to buffer density. The swelling properties are important not only for homogenising the buffer after installation of the bentonite blocks, but also after long time if openings in the buffer would appear. Such spaces may appear due to several processes: i) the unexpected event of missing bentonite rings; ii) erosion before closure of the repository caused by water inflow into deposition holes; iii) long term erosion of bentonite in fractures intersecting the deposition hole; iv) small channels caused by piping and rather limited short-term erosion. The swelling and sealing of bentonite cannot take place unhindered since there is a resistance to swelling caused by friction both internally in the bentonite and between the bentonite and the surrounding fixed walls represented by the rock surface and in some cases the canister. In order to investigate how well the buffer material seals the openings resulting from the mentioned processes a number of finite element calculations were performed by Åkesson et al. (2010a) using the code Abaqus and a mechanical material model consisting of a porous elastic and a Drucker-Prager plasticity model.

Cases in which a *large part of the bentonite buffer is missing,* corresponding to one, two or three missing bentonite blocks (0.5 m thick) were analysed with 2D axisymmetric HM models. These cases could also represent an extreme loss of bentonite by colloid erosion. In summary, the analyses showed that in the case where large amounts of bentonite is lost from a deposition hole, or missing from the start, the remaining bentonite will swell and fill the empty space, but the density and resulting swelling pressure will be rather low due to the friction in the buffer and the friction against the rock surface. For a 50 cm vertical opening in a deposition hole, the resulting swelling pressure will be in average 0.5–1 MPa in almost the entire former hole. This means that the system has reached equilibrium (with zero suction gradients) and that the dry density in the former hole has increased to a level which corresponds to this pressure level. However, if the rock surface is smooth and the resulting friction against the rock is halved, then the swelling pressure will be above 1 MPa in a most of the former space. For a 100 cm opening the swelling pressure will be rather low close to the canister with the pressure below 100 kPa and there may even be an unfilled part left, while a case with halved friction will yield a minimum swelling pressure of more than 300 kPa. If the opening is 150 cm, a large volume will have a swelling pressure below 100 kPa and may even be unfilled. However, the influence of the friction between the bentonite and the rock and canister is large and with halved friction almost the entire opening will be filled.

Cases with *loss of bentonite from erosion* were analysed with 2D axisymmetric HM models, with cavities with the shape of either a “half donut” or a “half sphere”. The calculations of the swelling and homogenisation of a half donut resulting from erosion showed that the swelling yields a strong decrease in density and swelling pressure due to the friction in the bentonite. However, the swelling pressure after completed homogenisation was not below 1 MPa for any of the cases with donut radius varying from 3.4 cm to 13.4 cm. The influence of the radius seemed to be insignificant due to the long distance to the bentonite boundaries. If half a sphere was created instead of a donut then the consequences would be more severe, since the radius of the sphere is larger for the same amount of bentonite, and thus the mass of bentonite left between the sphere and the canister is much less. However, in 2/3 of the distance between the buffer and the rock the buffer will have a swelling pressure higher than 1 MPa. The conclusion was thus that about 100 kg of dry bentonite may be lost from erosion without jeopardizing the function of the buffer. The effect of such a case with point erosion would be strong but rather unlikely.

Finally, cases with *self-sealing of long small channels* were analysed with 1D axisymmetric HM models. These showed that: i) a long open tube will *not* seal completely, but the density will decrease with decreasing radius, and the tube will remain just like for larger holes; ii) the final stage will be independent of the initial radius of the hole if the geometry is scaled to the radius; iii) all calculations yielded a remaining open pipe after completed homogenization; iv) there is a strong influence of element size on the remaining hole radius; and v) the remaining density gradient is caused by the shear resistance in the clay.

An investigation of the potential formation and growth of cavities in the buffer due to bentonite erosion has recently been presented by Börgesson et al. (2020b). The purpose of these calculations was to analyse how erosion affects the density distribution in a deposition hole as a function of time and erosion rate and to conclude how and when a cavity can be created during of the erosion process. Two erosion rates were considered: 10 g/year and 150 g/year (derived by Neretnieks et al. 2017). Two model approaches were presented: i) with Abaqus in which the bentonite was described with the Porous Elastic model and the Drucker-Prager Plasticity models as well as the Claytech Plastic Cap model; and ii) with hydro-mechanical numerical models, implemented in the MathCad software, in which the bentonite was described by the Hysteresis Based Material model (HBM). Both approached included a representation of mass loss at the boundary. The Abaqus model consisted of a 2D axis symmetric geometry in which the mass loss boundary was implemented as a horizonal plane at the canister mid-height stretching from the canister to the rock-wall. MathCad implemented models were developed for two different one-dimensional geometries, with either axial or radial swelling. With both approaches, cavity formation was observed once the void ratio had increased to a certain level, for the Abaqus models this resulted implicitly from the mechanical models and was found to be between 1.6 and 2.5, whereas in the MathCad models this was explicitly set to the value 3. The Abaqus calculations resulted in a total mass loss of between 5.1 and 7.6 tons dry bentonite before the contact between in the erosion front was lost depending on the material model and the erosion rate. The corresponding total mass loss required to reach cavity formation with the MathCad axial swelling model was approximately 5 tons, while the corresponding mass loss for the radial swelling model was 1.2 tons. Of special interest was the question whether a hypothetical cavity which exhibits a semi-circular shape and which precisely exposes the canister surface is realistic or not, but this could not be simulated with the presented models. However, based on the available results, it could be argued that the formation of such a cavity was not realistic.

Task 8. Buffer upward swelling

The mechanical interaction between the buffer material in the deposition hole and the backfill material in the deposition tunnel is an important process in the safety assessment since the primary function of the backfill is to keep the buffer in place and not allow it to expand too much and thereby loose too much of its density and barrier properties. The extent of the upward expansion is essentially a combined effect of the properties and dimensions of the deposition tunnel and the backfill on one hand, and the deposition hole and the bentonite buffer on the other. The influence of individual factors and their contribution to the upward swelling are described and assessed separately below.

Several hydro-mechanical finite element calculations of the buffer upward expansion have been presented by Börgesson and Hernelind (2009, 2017) and Åkesson et al. (2010a) using the code Abaqus; and by Sandén et al. (2020) using Code_Bright. All Abaqus buffer models have used a material model consisting of a porous elastic model and a Drucker-Prager, or a Claytech plastic cap plasticity model, and were described as water saturated from the start of the simulation. In contrast, all Code_Bright simulations of the buffer have used a material model based on the Barcelona Basic Model, and were described as unsaturated from start. All parameter values for the buffer material were adopted for MX-80 bentonite. It should be noted that all calculated buffer upward displacement values mentioned below were evaluated for a position 1.5 m above the canister.

The influence of the *water content of the backfill* has been investigated through modelling and experimental work. Börgesson and Hernelind (2009) presented several models with a saturated backfill and one model with a dry backfill; all cases assumed a saturated buffer density of 2 000 kg/m^3. The displacement for the dry case was counterintuitively found to be lower (90 mm) than for the saturated reference case (100 mm), but this was caused by similar stiffness values used for the backfill in those two cases, and also that no swelling pressure was assumed for the backfill in the saturated reference case. Åkesson et al. (2010a) presented three models with a dry backfill, two of which had a saturated buffer density of 2 000 kg/m^3, and the displacement in these models were also approximately 100 mm. Börgesson and Hernelind (2017) presented five 2D-models with a saturated buffer density of approximately 2 000 kg/m^3 and for dry a backfill which was represented with different stress-displacement relations (described below) and with different representations of the bevel (also described below). The displacement in these models was found to be between 120 and 240 mm, which is clearly higher than for the saturated reference case mentioned above. In addition to these model results, Sandén et al. (2020) presented tunnel scale tests (1:20) in which the compressibility of the backfill was investigated for different test conditions. The tests were performed by supplying water to the backfill

during a specific time period: from 0 (dry case) to 52 days, after which a deposition hole was simulated by pushing a piston upwards into the backfill at a constant rate, and by measuring the force and the displacement continuously. These tests clearly showed that the compressibility of the backfill decreased with an increasing water content (Figur 3-18). These observations therefore demonstrate that *a dry backfill is the most conservative case concerning the buffer upward swelling.*

The influence of the *thickness of the pellets bed on the tunnel floor* has also been investigated through modelling and experimental work. The models presented by Börgesson and Hernelind (2009) did not include any pellets on the tunnel floor, whereas those presented by Åkesson et al. (2010a) included a fairly thin pellets layer of 80 mm between the uppermost buffer block and the backfill blocks. In contrast, Börgesson and Hernelind (2017) analysed the influence of three different pellets bed thicknesses: 100, 250 and 500 mm. Together with a saturated buffer density of approximately 2 000 kg/m^3, these values resulted in a displacement of 150, 190 and 240 mm, respectively. These results were obtained by representing the entire backfill with a stress-displacement relation (Figur 3-19), which in turn was based on: i) a stress displacement relation evaluated from the full-scale Buffer Swelling Test which had a pellet bed thickness of 70–90 mm (Sandén et al. 2017), and ii) a stress-strain relation of a specific extruded pellets material which was scaled (depending on the thickness in question) and added to first relation. The Buffer Swelling Test was performed at Äspö HRL and involved a "simulated deposition hole" with a depth of about 1.5 meter which was excavated in the tunnel floor and equipped with four hydraulic jacks on the bottom of the hole, a steel plate resting on the jacks and a bentonite buffer block placed on the steel plate. The tunnel above the simulated deposition hole was filled with backfill blocks and pellets. The buffer block was then pushed upwards, while simultaneously measuring the vertical force, the displacement of the steel plate and the pressure against the rock surface. The calculated stress-displacement relations used in the models is to some extend independently supported by the stress-displacement relations obtained for a dry backfill material in the tunnel scale tests mentioned above. The pellets layer in the floor in those tests corresponded to a thickness of approximately 175 mm. An up-scaled displacement of for instance 200 mm yielded a stress level of 3 MPa, i.e. 7.2 MN for a deposition hole area, and this point is fairly consistent with the calculated stress-displacement relations for 100 and 250 mm. These results clearly show that the *thickness of the pellets bed on the tunnel floor has a major influence of the upward swelling of the buffer. Still, the current nominal thickness in the reference design (i.e. 100 mm) should result in a fairly limited displacement.*

The influence of the *thickness of the pellets layer in the tunnel ceiling* has been investigated through modelling work. Åkesson et al. (2010a) presented two 3D-models with different thickness in the ceiling (30 and 55 cm). Similarly, Börgesson and Hernelind (2017) also presented two 3D-models with different thickness (450 and 600 mm). These models resulted in quite similar displacements: 96 and 102 mm in the former case, and 195 and 204 mm in the latter case. *These models thereby show that the influence of the thickness of pellets in the ceiling is rather small.*

The stacking of the backfill blocks has been addressed in all 3D-models with a tunnel section and a dry backfill. The models presented by Börgesson and Hernelind (2009) and Åkesson et al. (2010a) did not assume any overlapping blocks, whereas the tunnel models presented by Börgesson and Hernelind (2017) did assume overlapping blocks. Moreover, both the Buffer Swelling Test (Sandén et al. 2017) and the tunnel scale tests (Sandén et al. 2017) were performed with overlapping backfill blocks. *These tests have demonstrated that use of overlapping blocks will lead to a lateral spreading of the pressure from the buffer and will therefore also limit the upward swelling.* The current reference design is based on a system with overlapping block.

The importance of the *compressive strength of backfill blocks* was observed in the Buffer Swelling Test (Sandén et al. 2017). This test displayed a fairly linear stress-displacement relation up to a maximum pressure level of 1 800 kPa which at a displacement of 75–80 mm, after which a residual stress of 1 200–1 400 kPa was measured up to a displacement of 150 mm (Figur 3-20). This relatively low compressive strength was subsequently found to be mainly caused by the low density and relatively low water content in the used backfill blocks. This data was subsequently used to adopt a stress-displacement relation which was used to represent a backfill in one of the 2D-models of a swelling buffer with an initial saturated density of approximately 2 000 kg/m^3 presented by Börgesson and Hernelind (2017). This relation resulted in a major increase of the displacement (300 mm). *These results therefore illustrate the importance of installing backfill blocks with a sufficiently high compressive strength.*

The *friction angle between the buffer and the rock wall* in the deposition hole will influence the density gradient that can be maintained, and therefore also whether a specific displacement at the buffer/backfill interface will affect the density in the vicinity of the canister. The models presented by Börgesson and Hernelind (2009) adopted a base case value of 8.7°, and did also investigate the influence of changing this value to 0°, 4.4° and 17.0°. The models presented by Åkesson et al. (2010a) and Börgesson and Hernelind (2017) were all based on the value of 8.7°. Subsequent 2D buffer swelling models presented by Sandén et al. (2020) adopted the slightly lower value of 7.5°. The value of 7.2° was evaluated from experimental results from the long tube tests presented by Dueck et al. (2019). *The representation of wall friction has in all models therefore been quite consistent with experimental data.*

The installed dry density of the buffer will influence the potential for upward swelling. All models presented by Börgesson and Hernelind (2009) were based of a saturated density (ρ_m) of 2 000 kg/m^3. Åkesson et al. (2010a) investigated the effect of reducing ρ_m from 2 000 to 1 950 kg/m^3, and found that the upward displacement decreased from 102 to 68 mm. By the same token, Börgesson and Hernelind (2017) presented several 2D models with different ρ_m values 1 965, 2 011, 2 041 kg/m^3. These models illustrate that a higher density generally results in a larger displacement. However, *this does not mean that the final density in the vicinity of the canister is lower. The installed density is therefore not a relevant factor for reducing the upward swelling.*

The influence of buffer homogenisation on the upward swelling was investigated by Börgesson and Hernelind (2017) by comparing a model in which the buffer was completely homogenized from start, with a model in which the initial density distribution was consistent with the reference design. The inhomogeneous model resulted in a significantly higher displacement, 180 mm, as compared to 130 mm for the homogeneous model. *This finding therefore demonstrates the importance of taking the initial heterogeneities into account in models, but does not have any real implications for the design.*

The influence of a localized water uptake in the buffer has been investigated through modelling and experimental work. Sandén et al. (2020) performed both scale-tests (1:10) and 2D HM modelling in which a case with localized water-uptake from a filter surrounding the lower buffer block was compared with a reference cases in which the entire lateral surface of the buffer could take up water. The compressibility of the backfill were in the scale tests represented with springs which were adopted from the stiffness observed in the Buffer Swelling test (Sandén et al. 2017). An equivalent stiffness in the HM models was implemented by adopting a special retaining system material. Both experiment and model with localized water uptake resulted in a significant localized swelling and reduction of dry density in the bentonite block below the canister; in the scale tests as low as 1 400–1 450 kg/m^3 (Figur 3-21). This density corresponded to a mean swelling pressure of 2.2 to 2.6 MPa. *The average dry density of the buffer volume was, however, high enough to fulfil the swelling pressure requirement (mean swelling pressure 3.8 MPa)*.

The *influence of the bevel* in the deposition hole has been investigated through different modelling work. Börgesson and Hernelind (2017) presented six 2D models of the buffer in which the backfill was represented with different stress-displacement relations, and in which the influence of the bevel was addressed by adding a 1.25 m high continuation of the buffer. This section thereby created an extra compressibility which was added to the original backfill stress-displacement relation, which corresponded to a 100 mm thick pellets bed. The dry density of this section was adopted by assuming complete homogenisation of the backfill blocks in the upper part of the deposition hole, and the bentonite material in the bevel. Two values were adopted by using different approaches: i) that the bevel was filled with pellets only, which yielded a total dry density of 1 364 kg/m^3; or ii) that the bevel was filled with both blocks and pellets, which yielded the value 1 488 kg/m^3. The approach with pellets only resulted in buffer displacements values 30–40 mm higher than for the second approach with higher density. The relevance of these assumptions was also investigated by analysing different 3D models which included backfill, buffer and a pellets-filled bevel. These models resulted in large horizontal swelling into the bevel. However, the density distribution after equilibrium was still very inhomogeneous in the upper part of the deposition hole and the bevel, and the assumption of complete homogenization used in the 2D models was thus very pessimistic. *Based on these results it was concluded that a design with a pellets bed with a thickness of 100 mm would be acceptable in combination with a pellets-filled bevel.*

Finally, the buffer upward swelling has implications for the dimensioning of both the buffer and the backfill. For the buffer an overall buffer/backfill displacement of 175 mm was adopted and used as input (Luterkort et al. 2017). This value was based on the initial heaving in the BÅT-experiment (Luterkort et al. 2017) and from results presented by Börgesson and Hernelind (2017). For the dimensioning of the backfill blocks a general displacement value of 150 mm was adopted from the results presented by Börgesson and Hernelind (2017). This value was in turn used to derive a swelling pressure of 3.8 MPa for the buffer under the condition that there is no friction along the rock wall. This pressure has thus been adopted as a requirement regarding the compressive strength of the backfill blocks (Eriksson 2020). A requirement for the allowed deformation of the entire tunnel backfill is being developed.

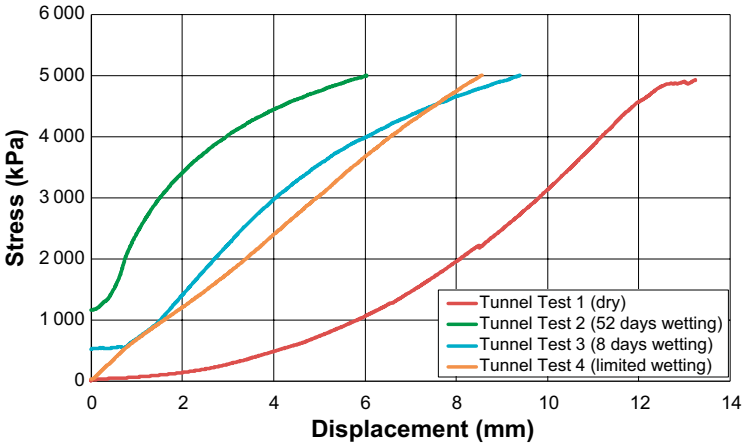

Figur 3-18. *The registered stress plotted versus displacement for all four tests (Sandén et al. 2020).*

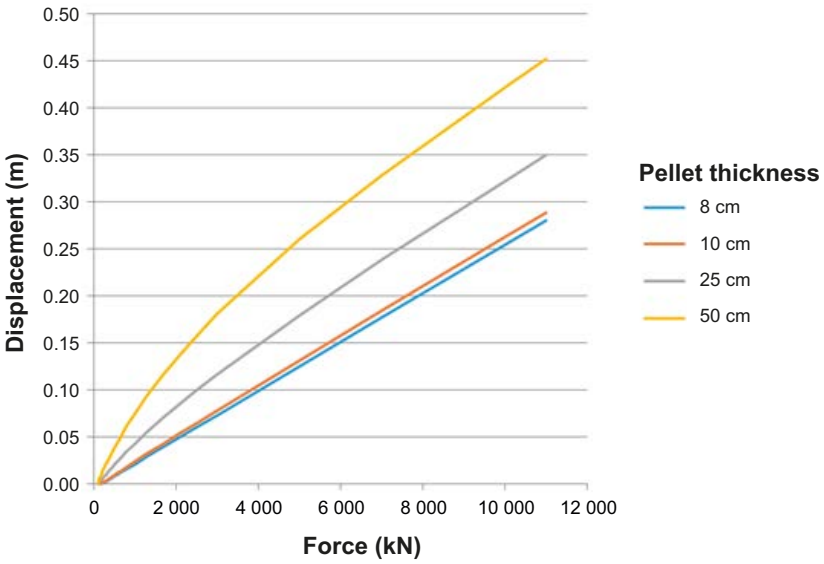

Figur 3-19. *Force-displacement relation used for modelling of the response of the dry backfill (Börgesson and Hernelind 2017).*

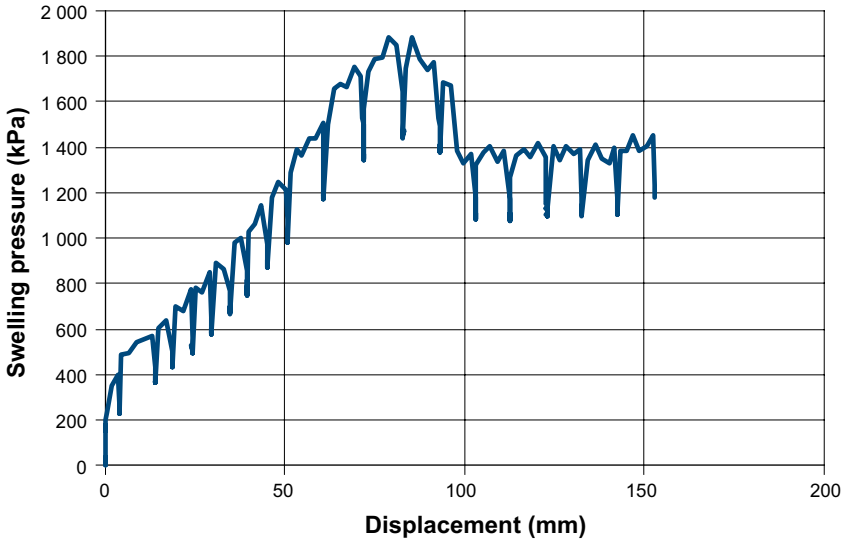

Figur 3-20. *Total average vertical stress from the buffer block plotted as function of the displacement (Sandén et al. 2017).*

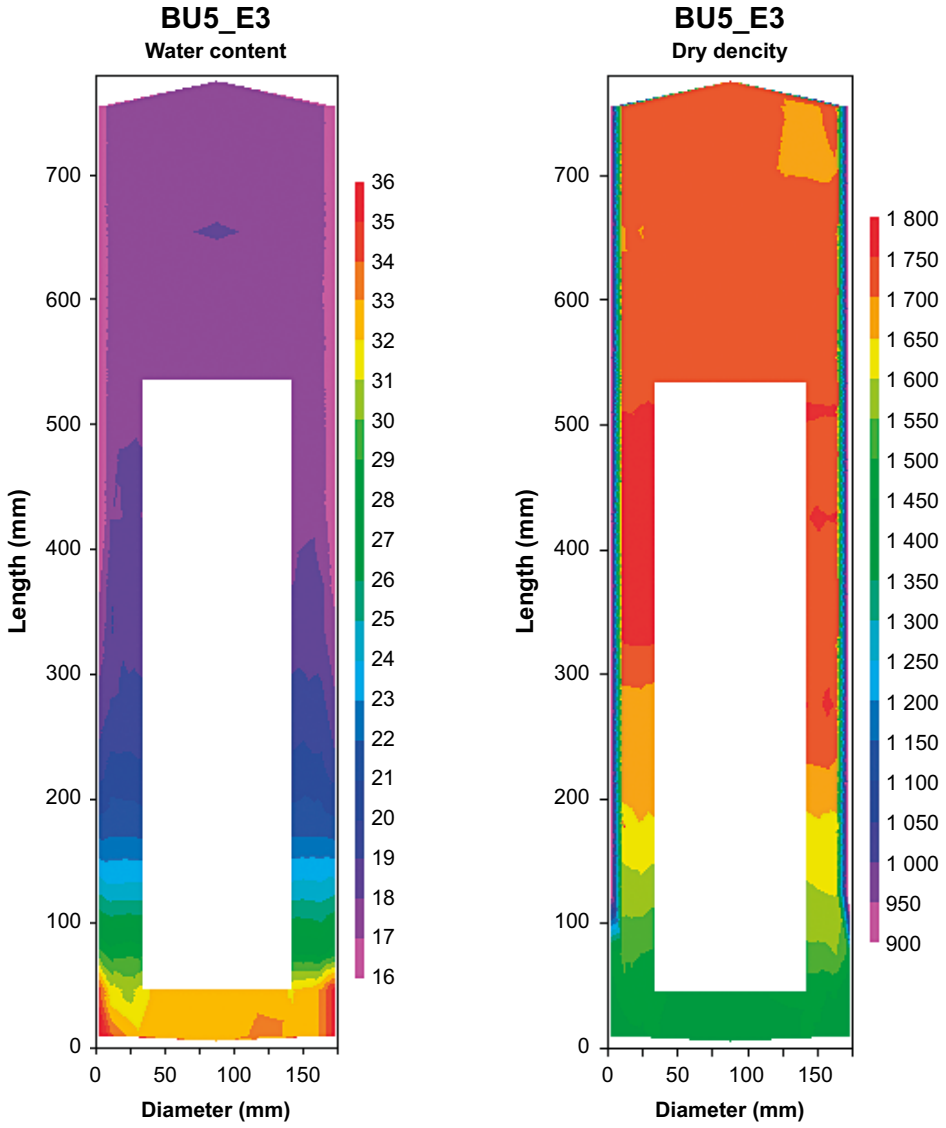

Figur 3-21. *Results from sampling of Test BU5_E3. Left: Water content distribution in a cross-section of the deposition hole. Right: Dry density distribution in a cross-section of the deposition hole (Sandén et al. 2020).*

Task 9. Canister sinking

One of the safety functions for the buffer is that it should prevent the canister from sinking in the deposition hole since this would render the canister in direct contact with the rock thus short-circuiting the buffer. The vertical displacement of the canister in the KBS-3V concept has been studied by Åkesson et al. (2010a) in a number of consolidation and creep calculations using the FE-program ABAQUS. The creep model used for the calculations was based on Singh-Mitchell's creep theory, which had been adapted to and verified for the buffer material MX-80 in earlier tests. A porous elastic model with Drucker-Prager plasticity was used for the consolidation calculations. For simplicity the buffer was assumed to be water saturated from start.

In one set of calculations, only the consolidation and the creep in the buffer were studied. In the other set of calculations, the interaction with a 30/70 backfill was also included. The two cases represented two extreme cases, one with a backfill that had a low stiffness and the lowest allowable swelling pressure, and one that had the highest possible swelling pressure and stiffness.

The base cases in the calculations corresponded to the final average density at saturation of 2 000 kg/m^3 with the expected swelling pressure of 7 MPa in a buffer. In order to study the sensitivity of the system to loss in bentonite mass and swelling pressure, seven additional calculations were performed with reduced swelling pressure down to 80 kPa corresponding to a saturated density of about 1 500 kg/m^3. The calculations were performed in two stages: i) the swelling and consolidation of the buffer so that force equilibrium was reached; and ii) the deviatoric creep in the buffer during 100 000 years.

The calculations showed that the canister settlement was very small even at low swelling pressure and density. The base case corresponding to the expected final swelling pressure of the buffer 7 000 kPa yielded a total settlement of the canister of only 0.35 mm for the fixed boundary case, while there was a heave of the canister of about 4.5 mm at the other case with 30/70 backfill due to the upwards swelling of the buffer. At reduced swelling pressure the settlement increased but was not more than about 23 mm at the very low swelling pressure 80 kPa for both cases.

The conclusion was thus that the expected displacement of the canister from consolidation and creep during 100 000 years is very small and for the case of 30/70 backfill actually will result in a heave of the canister. The sensitivity analyses with reduced swelling pressure corresponding to reduced density or reduced friction angle also showed that the canister displacement was very insensitive to such phenomena since the total settlement will be less than a few cm even at a saturated density of 1 500 kg/m^3 or at a friction angle of 0.3°.

Task 10. Rock shear through a deposition hole

Existing fractures crossing a deposition hole may be activated and sheared by an earthquake. The buffer material in a deposition hole will act as a cushion between the canister and the rock, which reduces the effect of a rock shear substantially. Lower density of the buffer yields softer material and reduced effect on the canister. However, at the high density that is suggested for a repository the stiffness of the buffer is rather high. The stiffness is also a function of the rate of shear, which means that there may be a substantial damage on the canister at very high shear rates. However, the earthquake induced rock shear velocity is lower than 1 m/s which is not considered to be very high.

The rock shear has been modelled with finite element calculations with the code Abaqus (Hernelind 2010). A three-dimensional finite element mesh of the buffer and the canister has been created and different cases of rock shear have been simulated. The bentonite buffer was modelled using only total stresses that do not include the pore water pressure due to the very fast mechanical processes. The bentonite was modelled as a linear elastic material combined with the von Mises plastic hardening, for which the hardening curve was defined as a function of the strain rate. The models also included detailed representations of the canister iron insert, the steel channels and the copper shell. The shear calculations were driven to a total shear of either 5 or 10 cm and the shear velocity for the buffer-canister system was pessimistically set to 1 m/s which was higher than the highest velocities deduced from target fractures (0.3 m/s) in earthquake simulations. Six different planes of rock shear were investigated:

- Perpendicular to the canister at ¾ height or ½ height from the bottom; or
- With tension of the canister and a shear plane at an angle of 22.5° to the canister axis, at ¼ height or at ½ height from the bottom, or
- With a horizontal movement of a vertical plane, at a ¼ of the diameter and through the centre of the canister

Important parameters among the results from the insert were the peak values for the equivalent plastic strain (PEEQ), the effective stress (von Mises) and the maximum axial tension stress (S33).

The largest effects on the insert (highest strains and stresses) were obtained with shearing perpendicular to the canister axis and with an intersection point ¾ of the height from the bottom. Lowering the density from 2 050 to 2 000 or 1 950 kg/m^3 lessened both the strains and stresses. All results were below the measured values of elongation and ultimate tensile strength suggesting that the integrity of the canister would not be jeopardized by such shear loads.

The canister also has to be designed to withstand the loads caused by a thick ice sheet. Besides rock shear the model has been used to analyse the effect of such glacial load (either combined with rock shear or without rock shear). In addition, the effect of creep in the copper shell was also investigated.

Bentonite exposed to high temperatures has shown tendencies of brittle failure. The influence of such behaviour on the shearing of the buffer and the stresses in the canister was therefore analysed with the same type of Abaqus models as described above (Sellin et al. 2017). The overall conclusion from this study was that brittle failure behaviour of the buffer will not have a strong effect on the consequences of a rock shear.

Task 18. Bottom plate 1 – Lifting of package

In order to achieve a sufficiently flat bottom of the deposition hole, a bottom plate is planned to be installed in each deposition hole. In the case where water can enter the deposition hole under the bottom plate, there might be a risk that the water pressure generated may be sufficient to lift the entire buffer-canister package.

Åkesson et al. (2010a) have studied the potential lifting of the buffer/canister package during the period from the termination of the drainage to the installation of the backfill, and a tailored analytical solution were developed based on the following assumptions:

1. The hydration of the buffer varies with time and distance from the bottom plate. The hydration of blocks at a certain height begins when the hydration of the outer slot has reached this height. The rate of hydration was assumed to be proportional to the remaining pore space.
2. The build-up of swelling pressure at a certain height starts at the same time of the hydration, and a cumulative lognormal distribution function was adopted for describing this evolution.
3. The water pressure beneath the package is equal to the swelling pressure at the bottom.
4. The build-up of the frictional forces along the rock wall is concurrent with the build-up of the lifting forces. The package will be lifted if the lifting forces exceed the sum of the frictional forces and the weight of the package.

These calculations indicated that the time to reach lifting conditions will be approximately one week. And the model also suggested that an inflow higher than approximately 100 litres per day will avoid lifting conditions, due to the rapid build-up of the frictional force along the rock wall. The time-scale to reach lifting conditions at low inflows was given directly by an adopted swelling pressure evolution, and the weight of the package (corresponding to 0.2 MPa). The swelling pressure should therefore not be allowed to reach this level as long as the backfill has not been installed.

Homogenization

The objective of the *homogenization project* has been to further improve the knowledge of the process of swelling and buffer homogenization. The project consisted of four parts; theoretical studies, fundamental laboratory tests, laboratory study of the influence of friction and medium scale tests of the scenario involving loss of bentonite (Dueck et al. 2011b, 2014, 2016, 2018). The laboratory tests have provided results that can be used for modelling some well-defined benchmark tests in order to improve the models or determine mechanical parameters for HM modelling of the behaviour of the buffer. The *fundamental swelling tests* were performed with water saturated bentonite specimens installed in test arrangements and confined except for one direction with a slot/cavity and with free access of water which enabled the specimen to swell into the slot. The following test geometries were studied: i) axial swelling in a device with constant radius and limited height; ii) radial swelling

of the outer surface in a device with constant height and limited radius; iii) radial swelling into a cylindrical cavity in a device with constant height and radius. The tests were mainly done with free swelling surfaces, i.e. no counteracting force until the swelling bentonite gel had reached the outer limited surface. Two test series with different dimension of the equipment were performed: i) basic series; and ii) high resolution series. For the latter series, a fourth test geometry was studied in which a cylindrical specimen was allowed to swell and homogenize in all directions. In all tests the friction was minimized by use of a mineral-oil based lubricant on relevant surfaces. The process was monitored by measuring stresses in different directions. After equilibrium was reached, the specimen was dismantled, and the density distribution was quantified. These tests generally exhibited clear remaining heterogeneities. The *friction tests* were carried out with a swelling pressure device consisting of a steel ring surrounding the specimen having filters on both sides. During the shearing phase the swelling pressure device was placed in a load frame where the ring was fixed while the specimen was moved upwards with a constant rate, i.e. the specimen was pushed upwards through the ring. During the shearing phase the required force to keep the ring in place as well as the deformation and swelling pressure were measured. The specimen had free access to water during both the saturation and the subsequent friction phase. After moving the specimen a distance similar to the height of the specimen, the test was finished and the bentonite specimen was dismantled. The distributions of water content and density over the specimen height were finally determined. The measured forces were ultimately evaluated as friction angles versus swelling pressure. The *self-sealing ability* of large and irregular cavities was studied in two tests of the last part of the project. These tests were performed on medium scale bentonite blocks (0.3 m diameter; 0.1 m height) installed in steel rings. A stiff filter was mounted to the inside of the ring with the purpose to provide water to the bentonite from the radial surface. Two cavities (approximately $70 \times 50 \times 40$ mm) were cut out from each block in two diametrical positions, to simulate loss of material. The blocks were instrumented for measuring the evolution of stresses and suction. The blocks were allowed to swell and homogenize during approximately 500 and 1 000 days, respectively. After equilibrium was reached, the tests were dismantled, and the density distribution was quantified. These tests also generally exhibited clear remaining heterogeneities.

These tests were used as a *modelling task for the SKB Task forces* on Engineered Barrier Systems (EBS). The aim of this task was to increase the knowledge of the homogenization processes and involved two subtasks: i) to model several small laboratory scale swelling tests (with axial, radial or spherical swelling), and ii) to model a large laboratory scale test that simulates bentonite lost in a deposition hole. Börgesson et al. (2020a) presented results from analyses from several approaches and with established material models. The most extensive contribution was performed with Abaqus (porous elastic + Plastic Cap material model) with which modelling results for all test types were presented. The overall conclusion of the calibration and evaluation models of the fundamental swelling tests (subtask 1) was that the model simulates bentonite swelling well within a limited density interval but also that the model does not work well for the unlikely case of completely isotropic swelling. Comparing with data from these tests, the Plastic Cap was found to give better agreement than the Drucker-Prager plastic model. A general conclusion for subtask 2 was however that the Plastic Cap model underestimated the self-healing ability (or the homogenization) of the bentonite in the test by yielding too high void ratio and too low stresses in the former cavity. The Drucker-Prager plastic model captured the homogenization better, with a void ratio distribution that agreed rather well with the measurements, and smaller remaining gaps in the former cavity. However, also this model yielded the same too low stresses in the cavity.

In addition, attempts to use Code_Bright, together with the BBM or the Barcelona Expansive model (BExM) showed that these models exhibited several limitations: i) none of the models have any implemented void ratio dependences of the parameters; ii) none can represent suction (> 0) at saturated conditions; iii) only BExM uses ”effective stress” (for micro voids) which means that only the expansive model has a consistent representation of simple unloading or loading at constant water content; iv) only the BExM can include a contraction of the yield surface during isotropic swelling, although this has to be attributed to the macro void, even at saturated conditions. These limitations motivated the development of a new material model for saturated conditions which is based on a body of empirical data, as well as thermodynamic relation for the chemical potential of the clay water. This lead to a description that the clay potential (i.e. stress + suction, Equation 1-5) for a specific void ratio is found in an interval which is bounded by two lines, for swelling and consolidation respectively. The actual state between these lines is controlled by a path variable, which in turn is governed by

the strain history. This means that hysteresis is at the core of the material model. Numerical solutions for homogenization problems have so far been limited to simple 1D geometries developed in advanced spreadsheet software. These results show that the material model seems to be able to capture all the essential behaviour of the homogenisation tests.

An evaluation of the homogenisation project was presented by Dueck et al. (2019). This covered the main tests and models mentioned above. In addition, it presented an evaluation of tests with homogenisation in long tubes. Ten almost identical tests of the homogenisation of bentonite with large density difference placed in long tubes with raw grooved inner surfaces have been running for 4–5 years, with the purpose to study the long term homogenisation process. One of those has been terminated and sampled. The results showed that the homogenisation process can be well modelled with remaining unaffected initial densities at both ends of the tube, if the average residual friction angle evaluated from friction tests is used. An important conclusion from these tests and calculations is that it is the residual friction angle and not the peak value that is valid between a bentonite and a surface even when the surface is so raw that the slip takes place in the bentonite itself. Moreover, the new hydro-mechanical material model, first defined in Börgesson et al. (2020b) and denoted the Hysteresis Based Material (HBM) model, intended for bentonite-based components, was further developed and implemented into the COMSOL Multiphysics platform. In order to evaluate the model implementation (and the material model itself) two laboratory experiments were simulated: i) one oedometer tests; and ii) one of the axial homogenisation test above (HR-A1). Both experiments were modelled successfully, and the simulation results agreed well with laboratory data. Dueck and Börgesson (2021) have subsequently presented results from three analyses related to buffer homogenisation: i) comparison of homogenisation and sealing behaviour of calcium and sodium bentonite, ii) comparison of homogenisation and sealing behaviour of bentonite after rapid and slow water uptake, and iii) comparison of homogenisation of bentonite in long steel tubes after two, four and six years. Finally, Dueck et al. (2022a) have presented a 5th status report from the homogenisation project, with results from three different test types: small-scale fundamental swelling tests, medium scale self-healing tests, and homogenisation tests in long tubes.

Uneven swelling

A number of different load cases that may be harmful for the canister have been investigated. Such load cases were derived from uneven swelling pressure in the buffer material, both during the water saturation phase and after full water saturation. Two main types of stress combinations have been investigated: i) bending due to uneven horizontal swelling pressure, which is critical to the cast iron insert, and ii) shearing due to uneven vertical swelling pressure, which potentially can harm the copper shell. Bending can be caused by a curved shaped deposition hole or by rock fall out, while shearing may be caused upward swelling. Both stress combination may be further enhanced by differences in block density and deposition hole geometry. Analytical analyses of such load cases have been presented by Börgesson et al. (2009) and Börgesson (2019).

The bending load cases were defined for situations in which the length of the canister was divided in three sections (two end sections with equal length and one central section, twice as long as each end section) with a net swelling pressure acting in the same direction on the end sections and in the opposite direction on the central section. The bending moment could thereby be calculated for the net swelling pressure and the dimensions (length and diameter) of the canister, while the bending stress could be calculated from the bending stress and sectional modulus. Analyses have been performed with rectangular or triangular stress distributions on the different section, representing water saturated and unsaturated conditions, respectively. The most severe load case presented by Börgesson (2019) was found to result in a moment of 15.4 MNm and a bending stress of 273 MPa. The latter load exceeded the yield stress of the iron insert of 270 MPa noted by Börgesson et al. (2009).

The shearing load cases were defined for situations in which the swelling pressure acting on the upper part of the canister was lower than on the lower part, and by counteracting the upward directed net force with shear stress along a section of the lateral surface. Moreover, the length of the lateral surface could be minimized by assuming a mobilized friction angle, which in turn maximized the shear stress. The most severe load case was found to result in a shear stress that varied from 1 920 to 1 270 kPa, which was significantly lower than the shear strength of the copper at 30–50 MPa.

Shear strength

Dueck et al. (2022b) presented a study on the compressive strength of bentonite, in which the influence of ion-exchange, different stress paths, drying and heating on the unconfined compressive strength was investigated for different bentonites. Eight different bentonites were used in the different test series: Asha505, Calcigel, Deponit CaN, FEBEX, GMZ, Ikosorb, Kunigel and MX-80. The main part of the specimens was saturated before testing but also a series with unsaturated specimens exposed to drying was included in the study. The shear strength has often been related to mean stress or swelling pressure for modelling purposes so the influence of swelling pressure on the strength was also studied.

Strength is to a large extent governed by the dry density and the type of bentonite. The results show that there are no indications that ion-equilibrium with an external salt solution ($CaCl_2$) will influence the strength and for the main part of the bentonites tested no large influence of an ion-exchange (to Ca-dominated bentonite) on strength was seen. In addition, there was no influence of stress path (swelling/consolidation) on the resulting strength when studied as function of final dry density.

When strength is plotted as a function of swelling pressure, the scatter between the results from different types of bentonites is lower than when plotted as a function of dry density. However, to have an unambiguous relationship between swelling pressure and strength for a bentonite, the swelling pressure should refer to a specific condition including e.g. saturation at constant volume condition and equilibrium with de-ionized water. At deviating conditions factors can be introduced into the relationship between average stress and strength although these do not influence the strength as a function of dry density.

Swelling into fractures

Börgesson et al. (2018) analysed the swelling of bentonite into a fracture that takes place when the chemistry of the groundwater is above the critical coagulation concentration (CCC). Under such conditions, a bentonite may swell until it becomes a non-swelling gel. Since the problem of colloid erosion is largest for homoionic Na-montmorillonite, limits have been determined for such types of systems. CCC for homoionic Na-montmorillonite (Wy-Na) extracted from MX-80 is circa 20 mM NaCl(aq), and at this concentration the swelling stops at a clay concentration of approximately 60 g/L. An expression of swelling pressure vs dry density was derived from DLVO theory and literature swelling pressure data, and for clay concentrations below 60 g/L the pressure was explicitly set to 0.

A theory was developed for the bentonite penetration into a horizontal fracture. The penetration depth was analysed in terms of the equilibrium situation where the swelling is completed, and the swelling pressure is balanced by the friction against the fracture walls. By using evaluated friction angles in the range 0.5 to 30° it was shown that the penetration into a 100 µm wide fracture is anyway limited to < 80 mm at the lowest friction angle. A comparison between theory and experimental swelling of Wy-Na into a 120 µm fracture gave the best agreement for the highest friction angle, 30° which gave a penetration depth in the vicinity of 1 mm. It was thus concluded that the shear resistance or a friction in bentonite and between bentonite and confining surfaces hinders the bentonite to swell deeply into any fracture in a groundwater with salinity above the CCC.

Moreover, through rotating-vane rheometry, the shear strength for a gel of 60 g/L was determined to be 40 Pa at CCC. It was thereby shown that the strength of the non-swelling bentonite gel that is formed at the swelling front is with large margin high enough to withstand both the gravitational forces and the erosional forces caused by ground water flow past the swelling front. The release of montmorillonite colloids may occur under conditions below CCC (see 3.5.11.).

Natural analogs/observations in nature

Mechanical processes in bentonite in nature have not been studied and would probably not contribute to the knowledge necessary for the assessment of these processes in a repository.

Time perspectives

The different mechanical processes are driven by different forces and mechanisms which imply that the time scales for the different processes also vary:

- Rock shear is the fastest process and is driven by displacements caused by an earth quake. The time scale is largely governed by the velocity of the rock shear (1 m/s) and the total shear displacement (e.g. 5 cm) which gives a time scale of 50 milli seconds.
- Homogenization of heterogeneities caused by differences in densities at installation is driven by the same suction gradients which drives the hydration of buffer. The time scale for this homogenization process is therefore the same as for buffer hydration, i.e. 10 years for wet conditions and orders of magnitude longer if there are few fractures and if the rock matrix has a low permeability. Once saturated conditions have been reached and the suction gradients are depleted, this means that there is no driving force for further homogenisation.
- The buffer upward swelling is caused by the density and suction differences in the buffer and the backfill, respectively. The time scale for upward swelling is therefore the same as for the hydration of the backfill, i.e. 80 years for wet conditions and orders of magnitude longer if there are few fractures and if the rock matrix has a low permeability.
- The time scale for homogenization of heterogeneities caused by loss of bentonite is governed by the loss rate and total mass loss. A loss rate of 0.1 kg/yr (Neretnieks et al. 2017) and a case with two missing bentonite rings á 1 200 kg (Åkesson et al. 2010a) gives a time frame of 24 kyrs. The very low suction levels observed in the cavity formation models presented by Börgesson et al. (2020b) imply that erosion and homogenisation occur virtually simultaneously.
- The time scale for homogenization of heterogeneities caused by disintegration of concrete in the bottom plate is governed by the chemical dissolution and the subsequent diffusion of dissolved species out of the concrete. The kinetics of these processes is however largely unknown and the time scale for this homogenization process is therefore also largely unknown.
- Finally, the canister sinking is probably the slowest process and is driven by gravity and governed by creep properties. Creep calculations presented by Åkesson et al. (2010a) simulated a tie period of 100 kyrs.

Handling in the PSAR

Homogenization: Heterogeneities in buffer density may arise in different ways, and in order to fulfil the requirement on density/swelling pressure it is important to assess the extent of homogenization (Åkesson et al. 2010a):

i. Heterogeneities will be caused by the installation due to the differences in density between blocks, pellets and open slots. THM models (analytical, Code_Bright and Abaqus) were therefore used to investigate the homogenization process and what remaining heterogeneities can be expected once full water saturation has been reached.

ii. Heterogeneities may be caused by the loss of bentonite, either due to missing bentonite blocks, or due to bentonite lost through erosion. HM models (Abaqus) was therefore used to investigate the homogenization process and what remaining heterogeneities/cavities can be expected once hydro-mechanical equilibrium has been reached.

iii. Heterogeneities may be caused by the disintegration of concrete in the bottom plate. HM models (Abaqus) was therefore used to investigate the homogenization process and to define a limit for allowable compression of the bottom plate in order to keep the buffer density within the tolerances.

Buffer upward swelling: The extent of the upward expansion is essentially a *combined effect* of the properties and dimensions of the deposition tunnel and the backfill on one hand, and the deposition hole and the bentonite buffer on the other. The process is analysed through hydro-mechanical modelling performed by Börgesson and Hernelind (2009, 2017) and Åkesson et al. (2010a) using the code Abaqus; and by Sandén et al. (2020) using Code_Bright. All Abaqus buffer models have used a material model consisting of a porous elastic model and a Drucker-Prager, or a Claytech plastic cap plasticity model, and were described as water saturated from the start of the simulation.

In contrast, all Code_Bright simulations of the buffer have used a material model based on the Barcelona Basic Model, and were described as unsaturated from start. All parameter values for the buffer material were selected as to describe MX-80 bentonite.

Creep/Canister settlement: The canister will potentially sink to the bottom of the deposition holes which will lead to the short-circuiting of the buffer. HM models (Abaqus) based on the Singh-Mitchell creep theory was therefore used to predict the settlement of the canister (Åkesson et al. 2010a).

Rock shear: The canister will potentially be damaged due to the shearing of the deposition hole during an earthquake. HM models (Abaqus) were therefore used to predict the mechanical impact on the canister. Different cases for different planes of rock shear, different total shears and different buffer densities have been analysed (Åkesson et al. 2010a). The influence of brittle bentonite behaviour on the shearing of the buffer and the stresses in the canister was subsequently analysed by Sellin et al. (2017).

Swelling into fractures: This process is handled in Section 3.5.11 Montmorillonite colloid release.

Handing of uncertainties in the PSAR

Mechanistic understanding

The processes of swelling/mass redistribution are generally well understood. However, the physical chemical basis for properties like swelling pressure, shear and tensile strength is still unclear. And regarding long term stability of creep, hysteresis and friction, there is still a significant lack of understanding.

Model simplifications

The BBM model exhibit several limitations: i) the parameters are not defined with any void ratio dependences of the parameters; ii) suction (> 0) cannot be represented at saturated conditions; iii) the use of net stresses (not effective stress) means that simple unloading or loading cannot be consistently representation; iv) no mechanism for contraction of the yield surface during isotropic swelling. Moreover, Code_Bright and BBM have no representation of chemical interaction. For ABAQUS, the shortcomings of the effective stress theory for unsaturated conditions can be compensated by the moisture swelling function. For saturated conditions, the model has some limitations to reproduce an accurate relation between the swelling pressure and the dry density, for instance due to the use of a constant kappa module value, and due to the inability to contract the extension of the yield surface during isotropic swelling.

Input data and data uncertainties

The empirical data on swelling pressure and retention properties display a hysteresis behaviour which has not been systematically investigated, especially at higher water contents (above 20 %). In addition, swelling pressure measurements generally display a scatter.

3.4.2 Liquefaction

Overview

This process was included in the Process report for SR-Can. However, it has been concluded that the phenomena cannot occur in a KBS-3 type buffer material. The reasoning justifying this conclusion was discussed in SKB 2010a (Section 3.4.1). Liquefaction is no longer regarded as a process in the buffer.

Handling in the PSAR

Since the process cannot occur, it will not be handled in the PSAR.

3.5 Chemical processes

3.5.1 Advective transport of species

Overview

In this context advection refers to the potential transport of any forms of additional substances, e.g. ions, molecules or colloids, with porewater flow. The transport direction is principally from volumes of high water pressure to volumes of lower pressure. The process leads to redistribution of solutes in the pore-water and thus affects the pore-water composition. There are several possible causes of pressure gradients in the buffer material, e.g. external water pressure, affinity for water in the bentonite and temperature induced volume change of the water. The advection is thereby closely related to water flow in the buffer, which is comprehensively described in Water transport under saturated condions (3.3.2). In quantitative terms, advective transport of ions and colloids may differ from the actual flow of water due to ion equilibrium effects the filtering in nano-sized pores, respectively.

Advection is of special importance in the buffer during the water saturation phase when a net inflow of water takes place in the buffer. The principal flow direction during this phase is towards the canister, provided that groundwater is supplied by the surrounding rock. After placement of a canister, a minor counter-flow may initially also take place in a direction away from the canister due to the temperature gradient.

Under saturated conditions, hydraulic gradients are significantly decreased and the transport of solutes in the porewater is expected to be dominated by diffusion, due to the low hydraulic conductivity of the buffer (see Section 3.5.2). Exceptions may be sudden events such as gas pulses or earthquakes, which can cause local pressure changes in the porewater. The improbable condition of a failure of a canister will lead to advective water flow into the canister due to the groundwater pressure. Corrosion of the steel insert will lead to hydrogen gas production, and the successively increasing gas pressure will reduce the inflow. Inflow will stop when the water level in the canister is below the canister damage region at the time when the gas pressure exceeds the groundwater pressure. Alternatively, the flow direction will be reversed towards the rock when the water level is located above the damage. Eventually the gas pressure may reach the sum of the swelling pressure and the groundwater pressure, which would lead to a significant water flow (See gas Section 3.3.3).

Dependencies between process and buffer variables

Table 3-9 summarises how the process influences and is influenced by all buffer variables and how these effects are treated in the PSAR.

Boundary conditions

The external boundary condition for this process is the hydraulic gradient across the buffer.

Model studies/experimental studies

Several studies by SKB and others have examined water flow in bentonite material, both during water uptake and after complete water saturation, and a wealth of quantitative data, which describe water transport under different physico-chemical conditions (e.g. density, salinity, temperature) and different sample preparation techniques, is available (Karnland et al. 2006, 2009, Cho et al. 1999) (see also Water transport under saturated conditions, Section 3.3.2).

The Long Term Tests of Buffer material (LOT) field test at Äspö HRL shows a total increase in ion concentration in the porewater compared to that originally present in the bentonite as a consequence of the salinity of the saturating groundwater (Karnland et al. 2000, 2009). Precipitation of calcite and gypsum close to the central heater indicate ion enrichment and cementation (Section 3.5.6).

Extensive data on primarily diffusive radionuclide transport with a notable advective component are available from percolation experiments with Boom Clay samples (see e.g. Maes et al. 2011 and references therein).

Table 3-9. Direct dependencies between the process "Advective transport of species" and the defined buffer variables and a short note on the handling in the PSAR.

Variable	Variable influence on process		Process influence on variable	
	Influence present? (Yes/No) Description	Handling of influence (How/Why not)	Influence present? (Yes/No) Description	Handling of influence (How/Why not)
Buffer geometry	Yes, major importance before full water saturation	Included in geochemical modelling. This variable may be considered constant after water saturation	No	
Pore geometry	Yes, interlayer distance and density is a decisive parameter	Included in geochemical modelling via the parameter hydraulic conductivity	No, but indirectly, through dissolution/precipitation	Included in geochemical modelling
Radiation intensity	No		No	
Temperature	Yes, through thermal expansion and viscosity	Viscosity effect is included in geochemical modelling	No	
Water content	Yes, major importance	Included in geochemical modelling	Yes, through dissolution/ precipitation	Included in geochemical modelling
Gas content	Yes, reduced flow in unsaturated clay	Neglected since the presence of gas generally will reduce advection	Yes, through transport/ precipitation of dissolved gas	Neglected, since it always reduce advection
Hydrovariables (pressure and flows)	Yes, by definition	Included in geochemical modelling	Yes, minor osmotic and viscosity effects possible	Neglected
Stress state	No, Indirectly through the coupling to pore geometry	Neglected	Yes, minor effect possible	Neglected
Bentonite composition	Yes, through montmorillonite content	Included in geochemical modelling	Yes, through dissolution/ precipitation	Neglected
Montmorillonite composition	Yes, minor at buffer density	Included in geochemical modelling	Yes, through ion exchange	Included in geochemical modelling
Porewater composition	Yes, by definition	Included in geochemical modelling	Yes, by definition	Included in geochemical modelling
Structural and stray materials	Potentially, as alternative transport paths	Neglected, since no stray materials are assumed to be present in the buffer	No	

Natural analogues/observations in nature

Sediments rich in smectite may maintain large chemical gradients over geological timescales (Neuzil 2000), indicating that advective transport of soluble constituents is (very) limited.

Time perspective

Advective transport in conjunction with water saturation takes place on a timescale of up to hundreds of years. Advective transport after water saturation is expected to be negligible in relation to diffusive transport.

Handling in the PSAR

Before saturation: No detailed modelling of advection is required. It should be noted that the composition of the bentonite porewater will be influenced by the composition of the intruding groundwater during saturation. The groundwater composition should be considered when defining initial conditions for modelling of the chemical evolution after saturation, see further Alteration of accessory minerals Section 3.5.6.

After saturation: Based on the scenario-specific evaluation of water transport under saturated conditions, (Section 3.3.2), advective transport can normally be neglected compared to diffusion. If the expected low hydraulic conductivity is for some reason not maintained, advective transport is included in the modelling of the canister corrosion and of radionuclide transport.

Handling of variables influencing this process: See Water transport under saturated conditions (3.3.2).

Failed canister: Advective flow away from the buffer due to hydrogen gas pressure is calculated as a special case in the radionuclide transport calculations.

Earthquakes: Neglected: pressure transients may arise, but will not prevail in the buffer over timescales that could lead to significant water flow.

Uncertainties

Uncertainties in mechanistic understanding

See Water transport under saturated conditions (Section 3.3.2) for uncertainties concerning water advective transport. The magnitude of geometrical and ion equilibrium effects are uncertain but both effects will only act to reduce the advective transport of species.

Model simplification uncertainties in the PSAR

Unsaturated conditions: see Section 3.3.1.

Saturated conditions: The process can be modelled with a standard mass-transfer approach. The main uncertainty lies in the coupling between the fractured rock and the porous buffer.

Input data and data uncertainties in the PSAR

Unsaturated conditions: see Section 3.3.1.

3.5.2 Diffusive transport of species

Overview

In clay barriers with very low hydraulic conductivity and in the absence of any relevant advective transport (see Section 3.5.1), solutes can be transported in the stagnant porewater by diffusion, following concentration gradients. Solutes move from areas of higher concentration to areas of lower concentration. The process leads to a redistribution of dissolved porewater constituents, including radionuclides, in the porewater. Therefore, diffusion is a critical process for radionuclide migration in the buffer, but also affects the actual porewater composition.

The diffusion process is strongly coupled to nearly all chemical processes in the buffer, since it accounts for the transport of reactants to and reaction products away from the canisters. Diffusion of Na^+ and Ca^{2+} ions is, for example, of crucial importance to ion exchange processes, diffusion of K^+ is an important limiting factor for illitisation etc. Diffusion is central to the entire chemical evolution in the buffer. Through the process osmosis (see Section 3.5.7), diffusion is also directly related to the development of swelling pressure in a KBS-3 buffer.

Diffusion in bentonite has been studied thoroughly in conjunction with radionuclide transport. Despite the substantial experimental and theoretical challenges arising from the inaccessibility of the pore space in compacted clay, to date there is a good phenomenological (macroscopic) understanding of the diffusion of trace constituents in compacted clays. Similarly, robust values for the diffusion rates of many radionuclides through clays under various conditions and the corresponding diffusion

coefficients are available (see below). On a macroscopic level, well-established equations are available for describing and quantifying the observable results of tracer diffusion and for linking diffusion with other macroscopic parameters, (K_d, density, porosity); these are described below.

On the other hand, the established macroscopic framework is not sufficient to explain the variations that can be observed for some diffusants (especially simple cations and anions) as a function of conditions, such as salinity. As a result, different microscopic or molecular-level models were developed to explain the observed phenomena. Controversies regarding diffusion models should rather be seen as controversies regarding the detailed environment in which diffusion takes place, rather than controversies regarding the nature of the actual diffusion process (see e.g. NEA 2012, Birgersson et al. 2017, Tinnacher et al. 2016). In terms of application to the performance of a bentonite barrier, different model concepts have been proven to be roughly equally well suited for describing the diffusion of trace constituents (Idiart and Pękala 2016, Idiart and Coene 2019).

Macroscopic-scale definitions: Fickian model

Diffusion equations for radionuclides (as well as some experimental measurement techniques relevant for determining the respective parameters) are described in detail in textbooks; a convenient summary can be found in Yu and Neretnieks (1997).

Diffusion in a porous medium takes place according to Fick's first law (Equation (3-18)):

$$J = -D_p \varepsilon \, dC_p/dx \qquad (3\text{-}18)$$

where: J is the diffusive flux, D_p the diffusion coefficient in the pore, ε is the (physical) porosity and C_p the concentration of the diffusing species in the pore.

The pore diffusion coefficient D_p in a solution-filled pore is lower than the diffusion coefficient in an unconfined volume of the same solution, D_w. This is mainly due to the tortuosity of the pores, which increases the length of the diffusion path. The relationship between D_p and D_w is:

$$D_p = D_w \, \delta/\tau^2 \qquad (3\text{-}19)$$

where: δ is the physical constrictivity and τ the tortuosity of the pores. The constrictivity takes into account any narrowing or widening of pores along the flow path. Since bentonite is viewed as a homogeneous porous medium on a macroscopic level, δ is usually set equal to unity.

Fick's second law, taking into account conservation of mass, describes changes in concentration of a diffusing species in time and space. For diffusion of a sorbing species in a porous material, it can be formulated as follows:

$$\varepsilon \, \partial C_p/\partial t + \rho \, \partial q/\partial t = \varepsilon \, D_p \, \partial^2 C_p/\partial x^2 \qquad (3\text{-}20)$$

where: ρ is the bulk density of the material and q is the tracer concentration in the solid phase. For conditions where sorption is linear (i.e., not dependent on the concentration of the diffusing tracer), can be written:

$$\partial C_p/\partial t = D_e/(\varepsilon + K_d \, \rho) \, \partial^2 C_p/\partial x^2 = D_a \, \partial^2 C_p/\partial x^2 \qquad (3\text{-}21)$$

where: K_d is the distribution coefficient (see Section 3.5.3), D_e is the effective and D_a the apparent diffusion constant, which are defined as follows:

$$D_e = \varepsilon D_p \qquad (3\text{-}22)$$

$$D_a = D_e/(\varepsilon + K_d \rho) \qquad (3\text{-}23)$$

The term ($\varepsilon + K_d r$) is also known as the capacity factor a of a porous medium. When sorbing solutes are present at trace levels, sorption is independent of their concentration (i.e. the concept of a linear sorption isotherm applies), and C_p can be replaced by the total concentration in the porous material, which gives:

$$\partial C/\partial t = D_a \, \partial^2 C/\partial x^2 \qquad (3\text{-}24)$$

where C is the total concentration of the diffusing ion.

Equation (3-23) is the relationship that is frequently used for describing the overall migration behaviour of radionuclides in bentonite. For diffusion of inert, non-interacting species (implying $K_d = 0$ in Equation (3-23), D_a is equal to D_e/ε.

Note that this relationship holds for most diffusing radionuclides and other species that are relevant in the present context but does not apply to inert anionic tracers, even though a formal $K_d = 0$ is typically assigned to these species. This is because the diffusion of anionic tracers through clay is influenced by the permanent negative charge of clay surfaces, which gives rise to the anion deficit/ Donnan potential in clay pores (see below and Section 3.5.7). In terms of using Equation (3-24) in the context of diffusive transport of trace contaminants, the effect of anion deficit is typically handled by assigning a value to ε which is lower than the physical porosity (see section on uncertainties).

Diffusion of anionic and cationic species

While the process of diffusion as such is well established, all available data indicate that the macroscopic model discussed above can be applied only in case of neutral diffusants in a straightforward fashion, whereas additional or different concepts and processes need to be invoked to explain the diffusion of purely cationic and anionic species (see model studies/experimental studies). I.e., the Fickian approach is sufficient for describing the diffusion of many radionuclides, but cannot explain the apparently diminished or enhanced diffusion of anions and cations (SKB 2010a, NEA 2012, Birgersson et al. 2017). This is to be expected, since the diffusion of charged ions is influenced by the electrical double layer (EDL) extending from the clay surfaces into the pores and because microscopic or molecular-level features, such as EDL-effects, are not considered by the Fickian model. The safety-related importance of the electrostatic effects is considerable – it is one of the few phenomena that limit the transport of non-sorbing anions from a damaged canister.

It needs to be noted in this context that the term neutral diffusant encompasses any element or radionuclide whose species distribution in bentonite porewater results in an overall approximately neutral charge (e.g., M^+, MOH, $M(OH)_2^-$). As purely cationic diffusants, alkali and to some degree alkaline earth elements have to be viewed. Chloride (Cl^-), sulphate (SO_4^{2-}) and pertechnetate (TcO_4^-) are typical examples of anionic diffusants. To explain the diffusion of such cations and anions, the macroscopic Fickian concept needs to be extended to include the effects of the permanent negative clay charge.

To compensate for the shortcoming of the Fickian concept, the following approaches are possible. Note that these approaches are not exclusive: often, a pragmatic methodology is followed while acknowledging the mechanistic concepts.

- A pragmatic way forward often used in the context of recommending radionuclide migration parameters for safety assessment calculations is to modify the Fickian model where needed to address anion exclusion and enhanced cation diffusion. In lack of a reliable model, such modifications have to be done on the basis of available experimental data and for a defined migration scenario and are therefore conditional. For example, Ochs and Talerico (2004) recommended values for diffusion-available porosity, effective diffusivity and distribution coefficient for 38 elements using the Fickian framework with modifications to handle anion exclusion and enhanced cation diffusion. To this end, a lower diffusion-available porosity and a lower D_e was recommended for anions, while a higher D_e was recommended for Cs.
- During the last two decades or so, much effort has been devoted to the determination of 1) specific experimental data and 2) to the development of fundamental physical-chemical models and conceps to describe various aspects of the observed diffusion phenomena. However, no sufficiently constrained concept of the underlying fundamental properties of bentonite pores is available to date. Due to this lack of constraint, different models which differ in fundamental aspects can be used, more or less equally well, to describe the diffusion of various ions (e.g. Idiart and Coene 2019). Once the choice of a basic model is made, the actual model parameters can be well underpinned by experimental diffusion data.

Dependencies between process and buffer variables

Table 3-10 summarises how the process influences and is influenced by all buffer variables and how these effects are treated in the PSAR.

Influence of pore geometry: The influence of pore geometry is included in the equations for diffusion coefficients through the parameters tortuosity and constrictivity.

Influence of temperature: Based on the influence of temperature on the diffusivity of ions in free water (Robinson and Stokes 1959), it can be expected that D_e will increase about twofold when temperature is increased from ambient conditions to about 50–60 °C.

Table 3-10. Direct dependencies between the process "Diffusive transport of species" and the defined buffer variables and a short note on the handling in the PSAR.

Variable	Variable influence on process		Process influence on variable	
	Influence present? (Yes/No) Description	Handling of influence (How/Why not)	Influence present? (Yes/No) Description	Handling of influence (How/Why not)
Buffer geometry	No		No	
Pore geometry	Yes	Porosity is included in the model	Possibly indirectly through influence on porewater composition and swelling	
Radiation intensity	No		No	
Temperature	Yes	Neglected for radio-nuclide transport – the temperature will be low when the process occurs	No	
Water content	Through pore geometry and porewater compo-sition	(saturated conditions assumed)	No	
Gas content	No	(saturated conditions assumed)	In case of dissolved gases such as CO_2 or CH_4	See Gaseous speciation and reactions 3.5.5
Hydrovariables (pressure and flows)	No		No	
Stress state	Indirectly through pore geometry		Possibly indirectly through influence on porewater composition and swelling	
Bentonite composition	Indirectly through porewater composition		Indirectly through influence on porewater composition	
Montmorillonite composition	Extent of EDL depends on magnitude of charge and physical pore width	Included in data selection	Composition of exchangeable ions: indirectly through influence on porewater composition	
Porewater composition	Extent of EDL depends on ionic strength	Included in data selection	Through diffusive transport of main constituents	Included in model, see Section 3.5.6
Structural and stray materials	Through influence on physical porewidth	No stray materials are assumed to be present within the buffer	Possibly indirectly through influence on porewater composition	

Influence of bentonite/montmorillonite composition and structural/stray materials: The diffusion properties are dependent on the interlamellar space in the bentonite which is in turn dependent on the permanent charge characteristics and the composition of the exchangeable cations. Soluble stray materials may exert an effect through influencing the porewater composition. Structural and stray materials may also influence pore geometry.

Influence of porewater composition and speciation: Different species of the same element can have radically different diffusivities. This holds for free water diffusivities, but in particular for diffusion in bentonite pores. Due to their interaction with the diffuse layer extending from negative clay surfaces, diffusivities increase in the order anionic species < neutral species < cationic species. For example, dissolved strontium has a lower diffusivity at high concentration of sulphate, which can be explained by the formation of the neutral aqueous complex $SrSO_4^0$ (Ochs et al. 2001). Changes in porewater composition that cause changes in ionic strength also influence diffusion by affecting the extent of the EDL.

Influence of sorption: The influence of sorption is taken into account in the equation for D_a.

Influence of buffer density: The transport of radionuclides in bentonite is influenced by the density of the material (the degree of compaction). This is a direct consequence of the corresponding change in porosity. In addition, the presence of soluble accessory minerals will lead to changes in porewater composition and, in particular, to an increase of ionic strength as a function of density. The influence of porewater composition is discussed above. In most experiments, the apparent diffusivity decreases with increasing density.

Influence on buffer variables: As pointed out above, the diffusion process is coupled to nearly all chemical processes in the buffer through the diffusive transport of reactants. How other chemical processes, such as exchange reactions of major ions, may further influence other buffer variables is discussed in Section 3.5.6.

Boundary conditions

Diffusive transport in the buffer is relevant with regard to the following aspects:

- Any ions or dissolved gases involved in geochemical alterations of the buffer material (as well as any corresponding reaction products) have to be transported through the buffer by diffusion.
- In case of canister failure, the dissolved concentration of most radionuclides will be limited by the formation of radionuclide-bearing solid phases, including pure solids (such as oxides, carbonates) and solid solutions. Migration of the traces remaining in solution towards the geosphere is limited by the slow diffusive transport through the buffer.
- Ions involved in osmotic equilibria have to be transported in or out of the buffer by diffusion.

The transfer of species from the bentonite to the surrounding rock can be visualised as the diffusion of dissolved species from the bentonite into flowing water in the near-field fracture network (equivalent flow rate or Q_{eq}). The equivalent flow rate can be derived by solving the boundary layer theory equations for diffusive transport into flowing water. The Q_{eq} depends on the geometry of the contact area, the water flux, the flow porosity and the water diffusivity.

Model studies/experimental studies

Experimental approaches and data situation

Diffusion is a slow process, and the diffusion of a tracer through even a small volume of compacted clay requires relatively long timeframes. As a result, Steady-state through-diffusion studies, which can yield directly the required input parameters D_e and porosity, are largely restricted to mobile tracers (HTO, anions, alkaline and alkaline earth elements). Most diffusion studies with moderately and strongly sorbing radionuclides are performed as transient in-diffusion experiments. These experiments yield D_a, which is a lump-sum representation of all processes relevant for radionuclide migration, including diffusion and sorption.

Different experimental set-ups for both transient and steady-state diffusion experiments are described in the literature. Yu and Neretnieks (1997) give a detailed discussion of different experimental methods and how the results can be interpreted. For comparison of data from different studies, it is important to observe which technique has been used and how the diffusivities have been determined. If, for example, metal filters have been used, they can greatly influence the results (Glaus et al. 2010). It also has to be realised in this respect that the extraction of diffusion coefficients invariably involves fitting of experimental data to the diffusion equations described above.

A large number of investigations are described in the literature concerning diffusion experiments in bentonite and similar clays. Yu and Neretnieks (1997) provide a good overview and compilation of older literature on diffusion coefficients. Further results are compiled and discussed in Ochs and Talerico (2004). More recently, results of through-diffusion experiments have become available especially for clay rocks (argillites) as well as some bentonites. These new data were considered in SKB (2010a) to update the selection of diffusion parameters. Nearly the same database was considered by Wersin et al. (2014a, b). Further data became available recently from studies aimed at elucidating diffusion mechanisms and clay porespace characteristics, see following section.

Model concepts

Tracer through-diffusion experiments demonstrate that anions such as chloride show lower diffusive fluxes than neutral tracers (e.g. HTO), whereas simple cations, such as Cs^+, tend to show higher diffusive fluxes. It is established that these effects are primarily related to electrostatic effects in the narrow pore spaces that are caused by the negatively charged clay surfaces (NEA 2012 and references therein, Tachi and Yotsuji 2014, Idiart and Pękala 2016, Tinnacher et al. 2016, Birgersson et al. 2017). The magnitude of the electrostatic effects depends on the composition of the external solution and on the permanent clay charge (i.e., is more pronounced for montmorillonite than for illite (Glaus et al. 2010)).

While it is thus clearly established that the diffusion behaviour of anions and cations is caused by electrostatic effects, different model concepts have been developed to explain the diffusion data, and controversies regarding diffusion mechanisms as well as the model representation of the underlying clay properties remain to date. This diversity of concepts can be traced directly to significant uncertainties and under-constraint by experimental evidence regarding the micro-/nanostructure of compacted clays and especially regarding the nature and distribution of pore types and porewater types (NEA 2012, Wersin et al. 2014a, b, Idiart and Pękala 2016, Tinnacher et al. 2016, Birgersson et al. 2017).

The different model concepts can be grouped according to their handling of electrostatic effects and their consideration of single and multiple pore types. To date, the disagreement between these different conceptual representations of the bentonite porespace is seen as the main hurdle for a further improvement and consolidation of diffusion models.

Conventional porewater (Fickian) model

The conventional Fickian model (as typically applied for performance assessment calculations) does not take into account electrostatic effects in the porespace. Therefore, diffusion of anions and cations is formally handled by a reduction of accessible porosity and a lower D_e for anions and an increased D_e for cations (see e.g. Yu and Neretnieks 1997, Schwyn 2003, SKB 2010a, Wersin et al. 2014a, b). Note that for pragmatic approaches, the outcomes of the more sophisticated model concepts outlined below can still be translated into Fickian model parameters.

Models based on anion deficit/cation excess in a single porosity

Starting from the accepted premise that enhanced cation diffusion and anion exclusion are mainly influenced by electrostatic effects in the porespace, two research groups independently developed models to explain these effects by considering differences in anion and cation concentration between external and pore solutions rather than by a different diffusion process or differences in the diffusion-available porosity. Both approaches consider diffusion of both cations and anions in a single type of (interlayer) porespace and porewater.

- JAEA (Sato et al. 1995, Ochs et al. 2001, Tachi et al. 2010, 2014, Tachi and Yotsuji 2014) developed a surface chemical electric double layer (EDL) model considering the distribution of ions between bulk solution, diffuse layer (extending from planar surfaces) and Stern layer/ ion exchange (or surface complexation) sites to calculate the concentrations of species in the porespace (integrated sorption-diffusion model ISD). The model is able to describe enhanced cation diffusion and anion exclusion in compacted bentonite based on cation excess and anion deficit in the EDL.
- Birgersson and Karnland (2009) developed a Donnan-equilibrium model that treats compacted smectite clay like a homogeneous solution containing immobile negative charges (clay platelets) inside a semi-permeable membrane. While also calculating cation excess and anion deficit, the Donnan equilibrium concept is based on chemical potentials rather than detailed surface chemistry, which is an advantage in the complex clay system. This model successfully describes the diffusion of both cations and anions in compacted clay. To date, it appears to be the only model that is able to correctly reproduce the diffusion of a tracer according to the concentration gradient inside the clay but against a gradient in the external solutions (Glaus et al. 2013). An update and more comprehensive treatment of chemical equilibria between compacted bentonite and aqueous solutions, including a rigorous handling of activity coefficients, is reported by Birgersson (2017). At the same time, the Donnan model is able to explain macroscopic clay behaviour, such as swelling pressure development as a function of compaction and salinity (Karnland et al. 2005, see also the overview given in Birgersson et al. 2017).

Multiporosity-models based on anion exclusion and increased cation diffusion

A number of multi-porosity models have been developed (e.g. Appelo 2013, Wersin et al. 2004, Appelo and Wersin 2007, Bourg et al. 2006) which generally consider diffusion in different porosities giving rise to three different porewater types. In detail, the fraction of each porewater type is not fixed but depends on a number of factors, such as the density of the clay and the composition of the clay and external solution (Appelo 2013).

- Bulk (or “free”) porewater, which is charge balanced and can be treated like any external solution (corresponding to the porewater in the Fickian model).
- Diffuse double layer water containing an excess of cations and a deficit of anions due to the charge of the clay surface (corresponding essentially to the porewater considered in the Donnan and ISD models).
- Interlayer water containing only water molecules and cations balancing the charge of the siloxane surface of smectite (this corresponds approximately to the exchanger complex or Stern layer in the ISD model and can be seen as part of the clay structure).

While differing in detail, all multi-porosity models consider the complete exclusion of anions from a part of the total porosity, giving a lower diffusion-accessible porosity and a lower D_e relative to neutral diffusants. The enhanced diffusion of cations on the other hand is explained by various processes:

- Appelo and Wersin (2007) consider an increased diffusional gradient of cations between the diffuse layer and the free water.
- Bourg et al. (2006) and Glaus et al. (2010) propose an additional diffusion pathway for cations in the interlayer.
- Gimmi and Kosakowski (2011) inferred from an evaluation of published diffusion data that cations sorbed to clay surfaces exhibit a cation specific surface mobility (sometimes termed surface diffusion).

Because of the assumed presence of different pore volume fractions, water types, and diffusion pathways, multi-porosity models offer a greater flexibility in data interpretation and modelling. In particular the presence of a volume of free water allows to make a direct connection to standard chemical equilibrium calculations in a bulk water phase (Idiart and Pękala 2016).

Structure of compacted bentonite

The main difference between single- and multi-porosity models is that each of the different porewater types of multi-porosity models is considered as a separate compartment, possessing its own physico-chemical properties. This concept is in turn based on a heterogeneous structural model of compacted bentonite that includes interlayer space, intraparticle space and external space as distinct, separate regions (Appelo 2013). This concept is based on Bradbury and Baeyens (2003) and is supported by microscopic observations (Tessier 1990, Melkior et al. 2009) indicating a heterogeneous microstructure consisting of a gel phase and hydrated clay layers.

On the other hand, Tachi and Yotsuji (2014) point out that the microstructure of water-saturated, compacted montmorillonite is controlled by the interlayer swelling behavior, which is dependent on the hydration of the interlayer cations. The size of the larger pores (interparticle pores in the heterogeneous model) can be reduced by swelling to approach the size of intraparticle pores, giving a near-homogeneoius pore size distribution. High resolution nano X-ray CT (Takahashi 2013) shows that individual montmorillonite particles in the dry state swell upon saturation to give a relatively homogeneous pore distribution. X-ray signal intensity distributions recorded in the dry and saturated state (Takahashi 2013) also indicate that swelling leads to a homogenisation of the pore size distribution. Holmboe et al. (2012) showed with XRD profile modelling that Na-montmorillonite with a dry density of 780 kg/m^3 saturated with 0.001M NaCl has a nearly uni-modal pore size distribution.

Diffusion of charged species

Enhanced apparent cation diffusion

It has been known for many years (cf. Yu and Neretnieks 1997) that the apparent diffusion coefficient (D_a) for cations and their respective distribution coefficient (K_d) do not correspond as expected (i.e., cannot be explained by a Fickian model). D_a has been higher than expected from K_d values and Fickian porewater diffusion-sorption theory. While several explanations of this phenomenon have been proposed (see below), it is of foremost importance to recognise that an agreement of D_a and K_d is only to be expected for datasets that are self-consistent in terms of chemical conditions. I.e. both D_a and K_d need to correspond to the same set of conditions, in particular to the same porewater composition. Thus, several of the discrepancies between D_a and K_d observed in the past can be traced to the fact that incompatible conditions have been compared. In particular, D_a values that invariably correspond to the porewater composition in compacted bentonite have been compared directly with K_d values from batch experiments involving typically much more dilute solutions. Given that K_d values are derived for relevant porewater conditions, sorption and apparent diffusion coefficients for most elements agree within the overall data uncertainty.

Nevertheless, there are cases where it seems clear that certain cations may have apparently enhanced diffusivities, which must be taken into consideration in safety assessments. The presently available information suggests that these cases are largely restricted to mobile and cationic elements interacting with the clay surface mainly by ion exchange: alkali elements and sometimes alkaline earth elements (Ochs and Talerico 2004, SKB 2010a, Wersin et al. 2014a, b).

Enhanced cation diffusion can be explained by a cation excess in the electrical double layer (EDL) extending from negatively charged clay surfaces into the pore space (see Birgerson and Karnland 2009, Glaus et al. 2013, 2015, Tachi and Yotsuji 2014, Tachi et al. 2014), as well as Section 3.5.8). The enhanced mass transfer of cations is thus due to a higher concentration and not to a higher diffusivity. Note that cation excess (as well as anion deficit, see below) have been well established in clay chemistry (see e.g. van Olphen 1991) and that the mean cation excess/anion deficit in the EDL corresponds to the differences in cation/anion concentrations in compacted clay pores as calculated through Donnan equilibrium (see Section 3.5.8).

Because these electrostatic effects increase the dissolved concentration of cations in the pore space in comparison to the corresponding (external) bulk solution and in comparison to neutral and anionic species, diffusing cationic tracers have higher concentration gradients and therefore higher diffusion rates than would be expected in the absence of the electric charge effects in the clay pores. Note that this holds for cations that accumulate in the diffuse layer, thereby retaining their mobility parallel to (but not perpendicular to) a mineral surface; but does not hold for specifically (i.e. chemically) sorbed surface species formed at surface complexation or ion exchange sites. For an evaluation of

diffusive transport in compact clays, the simple accumulation in the counter-ion swarm of an electrical field near a surface and actual sorption (represented by K_d) need to be distinguished (Ochs et al. 2004, Glaus et al. 2015, Birgersson et al. 2017).

While presumably based on the same underlying process, the so-called surface diffusion mechanism (Muurinen 1994, Eriksen and Jansson 1996, Yu and Neretnieks 1997) makes a direct link with actual sorption by introducing an additional surface diffusion coefficient that is multiplied by K_d. More recently, Gimmi and Kosakowski (2011) proposed an alternative surface diffusion model, where the mobility of sorbed cations is inversely related to their sorption affinity. This concept is actually compatible with the notion (Ochs et al. 2004) that ions accumulated in the EDL retain their mobility whereas specifically sorbed species are immobilised. This was also confirmed by the recent experimental study of Glaus et al. (2015).

At the onset of the discussion of enhanced cation mass transfer, a reduction of K_d in highly-compacted bentonite due to a decreased accessibility of surface sites has also been discussed as a possible explanation for the disagreement of diffusion data with batch K_d values (Wanner et al. 1996), but the data by Kato et al. (1995) allowed the conclusion that the entire physical porosity in compacted bentonite is accessible to porewater. Bradbury and Baeyens (2003) also determined that compaction is not expected to lead to a reduction of sorption capacity, based on BET measurements for dispersed/compacted bentonite and by comparing batch and diffusion-derived K_d values.

Anion exclusion

The various concepts being used at present to explain the phenomenon of anion exclusion have already been discussed above.

It is assumed that in compacted bentonite, the pore width is small enough to cause a superimposition of the electrical double layers between two negatively charged pore walls. i.e., the EDLs in compacted clay are overlapping and no free (bulk) porewater exists (Ochs et al. 2004, Birgersson and Karnland 2009, Tachi and Yotsuji 2014, Birgersson 2017). Under such conditions, the anion deficit in the diffuse layer applies to the entire pore space (see above and Section 3.5.8) and causes, for anions, the opposite effect as was explained above for cations: Diffusing anionic tracers have lower concentration gradients, and therefore lower diffusion rates than would be expected in the absence of the electric charge effects in the clay pores.

An alternative view of the same phenomenon taken in case of multi-porosity models is that the anion deficit in the clay pores decreases the available diffusion pathways for an anionic tracer. The interlayer would not be available at all to transport of anionic species (Appelo 2013).

Evidence from activation energy measurements suggests that the overlap of EDL's may occur at a dry density of about 1 200–1 500 kg/m^3 (Kozaki et al. 1998). The effect of anion exclusion becomes less at high salinities, because high ionic strength leads to a depression of the EDL (Stumm and Morgan 1996), and in sand-bentonite mixtures it is negligible.

Natural analogues/observations in nature

The usefulness of natural analogues for evaluating diffusion behaviour and for determining constants is limited due to the difficulty of determining the conditions that existed in the past. Natural analogues can illustrate that diffusive transport is greatly slowed down for many sorbing radionuclides (e.g. Smellie and Karlsson (1996), see also Section 3.5.3).

Time perspective

Diffusion processes in the buffer material are of the greatest importance on all timescales. If the canister is intact, the process is of importance for the stability of the canister and the buffer. In the event of a defective canister, slow diffusion is very important in delaying, reducing and in many cases completely preventing releases of radionuclides.

Handling in the PSAR

Before saturation: The process is neglected since advection dominates.

After saturation: The process is included in the scenario-specific modelling of the buffer chemical evolution for the thermal phase and the post-thermal long-term phase, see heading “Handling” for process alteration of accessory minerals (Section 3.5.6). The process is treated in a simplified way with identical diffusivity for all elements in the buffer chemical evolution.

Failed canister: Included in the modelling of radionuclide transport for the long-term phase, see heading “Handling” for process transport of radionuclides in water phase 3.6.2. For the treatment of radionuclide diffusion, element-specific effective diffusivities are used together with corresponding porosities (see Ochs and Talerico (2004) and SKB (2010a) for the definition of data and associated uncertainties).

Boundary conditions: See referred to above.

Influences and couplings: Dependence on buffer density and bentonite type, expected ionic charge of diffusing species, ionic strength and temperature is considered in selecting diffusion constants for transport of radionuclides. For the treatment of diffusion within the buffer chemical evolution, see alteration of accessory minerals 3.5.6.

Uncertainties

Uncertainties in mechanistic understanding

Because of the experimental inaccessibility of bentonite pores, diffusion data are of macroscopic nature and are not well suited for any mechanistic interpretation. On a mechanistic level, the main shortcomings probably lie in the understanding of pore structure as well as porewater and EDL properties in compacted bentonite (NEA 2012, Tinnacher et al. 2016, Birgersson et al. 2017). This is particularly true for higher densities that may lead to the disappearance of free water.

The basic processes of enhanced cation diffusion and anion exclusion have been discussed above. All available evidence suggests that the processes giving rise to these phenomena are the establishment of a cation excess and an anion deficit in the porespace. However, several conceptual models are available to interpret these phenomena, as detailed in the section model studies/experimental studies above. In contrast to the various multi-porosity models, both types of the single-porosity models (Donnan/homogeneous mixture, ISD) are based the same effect (cation excess/anion deficit) to explain cation and anion diffusion, but use very different approaches to implement this concept. Further, by considering cation excess/anion deficit one does not need to invoke a different or modified diffusion process or modified porosity to explain diffusion of charged species. Based on recent developments (Glaus et al. 2013, Tachi and Yotsuji 2014), these model concepts are viewed as reasonable approximations of the actual processes. However, as pointed out above, the porespace of compacted bentonite is essentially inaccessible to direct experimental observation, and the microstructure of compacted bentonite is still poorly known. The unfortunate existence of several different approaches for explaining diffusion phenomena is a direct consequence of this lacking constraint.

It further has to be realized that within the overall experimental uncertainty

- the diffusion of most radionuclides can be described sufficiently well by a Fickian model,
- additional processes caused by electrostatic effects are relevant for a few elements only, and model-specific results can be converted to parameters of the Fickian approach (for example, an anion deficit can be formally expressed as a decrease in porosity).

In the end, several model concepts can be used to guide the selection of input data for consequence analyses. In view of the above discussion, it is essential that sufficiently detailed arguments are provided regarding selection of the model concept, and that the chosen concept is used in a consistent fashion. For the selection of radionuclide diffusion data and uncertainties for the PSAR (**Data report**) and Ochs and Talerico (2004)), the anion deficit is taken into account through a decrease in D_e and a reduced diffusion-available porosity. Enhanced cation diffusion is accounted for by an increase in D_e in combination with the physical porosity.

Model simplification uncertainties in the PSAR

As pointed out above, diffusion is represented in a simplified way, through the use of selected constant effective diffusion coefficients and available porosities in the relevant transport codes (see alteration of accessory minerals 3.5.6 and Transport of radionuclides in water 3.6.2). In that sense, the diffusion input parameters have to be viewed as conditional; i.e. their application will only be valid under the conditions considered in data derivation. A selection of diffusion parameters based on relevant experimental data can be supported by essentially any of the models discussed in the model studies/ experimental studies section, as long as this is done in a transparent fashion and as long as arguments are provided for preferring one model over another.

Overall, uncertainties will be related to considering consistent conditions in the selection of diffusion parameters rather than to uncertainties related to model simplification. If, for example, the processes occurring during buffer evolution would lead to a significant alteration of bentonite properties, it may be necessary to use input parameters that differ from those for standard MX-80 bentonite.

In principle, this situation could be resolved by directly including diffusion processes in the model used for consequence calculations, which would require a THMC model approach. However, difficulties remain to date with regard to fully coupling THM processes on the one hand and C processes on the other in view of modelling permeability and porosity changes in bentonite (Savage 2012). More importantly, the present lack of consent regarding the micro- and pore-structure of compacted bentonite would not allow discriminating between very different models, similar to the present situation regarding diffusion modelling.

Input data and data uncertainties

Input data to the PSAR are effective diffusivities and available porosities to be directly used in consequence calculations. Data and uncertainties as a function of bentonite density are given in Ochs and Talerico (2004), from which data for consequence calculations are chosen.

3.5.3 Sorption (including ion-exchange of major ions)

Overview

Radionuclides and major ions in the buffer porewater can be bound to the surfaces of the bentonite material in several ways (see below). Together, these processes are termed sorption and are of essential importance for the function of the buffer, since they drastically affect the mobility of most radionuclides and also of major ions, which is, in turn, related to the evolution of the buffer. The principal mineral in bentonite is montmorillonite, which consists of octahedral alumina sheets sandwiched between tetrahedral silica sheets (2:1 clay). Expandable 2:1 clay minerals feature two distinctly different types of surface, where two main types of sorption take place (e.g. Sposito 1984, Stumm and Morgan 1996, NEA 2012).

Siloxane or basal surfaces: The siloxane (‘layer’) surfaces of clay minerals are *permanently charged surfaces*. These charges derive from isomorphous substitutions, which result in a constant negative surface charge. This charge is largely compensated for by cations simply accumulated in a counter-ion swarm and partly by cations located at (and in some cases bound to, e.g. at the di-trigonal cavity) the clay surface ((Sposito 1984), and. The counter ion swarm is equivalent to an electrical double layer (EDL) extending from the surface (see Section 3.5.7). Note that the permanent charge of the siloxane surface gives rise to the electrostatic phenomena that are operative in the anion and cation diffusion process and in Donnan equilibria in clays (see Section 3.5.2 and Section 3.5.7).

Macroscopically, sorption takes place when compensating ions are exchanged. *Ion exchange models* of the site-binding type have been used in soil science since the first quarter of the 20th century. Several formalisms have been developed to correct for activity changes of the exchanger as a function of the composition of the charge-compensating ions. The most common are the equivalent fraction (Gaines-Thomas, GT) and mole fraction (Vanselow) models.

Edge surface: The edge surfaces of clay minerals are variably charged surfaces. They carry a net positive or negative surface charge depending on the species sorbed to their surfaces (potential-determining ions), often involving surface-bound OH^- groups. *Surface complexation and ligand*

exchange models were established by Stumm, Schindler and co-workers in the 1970s by extending proton-binding and metal coordination chemistry in a rigorous fashion to surface chemistry.

Typically, the process implicitly refers to the formation of inner-sphere complexes. Surface complexation refers to the formation of coordinative bonds between hydrolysable elements (typically aqueous metal species) and surface –OH groups. Analogously, ligand exchange refers to the coordinative binding of inorganic or organic ligands to surface metal centers (typically Al or Si-atoms, or their substituting atoms), thereby replacing the –OH surface functional groups (Stumm and Morgan 1996). To account for the electrostatic field, the mass laws for surface equilibria often include an electrostatic correction term. The scientific basis for these corrections is again derived from Electrical Double Layer (EDL) theory (Stumm and Morgan 1996). In addition, ions (both anions and cations, depending on pH) can accumulate in the EDL extending from the edge surface (outer-sphere complexation).

Note that montmorillonite is a fully expandable clay mineral. Therefore, the edge of montmorillonite does not contain any sterically restricted site types, such as the frayed edge sites (FES) found on illite (van Olphen 1991).

Sorbing species, electron transfer, reversibility: Ion exchange is the typical sorption mechanism for alkali and alkaline-earth elements, as well as transition metals at low pH values where positive species are predominant. Surface complexation is generally the more relevant process for all hydrolysable elements (transition metals, actinides, lanthanides, reactive anions such as carbonate). Note that both ion exchange and surface complexation take place simultaneously, but at different surfaces (see above).

As ion exchange is relevant for both trace radionuclides as well as major system cations, this process influences both radionuclide transport as well as the overall composition of cations in the buffer system. This includes the porewater composition and the composition of the exchange complex on the clay surface, which has an influence on bentonite properties. The composition of porewater and clay surface is principally determined by the original cations in the exchange positions of the montmorillonite, soluble minerals in the original bentonite material, and the surrounding groundwater.

In analogy to aqueous acid-base reactions, H^+ ions are bound to the surface –OH groups on the edge sites of clays (as well as to ion exchange positions at very low pH), which means that pH changes can occur due to surface chemical reactions (Stumm and Morgan 1996). Owing to its amphoteric properties, i.e. ability to both accept and donate hydrogen ions, the montmorillonite can buffer external changes in pH (Wanner et al. 1992, NEA 2012).

Redox-reactions taking place upon sorption have received relatively little attention to date. Many montmorillonites contain redox-active sites (mainly Fe atoms) which are able to participate in redox reactions of clay minerals with sorbed species and therefore, with the surrounding environment (Soltermann et al. 2014a). Both the total Fe content of clay minerals and the absolute redox state of the mineral are important factors influencing redox reactions between constituents in the clay structure and surface-bound metals.

Reversibility of sorption is a fundamental paradigm with regard to

- quantitatively expressing solid/liquid partitioning of solutes through K_d values,
- the use of K_d values in transport models (for dissolved radionuclides and any other solutes).

Therefore, the available evidence for the processes relevant for radionuclide sorption to clays – surface complexation and ion exchange – is discussed in more detail in the following sections.

In the absence of any evidence to the contrary, a fundamental and widely accepted principle is that cation exchange and surface complexation on clay and oxide-type minerals is reversible, which follows directly from analogies with corresponding exchange and complexation reactions in homogeneous aqueous solutions (see e.g. Sposito 1981, 1984, Stumm and Morgan 1996). Sorption/desorption kinetic experiments indicate that desorption from surface complexation sites tends to be kinetically slower in comparison to sorption (e.g. Np(V) sorption/desorption on Fe-oxides (Nakata et al. 2000). Accordingly, most studies concerning surface reactions on these minerals focus on sorption, whereas much fewer studies have been published that systematically investigate the degree of reversibility in sorption experiments. On the other hand, the pertinent literature offers several examples where some type of

irreversibility was observed. Below, in the Model studies/experimental studies section, several examples are examined and their relevance with respect to radionuclide sorption on clays is evaluated. While this discussion is not based on an exhaustive review of the literature, it shows that sorption on clays and clay-like substrates is typically found to be reversible if the experimental boundary conditions are carefully evaluated.

Dependencies between process and buffer variables

Table 3-11 shows how the process influences and is influenced by all buffer variables.

Table 3-11. Direct dependencies between the process "Sorption" and the defined buffer variables and a short note on the handling in the PSAR.

Variable	Variable influence on process		Process influence on variable	
	Influence present? (Yes/No) Description	Handling of influence (How/Why not)	Influence present? (Yes/No) Description	Handling of influence (How/Why not)
Buffer geometry	No	(Total buffer mass is a parameter in the RN-transport model)	No	
Pore geometry	Possibly indirectly through influence on EDL properties		Possibly indirectly, through influence on EDL properties/ swelling	
Radiation intensity	Possibly indirectly, through influence on mineral properties		No	
Temperature	Influence of temperature on sorption must be acknowledged, but effect is not clear		No	
Water content	Indirectly through porewater composition		No	
Gas content	Indirectly through porewater composition (CO_2)		Possibly indirectly, through influence of Ca-exchange on carbonate equilibria	
Hydrovariables (pressure and flows)	Indirectly through porewater composition		Possibly indirectly, through porewater composition/swelling	
Stress state	Indirectly through influence on porewater composition and EDL properties		Indirectly through influence on porewater composition and EDL properties/swelling	
Bentonite composition	Yes	Used for derivation of K_d	Yes	Included in geochemical transport model
Montmorillonite composition	Yes	Used for derivation of K_d	Yes	Included in geochemical transport model
Porewater composition	Yes	Used for derivation of K_d	Yes	Included in RN-transport model (Section 3.6.2) and geochemical transport model (Section 3.5.6)
Structural and stray materials	No stray materials are assumed to be present within the buffer		Indirectly through influence on pore-water composition and related mineral equilibria	

Influence on buffer variables: Exchange reactions of major cations directly influence the surface composition of the clay minerals as well as the porewater composition. In turn, changes in the porewater chemistry may induce further changes in the bentonite composition through mineral dissolution and precipitation. On the other hand, the pore geometry, and thereby also the hydraulic conductivity, are not expected to be significantly altered by ion exchange processes, because the volume of the buffer at reference density is so constrained that a maximum swelling of the bentonite cannot be achieved even after complete conversion to the Ca-form (or in the presence of high ion concentrations in the porewater). At saturated densities below 1 800 kg/m^3, these processes may lead to a significant reduction in the swelling pressure due to osmotic effects and a suppression of the EDL, and to an increase in the hydraulic conductivity (see Sections Water transport under saturated conditions (3.3.2) and Osmosis (3.5.7).

Influence of bentonite and porewater composition: The two most important variables with regard to radionuclide sorption and exchange of major ions are the bentonite and porewater composition. The mineralogical composition of bentonite is directly related to the number of sorption sites available and their specific properties. The porewater composition is the result of groundwater-bentonite interaction (ion exchange, surface acid-base reactions, mineral equilibria) and, in turn, exerts a major influence on radionuclide sorption. As described in the previous chapter on diffusion, different model concepts of porosity in compacted bentonite would also lead to different corresponding approaches for modelling porewater chemistry (Wersin et al. 2004, NEA 2012, Birgersson 2017).

On the other hand, K_d is clearly independent of the solid/water ratio and, therefore, of the buffer density (given that the solution composition remains constant). Under a given set of conditions, the sorbed amount of a radionuclide increases if the amount of bentonite (i.e. the solid/water ratio) is increased. By expressing sorption through K_d (see below), which includes the solid/water ratio, this effect is already taken into account. It appears from diffusion experiments that the apparent K_d is influenced by density, for example the K_d for caesium is halved when the density of the water-saturated system changes from 1 300 to 1 950 kg/m^3. However, this can be entirely attributed to an increase of ionic strength caused by the dissolution of accessory minerals from an increasing mass of bentonite, and is easily reproduced by simple thermodynamic sorption models (see e.g. Ochs et al. 2001). This effect is mostly relevant in the case of dilute groundwaters. Tachi and Totsuji (2014) show that both diffusion data (D_a and D_e) as well as batch-derived K_d values for Cs on bentonite can be modelled consistently as a function of ionic strength.

Influence of temperature: Most experiments have been carried out at room temperature, and not enough sorption data as a function of temperature are available to clearly evaluate temperature effects. Tertre et al. (2006) found no significant difference in the surface acid-base chemistry of kaolinite and montmorillonite between 25 °C and 60 °C. Similarly, Morel et al. (2007) observed only a negligible influence of temperature on the exchange of traces of Cs by a Na-clay. On the other hand, studies aimed at investigating the effect of temperature on the sorption of actinides/lanthanides (Lu et al. 2003, Schott et al. 2012) show that sorption increases with temperature. Thus, an increase or decrease of the temperature is potentially of importance for sorption, but the effects within the temperature range expected in the repository are deemed to be covered with good margin by other uncertainties.

Boundary conditions

There are no particular boundary conditions to discuss for this process. The relevant boundary conditions in order to treat the process quantitatively are those of the transport processes that control the exchange of solutes between the buffer porewater and the water in its adjacent components, i.e. the boundary conditions of the processes diffusion and advection.

Model studies/experimental studies

Ion exchange and surface complexation are well-established processes and quantitative thermodynamic models exist for calculation of equilibrium states. The relationship of these sorption processes to the different surfaces of montmorillonite has been discussed above. During the last decades, a vast amount of literature has accumulated on various specific aspects of sorption reactions and modelling, including kinetic aspects, the structure of surface species, kinetics, and so on. A detailed discussion would be drastically outside the scope of the present chapter. More importantly, the vast majority of

the research carried out so far is concerned with dilute suspensions rather than compacted clays. A state-of-the-art overview of i) radionuclide sorption on natural substrates including clays and ii) of the additional complexity to be considered in compacted systems is given in NEA (2012).

As described in the overview section, ions present in the cation exchange complex (mainly alkali plus alkali earth elements) are accumulated near the clay surface rather than chemically sorbed. In all diffusion or porewater concepts, these ions retain therefore a certain mobility along the surface (cf. references in NEA 2012) and ion exchange should not be interpreted as sorption in the sense of immobilization. Very few studies are available addressing chemical sorption (i.e., coordinative binding, mainly to edge sites) in compact bentonite or montmorillonite. Tachi et al. (2010) measured and modelled the diffusion and sorption of Np(V) in compacted montmorillonite under different salinity and carbonate concentrations. According to their study, a sorption model based on data from dispersed clay systems can fully explain the measured diffusion-derived K_d values; the degree of compaction was fairly low, however (800 kg/m^3). To our knowledge, no other study is available concerning fully expandable clays.

It is pointed out that additional data are available from systems with non-swelling clays and clay rocks. These are not discussed here as the relevance of these materials to fully swelling clays is questionable (and may help to obscure rather than to clarify concepts).

Effect of sorption/exchange processes on buffer properties

Of primary relevance for the properties of the buffer is the exchange of major cations between groundwater and bentonite pores, as well as pH-buffering by edge site protolysis equilibria. This is discussed under process alteration of accessory minerals (Section 3.5.6).

Effect of sorption on radionuclide transport

In assessing radionuclide transport from a repository, sorption is normally described as a linear, equilibrium relationship between the sorbed concentration and the concentration in solution, characterised by a distribution coefficient K_d, which is defined as:

$$K_d = \frac{q}{C_w} = \left(\frac{C_{init} - C_{equil}}{C_{equil}}\right)\frac{v}{m} \text{ (for batch experiments)} \quad (3\text{-}25)$$

where:

C_{init} is the initial aqueous concentration of a key element [mol/m^3] as measured in the reference solutions without solids

C_{equil} is the final equilibrium aqueous concentration of this element [mol/m^3]

C_w is the concentration in solution

v is the volume of the solution used for a batch experiment [m^3]

m is the mass of the solid phase used for a batch experiment [kg]

q is the sorbed concentration as mass per weight unit of solid phase.

When the concentration of the species in solution is low (more specifically, at a state sufficiently far from surface saturation), which is normally the case for radionuclides, the linear approximation is justified. K_d can also be calculated in a straightforward fashion from the output of thermodynamic sorption models (NEA 2012):

$$K_d[m^3/kg] = \frac{stoichiometric\ sum\ of\ surface\ species\ of\ element\ X\ [mol/kg]}{stoichiometric\ sum\ of\ solution\ species\ of\ element\ X\ [mol/m^3]} \quad (3\text{-}26)$$

Surface complexation models with parameters from well-controlled experiments that include sufficient variation of key geochemical parameters can often be used to describe the dependence of sorption on external parameters such as pH or carbonate concentration. The applicability of such models is mainly limited by the lack of sufficiently complete experimental datasets that can be used for parameterization (NEA 2012).

Reversibility

As pointed out in the overview section, reversibility is a central issue in view of the handling of sorption through K_d in transport models. While the process of sorption is regarded as clearly reversible, there are several examples in the literature where apparent effects of irreversibly have been observed. Some examples are discussed in the following, but it has to be noted that systematic studies regarding reversibility are still scarce to date.

The following examples suggest that apparent irreversibility is related to processes other than sorption, which are caused by a high surface- or interlayer-loading (see below for details):

- Complete exchange of compensating cations in clay can lead to aggregation, which hampers further exchange/desorption.
- In certain clays, but notably not in montmorillonite, sorption of cations like Cs can lead to a collapse of the clay structure.
- In some systems investigated to date, new minerals can form on the clay surface following sorption. The available data suggest that this is not likely to occur when sorption of radionuclides occurs from trace levels. It is also not finally resolved whether these minerals form as a direct consequence following a sorption complexation reaction, or whether the clay merely provides a nucleating surface.

Alkai and alkali earth element sorption to clays

With regard to the reversibility of cation exchange, Verburg and Baveye (1994) published a critical review of a number of studies where hysteresis (i.e., irreversibility) had been observed in simple cation exchange experiments. In their analysis, Verburg and Baveye (1994) come to the conclusion that the observed effects are related to hysteresis in clay swelling and aggregation in disperse laboratory systems (formation of quasi-crystals when the supporting electrolyte cation is changed from e.g. Na to Ca), rather than to the actual exchange process. Aggregation processes influence the exchange behaviour of clays, and their kinetics are much slower than the kinetics of exchange reactions (roughly, weeks instead of seconds).

At this point, it is important to distinguish the conditions in classical exchange experiments from those relevant for the adsorption of traces:

- The classical exchange experiments typical involve i) a complete change of the exchangeable ions (e.g., conversion of Na-clay to Ca-clay) and, concomitantly, a change of the supporting electrolyte solution (e.g. from NaCl to $CaCl_2$).
- On the other hand, under PA-relevant conditions, traces of a radionuclide (Sr, Cs…) are exchanged against other cations in a electrolyte solution of constant composition. Also, the exchanged trace cations do not influence the surface composition of the exchanger. In this case, no change in the clay's aggregation state has to be expected.

A somewhat special case where reversibility has been questioned is the sorption of Cs to clays. This is largely caused by a failure to distinguish between sorption on low charge, expandable 2:1 clays (e. g. smectites) and high-charge (e.g. vermiculite) or non-expandable clays (e. g. chlorite or illite). While it is well accepted that micaceous clays, such as illite, possess so-called 'frayed edge sites' (FES) that are only accessible to few ions (Cs+, K+, protons) for steric reasons (Sposito 1984, Baeyens and Bradbury 2004), the effect of changes in the structural properties of such clays are often not taken into account. Durrant et al. (2018) compared Cs sorption/desorption reversibility on illite, montmorollonite and kaolinite. Under all studied conditions, they observed full reversibility for Cs interaction with montmorillonite and kaolinite. On illite, they found irreversible sorption at high Cs loading, which presumably caused collapse of FES. This is consistent with earlier findings by Grütter et al. (1990) who demonstrated that sorption of Cs ions at high surface loadings may lead to a collapse of the interlayer of vermiculite-like clays, trapping sorbed Cs in the mineral structure and rendering desorption impossible. In the same study reversible sorption was observed at low surface loadings (i.e., where no collapse of the interlayer occurs).

There is also clear evidence that the above issues are specific to a few cations that easily loose their hydration shell and are not relevant for other ions. In an interesting study, Cui and Eriksen (1995) showed the reversibility of Sr(II) sorption as well as isotope exchange on several fractions of infill material(feldspar, quartz, muscovite, Fe-chlorite, probably also other Fe-minerals) from the Stripa mine, Sweden. Using reaction times between ca. 30–100 d they observed complete reversibility of Sr sorption with regard to 1) Sr concentration (no hysteresis for sorption and desorption isotherms covering 5 orders of magnitude in terms of Sr concentration), 2) pH change (from pH 4 to ca. 12.5 and back), 3) Sr isotope exchange.

Ni and Co sorption to clays

Scheidegger and Sparks (1996) examined the sorption/surface precipitation and detachment of Ni by pyrophyllite (a low-charge 2:1 clay mineral) as a function of time. Deviations from reversibility were attributed to the formation of a surface precipitate. In a follow-up study, Scheidegger et al. (1997) confirmed with EXAFS spectroscopy that the surface precipitate was a newly formed mixed Ni/Al-hydroxide phase similar to the mineral takovite. While it can thus be excluded that surface precipitation was simply due to formation of $Ni(OH)_2(s)$ by high dissolved Ni concentrations, it has to noted that Ni concentrations were very high rather than at trace levels.

Livi et al. (2009) re-examined the same system with a more detailed microscopic and spectroscopic investigation, working again at dissolved Ni concentrations just below supersaturation of Ni-hydroxide. They identified the surface precipitate as an amorphous phase similar to a layered Ni-Al layered double hydroxide (LDH) phase.

It appears that multinuclear surface complexes can be seen as a precursor to the formation of surface precipitates. In this context, the results of O'Day et al. (1994) are important. They observed (also by EXAFS) multinuclear surface complexes of Co on kaolinite at high surface loading (just below complete monolayer coverage), whereas only mononuclear surface complexes were observed at low coverage.

Scheidegger and Sparks (1996) conducted also a systematic study of reversibility. It was observed that Ni uptake was initially fast, followed by a slow process; overall equilibrium was reached after ca. 200 h (pH 7.5). The fast and slow processes were attributed to surface complexation and surface precipitation, respectively. Desorption experiments were initiated by lowering the pH from 7.5 to 6 after equilibrated samples had been stored for an additional 1–8 weeks. These experiments showed that:

- a few percent of Ni were removed within the first 2–3 h, presumably by desorbing from the surface complexation sites,
- the remaining Ni was removed much slower (based on the observed constant rate, complete removal would need about 250 days), which was ascribed to the dissolution of a Ni-surface precipitate (hypothesized as mixed Ni-Al-hydroxide),
- in comparison to experiments where the reaction products were removed every 24 h, Ni detachment was significantly slower when the reaction products were not removed, probably because of re-adsorption.

Overall, this shows that Ni adsorption onto clay surfaces is fast and reversible within similar time-frames. Similarly, Baeyens and Bradbury (1997) studied the sorption of trace concentrations of Ni onto Na-montmorillonite at pH 4.5–10. They report that no kinetic effects were observed for reaction times between 1 and 18 days and further state that reversibility of Ni sorption was confirmed (without giving specific data).

On the other hand, the data by Scheidegger and Sparks (1996) suggest that reversibility, albeit over longer time scales, may also be given under conditions where surface precipitates are formed. While this process is somewhat outside the scope of sorption, and presumably not likely to occur at trace levels, this is an important result in view of the use of the K_d concept.

The studies discussed above also point to a potential methodological problem: while the experimental systems are checked for potential oversaturation of simple radionuclide-bearing phases (e.g. Ni-hydroxide), they are typically never screened for supersaturation of more complex minerals, such as mixed radionuclide-Al layered double hydroxides. Therefore, much of the available evidence may come from systems that are essentially oversaturated with respect to more complex radionuclide mineral phases.

For example, Rabung et al. (2005) determined through spectroscopy (TRLFS) in their study of Cm(III)/Eu(III) sorption on Ca-montmorillonite that at high pH, Cm can become incorporated in a freshly formed portlandite or CSH-precipitate.

While the clay surface may thus serve as a nucleation template, it can be doubted that the radionuclide minerals would not form in the long term in the absence of the clays (given the same solution composition). Thus, the formation of new mineral phases in sorption experiments may be related more to uncertainties in the overall geochemical characterisation of the pore solution rather than to actual sorption processes.

Sorption competition, redox reactions, influence of ligands

In the actual KBS-3 concept, several radionuclides, inactive metals (corrosion products and other-contaminants) and groundwater components will be present simultaneously in the porewater of the bentonite buffer. Competitive sorption effects may influence the migration of radionuclides. Bradbury and Baeyens (2005) performed a systematic experimental evaluation of sorption competition on montmorillonite. Basically, they matched a number of elements at various concentration levels in sorption experiments (with pH generally > pH 6) to examine which combinations would show competition effects. Concentrations of the competing element were chosen so that the so-called strong sites (or high-energy sites HES according to the model by Bradbury and Baeyens (1997)) would be saturated. Further experiments were done by Soltermann et al. (2014b). Competition effects were detected within the following groups listed below, but notably not between these groups:

- Divalent – Co(II), Ni(II), Zn(II), Fe(II).
- Trivalent – Eu(III), Nd(III), Am(III).
- Tetra/hexavalent – Th(IV), U(VI).

The still preliminary conclusion from these data is that competitive effects are selective, i.e. metals with similar chemistries (valence state, hydrolysis behaviour) compete with one another, but metals with dissimilar chemistries do not.

Soltermann et al. (2014a, b) investigated competition in a redox-sensitive system. Under reducing conditions, traces of Zn(II) sorbed on montmorillonite were efficiently competed against by higher concentrations of Fe(II). On the contrary, trace concentrations of Fe(II) did not experience competition by Zn. Spectroscopic investigations showed that the adsorbed traces of Fe(II) had been oxidised to Fe(III) by structural reduced Fe present in the montmorillonite structure.

It is pointed out in NEA (2012) that the quantitative understanding of sorption in complex systems is hampered by the lack of systematic experimental data in the presence of typical groundwater constituents. For example, carbonate is one of the most important inorganic ligands for lanthanide and actinide ions, and thermodynamic modeling would suggest that complexation strongly decreases radionuclide sorption. However, sorption data for lanthanids and actinides obtained as a function of pH in the presence of carbonate show that sorption decreases less than expected, which points to the formation of ternary metal-carbonate-surface complexes, which need to be included in the models (Marques Fernandes et al. 2008). Follow-up spectroscopic analysis confirmed these findings, providing clear evidence for the formation of ternary Cm(III)-carbonate surface complexes (Marques Fernandes et al. 2010).

Time perspective

Sorption in the buffer is an important process for the retention of many radionuclides. The timescales that are of interest are dependent on the half-life of the individual nuclide. If the travel time through the buffer is of the same order of magnitude or longer, sorption is of great importance for the amount released. If the travel time through the buffer, including retardation from sorption, is short in comparison to the half-life of the radionuclide, the sorption process is less important.

An ion exchange process is fast, so the dissolution rate of other minerals and the transport rate in groundwater and bentonite pores will control ion exchange from Na^+ to Ca^{2+} end member. Relevant changes in buffer properties are expected to occur on the hundred-thousand-year scale (Bruno et al. 1999). It has to be pointed out further that modelling the conversion of Na- to Ca-bentonite by

implementing ion exchange in a mixing-tank type of model, as in Bruno et al. (1999), is in all likelihood a pessimistic approach, in the sense that it overestimates the rate of the exchange process: A certain cation concentration is required to compensate for the diffuse layer charge in the pore space (Ochs et al. 2004, Birgersson and Karnland 2009). While the maximum concentration of Ca is limited by the solubility of calcite or gypsum, the concentration of Na is not limited, and it is doubtful that a full conversion to the Ca-form is possible under these conditions.

Natural analogues/observations in nature

While a detailed interpretation of sorption processes is often not possible, natural analogues offer clear evidence that migration of sorbing radionuclides occurred only over limited distances away from a source in clay-rich substrates (Smellie and Karlsson 1996). Many bentonite deposits contain porewater with high salinities, indicating that soluble accessory minerals are not leached over very long timescales.

Handling in the PSAR

Before saturation: The process is neglected.

After saturation: Ion exchange is included in the scenario-specific modelling of the buffer chemical evolution for the thermal phase and the post-thermal long-term phase, see heading “Handling” for process alterations of impurities (3.5.6).

Failed canister: Sorption is included in the modelling of radionuclide transport for the long-term phase, see heading “Handling” ” for the process transport of radionuclides in the water phase (3.6.2). Sorption is treated through element-specific K_d values derived for specific conditions (see the **Data report** and Ochs and Talerico (2004) for the definition of data and associated uncertainties).

The fundamental assumption of reversibility, brought up at the beginning of this section, can be confirmed if:

- at least similar timeframes are considered for sorption and for desorption; but it seems that in many cases, desorption will be somewhat slower than sorption;
- there is a significant gradient or driving force for desorption (e.g. dilution, change in chemical conditions, presence of a competing sorbent), with removal of desorption products being a prerequisite for maintaining such gradients,

Exceptions to this are mainly reactions that lead to additional processes other than sorption, in particular incorporation or precipitation. For the case of alkali elements, the main mechanism would be the collapse of certain expandable 2:1 layer structures at high surface loading. However, this is not relevant for smectite clays, due to their relatively small permanent layer charge. With regard to the formation of surface precipitates of hydrolysable elements, the available evidence suggests that this may be mainly important at relatively high dissolved concentrations. Whether this process may also be important at radionuclide trace concentrations cannot be concluded with certainty to date. Further, surface precipitates may re-dissolve over sufficiently long timeframes. Based on the presently information, there is no reason to assume irreversibility of sorption reactions of radionuclides on clays under relevant conditions.

Boundary conditions: See sections referred to above.

Influences and couplings: Dependence on buffer properties as well as composition and pH of the porewater in the buffer, resulting from bentonite-groundwater interaction, is considered in selecting sorption constants for radionuclide transport. Because of the conditional nature of sorption constants, the data selected can be derived for several sets of relevant safety assessment conditions, if appropriate. Temperature effects are not considered explicitly, but the effects within the temperature range expected in the repository are deemed to be covered with good margin by the uncertainties associated with the selected K_d values. For the influence of ion exchange and surface acid-base equilibria on buffer chemical evolution, see Alteration of accessory minerals (3.5.6); these processes are also taken into account in the derivation of radionuclide K_d values.

Uncertainties

Uncertainties in mechanistic understanding

Both conceptual understanding and a large quantity of measurement data exist for simplified systems. Detailed reviews of sorption processes, underlying experimental data, model results, as well as the relationship to performance assessment can be found in e.g. NEA (2012). In particular, it has been shown that thermodynamic sorption models developed for purified Na-montmorillonite can be applied to Ca-montmorillonite (Bradbury and Baeyens 1999), and that such models give results for compacted bentonite that are compatible with diffusion data (Tachi et al. 2014, Tachi and Yotsuji 2014). To date, there is no doubt that sorption processes are well understood in a quantitative way and in terms of thermodynamic description, and that this understanding can be used to make educated and robust predictions of K_d values to be used in safety assessment calculations (see e.g. Marques Fernandez et al. 2016 and the overview given in NEA 2012). Due to the sheer number of possible combinations of relevant parameters there will nearly always be a lack of experimental data for understanding and predicting the influence of all relevant variables on radionuclide sorption, and this has to be taken into account in evaluating uncertainties of K_d values (**Data report**, Ochs and Talerico 2004, NEA 2012).

In the case of some of the more "exotic" radionuclides, the underlying thermodynamic database is insufficient to quantitatively evaluate their behaviour for different conditions.

Model simplification uncertainties in the PSAR

As pointed out above, the K_d concept for radionuclide transport modelling is basically justified under conditions far from surface saturation, which can be expected in the case of diffusion-limited radionuclide migration in a bentonite buffer. At the same time, it is clear that a K_d is a highly conditional parameter in terms of chemical conditions (pH, ionic strength, etc) and has to be derived for each set of conditions. This was done in the case of data selection for the SR-Can assessment using a semi-quantitative, traceable procedure to transfer K_d data from experimental to safety assessment-specific conditions (Ochs and Talerico 2004). The same approach will be used in the PSAR. For several elements, it was possible to use state of the art thermodynamic sorption models to derive K_d values for the specified conditions. The model-derived data were in all cases within the uncertainty range of the values that had been derived using the semi-quantitative conversion procedure. This strongly suggests that for the specified conditions, use of a sorption model and direct use of recommended K_d values would lead to consistent results (i.e., use of K_d would not introduce additional uncertainties, provided the conditions remain constant). To avoid potential problems related to the direct use of K_d in cases where conditions may vary to some degree (or to avoid re-derivation for each condition), thermodynamic sorption models could be directly coupled with transport codes (see Section 3.5.6). Again, for some radionuclides, not enough systematic sorption data for the relevant conditions are available to date to develop or sufficiently constrain thermodynamic models.

As long as the bentonite buffer can be expected to represent a homogeneous geochemical compartment, no spatial variability needs to be taken into account.

Input data and data uncertainties in the PSAR

K_d values are input directly to the PSAR for use in consequence calculations. K_d values for radionuclides for various conditions, as well as the associated uncertainties are given in Ochs and Talerico (2004), from which data for consequence calculations are chosen in the **Data report**.

3.5.4 Aqueous speciation and reactions

Overview

When the buffer is saturated, the water content is about 40 vol%. The composition of this water will be determined by the composition of the porewater present at deposition, the composition of groundwater at the site, reactions with the buffer and canister material and the accessory minerals in the bentonite. Within the aqueous phase, chemical reactions will take place and the final composition of the water can be determined by thermodynamic and kinetic calculations. Usually aqueous speciation reactions are fast, i.e. controlled by thermodynamics. Examples are reactions such as:

$HCO_3^- \leftrightarrow CO_3^{2-} + H^+$ and $HS^- + H^+ \leftrightarrow H_2S(aq)$

Dependencies between process and buffer variables

Table 3-12 summarises how the process influences and is influenced by all buffer variables and how these effects are treated in the PSAR.

Boundary conditions

By definition, this process takes place in the porewater. The boundary conditions will be the canister, the groundwater, the bentonite and the accessory minerals.

Model studies/experimental studies

Direct measurements of the porewater composition in compacted bentonite are virtually impossible. Limited amounts of water can be squeezed out under high pressure, but the composition of that water may not be representative of the porewater in situ. The concentration of non-sorbing elements with high solubility can be measured by total dispersion of the bentonite sample in water. Still, this only gives the total amount and reveals nothing about the speciation in the bentonite.

Modelling of the chemical composition/speciation of the porewater is done with an integrated model for the chemical evolution in the near field. This is described in Section 3.5.6. Speciation of radionuclides is discussed in the **Fuel and canister process report** (process Speciation of radionuclides).

Natural analogues/observations in nature

Not applicable, since natural analogues are usually studied for water rock interactions and not for the water phase alone.

Time perspective

The process is important for all repository timescales.

Handling in the safety assessment the PSAR

Before saturation: Geochemical processes will be the same before and after saturation. This is just a matter of water flow and solute transport, something to be considered in other sections. Temperature is another variable of high relevance for aqueous speciation and reactions, as all thermodynamic constants are temperature dependent.

After saturation: The process is included in the scenario-specific modelling of the buffer chemical evolution for the thermal phase and the post-thermal long-term phase. This is described in Section 3.5.6.

Failed canister: In the case of a failed canister, vast amounts of metallic iron, originating from the cast iron canister insert, will be added to the geochemical system. This will be included in the model mentioned above, as a dedicated calculation case.

Boundary conditions: See Alteration of accessory minerals (3.5.6).

Handling of variables influencing this process: The modelling is in itself a coupling of the four (groups of) processes mentioned above and thus a coupled modelling of most of the significant long-term chemical processes. A large number of the variable influences related to the chemical conditions (porewater composition, montmorillonite composition, and bentonite composition) are also included.

Handling of variables influenced by the process: The chemical composition of the porewater is calculated. The result may have influence on the processes osmosis (3.5.7), montmorillonite alteration (3.5.8) and Iron-bentonite interaction (3.5.9)

Table 3-12. Direct dependencies between the process "Aqueous speciation and reactions" and the defined buffer variables and a short note on the handling in the PSAR.

Variable	Variable influence on process		Process influence on variable	
	Influence present? (Yes/No) Description	**Handling of influence (How/Why not)**	**Influence present? (Yes/No) Description**	**Handling of influence (How/Why not)**
Buffer geometry	Yes, the total amount of minerals in the buffer and the bentonite/ porewater ratio affects the process	The geometry and the bentonite mass, as well as the bentonite/ porewater ratio is considered in the model	No	
Pore geometry	Yes. the ratio between accessory minerals and porewater	Included in the initial conditions	Yes. Precipitation-dissolution of minerals	Variation in porosity is considered through the effect of "cementation", which is included in the model
Radiation intensity	No	Only very high radiation fields could influence the processes	No	
Temperature	Temperature strongly influences the extent of mineral – porewater reactions	Temperature and temperature gradient is included in the chemical model	No	
Water content	Yes, could affect concentrations	The saturation phase will be considered	Precipitation-dissolution of accessory minerals modifies the porosity	The effect on the overall porosity is small and not accounted for
Gas content	An indirect effect from water content variations		Yes	Dissolved gases are included in the model
Hydrovariables (pressure and flows)	Yes	Darcy flow is included in the model	No	
Stress state	Yes	Partial pressures of gases are included in model	Yes	The results from the model are evaluated to consider effects on swelling pressure
Bentonite composition	Yes	Compositional data are considered in model	Yes	The evolution of the composition is calculated with the model
Montmorillonite composition	Yes	Compositional data are considered in model	Yes	The evolution of the composition is calculated by the model
Porewater composition	Yes	Compositional data are considered in model	Yes	The evolution of the composition is calculated by the model
Structural and stray materials	Potentially, The degradation of these materials can affect the chemical evolution of the system	No stray materials are considered in the buffer. However, effects of other system components are considered	Potentially, Secondary mineral formation/ dissolution may influence the alteration of structural and stray materials	Secondary mineral formation/dissolution is considered

Uncertainties

Uncertainties in mechanistic understanding

The model assumes that the chemistry of the porewater is identical to the chemistry in free water. The effect of the bentonite surface and structure is not included (except ion-exchange). It is not clear if or how this will affect the chemistry. See also Osmosis (3.5.7).

Model simplification uncertainties in the PSAR

For uncertainties regarding mineral reactions and porewater composition Section Alteration of accessory minerals (3.5.6).

Input data and data uncertainties in the PSAR

For uncertainties regarding mineral reactions and porewater composition see Alteration of accessory minerals (3.5.6).

3.5.5 Gaseous speciation and reactions

Overview

The buffer is installed with a water ratio of ~17 %. The volume of air in a deposition hole after installation is 2.6 m^3 (Table 2-4). This volume will decrease with time as the buffer takes up water from the surrounding rock (see Section 3.3.1). At the Forsmark site, the time for full saturation of the buffer is expected to vary between a few tens of years and a few thousands of years depending on the local hydrogeological conditions (Sellin et al. 2017). This means that a gas phase will persist over this period. The original gas composition is basically air, but this may evolve with time as the gas interacts with the other system components.

As the pressure in the repository increases, the gas will dissolve in the porewater in the bentonite according to Henry's law. Gas components dissolved in the porewater may also enter the gas phase. This means that the gas composition will change in time. The gas phase will be in equilibrium with the aqueous phase. In the chemical modelling in SR-Site, the gas composition was calculated as equilibrium partial pressures with the water phase, but the results were not used further in the assessment. For chemical reactions within the bentonite, this treatment is sufficient. However, the gas may interact with the copper canister and from that respect it may be important to assess the composition of the gas phase. The corrosion mechanism may be different in an unsaturated environment and the diffusivity of gaseous species in the bentonite is significantly higher in the gas phase than for dissolved species in the aqueous phase.

The main component in air is nitrogen which is expected to have a limited chemical effect in the repository environment. Dissolved oxygen, on the other hand, is potentially reactive with the copper canister and minerals in the buffer (see 3.5.6). Oxygen molecules will then be transferred from the gaseous phase to the aqueous to maintain the equilibrium. Carbon dioxide is present in the air and dissolved CO_2 may react with components in the water to form minerals (e.g calcite). CO_2 may also form from dissolution of minerals already present in the buffer (see 3.5.6). The content in the gas phase may increase and decrease dependent on the chemical conditions. Gaseous hydrogen sulphide (H_2S) is one of the more interesting gaseous species since it may react with the copper canister. Normal air contains no H_2S, but aqueous H_2S could potentially be formed by dissolution of sulphide minerals in the buffer or by microbial sulphate reduction (see 3.5.15). Other gaseous components that could be considered are hydrogen, methane and possibly other organic gases.

The composition of the gas phase will be determined by the composition of the gas present at deposition, the composition of groundwater at the site, reactions with the buffer and canister material and the accessory minerals in the bentonite. The reactions are assumed to occur in the water phase, while the gas phase is assumed to be in equilibrium with the water.

Dependencies between process and buffer variables

Table 3-13 summarises how the process influences and is influenced by all buffer variables and how these effects are treated in the PSAR.

Table 3-13. Direct dependencies between the process "Gaseous speciation and reactions" and the defined buffer variables and a short note on the handling in the PSAR.

Variable	Variable influence on process		Process influence on variable	
	Influence present? (Yes/No) Description	**Handling of influence (How/Why not)**	**Influence present? (Yes/No) Description**	**Handling of influence (How/Why not)**
Buffer geometry	Yes, the total amount of gas in the buffer and the bentonite/ porewater ratio affects the process	Included in the calculations of canister corrosion. The volume is included in the expression. (See the **Fuel and canister process report**).	No	
Pore geometry	Yes. Affects the volume available for gas	Included in the calculations of canister corrosion. The volume is included in the expression. (See the **Fuel and canister process report**).	No	
Radiation intensity	Yes, radiolysis may affect the gas composition	Included in the calculations of canister corrosion (See the **Fuel and canister process report**).	No	
Temperature	Temperature influences pressure and the equilibrium constant	Fixed temperature is assumed in the calculations	No	
Water content	Yes, will affect gas volume	The saturation phase will be considered	No	
Gas content	An indirect effect from water content variations	The saturation phase will be considered	Yes	Dissolved gases are included in the model
Hydrovariables (pressure and flows)	Yes, the pressure will affect the equilibrium	Henry's law	No	
Stress state	No		No	
Bentonite composition	Indirectly through Aqueous speciation and reactions (3.5.4)	Compositional data are considered	Indirectly through Aqueous speciation and reactions (3.5.4)	The evolution of the composition is calculated with the model
Montmorillonite composition	Indirectly through Aqueous speciation and reactions (3.5.4)	Compositional data are considered in model	Indirectly through Aqueous speciation and reactions (3.5.4)	The evolution of the composition is calculated by the model
Porewater composition	Yes	Henry's law	Yes	Henry's law
Structural and stray materials	Indirectly through Aqueous speciation and reactions (3.5.4)	No stray materials are considered in the buffer. However, effects of other system components are considered	Indirectly through Aqueous speciation and reactions (3.5.4)	Secondary mineral formation/dissolution is considered

Boundary conditions

By definition, this process takes place in the in the unsaturated part of the buffer. The boundary conditions will be the canister, the porewater, the bentonite and the accessory minerals.

Model studies/experimental studies

Svensson et al. (2017b) performed experiments with Ibeco backfill (Milos, Greece) and MX-80 (Wyoming, USA) bentonite and in selected cases sulphide solutions. The main target was to determine the solubility of the sulphides in the bentonites and their equilibrium concentrations. The concentration was determined to be lower than the limit of quantification of the methylene blue method, however, oxidation and/or H_2S loss, may have caused a lowering of the sulphide concentration in the samples, thus introducing an uncertainty (Figure 3-22). Sulphide was also added in some samples, and when sulphide was added as Na_2S solution, the results indicated that the bentonite reduced the amount of sulphide in the solution. The mechanism of this can be absorption or some kind of transformation or reaction with the sulphide, but these details are currently unknown. The observation that bentonite reduces the amount of sulphide in solution when Na_2S is added supports that no sulphide could be detected when Na_2S was not added.

From the sulfide content in the water, the H_2S content in the gas phase can be calculated by Henry's law. A total sulfide content (sum of H_2S and HS^-) of 10^{-6} M, a pessimistic value based on the detection limit in the previous paragraph, in the pore water and with pH=7 (pessimistic pH of the bentonite, see, for example, Figure 5-14 in Sena et al. 2010a) corresponds to an H_2S concentration of 3.9×10^{-7} mol/L, which gives a gas phase in contact with the pore water a partial pressure of H_2S at $10^{-5.4}$ atm, that is, a sulfide content in the gas phase of 1.7×10^{-4} mol / m^3.

Eriksson and Hedin (2019) studied how sulphide in the form of gaseous H_2S diffuses in the gas phase of the unsaturated bentonite backfill and buffer to the copper canister where it is assumed to react with the copper and cause corrosion. Primarily, a case where the initial water content of the clay system is unchanged was considered. This is relevant for a dry site, as Forsmark in Sweden, where saturation may take hundreds of years or longer (Sellin et al. 2017). As the bentonite saturates, the air phase in the bentonite will be reduced and the diffusion of H_2S will slow down and finally, when full saturation is reached, the diffusion in the gas phase will stop. Such a case was also studied, to illustrate the impact of saturation.

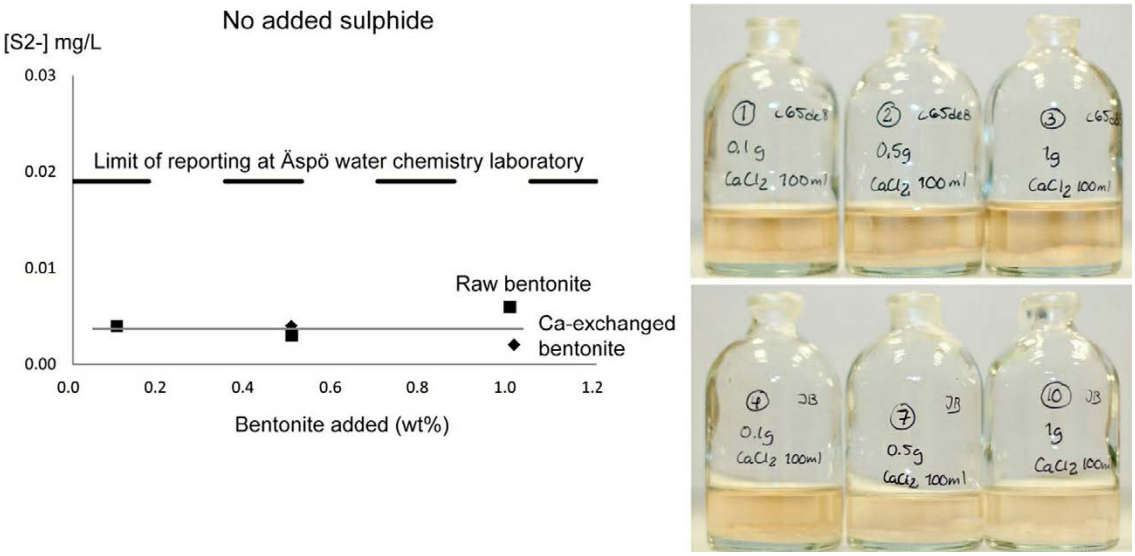

Figure 3-22. *The measured sulphide content in the solution after the addition of different amounts of Ibeco BF bentonite. All points below limit of quantification (LOQ) 0.019 mg/L. Limit of detection is 0.006 mg/L. Uncertainty in the measurements is approximately ± 32 %. Lines were added as guides for the eyes.*

The Full-scale Emplacement (FE) experiment is a spent fuel emplacement drift constructed at full scale according to the Swiss concept for radioactive waste disposal. The experiment is located in the Underground Rock Laboratory at Mont Terri (Switzerland). During backfilling and after sealing of the FE experiment, the gas composition in the bentonite buffer pore space showed very rapid changes. A decrease of the O_2 concentration from the atmospheric value of 21 % v/v to less than 0.1 % v/v within a few months was observed (see Figure 3-23) (Giroud et al. 2018). Hydrogen gas, which indicates anaerobic conditions, was detected less than two months after the construction of the retaining wall. Until recently, aerobic conditions were expected to prevail for a period ranging from a few years to a few decades (Wersin et al. 2003, Landolt et al. 2009, Senger 2015). This considerable mismatch between prediction and measurement indicates that there is a lack of understanding of in-situ processes which influence the evolution of the gas phase in a deep geological repository. Oxygen sensors located closest to the plug in the bentonite buffer show higher concentrations than sensors located at the far end of the FE tunnel and a positive correlation with the atmospheric pressure in the FE access niche has been observed. This may indicate either an experimental artefact which might potentially affect the other gases (gas flow along sensor lines or through the plug) or show transport of gases within the Excavation Damaged Zone (EDZ).

Giroud et al. (2018) reports experiments where about 15 g of granulated bentonite were filled in open glass vials which were placed into the stainless-steel bottles that were subsequently sealed airtight. The initial gas phase in the sealed bottles was atmospheric air at ambient pressure. In the experiment presented in this section all bottles were kept at laboratory temperature (~ 23 °C). The relative humidity in the laboratory atmosphere is about 55 %. As the used granular buffer material (GBM) was rather dry (approximately 6 % water ratio), the RH in the bottles was not expected to exceed this value during the measurements at ambient temperature. The experiment lasted approximately 17 days. The second bottle containing a bentonite aliquot was treated slightly differently. Starting from day 14, all the measurements were stopped, and the second bottle was heated at 100 °C for one day. From day 15 the measurements started again and were performed until day 17. Figure 3-24 summarizes the results of this heated experiment. The observation of a decrease in the partial pressure of Ar and Kr (i.e., chemically inert gas species) makes the case that bentonite can adsorb gases.

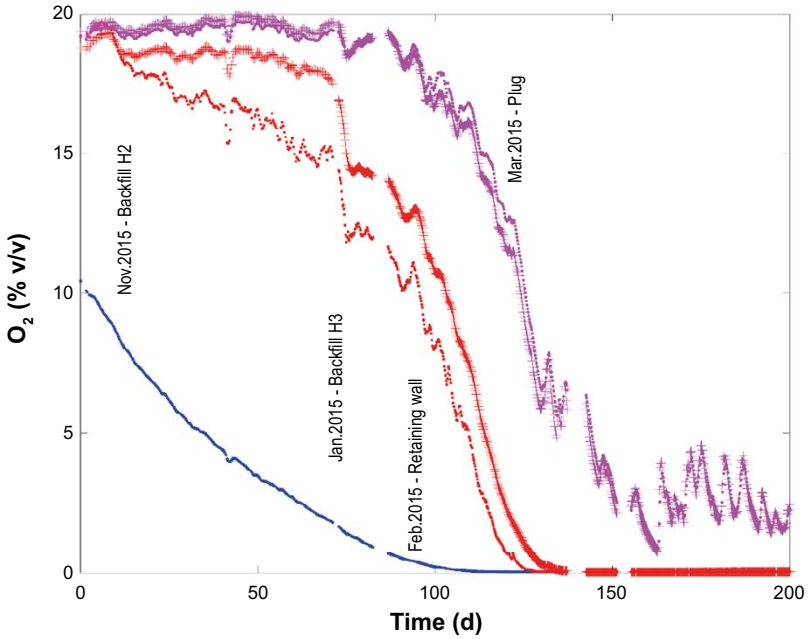

Figure 3-23. *Oxygen concentrations measured in the backfill pore space of the FE experiment. Different colors correspond to different depth ranges within the FE drift (Giroud et al. 2018).*

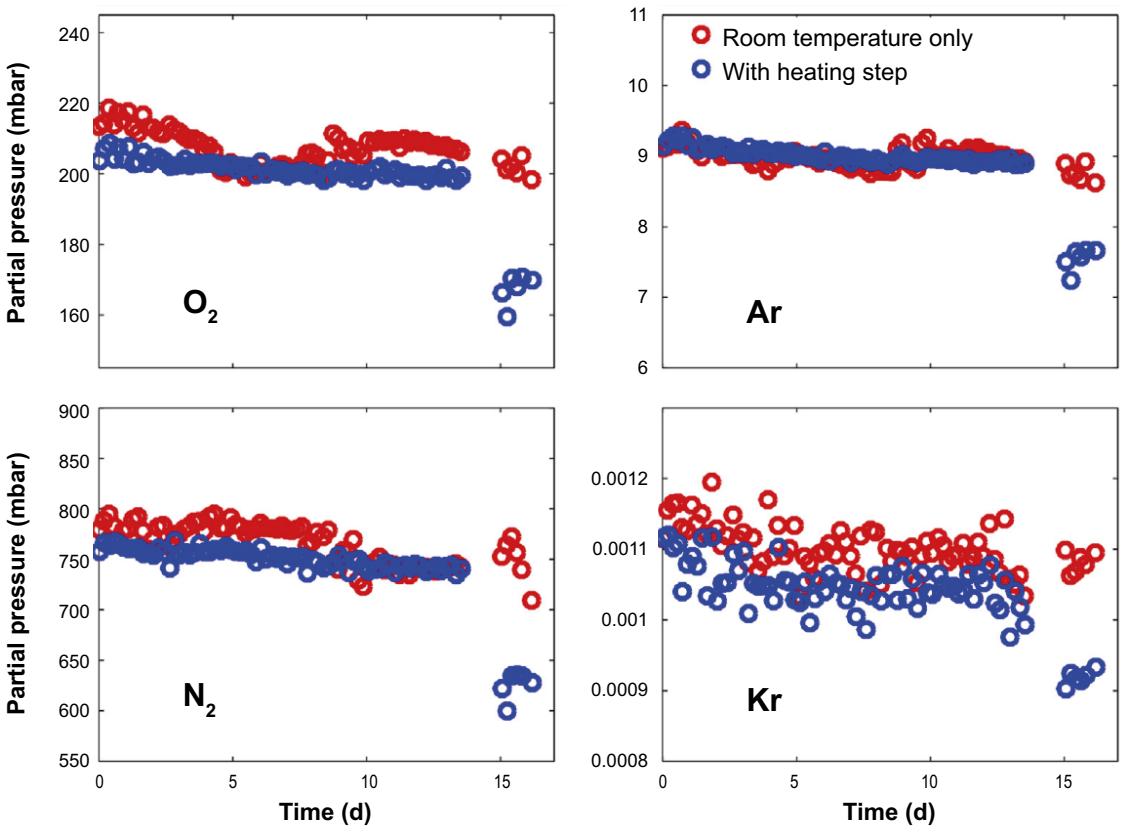

Figure 3-24. *Gas partial pressures determined during the measurement of the gas composition in airtight sealed bottles containing untreated bentonite. After a heating step of 1 day at 100 °C, the partial pressures of all gases in the respective bottle (blue circles) drop significantly compared to the partial pressures in the bottle kept at ambient temperature (red circles) (Giroud et al. 2018).*

Birgersson and Goudarzi (2018) reports about two tests that were designed and conducted in order to investigate the possible evolution of gases in the buffer of an unsaturated KBS-3 repository. One of the tests included a central heater in form of a copper tube as well as IBECO RWC bentonite blocks and pellets, configured to form a scaled model of an isolated unsaturated KBS-3 buffer (10 cm copper tube, approximately 30 cm bentonite block diameter). The other test was conducted in isothermal (room temperature or 50 °C), isolated conditions, and involved only bentonite pellets. The evolution of the oxygen concentration in the tests was monitored by occasional measurements using an in-situ system. At the end of the tests, gas was sampled and analysed in a dedicated accredited laboratory (Table 3-14). The tests were conducted over the course of approximately one year. Although the bentonite used was chosen due to its rather high sulfur content, no sulphide gas was detected in any of the samples. This result is a strong indication that such gas is not to be expected under semi-dry repository conditions. Furthermore, pronounced oxygen consumption was noted in the test involving a copper tube – after approximately 50–60 days, the oxygen concentration was about 1 % (Figure 3-25). In contrast, the test which did not include a copper component showed no noticeable oxygen consumption at room temperature. From this difference in behaviour it can be concluded that oxygen is mainly consumed as a consequence of aerobic copper corrosion. The gas samples were also analysed for carbon monoxide, methane, and other light hydrocarbons. None of these compounds were detected. A noticeable carbon dioxide level was detected in both tests (above 1 %). A tentative explanation for this is carbonate dissolution as a consequence of pyrite oxidation and associated acidification.

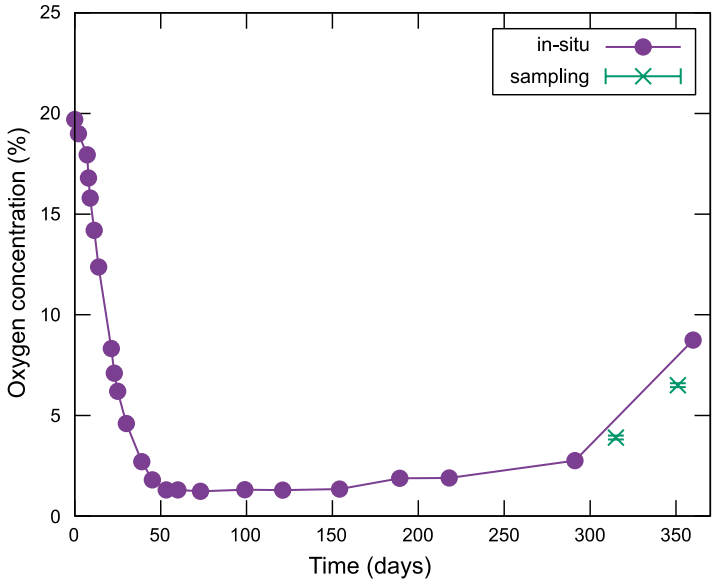

Figure 3-25. *Oxygen evolution in the thermal gradient test. The heater was switched on after 7 days. Sampling was performed at day 315 and day 351 (Birgersson and Goudarzi 2018).*

Table 3-14. Gas composition of the analysed samples. Unit is vol-% except for H_2S. TG are tesst with copper heater and a temperature gradient. IT are isothermal tests with pellets (Birgersson and Goudarzi 2018).

Sample	TGT01	TGT02	IT01	IT02
O_2	3.9	5.9	19.1	19.5
N_2	94.6	91.0	79.7	77.8
H_2	0.1	0.1	0.1	0.1
CO_2	1.5	1.3	1.2	0.9
CO	< 0.1	< 0.1	< 0.1	< 0.1
CH_4	< 0.1	< 0.1	< 0.1	< 0.1
H_2S	< 0.1 ppm	< 0.1 ppm	< 0.1 ppm	< 0.1 ppm

There are two reported experimental determinations of the oxygen consumption rate in bentonite. Lazo et al. (2003) performed their experiments in bentonite/water slurries of different densities. Two kinds of bentonite were studied, MX-80 and Montigel. The dissolved oxygen disappeared in about five days in these experiments. It was observed, however, that pyrite oxidation is perhaps not the main process for O_2 consumption, as MX-80 contains 0.3 % FeS_2 while Montigel bentonite has a negligible amount. Another possible mechanism for O_2 consumption could be oxidation of Fe(II) from siderite or in the alumino-silicate framework of the bentonite. The microbial activity was suppressed by the use of a microbial inhibitor (NaN_3). The microbial O_2-consumption may not have been completely eliminated, but the results suggest that microbial O_2 consumption was very limited in the bentonite suspensions (Lazo et al. 2003). Preliminary determinations of oxygen depletion in bentonite by Muurinen and Carlsson (2007, 2010) also indicate rapid oxygen consumption.

Åkesson and Laitinen (2022) investigated the temperure dependence of O_2 consumption in a Milos bentonite. The experiments were performed in an isothermal setup with a glass container in a heating cabinet. The temperature dependence of the rate of O_2 consumption was evaluated from data measured during the initial phase of five of the tests performed in glass container. Two of these were performed at 70 °C, two at 50 °C and one at 40 °C. The oxygen consumption rates used in the evaluation was simply defined as the concentration decrease per unit time (i.e. %/day). This was deemed to be sufficiently detailed, since the bulk mass and the water content in the different tests were quite similar.

From these evolutions, the following consumption rates were evaluated: 4.5, 1 and 0.1 %/day for 70, 55 and 40 °C, respectively (Figur 3-26, upper row). By plotting the logarithm of these consumption rates versus the inverse of the absolute temperature (Figur 3-26, lower left), an activation energy of approximately 0.11 MJ/mol can be evaluated. A comparison of an exponential temperature dependence with this activation energy and the evaluated consumptions rates is shown in Figur 3-26 (lower right).

In all tests, relatively high amounts of CO_2, together with measureable quantities of H_2S and SO_2 were detected. Since there were no metals in the glass container, and since a clear generation of SO_2 could be measured, it appears to be quite evident that oxygen is consumed through pyrite oxidation. This process probably occurs in the presence in water, since the O_2 concentration reduction exceeds by far the concentration of SO_2. The formation of CO_2 indicates the dissolution of calcite. This process requires the formation of H^+, which in turn also indicates pyrite oxidation in the presence of water. Pyrite oxidation would though not lead to the formation of H_2S, if the sulphur is oxidized. Pyrite dissolution, possibly aided by a local low pH, could be the source of H_2S, and thus both reactions seem operable at the same time.

Natural analogues/observations in nature

Not applicable, since natural analogues are usually studied for water rock interactions and not for the gas phase alone.

Time perspective

The process is only relevant until the buffer is saturated. The time for buffer saturation will vary strongly between different deposition holes. The minimum value is around 10 years and the maximum is less than 10 000 years (Sellin et al. 2017).

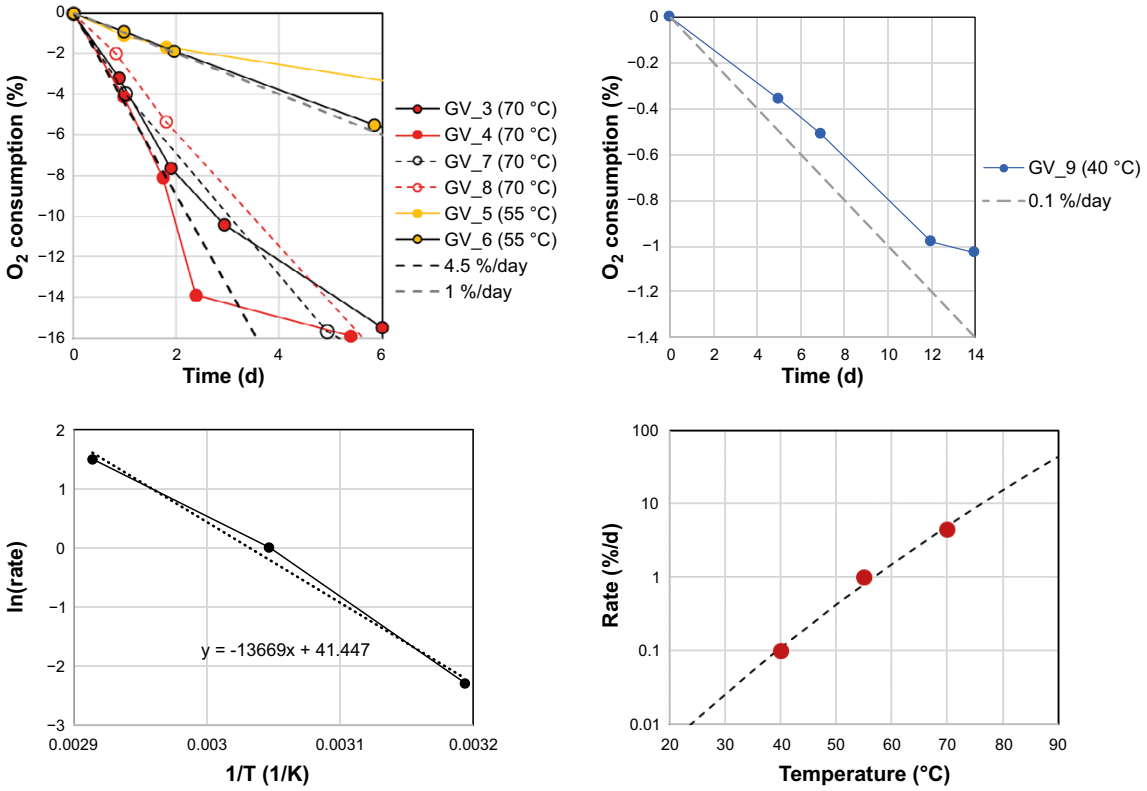

Figur 3-26. *Evaluation of temperature dependence of the rate of oxygen consumption in tests in glass containers. Evolution of O2 consumption in five tests (upper row). Arrhenius plot (lower left) and exponential temperature dependence together with measure consumptions rates (lower left) (Åkesson and Laitinen 2022).*

Handling in the PSAR

Before saturation: Canister corrosion from O_2 and H_2S in a gas phase is included in the assessment of canister lifetime (see the **Fuel and canister process report**).

After saturation: Excluded by definition.

Failed canister: In the case of a failed canister, hydrogen will be generated from the corrosion of the canister insert. Radionuclides may enter the gas phase. This is not included in the discussion in this section is covered by the processes Gas dissolution/transport (3.3.3) and Transport of radionuclides in a gas phase (3.6.3).

Boundary conditions: The process is limited to the unsaturated part of the buffer.

Handling of variables influencing this process: Gas volumes are given as initial condition and calculated as a function of saturation (e.g. Eriksson and Hedin 2019). The gas composition can be calculated with Henry's law together with the composition of the porewater. The composition of the porewater is dependent on reactions with minerals in the buffer; see processes Alteration of accessory minerals (3.5.6) and Aqueous speciation and reactions (3.5.4).

Handling of variables influenced by the process: The chemical composition of the porewater is calculated with Henry's law together with the composition of the gas phase.

Uncertainties

Uncertainties in mechanistic understanding

The key uncertainty regarding oxygen is the consumption by the bentonite. Some references show a rapid consumption, while others show no reactivity. This is discussed further in the **Fuel and canister process report**.

The key uncertainty regarding hydrogen sulfide is the concentration of dissolved sulfide species in the porewater. The concentration is expected to be low based on low solubilities of sulfide minerals and this is probably the case based on the findings in Svensson et al. (2017b).

Sorption of gaseous species onto the bentonite would potentially lower the concentrations in the gaseous phase. This is pessimistically neglected in the assessment. The relative effect is also rather small as seen in Figure 3-24.

Model simplification uncertainties in the PSAR

Henry's law is sufficiently accurate. For uncertainties regarding mineral reactions and porewater composition see Section Alteration of accessory minerals (3.5.6).

Input data and data uncertainties in the PSAR

As seen in Sander (2015) the uncertainties for the Henry's law constants for O_2 and H_2S are very low. For uncertainties regarding mineral reactions and porewater composition see Section Alteration of accessory minerals (3.5.6).

3.5.6 Alterations of accessory minerals

Overview

The buffer material consists not only of montmorillonite, but also accessory minerals as well as accessory minerals. The mineral composition of MX-80 bentonite can be found in Section 2.2.1. In the repository environment, these accessory minerals can dissolve and sometimes re-precipitate depending on the prevailing conditions.

The behaviour of these bentonite accessory minerals and their effect on the overall performance of the barrier depends on the interaction of groundwater with the bentonite buffer. The accessory minerals in bentonite are either stable or metastable in the environment where they were originally

mined. In the repository, however, they will be exposed to a fluid that differs in some respects from that at the original site, in terms of both composition and temperature. Most accessory minerals in the bentonite are nevertheless stable in contact with the granitic groundwaters prevailing in the Fennoscandian shield. The main potential effects on the bentonite buffer are cementation of the barrier (i.e. precipitation of large amounts of accessory minerals in specific parts of the buffer), changes in the montmorillonite composition, especially the exchangeable ions that can affect the swelling capacity of the bentonite and changes in the chemical composition of porewater, which can affect the retention capacity of the near-field system.

Moreover, evaporation of incoming groundwater during the saturation phase in the warmer parts may lead to different concentrations of dissolved elements at different positions in the buffer and the consequent redistribution of accessory minerals and changes in the montmorillonite composition, resulting in an overall heterogeneous composition of the bentonite.

Another aspect of interest is the behaviour of the buffer in contact with the potential corrosion products of the cast iron insert (see Section 3.5.9 Iron-bentonite interaction). Anoxic corrosion of the cast iron insert will generate iron in solution and hydrogen, both diffusing into the bentonite. Dissolved iron entering the bentonite can precipitate as new accessory minerals (e.g. magnetite), replace other major cations in the montmorillonite interlayer sites (cation exchange), or replace octahedral cations in the montmorillonite, which can result in montmorillonite transformation towards iron-rich clay minerals (see Section 3.5.8Montmorillonite transformation).

Dependencies between process and buffer variables

Table 3-15 summarises how the process influences and is influenced by all buffer variables and how these effects are treated in the PSAR.

Buffer geometry: The geometry of the buffer can affect the alteration of accessory minerals indirectly through transport of solutes in the groundwater and bentonite porewater, thus affecting geochemical reactions during its interaction. Moreover, buffer geometry determines the total proportion of accessory minerals able to react in the system due to the interaction of groundwater and bentonite.

Pore geometry: The pore geometry of the bentonite buffer affects the diffusive transport of solutes, which in turn affects the chemical composition of porewater at different points within the buffer and, therefore, the geochemical reactions taking place in the buffer. In addition, precipitation-dissolution of accessory minerals can modify the porosity distribution in the buffer as well as the pore geometry.

Radiation intensity: Only in the case of very high radiation fields; the chemical composition of buffer porewater can be modified and thus affects geochemical reactions involving accessory minerals.

Temperature: Thermodynamic constants of chemical reactions are dependent on temperature. The temperature gradient exerted by the waste canister will have a large impact on the dissolution-precipitation behaviour of accessory minerals, especially in those areas of the bentonite close to the canister. The effect of temperature on diffusion has not been considered.

Water content: The water content has an indirect effect on the alteration of accessory minerals. As the saturation process affects the transport of solutes, this in turn affects the chemical reactions. In addition, the coupled effect of temperature and saturation can result in significant changes in the redistribution of accessory minerals and on the chemical composition of buffer porewater. Precipitation-dissolution of accessory minerals can result in minor changes of porosity, and therefore the water-solid ratio or available porosity for water uptake. However, this change in porosity is expected to be very small.

Table 3-15. Direct dependencies between the process "Alteration of accessory minerals" and the defined buffer variables and a short note on the handling in the PSAR.

Variable	Variable influence on process		Process influence on variable	
	Influence present? (Yes/No) Description	**Handling of influence (How/Why not)**	**Influence present? (Yes/No) Description**	**Handling of influence (How/Why not)**
Buffer geometry	Yes, the total amount of minerals in the buffer and the bentonite/ porewater ratio affects the process	The geometry and the bentonite mass, as well as the bentonite/ porewater ratio is considered in the model	No	
Pore geometry	Yes. the ratio between accessory minerals and porewater	Included in the initial conditions	Yes. Precipitation-dissolution of minerals	Variation in porosity is considered through the effect of "cementation", which is included in the model
Radiation intensity	No	Only very high radiation fields could influence the processes	No	
Temperature	Temperature strongly influences the extent of mineral – porewater reactions	Temperature and temperature gradient is included in the chemical model	No	
Water content	Yes, could affect concentrations	The saturation phase will be considered	Precipitation-dissolution of accessory minerals modifies the porosity	The effect on the overall porosity is small and not accounted for
Gas content	An indirect effect from water content variations		Yes	Dissolved gases are included in the model
Hydrovariables (pressure and flows)	Yes	Darcy flow is included in the model	No	
Stress state	Yes	Partial pressures of gases are included in model	Yes	The results from the model are evaluated to consider effects on swelling pressure
Bentonite composition	Yes	Compositional data are considered in model	Yes	The evolution of the composition is calculated with the model
Montmorillonite composition	Yes	Compositional data are considered in model	Yes	The evolution of the composition is calculated by the model
Porewater composition	Yes	Compositional data are considered in model	Yes	The evolution of the composition is calculated by the model
Structural and stray materials	Potentially, the degradation of these materials can affect the chemical evolution of the system	No stray materials are considered in the buffer. However, effects of other system components are considered	Potentially, Secondary mineral formation/ dissolution may influence the alteration of structural and stray materials	Secondary mineral formation/dissolution is considered

Gas content: The formation of a gas phase (i.e. water vapour due to high temperature close to the canister) can modify the concentration of solutes in the porewater, and therefore the stability of accessory minerals. However, this process is only expected for the water saturation stage. Other gases are not expected to affect the behaviour of accessory minerals significantly. The formation of $H_2(g)$ can affect the chemical evolution of the system only in the case of anoxic corrosion of the cast iron insert or other steel components in the system.

Hydrovariables (pressure and flows): Transport of dissolved chemical species in the system can modify the dissolution-precipitation rates of accessory minerals by maintaining the saturation state of these phases far from equilibrium (i.e. fast water flows around the buffer).

Stress state: Increase in the partial pressure of gases can affect the stress in the system. The build-up of such partial pressures could be a direct consequence of the alteration of buffer accessory minerals.

Bentonite composition: This is one of the most relevant variables influencing the alteration of accessory minerals. The type and amount of accessory minerals (in addition to the montmorillonite content) determines how their dissolution-precipitation behaviour will affect the chemical evolution of the system. Moreover, the dissolution-precipitation of these mineral phases will modify the bentonite composition through their interaction with porewater.

Montmorillonite composition: The composition of montmorillonite, especially the cation exchangeable (type of cations and occupancy) is very relevant, as interaction with buffer porewater will modify the chemical composition of this porewater and, hence the dissolution-precipitation of accessory minerals in the bentonite. In addition, the alteration of bentonite accessory minerals will modify the chemical composition of bentonite porewater and hence the montmorillonite composition.

Porewater composition: The porewater composition will determine which of the accessory minerals in the bentonite will dissolve or precipitate.

Structural and stray materials: The interaction of bentonite porewater with structural and stray materials can result in modification of the chemical composition of porewater and, therefore, in the behaviour of accessory minerals and vice versa.

Boundary conditions

There are no particular boundary conditions to discuss for these processes. The relevant boundary conditions in order to treat the process quantitatively are those of the transport processes that control the exchange of solutes between the buffer porewater and the water in its adjacent components, i.e. the boundary conditions of the processes diffusion and advection.

The exchange of a number of solutes such as sodium and calcium ions, carbonate and oxygen is relevant to the alteration of accessory minerals.

Model studies/experimental studies

Experimental studies regarding cementation

Hydrothermal tests with purified standard bentonite (SWY-1) heated to 150–200 °C have shown that cooling leads to precipitation of siliceous compounds in various forms. The precipitation is assumed to cause cementation effects, including a strength increase, which has been demonstrated in several laboratory investigations (Pusch and Karnland 1988, Pusch et al. 2010).

According to these investigations, the extent of precipitation is dependent on the temperature. At the highest temperature in the buffer (90 °C), cementation was not of such a great extent that it could be regarded as problematic. The tests were carried out without a temperature gradient, which cannot be regarded as pessimistic conditions.

Precipitation of sulphate and carbonate could be observed in one-year experiments with hydrothermal treatment of MX-80. XRD analyses indicated that sulphates and calcite had gone into solution and had been transported to the hot iron surface, where they had precipitated. Based on a geochemical model (Pusch et al. 1993a), it is likely that feldspars dissolved, and quartz was enriched at the colder boundary. In the Buffer Mass Test in Stripa (max 90 °C), the buffer was analysed with respect to the

distribution of silica, but no definite conclusion could be drawn regarding possible enrichment in the coldest part (Pusch 1985). However, the study of cooling-related precipitation of silica predicted by the Grindrod/Takase/Pusch model was confirmed by the Kinnekulle case (Pusch et al. 1998).

In the LOT tests at Äspö HRL, buffer material is exposed to high temperature gradients (maximum 130 to 80 °C over a 10 cm distance). Material from the one year tests was analysed at 25 positions with respect to elemental distribution and rheological properties. No significant gradients were found for silica content. The tensile strength was slightly reduced and the tensile strain was slightly increased, which shows that no cementation had taken place in the major part of the buffer material. However, precipitation of (mainly) anhydrite was found in a 1–2 mm thick rim around the copper tube. The ongoing evaluation of the twenty-year tests (Sandén and Nilsson 2020) is expected to provide information on whether the precipitation is an effect of evaporation of the inflowing water as part of the saturation process, or if the process also continues after full water saturation.

Further large-scale tests conducted in Äspö HRL, as Canister Retrieval Test (Dueck et al. 2011a), Alternative Buffer Material (ABM) (Svensson et al. 2011), Temperature Buffer Test (Åkesson 2012) and Prototype Repository (Olsson et al. 2013) show similar results. All these tests were included temperature gradients (with maximum temperatures ranging from 95 to 166 °C) and *in situ* bentonite hydration (natural or forced). In all cases dissolution of gypsum occurs in the outer rim of the buffer and sulphate precipitates as anhydrite in the warmer part of the bentonite. Another effect reported in all these experiments is the increase in magnesium content in the inner bentonite rim, in the warmer part. The sink for this magnesium is still unknown, although the increase in the exchangeable sites has been discarded. In all cases magnesium seems to be incorporated in insoluble form, in octahedral sites of the smectite or as a newly precipitated phase. Another effect recorded in some of these experiments is the dissolution of carbonate minerals (i.e. calcite) near from the heated part of the buffer. However, this effect has only been described in those experiments with maximum temperatures exceeding 140 °C (Alternative Buffer Material and Temperature Buffer Test). None of these experiments reported the precipitation of additional siliceous phases.

Geochemical models

There are several types of models describing bentonite – porewater interaction:

1. Donnan equilibrium (osmosis) models, considering the entire layer charge (CEC) to be available for influencing solution chemistry; i.e. the CEC is balanced entirely by cations in solution. Clay pores are assumed to contain no bulk water at all. See Section 3.5.8 on osmosis.
2. Diffuse layer (DDL) models, where the CEC is assumed to be partly compensated by cations immobilised at ion exchange sites (giving rise to sorption of alkali and alkali earth elements) and partly by ions in a diffuse layer extending from the layer surface. Bulk solution in the pores can exist at low density and/or high ionic strength (Ochs and Talerico 2004, Wersin et al. 2004, 2016, Alt-Epping et al. 2014).
3. The ion exchange models used in the context of calculating clay alterations assume that the CEC is completely balanced by exchangeable cations. As a result, the layer surface is electrically neutral to the contacting solution, and bulk water can exist between clay platelets.

The validity of the different type of models is still under debate (Wersin et al. 2004, 2014a, b, Birgersson and Karnland 2009, Idiart and Pękala 2016), being the different conceptualizations of the transport through the bentonite and its different pore spaces the main point of controversy.

In this context, geochemical models for use with the LOT experiment at Äspö (Arcos et al. 2003, Sena et al. 2010b) have been developed and generated results like those obtained in previous models. The calibration against experimental results improved the model both from the conceptualization of the geochemical processes and the parameters considered (Sena et al. 2010b). Also, the results from several of the large-scale experiments introduced above (i.e. LOT and ABM) have been modelled in terms of transport, cation exchange and concentration of conservative anions (i.e. chloride) using the different model approaches (Idiart and Pękala 2016). The results indicate that none of the modelling approaches can reproduce all the different experiments within a reasonable uncertainty range.

The redox buffering capacity of the bentonite is also controversial. Some of the models predict that redox buffering is due to pyrite oxidation and iron (III) hydroxide precipitation; whereas other models point to iron carbonate (siderite) dissolution and iron (III) oxy-hydroxides as controlling the redox buffering capacity of the system. Experimental data obtained in the frame of the integrated project NF-PRO (Muurinen and Carlsson 2007, Arcos et al. 2008) indicate that there is a fast and reversible redox buffering reaction occurring in the bentonite. When compacted bentonite was placed in contact with an external solution under aerobic conditions, higher Eh values were only recorded in bentonite near the contact with the external solution. Moreover, when changing the aerobic external water for another under anaerobic conditions, Eh values in the most external part of the bentonite rapidly decrease to initial values, equivalent to those in the rest of the bentonite block. These results do not allow the chemical reaction responsible for such a redox buffering effect to be identified, although the fast response of the system to changes in redox external conditions indicates that pyrite-involved reactions can be disregarded, whereas an additional process related to the oxidation-reduction of iron in the octahedral sites of montmorillonite must be considered and investigated (Anastácio et al. 2008).

The ion exchange model approach has been applied to assess the long-term evolution of the buffer for the KBS-3 concept. Some of the models are based on a mixing tank concept (Wanner et al. 1992, Bruno et al. 1999) where the thermal stage has not been considered. Other models are reactive transport models where the thermal stage is considered (Arcos et al. 2000). All these models suggest that cation exchange is the dominant process in the buffer resulting in direct control on calcite precipitation-dissolution, thus buffering the pH of the system. Also, the effect of protonation-deprotonation of montmorillonite edge sites can play a role in pH buffering. However, earlier models (Bruno et al. 1999, Arcos et al. 2000) indicate that calcite equilibrium is the main process buffering pH, and only if calcite is exhausted will edge sites be able to buffer pH in the system. This is in agreement with experimental data obtained in the frame of the EC integrated project NF-PRO (Muurinen and Carlsson 2007, Arcos et al. 2008), where compacted bentonite was put in contact with an external solution at high-pH and pH was measured in the bentonite at different distances from the bentonite – external water interface. The data showed that high pH values in porewater were only recorded near the interface, but pH in this zone rapidly decreased over 100 days, indicating that a chemical reaction in the bentonite is buffering the pH. Unfortunately, no information was provided on the type of reaction buffering the pH; the most likely reactions are either precipitation of calcite or protonation-deprotonation reactions on the montmorillonite surface.

The integrated geochemical evolution of the buffer was modelled in the SR-Can assessment (Arcos et al. 2006) and in the SR-Site Safety Assessment (Sena et al. 2010a). An example of the results can be found in Figure 3-27.

Natural analogues/observations in nature

Development of salt crusts in arid regions resembles in some respects certain conditions during the water saturation phase. Specific SKB-related studies have not been conducted, but a large body of literature exists on the subject. The information from these natural systems could be of interest to support information on the processes occurring during the saturation phase, as indicators of the type of minerals that can potentially precipitate in the bentonite.

Silica precipitation occurs at a large number of locations where hydrothermal transformation of bentonite has taken place. Numerous scientific articles have been published, some directly linked to repository questions, see for example (Pusch et al. 1998).

SKB was involved in the study of a bentonite natural analogue in Spain, the BARRA Project, under the coordination of ENRESA. Two processes were studied in this natural system: 1) changes in the bentonite induced by long time exposure to a very high salinity environment, and 2) the thermal effect induced on bentonite properties by a sub-volcanic intrusion and its interaction with iron-rich fluids. The initial results from this study indicate that exposure to very high salinities does not alter the properties of the bentonite. The interaction of bentonite with iron-rich fluids at a relatively high temperature (~100 °C) resulted in changes to the smectite composition, which shifted to iron-rich members due to octahedral substitution (Pérez del Villar et al. 2005). These studies of natural systems can give very valuable information on the long-term effect on the bentonite-porewater system of several processes that are likely to occur in the repository system, thus validating the geochemical models based on laboratory experiments.

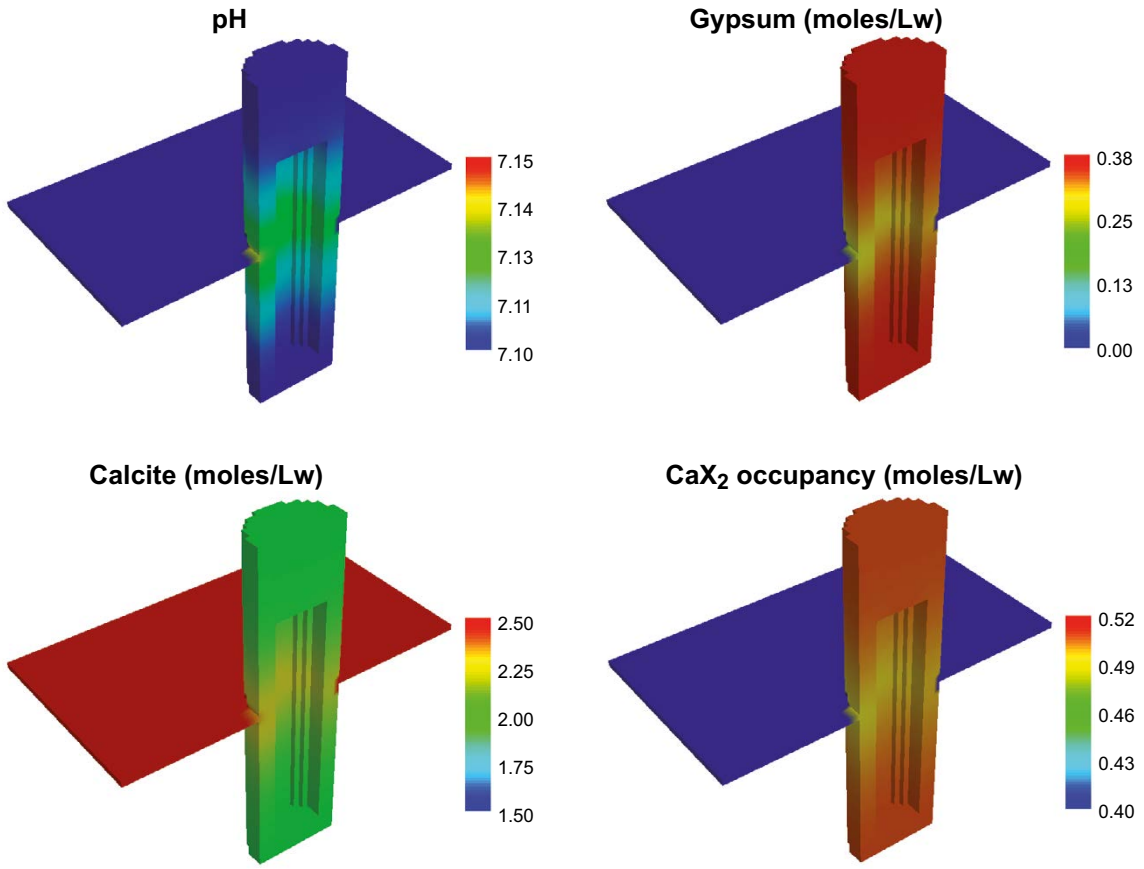

Figure 3-27. *Graphics from SR-Can showing the predicted evolution in the simulated domain (Deponit CA-N bentonite) for pH, calcite and gypsum content and calcium occupancy in the cation exchanger of montmorillonite after 10 000 years of simulation. Groundwater is simulated to contact the buffer through a conductive fracture perpendicular to the deposition hole (units in moles per litre of porewater). Note that as gypsum dissolves and calcium occupancy in the exchanger is depleted calcite precipitates and pH slightly decreases (Arcos et al. 2006)*

Time perspective

Chemical precipitation/dissolution processes are likely to be most important at an early stage of repository evolution when temperature and temperature gradients are high, water saturation occurs, and oxygen remains in the repository tunnels. At later stages, most of the processes approach equilibrium. The accessory minerals in the bentonite are, however, also important over timescales of hundreds of thousands of years if the chemistry in the repository should be disturbed for some reason; both pH and Eh are buffered effectively by the accessory minerals that are common in different bentonite materials.

Handling in the PSAR

Model

Before saturation: Although the same geochemical processes will occur both before and after saturation phases, the combination of saturation and thermal gradients increase the reaction rates, resulting in larger geochemical changes (precipitation/dissolution) associated to the saturation phase. Therefore, the need of knowledge of the processes occurring during this phase is essential to reduce the uncertainty, which can propagate for the long-term evolution.

After saturation: The processes are included in the scenario-specific modelling of the buffer chemical evolution for the thermal phase and the post-thermal long-term phase. This modelling includes, in addition to alterations of accessory minerals, the processes of diffusion (Section 3.5.2), ion exchange (Section 3.5.3), aqueous speciation and reactions (Section 3.5.4). The initial intrusion of groundwater during buffer saturation should be considered in formulating initial conditions. The geochemical model

applied is a 3D reactive transport model based on the results of the LOT experiment (Arcos et al. 2003, 2006, Domènech et al. 2004, Sena et al. 2010b). The model handles advective flow in a fracture in granite intersecting the deposition hole, diffusive transport in the bentonite, dissolution-precipitation of the main bentonite accessory minerals, cation exchange in the bentonite, protonation-deprotonation reactions in the smectite fraction and precipitation of potential secondary phases in both bentonite and the granitic fracture. Prior to application in SR-Site, the reactive transport model was validated by comparing its results with experimental data from the LOT test (Sena et al. 2010b).

The following is a description of the main geochemical processes considered in the alteration of accessory minerals and how they are handled within the PSAR.

Precipitation of carbonates and sulphates in the areas nearest to the canisters may lead to the formation of a porous contact zone between the buffer and the canister surface and an increase in the stiffening of the buffer. When the thermal period is over and temperature gradients no longer exist to any substantial extent in the buffer, it is likely that the previously precipitated solids will be re-dissolved to some degree and then diffuse in ionic form through the buffer. Precipitation of silica may reduce the swelling potential, as well as decrease bentonite porosity, although this process has not been observed in any of the experiments conducted up to date.

The carbonate and pyrite contents are of decisive importance for determination of pH, Eh and alkalinity in the near field. Bentonite also contains small quantities of gypsum ($CaSO_4 \cdot 2H_2O$), which may be of importance at an early phase during the high temperature transient.

Calcite dissolution: Calcite is stable in groundwater. In the bentonite, however, the ion exchange process will compete for free calcium ions Sorption (3.5.3). The reaction

$$2XNa + Ca^{2+} \leftrightarrow X_2Ca + 2Na^+$$

competes with

$$Ca^{2+} + HCO_3^- \leftrightarrow CaCO_3(s) + H^+$$

The carbonate content of the groundwaters that may be encountered is sufficiently low for the ion exchange process to dominate and calcite will be dissolved. This will entail net proton consumption, i.e. an increase in pH. The water flux in the buffer is very low, and the reactions are close to equilibrium. Additionally, the presence of thermal gradients can affect the solubility of calcite, which is more insoluble at the higher temperature expected in the near field, allowing its dissolution from the buffer/ rock interphase and its precipitation close to the canister, during the thermal period.

Siderite dissolution and iron hydroxide precipitation: The presence of pure siderite or ankerite, a mixed calcium-iron carbonate, is of paramount importance for redox control of the system through the following reaction

$$FeCO_3(s) + ¼O_2(aq) + 2½H_2O \leftrightarrow Fe(OH)_3(s) + HCO_3^- + H^+$$

Siderite oxidation leads to an increase of iron in solution allowing the precipitation of iron (III) hydroxides and thus controlling the redox of the system. However, during the early stage, when high temperatures are expected in the buffer, hematite would be the stable iron (III) phase instead of iron (III) hydroxide, leading to the precipitation of hematite close to the canister and increasing the strength/ stiffness of the buffer.

Pyrite oxidation/dissolution: Pyrite is also stable in groundwater. However, penetrating oxygenated water can oxidise pyrite in accordance with

$$2\ FeS_2(s) + 7½O_2(aq) + 7H_2O \leftrightarrow 2Fe(OH)_3(s) + 4SO_4^{2-} + 8H^+$$

Pyrite oxidation releases protons and can thereby lower the pH, but this is buffered by the dissolution of calcite previously discussed. There is enough pyrite in the buffer to consume all initial oxygen left after closure of the repository. The air content in the bentonite buffer is 12 % by volume (SKB 2004), corresponding to 1.9 moles of oxygen gas per cubic metre of bentonite, thus 0.51 moles of pyrite in 1 m^3 of bentonite are needed to consume all this oxygen, which is equivalent to a pyrite content of 0.004 % by weight, which is 20 times lower than the pyrite content of MX-80 bentonite or 125 times lower than the pyrite content of Deponit-CaN bentonite. The quantity is also sufficient to prevent any

penetrating oxygenated water from coming into contact with the canister for hundreds of thousands of years. However, as this process is kinetically driven, it is likely that pyrite oxidation exerts a minor effect on the redox of the system, which will be controlled by the iron carbonate dissolution process.

Pyrite is a source of sulphide that could act as a corrodant on the copper canister. Under reducing conditions pyrite dissolves as:

$FeS_2(s)+H^+ \leftrightarrow Fe^{2+} + HS^- + S^0$

The concentration of HS^- is an important parameter for canister corrosion.

Dissolution of calcium sulphates: Calcium sulphates (gypsum and anhydrite) and calcite have lower solubility at high temperatures. At an early stage, when the canister temperature is high, it is possible that they will be dissolved in the colder portion of the buffer and precipitate near the canister surface.

Precipitation/dissolution of silica: The main accessory minerals in the bentonite are quartz and feldspars. Feldspars are not stable in the repository environment, although the kinetically driven dissolution is a relatively slow process that is accompanied by the precipitation (or replacement) of clay minerals, i.e. kaolinite. The low water flux in the buffer is likely to minimise the kinetic dissolution of feldspars. Quartz is normally stable in the natural repository environment, but its solubility increases with increasing temperature. Silica will dissolve due to high temperature close to the canister and will be transported by diffusion outwards into the colder parts where precipitation may take place. In the Buffer Mass Test in Stripa, the buffer was analysed with respect to the distribution of silicon, but no definite conclusion could be drawn regarding possible enrichment in the coldest part (Pusch 1985).

Failed canister: In the case of a failed canister, vast amounts of metallic iron, originating from the corroding cast iron canister insert, will be added to the geochemical system. This was not included in the model mentioned above. The reaction between iron and bentonite is also discussed in Section 3.5.9.

Boundary conditions: The diffusive transfer of species between the flowing water and the bentonite is modelled explicitly. The near-field evolution model uses the Q_{eq} concept to handle the boundary conditions. This is sufficient to estimate a general timescale on which the evolution occurs.

Handling of variables influencing this process: The modelling is in itself a coupling of geochemical, hydraulic and transport processes and is thus a coupled modelling of most of the significant long-term chemical processes. A large number of the variable influences related to the chemical conditions (porewater composition, montmorillonite composition, bentonite composition) are also included.

Handling of variables influenced by the process: The geochemical conditions in the near-field as a function of time and space will be calculated.

Changes in the accessory mineral content of the buffer as a consequence of the thermal stage has been modelled, but not fully validated through a comparison with experimental and/or natural analogue data. Moreover, the discrepancy between different modelling approaches increase the uncertainty on the modelling results. This makes it difficult to ensure that changes due to the thermal stage are minor or that these results should be assumed to be the same as the initial conditions for the low temperature stage.

In addition to the processes discussed above, the behaviour of silica and clay minerals and their effect on cementation should be addressed by performing some scoping calculations considering the present knowledge of kinetic dissolution-precipitation of smectite, silica-phases and the precipitation of alternative clay minerals (kaolinite and/or illite). These scoping calculations should give some qualitative information on the relative importance of these processes and the effect on bentonite properties, e.g. porosity changes. See also Cementation (3.5.10).

Uncertainties

Uncertainties in mechanistic understanding

Some critical uncertainties remain concerning the mechanistic understanding of the processes that control the redox state of the bentonite system. It is not clear yet to what extent pyrite and/or siderite are the main redox controlling phases, although either process, or their combination, will scavenge

the remaining oxygen in the near field. This should be discerned by comparative modelling of pyrite and siderite kinetic availability.

In addition, most of the secondary precipitation/dissolution processes that are temperature driven are thermodynamically controlled. Hence, there is no need for a detailed mechanistic understanding. However, some of the silicate transformations are kinetically controlled and their mechanistic understanding in compacted bentonite conditions is poor. This is mainly related to clay mineral transformations (dissolution of smectite and precipitation of illite and/or kaolinite). Although these reactions occur at a very slow rate, their effect on the overall geochemical evolution is not yet clear.

Most of the conceivable processes are in themselves well known and can be modelled for less complex systems. However, conditions in the buffer, as far as transport and reaction kinetics are concerned, are not fully understood for all processes. The conceptualization of the transport of solutes is still under debate and, therefore different modelling approaches considering different concepts give different results. Modelling of the system must therefore be coupled to the THM processes that proceed in parallel with transport and reaction kinetics.

Silicon is the most common element in the buffer and occurs in a number of different minerals and phases. The following processes are not fully understood:

- release of silica by dissolution from different minerals,
- transport of dissolved silica driven by the prevailing temperature gradient,
- precipitation of silica minerals.

Precipitation of silica is particularly complex, since it is dependent on several interacting factors and since several conceivable forms occur, both crystalline and amorphous.

The greatest uncertainty concerns the scope for cementation as a consequence of dissolution, transport and precipitation of silica or aluminosilicate minerals. The scope and consequences of cementation cannot be predicted with reasonable certainty at present.

Finally, it is assumed that pH is buffered by equilibrium with calcite. However, the amount (or even the presence) of this mineral phase is somewhat uncertain, depending on the bentonite type selected for the buffer, thus the pH buffering capacity of the clay barrier could be affected.

Model simplification uncertainties in the PSAR

One of the major uncertainties concerns the conceptual model of the solute transport through the buffer. As stated previously, there are several conceptual models regarding the way the bentonite – porewater is considered (Donnan equilibrium models, diffuse layer models and ion exchange models). The effect of such different models on the geochemical evolution of the system should be evaluated.

Secondary dissolution and precipitation processes have not been fully implemented in a coupled model of buffer evolution. The processes are only considered when required for the definition of critical master variables in the system (pH and pe). One possibility could be to couple the THM processes occurring with the key chemical processes that will control the geochemical evolution of the buffer system.

There are some accessory minerals, such as framework silicates, which are not included in the models, as most tend to dissolve at a very slow kinetic rate. Other silicates (usually clay minerals) precipitate at similarly slow rates. However, the dissolution-precipitation processes involving these two types of minerals could affect the stability of montmorillonite as well as the chemical composition of the buffer porewater, thus affecting the chemical long-term evolution of the buffer. See also Montmorillonite transformation (3.5.8).

There is no model to account for the dissolution/precipitation of accessory minerals during the water saturation stage of the buffer. As water flux will be faster than when the buffer is water saturated, the buffer composition won't be at equilibrium with incoming water and there will be a thermal gradient in the buffer; some changes will occur faster. These changes will account for step compositional

gradients in the buffer and changes in porosity as accessory minerals dissolve and/or precipitate, leading to changes in the hydraulic properties of the buffer. Thus, modelling of the system must be coupled to the THM processes that proceed in parallel with transport and chemical reactions. A submodel dealing with the saturation stage of the bentonite will, at least, give an indication of the magnitude of these changes.

Input data and data uncertainties in the PSAR

Key thermodynamic data are well established and thought to be reliable. The main uncertainties remain in the definition of the kinetically controlled processes. These are linked to the mechanistic uncertainties mentioned previously.

Reliable data for surface reactions (i.e. cation exchange and edge site reactions) are of paramount importance for the correct assessment of bentonite behaviour. Two types of information are needed for geochemical modelling: i) Cation occupancy of the CEC and the protonation state of the smectite surface, and ii) Exchange and protonation-deprotonation constants. The main uncertainty associated with these data is related to the experimental conditions used for their determination (i.e. low bentonite density and high solid/liquid ratios). Recent experiments have addressed this problem, but there is still a large uncertainty related to the determination of cation exchange constants and their variation as a function of bentonite density.

3.5.7 Osmosis

Overview

A classical view of osmosis, as shown in Figure 3-28, may be used in order to illustrate the conditions in a bentonite buffer. The two sides of the water system are divided by a semi-permeable membrane permeable only to water molecules. If salt is added to the left-hand side, the water activity is reduced and transport of water from right to left will take place. The water table on the left will rise and a hydrostatic pressure develops (a). If salt is now added to the right-hand side, there will be a levelling of the water tables on both sides (b). If the initial volume change on the left-hand side is prohibited by an external force, pressure will rise in the salt solution (c), corresponding to the previous hydrostatic pressure. Introduction of salt into the right hand side of the membrane will lead to a drop in pressure. A complete loss of pressure will evidently take place when the two concentrations become equal (d).

By analogy, assumes that the left-hand side of the system represents the bentonite buffer and the right-hand side an external groundwater solution (Figure 3-29). An external solution would reduce the pressure produced by the clay, to an extent equal to the osmotic pressure of the solution, if no ions could pass into the clay. A sodium chloride concentration of around 1.7 M (~10 % by weight) would then result in a complete loss of swelling pressure in a KBS-3 buffer. On the other hand, if ions could pass freely into the clay, without restriction, then the final conditions would be equal concentrations on both sides and no effect on swelling pressure would be found. Laboratory experiments show that neither of these conditions prevail and that there is a systematic reduction of swelling pressure, which indicates that ions from the external solution do pass into the clay to a certain extent (Karnland et al. 2005).

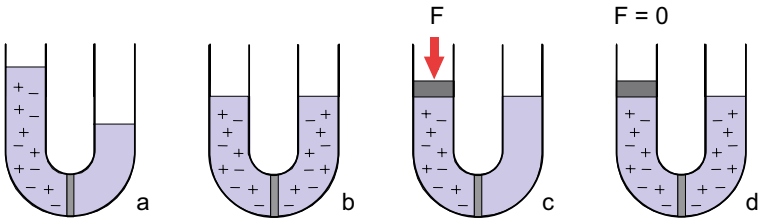

Figure 3-28. *The basic principles of osmosis as an analogy of bentonite swelling pressure (Karnland et al. 2005).*

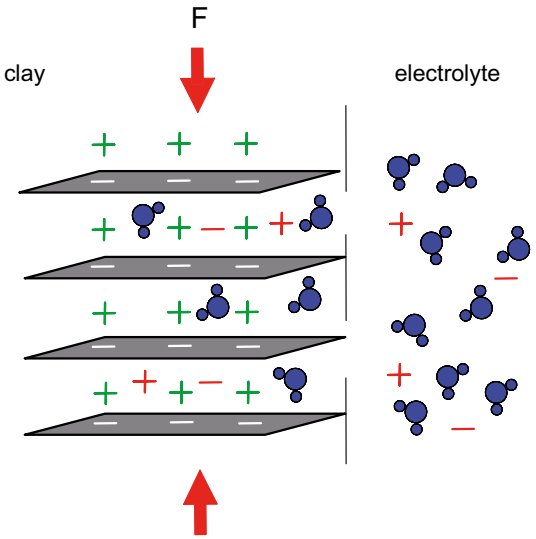

Figure 3-29. *Principle drawing of the clay-water-ion system. Clay mineral flakes and charge compensating cations on the left side, and sodium and chloride ions on both sides of a semi-permeable membrane (buffer-rock interface), which is permeable to dissolved ions and water, but not to the individual montmorillonite layers (Karnland et al. 2005).*

The conditions in the bentonite/groundwater system are typical of what is often referred to as a Donnan equilibrium system (Donnan 1911). The equilibrium is governed by the fact that some, but not all, ions can pass between the system parts, usually because of their large size. The condition leads to prevailing concentration differences between the two parts, including the ions which can move freely in the system. In a repository, the individual negatively charged montmorillonite mineral layers have a restricted mobility because of their relatively large size compared to the mean pore size; see Diffusive transport of species (3.5.2) while the charge compensating cations and excess electrolyte ions may move in the bentonite/groundwater system (Figure 3-24).

The condition for equilibrium is that the electrochemical potential is equal in all system parts for all ions that can move. Since the negatively charged macro-sized mineral layers are immobile, equilibrium will be established between ions in the external solution and charge compensating cations in the montmorillonite. Ideally, for a sodium chloride solution and sodium montmorillonite these will be only Na^+ and Cl^-. The condition of electrical neutrality in the entire system is:

$$0 = z \cdot C_m + C_{Cl^-} - C_{Na+} \qquad (3\text{-}27)$$

where z is the valence of the macromolecule, C_m, C_{Na+} and C_{Cl-} are the concentration of the macromolecules, sodium ions and chloride ions, respectively. In terms of ion activity, the equilibrium condition for the diffusible ions is:

$$\{Na^+_c\}\{Cl^-_c\} = \{Na^+_e\}\{Cl^-_e\} \qquad (3\text{-}28)$$

where the indices c and e refer to the clay-water system and to the surrounding electrolyte, respectively. The $\{Na^+_c\}$ factor is the sum of the activities of original charge compensating ions $\{Na^+_{cc}\}$ and introduced electrolyte ions $\{Na^+_{ie}\}$. The constraint of local electrical neutrality gives $\{Na^+_e\} = \{Cl^-_e\}$ and $\{Na^+_{ie}\} = \{Cl^-_{ie}\}$ which in turn gives:

$$(\{Na^+_{cc}\}+\{Na^+_{ie}\})\ \{Na^+_{ie}\} = \{Na^+_e\}\ \{Na^+_e\}) \qquad (3\text{-}29)$$

Rearranging gives the introduced sodium ion activity:

$$\{Na^+_{ie}\} = \frac{-\left[\{Na^+_{cc}\} \pm \sqrt{\{Na^+_{cc}\}^2 + 4 \cdot \{Na^+_e\}^2}\right]}{2} \qquad (3\text{-}30)$$

Consequently, it is possible to calculate the activity of sodium ions introduced in the clay-water system if the activity of the original cations $\{Na^{+}_{cc}\}$ in the clay and the activity of the ions in the external solution $\{Na^{+}_{e}\}$ are known. The resulting drop in swelling pressure can be calculated approximately if the activity of both the groundwater and the interlayer cations can be determined (Karnland et al. 2005). Figure 3-30) shows measured and calculated results for the above conditions assuming an activity coefficient of unity. The same principle may be applied to divalent ions, which leads to a more complicated expression, but both measured and calculated values for calcium show similar osmotic effects to sodium.

Dependencies between process and buffer variables

Table 3-16 summarises how the process influences and is influenced by all buffer variables and how these effects are treated in the PSAR.

Boundary conditions

The process occurs at the interface between the bentonite and an external solution, mainly the rock/bentonite interface, but could also occur at the bentonite/canister interface in the case of a defective canister.

Model studies/experimental studies

The first preliminary study concerning influence of external groundwater salinity on swelling pressure was reported in Karnland (1997). A comprehensive model and experimental study of MX-80 bentonite converted to a pure sodium state has been made by SKB (Karnland et al. 2005). An additional experimental study of the two reference bentonites MX-80 and Deponit-CaN in their natural state and after conversion to pure sodium and calcium forms has been made by SKB (Karnland et al. 2006).

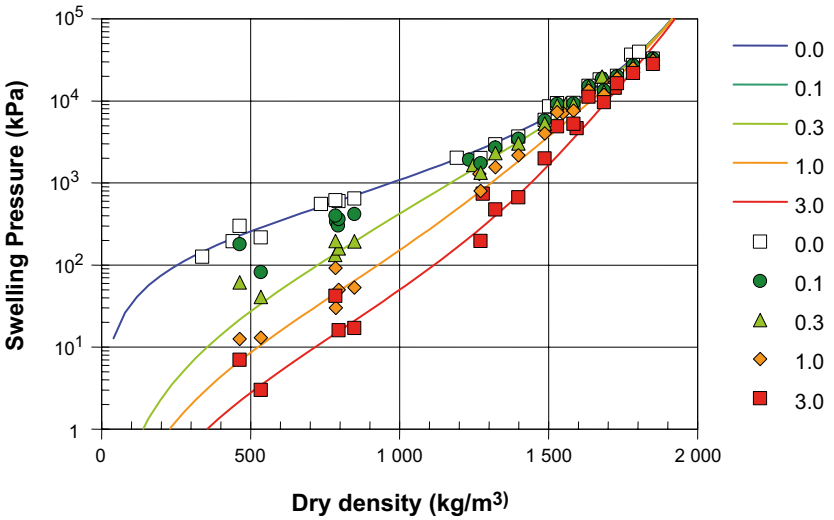

Figure 3-30. *Measured (symbols) and calculated (lines) swelling pressure versus dry density of clay for different concentrations of a NaCl solution in equilibrium with Na-montmorillonite. Legends show external solution concentration in mol/dm³(Karnland et al. 2005).*

Table 3-16. Direct dependencies between the process "Osmosis" and the defined buffer variables and a short note on the handling in the PSAR.

Variable	Variable influence on process		Process influence on variable	
	Influence present? (Yes/No) Description	Handling of influence (How/Why not)	Influence present? (Yes/No) Description	Handling of influence (How/Why not)
Buffer geometry	No		No, but indirectly through stress state	
Pore geometry	Yes, interlayer distance is a decisive parameter	Included as a function of buffer density	No, but indirectly through stress state	
Radiation intensity	No		No	
Temperature	Yes, linear dependence	Neglected due to small variations	No	
Water content	Yes, equivalent to pore geometry in saturated buffer	The buffer is assumed to be saturated for this process	No, not at high buffer densities	
Gas content	No, the process is not well defined in unsaturated buffer		No	
Hydrovariables (pressure and flows)	No, but indirectly through porewater composition		Yes, hydraulic conductivity effects	The effect of salinity on hydraulic conductivity is evaluated
Stress state	No, but indirectly through charge compensating cation concentration (montmorillonite composition)		Yes, by definition	The effect of salinity on swelling pressure is evaluated
Bentonite composition	Yes, through montmorillonite content	Included in data	No	
Montmorillonite composition	Yes, through type and number of charge compensating cations	Included in data	Yes, counter-ion distribution	Ion-exchange is considered
Porewater composition	Yes, by definition	Included in data	Yes, by definition	Included in data
Structural and stray materials	No		No	

Time perspective

The process is relevant for all timescales over the lifetime of the repository. The swelling pressure response of a change in groundwater salinity is expected to be instantaneous.

Natural analogues/observations in nature

Osmotic effects related to clay are discussed in several articles, but they are only peripherally relevant for repository conditions. Osmotic induced pressure effects are discussed in Neuzil (2000).

Handling in the PSAR

The osmotic swelling pressure effects are handled by direct application of empirical data for relevant, scenario-specific conditions.

Model: The relationship presented above may be used to estimate swelling pressure and hydraulic conductivity for the buffer.

Boundary conditions: The important boundary condition for this process is the composition of the groundwater.

Handling of variables influencing this process: The montmorillonite composition and the groundwater/ porewater composition are directly included in the model.

Handling of variables influenced by the process: The buffer swelling pressure and hydraulic conductivity are measured for all relevant conditions.

Uncertainties

Uncertainties in mechanistic understanding

The process is based on well-established theories and generally well understood. However, detailed treatment of ion activity in the buffer is not clear.

Model simplification uncertainties in the PSAR

The ion equilibrium model for predicting swelling pressure is based on the assumption that the system is relatively homogeneous with respect to pore geometry. This assumption is strongly supported by comparison of calculated and experimental data for swelling pressure, freezing (Section 3.2.2) and Diffusive transport of species (Section 3.5.2).

Input data and data uncertainties in the PSAR

The input data to the model are the activity of ions in the groundwater and the activity of the interlayer cations in montmorillonite. The model is relatively insensitive to the difference in activity and concentration of groundwater and standard methods may be used for calculating this activity. The relevance of calculating the activity of interlayer ions by standard methods (Debye-Hückel, Davis, Pitzer etc) is not obvious. Uncertainties still remain as to how this activity should be treated in a relevant way.

3.5.8 Montmorillonite transformation

Overview

The advantageous physical properties of the buffer, principally swelling pressure and low hydraulic conductivity, are determined by the capacity for water uptake between the montmorillonite layers (swelling) in the bentonite, see Swelling 3.4.1 and Water transport for saturated conditions 3.3.2. Montmorillonite can transform into other minerals (Figure 3-31) of the same principal atomic structure but with less or no ability to swell in contact with groundwater. The transformation processes usually consist of several basic mechanisms , depending on the situation, e.g. metal-bentonite interaction, cement-bentonite interaction. At the physico-chemical conditions expected in a repository, the following possible mechanisms have been identified.

Congruent dissolution

Montmorillonites will not necessarily be in chemical equilibrium with repository groundwater (Figure 3-32). As mineral solubility is low, no significant mass loss is expected from this mechanism. However, solubility is temperature and pH dependent (Aagard and Helgeson 1983).

Reduction/oxidation of iron in the mineral structure

This process alters the layer charge and may destabilize the mineral structure (Stucki et al. 1984). Corrosion of metallic iron or bacterial activity (Kim et al. 2004) could promote the process (see Section 3.5.10).

Atomic substitutions in the mineral structure

This process alters the layer charge by e.g. Al replacement of Si in the tetrahedral sheets, or Al replacement by Mg.

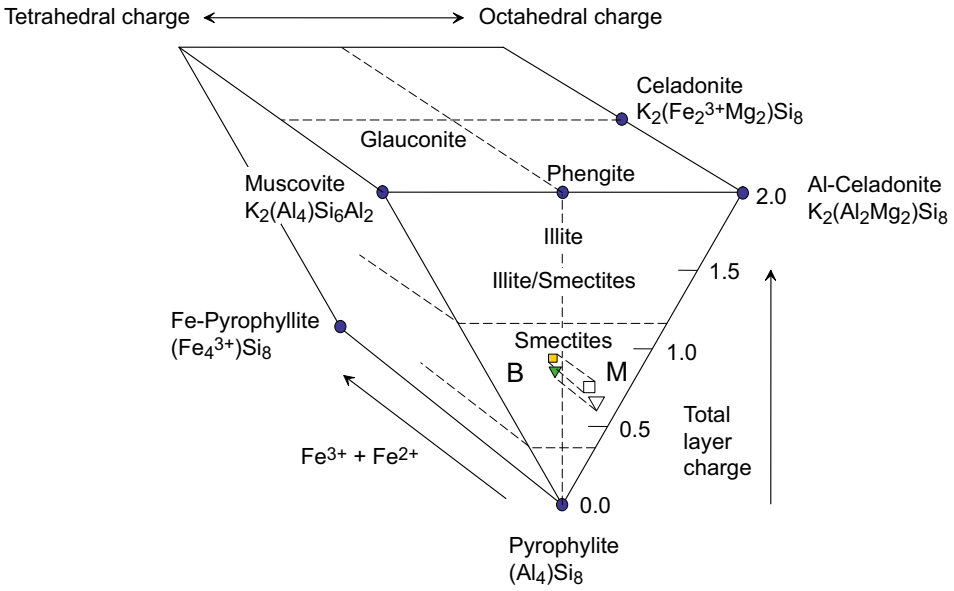

Figure 3-31. *Ideal end-member minerals in the pyrophyllite – mica series with potassium as charge compensating cation, and approximate compositional ranges for illite and smectite (modified from Newman and Brown 1987). B denotes beidellite, M denotes montmorillonite. The compositional positions of the montmorillonite minerals in the reference bentonite materials are indicated by a triangle (MX-80) and by a square (IBECO RWC). All formulae contain the basic $O_{20}(OH)_4$ unit.*

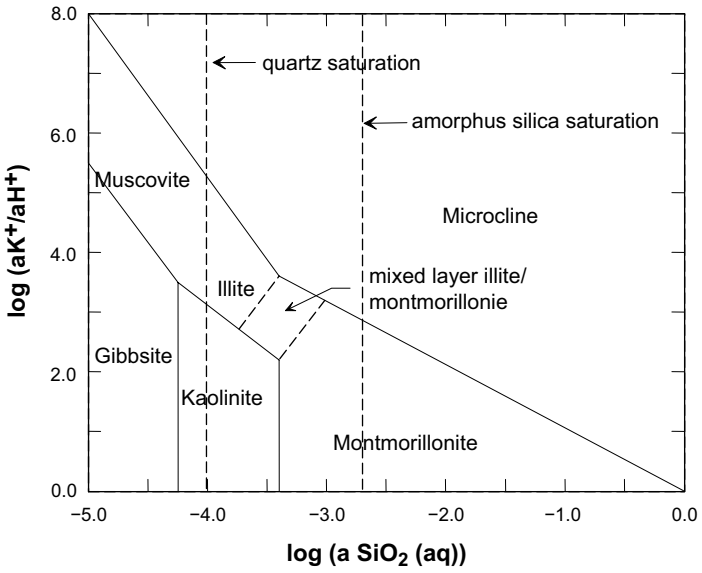

Figure 3-32. *Silicate mineral equilibria with the partial component potassium at 25 °C (Simplified from Aagard and Helgeson 1983).*

Octahedral layer charge elimination by small cations.

At high temperatures, e.g. Li^+ may penetrate into the octahedral sheet, which reduces the layer charge (Greene-Kelley 1953).

Replacement of charge compensating cations in the interlayer.

Substitution of counter ions is referred to as exchange and is treated elsewhere (see ion exchange process 3.5.5). Due to charge balance, any mechanism which alters the layer charge must be compensated by addition or removal of counter ions in the interlayer. Such compensation is fundamentally coupled to processes governing transport in the porewater, see diffusion, 3.5.2.

Transformation from montmorillonite to illite, which is the most common alteration observed in natural sediments, is well documented in different geological environments, and has been reproduced under laboratory conditions. The illitization process may be seen as the first step in a transition from montmorillonite to mica (muscovite/celadonite) minerals (Figure 3-31, and all intermediate stages from swelling to non-swelling material may be found (mixed layer smectite-illite). The conversion always involves a layer charge increase, mainly due to a decrease in silica content, and an uptake of charge compensating potassium ions. However, there is no general consensus concerning the detailed mechanisms in the conversion, and several models have been proposed.

Advanced illite replacement may be illustrated by the mineralogical composition of a natural illite from Montana, US, with less than 10 % swelling layers (Hower and Mowatt 1966):

$(Si_{6.81}\,Al_{1.19})$	$(Al_{3.25}\,Fe_{0.14}\,Mg_{0.59})$	$O_{20}\,(OH)_4$	$Ca_{0.1}\,Na_{0.02}\,K_{1.53}$
tetrahedral	octahedral		interlayer

This illite mean structural formula can be compared with the mean structural formula for the montmorillonite in the MX-80 the PSAR reference bentonite (Karnland et al. 2006):

$(Si_{7.94}\,Al_{0.06})$	$(Al_{3.10}\,Fe_{0.37}\,Mg_{0.50})$	$O_{20}\,(OH)_4$	$Ca_{0.05}\,Mg_{0.02}\,K_{0.01}\,Na_{0.46}$
tetrahedral	octahedral		interlayer

The main mineralogical differences are that illites have approximately one unit higher tetrahedral charge, and potassium as the main charge compensating cation. Simplified, the total illitization reaction may be expressed:

Ca^{2+}/Na^{+}-montmorillonite + K^{+} + (Al^{3+}) → Illite + Silica + Ca^{2+}/Na^{+}

In massive natural sediments the physico-chemical conditions are similar over huge volumes and concentration gradients are generally insignificant. The total reaction therefore involves a series of sub-reactions; release of silica from montmorillonite, release of potassium from e.g. feldspars, potassium fixation and precipitation of new silicate minerals. The total reaction rate is governed by the slowest of the sub-reactions.

According to the equilibrium conditions for 25 °C (Figure 3-32), montmorillonite may be thermodynamically stable for silica activities above 6×10^{-4}. Amorphous silica, with an equilibrium activity of around 2×10^{-3} may consequently be in equilibrium with montmorillonite. However, quartz with an activity of 1×10^{-4} will not be in equilibrium with montmorillonite. Precipitation of quartz may therefore destabilize the montmorillonite, and the precipitation rate may be the kinetically controlling mechanism in illitization of montmorillonite (Abercrombie et al. 1994). Figure 3-33 shows the decrease in silica activity in sediment porewater, as a function of temperature (depth in the sediments). At temperatures below 40 °C the porewater is in equilibrium with amorphous silica, and at temperatures higher than 60 °C the porewater is in equilibrium with quartz. The onset temperature of quartz precipitation in this system should consequently be in the range 40 to 60 °C.

However, at low temperatures the precipitation of quartz is very slow and the porewater may stay strongly supersaturated with respect to quartz. Consequently, a high smectite content is commonly found in old formations exposed to repository temperatures. For example, Velde and Vasseur (1992) studied the time-temperature distribution of illitization in seven deep wells in four sedimentary basins in the US, Japan and France. In all wells there was a typical reduction of smectite content with depth, which represents an increase in both age and temperature (Figure 3-34). The prerequisites for transformation are obviously present in the sediments with time and temperature the governing parameters. A decrease to around 60 % smectite was observed in the Californian Norwal formation after 4.5 million years at a depth of 5 km, representing a final temperature elevation of over 100 °C. The same transformation took around 60 million years at a depth of 2 km and a temperature elevation of around 70 °C in the Texan Peelan sediments. The reaction rate at these repository relevant temperatures is consequently very slow in relation to the timescale of a repository.

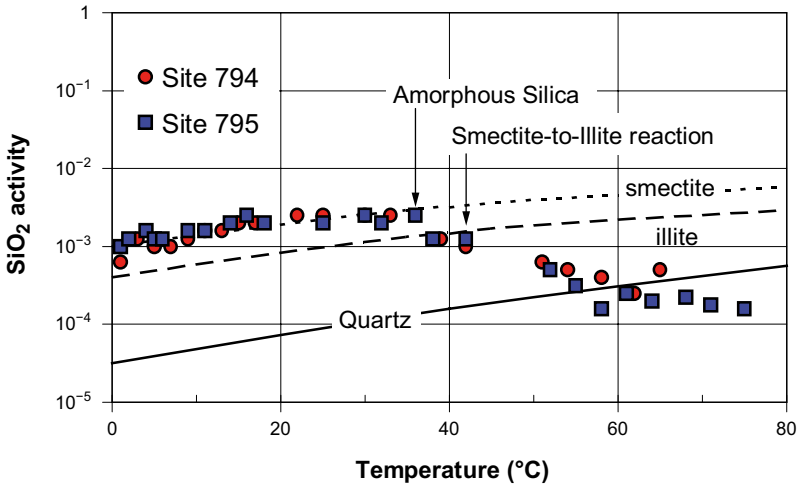

Figure 3-33. *Silica activities for waters from Ocean Drilling Program sites 794 and 795 and saturation curves for amorphous silica, smectite-to-illite reaction, and quartz. Modified from Abercrombie et al. (1994).*

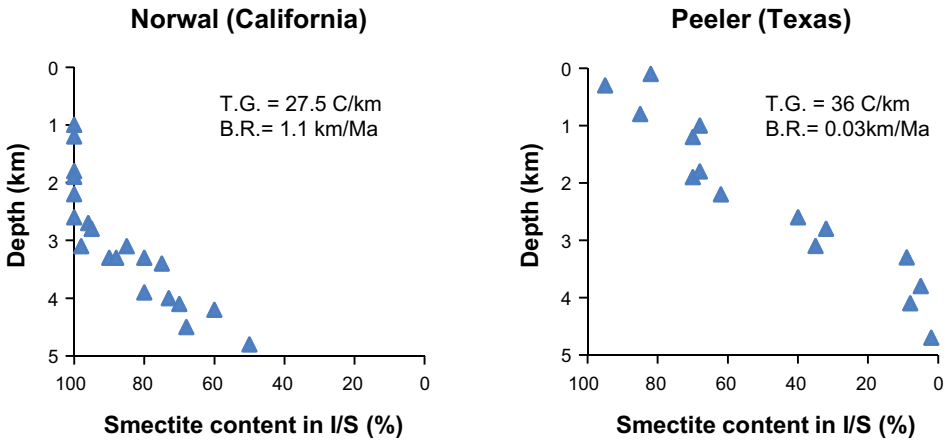

Figure 3-34. *Smectite content versus depth in smectite-illite mixed layer material in two sediments representing relatively fast burial rate (left) and slow burial rate (right). T:G: indicate the present temperature gradient and B.R. indicates the burial rate. Redrawn from Velde and Vasseur (1992).*

Brammallite/rectorite may be seen as a sodium equivalent to illite. The mean layer charge is higher than in illite, normally close to 2 unit charges per $O_{20}(OH)_4$. It is expected that the transformation from montmorillonite into brammallite/rectorite is governed by the same basic mechanisms as in illitization. The release of silica from the montmorillonite may theoretically continue until the required tetrahedral charge is reached in the absence of potassium. In consequence, brammallite/rectorite are less commonly found as alteration products in natural sediments compared to illites, and there are no indications that the basic mechanisms should be faster than in illitization.

Chlorites have the same basic structure as montmorillonite, but the layer charge is normally close to 2 unit charges per $O_{20}(OH)_4$. The layer charge is balanced by positively charged, octahedrally coordinated, hydroxide sheets, where the central ion may be any di- or tri-valent metal ion, normally Mg, Al or Fe. Transformation from montmorillonite to chlorite is occasionally found in parallel with illitization, and it is expected that both transformations are governed by similar basic mechanisms. It cannot be excluded that chlorite may be formed from montmorillonite without illitization in the absence of potassium, but there are no indications that this process would be faster than the illitization process under repository conditions.

Silica solubility increases significantly above pH 9 due to the H_4SiO_4 -species losing one or two of its protons. The total equilibrium SiO_2 concentration ($[H_4SiO_4] + [H_3SiO_4^-] + [H_2SiO_4^{2-}]$) is given by the law of mass action:

$$[SiO_2]_{TOT} \approx \{H_4SiO_4\}\ (1+K_1/\{H^+\}+K_1K_2/\{H^+\}^2)$$

where $K_1 = 10^{-9.9}$ and $K_2 = 10^{-11.7}$ denote the equilibrium constants for the dissociation reactions. The total SiO_2-concentration as a function of pH is shown in Figure 3-35, assuming an H_4SiO_4 activity for saturated amorphous silica.

The tetrahedral silica in the montmorillonite consequently equilibrates at higher concentrations above pH 9. Diffusive removal of silica or precipitation of new silica minerals thereby lead to a faster increase of the tetrahedral layer charge compared to near neutral conditions. The corresponding increase in concentration of charge compensating cation leads to a change in the interaction with water and thereby to a change in sealing properties. The layer charge may reach the critical value for collapse, which results in total loss of expandability and in principle, to the same consequences as for illitization. Eventually, the process may lead to a general dissolution of the montmorillonite (ECOCLAY II) (Karnland et al. 2005).

At pH 11, the divalent anion $H_2SiO_4^{2-}$ starts to play an important role leading to a dramatic increase in silica solubility. At pH 11 the total silica concentration is calculated to be approximately 16 times greater than at neutral pH conditions, and at pH 12.4, representing matured Portland cement, the theoretical increase in total silica solubility is more than 3 orders of magnitude higher than at near neutral conditions. The total difference in silica concentration between the bentonite porewater and the groundwater increases approximately by the same factor, assuming the groundwater is in equilibrium with quartz. This leads to diffusional transport of aqueous silica from the bentonite into the groundwater. Besides the difference in equilibrium concentration, the limiting factors for this mass loss will likely be the contact area between the buffer and the groundwater and the groundwater flow. Huertas et al. (2005) studied the dissolution rate of smectite as a function of pH. Figure 3-31 plots log dissolution rate vs. pH at 25, 50, and 70 °C. In alkaline solutions, the smectite dissolution rate increases as pH increases, showing a steeper slope for pH values higher than 11, which seems to be a critical value for smectite dissolution and stability. The conclusion from Huertas et al. (2005) is that the results indicate that dissolution rates are strongly affected by both pH and temperature. This effect is particularly important for pH values above 11. The effect of the alkaline plume should be especially strong for young cement waters and for a repository concept in clay rocks, where the vousoirs surrounding the bentonite are closer to the canister that the concrete plug in the granite concept, and therefore subjected to higher temperatures. In cooler regions and slightly alkaline solutions, the bentonite components should be much more stable.

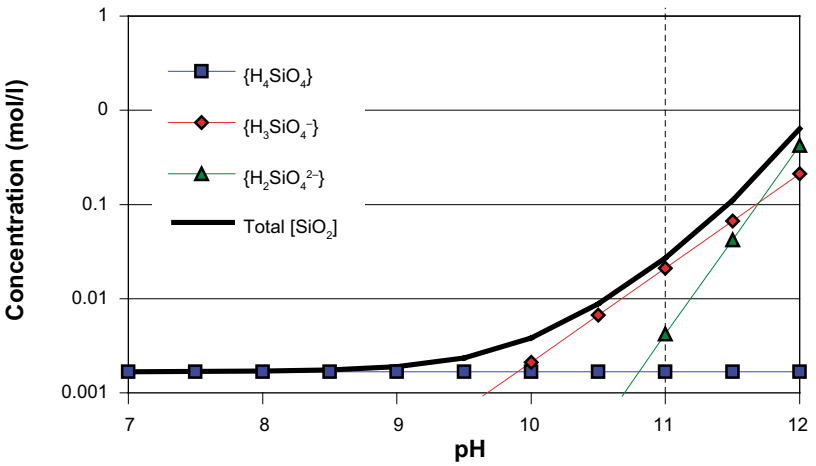

Figure 3-35. *Total concentration of silica as a function of pH assuming H_4SiO_4activity for saturated amorphous silica at 25 °C. At pH=9.9 $H_3SiO_4^-$ starts to dominate and above pH=11.7 $H_2SiO_4^{2-}$ dominates. The upper limit for the KBS-3 design criterion, pH=11, is indicated (Karnland et al. 2006).*

Effects of montmorillonite transformation

If montmorillonite transformation occurs the buffer functions will alter. A layer charge change in the montmorillonite lead to changes in the interplay with water and thereby affects the swelling pressure. During the early stages of illitization and similar transformations, montmorillonite/water interaction may become stronger due to moderate layer charge increase. However, as the transformation progresses, fixation of K^+ between sufficient highly charged layers leads to loss of interaction with water. The pore geometry is thereby changed towards fewer and larger pores, which in turn leads to a successive general deterioration of the buffer properties. A total transformation of all the montmorillonite in the buffer into illite or similar minerals would lead to complete loss of buffer function.

Many transformation processes and also congruent dissolution of the montmorillonite mineral releases solutes which could precipitate as new minerals which may act as cementing agents. Cementation could be enhanced due to transport of material from high solubility to low solubility regions, in situations where a solubility gradient prevails across the buffer, e.g. due to temperature and pH differences (Karnland and Birgersson 2006). For instance, in the case of silica, solubility increases dramatically at pH above 11 due to deprotonisation. Cementation may lead to a deterioration of the buffer's rheological properties as well as decreased capacity to swell , but these effect were expected to be small since montmorillonite transformation is expected to be minor (see Cementation 3.5.10).

Table 3-17 summarises how the process influences and is influenced by all buffer variables and how these effects are treated in the PSAR.

Boundary conditions

The relevant boundary conditions for the buffer are temperature and solute concentrations in the adjacent components, i.e. the same boundary conditions as for the processes heat transport, diffusion and advection.

Model studies/experimental studies

The illitization process is of great commercial importance in connection with prospecting and extraction of oil deposits which has led to very extensive research since the 1960s.

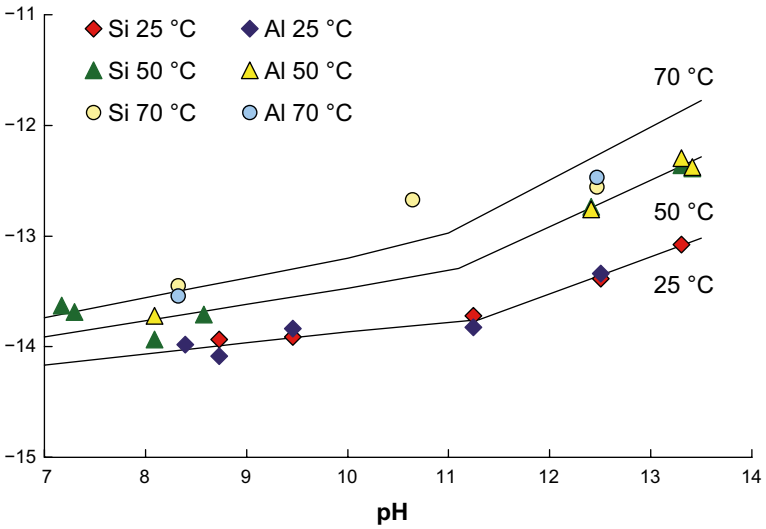

Figure 3-36. *Dissolution rates of smectites as a function of pH and temperature. Experimental (symbols) and estimated (lines) dissolution rates (Huertas et al. 2005).*

Table 3-17. Direct dependencies between the process "Montmorillonite transformation" and the defined buffer variables and a short note on the handling in the PSAR.

Variable	Variable influence on process		Process influence on variable	
	Influence present? (Yes/No) Description	Handling of influence (How/Why not)	Influence present? (Yes/No) Description	Handling of influence (How/Why not)
Buffer geometry	Yes, the size affects the transport of dissolved species and total buffer mass	Total mass considered. Transport resistances are pessimistically neglected	Yes, for extreme (unexpected) transformation	Separate scenario
Pore geometry	Yes, the density will affect the transport of dissolved species and ion equilibrium	A kinetic expression is used. Transport resistances are pessimistically neglected	Yes, by definition	Separate scenario
Radiation intensity	Possible minor effect	Neglected, see Radiation induced transformation 3.5.13	No	
Temperature	Yes, major impact	A kinetic expression is used.	No	
Water content	Yes, direct effect on hydraulic conductivity	Irrelevant for the time-frames considered	Yes, for extreme (unexpected) transformation	Separate scenario
Gas content	Yes, direct effect on hydraulic conductivity	Irrelevant for the time-frames considered	No	
Hydrovariables (pressure and flows)	Yes, minor through transport of dissolved species	Transport resistances are pessimistically neglected	Yes, major impact	Separate scenario
Stress state	No, pressures are too small to be significant		Yes, major impact	Separate scenario
Bentonite composition	Yes, through available species in accessory minerals	Minor importance, included in the assessment of effects of cementation	Yes, by definition	Separate scenario
Montmorillonite composition	Yes, by definition	Included in assessment	Yes, by definition	Separate scenario
Porewater composition	Yes, by definition	Included in the assessment of effects of cementation	Yes, by definition	Minor change that has little impact on performance
Structural and stray materials	Yes, indirectly through dissolved species. Especially pH effects from cement	Neglected in this case, since no stray materials are assumed to be present	No	

Kinetic models have been developed for the smectite-to-illite transformation. Relationships and constants have been established by means of laboratory batch experiments and comparisons with natural systems (e.g. Eberl and Hower 1976, Pytte 1982, Velde and Vasseur 1992, Huang et al. 1993). Most models take the form of an Arrhenius expression and the Huang et al. model may be shown as an example:

The overall kinetics of the smectite-to-illite reaction can be described by Equation 3-31:

$$-dS/dt = A \cdot [K^+] \cdot S^2 \cdot \exp(-E_a/RT) \qquad (3\text{-}31)$$

where S is the smectite fraction in the illite/smectite material, A is the frequency factor, E_a is the activation energy, R is the universal gas constant, and T is the temperature. After integration of Equation 3-31 the smectite content at a certain time can be calculated if the temperature and potassium concentration in the porewater are known. The potassium concentrations in the Äspö groundwater have been measured and found to be in the range of a few ppm up to 45 ppm (Laaksoharju et al. 1995). According to the model, practically no clay conversion is possible in a KBS-3-type repository under these conditions as shown in Figure 3-37.

The mineralogical stability of montmorillonite is being studied by SKB in the LOT tests at Äspö HRL (Karnland et al. 2009). The test series represents both anticipated repository and adverse conditions. The latter are used to accelerate possible degradation processes by use of:

- Higher temperature.
- Higher temperature gradient.
- Higher content of accessory minerals (calcite, gypsum, K-feldspar).
- New substances (Portland cement).

At the highest temperature (~130 °C), a test period of 10 years corresponds to the entire period of elevated temperature in a KBS-3 repository with respect to illitization according to the Huang model. The introduction of additional substances and increased temperature gradients is made in order to accelerate mass transport processes. The effect of the temperature gradient is, however, not possible to describe in a simple and generalised way by means of increased temperature and concentrations of reactants. No mineral transformation to illite has been detected in the tests performed at standard or adverse conditions by use of standard clay mineralogical analyses, nor has any K^+-fixation been observed by the performed mineralogical and chemical analyses. However, the MgO content of the clay fractions displayed a clear gradient towards the Cu-tube in the hot blocks and has increased from 2.35 % (mean of references) to ca. 2.6 % in the innermost samples, whereas the peripheral parts of the blocks appear to be depleted in magnesium. No mineral phase could be connected to this MgO increase. MgO was also noticed to increase towards the copper heater in the Prototype Repository experiment at Äspö (Olsson et al. 2013), an experiment using full scale buffer blocks and running at a temperature of approximately 90 °C excavated in 2010–2011 after about 8 years of heating. No mineral phase could be identified connected to the MgO increase. A similar increase was also observed in ABM1 (iron heater, LOT scale experiment at 130 °C at Äspö iron (Kaufhold et al. 2013, Svensson et al. 2011)). In these studies it was observed that the MgO increase seems to correlate with changes in the 060 region of the powder X-ray diffractograms (XRD patterns), possibly indicating structural changes to the montmorillonite or neoformation of a new trioctahedral phase. Also in the Febex experiment at the Grimsel site, Switzerland similar changes were observed in the XRD patterns and accumulation of Mg and Fe towards the Fe-heater (Wersin and Kober 2017). In the ABM2 experiment samples were found on the surface of the corroding iron heater with a much higher occurrence of this new phase that was identified as a trioctahedral smectite most likely it was ferrosaponite (Svensson 2015). This phase was possibly neoformed from available interlayer Mg^{2+} cations, corroding iron products and dissolution of cristobalite and volcanic glass. Synthetic saponites can be produced fairly simple in the laboratory at 90 °C in only 20h (Vogels et al. 2005) when right precursors are available. The production of saponite observed in ABM2 and possibly also in the other experiments is expected to be limited by the available amount of precursors, hence the amount is expected to stay very low and have no significant impact on the buffer performance. In ABM5 the temperature was much higher compared to ABM2 (> 200 °C compared to approx. 130 °C) and no significant changes in the smectite content could be identified or any formation of trioctahedral smectite (Fernández et al. 2022, Kaufhold et al. 2021, Sudheer Kumar et al. 2021).

Laboratory experiments with pure montmorillonite in a compacted state at 90–150 °C showed that that silica was released during (i) leaching with constant water flow at the boundaries at 90 °C or (ii) in direct contact with a NaCl test solution at high liquid to solid ratio at 150 °C (Leupin et al. 2014). The silica release was interpreted as coming from montmorillonite resulting in a layer charge increase located in the tetrahedral sheets, and it was concluded that the montmorillonite consequently was altered in the direction towards a beidellite type smectite mineral. However it was also stated that the silica release could have its cause from e.g. cristobalite dissolution (something that is commonly observed in the field experiments described above), and the stated layer charge increase of the investigated material was not confirmed e.g. by using X-ray diffraction with alkylammonium ions or other interlayer cations suitable for layer charge determination.

Another series of experiments were performed using hot steam at temperatures up to 200 °C on water unsaturated bentonite (Leupin et al. 2014), with the conclusion that the hot steam had no significant impact on the water uptake capacity of the montmorillonite.

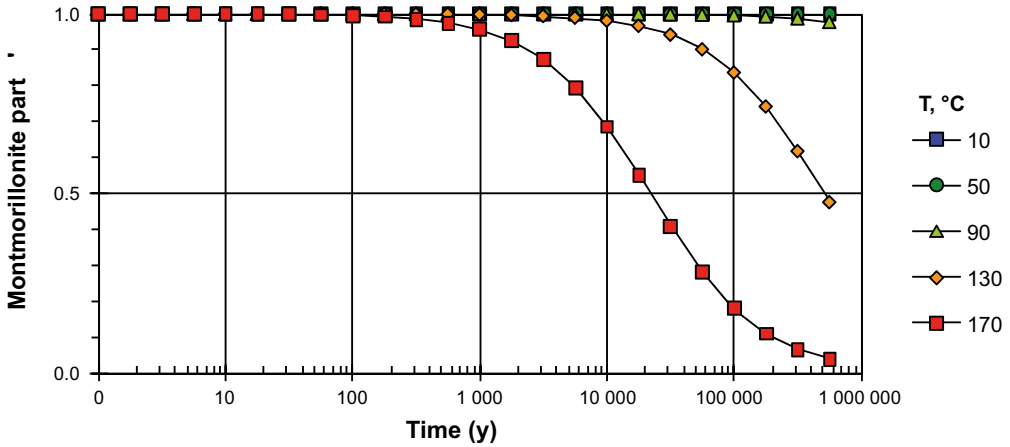

Figure 3-37. *Remaining smectite fraction for different temperatures in a hydrothermal system with $[K^+] = 0.0012$ mol/liter (45 ppm) according to the Huang et al. kinetic model and laboratory determined constants ($E_a = 28$ kcal · mol^{-1} and $A = 8.08E4$ L · s^{-1} · mol^{-1}) (Karnland and Birgersson 2006). Legend shows temperature in °C.*

Natural analogues/observations in nature

Apart from SKB-related investigations, the transformation of smectite to illite is well-documented in a large number of geological formations. Natural sediments have been studied by, among others, Burst (1969), Perry and Hower (1970), Hower et al. (1976), Colten-Bradley (1987), Velde and Vasseur (1992) and Lynch (1997). The studies show that increased sediment depth (increasing temperature) leads to increased illite content and that low availability of potassium can be linked to reduced transformation. Silica activity as a kinetically controlling factor has been studied in sediments (Abercrombie et al. 1994). Formations where temperature effects have been obtained from e.g. volcanic activity have revealed a similar transformation (e.g. Pytte 1982, Lynch and Reynolds 1985, Brusewitz 1986). Cementation may be a consequence of mineral alteration or precipitation reactions.New potential natural analogues have been identified in the Malmberget and Kiruna mines in northern Sweden, were clays rich in montmorillonite have been identified to occur from the surface level down to about 1 000 m deep in the ground. Chemical stability of montmorillonite in Swedish crystalline host rock over very long time periods is a valuable complement to laboratory studies and theoretical calculations. There will be efforts to determine the age of the montmorillonite rich clays in the coming years.

Time perspective

Reduction/oxidation reactions of iron may take place on a short time scale. Montmorillonite layer charge changes and associated precipitations may take place during the initial elevated temperature phase. Changes in montmorillonite content are relevant for the whole life-time of the repository.

Handling in the PSAR

The montmorillonite transformation in a KBS-3 repository is assumed to be small based on the following observations and arguments:

1. The time scale for significant montmorillonite transformation at repository temperatures in natural sediments is orders of magnitude longer than the period of elevated temperature in a KBS-3 repository (e.g. Velde and Vasseur 1992).
2. The bentonite material is close to mineralogical equilibrium to start with (e.g. Fritz et al. 1984).
3. Transformation is limited by low transport capacity, principally regarding potassium (Hökmark et al. 1997) and silica (Karnland and Birgersson 2006).
4. All published kinetic models, based both on natural analogues and laboratory experiments indicate that the transformation rate is very slow under repository conditions (e.g. Huang et al. 1993).

The montmorillonite transformation process can also be quantified by modelling, as exemplified above. Based on the above description, no mineral transformation is expected to be faster than illitization as a result of elevated temperature. Consequently, the maximum temperature effect is modelled by the kinetic expression for illitization proposed by Huang et al. and by use of different but realistic potassium concentrations. Adverse pH conditions could lead to increased dissolution of the montmorillonite and possible mass loss.

Two safety function indicator criteria have been defined. As long as the maximum temperature is below 100 °C and the pH of the water in the rock is below 11 the montmorillonite in the buffer is assumed to be stable for the timescale of the repository.

In the reference evolution, alteration is not expected to proceed to a level where it will affect the properties of the buffer. Alteration is therefore treated as a separate scenario.

Boundary conditions: The temperature and the composition of the groundwater.

Handling of variables influencing this process: See Model in Figure 3-33.

Handling of variables influenced by the process: The amount of remaining montmorillonite as a function of time will be calculated. The content of neoformed silica accessory minerals will also be calculated.

Uncertainties

Uncertainties in mechanistic understanding

There is a generally accepted explanation of the digenetic processes by which smectite is converted into illite accompanied by a release of silica, water and cations. There is, however, no general consensus concerning the details in the smectite-to-illite transformation mechanisms in a repository environment and a number of explanations for the character and mechanisms of the smectite-to-illite conversion have been proposed (Moore and Reynolds 1989):

Model simplification uncertainties for the above handling in the PSAR

Laboratory experiments have shown transformation rates that are faster than predicted by the kinetic models under the following extreme conditions. Consequently, these are not covered by the present models:

- Influence of low water content (Couture 1985).
- Extreme potassium ion concentration (Lee et al. 2010)
- pH effects:
  - High pH: (Velde and Vasseur 1992, Savage et al. 2002, Gaucher et al. 2004, Karnland et al. 2007, Savage et al. 2010).
  - Low pH: (Zysset 1992).

Input data and data uncertainties for the above handling in the PSAR

Thermodynamic and kinetic data for modelling silica dissolution/precipitation are not readily available especially for high pH and high temperatures. In transport calculations, the diffusion constants in rock and bentonite constitute an uncertainty. For obvious reasons, the kinetic constants are determined in laboratory experiments performed over relatively short durations and at higher temperatures and potassium concentrations when compared to the conditions they aim to simulate. The various illitization models currently available show a large variety in constant values and model formulae, which indicates conceptual problems. However, the set of determined constants and formulae generally results in similar long-term predictions (Karnland and Birgersson 2006).

3.5.9 Iron – bentonite interaction

Overview

Metallic iron will be present in several places in the repository; the iron insert in the canister and in rock reinforcements. The amount of iron is considerable. The fact that metallic iron is not thermodynamically stable in the repository ($E^0 < 0$ V) raises the questions: where does it go and what does it do? The answer is complex and implies that it depends on several factors such as the redox potential, the temperature, the pH, solute concentrations and the composition of the buffer (type of bentonite). Other less obvious factors may also be important such as the buffer density, liquid to solid ratio, temperature gradients, transport rates and microbes.

Standard iron corrosion in the absence of bentonite

The initial step in anaerobic corrosion takes place as follows:

$$Fe(s) + 2\ H_2O \leftrightarrow Fe^{2+} + 2\ OH^- + H_2(g)$$

If any oxygen is present, the reaction that follows is:

$$Fe(OH)_2(s) + ½\ O_2(g) \leftrightarrow Fe(OH)_3\ (s)$$

If carbonate concentrations are sufficiently high, carbonates will precipitate:

$$HCO_3^- + OH^- \leftrightarrow CO_3^{2-} + H_2O(l)$$

$$CO_3^{2-} + M^{2+} \leftrightarrow MCO_3(s)$$

If carbonic acid is absent, $Fe(OH)_2$ will precipitate, which is stable in the absence of oxygen at low temperatures. At higher temperatures (> 373 K), it will convert to the thermodynamically more favoured magnetite phase. The reaction is also possible at lower temperatures but is then much slower.

$$3\ Fe(OH)_2(s)\ Fe_3O_4(s) + H_2(g) + 2\ H_2O(l)$$

This possible build-up of magnetite and other corrosion products can passivate the iron surface and decrease the corrosion rate.

Iron corrosion in the presence of bentonite

The anaerobic corrosion of iron does not seem to be passivated in the same way in bentonite. The corrosion rate seems to be increased by the presence of bentonite. This is possibly due to the cation exchange capacity of the clay minerals which allows them to adsorb iron ions thereby minimising precipitation. In addition, corrosion and/or its products seem to react with the clay minerals creating new non-swelling minerals (Lantenois et al. 2005, Perronnet et al. 2008).

The most probable scenarios are:

- Formation of ion exchanged iron-montmorillonite.
- Reduction of the iron in the octahedral sheet of the montmorillonite structure, possibly coupled to dehydroxylation (reversible or irreversible).
- Dissolution and/or transformation of the montmorillonite.
- Formation of corrosion products with possible cementation of the buffer.

All scenarios will probably affect the buffer performance to some extent. The rate and degree of destabilisation of the smectite seems to depend on the nature of the smectite (dioctahedral/trioctahedral, counter ion and Fe^{III}-content) (Lantenois et al. 2005). The effect of iron reduction may have a negative impact on the hydraulic conductivity and the swelling properties. The cation fixation capacity has been observed to increase (Khaled and Stucki 1991).

Dependencies between process and buffer variables

Table 3-18 summarises how the process influences and is influenced by all buffer variables and how these effects are treated in the PSAR.

Boundary conditions

The relevant boundary condition for this process is the presence of iron in the adjacent system components. As long as the canister is intact, the only source of iron is in the construction materials within the repository. In the case of a failed canister, there will be large amounts of iron in close contact with the buffer.

Table 3-18. Direct dependencies between the process "Iron – bentonite interaction" and the defined buffer variables and a short note on the handling in the PSAR.

Variable	Variable influence on process		Process influence on variable	
	Influence present? (Yes/No) Description	Handling of influence (How/Why not)	Influence present? (Yes/No) Description	Handling of influence (How/Why not)
Buffer geometry	Yes, through transport of dissolved species and total buffer mass	Included in mass balance	Yes, for extreme unexpected transformation	Separate scenario
Pore geometry	Yes, through transport of dissolved species and ion equilibrium	Included in model/ expression used	Yes, by definition	Separate scenario
Radiation intensity	No		No	
Temperature	Yes	Neglected, since the reaction will occur late in the repository evolution	No	
Water content	Yes, through transport of dissolved species	Full saturation assumed	Yes, for extreme unexpected transformation	Neglected, importance is minor
Gas content	Yes, through transport of dissolved species	Neglected, since the reaction will occur late in the repository evolution	No	
Hydrovariables (pressure and flows)	Yes, minor through transport of dissolved species	Neglected since the major source of iron is present inside the canister	Yes, for extreme unexpected transformation	Separate scenario
Stress state	No, pressures are too small to be significant		Yes, for extreme unexpected transformation	Separate scenario
Bentonite composition	Yes, through available species in accessory minerals	Neglected, due to small effect compared to other sources	Yes	Precipitation of iron phases can be calculated
Montmorillonite composition	Yes, by definition	Included in model/ expression used	Yes, at extreme unexpected transformation	Separate scenario
Porewater composition	Yes, by definition	Included in model/ expression used	Yes, by definition	Included in model/ expression used
Structural and stray materials	Yes, determines availability of iron	No iron is assumed to be present as stray material in buffer	(No)	

Model studies/experimental studies

Most of the published results are based on experiments were the kinetic limitations have been reduced in some way. The most common ways to accelerate the processes are to increase the temperature, increase the liquid/solid ratio or to increase the reactive surface area by intimately mixing iron and clay powders. However the experimental results are very sensitive to the conditions and hence the results from the studies are rather scattered (Mosser-Ruck et al. 2010). It is clear that in laboratory studies with high liquid-solid ratio various clay minerals form fairly quickly, while in experiments using compacted bentonite and lower liquid-solid ratios, no or very few mineralogical changes occur. Hence, field experiments (e.g. ABM, TBT, Febex) using water saturated compacted bentonite at high temperatures are identified as most important sources of information as they are the closest to the real application. Compared with experiments using copper heaters there are more things happening in the bentonite when metallic iron is present, however so far, no significant decrease in the bentonite buffer performance have been observed:

Typical experimental results are the following examples:

(i) Iron powder mixed with different bentonites in deionised water was heated at 80 °C for 45 days. Ion exchange was noticed, and also magnetite and 7 Å phyllosilicate formation (Lantenois et al. 2005).

(ii) Carbon steel (coupons and wires) in compacted MX80 bentonite was heated (30 and 50 °C) with artificial groundwater for up to 900 days. No transformation of the montmorillonite was observed. Magnetite, hematite and goethite were identified as corrosion products. The results were consistent with sodium to iron ion exchange of the montmorillonite (Carlson et al. 2007).

(iii) FoCa7 bentonite was mixed with various ratios of powdered metallic iron in Evian water and heated for 45 days at 80 °C. The ratio of clay and iron seems to have an impact on the new phases formed. SiAlFe gels were created, which matured into Fe-rich phyllosilicates (identified as odinite or greenalite) (Perronet et al. 2008).

(iv) The Alternative Buffer Materials (ABM) experiments at Äspö HRL. More than ten different compacted clays were placed in contact with an iron heater at 130 °C in three packages in 2006 and in three more in 2012. ABM1 was excavated in 2009 and showed no proof of montmorillonite alteration, only minor increase in Mg-content in the bentonite closest to the heater, and increase in Fe(II)/Fe(III) ratio due to the corroding iron (Svensson and Hansen 2013a, Kaufhold et al. 2013, Svensson et al. 2011). In ABM2 the results were fairly similar to ABM1 with little or no alteration of the montmorillonite (Kaufhold et al. 2017, Kumpulainen et al. 2016). However, Svensson (2015) found formation of trioctahedral smectite in the vicinity of the corroding iron heater at one block interface with a Spanish bentonite. The amount of trioctahedral smectite was very low, the smectite type was identified as a ferrosaponite which also is a swelling clay just like montmorillonite. The ferrosaponite was most likely neoformed from accessory minerals together with the corroding iron and Mg^{2+} from the interlayer cations, and not formed by alteration from montmorillonite. The extent of ferrosaponite formation is expected to have no impact on the buffer performance. ABM5 was excavated in 2017 and more data is expected in the coming years.

(v) Temperature Buffer Test (TBT) at Äspö HRL. Minor increase in non-exchangeable Mg was found towards the 150 °C iron heater (Åkesson et al. 2012), dissolution of accessory minerals such as cristobalite, accumulation of Fe-corrosion products close to the heater. No neoformation of any clay minerals, no signs of montmorillonite alteration.

(vi) The Febex experiment at the Grimsel site, Switzerland. Minor changes in the XRD patterns indicating possible formation of trioctahedral smectite, accumulation of Mg and Fe towards the Fe-heater, minor decrease in CEC due to the dilution effect from the corroding iron heater (Wersin and Kober 2017).

Natural analogues/observations in nature

Possible analogues could be naturally occurring native iron (meteoritic or non-meteoritic) or perhaps old archaeological artifacts in contact with bentonites or other clays. However because of the rare nature and the uncertain history of the objects they are probably of limited value. Other natural analogues could be soils in anaerobic environments in rice fields where Fe-rich chlorites or 1:1 minerals have been identified (Favre et al. 2002).

Time perspective

The process may occur as long as iron is present in the repository.

Handling in the safety assessment in the PSAR

Since there will be very small amounts of iron present in the vicinity of the deposition hole, the process is assumed to be of insignificant importance to the buffer properties as long as the canister is intact.

For the case of a defective canister, alteration of some of the buffer caused by the interaction with metal iron cannot be ruled out based on current knowledge.

Iron-clay interaction was not assumed to change the major properties of the buffer in the SR-Site assessment. This will still be the assumption in the PSAR. However, since there are uncertainties regarding this process a sensitivity discussion will be included in the montmorillonite transformation scenario.

Uncertainties

Uncertainties in mechanistic understanding

There are uncertainties in the mechanistic understanding and the total possible impact from the metallic iron on buffer properties.

Model simplification uncertainties in the PSAR

No quantitative model is available. The possible consequences will be discussed with simple sensitivity studies.

Input data and data uncertainties in the PSAR

Not really applicable in this case.

3.5.10 Cementation

Overview

The term “cementation” has often been used in a broad sense to describe processes, which lead to specific changes in rheology and swelling properties of the buffer material. A number of quite different chemical/mineralogical and mechanical processes could conceivably cause cementation, and these are treated here. The accompanying sections dealing with related processes, i.e. montmorillonite stability, ion exchange, accessory mineral alteration, diffusive transport etc are consequently of most relevance for the cementation process. The main concerns regarding the effects of cementation of the bentonite buffer are increase in hydraulic conductivity reduction of swelling ability and increase of shear strength.

Cementation due to precipitation of minerals and amorphous compounds commonly leads to lower porosity, which in turn usually leads to lower hydraulic conductivity in soil and rock materials. However, the porosity in the bentonite buffer is as high as 43 %, and so the low hydraulic conductivity is obviously not due to low porosity but to montmorillonite/water interaction. Consequently, a large reduction in porosity caused by cementation may still lead to an increase in hydraulic conductivity if the montmorillonite/water interaction is reduced or counteracted by cementation.

Bentonite buffer rheology is characterized by low shear strength, i.e. the material deforms at relatively low shear forces. Precipitates may be expected to increase the shear stress and decrease the strain at failure, i.e. the material becomes more brittle. A rock displacement may thereby transmit higher shear stresses to the canister.

The most obvious cause of cementation is precipitation of minerals and amorphous solids in the bentonite. Potential mineral phases include gypsum, or anhydrite at high temperatures, calcite and silica minerals/compounds and iron oxide/hydroxide minerals/compounds. The underlying source

of ions may be the molecular structure of the montmorillonite mineral layer, the interlayer space, accessory minerals and the groundwater. The resulting cementation does not necessarily have to appear in the same volume, since released species can be transported in the buffer owing to the prevailing thermal and concentration gradients.

In addition to the mineralogical causes of cementation, there is a (principally) mechanical effect which may be of importance. The swelling pressure at a certain clay density is significantly dependent on the stress history of the bentonite material (Börgesson et al. 1995). A similar hysteresis may also be apparent in the rheological properties and the mechanical strength in consolidated clay would therefore have higher shear strength than a swollen sample at the same density. Such a purely mechanical cause of rheological changes is expected to have a limited and relatively small effect on buffer performance.

The mineralogical processes that lead to cementation may take place at relatively low temperatures, but all experimental data indicate that the processes are only of importance at relatively high temperatures, in response to temperature gradients or after relatively large temperature changes.

Dependencies between process and buffer variables

Table 3-19 summarises how the process influences and is influenced by all buffer variables and how these effects are treated in the PSAR.

Boundary conditions

The boundary conditions for the cementation process are the porewater composition, groundwater composition, temperature in different parts of the buffer and the buffer composition.

Model studies/experimental studies

The principal mineralogical processes that may cause cementation are treated separately in the descriptions of underlying processes; mainly Montmorillonite Transformation (Section 3.5.9), Alteration of Accessory minerals (see Section 3.5.6), and Sorption (Section 3.5.3). In general, there is extensive knowledge concerning precipitation in soil material and a vast number of publications with regard to natural systems, experimental work and modelling. There are also a number of publications dealing more specifically with cementation in radioactive waste repositories and several are related to SKB projects (e.g. Pusch 1977, Pusch et al. 1998). The CEA/SKB field test at high temperatures (170 °C) relative to KBS-3 conditions, which were performed in the Stripa mine, showed extensive precipitation of especially anhydrite but also of silica compounds in the warmest part. The ductility of the innermost centimetre was completely lost and the hydraulic conductivity dramatically increased (Pusch et al. 1993a). Material from the one year LOT S1 test, performed at a maximum temperature of 90 °C at the Äspö HRL, did not show any increase in shear strength or in hydraulic conductivity (Karnland et al. 2000). Material from the LOT A2 test, exposed to a maximum temperature of 130 °C for 6 years, had slightly altered rheological properties in the form of reduced strain at failure, but no changes in hydraulic conductivity were found (Karnland et al. 2009). Minor mineralogical changes were found in the warm sections in this material; calcium sulphate, in particular, was redistributed and precipitated in the form of anhydrite in the warm sections. No clear correlation was found, however, between the calcium sulphate content and reduced strain. Similar behaviour was also observed by Dueck (2010) in short term laboratory tests. Dueck made the observation that the observed influence of temperature occurred already after very short term heating (a couple of hours) and that milling and re-compaction after heating restored the original properties of the bentonite (indicating no mineralogical changes). Further, the influence of temperature on the maximum stress at failure was in the same range as the difference between the tested bentonites, indicating that the observed changes in the properties in the experiments were in the range of the detection limit of the method. Unconfined compression tests were performed on samples from the Prototype Repository experiment at Äspö (Olsson et al. 2013) and it was concluded that the scatter in the method was relatively large in relation to the possible minor differences in strength between the reference specimens and the field-exposed material.

Arthur and Zhou (2005) have performed geochemical modelling and concluded that the total extent of mineral mass transfer, represented by spatial and temporal variations in porosity, may be small in a KBS-3 repository throughout the non-isothermal period. Assessing the effects of such changes on buffer performance is problematic, however, because it is unclear how mineralogical changes affect the physical, mechanical and rheological properties of these materials. Further relevant geochemical modelling is presented in the section on Alteration of Accessory minerals 3.5.6.

Table 3-19. Direct dependencies between the process "Cementation" and the defined buffer variables and a short note on the handling in the PSAR.

Variable	Variable influence on process		Process influence on variable	
	Influence present? (Yes/No) Description	Handling of influence (How/Why not)	Influence present? (Yes/No) Description	Handling of influence (How/Why not)
Buffer geometry	No		No	
Pore geometry	Yes, through ionic equilibria	See Sections 3.5.6 and 3.5.9, Alteration of accessory minerals and montmorillonite transformation	Yes, main effect	See Section 3.5.6, Alteration of accessory minerals
Radiation intensity	No		No	
Temperature	Yes, major impact	See Sections 3.5.6 and 3.5.9, Alteration of accessory minerals and montmorillonite transformation	Yes, minor effects through changes in thermal conductivity.	Neglected unless modeling shows significant amounts of precipitation
Water content	Yes, Major impact	See Section 3.5.6, Alteration of accessory minerals	Yes, through changes in porosity	See Section 3.5.6, Alteration of accessory minerals
Gas content	Yes, through concentration	See Section 3.5.6, Alteration of accessory minerals	No	
Hydrovariables (pressure and flows)	Yes, through transport of species	See Section 3.5.6, Alteration of accessory minerals	Yes, indirect through pore geometry, central impact	See Sections 3.5.6, 3.5.5 and 3.5.9, Alteration of accessory minerals, sorption and montmorillonite transformation
Stress state	Yes, through ionic equilibria	See Section 3.5.6, Alteration of accessory minerals	Yes, major possible impact by changed rheological properties	See Section 3.5.6, Alteration of accessory minerals
Bentonite composition	Yes, accessory minerals are of major importance	See Section 3.5.6, Alteration of accessory minerals	Yes, by definition in case of precipitation	See Sections 3.5.6 and 3.5.9 , Alteration of accessory minerals and montmorillonite transformation
Montmorillonite composition	Yes, through mineral composition and ionic equilibria with charge compensating ions	See Sections 3.5.6, 3.5.5 and 3.5.9, Alteration of accessory minerals, sorption and montmorillonite transformation	Yes, by definition if the underlying process is montmorillonite alteration	See Sections 3.5.5 and 3.5.9, sorption and montmorillonite transformation
Porewater composition	Yes, by definition	See Sections 3.5.6, 3.5.5 and 3.5.9 , Alteration of accessory minerals, sorption and montmorillonite transformation	Yes, by definition in case of precipitation	See Sections 3.5.6, 3.5.5 and 3.5.9 , Alteration of accessory minerals, sorption and montmorillonite transformation
Structural and stray materials	Yes, especially the concrete and iron	See Sections 3.5.6, 3.5.5, and 3.5.9 , Alteration of accessory minerals, sorption and montmorillonite transformation	No	

Effects on material properties from slow re-saturation

The bentonite in the buffer consists of mainly of the clay mineral montmorillonite together with a minor proportion of common used minerals such as quartz, feldspar, gypsum etc. The sealing properties of the bentonite are essentially linked to the montmorillonite, mainly through interaction between montmorillonite counter-ions and water.

Studies of bentonite materials under full water saturation have strongly dominated the general research efforts, as this is the common condition in natural systems. Studies for final repositories have also mainly considered a water saturated buffer. However, a few studies specifically relating to structural and/or mineralogical conversion of bentonite under unsaturated conditions have been conducted.

Some studies have also touched on the special conditions, with elevated temperature and varying degrees of saturation, which may be prevailing in a final repository.

Slow water saturation generally causes transient conditions and gradients to prevail for a longer period than in the case of a rapid water saturation. High temperature conditions could potentially affect the buffer properties in a negative direction, through steam, bacterial activity, transport and enrichment of dissolved species. This is discussed and investigated in both laboratory trials and field trials. Sellin et al. (2017) has made a summary of the studies available and underway that deal with these processes:

- In terms of physical properties such as shear strength, shear elongation, swelling pressure and hydraulic conductivity as a result of short-term elevated exposure (up to 150 °C) it appears that there is an tendency of increased shear strength and a significant change in maximum strain failure as a result of short-term hydrothermal treatment. However, the effect is equal to or greater for samples heated under saturated conditions compared to those heated without an external water pressure. Swelling pressure and hydraulic conductivity are not affected by short-term heating irrespective of hydraulic conditions.
- Vapour transport tests in bentonite show that vapour condensed under all investigated conditions, and that water absorption from condensation water totally dominated over water absorption directly from vapour. All tests showed that water absorption decreased over time, indicating that the pellet system was sealed and that vapour transport decreased with time.
- Test series of material exposed to temperatures of up to 200 °C at different water saturation levels show no clear differences due to hydrothermal treatment between unsaturated and water-saturated samples with respect to swelling capacity (Figure 2-8).
- Generally, differences in measured swelling properties due to hydrothermal treatment are negligible in comparison to the differences between sodium dominated and calcium-dominated materials. The effects of short-term vapour pressure on free swelling are therefore not considered to be a problem for a KBS-3 repository. One study included experiments with bentonite at different degrees of water saturation (0, 50, 85 and 100 %) exposed to temperatures up to 150 °C. After hydrothermal treatment, the samples were saturated and swelling pressure and hydraulic conductivity was determined both at elevated temperature and at room temperature. In no case was any significant change in the properties compared to the reference materials.
- Precipitation of secondary minerals in the buffer, e.g. $CaSO_4$, in a temperature and water saturation gradient has been observed in field tests. However, these reactions are reversible and the precipitated minerals will be dissolved when water saturation increases. The precipitates are therefore not expected to affect the performance of the buffer.

There is nothing in the above-mentioned studies suggesting that there would be changes in the properties caused by mineralogical changes due to short-term exposure to dry or semi-dry conditions at high temperatures. The transport capacity of dissolved species can generally be expected to be lower at low water content than at full water saturation, which counteracts most known transformation processes.

Natural analogues/observations in nature

There is a vast literature on soil cementation due to mineral precipitation, and it concerns a variety of mineralogical alterations. The challenge is therefore to discriminate processes relevant for repository conditions and to determine the prevailing geological conditions under which the cementation took

place; attempts have been made by several groups (e.g. Pusch and Madsen 1995, Metcalfe and Moore 1998, Pellegrini et al. 1999, Henry et al. 2007). Cementation effects as a consequence of illitization have been studied by, among others, Hower et al. (1976) and Boles and Franks (1979).

Time perspective

Cementation is expected to take place mainly during the water saturation phase and within the non-isothermal period. The effects may, at least to some extent, remain during the whole life-time of the repository.

Handling in the PSAR

The mineralogical evolution in the buffer is presently being modelled, and cementation effects will be judged based on the extent of precipitation. Presently, the process is neglected based on the modelling performed previously and experimental results for rheology.

Uncertainties

Uncertainties in mechanistic understanding

The role of bentonite pore structure and the handling of pore space in geochemical modelling are subject to debate. There is a general problem of how to assess changes in mineralogy on buffer performance, because it is not clear how all possible changes affect the physical, mechanical and rheological properties of the bentonite buffer.

Model simplification uncertainties for the above handling in the PSAR

See Section 3.5.6 (Alteration of accessory minerals) concerning the geochemical modelling.

Input data and data uncertainties for the above handling in the PSAR

See Section 3.5.6 (Alteration of accessory minerals) concerning the geochemical modelling.

3.5.11 Montmorillonite colloid release

Overview

This process covers expansion of bentonite into fractures, erosion of bentonite under dilute water conditions, as well as the sedimentation of bentonite in sloping fractures under dilute water conditions.

The uptake of water and resulting swelling of the bentonite buffer is counteracted by the walls of the deposition hole, and a swelling pressure is developed in the bentonite (see Section 3.4.1 Swelling/ mass redistribution). Fractures intersecting the deposition hole mean that rigid swelling restrictions are not present everywhere, and that localized swelling continues into the fractures until an equilibrium or steady state is reached. This free swelling may lead to separation of individual montmorillonite layers (dispersion) and part of the buffer could be transported away by groundwater.

The maximum free swelling of the bentonite is strongly dependent on the valence and concentration of the ions in the interlayer space. At sufficiently low groundwater cation concentrations, the interlayer distance between the individual montmorillonite layers may increase enough to give the clay/water system a sol character, i.e. single or small groups of montmorillonite layers act as individual colloidal particles.

The maximum interlayer distance, when only monovalent cations are present in the solution, may be discussed in terms of the Debye-Hückel screening length, which is inversely proportional to the square root of solution concentration. The same dependence on interlayer separation with solution concentration has been experimentally determined (Norrish 1954a, b). The forces between parallel montmorillonite layers with only monovalent ions present can be calculated for an ideal system from DLVO theory (Derjaguin and Landau 1941, Verwey and Overbeek 1948), in which the entropic repulsive effects from ions and the attractive van der Waals forces are taken into account. In the case

that only divalent ions are present in the system, additional attractive forces become significant, which restrict the swelling to relatively short interlayer distances and prevent release of individual colloid particles (Guldbrand et al. 1984, Kjellander et al. 1988). However, a relatively small content of monovalent ions in a calcium-dominated system may still lead to general colloidal sol formation in deionised water or at very low ion concentrations (Birgersson et al. 2010, Hedström et al. 2011).

For simple model systems such as charged spheres or parallel extended flat charged surfaces, the concept of a critical coagulation concentration (CCC) is readily defined within the DLVO theory as the salt/electrolyte concentration where the energy barrier for particle-particle association approached zero (e.g. Evans and Wennerström 1999). At the CCC and higher salt concentrations the attractive van der Waals forces dominate the system and colloidal particles will be held together and not disperse spontaneously. If one considers montmorillonite as extended negatively charged surfaces ordered in parallel, the calculated CCC for a 1:1 salt e.g. NaCl within DLVO theory turns out to be in the range 1–2 M. However, experimentally the transition from sol to attractive gel is observed to take place at much lower concentrations (van Olphen 1963, Le Bell 1978, Hetzel and Doner 1993, Abend and Lagaly 2000, Wold 2003, Lagaly and Ziesmer 2003, Tombács and Szekeres 2004). This strongly suggests interactions other than face-to-face DLVO forces, in real montmorillonite systems. It has been proposed (van Olphen 1963) that flocculation of clay could be a result of the interactions between positive charges present on the edges of clay particles and negative charges on the faces of the clay particles. Missana and Adell (2000) have shown that the small fraction of the pH-dependent charges on the edge greatly influence the stability behaviour of the clay colloids and that the standard DLVO theory for parallel clay layers is not particularly suitable for predicting the stability, mainly because it is not able to account for this charge contribution. However, the concept of a CCC need not be defined within the framework of a particular theory but from observations alone as the concentration where an attractive gel can be formed (e.g. Abend and Lagaly 2000).

A CCC may be determined for monovalent systems and used as a pessimistic concentration limit for spontaneous colloid particle release. Governing variables are the concentration and the layer charge of the montmorillonite. Laboratory results have shown that montmorillonite extracted from MX-80 bentonite and ion-exchanged to Na^+-state has a CCC of around 25 mM in NaCl solution, i.e. an attractive gel is formed (Birgersson et al. 2010). Two other Na- montmorillonites analysed in the same study with higher layer charge than in MX-80 were found to have lower CCC, in contrast to predictions from DLVO theory for parallel layers (Evans and Wennerström 1999). For systems with only divalent counterions the CCC concept is not really valid, and the CCC may be considered zero, i.e. no excess ions are needed in order to prevent colloidal sol formation of colloidal particles as demonstrated in e.g. Ch 4 in Birgersson et al. (2010) or from theoretical considerations (Kjellander et al. 1988). For a mixed system with both mono and divalent counterions one also needs to consider ion equilibrium (Kahn 1958). Thus one cannot speak in terms of a CCC for Ca^{2+} for Na-montmorillonite as such a value cannot exist. The limiting condition for colloidal sol formation is thereby given by combinations of ion concentrations and monovalent/divalent ion ratios in the clay/water system illustrated in Figure 3-38.

The central conditions for possible colloid formation in a repository are consequently the local porewater concentration and the ratio between mono and divalent ions in the montmorillonite at the bentonite/groundwater interface. The governing processes are ion exchange of the original montmorillonite counterions by ions originating from the accessory minerals and from the surrounding groundwater.

Based on present knowledge, significant formation of colloids and subsequent buffer mass loss cannot be excluded over the time scale of several glaciations.

Table 3-20 summarises how the process influences and is influenced by all buffer variables and how these effects are treated in the PSAR. Note though that the process occurs at the boundary between buffer and rock, within rock fractures making the boundary conditions described below of prime importance for the understanding and quantification of the process.

Boundary conditions

The boundary conditions are the cation concentration and cation valence of the groundwater in direct contact with the outermost part of the bentonite buffer and also the cation pool in the bentonite itself.

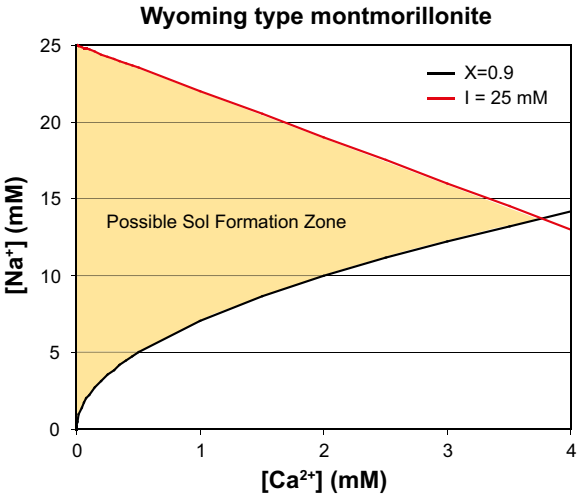

Figure 3-38. *Limitations of a possible sol formation zone for Wyoming type montmorillonite in equilibrium with an external Ca/Na-solution and monovalent anions (e.g. Cl-). The lower curve (X=0.9) represents the experimental finding that when the Ca fraction is 0.9 or higher in the clay no sol is formed irrespective of the ionic strength in the external solution. On the upper curve the ionic strength equals 25 mM, which is the CCC value for Wyoming-type montmorillonite in NaCl solution (Birgersson et al. 2010, 2011).*

Table 3-20. Direct dependencies between the process "Montmorillonite colloid release" and the defined buffer variables and a short note on the handling in the PSAR.

Variable	Variable influence on process		Process influence on variable	
	Influence present? (Yes/No) Description	Handling of influence (How/Why not)	Influence present? (Yes/No) Description	Handling of influence (How/Why not)
Buffer geometry	Yes, the amount of buffer present	Included in modelling	Yes, at extreme process magnitude	Included in modelling
Pore geometry	Yes, governs the dispersing forces	Included in modelling	Yes, by definition	Included in modelling
Radiation intensity	No		No	
Temperature	No, negligible		No	
Water content	Yes, by definition	Full saturation assumed	Yes, by definition	Full saturation assumed
Gas content	Yes, no dispersion possible from unsaturated clay	Full saturation assumed	No	
Hydrovariables (pressure and flows)	Yes, by definition	Included in modelling	Yes, indirect through pore geometry, central impact	Evaluated from modelling results
Stress state	Yes, by definition	Included in modelling	Yes, major impact	Included in modelling
Bentonite composition	Yes, accessory minerals may govern the ion type and concentrations	Included in modelling	Yes, selective loss of the clay component	Included in modelling
Montmorillonite composition	Yes, important variables are magnitude and distribution of layer charge, and type of cations	Included in modelling	Yes, possible through selective formation of colloids	Neglected
Porewater composition	Yes, major importance both with respect to cation type and concentration	Included in modelling	Yes, through pore geometry	Included in modelling
Structural and stray materials	Yes, concrete, especially, may provide calcium ions	Neglected, no concrete assumed in buffer	Yes, minor effects possible through calcium uptake	Neglected

Water flow in the fractures will not affect the stability of the sol phase. However, the interlayer distance between the montmorillonite layers is continuously increasing with decreasing electrolyte concentration and layers at large separation are more sensitive to erosion than layers at close separation. Water flow may tear loose montmorillonite even before the clay formally turns into a sol. The extent of such particle release by flow is dependent on the flow velocity. Without flow the particles will sediment. The treatment of erosion under such condions is presented in Section 3.3.4.

Model studies/experimental studies

Background

Expansion of bentonite into fractures for groundwater conditions above CCC was not treated in SR-Site (SKB 2011). The overall assumption was that the friction between the bentonite and the rock would be sufficient to limit the expansion to negligible values.

The principles for swelling of montmorillonite in 1:1 electrolyte solutions have been reported in a large number of publications. The basic theoretical principles are described by the DLVO theory (Derjaguin and Landau 1941, Verwey and Overbeek 1948). For divalent cations additional attractive correlation forces come in to play which necessitates a theoretical treatment beyond the DLVO theory (Guldbrand et al. 1984, Kjellander and Marčelja 1984, Kjellander et al. 1988). Interlayer distances were experimentally determined by Norrish (1954a, b), and several subsequent studies have in principle confirmed these results, e.g. those by Zhang and Low (1989). Several laboratory studies have been made in order to determine the critical coagulation concentration for montmorillonite in sodium chloride solutions (van Olphen 1963, Le Bell 1978, Hetzel and Doner 1993, Abend and Lagaly 2000, Wold 2003, Lagaly and Ziesmer 2003, Tombács and Szekeres 2004, Laaksoharju and Wold 2005, Birgersson et al. 2010). A large body of work suggests the mechanism for montmorillonite coagulation in NaCl is edge-face interactions (e.g. Lagaly and Ziesmer 2003, Tombács and Szekeres 2004, Birgersson et al. 2010) although opinions differ concerning the pH range where the edge charges may be positive.

For to the SR-Site assessment (SKB 2011) a DLVO based force-balance model for spherical colloids (Petsev et al. 1993) was adapted to parallel clay layers (Liu et al. 2009, Neretnieks et al. 2009) and used to calculate the swelling of Na-montmorillonite into fractures filled with water of low ionic strength (1:1 salt). The force-balance model uses DLVO to describe swelling pressure and Kozeny-Karman-like expression fitted to experiments to describe hydraulic conductivity. The model was adjusted and tested towards free-swelling experiments obtained through magnetic resonance imaging (MRI) (Dvinskikh et al. 2009). Advective loss of montmorillonite was modelled by combining the force-balance model for swelling with a viscosity model for the repulsive montmorillonite gel and the Darcy equation for two-dimensional flow in a fracture intersecting the deposition hole. It was found that the continuous ion exchange could be neglected because at the rim, where the expanding clay turns to sol, the ion concentration becomes essentially the same as that of the approaching water. Even so, the very nonlinear PDE is difficult to solve with high accuracy with finite element or other discretization methods because the location of the rim constantly moves and the rim-zone, i.e. the location where the solubilisation and onset of sol flow occurs is very thin compared to the region that needs to be modelled to follow the expanding clay.

For application in the safety assessment SR-Site, a simple analytical expression for the loss at the rim was fitted to the results of the numerical model. The loss rate, $N_{Erosion}$, is described by (Neretnieks et al. 2009)

$$N_{Erosion} = A \cdot \delta \cdot v^{0.41} \tag{3-32}$$

where $A = 27.2\ \mathrm{kg \cdot m^{-1.41} \cdot yr^{-0.59}}$, δ (m) is the fracture aperture and v (m/yr) is the water velocity.

Due to the computational difficulties with the numerical model, potentially leading to considerable errors, a need for further model development was seen.

In the models described in Neretnieks et al. (2009), the expansion was taken to be horizontal, thus neglecting gravity. Scoping calculations suggested that gravity will give small effects as in the model the smectite sheets have separated into essentially individual colloid particles. For gravity to have an effect the particles must be considerably larger.

The general significance of clay expansion, erosion and sedimentation for the KBS 3 concept has led to considerable both experimental and theoretical efforts in the past decade. That work is summarised and discussed below.

Expansion into fractures for ionic strengths above CCC and no flow

According to Neretnieks et al. (2017) for ion strengths above CCC, the expansion only depends on time as the loss at the rim is zero. Furthermore it is assumed that the loss is small compared to the total amount of clay in the deposition hole so that the volume fraction of clay in the deposition hole is essentially constant. The approach is the same as that in Liu et al. (2009) and in Neretnieks et al. (2009). The radius r_R (metres) of the expanded clay sheet in the assumed circular fracture after time t (years) can then be well fitted by the following expression:

$$r_R(t) = 1.300 + 0.3428\sqrt{t} - 0.0000335t \qquad (3\text{-}33)$$

According to Equation (3-33) the expansion would extend to > 100 m in a period of 100 000 years even for groundwater concentrations above CCC.

This approach is in conflict with the view of Börgesson et al. (2018), where a theory is developed for the bentonite penetration into a horizontal fracture. The penetration depth is analysed in terms of the equilibrium situation where the swelling is completed, and the swelling pressure is balanced by the friction against the fracture walls. There are several ways of estimating the friction angle at the low dry densities relevant for the non-swelling gel. Depending on the approach taken and the swelling pressure chosen the evaluated friction angles show large variations; from 0.5° to 30°. However, by using these large variations in the sensitivity analyses it was possible to show that the penetration into a 100 µm wide fracture is anyway limited to < 80 mm at the lowest friction angle. Comparison between theory and experimental swelling of Wy-Na into a 120 µm fracture gives best agreement for the highest friction angle, 30° which gave a penetration depth in the vicinity of 1 mm. Thus, it was concluded that above the CCC the bentonite swelling into fractures is limited to distances very much smaller than the deposition hole diameter. Other tests above and below CCC have confirmed this conclusion. The two approaches give totally different results. Neretnieks et al. (2017) gives a substantial mass loss, while the calculated loss from Börgesson et al. (2018) is negligible. It is noted that all available experimental results support the approach by Börgesson et al. (2018).

Expansion into fractures for ionic strengths below CCC and no flow

In Alonso et al. (2019) it is shown that in the experiments, where the clay extrusion in the fracture was followed during 30 days, periodical photographs were taken to measure extrusion distances. Eroded masses and physico-chemical evolution were evaluated by post-mortem analyses. All erosion experiments carried out within narrow fractures with apertures smaller than 1 mm, showed that clay extrusion in the facture was stopped at some time. Clay expansion was favoured within fractures of wider apertures. In general, Na-rich bentonites (Nanocor® or Na-exchanged MX-80) exhibited longer extrusion distances than raw MX-80 or Ibeco. Extrusion distances measured for Ca- exchanged bentonites, or other clays as saponite, were clearly shorter, but not null. As suggested by previous studies, which related clay erosion capability to its intrinsic characteristics, the relevance of clay properties is again pointed out.

Erosion experiments (Schatz et al. 2013)

Schatz et al. (2013) performed laboratory tests using purified, homo-ionic sodium and calcium montmorillonites. Wyoming bentonite sold as the commercial product Volclay MX-80 was used as starting material for the preparation of homo-ionic montmorillonite fractions used in these experiments. Experiments were conducted using custom-designed, small-scale, flow-through artificial fracture cells. The aim of this work was to perform experiments which would examine the extrusion/erosion behaviour of bentonite buffer material into an intersecting, transmissive fracture environment over a range of solution chemistry (salt concentration and composition), material composition (sodium montmorillonite and admixtures with calcium montmorillonite), and flow velocity conditions. Clear distinctions were observed between those tests for which erosive mass loss was observed and those for which it wasn't. Specifically, no erosion was observed for sodium montmorillonite against solution

compositions from 10 g/L to 0.5 g/L NaCl. Most reports in the literature indicate that a concentration of 0.5 g/L NaCl (8.6 mM) is below, in some cases well below, the (experimentally observed) critical coagulation concentration (CCC) for the colloidal sodium montmorillonite/sodium chloride system. The reported CCC values were all obtained under batch conditions whereas the artificial fracture test results correspond to spatially confined, dynamic conditions which are of more relevance to the erosion scenario. No erosion was observed for 50/50 calcium/sodium montmorillonite against 0.5 g/L NaCl either (see Section 3.2.7).

Although it has been demonstrated that a CCC value for clay/water systems containing both mono and divalent counterions cannot be defined in terms of a single, aqueous cation concentration due to ion exchange (Birgersson et al. 2009), erosion tests on such mixed electrolyte systems can be used to establish stability. A number of tests were conducted for which measurable erosion was observed (Schatz et al. 2013). For most of these tests erosion was observed to begin almost immediately upon contact between the compacted material and the dilute solution and continue throughout. The sole exception to this characteristic was 50/50 calcium/sodium montmorillonite against a flowing 4 mM NaCl solution where erosive conditions first developed only after a much longer period of time. The overall mass loss rates for the tests with the highest levels of observed erosion, appear to be well-correlated to flow velocity (in terms of a power law relationship with $y = 2.5 \times 10^{-5} x^{0.27}$). Interestingly, 50/50 calcium/sodium montmorillonite against flowing deionised water erodes with the same functionality as does sodium montmorillonite against flowing deionised water. In other words, no effect on erosion due to material composition (at the levels examined here) was observed at zero ionic strength. Similarly, sodium montmorillonite against flowing Grimsel groundwater simulant erodes with the same functionality as sodium montmorillonite against flowing deionised water. As such, no effect on erosion due to solution composition was observed up to the ionic strength of Grimsel groundwater. Other tests, for which erosion was also observed, are not equivalently associated to the flow rate. The erosive mass loss for these tests was attenuated by factors of 2–10, relative to the correlated behavior of the test showing the highest erosion. This attenuation can be attributed solely to solution composition effects, i.e., increased ionic strength, and to solution and material composition effects, possibly in combination. The difference in erosive mass loss between the test 50/50 calcium/sodium montmorillonite against a flowing 4 mM NaCl solution) and the test with sodium montmorillonite against a flowing 4.3 mM NaCl solution indicates that both material and solution composition can significantly affect erosion rates. Based on the results of the flow-through, artificial fracture tests, stability to erosion was observed down to a dilute concentrations between 8.6 and 4.3 mM NaCl solution for sodium montmorillonite and 8.6 and 4 mM NaCl for 50/50 calcium/sodium montmorillonite. The latter limit compares favorably with that postulated by Birgersson et al. (2009) for montmorillonite with calcium content greater than 20 % based on observations using a completely different experimental technique, i.e., a modified swelling pressure test. Two additional tests were performed using as-received, MX-80-type bentonite in contact with the Grimsel groundwater simulant. The aggregate erosion rates for these tests were slower by more than an order of magnitude compared to that observed for the sodium montmorillonite system under similar solution and flowrate conditions. These observations are likely attributable to soluble salts in the as-received material. As observed in every test in the artificial fracture systems, material extruded into the fracture and, furthermore, this material (as often demonstrated, even under erosive conditions) was impermeable to water flowing in the fracture. In other words the zone of extruded buffer material forms an extended diffusive barrier around the intersecting fracture/buffer interface.

Sedimentation experiments (Schatz and Akhanoba 2016)

Schatz and Akhanoba (2016) made an effort to address the potential effect of gravity on the extrusion/erosion behaviour of bentonite buffer material in contact with dilute groundwater flowing through intersecting, transmissive fractures in sloped fracture environments, a series of experiments were performed in flow-through artificial fracture systems positioned at steep slope angles. 52 experiments were made to specifically study erosion under impact of gravity. This was done in fractures at 0, 45 to 90 degree angle from the horizontal. Concentrations covered 0–171 mM NaCl using NaMt as well as NaMt/CaMt in proportion 50/50. Water velocities were 7.1×10^{-6} m/s (230 m/yr) in most experiments with 1 mm aperture fractures. Three experiments were made in a fracture about five times the area of the smaller ones with about the same velocity. Two experiments were made in 0.1 mm aperture fractures, one with 10 times higher velocity and one with stagnant water.

Figure 3-39 shows examples of expanding clay, which releases flocs that sediment in a 45 degree fracture. It is seen that in the narrow fracture the flocs have agglomerated to form a coherent structure that can be broken up in larger sections that move independently. In the larger aperture fracture the small, hardly visible, flocs have not joined into a coherent "agglomerate fluid". In an effort to determine whether extrusion and erosion behaviour in sloped fractures is affected by the presence of non-swelling clay accessory minerals, results between tests performed with montmorillonite samples and those with samples containing accessory minerals as well can be compared. In the horizontal fracture test, the formation of a uniform layer of sand particles near the extrusion/erosion interface can be observed. Moreover, this layer grew progressively in thickness over the course of the test. These results provide evidence that, following erosive loss of montmorillonite through contact with sufficiently dilute groundwater at a transmissive fracture interface, non-erodible accessory phases (within bentonite) remain behind and form into layers at the solid/solution interface. In the sloped fracture test, on the other hand, no such sand layering is observed except at the very top of the extruded ovoid body. This observation indicates that sand particles, similar to those of montmorillonite, are released due to gravity whenever they are exposed at the solid/liquid interface. The (total) mass loss rates determined from the sloped fracture tests with these samples indicated that the resulting rate was faster in the case of the montmorillonite/sand mixture (2.37×10^{-9} kg/s) than for that with montmorillonite alone (2.00×10^{-9} kg/s) by nearly 20 %. This increase can possibly be attributed to the presence of the large sand particles (narrowly distributed around a mean value of ~250 μm) in the extruding matrix. The results support earlier findings qualitatively in several important ways. Erosion is only found at ion concentrations below somewhat less than 10 mM NaCl and for all bentonites with mostly Na as charge balancing ion. Clay expansion into the fractures is observed with all clays up to several cm before again receding when there is erosion and the source is partially depleted. When there is erosion, the rate of erosion seems to be correlated to the area of the clay/water interface i.e. perimeter times aperture irrespective of whether the fracture is horizontal or has a slope of 45 or 90 degrees. Sloping fractures practically always give larger erosion rates than horizontal fractures.

Experimental and theoretical studies of montmorillonite phase behaviour (Hedström et al. 2016)

Hedström et al. (2016) reported several studies aiming at understanding the phase behaviour of montmorillonite. Of the three main montmorillonite phases (paste, gel, and sol), colloid erosion is only likely to occur when the montmorillonite turn into a sol, which is liquid, and the transformation to a sol is linked to the aqueous chemistry of the groundwater. For homoionic Na-montmorillonite the sol phase is possible when the ionic strength (NaCl concentration) is below the CCC. For homoionic Ca-montmorillonite the sol phase is absent due to correlation forces. In the study, further investigations were done on the break-up behaviour by mixing suspensions of Na-montmorillonite with Ca and Mg-montmorillonite, using montmorillonite from three different origins (Wyoming; Milos, Greece; Kutch region, India). For both Wy- and Mi-montmorillonite the 20 % Na^+ limit was confirmed, while the Ku-80/20 montmorillonite show less break-up than the other two. This is also in accordance with the theory for correlation effects, which are stronger the higher the CEC. The experiments also show that the break-up process is fast: within 10 minutes the turbidities of the mixed suspensions have stabilized. Furthermore, these experiments on break-up were performed using DI water thus showing that excess ions are not needed to mix the ions. Na^+ diffuses into the interlayer of the Ca-montmorillonite tactoids and Ca^{2+} diffuses out and eventually all the clay is a mixed Ca/Na-montmorillonite. A large part of the study was devoted to increase the understanding of the gel state. From a theoretical perspective it was shown that standard DLVO theory for parallel layers is not applicable to smectite clays in low particle volume fraction (ϕ_c) region where gels are formed. The van der Waals interaction (using a relevant Hamaker constant and a representative clay layer area) becomes weaker than thermal fluctuations at $\phi_c \approx 1/17$, while we herein have presented gels formed at $\phi_c \approx 1 \times 10^{-4}$. The only plausible force responsible for gelation of montmorillonite is electrostatic edge-to-face attraction. In order for modelling work on bentonite erosion under low salinity conditions to be relevant, this interaction must be included. Models based on DLVO for parallel layers cannot explain, e.g., the low CCC values that are found in experiments or the complex behaviour of the phase diagram.

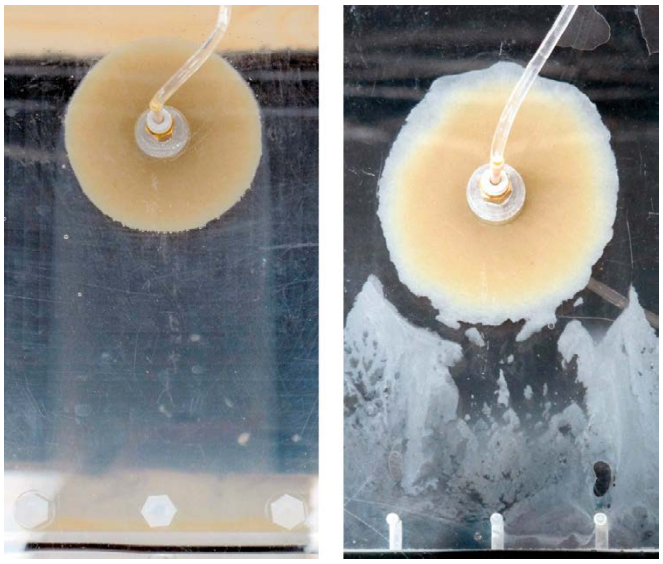

Figure 3-39. *Images of extrusion and mass loss of sodium montmorillonite in 45° sloped fractures with 1 mm apertures, left and 0.1 mm. Simulated Grimsel water, GGWS, with Na^+ 0.68 and Ca^{2+} 0.14 mM (Schatz and Akhanoba 2016). (Image from Neretnieks and Moreno 2018.)*

New evidence are presented that support the notion of positive edge charges and the spillover model, which states that at low salinity the spillover of the negative potential from the face to the edge creates a barrier for edge-to-face interaction. Above the CCC this barrier is overcome and the positive edge of one clay layer is discernible to a second clay layer. Erosion experiments using artificial fractures also demonstrate that material is lost when the ionic strength is below the CCC. This erosion occurs both under flowing conditions (horizontal fracture) or under stagnant water conditions provided that the fracture is sloped (in this study 45 degrees). The tests using Wy-Ca/Na (50/50) gave an order of magnitude larger erosion rates using a sloped fracture compared to a horizontal fracture. Assuming that the results from the laboratory tests can be scaled up (0.1 mm aperture and clay radius 3 cm) to a pessimistic repository condition (1 mm aperture and radius 1 m) the bentonite loss due to colloidal sol formation is approximately 1 kg/yr. As long as the sol is removed from the repulsive paste/sol interface the transition from paste to sol progresses and erosion continues. A factor that may lessen the impact of gravity would be accumulation of clay aggregates in uneven fractures. This has not been addressed with the planar fractures used in this study. Furthermore the rheological properties of an accumulation aggregate is unknown as well as the intrinsic stability of individual aggregates. The sol that is in quasi equilibrium with the repulsive paste appears as a dense liquid which is why it is so readily affected by gravity. The emergence of a Rayleigh-Taylor instability in the swelling tests under stagnant conditions is another manifestation of the liquid qualities of the sol. Clearly the montmorillonite layers in the dense sol interact. Presumably the interaction is again related to the positive edge charge; further highlighting the need to extend the theoretical study beyond regular DLVO based models. As suggested by this study, the rate-limiting factor for erosion is the repulsive paste to sol transfer rate and the rate by which the sol is removed. Above the CCC there is no detectable erosion. This observation is also made under high pH conditions. The lowest CCC value found in this study was ~4 mM NaCl for Ku-Na, followed by 6 to 8 mM for Mi-Na. In contrast, the highest CCC value was found for Wy-Na at 20 mM NaCl.

Additional erosion studies

Reid et al. (2015) investigated the mechanisms governing bentonite erosion in a fracture with a naturally varying aperture. The flow cell was constructed by taking a cast of a natural fracture present in a core of microgranite. The study has demonstrated that the accumulation of a ring of accessory minerals does indeed provide a mitigating effect against erosion of MX-80 bentonite extruded into fractures. The erosion process, in which an accessory-mineral ring forms, is governed by a two-stage cyclic erosion mechanism: increasing swelling pressure causes a breach in the accessory-mineral ring, triggering a subsequent erosive period. During this period, the mineral ring is supplemented and the breach is healed.

The cycle repeats until the ring is sufficiently strong that the ring remains intact. This observed process of mineral-ring formation results in somewhat decreased erosion rates, but the ring does not cause the erosion to stop.

Alonso et al. (2019) studied the erosion behaviour of different raw bentonites, compacted at high density, and analysed in a confined system under chemical conditions favourable for colloid stability. A complete physical and geochemical characterisation of clays was carried out to overall relate clay physico-chemical characteristics and structure to their erosion behaviour. The bentonite erosion results obtained in compacted and confined conditions were compared to those determined for the same clays under free dispersed conditions, where maximum erosion is achieved. The masses eroded measured under compacted and confined conditions and subjected to favourable chemical conditions for erosion (low ionic strength water in absence of divalent cations: deionised water) were in all cases very low. At maximum, eroded mass measured corresponds to a 1 % of the initial mass installed. Obtained values are by far lower than those obtained under free-dispersed conditions, indicating that processes related to the compacted and confined conditions were limiting erosion. When appreciable erosion was measured, the average diameter of the eroded particles was around 300–500 nm, values that are by definition, in the colloid range (< 1 μm), such that it would affect their stability and transport behaviour.Negligible erosion was measured from Ca/Mg-clays (Ca^{2+} + Mg^{2+} > 90 %), independent of their smectite content or charge distribution, indicating that high content of divalent cations in exchangeable positions is a dominant aspect affecting smectite erosion, in this case inhibiting it. All clays which showed appreciable erosion have smectite content higher than 70 wt%. In addition, all erodible clays have tetrahedral charge lower than 0.1 e/h.u.c (in absolute value). Eroded masses decreased as tetrahedral charge (in absolute value) increases, because clay layers interactions are strengthened, limiting detachment. However, eroded masses were not straightforwardly related to the main exchangeable cation, in contrast to that observed under free dispersed conditions. The chemical analyses carried out at equilibrium revealed salt dissolution and cation exchange processes took place. Ionic strengths measured at equilibrium partially explained the limited erosion measured under compacted conditions, in comparison to free dispersed conditions. In particular, the ionic strength of water in contact with studied Na-clays was higher, in agreement to the higher concentration of soluble salts in their inventory. This means that, under repository conditions, where solid to liquid ratio is high, the clays' salt inventory and clay/water interactions may play a very relevant role on erosion despite the structural characteristics of the clays. This is, however, a transient effect and residual salt in the caly will eventually be washed out during periods with dilute groundwaters.

Expansion/Erosion model (Neretnieks et al. 2017)

To overcome the computational problems with the model by Neretnieks et al. (2009b) discussed in the introductory section, a modified solution method was developed where two regions were considered; the expanding clay region and the rim region (Neretnieks et al. 2017). The latter was, using some simplifying assumptions, solved by a technique that can resolve the details in the rim zone with very high accuracy. The rim region model is then used as a boundary condition to the expanding clay region. The latter is solved using a technique that starts with a very small region, which is allowed to expand depending on how much clay enters from the deposition hole and how much is simultaneously lost at the rim region. It can be visualised as an expanding system in which nothing exists beyond the rim zone. This model gave quite different results from the original one. This model was used to simulate a series of laboratory experiments in which a compacted clay tablet was allowed to expand into a 1 mm aperture slot in transparent equipment where the expanding clay could be observed and where the loss of clay by erosion could be measured over time and at different chemical and hydrodynamic conditions. The model predicted the expansion of clay well into stagnant water but grossly underestimated the rate of erosion under flow conditions. Inspection of the pictures taken of the expanding and eroding clay showed that the sol that formed at the rim very quickly formed agglomerates (flocs) that flowed downstream with the same velocity as water. There seemed to be no viscosity increase of the water containing the flocs as would be the case if the sol were stable and did not agglomerate. The flowrate and velocity of the agglomerate fluid (AF) is thus much larger than what the sol model predicts. The flocs are voluminous and contain a low volume fraction of smectite particles. Although such behaviour has been observed earlier and speculation about the reasons have been discussed, only recently it has been firmly established that the edges of smectite particles, even

at near neutral pH, are positively charged (Hedström et al. 2016). This leads to edge to face attraction and formation of loose, space filling structures. The formation of such flocs is promoted by the presence of velocity gradients, such as exist in narrow fractures, which make the flat particles rotate and come in contact with each other.

These observations led to a modification of the model. As the small flocs flow with the water the impact on AF viscosity was assumed to be negligible. This implies that when the particles are released from the rim the sol quickly turns to AF and carries the particles away with the velocity of water. The two-region model was modified accordingly. The model then is simplified, but an important questions arises, namely how does the rapid floc formation influence the preceding sol formation, i.e. the release rate of particles at the rim. In the rim model without floc formation the release rate is determined by the smectite expansion model, which is formulated as a diffusion model with a diffusivity that is strongly influenced by the volume fraction of smectite and by the ion concentration. The diffusivity spans over three orders of magnitude at least in the region of interest. When the sol is stable the smectite particle diffusivity can be calculated by the model, which at the same time gives the volume fraction at which the sol can start to flow according to the viscosity model. This volume fraction lies in a range about 0.3 to 1 volume % smectite in water depending on the ion concentration. Simulations with these data did not give a sufficient increase in erosion compared to the experiments. However, using a volume fraction of 1.5 % for all experiments irrespective of flow velocity and ion concentrations gave a surprisingly good agreement (Figure 3-40).

In addition it results in a very simple expression for determining the loss at the rim. Wall friction is accounted for by not allowing the paste in the deposition hole to be pressed into the fracture more than the short distance determined by the balance between wall friction and intrusion force. The intrusion distance is about 2–3 times the aperture of the fracture. The clay expansion into the water starts at the tip of the extruded paste. This expansion is modelled by the expansion of the clay by the extremely strong osmotic forces sucking water in between the particles that drive them apart. The size of the colloid particles is much smaller than the aperture of fractures. The "swelling" of the montmorillonite, MMt, can be conceived as a diffusional mixing between the MMt and water, although the forces are partly different. There is no net movement of the fluid (the mixture of smectite and water). It is only a dilution process. Where an MMt particle vacates a space an identical volume of water replaces it moving in the other direction. No pressure gradient driving the fluid into the fracture results. Friction is again accounted for to determine the flow resistance of the expanded clay in the fractures, which is subject to a hydraulic gradient driving the water seepage in the fracture. Flow of the expanded clay essentially stops where the volume fraction of smectite is above about 1 %. Below 1 % the viscosity of the sol drops from very high to that of water with decreasing volume fraction smectite.

The mathematical model is formulated according to the following, once a steady state where the loss at the rim is balanced by the outward transport in the extrusion zone has been established.

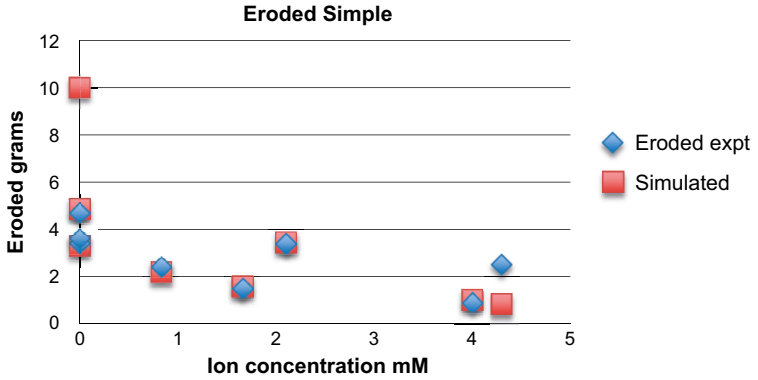

Figure 3-40. *Eroded mass from experiments and simulations of model variant c as function of ionconcentration mM with $\phi R,f = 0.015$ (Neretnieks et al. 2017)*

The erosion rate at the rim depends on water velocity, aperture, radius to the rim and ion concentration. (The model for diffusivity is based on Na^+ ion concentration, but is applied to total cation concentration, not cation charge (Neretnieks et al. 2017)) It can be determined by Equation (3-34).

$$N_{Erosion} = \rho_s \delta \theta_R 4\sqrt{D_R(c_{ion})\pi r_R u_0} \quad (3\text{-}34)$$

$D_R\ (c_{ion})$ is obtained by solving the equations for clay diffusion properties. The value of the volume fraction at the rim $\phi_R = 0.015$, the volume fraction found to give the best fit to experiments.

The solution for $D_R\ (c_{ion})$ for a given clay, in this case MX-80, when fitted gives the following equation where $x = Log10(c_{ion})$ in mM and D_R in m^2/s. It is valid for $0.1 < c_{ion} < 4$, which is within the region in which erosion occurs by flow and by floc sedimentation.

$$D_R(c_{ion}) = 10^{-9.42911 - 1.5309x - 1.88737x^2 - 0.783596x^3} \quad (3\text{-}35)$$

D_R is practically constant below $c_{ion} = 0.5$ and it can be set to D_R(0.1 mM) for $c_{ion} < 0.1$, but drops considerably approaching 4 mM.The diffusivity function plays an important role in the modelling. At low sodium ion concentrations the diffusivity is essentially constant and around 0.3×10^{-9} m^2/s for all volume fractions in the region of the plot. For concentration c_{ion} = 1 mM at a volume fraction 0.015 it drops by about a factor of 5. For c_{ion} = 10 mM it drops by more than 3 orders of magnitude.

A transition period starts after dilute water intrusion. After some time a steady state is reached where the intrusion rate from the deposition hole is equal to the erosion rate at the rim. The distance to the rim, r_R stabilises at r_{RSS} and the loss rate from the deposition hole becomes constant. The time to reach this *SS* is short when erosion is large. This happens for high velocity for horizontal fractures and for large apertures for inclined fractures with floc sedimentation. For $c_{ion} < 0.5$ mM it can be illustrated by the following. For $u_o > 10^{-5}$ m/s steady state conditions are reached in less than 20 years in horizontal fractures. For $u_o = 10^{-6}$ m/s it takes about 200 years and for $u_o = 10^{-7}$ m/s it takes about 2 000 years. For low water velocities the loss rate will be small and it is reasonable to neglect the higher loss rate during the initial period and use the *SS* loss rate also for the entire period to avoid the need to solve the time dependent equations. For $u_o = 10^{-7}$ m/s this would underestimate the loss during 1 000 years by less than 10 % and increasingly less for longer times. With this approximation a very simple expression results that can be used to calculate the *SS* loss rate for apertures, velocities and ion concentrations in the ranges expected.

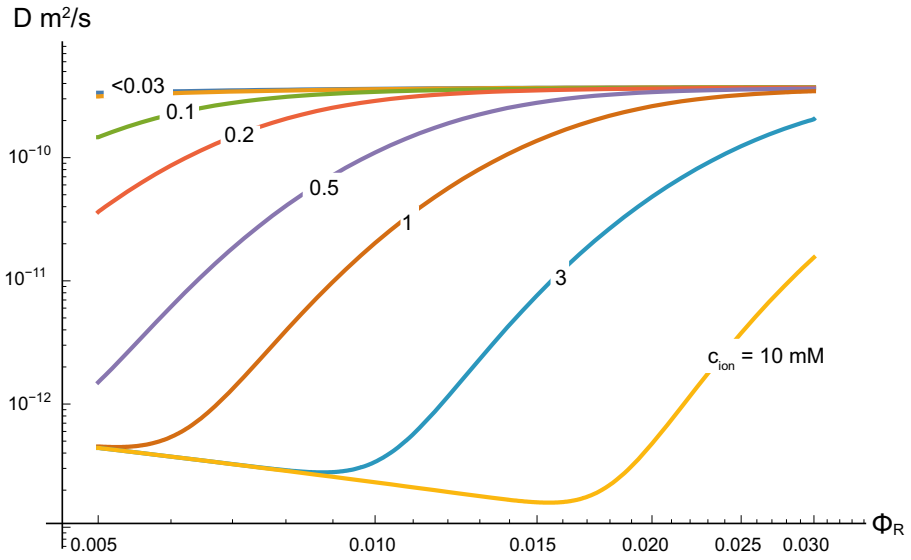

Figure 3-41. *Diffusivity function influenced by volume fraction and sodium ion concentration. Smectite diam. 200 nm (Neretnieks et al. 2017)*

The procedure is as follows. When *SS* is reached the intrusion rate into the fracture is equal to the erosion rate at the rim. This is obtained by equating the loss rate by erosion with the intrusion rate $N_{erosion} = 2N_{rim} = N_{in}$. G is defined as: $G = \frac{\varrho_s D_i \delta(\phi_i - \phi_R)}{N_{rim} r_i} = \frac{D_i \pi(\phi_i - \phi_R)}{2\phi_R \sqrt{D_R(c_{ion}) r_i u_0}} = \ln\left(\frac{r_{RSS}}{r_i}\right)\sqrt{\frac{r_{RSS}}{r_i}}$ (3-36)

Noting that G contains only known entities G is constant for a given case it has the solution

$$\frac{r_{RSS}}{r_i} = \left(\frac{G/2}{ProductLog\left(\frac{G}{2}\right)}\right)^2 \quad (3\text{-}37)$$

ProductLog(z) gives the principal solution for w in $z = we^w$. It is also called the Lambert W function $z = \frac{G}{2}$ in this case. This gives the solution of r_{RSS} at steady state when D_i and ϕ_i are constant. D_i and ϕ_i are the smectite diffusivity and the volume fraction at the conditions in the deposition hole respectively. With the radius to the rim from Equation (3-37) the SS rate of loss is obtained by Equation (3-34). Figure 3-42 shows loss rate as function of water velocity for different ion concentrations for a 0.1 mm aperture fracture. Steady state is well reached for $uo > 10^{-7}$ m/s in 1 000 years. The dashed line shows the old model results from Neretnieks et al. (2009) that was used in the SR-Site assessment for all cation charge concentrations below 4 mM.

Figure 3-43 shows the steady state radius to the rim as function of velocity and ion concentration.

Sedimentation model (Neretnieks et al. 2017)

In the above description and modelling no account is taken of gravity effects. This is because it was found that in stable sols gravity has a negligible effect (Neretnieks et al. 2009). However in the simulated fracture experiments mentioned above it was seen that when the fracture was turned vertical the flocs sedimented and new flocs were released from the expanding clay. The erosive loss was comparable to or larger than that in the horizontal fractures (Schatz et al. 2013). A simple model was devised that accounts for the sedimentation rate of small floc particles in a fluid in a fracture (Neretnieks et al. 2017). The model also gives the sedimentation velocity of large flocs in contact with the wall. This applies to cases with sodium-dominated clays that form flocs. In calcium dominated clays, even in deionised water, flocs are not observed. Instead it seems that heavy stacks form that may in turn agglomerate to even larger dense particles of up to a few tenths of mm size, which rapidly sediment. These particles can also be released from expanding calcium dominated clay and they sediment rapidly in inclined or vertical 1 mm aperture fractures.

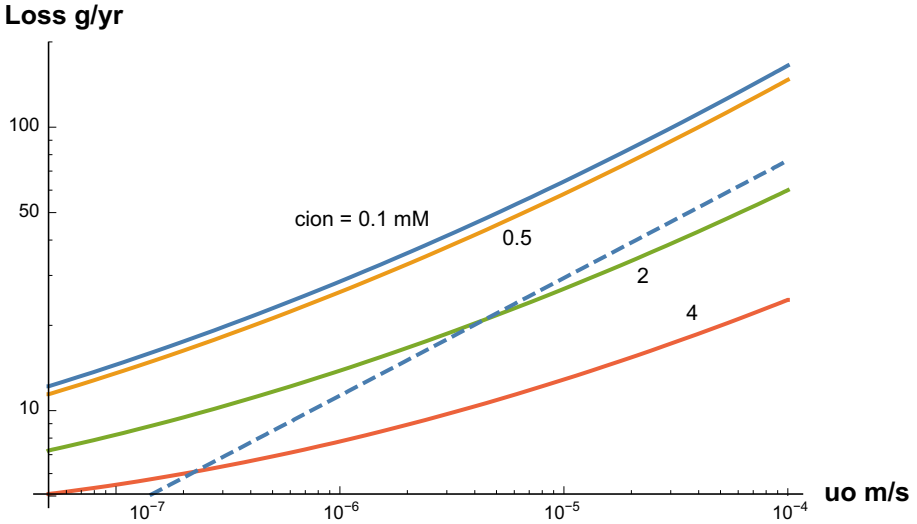

Figure 3-42. *Loss rate as function of water velocity for different ion concentrations in mM for a 0.1 mm aperture fracture. Dashed line shows the old model results from Neretnieks et al. (2009) (Neretnieks et al. 2017).*

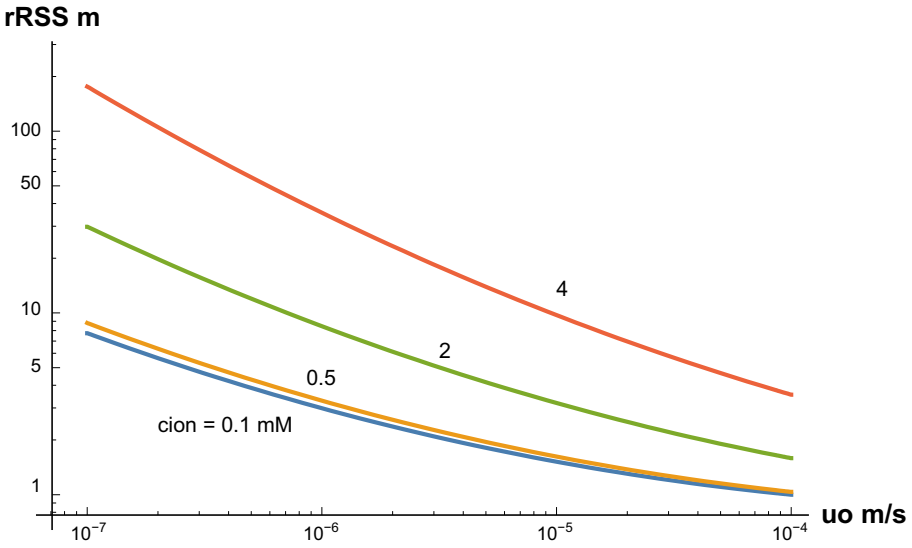

Figure 3-43. *r_R at steady state for different ion concentrations (Neretnieks et al. 2017).*

The sedimentation model in Neretnieks et al. (2017) is in brief according to the following. It is shown that it is possible to find an upper bound on the formation and release of agglomerates but that this is probably very pessimistic. At present it is only possible to use direct experimental results on the loss rate from small cylindrical sources and assume that these results can be extrapolated to much larger dimensions. Experiments in sloping fractures show that in low ionic strength waters tiny smectite agglomerates are constantly released and they sediment in the fracture (Schatz et al. 2013, Schatz and Akhanoba 2016)[5]. The results can be summarised as follows for 45 and 90° slopes from the horizontal, Equation (3-38). The release rate is proportional to the circumference of the extruded clay times the aperture.

$$N_{Exp} = J_{Exp}\delta 2\pi r_{RSS} Sin(\alpha) \tag{3-38}$$

J_{Exp} was found to be 850 and 1 550 kg/m^2/year by Schatz and Akhanoba (2016) for different clays in fractures with slopes of 90 and 45° from horizontal. The Steady State radius to the rim (rRSS) is obtained by solving:

$$N_{Exp} = N_{In} \tag{3-39}$$

With N_{In} from:

$$N_{In} = D_i 2\pi \varrho_s \delta \frac{\phi_i - \phi_R}{ln\left(\frac{r_R}{r_i}\right)} \tag{3-40}$$

this has an analytical solution:

$$r_{RSS} = \frac{F_{Exp}}{ProductLog\left(\frac{F_{Exp}}{r_i}\right)} \tag{3-41}$$

where:

$$F_{Exp} = \frac{D_i \varrho_s (\phi_i - \phi_R)}{J_{Exp} Sin(\alpha)} t_y \tag{3-42}$$

$t_y = 3.15 \times 10^7$ s/year.

[5] Schatz and Akhanoba do not account for the angle in their summary of results. Without access to the detailed data the effect of slopeis omitted in Equation (3-38).

The rate of loss is then directly obtained by inserting the value in Equation (3-38). The next step is to see if that rate of released smectite can be transported away in the fracture as an agglomerate fluid. Then

$$N_{Sed} = \frac{\delta^3}{12\mu_{agg}}\left(\varrho_{agg} - \varrho_W\right) g \phi_R \varrho_s W_{AF} \qquad (3\text{-}43)$$

with $W_{AF} = 2\, r_{RSS}$ is used to calculate N_{sed}. μ_{agg} and ϱ_{agg} are the viscosity and density of the AF respectively.

Based on Schatz and Akhanoba (2016) it appears that, irrespective of whether mass loss occurs in a horizontal or 45° sloped fracture, at cation charge concentrations ≥ 8.6 meq/L the rate of erosion for all of the tested materials is effectively zero assuming that the small amounts of mass loss detected in some of the cases can be ascribed to slaking (or other phenomena not associated with a continuous mass loss process).

Figure 3-44 left frame, shows how the loss would increase with increasing aperture based on the experiment according to Equation (3-38) for a vertical fracture and with J_{Exp} = 1 000 kg/m^2/year, the full line. The dashed line shows the maximum rate of sedimentation of the AF according to Equation (3-43). For fractures narrower than 0.016 mm the sedimentation rate is not sufficient to carry away the released smectite. The right frame shows the maximum loss from the source accounting for these limitations. The maximum loss in a 0.1 mm aperture is 0.61 kg/year.

It is seen that the loss is very sensitive to the release rate and that the increase in agglomerate viscosity only starts to matter when the agglomerate fluid viscosity is very large as seen in the last three rows in Table 3-21 The loss by sedimentation in the central case (row 1) is about two to three times higher than for horizontal fracture with flow for the highest considered water velocities in horizontal fractures. This loss occurs even without any flow in the sloping fractures, provided the sediments can move away continuously. Such further movement may not be assured if the sediments have a non-zero friction angle and cannot move on at intersections with fractures with slopes less than the friction angle.

Table 3-21. Smectite loss by sedimentation in a vertical fracture for different combinations of CExp and μagg. The figures in parentheses show what the loss would be if it were not limited by the rate at which the sediments can move away.

C_{Exp} kg/m^2/year	μ_{agg} mPa s	N_{loss} kg/year
1 000	1	0.61
10 000	1	6.1
1 000	10	0.61
10 000	10	2.3 (6.1)
1 000	100	0.23 (0.61)
10 000	100	0.23 (0.61)

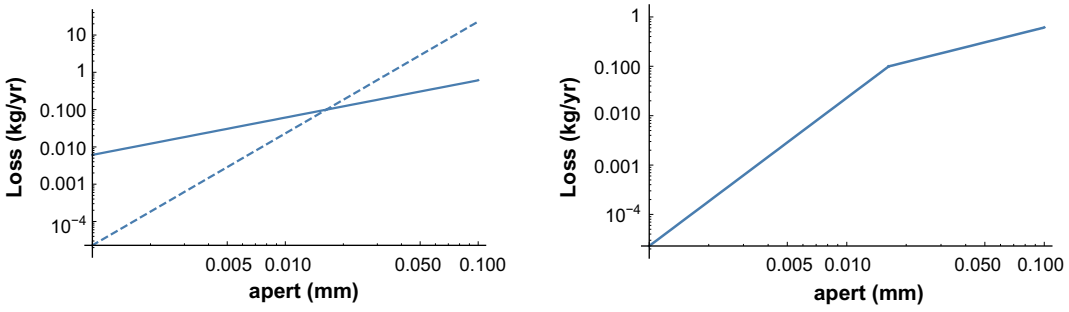

Figure 3-44. *Left frame, Maximum possible release rate of smectite, full line and possible sedimentationrate of the agglomerate fluid, dashed line. Right frame, maximum loss from source taken from left frame (Neretnieks et al. 2017).*

The BELBaR project Summary

The BELBaR project (2012–2016) was a collaborative effort based on the desire to improve the long-term safety assessments for geological disposal facility concepts for spent fuel/high level waste that combine a clay engineered barrier system (EBS) with a fractured rock. BELBaR partners included national radioactive waste management organisations (WMOs) from a number of countries, research institutes, universities and commercial organisations working in the radioactive waste disposal field. A summary of the conclusions from BELBaR can be found in Shelton et al. (2018). Much of the studies cited in the preceding sub-sections were carried out as part of the BELBaR project and the following brief account of the findings in the project also serves as a summary of the current understanding of the expansion, erosion and sedimentation phenomena.

In the BELBaR project a considerable number of experiments were made in which bentonite clay was allowed to intrude a fracture with either stagnant water or slowly seeping water. The intrusion of the clay into artificial fractures and the release of smectite into the water in the fractures were studied. An important aim of these experiments was to obtain data that could be used to develop models that can be used to assess the loss rate of bentonite from deposition holes and tunnels hosting radioactive waste canisters. In addition a number of experiments were made to study the underlying mechanisms for bentonite swelling and smectite solubilisation. Previously derived conceptual, mathematical and numerical models were refined and modified based on the experimental results. The vast amount of information gathered during the four-year project has been reported in a number of reports, deliverables, and in publications in journals. Not all this information and experimental results could be fully digested by the participants during the final phases of the project. Neretnieks and Moreno (2018) made an evaluation of how well the model developed by Neretnieks et al. (2017) matches the experimental data from the BELBaR project. The main purpose was to collect and compile available data, mainly from the BELBaR project but if possible also from other sources, to be able to use them for model testing and to verify the model by Neretnieks et al. (2017) against experimental data from the BELBaR project. The BELBaR project has confirmed and strengthened earlier understanding of smectite behaviour in different waters. The experimental findings that very calcium rich bentonites will not release colloids have been confirmed by modelling of the behaviour of mono- and divalent ions in the narrow space between smectite sheets (Yang et al. 2016). The formation and properties of very loose smectite flocs has been experimentally shown to be caused by the presence of positively charged edges on the smectite sheets (Hedström et al. 2016). The concept of critical coagulation concentration CCC, as commonly used, has been shown to be oversimplified and potentially considerably misleading. Instead a practical ion concentration range together with information on clay composition, i.e. the ratio of mono- to divalent ions needed to neutralise the permanent negative charge of the smectite was found to well define the condition under which colloid sol can form (Hedström et al. 2016). Under conditions allowing sol to form, flocculation of the smectite colloids was found to be an important process that strongly influences erosion in stagnant and seeping water in sloping fractures as well as in horizontal fractures with flow (Schatz et al. 2013, Schatz and Akhanoba 2016). Flocculation has been incorporated in the updated model for bentonite expansion and erosion (Neretnieks et al. 2017). The released montmorillonite particles form flocs, which in narrow fractures join to become a viscous fluid that is slowed by friction against the fracture walls. It has been reported in the literature that the viscosity of such fluids increases with time. The sedimenting flocs could even form sufficiently strong complex space-filling structures characteristic of gel and develop sufficient yield strength to essentially stop floc movement in fractures. This may considerably decrease the flowrate of the released montmorillonite and possibly even in practice stop further erosion. In the experiments with clays that contain accessory minerals these are invariably found to clog filters and narrow passages in fractures. This suggests that natural narrow fractures in crystalline rocks will be clogged by the accessory minerals when montmorillonite escapes as colloidal particles leaving the non-colloidal minerals behind. The accessory minerals eroded in sloping fractures sediment and collect at the bottom of the fracture unless the sediment can enter the next intersecting fracture. If the slope of the next fracture is smaller than the angle of repose of the sediment it cannot migrate further.

Considering the large variations in observed erosion rates, no information has been found in the BELBaR investigations or in other relevant literature on montmorillonite suspension properties and behaviour that could seriously increase the erosion rate above that in the model of Neretnieks et al. (2017).

Recent model development

The model proposed by Neretnieks et al. (2017) has been developed further and the result is available in Pont et al. (2020) and Pont and Idiart (2022). There, a numerical model is presented which handles wall friction, flow along chemical erosion, and sedimentation due to gravity. The model has been developed and partially validated with experimental data from small-scale tests. This model is still in a development stage and has not been utilised in the PSAR.

Natural analogues/observations in nature

In principle, a large number of analyses of Swedish groundwater may serve as natural analogues since they show low contents of clay colloids despite the fact that swelling clay is often found in fractures. Specific studies have been made at the Äspö HRL (Laaksoharju 2003) and at Grimsel HRL (Degueldre et al. 1996).

A literature review of bentonite deposits with the objective of finding natural analogues was done as a part of the Bentonite Erosion Project (Puura and Kirsimäe 2010). However, the conclusion was that relevance to the Bentonite Erosion Project was still questionable because of the uncertainties related to the changes during tens and hundreds of millions of years.

Time perspective

Colloid formation is only relevant at low ion concentrations and likely to be relevant only in conjunction with a glaciation, or possibly after long periods of intrusion of meteoric water. The effects may be significant only in the long-term perspective.

Handling in the PSAR

Expansion of clay into fractures intersecting the deposition hole, erosion due to colloid formation and clay loss due to sedimentation all have to be addressed in the safety assessment, in an appropriate context including site specific data concerning fracture apertures, groundwater velocity and chemical composition. The spatial distributions of these entities over the ensemble of canister positions need to be taken into account as do the temporally varying conditions, largely driven by glaciation cycles.

Water with cation content higher than 4–8 mM charge equivalents is considered to prevent colloidal sol formation provided that the calcium content in the montmorillonite is above 20 %, irrespective of whether the montmorillonite is of Wyoming, Milos or Kutch type. Ion exchange processes during the operation of the repository may alter the counterion content relative to the initial state. The content of calcium in the cation exchanger is, however, not expected to fall below 20 %, since the ion-exchange to a calcium form is promoted at low concentrations. Thus the process of colloidal sol formation can be neglected during operation of the repository. Present day ground water at the Forsmark site fulfils this condition as does Baltic Sea water. During glacial conditions the cation content may possibly fall below 4–8 mM charge equivalents, and colloidal sol formation can therefore not be excluded. It is also possible that deposition positions intersected by fractures with prolonged high groundwater flow rates during temperate conditions could be exposed to sufficiently dilute groundwaters that erosion and sedimentation occurs.

Expansion

As regards expansion of clay into fracture for above CCC conditions, the approach by Börgesson et al. (2018) is used since all experimental evidence supports that approach rather than the one put forward in Neretnieks et al. (2017). Expansion is thus assumed to be negligible above CCC.

The approach by Börgesson et al. (2018) is not valid at conditions below CCC, since it contains an assumption about the formation of a stable gel. As stated in the previous section, experimental results, e.g. Alsonso et al. (2019) shows that expansion is restricted even at dilute conditions. Therefore, in the PSAR, it is assumed that expansion will be limited to 5 cm for all conditions.

Erosion by flowing water

As is evident from the discussion in the preceding sections, erosion is a complex phenomenon dependent on a number of material specific and environmental factors. In the PSAR a thorough analysis of the extent of mass loss due to erosion given site specific, spatially and temporally varying data is required. In terms of models for the safety assessment, the simpler model in Neretnieks et al. (2009) and the more detailed model in Neretnieks et al. (2017), taking also ion concentration into account, are available. As seen in Figure 3-42 the two give fairly similar results for cation concentrations around 1–2 mM. Both can be used in their appropriate context to assess the extent of mass loss under repository conditions.

As noted in the discussion of the erosion experiments by Schatz et al. (2013) above, the zone of extruded buffer material forms an extended diffusive barrier around the intersecting fracture/buffer interface. This barrier function is neglected in the safety assessment.

As also noted in the preceding text, clogging of fractures by detritus material released from the clay due to erosion may be expected. The limiting effect of this phenomenon on the extent of erosion is not taken into account in the PSAR since the effect is difficult to quantify, and since no requirement on the contents of such detritus has been formulated for the clay materials considered in the PSAR.

Erosion due to sedimentation

Erosion due to sedimentation cannot be neglected in the safety assessment, given the current understanding of the phenomenon. The only available quantitative model is that described in Neretnieks et al. (2017), as discussed above. The extent of mass loss due to sedimentation according to this model needs to be illustrated in the PSAR for site specific, spatially and temporally varying data.

It is noted that in the sedimentation model in Neretnieks at al. (2017) the finite extent of the fractures to which the loss occurs and the aforementioned effect of clogging due to release of detritus are both pessimistically neglected.

Uncertainties

Uncertainties in mechanistic understanding

Knowledge concerning colloidal sol formation and colloid stability is good concerning the effects of mono- and divalent ions. However, modelling of the correlation effects caused by divalent ions is demanding. The prevention of sol formation at low ionic strength when the calcium content in the montmorillonite is above 20 % has been verified experimentally. Detailed understanding of this effect is less well developed and handling edge-face interactions in modelling is complicated. The force-balance model is based on parallel layers and furthermore only tested versus vertical swelling experiments and for short swelling times, up to 5 weeks.

The possible transport of colloids by diffusive and flow transport is less well known. The effects of mechanical erosion of loose gels close to sol forming conditions have not been fully examined. Experiments show that montmorillonite does not penetrate filters with pore-sizes of 0.5 mm. However, it has not been shown that accessory minerals could actually form an effective filter in the fractures. The understanding of the effect of pH on colloidal sol formation is incomplete.

The role of friction between the expanding clay paste and the fracture surface is also an important uncertainty. Börgesson et al. (2018) demonstrates well the role of friction for groundwater concentrations > CCC. However, the importance below CCC has not currently been assessed.

Sedimentation of clay particles in sloping fractures below CCC is an area where the mechanistic understanding is very limited. So far only empirical models are available.

The experimental observations are not always consistent, which makes interpretation as well as verification or validation of models difficult.

Model simplification uncertainties for the above handling in the PSAR

The treatment for quantifying montmorillonite loss during dilute conditions in the PSAR is mainly based on the models in Neretnieks et al. (2017). It should be noted that a number of simplifying assumptions have been made.

The following assumptions must be revisited and checked for reasonableness:

1. The assumption that the force-balance model is pessimistic for the swelling of Na-montmorillonite. Predicted CCC is claimed to be about 50 mM whereas the underlying DLVO model gives 1–2 M.
2. Assumption of Darcy flow. the application of Darcy's law on the boundary between bentonite and dilute (colloidal) bentonite solution may be an oversimplification relative to more detailed approaches, e.g., applications of Stokes equation or direct application of Navier-Stokes equations.

The following could act to decrease the dispersion rate:

1. The change of composition in the diffuse layer, which is not accounted for.
2. The presence of 20 % or more Ca in the clay.
3. A model beyond DLVO for parallel clay layers. Correlation as well as edge-face interactions.
4. Physical hindrance of clay particle dispersion in the fracture.
5. Clogging of pathways by the clay being pressed out into the fracture.

Input data and data uncertainties for the above handling in the PSAR

The evolution of groundwater composition, and groundwater flow conditions are the most important factors. These will be evaluated in integrated assessment modelling.

The magnitude of the empirical sedimentation rate has a very strong effect on the loss of buffer mass from a deposition hole. One pessimistic and one more reasonable value is used in the assessment.

3.5.12 Colloid transport/filtration

Overview

Particles with sizes of the order of 10^{-9} to 10^{-6} m (colloids) could form on dissolution of the fuel and/or reaction between radioelements and canister corrosion products or bentonite colloids. If radioelements can be transported in the near-field as colloids, the concept of elemental solubility would not be valid. The diffusive transport of these colloids through highly-compacted bentonite is, however, assumed to be negligible, due to the tortuosity and small size of the bentonite pores. The fundamental (dispersed in water) particle size of the bentonite is < 2 μm. At emplacement, the bentonite has a water ratio of 17 % (weight of water divided by weight of solid), which corresponds to a water film with a mean thickness of 6×10^{-10} m between the individual montmorillonite flakes (interlayer distance). Larger pores, between the original bentonite grains from which the blocks are produced, make up the remaining pore space. The water film thickness increases during water saturation, and the final theoretical mean interlayer distance is around 10^{-9} m, which obviously would dramatically reduce colloid transport. However, a complete homogenisation of the bentonite cannot be expected, and a certain variation in the final pore size will remain also at full saturation.

Colloid filtration is defined as a safety function for the buffer, to ensure the validity of the elemental solubility concept in the waste form. The minimum required dry density is set as the performance target.

Dependencies between process and buffer variables

Table 3-22 summarises how the process influences and is influenced by all buffer variables and how these effects are treated in the PSAR.

Boundary conditions

The process only considers the transport of colloids from the canister interior to the rock contact.

Model studies/experimental studies

Kurosawa et al. (1997) reports that 15 nm gold colloids are effectively filtered out at a dry density of 1 000 kg/m^3 for bentonite/sand mixtures with a sand content of up to 40 %. At 50 % sand there is an indication of colloid breakthrough, but even there the retention is strong. No colloid breakthrough is observed for a 50/50 mixture when the dry density is increased to 1 800 kg/m^3.

Wold (2003) reports on diffusion experiments with organic colloids through MX-80 bentonite with a range of dry densities from 600 to 1 800 kg/m^3. The lignosulfonate (LS) and humic acid (HA) colloids used had an average size of 80 and < 10 nm, respectively, but the size distribution was broad. The LS and HA colloids showed diffusivities in the same range as negatively charged ions like Cl^- and I^-, which is surprising, especially for the large LS, since the mean interlayer spacing in a saturated bentonite is between ~ 5 and 10 Å. One possible explanation for lack of colloid filtration could be the presence of larger pores, the broad size distribution of the LS colloids, or transformation of the molecules during the course of the experiment. The issue of organic colloid-related transport of radionuclides is one that warrants further examination.

Holmboe et al. (2010) examined diffusion of negatively charged 2-, 5-, and 15-nm gold colloids in 4-month diffusion experiments using MX-80 Wyoming bentonite compacted to dry densities of 0.6–2.0 g/cm^3. Breakthrough of gold colloids was not observed in any of the three diffusion experiments. In a gold-concentration profile analysis, colloid diffusion was only observed for the smallest gold colloids at the lowest dry density used (estimated apparent diffusivity Da ≈ 5×10^{-13} m^2/s). The results from a microstructure investigation using low-angle X-ray diffraction suggest that at the lowest dry density used, interlayer transport of the smallest colloids cannot be ruled out as a potential diffusion pathway, in addition to the expected interparticle transport. In all other cases, with either greater dry densities or larger gold colloids, compacted bentonite will effectively prevent diffusion of negatively charged colloids due to filtration.

Time perspective

The process is important for all repository timescales, but only if canisters have failed.

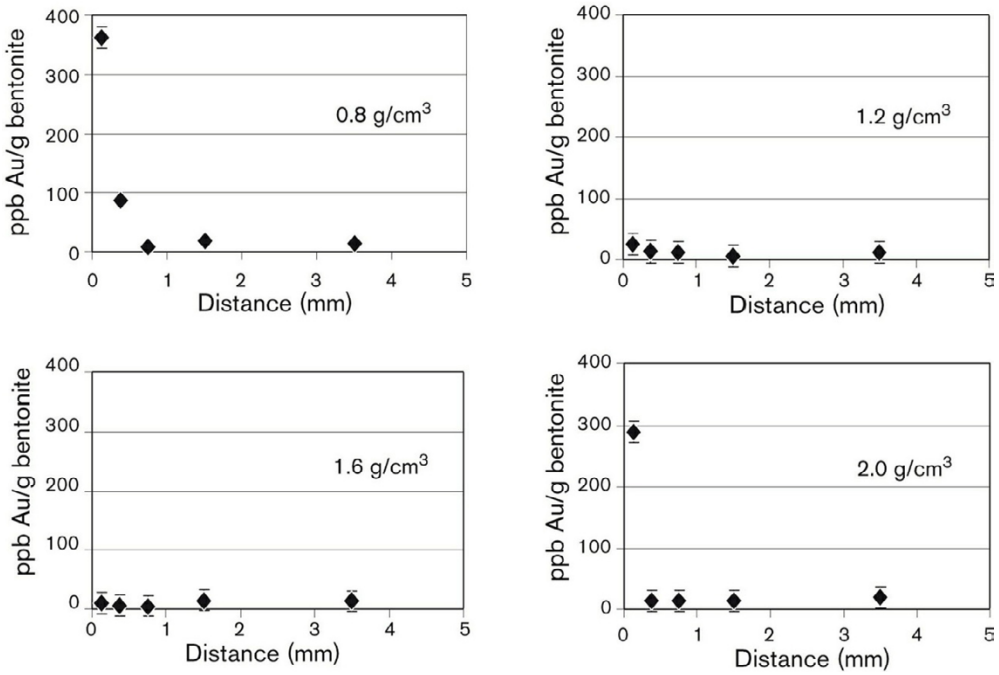

Figure 3-45. *Concentration profiles of gold in the compacted bentonite pellets that were used in the diffusion experiment. The high value for the first data point in the graph, 2.0 g/cm^3, is presumably the result of contamination, since the swelling pressure at the high dry density caused deformation of the metal filter (Holmboe et al. 2010).*

Table 3-22. Direct dependencies between the process "Colloid transport" and the defined buffer variables and a short note on the handling in the PSAR.

Variable	Variable influence on process		Process influence on variable	
	Influence present? (Yes/No) Description	Handling of influence (How/Why not)	Influence present? (Yes/No) Description	Handling of influence (How/Why not)
Buffer geometry	No Colloid filtration is assumed to be on or off		No	
Pore geometry	Decisive importance	The lowest buffer density to facilitate colloid transport is defined	No	
Radiation intensity	No		No	
Temperature	Very minor	Excluded – No data available and temperature range will be narrow	No	
Water content	No (if saturated conditions assumed)		No	
Gas content	No (if saturated conditions assumed)		No	
Hydrovariables (pressure and flows)	No (if saturated conditions assumed)		No	
Stress state	Indirectly through pore geometry		No	
Bentonite composition	Indirectly through pore geometry		No	
Montmorillonite composition	Through layer charge	The lowest buffer density to facilitate colloid transport is defined	No	
Porewater composition	Possibly a very minor effect through viscosity	Excluded	No	
Structural and stray materials	No		No	

Natural analogues/observations in nature

No applicable observations of the colloid filtration effect are available from nature.

Handling in the PSAR

The concern in the safety assessment is the transport of radionuclides with colloids from a potentially failed canister, in particular fuel colloids. This transport mechanism is neglected, provided the buffer completely envelops the canister and has a dry density of at least 1 000 kg/m^3, i.e. a saturated buffer density of at least 1 650 kg/m^3. This is based on the experimental results from Kurosawa et al. (1997) and is clearly confirmed by Holmboe et al. (2010). A dry density of 1 000 kg/m^3 is set as the performance target for the safety function: "Filter Colloids".

The consequence of a loss of the colloid filtration effect is treated as a separate case with transport of radionuclides in/sorbed on a colloid phase. This would mean that the concept of solubility limits is not valid. Radionuclide solubilties as well as sorption coefficients are adjusted for that case.

Uncertainties

Uncertainties in mechanistic understanding

As seen in the Model/Experiment section above, different types of colloids behave very differently. It is not clear why there is such a large difference between inorganic and organic colloids.

Model simplification uncertainties in the PSAR

If the buffer density is high enough to exclude colloid transport, no model is needed in the assessment. Bounding calculations can be done by adjusting input data.

Input data and data uncertainties in the PSAR

No data is used for the same reasons as are outlined above.

3.5.13 Radiation-induced transformations

Overview

This process covers the direct effect of radiation on the stability of the montmorillonite component of the buffer material. Indirect effects through the radiolysis of porewater are covered in that process (3.5.14).

Montmorillonite in the buffer can potentially be broken down by γ-radiation. The result is a decrease in the montmorillonite component of the buffer.

In the case of a failed canister, radionuclides sorbed in the buffer could possibly affect the properties by α-radiation.

Dependencies between process and buffer variables

Table 3-23 summarises how the process influences and is influenced by all buffer variables and how these effects are treated in the PSAR

Boundary conditions

A quantitative treatment of the process requires knowledge of the radiation field in the buffer, which is obtained from the process Radiation attenuation (3.1.1).

Model studies/experimental studies

Experimental studies concerning γ-irradiation of bentonite with low water contents (Huang and Chen 2004, Negron et al. 2002, Plötze et al. 2003, Pusch et al. 1993b, Pushkareva et al. 2002), have only found small or insignificant effects on both the physical and chemical properties of bentonite and montmorillonite, even at very high doses (several MGy, 1 Gy = 1 J/kg).

The buffer will not be exposed to α- and β-radiation as long as the canister is intact. In the case of a failed canister, radionuclides that migrate out will be sorbed in the buffer and may expose it to a radiation dose.

In the radionuclide calculations for SR 97 (SKB 1999), it was found that the total concentration of α-emitters in the buffer closest to the canister would give a total dose of 8×10^{15} alphas/g of bentonite for the first million years with the assumption of an early canister failure. In most parts of the buffer, the α-dose will be much less since the α-emitters are strongly sorbed and will stay in the vicinity of the canister. 8×10^{15} alphas/g corresponds to an absorbed dose of 8 MGy. Gu et al. (2001) show that the amorphisation dose for montmorillonite is 30 GGy. Since the total dose received is more than three orders magnitude lower than the amorphisation dose, the impact on the properties of the buffer can be expected to very small.

Table 3-23. Direct dependencies between the process "Radiation-induced transformations" and the defined buffer variables and a short note on the handling in PSAR.

Variable	Variable influence on process		Process influence on variable	
	Influence present? (Yes/No) Description	Handling of influence (How/Why not)	Influence present? (Yes/No) Description	Handling of influence (How/Why not)
Buffer geometry	Total buffer mass available	Dose rates are too low to cause any significant transformations – the process is excluded from the PSAR	No	
Pore geometry	No		No	
Radiation intensity	Yes	Dose rates are too low to cause any significant transformations – the process is excluded from the PSAR	No	
Temperature	No		No	
Water content	No		No	
Gas content	No		No	
Hydrovariables (pressure and flows)	No		No	
Stress state	No		No	
Bentonite composition	Not detected		(Yes)	Dose rates are too low to cause any significant transformations – the process is excluded from the PSAR
Montmorillonite composition	Not detected		(Yes)	Dose rates are too low to cause any significant transformations – the process is excluded from the PSAR
Porewater composition	No		No	
Structural and stray materials	No		No	

Natural analogues/observations in nature

No studies of systematic studies of clay mineralogy under the influence of alpha radiation are available.

Time perspective

See Section 3.1.1.

Handling in the PSAR

Based on the experimental and modelling studies mentioned above it is shown that the effect of radiation on buffer properties is insignificant and the process is therefore neglected.

Uncertainties

Fourdrin et al. (2010) used beams of 925 MeV Xenon ions with radiation dose reaching 73 MGy were used to simulate the effects generated by alpha recoil. The results showed increased dissolution of the smectite. The dose rates in the experiments were however extremely high and may not be relevant to the conditions in a repository.

3.5.14 Radiolysis of porewater

Overview

Gamma radiation from the fuel that penetrates through the canister can decompose porewater by radiolysis, forming OH radicals, H_2, O_2 and several other components. The oxygen is consumed rapidly by oxidation processes that affect the redox potential, while the hydrogen may be transported away. The canister wall thickness is, however, sufficient so that the effect of γ-radiolysis on the outside is negligible (Werme 1998). This process is also described in the **Fuel and canister process report**.

Irradiation of moist air before saturation leads to the formation of nitric acid, which is an oxidant for copper and thus a potential corrosive agent. This is discussed further in the **Fuel and canister process report**.

Dependencies between process and buffer variables

Table 3-24 summarises how the process influences and is influenced by all buffer variables and how these effects are treated in the PSAR

Boundary conditions

A quantitative treatment of the process requires knowledge of the radiation field in the buffer, which is obtained from the process Radiation attenuation.

Model studies/experimental studies

Corrosion of copper in water in the presence of γ-radiation has been studied in a few experiments. These are summarised in King et al. (2001). The results show no effect on the corrosion rate even with higher doses than those expected in the repository.

Natural analogues/observations in nature

Not applicable.

Time perspective

γ radiation is significant during the period approximately 1 000 years following canister installation.

Handling in the PSAR

Before saturation, radiolysis of moist air leads to the formation of nitric acid, which is an oxidant for copper and thus a potential corrosive agent. After water saturation, radiolysis of water near the canister will occur. This will lead to the formation of oxidants and hydrogen. If these radiolysis products are not removed, equilibrium will soon be reached whereby further production of hydrogen and oxidants ceases. If the radiolysis products are removed, however, for example by the diffusion of hydrogen away from the canister or by reaction of the oxidants with copper or other oxidisable species in the system, radiolysis can continue. The handling of this process is discussed in the **Fuel and canister process report.**

Uncertainties

There are no uncertainties currently identified that are of relevance to the safety assessment.

Table 3-24. Direct dependencies between the process "Radiolysis of porewater" and the defined buffer variables and a short note on the handling in the PSAR.

Variable	Variable influence on process		Process influence on variable	
	Influence present? (Yes/No) Description	Handling of influence (How/Why not)	Influence present? (Yes/No) Description	Handling of influence (How/Why not)
Buffer geometry	(Determines the total amount of water in the radiation field)		No	
Pore geometry	No		No	
Radiation intensity	Yes	Dose rates are too low to cause any significant radiolysis outside canister – the process is excluded from the PSAR	No	
Temperature	No		No	
Water content	Yes, determines the amount of water available	Dose rates are too low to cause any significant radiolysis outside canister – the process is excluded from the PSAR	No	
Gas content	No, but indirectly through water content		No	
Hydrovariables (pressure and flows)	No		No	
Stress state	No		No	
Bentonite composition	No		No	
Montmorillonite composition	No		No	
Porewater composition	Determines the reactions	Dose rates are too low to cause any significant radiolysis outside canister – the process is excluded from the PSAR	Yes	Dose rates are too low to cause any significant radiolysis outside canister – the process is excluded from the PSAR
Structural and stray materials	No		No	

3.5.15 Microbial processes

Overview

Under certain conditions, microbial processes can result in the formation of gas and sulphide (Pedersen 2002). Gas formation can give rise to pore pressure and mechanical effects in the bentonite buffer and sulphide from sulphate reducing bacteria (SRB) can corrode the copper canister. Sulphide formation must take place in the buffer, near the canister and be of considerable extent for corrosion to be a threat to canister integrity. This is mainly due to the fact that sulphide is commonly precipitated with ferrous iron. Therefore, sulphide concentrations do not occur at high concentrations in groundwater and its diffusive transport capacity is very low. In order for the processes described above to take place, the bacteria must be active and have access to water, nutrients and space (Pedersen 2002).

Sulphate-reducing bacteria are very common in deep Fennoscandian groundwater. They are reported to occur abundantly down to depths of at least 600 to 700 m (Haveman and Pedersen 2002, Pedersen 2001, Pedersen et al. 2008). In addition, about 2×10^6 SRB will be introduced per m^3 bentonite in the repository. Microbes are generally very robust and can withstand harsh conditions. The cells can remain dormant, either desiccated or as spores, in the clay for decades or even centuries until conditions become more favourable. The potential for sulphide production is significant at repository depth and possible effects on the repository function must be considered in the safety assessment (Hallbeck and Pedersen 2008).

A safety function for the buffer was defined in SR-Site (SKB 2011), which involves the limitation of microbial activity. The safety function indicator was defined as high swelling pressure due to the uncertainties associated with the mechanism. In Posiva SKB (2017), the question was discussed further, and it was established that the conclusions regarding swelling pressure/dry density and potential other factors that limit microbial activity are somewhat incomplete. There are, however, results indicating a clear threshold where microbial sulphate reduction ceases in MX-80 bentonite (Bengtsson et al. 2015). The function indicator criterion for limiting microbial activity (Buff2) is defined as a swelling pressure > 2 MPa and applies to the entire buffer volume. This value is relevant for MX-80 bentonite, but may have to be revised for other materials.

Dependencies between process and buffer variables

Table 3-25 summarises how the process influences and is influenced by all buffer variables and how these effects are treated in the PSAR.

Table 3-25. Direct dependencies between the process "Microbial processes" and the defined buffer variables and a short note on the handling in the PSAR.

Variable	Variable influence on process		Process influence on variable	
	Influence present? (Yes/No) Description	Handling of influence (How/Why not)	Influence present? (Yes/No) Description	Handling of influence (How/Why not)
Buffer geometry	No, indirectly through pore geometry		No	
Pore geometry	Yes. Microbial activity decreases exponentially with increasing buffer densities and approach nil at densities above 2 000 kg/m^3	Maximal possible production of sulphide and gas is calculated for all possible pore geometries (densities) and the amounts produced are compared with the amount needed to corrode a copper canister	No	
Radiation intensity	Yes	Lethal effects from the radiation field are not considered	No	
Temperature	Yes. Microbial activity is positively correlated with temperature and will be higher during the thermal period compared to the ambient temperature period	Maximal possible production of sulphide and gas is calculated for high and low temperatures and the amounts produced are compared with the amount needed to corrode a copper canister	No	
Water content	Yes. Decreasing water availability reduces the diversity and the possibilities for microbial activity. At the same time, increasing water content increase the stress state (swelling pressure)	Maximal possible production of sulphide and gas is calculated for all possible water contents and the amounts produced are compared with the amount needed to corrode a copper canister	No	

Variable	Variable influence on process		Process influence on variable	
	Influence present? (Yes/No) Description	Handling of influence (How/Why not)	Influence present? (Yes/No) Description	Handling of influence (How/Why not)
Gas content	Yes Microbial activity is possible with hydrogen and methane as sources of energy	Maximal possible production of sulphide is calculated for all possible gas contents and the amounts produced are compared with the amount needed to corrode a copper canister	Yes. Microbial activity may result in the production of carbon dioxide and methane	Only effects on the buffer/canister are considered
Hydrovariables (pressure and flows)	(No)		Yes. induced gas pressure induces water flow	Neglected since the effect is very small.
Stress state	Yes. Microbial activity decreases exponentially with increasing buffer densities and approach zero at densities above 2 000 kg/m^3	Maximal production of sulphide is calculated for all possible pore geometries and the amounts produced are compared with the amount needed to corrode a copper canister	No	
Bentonite composition	Yes. Organic carbon can be utilised and several types of commercial bentonites contain viable bacteria including thermophilic sulphate reducing bacteria	Microbial activity can be possible.Maximal production of sulphide is calculated for the bentonite in use and the amounts produced are compared with the amount needed to corrode a copper canister	Yes.	Neglected since the effect is very small
Montmorillonite composition	Yes. Iron reducing bacteria can use Fe(III) in smectite as an electron acceptor in their respiration	The risk maximum layer charge change is evaluated for the bentonite used	Yes. Iron reducing bacteria may degrade montmorillonite which will decrease the swelling properties of the bentonite	The risk for illitisation is evaluated for different combinations of bentonite process variables. Discussed in the bentonite transformation scenario
Porewater composition	Yes	Maximal production of sulphide and gas is calculated for all possible porewater compositions and the amounts produced are compared with the amount needed to corrode a copper canister	Yes	Only the indirect effects on the buffer/canister are considered
Structural and stray materials	Yes	No stray materials are assumed to be present within the buffer material	Yes	No stray materials are assumed to be present within the buffer material

Buffer geometry: The overall dimension of the buffer will have no direct impact on the process. An expanding buffer – into fractures or into the tunnel could however affect the pore size and impact the pore geometry.

Pore geometry: The density of the buffer affects the pore size. Pores with sizes smaller than about 200 nm cannot be penetrated or inhabited by microbes. Microbes vary in size from about 200 nm up to 600 µm, however the dimensions of the average prokaryote (Bacteria and Archaea) is in general between about 0.2 and 2 µm (e.g. Madigan et al. 2012). The cut-off in sulphide-producing activity by SRB has been observed over increasing wet density at discrete wet density intervals that differ from clay to clay. Bengtsson et al. (2015, 2017a, b) and Bengtsson and Pedersen (2017) have shown that sulphide production drop from high to very low or below detection in the wet density interval 1 740–1 880 kg m^{-3} for the MX80, Asha, Calcigel and Rokle. Similar decrease in activity was also observed for Boom Clay in the interval 1 800–1 900 kg m^{-3} (Bengtsson and Pedersen 2016). For the Gaomaiaozi bentonite the cut-off could not be found within any of these intervals (Bengtsson et al. 2017b).

Radiation intensity: Microbes are generally radiation resistant, but it varies from species to species. Increasing dose will decrease the number of surviving microbes. Spores and desiccated cells have even higher resistance against radioactivity.

Temperature: All microbes have a temperature range within which they are active. Increasing the temperature will increase microbial activity. Temperatures above the maximum tolerable temperature are let al. The highest demonstrated temperature for active microbial life is 113 °C (Stetter 1996). Previous and ongoing investigations of materials from the Alternative Buffer Materials project at Äspö show that sulphate reducing bacteria are common in many clays. Several of the alternative materials appear to have thermophilic sulphate reducers that grow much better at temperature above 50 °C, than at room temperature. It is obvious that many of the buffer materials come with sulphate reducers of which several withstand high temperatures (Masurat et al. 2010a).

Water content: Decreasing water availability reduces microbial diversity. Many microbes can compensate for low water content using metabolic, energy consuming processes but some water is needed for active life. A combination of low energy availability and low water content is detrimental to many microbes (Potts 1994).

Gas content: Hydrogen and methane can be consumed by microbes; a large effect is obtained if oxygen is present. Active microbes can produce gas if organic carbon is available for metabolism. Methanogens generate methane from hydrogen and carbon dioxide. Anaerobic methane oxidation (ANME) has been identified as a crucial microbial process. This process outputs sulphide when methane is oxidised with sulphate in the ANME process. Therefore, methane may imply sulphide production where microbial life is possible in the buffer. As judged from results from Olkiluoto, Finland (Pedersen et al. 2008), and also from the Äspö hard rock laboratory (HRL), the rate can be high. Similarly, hydrogen from depth and/or corroding iron may result in sulphide via microbial processes. When oxygen is present, methane is oxidised with concomitant reduction of oxygen (Eriksson 2007).

Hydrovariables (pressure and flows): Most microbes tolerate large variations in hydrostatic pressure and flow.

Stress state: Microbes tolerate limited mechanical pressure. Swelling clay will disrupt microbes when the pore size becomes smaller than the size of the microbe.

Bentonite composition: There is a positive correlation between microbial activity and the concentration of organic carbon. The organic material in the bentonite is assumed to be mostly humic and fulvic acids, i.e.presumably plant-derived waxes and highly aromatic carbon with low contributions from small molecules (Marshall et al. 2015). It is not known how much of it will be subject to biodegradation.

However, in the study by Marshall et al. (2015) it was concluded that since the majority of the natural organic matter in the bentonite clay is recalcitrant and already diagenetically altered, it is unlikely to serve as microbial substrate. Due to the low concentration of water-extractable organic carbon, which was less than 0.01 %, of the total organic amount, the bioavailability of these compounds in the repository will be low. The low solubility of organic carbon was also confirmed by Maanoja et al. (2020).

Montmorillonite composition: Iron-reducing bacteria have been demonstrated to dissolve iron-rich smectite through reduction of structural Fe(III) at room temperature and 1 atmosphere within 14 days under good growth conditions (Kim et al. 2004). Microbial processes may consequently have an influence on the variable if the montmorillonite is rich in Fe(III). However, the laboratory-optimized conditions may be satisfied only in certain geological environments. The lack of these conditions may be the reason why smectite in soils and sediments persists despite the presence of active microbial processes (mostly non-iron-reducing activity). Likewise, illite in modern sediments is mostly derived from the erosion of sedimentary rocks and is not necessarily biogenic in origin (Dong 2012).

Porewater composition: There is a positive correlation between microbial activity and the concentration of organic carbon. There is a limited effect on the porewater chemistry if the microbes are metabolically active. Gas and sulphide production can occur.

Structural and stray materials: There is a positive correlation between microbial activity and organic carbon present in stray material. Microbial degradation of organic stray material is possible. See previous discussion under Bentonite Composition. No stray materials are assumed to be present in the buffer.

Boundary conditions

The relevant boundary conditions in order to treat the process quantitatively are those of the transport processes that control the exchange of solutes (microbe nutrients) and dissolved gas (sources of energy) between the buffer porewater and the water in its adjacent components, i.e. the boundary conditions of the processes diffusion and advection.

Model studies/experimental studies

A Large scale Canadian buffer experiment: A full-scale experiment (Buffer-Container Experiment, BCE), with buffer material consisting of 50/50 % bentonite/sand was performed at Atomic Energy of Canada Limited's (AECL) underground laboratory in Canada. The results showed that microbes, with a few exceptions, could only be cultured from buffer samples with a gravimetric water content of 15 % or more, which is approximately equivalent to the water content in a 100 % bentonite having a saturated density of 2 000 kg/m^3 (Stroes-Gascoyne et al. 1997). Elevated temperatures had no effect on the microbes. These results were interpreted as an effect of limited availability of water. The result of the BCE raised questions about the survival of microbes, and especially SRB, in buffer materials with 100 % bentonite and has subsequently led to detailed laboratory experiments.

Laboratory experiments exploring the survival of bacteria in buffer: The Canadian field experiment was followed up by laboratory experiments. Two species of sulphate-reducing bacteria were mixed with MX-80 bentonite at varying saturated bentonite densities, from 1 500 kg/m^3 to 2 000 kg/m^3 (Motamedi et al. 1996). The species were *Desulfovibrio aespoeensis* and *Desulfomicrobium baculatum*, both isolated from deep groundwater at the Äspö HRL. None of the species survived 60 days at densities above 1 800 kg/m^3. *D. baculatum* survived the better of the two, remaining culturable for 60 days at 1 500 kg/m^3. Although microbial activity diminished rapidly, it was argued that this was due to the laboratory conditions during this experiment, which may have added some extra constraints to the ones found in the field situation. The laboratory experiment represents a closed situation with an artificial microbial population, while field conditions would be of the open system type with a natural microbial population. A long-term field experiment was therefore initiated to assess microbial issues.

Survival of microbes in long term buffer tests with in situ conditions: The long-term test (LOT) of buffer performance aims to study models and hypotheses of the physical properties of a bentonite buffer. Several species of bacteria with different relevant characteristics were introduced into the LOT bentonite. Mesophilic, thermophilic and spore-forming sulphate reducing bacteria, together with desiccation resistant, chemo-organotrophic or chemolithotrophic spore- and non-spore forming bacteria were mixed with bentonite clay to give approximately 100 million bacteria per gram (dry weight) of clay (Pedersen et al. 2000a). The clay with bacteria was subsequently formed into cylindrical plugs of 20 mm length and diameter, and installed in bentonite blocks exposed to low (20–30 °C) and high (50–70 °C) temperatures. The blocks were installed in the LOT boreholes immediately after the bacterial plugs were introduced (Pedersen et al. 2000a). The experiment was terminated after 15 months. The major outcome was the effective elimination, to below detection limits, of all bacteria except the spore-forming populations. All of the three spore formers survived at the lower temperature. The numbers remaining were, however, much lower than those initially introduced. The approximately 100 million spore-forming bacteria per gram (dry weight) of clay were reduced 100- to 10 000-fold. This can be interpreted as showing that the cell death rate was higher than the growth rate, which may have been zero, or close to zero. The spore-forming sulphate-reducing bacterium was the only one of the three that survived at high temperature. It was concluded that the spore formers most probably survived as spores, and spores do not produce sulphide. Survival is not equivalent to activity. Since the methods used in this experiment did not reveal activity, additional experiments were set up to include measurement of sulphide production in simulated repository conditions.

Survival of microbes in Full-scale Engineered Barrier Experiment (FEBEX): Full-scale Engineered Barrier EXperiment mimicking a typical High Level Radioactive Waste (HLRW) repository concept for spent nuclear fuel disposal. The experiment has been excavated in two steps, the first, partial dismantling of the FEBEX "in situ" test, FEBEX-I, was carried out during de summer of 2002, following 5 years of continuous heating and the second and final excavation, FEBEX-II, took place 2015 and has been investigated in terms of bacterial diversity and bacterial numbers. Lopez-Fernandez et al. (2015) found high bacterial diversity in bentonite dominated by phyla Proteobacteria, Bacteroidetes and Actinobacteria in samples of FEBEX bentonite. The phylum Proteobacteria contains many species of the Desulfovibrio genus which all are sulphide-producers. During the partial dismantling of the FEBEX repository in 2002, sulphate-reducing bacteria (SRB) could be cultivated from FEBEX bentonite samples in numbers ranging from 30 to 10 000 cells per gram depending on temperature and water content (Fuentes-Cantillana and García-Siñeriz 2000, Madina and Azkarate 2004).

Even after 18 years of simulation in full-scale of a HLRW repository, anaerobic mesophilic bacteria were found in numbers of over thirty thousand per gram of bentonite in some core samples (Bengtsson et al. 2017c). Specific bacterial groups important for the safety case of a HLRW repository like iron reducing bacteria (IRB), nitrate reducing bacteria (NRB) and sulphate reducing bacteria (SRB) could also be cultivated from several bentonite core samples. However, these were mainly found in the dismantling sections where the water content was elevated and temperature and dry density was lower than in the hot and dry sections adjacent to the heater (Villar et al. 2016).

Laboratory experiments exploring microbial sulphide production in buffer: The worst-case scenario for copper canister corrosion would be if SRB formed biofilms on the canisters or grew intensively in the buffer close to the canister. To mimic this situation, several experiments have been executed and evaluated. In a first series, swelling pressure oedometers were loaded with bentonite at different densities, corresponding to different water activity values (Pedersen et al. 2000b). A copper disc was placed between the bottom lid and compacted bentonite. Different SRB were added to the clay and the discs, together with $^{35}SO_4^{2-}$. The species used were laboratory cultures. Finally, oxidised silver foil was placed between the disc and the clay. The oedometers were reassembled and incubated for 4 weeks at the respective optimum temperatures and three different saturated bentonite densities: 1 500, 1 800 and 2 000 kg/m^3, corresponding to water activities at the unpressurised condition of 0.999, 0.994, and 0.964, respectively. After incubation, ^{35}S-Ag_2S was localised on the silver foils and quantified by electronic autoradiographic imaging (Packard instant imager electronic autoradiography system, Meriden, U.S.A.). The amount of Ag_2S formed was used as a measure of the sulphate-reducing activity.

The SRB used were active at a saturated bentonite density of 1 500 kg/m^3, but sulphide production was virtually absent at higher densities. This experiment indicated that SRB probably cannot be active at the canister surface at a repository bentonite density of 2 000 kg/m^3 at full water saturation. However, the experiment was run with two laboratory species and it may be possible that other species that were not tested could survive better. Therefore, additional experiments were carried out using natural groundwater that commonly contains many hundreds of different microbial species, including several naturally occurring species of SRB.

There seems to be a correlation between swelling pressure and microbial activity. This correlation has not been sufficiently investigated and it is currently not clear which buffer characteristics limit microbial activity. In the SR-Can safety assessment, the limit for controlling microbial sulphide production was set as a saturated clay density of 1 800 kg/m^3. This gives a pore space and swelling pressure that lie close to the low pore space and high swelling pressure reported to suppress microbes in Masurat (2006). (The limit was not further specified in the SR-Site assessment.)

The lower limit of bentonite density and thereby the swelling pressure for which the microbial sulphate reduction can be considered to be insignificant have been studied. Conclusions concerning the swelling pressure and/or dry density and potential additional constraints limiting microbial activity are, however, somewhat incomplete. There are preliminary results that indicate a sharp limit in dry density where microbial sulphate reduction ceases in MX-80 as well as in other bentonites (Bengtsson et al. 2015, 2017a, b). The limit seems to be dependent on the type of bentonite (Figure 3-46). The findings presented in Bengtsson et al. (2017a, b) have been verified by Haynes et al. (2019).

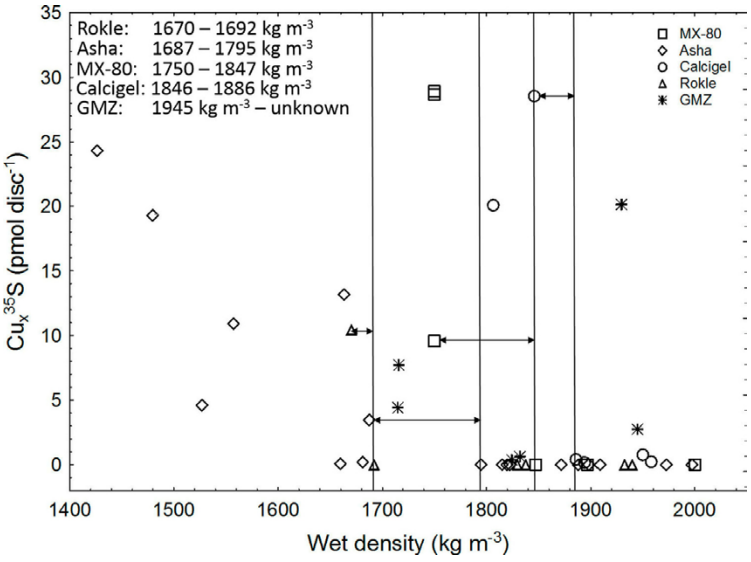

Figure 3-46. *Accumulated $Cu_2{}^{35}S$ on copper discs (pmol) over wet density. The respective intervals where sulphide-production shifts from high to low are indicated with arrows. The corresponding analysed wet density intervals are inserted, for GMZ all tested wet densities shows high sulphide production. (Bengtsson et al. 2017b).*

Field experiments exploring microbial copper sulphide production in buffer: The activity of SRB was again investigated in compacted bentonite with densities of 1 500, 1 800 and 2 000 kg/m^3 at full water saturation using stainless steel oedometers with $^{35}SO_4{}^{2-}$ as an oxidised sulphur source for the SRB respiratory processes (Masurat and Pedersen 2003, Masurat et al. 2010b). This time, the investigations were performed under in situ conditions, including a hydrostatic pressure of 25 bars at a depth of 450 m at the Äspö Hard Rock Laboratory. The sources of SRB were the groundwater and the bentonite. Cultured SRB were not added. Canister type, copper plates were placed in the oedometers, with the top either in contact with the added groundwater (exposed) or with 3–4 mm bentonite between the plate and the added groundwater (embedded) (experiment B). The initial slot between bentonite and rock in a repository was simulated by a gap between the water inlet filter and the compacted bentonite. The bentonite density was thereby initially low at this end of the sample. The water uptake into the sample led to a density homogenisation and a successive increase of density to the final test density. Radioactive hydrogen sulphide formed by the SRB reacted with the copper and formed radioactive copper sulphide, which was measured by electronic radiography as described for the lab experiments above. A similar set-up (experiment G) with filter-sterilised groundwater (0.2 µm) was used as control. Finally, a third bentonite set-up was heat treated at 120 °C for 12 h and sterile groundwater added. The results showed that SRB were active and produced hydrogen sulphide during the initial phase of bentonite swelling, which was monitored for about 70 days. The copper sulphide production by the SRB was inversely related to the final density of the bentonite, as the highest density had the lowest overall SRB activity (Figure 3-47).

The experiments with sterile groundwater on the one hand, and sterile groundwater and heat treatment of the bentonite on the other, showed that SRB were present in a dormant state in the commercial MX-80 bentonite. By addition of water, these dormant SRB became active and started to produce hydrogen sulphide. It is obvious that there are two sources of SRB to buffer material; the groundwater and the bentonite itself.

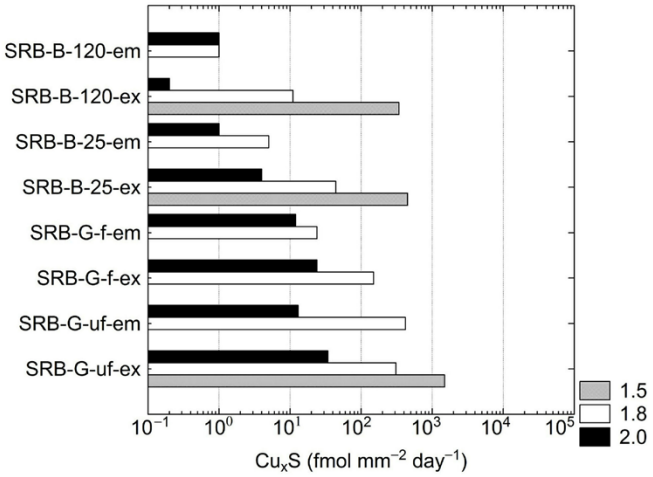

Figure 3-47. *Graphic representation of the mean copper sulphide production rates on copper plates that were exposed (ex) and embedded (em) at different saturated bentonite densities (1 500, 1 800 and 2 000 kg m^{-3}). The treatments were un-filtered (uf) filtered (f) in experiment G and exposure to 25 °C (25) and 12 °C (120) during 15 h. See text for details. Figure is from Masurat et al. (2010b).*

Microbial sulphide formation under unsaturated conditions: a series of experiments were conducted (Svensson et al. 2020) to investigate the activity of sulphate-reducing bacteria (SRB) in bentonite as a function of the availability of water (liquid and different relative humidities). The focus was on experiments with the commercially available Pseudodesulfovibrio aespoeensis (previously called Desulfovibrio aespoeensis), which was originally isolated from the Äspö HRL, but experiments were also performed with an enrichment fromnatural groundwater from a borehole in the Äspö HRL. The experiments were performed in small glass tubes placed in larger plastic tubes (Figur 3-48), which were then stored in an oxygen-free environment. When gypsum, lactate (a source of both carbon and energy), nutrients and liquid water were added, sulphate reduction was observed regardless of whether bentonite had been added or not. There were strong indications that the bentonite reacted with sulphide since the amount of formed sulphide was lower or below the detection limit in the presence of bentonite. The conclusion of this study is that both an energy source (lactate in this case) and liquid water is required for sulphate reduction to take place. Not even with 100 percent humidity could sulphide be observed during the test period.

Natural analogues/observations in nature

There is a natural analogue in Dunarobba, Italy, where a bentonite slide buried a forest approximately one and a half million years ago. Trees that have not been decomposed by microorganisms can still be found. This indicates that conditions for microbial activity in bentonite clay are unfavourable.

Time perspective

The time perspective concerning survival and activity of microbes in compacted bentonite has been summarised in a conceptual model as follows (confer Figure 3-4 in Pedersen 2002). At the time of deposition, there will be a canister, bentonite blocks and a hole in the rock. The next step will be to allow water to fill all the void volume. This water can be groundwater from the rock or, alternatively, groundwater or process water added from above at the time of container deposition. Irrespective of the source, microbes will be present in the water and these microbes will mix with the buffer, as described above.

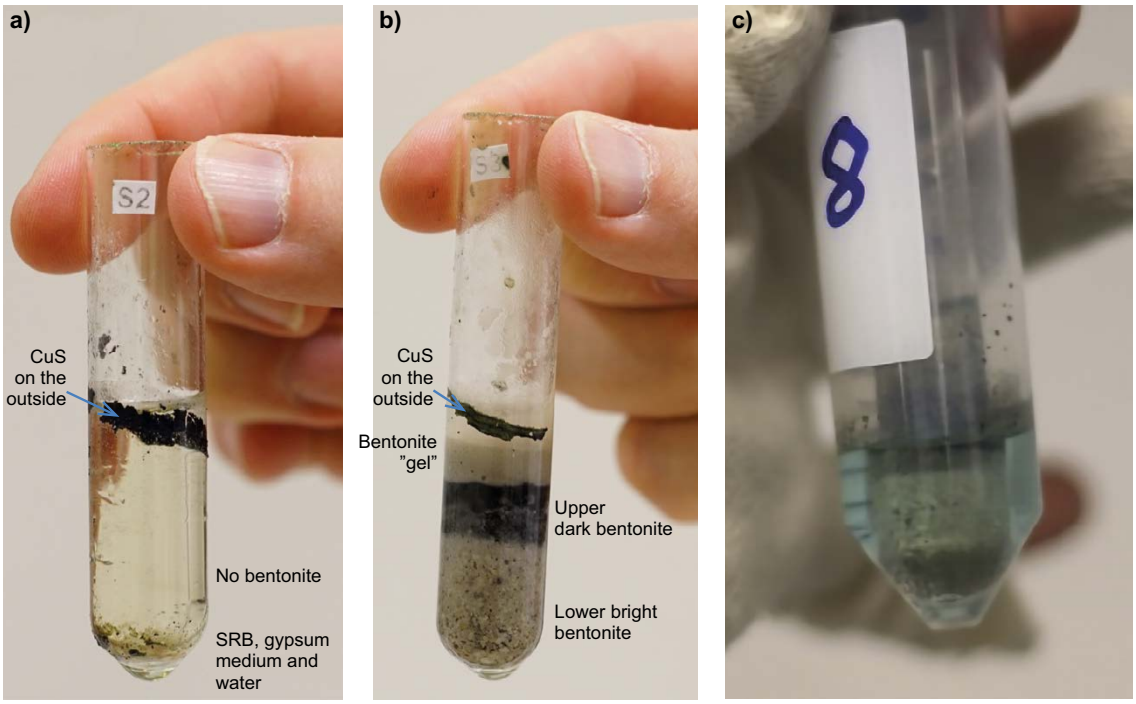

Figur 3-48. *Picture a) and b) show two glass tubes with newly formed copper sulphide from microbial transformation of sulphate. Picture c) shows how one of these glass tubes has been placed in a plastic tube with liquid to provide the relative humidity in the system. The liquid also captured any formed hydrogen sulphide in the stable phase copper sulphide. There is no bentonite in the left glass tube, while the glass tube in the middle contains bentonite. Liquid water was available for the microbes in both cases. These tests were performed in an oxygen-free atmosphere (Svensson et al. 2020).*

Swelling of the clay will introduce groundwater microbes into the clay, to a depth that is dependent on the initial slot, on both the rock and the canister side of the bentonite. Additionally, the microbes indigenous to the bentonite will be present in the entire bentonite buffer, as spores, dormant cells, metabolically active cells and as desiccated cells in dry clays. The experimental data on survival and activity of microbes in bentonite suggest that the number of viable microbes will decrease rapidly during swelling and that very few viable cells will be present at full compaction. Sulphate-reducing activity will also approach zero when full compaction is achieved. An endospore (often shortened spore) is a dormant, tough, and non-reproductive structure produced by some bacteria eg some species of SRB . Under harsh conditions and when the environment becomes more favorable, the spore can reactivate itself to the vegetative state. Our results indicate that viable cell activity will be impossible at full compaction, as spores are inactive. Although spores generally are very resistant to difficult environmental conditions they can be killed by eg. autoclaving. . The experiments by Pedersen et al. (2000a) indicated a decrease in the number of viable spores at full compaction so that a slow, but significant, death rate of spores would eventually lead to the complete eradication of life in the buffer. It has not yet been clarified, however, whether this would occur within the lifetime of a HLW repository. The theoretical pore size of the clay is 100–1 000 times smaller than the average-sized microbe, meaning that no new microbes can enter into an intact buffer.

Handling in the safety assessment the PSAR

There is a limit to the rate of microbial sulphide corrosion that must not be exceeded. This rate is defined by the thickness of the canister and is based on the assumption that sulphide corrosion of copper is of a non-pitting type. Based on the results in Bengtsson and Pedersen (2016, 2017) which show shown that sulphide production drop from high to very low or below detection in the saturated density interval 1 740–1 880 kg/m^3 for the MX80, Asha, Calcigel and Rokle bentonites, microbial sulphide production can be treated as an on-off process. If the buffer density is sufficient the process can be neglected. If the buffer density is too low it has to be pessimistically assumed that the rate of microbial sulphide production is unlimited. In this case the rate will depend on the availability and diffusion rate of nutrients and sulphate from groundwater.

In the PSAR, MX-80 bentonite is used as reference material. According to Bengtsson et al. (2017b) the limit of saturated density to prevent microbial sulphide production for MX-80 lies in the interval 1 750–1 847 kg/m^3 for that material. Hence, a saturated density of 1 850 kg/m^3 is selected as the safety function indicator criterion in the PSAR. This means that no sulphate reduction will occur in the buffer as long as the saturated density is higher than 1 850 kg/m^3.

Microbial sulfate reduction will be neglected under unsaturated conditions based on the findings in Svensson et al. (2020).

Uncertainties

Uncertainties in mechanistic understanding

The rate of microbial copper sulphide production (if any) at the final swelling pressure remains to be determined. Rate limiting factors such as diffusion of nutrients, energy and sulphide, radiation, water content and heat stress (temperature) must be clarified and defined.

Migration of microorganisms through compacted bentonite is not likely as they need a liquid medium order to be motile. The restrictions due to a low pore size may need to be defined experimentally. Many microbes prefer to grow attached to surfaces, but formation of biofilms on clay particles is not well studied.

Formation of biofilms on the canister surface has been suggested to occur. This may be the case during the initial swelling phase. However, those microorganisms will obey the same restrictions as any microbe in other parts of the buffer. The stress from heat and radiation will be more severe at the canister surface than anywhere else in the buffer.

The mechanisms for survival of microbes in bentonite and buffer materials are not fully understood. Evidence for the presence of viable microbes in commercial MX-80 bentonite suggests that SRB and also other species can withstand the very dry conditions (10 %) in commercial bentonite. The present hypothesis is that microbes are introduced to the clay during mining and processing. The clay causes dehydration, which will gently remove water from the cell. The cells will be inactive, but viable. This process is similar to freeze drying of cells, which also results in inactive but viable cells, e.g. freeze dried baker's yeast. Adding water revives the microbes to an active life.

The observed disappearance of microbial activity and viability in highly compacted bentonite under repository conditions is hypothesised to be a combined effect from desiccation, mechanical pressure and other stress factors. The sum of stress factors, radiation, heat, low initial water availability and a high mechanical pressure after saturation of the buffer results in death of the microbes. However, the exact mechanisms for the observed disappearance of viability of microorganisms remain to be clarified. At full water saturation, water activity is fully restored, but a mechanical pressure develops which corresponds to the water activity in the unpressurised clay according to the Kelvin equation.

The low concentration of sulphide observed in many groundwater samples depends on the availability of ferrous iron, if the availability of iron decreases, the aqueous concentration of sulphide will increase, as it does at some depths in Olkiluoto and recently found also in monitored boreholes at Forsmark and Laxemar, where concentrations approach 10–20 mg sulphide/L. pH must be taken into consideration as dissociation of hydrogen sulphide (gas) depends on pH.

Model simplification uncertainties in the PSAR

A simplified model which assumes 0 or ∞ is used.

Input data and data uncertainties in the PSAR

The main uncertainty is the buffer density/swelling pressure where the process turns on or off.

3.6 Radionuclide transport processes

3.6.1 Speciation of radionuclides

Overview

This process discusses the speciation of radionuclides in the aqueous phase. Speciation of radionuclides is of importance for sorption and diffusion processes in the buffer. These processes depend on the aqueous radionuclide species that are kinetically and thermodynamically stable under the conditions of interest at the boundary of the buffer, i.e. inside the canister and also on the chemical conditions in the buffer.

Dependencies between process and buffer variables

Table 3-26 summarises how the process influences and is influenced by all buffer variables and how these effects are treated in the PSAR.

Boundary conditions

The boundary conditions for the process are the source term from the canister/fuel, i.e. the speciation inside the canister.

Table 3-26. Direct dependencies between the process "Speciation of radionuclides" and the defined buffer variables and a short note on the handling in the PSAR.

Variable	Variable influence on process		Process influence on variable	
	Influence present? (Yes/No) Description	Handling of influence (How/Why not)	Influence present? (Yes/No) Description	Handling of influence (How/Why not)
Buffer geometry	No		No	
Pore geometry	No		No	
Radiation intensity	(The effect from radiolysis in the buffer will be small)		No	
Temperature	Yes. Chemical reactions are temperature dependent	The uncertainty with respect to temperature is considered. However, the temperature range in the repository is expected to be narrow	No	
Water content	No, but indirectly, because porewater composition changes with water content		No	
Gas content	No, but indirectly through porewater composition		No	
Hydrovariables (pressure and flows)	No		No	
Stress state	No		No	
Bentonite composition	Indirectly through porewater composition		No	
Montmorillonite composition	Indirectly through porewater composition		(Sorbed radionuclides will change the smectite composition, but the effect is limited)	
Porewater composition	Yes. Direct dependence	Used in calculation	Yes	Results from calculations
Structural and stray materials	Indirectly through porewater composition		No	

Model studies/experimental studies

If the water chemistry in the buffer is known, the speciation of radionuclides can be calculated with a thermodynamic equilibrium model, such as PHREEQC or EQ3/6 together with a self-consistent thermodynamic database.

Time perspective

This process is relevant for the whole assessment period, but only if there is a canister failure.

Natural analogues/observations in nature

Natural analogues are usually studied for water rock interactions – not for the water phase alone.

Handling in the safety assessment the PSAR

The solubility and speciation of radionuclides is calculated and used as a source term for the modelling of release from a defective canister. This is done for a wide range of water compositions.

In the buffer, the speciation is used to determine the transport properties of the radionuclides. However, the parameters for the transport properties used in the PSAR are selected based on experiments done under relevant conditions or from thermodynamic sorption models; see Sections 3.5.3 and 3.5.4. The consistency of the predicted speciation with the speciation calculated in the source term will be checked.

Uncertainties

Uncertainties in mechanistic understanding

See processes Sections 3.5.3and 3.5.4.

Model simplification uncertainties in the PSAR

See processes Sections 3.5.3 and 3.5.4.

Input data and data uncertainties in the PSAR

See processes Sections 3.5.3 and 3.5.4. There may also be uncertainties in thermodynamic data. This is discussed in Sections 3.5.3 and 3.5.4.

3.6.2 Transport of radionuclides in the water phase

Overview

A number of processes will or could influence the transport of radionuclides in the water phase:

- advection, if the hydraulic conductivity of the buffer is high,
- diffusion, will generally be the main transport mechanism through the buffer,
- sorption, will have a strong effect on retarding the transport of most radionuclides,
- speciation, will determine the form (including oxidation state) in which the radioelements exist and therefore also its maximum solubility, as well as how the radioelements are sorbed and transported (sorption can thus be viewed as a part of the speciation),
- colloid transport, could enhance the transport of radionuclides,
- radioactive decay will determine how much of the radionuclide inventory will eventually leave the buffer.

All these have been discussed above among the processes occurring in the buffer, or, in the case of decay, under fuel processes.

Dependencies between process and buffer variables

Table 3-27 summarises how the process influences and is influenced by all buffer variables and how these effects are treated in the PSAR.

Boundary conditions

The inner boundary for this process is the concentration of radionuclides within a defective canister. The outer boundary is the fractures in the wall of the deposition hole or the deposition tunnel.

Model studies/experimental studies

Not done for relevant conditions. However, the individual processes are studied; see for example Sections 3.5.3 and 3.5.5.

Table 3-27. Direct dependencies between the process "Transport of radionuclides in the water phase" and the defined buffer variables and a short note on the handling in the PSAR.

Variable	Variable influence on process		Process influence on variable	
	Influence present? (Yes/No) Description	**Handling of influence (How/Why not)**	**Influence present? (Yes/No) Description**	**Handling of influence (How/Why not)**
Buffer geometry	Yes. Gives the volumes and geometries available for transport	Geometry is included in RN-transport calculations	No	
Pore geometry	Yes. Determines diffusivity.	Included in data	No	
Radiation intensity	No		No	
Temperature	Yes, transport and chemical processes are generally temperature dependent	Neglected. RN-transport occurs after thermal pulse. The temperature range in the repository will be narrow	No	
Water content	Yes.	Radionuclide transport is assumed to take place when the buffer is saturated	No	
Gas content	Yes.	Radionuclide transport is assumed to take place when the buffer is saturated	No	
Hydrovariables (pressure and flows)	Yes. Determines the exchange with groundwater	Near field flow is considered in calculations	No	
Stress state	No		No	
Bentonite composition	Yes. Determines sorption and transport properties	Included in data See 3.5.3 and 3.5.5	No	
Montmorillonite composition	Yes. Determines sorption and transport properties	Included in data See 3.5.3 and 3.5.5	Yes.By cation exchange	Neglected since effect from radio-nuclides is small
Porewater composition	Yes. Determines sorption/speciation	Included in data See 3.5.3 and 3.5.5	Yes. Contamination	Output from RN-calculations
Structural and stray materials	Indirectly through porewater composition	–	No	

Natural analogues/observations in nature

By definition, this process cover the integrated treatment of radionuclide transport in the near field and it is therefore difficult to find applicable natural analogues. Natural analogues could however by used to study the individual processes, e.g. sorption or solubility.

Time perspective

The process is active at all timescales after canister failure.

Handling in the PSAR

Radionuclide transport in the buffer is handled in the integrated modelling of radionuclide transport for the repository.

Model: The near field code COMPULINK/COMP23 (Romero et al. 1999) and the **Model summary report** is used for the calculations. The code calculates the non-stationary nuclide transport in the near field of a repository. The system is divided into compartments, where the only restriction is that a compartment is formed of the same material. The model, which is basically a coarsely discretisised Integrated Finite Difference Model, embeds analytical solutions at locations which otherwise would require a very fine discretisation, such as entrances and exits from small holes and fractures. In the repository, radionuclides leaking out through a small hole in the canister wall diffuse into the buffer and then may migrate through various pathways into the flowing water in the rock fractures.

The buffer processes that need to be considered are treated in the following way:

- Advection is neglected if the buffer conductivity is $< 10^{-12}$ m/s, see Section 3.5.1.
- Diffusion is treated with element-specific diffusivities and porosities (considering specific oxidation states), see Section 3.5.2.
- Sorption is treated with linear sorption coefficients (K_d) for all elements (considering speciation as well as bentonite and porewater composition), see Section 3.5.3.
- Colloid transport is neglected in the buffer, provided the buffer completely envelops the canister and has a dry density of at least 1 000 kg/m^3, see Section 3.5.12.
- Speciation of radionuclides is directly included in the calculation of the source term from the inner boundary condition. The speciation is also included in the determination of the sorption coefficient.
- Radioactive decay and chain-decay are considered in the calculations.

Boundary condition: Radionuclide transport in the buffer is strongly dependent on the conditions at the inner and outer boundaries. The geometry of defects and fractures will determine the rate of mass transport.

Handling of variables influencing this process: The buffer geometry is included as compartments in the model. The buffer variables, montmorillonite composition, bentonite composition and porewater composition will together determine the transport parameters. These include: porosity, diffusivity and sorption coefficients.

Handling of variables influenced by the process: The concentrations and mass flows of radionuclides are calculated.

An earthquake of large magnitude may potentially change the boundary conditions for the process, while the radionuclide transport within the buffer will remain the same.

Uncertainties

Uncertainties in mechanistic understanding

This process is an integration of several other processes all of which have uncertainties (see above).

Model simplification uncertainties in the PSAR

The COMPULINK/COMP23 code uses rather a coarse discretisation of the buffer and analytical solutions for the boundary conditions at the canister and the rock.

Input data and data uncertainties in the PSAR

The data uncertainties for the transport parameters in the buffer are presented in Sections 3.5.2 and 3.5.3. All input data to the radionuclide transport calculations will be handled in the **Data report**.

3.6.3 Transport of radionuclides in a gas phase

Overview

A pulse of hydrogen gas can be released from a defective canister see Section 3.3.3. Some radionuclides could potentially enter the gas phase and thereby be transported to the surface much more rapidly than would be the case for the aqueous pathway. In principle, only C-14 and Rn-222 can enter the gas phase. Theoretically, I-129 could also be present as elemental iodine, but the amount will be negligible.

Dependencies between process and buffer variables

Table 3-28 summarises how the process influences and is influenced by all buffer variables and how these effects are treated in the PSAR.

Boundary conditions

The inner boundary for this process is the gas pressure within a defective canister. The outer boundary is the fractures in the wall of the deposition hole.

Model studies/experimental studies

Not done for relevant conditions.

Natural analogues/observations in nature

Not relevant.

Time perspective

The process will only occur if there is a defect in a canister and if a sufficient amount of water is supplied to the iron insert to generate, over time, a gas pressure that is higher than the opening pressure of the bentonite.

Table 3-28. Direct dependencies between the process "Transport of radionuclides in the gas phase" and the defined buffer variables and a short note on the handling in the PSAR.

Variable	Variable influence on process		Process influence on variable	
	Influence present? (Yes/No) Description	Handling of influence (How/Why not)	Influence present? (Yes/No) Description	Handling of influence (How/Why not)
Buffer geometry	Yes. The buffer volume determines the transport	See 3.3.3	No	
Pore geometry	No. Only for dissolved gases. Indirectly through stress state		No	
Radiation intensity	No		No	
Temperature	Yes, but the thermal phase will be over before high enough gas pressures can be reached	Neglected	No	
Water content	Yes.	The process is assumed to occur only when the buffer is saturated	No	
Gas content	Yes.	The process is assumed to occur only when the buffer is saturated	Yes	Output from transport estimate
Hydrovariables (pressure and flows)	Yes. The gas pressure will be dependent on the hydrostatic pressure	The pressure build up determines the time for gaseous releases	No	
Stress state	Yes. The opening pressure is dependent on the swelling pressure	The pressure build up determines the time for gaseous releases	No	
Bentonite composition	Indirectly via stress state		No	
Montmorillonite composition	Indirectly via stress state		No	
Porewater composition	Yes and also indirectly via stress state that affects solubility/ speciation of gases, especially CO_2	Pessimistically neglected	No	
Structural and stray materials	No		No	

Handling in the PSAR

Radionuclide transport in a gas phase is treated as a separate case in the PSAR. The handling is based on the experiment by Harrington and Horseman (2003) presented in Section 3.3.3. It is assumed that if gas production exceeds the ability of the surrounding groundwater to take it into solution and transport it away from the container, a pressure will build up within and adjacent to the container. The bentonite is assumed to ultimately open and release gas when the internal pressure exceeds 20 MPa. A rapid outflow will occur until the pressure falls to 10 MPa. This means that half of the gas inside the canister will be released instantaneously together with the radionuclides contained in that amount of gas. The only important radionuclides that can be transported in a gas phase are C-14 and Rn-222. Since the half-life of C-14 is 5 568 years, neither the buffer nor the geosphere is expected to significantly delay the transport to the biosphere. Isotope dilution in a gas phase is not considered. Rn-222 has a very short half-life, but is always present inside the canister. Hence, delay in the geosphere could affect the releases, but is pessimistically neglected in the PSAR.

The pathway may either stay open as long a there is a gas production in the canister or open and close as the buffer reseals leading to repeated pulses of gas (see Section 3.3.3). In the first case, the gas is expected to be released at the same rate as it is produced by corrosion after the breakthrough pulse. The second case will lead to repeated pulses of about equal magnitude.

Uncertainties

Uncertainties in mechanistic understanding

The mechanisms for gas release through bentonite are still not fully understood, see Section 3.3.3. Theoretically, I-129 could also be present in a gas phase as elemental iodine, but the amount will be negligible. Some metals and metalloids form volatile methylated and/or permethylated species, whether these could appear in the fuel at low temperature has not been discussed.

Model simplification uncertainties in the PSAR

The handling of the gas transport pathway in the PSAR is based on a few experiments only. The values for opening and steady-state pressures have been selected from these experiments.

Input data and data uncertainties in the PSAR

As mentioned above, the values for gas opening and steady-state pressures are based on experimental evidence. However, under any conditions, the gas pressure differential should be in the range of 5–15 MPa. Another uncertainty is the fraction of C-14 that can enter a gas phase. For the time being, this fraction is pessimistically assumed to be 100 %. For Rn-222, it is probably fair to assume that all of the inventory will be in the gas phase.

4 Processes in the tunnel backfill

4.1 Thermal processes

4.1.1 Heat transport

Overview

Heat is transported from the canister surface to the buffer, through the buffer and finally from the buffer to the rock, both directly and via the tunnel backfill. The thermal evolution within the backfill is determined by the canister power, the canister spacing and the rock thermal properties while the thermal processes conditions in the deposition holes are unimportant.

The process description for the buffer (Section 3.2.1) is valid for the backfill as will.

Handling in the PSAR

There is no specific handling of heat transport in the backfill during the thermal phase since the backfill temperature is not directly related to the performance of the barrier and the temperature increase will be modest. Results from thermal analyses, obtained using either rock mass values or generic values of the backfill heat transport parameters, give sufficient information on the backfill temperature range during the thermal phase.

4.1.2 Freezing

Overview

The overview and general description of the corresponding buffer process, Section 3.2.2, are also valid for the backfill. Since also the backfill material exerts a swelling pressure, freezing (ice formation) is expected to occur at a temperature lower than 0 °C.

However, because backfill materials might have a lower content of swelling mineral (montmorillonite), it is crucial to empirically verify that the swelling pressure dependence on temperature still follows the thermodynamic description as described by Birgersson et al. (2008).

The swelling pressure of the backfill can be significantly lower than that in the buffer, and it cannot be excluded that it will be frozen in certain time intervals during periods of permafrost. Furthermore, the backfill is extended vertically in ramp and shafts and therefore parts of it will experience temperatures lower than those at repository level.

There is a requirement that the freezing of the backfill in the deposition tunnels should not lead to excessive pressures on the surrounding rock. The mean crack initiation stress level for the main rock type in Forsmark is 116 MPa and the minimum is 60 MPa SKB (2008). According the Clausius-Clapeyron equation, 60 MPa is generated when ice is cooled by 4.4 °C below the freezing point of water. As for the buffer, the critical temperature is dependent on the swelling pressure. The swelling pressure of the installed backfill at average density of 1 488 kg/m^3 is > 4 MPa and the swelling pressure for the minimum backfill density 1 361 kg/m^3 is ~2 MPa for deionised water. 2 MPa yield a critical temperature of −1.6 °C . The temperature of concern for the backfill is then −6 °C (−4.4−1.6)This is based on pure water and the salinity at the Forsmark site may reduce the freezing temperature further. For the deposition tunnel backfill, this requirement is primarily related to the retardation function, since i) freezing may damage the walls of the tunnel thus creating new transport paths for radionuclides and ii) the transport properties of a frozen and thawed backfill may be less favourable than those before freezing.

Handling in the PSAR

The current backfill will have a minimum swelling pressure of ~2 MPa, using the description in this section the temperature when the freezing of the backfill could cause damage to the rock of would be around –6 °C. For the backfill itseld it has been demonstrated that the freezing process is reversible.

4.2 Hydraulic processes

4.2.1 Water uptake and transport under unsaturated conditions

Overview

Water transport in the backfill under unsaturated conditions is a complex process that is dependent on temperature, smectite content, degree of water saturation and water content in the different parts of the backfill. The most important driving force for water saturation under deep repository conditions is the external water pressure from the water in the rock fractures and the negative capillary pressure in the pores of the backfill that lead to water uptake from the surrounding rock. The hydraulic sub-processes are identical to those of the buffer (Section 3.3.1).

Transport of water in vapour form controlled and driven by a temperature gradient, is probably insignificant for a major part of the backfill due to the low temperature gradient. However, it can be of importance for the backfill just above the buffer in the deposition hole and lead to drying if the supply of water from the rock is small.

Compression of air, may be more important for the water saturation process (Boyle's law) of the backfill than the buffer if the backfill is composed of clay with lower smectite content. If the air is trapped, it must be compressed and go into solution in the water in order for water saturation to be achieved. In highly compacted smectite rich bentonite, the suction potential appears to be sufficiently high for this to occur and full water saturation is achieved without any external water pressure. The backfill material has lower suction, which means that a pressurised air volume may remain if the air cannot seep out. Due to compression of the air, a large part of the volume will disappear when full water pressure has developed, but the remaining part of the entrapped air must be dissolved and diffuse out through the backfill and the rock.

When trapped air is compressed during the water saturation phase, a portion of the volume is dissolved in the water. This solubility (Henry's law) is approximately 2 percent at room temperature but decreases rapidly at increasing temperature. In order for additional air to be dissolved, the dissolved air must be transported away, which takes place by diffusion. The rate of diffusion in the backfill is partly limited by the transport capacity (diffusion and flow) in the rock. If gases are dissolved in the groundwater in the rock, the diffusion rate may be very low and the time to saturate the backfill very long.

Handling in the PSAR

The handling in the PSAR is based on the modelling of the process in Åkesson et al. (2010a). The saturation of the backfill was modelled for a number of different geometries and assumptions about data and boundary conditions. A summary of the investigated variations is given in Table 4-1. The primary purpose of the modelling was to analyse the time needed to saturate the backfill. 40 different cases were investigated in the primary variation, including combinations of tunnel sections, backfill representations, and fracture inflow (or boundary pressure). 25 different cases were investigated in the secondary variations using base case models and modified features including an EDZ, removal of fractures as well as modified permeabilities and retention properties. The approach with primary variations was largely an attempt to map the effects of different combinations of section areas, backfill representations, and fracture inflows (or boundary pressures) for different geometries. The secondary variations were mainly performed with 1D models with altered bentonite properties, and with large plane geometries, with or without fractures, and with altered rock properties.

The associated uncertainties are similar to those for the buffer and are described in Section 3.3.1.

Table 4-1. Summary primary and secondary variations.

Variation		
Primary	Tunnel section area	Two different tunnel sections
	Backfill representation	Two and in some cases three different representations
	Fracture distance and orientation	Two different orientations: vertical and horizontal. Two different distances for the vertical orientation
	Fracture transmissivity	Two different transmissivities
Secondary	Rock permeability	Several cases with different rock permeabilities
	Presence of EDZ	Two cases with EDZ
	Absence of fractures	Five cases with no fracture
	Water retention in the rock	Two cases with differerent retention curve
	Bentonite permeability	Four cases with differerent permeabilities
	Bentonite relative permeability	Two cases with differerent relative permeability
	Thermal evolution	One case with thermal evolution
	Hydromechanical processes	One case with hydromechanical processes
	Bentonite retention	Two cases with steeper retention curve
	Tunnel ventilation	One case with 10 years of RH 70 %

4.2.2 Water transport under saturated conditions

Overview

Water transport under saturated conditions is mainly driven by a water pressure gradient. The process can be described by Darcy's law. Any deviations from Darcy's law, which can occur at low gradients, are favourable in that they lead to a reduced through flow rate. The hydraulic conductivity K depends on the composition of the buffer, the void ratio e, the ion concentration in the porewater i_c and the temperature T.

Water transport in saturated backfill is a complex interplay between several sub-processes on a microscopic scale. On a macroscopic level, the result is that the permeability of a saturated backfill is low, and this is also the essential result for the safety assessment. Water flow in saturated backfill is a special case of unsaturated flow. The processes involved are *essentially* the same as for unsaturated conditions, *albeit without any vapour transport*..

The process is in general identical to the corresponding process in the buffer (Section 3.3.2) and the behaviour is expressed by the hydraulic conductivity, K. The difference in hydraulic conductivity between the backfill and the buffer is mainly the magnitude. The influence of groundwater salinity is stronger for the backfill than for the buffer; since the clay density is lower (see Section 3.5.7).

In order to prevent the deposition tunnels from being conductive pathways that influence the water movement in the repository, the backfill shall, over the entire length and cross-section of the tunnel, have a hydraulic conductivity that is in the same order of magnitude as that of the surrounding rock, or so low that diffusion is the dominating transport mechanism. A hydraulic conductivity target $K < 10^{-10}$ m/s is a limit that will ensure limited advective transport trough the backfill. A swelling pressure target of 0.1 MPa is required to be satisfied at all points in the deposition tunnel, ensuring the self-sealing ability of piping channels in conditions prevailing after closure and saturation of the repository when the hydraulic gradient is estimated to be small (Posiva SKB 2017).

Handling in the PSAR

The backfill material has a very low hydraulic conductivity that fulfils the conductivity requirements with high margins. The base case with an unaltered backfill that has not lost any material will thus not be investigated in any special way. However, sensitivity analyses are performed where the objective is to identify the parameter space where changes in conductivity result in changes in performance.

4.2.3 Gas transport/dissolution

Overview

The backfill will be emplaced with a water saturation of 40–80 %, which means that there is a substantial amount of air that needs to be dissolved and transported away. Also the groundwater in the rock may contain dissolved gas. This is covered by the cases discussed in Section 4.2.1.

Hydrogen gas from the corrosion of the cast iron insert could potentially escape from the repository by transport through the tunnel backfill. Wikramaratna et al. (1993) has estimated the gas transport and gas storage capacity of the backfill. The backfill could act as a passageway for gas under certain conditions. The backfill could then act as a sink and decrease the gas pressure in the near field of the repository. However, it is not evident that gas from the canister will ever reach the tunnel.

Handling in the PSAR

The influence of trapped air on the saturation time of the backfill is investigated in the PSAR. The process involving trapped air is only relevant during the saturation phase (see Section 4.2.1).

The backfill could potentially act as a sink for the escape of corrosion gas from the canister. However, the beneficial effect is rather limited (Wikramaratna et al. 1993) and the process is not considered in the PSAR. The desaturation of the backfill from gas transport is expected to be very minor with the same reasoning as for the buffer (see Section 3.3.3).

4.2.4 Piping/erosion

Overview

Water inflow into the deposition tunnel will take place mainly through fractures and will contribute to the wetting of the backfill. However, if the inflow is localised to fractures that carry more water than the backfill can absorb, there will be a build-up of water pressure in the fracture and therefore an increase in the hydraulic gradient across the backfill. This seems likely to occur at least locally at most conductive fractures. The backfill close to the rock surface initially consists of pellets with low density. As a result the backfill will probably not be able to stop the water inflow due to the high water pressure that will be achieved in the fracture. The results will be piping, formation of a channel and a continuing water flow, water filling of the space between the pellets and erosion. The processes are described in Section 3.3.4 (buffer). The knowledge of this process and its consequences for the backfill seems to be sufficient today (Börgesson et al. 2015).

Handling in the PSAR

Piping and erosion could lead to a loss or redistribution of the swelling clay component in the backfill. The implication of this is an increased hydraulic conductivity and a decreased swelling pressure.

The erosion model described in Section 3.3.4 can be used for the deposition tunnel as well. With a total tunnel void volume of 1 250 m^3, the largest possible erosion will be 1 640 kg. Erosion in the backfill will basically mean that material is redistributed within the tunnel itself. In SR-Site the total mass of backfill in a 300 m tunnel was estimated to be ~10 200 tonnes. Considering the large mass of backfill in the tunnel, a redistribution of 1 640 kg is assessed to have no impact at all on the backfill performance.

4.3 Mechanical processes

4.3.1 Swelling/mass redistribution

Overview

Water is absorbed by both unsaturated and saturated swelling backfill materials and causes swelling. If the backfill is unable to expand freely, a swelling pressure develops, which locally reaches its peak at full water saturation. The process is described in Section 3.4.1 for the buffer. The same basic process description is valid for the backfill. Creep is not a very important factor for the backfill since it is smaller than for the buffer and does not affect the tunnel filling function of the backfill.

Handling in the PSAR

One of the main design requirements of the backfill is to keep the buffer in place and prevent it from swelling upwards so that the buffer will not lose too much of its density. Some upwards swelling is expected since the backfill has a lower swelling pressure than the buffer and a certain degree of compressibility. A summary of different studies regarding this process, and the handling of this in the PSAR are presented in Section 3.4.1

It is important to ensure that there is a tight connection between the backfill and the tunnel wall. This is achieved by the swelling pressure of the backfill material. The evolution of backfill density and composition together with the composition of the groundwater/ porewater is studied. The hydraulic conductivity and the swelling pressure will be evaluated for the changing conditions caused by the chemical evolution. In SR-Site (SKB 2011) it was shown that backfill hydro-mechanical properties will be maintained for the expected geochemical evolution at the Forsmark site. The exception to this could however be mass loss due to chemical erosion, where relatively large mass losses could occur (Section 3.5.11). Homogenisation after loss of large masses of backfill after colloid erosion or plug disintegration is modelled for the PSAR (Åkesson et al. 2010a).

The deposition tunnels will have a varying cross section. Since the ratio of backfill blocks/pellets will vary in the installed backfill, density will vary in the axial direction of the tunnel. The homogenisation of the backfill was studied by Åkesson et al. (2010a).

The possible loss of backfill material expected during the installation and saturation phase is estimated as described in 4.2.4. The channels and possible holes caused by the lost backfill are expected to be healed by swelling and homogenisation of the backfill.

The cement and other substances in the concrete tunnel plugs may be dissolved with time and transported away (Section 5#), which means that the stiffness and strength of the plugs will be dramatically reduced. This disintegration will affect the backfill material on both sides of the plug. When the plug cannot withstand the swelling pressure of the backfill it will be compressed and the backfill will swell, which leads to a loss in density and swelling pressure of the backfill. Since there is friction against the rock surface the loss in density may be significant close to the plug but will be reduced with distance from the plug. In order to understand how this affects the backfill and the location of the first deposition hole a number of finite element calculations have been carried out (Åkesson et al. 2010a).

The uncertainties regarding these processes are similar to those described in Section 3.4.1.

4.3.2 Liquefaction

Overview

This process was included in the Process report for SR-Can. However, it has been concluded that the phenomena cannot occur in a KBS-3 type backfill material. The reasoning justifying this conclusion was discussed in SKB 2010a (Section 3.4.1). Liquefaction is no longer regarded as a process in the backfill.

Handling in the PSAR

The process is neglected.

4.4 Chemical Processes

4.4.1 Advective transport of species

Overview

In this context, advection refers to transport of any forms of additional substances, e.g. ions, molecules or colloids, with porewater flow. The transport direction is principally from volumes of high water pressure to volumes of lower pressure. The process leads to redistribution of solutes in the porewater and thus affects the porewater composition. There are several possible causes of pressure gradients in the tunnel backfill material, e.g. external water pressure, affinity for water in the bentonite and

temperature induced volume change of the water. Advective transport is closely related to water flow in the tunnel backfill, which is described in Section 4.2.2. In quantitative terms, advective transport of ions and colloids may differ from the actual flow of water due to ion equilibrium effects the filtering in nano-sized pores, respectively.

In principle, advective transport in the tunnel backfill material is governed by the same variables as in the buffer material (se Section 3.5.1). However, advective transport in the tunnel backfill material is expected to be more important than in the buffer since the backfill bentonite is of lower quality. Still, the transport of solutes in the backfill is expected to be dominated by diffusion (see Section 4.4.2).

Handling in the PSAR

Advective transport of species in the tunnel backfill is included in the integrated modelling of the chemical evolution of the near field (Section 3.5.6).

Radionuclide transport in the backfilled tunnels is modelled by assuming transport controlled by advection-dispersion with sorption. The sorption coefficient will be based on the assumption of equilibrium sorption on the backfill material. As an alternative, transport dominated by diffusion into the backfill material with subsequent sorption on backfill material can be assumed.

4.4.2 Diffusive transport of species

Overview

An overview of diffusion processes and phenomena as relevant for the buffer is given in Section 3.5.2; these considerations also apply to a backfill consisting of lower grade bentonite (Asha 2012).

While diffusion processes for Asha 2012 have not been studied in detail so far, the alternative buffer material (ABM) test (Svensson et al. 2011).

The diffusion data compiled for HTO, cations and anions in SKB (**Data report**) show similar behaviour of all species as a function of density for a wide range of clays. This includes data for some illitc materials. Similarly, Wersin et al. (2014a, b) used essentially the same approach for defining diffusion parameters for buffer and backfill material.

It can generally be assumed that the EDL-effects on enhanced cation diffusion and anion exclusion will decrease with decreasing content of expandable 2:1 minerals and decreasing compaction/density (increasing pore size). In sand-bentonite mixtures EDL-effects are expected to be negligible (except at sufficiently high bentonite/sand ratios). In the proposed backfill of low-grade bentonite, the content of smectite is about 50–60 %, (plus < 10 % smectite/illite mixed layer, see Section 2.4) and a dry density of about 1 500 kg/m^3 (clay fraction) is envisaged.

Handling in the PSAR

Most general issues relevant for handling diffusion in the backfill are discussed in the Sections 4.4.4 and 3.5.2. All radionuclide-specific data (effective diffusivities and porosities) are taken from SKB reports (Ochs and Talerico 2004) and the **Data report**. The backfill material has changed in the PSAR, but the data should still be reasonable for the Asha backfill as well. Sets of diffusion-available porosities and effective diffusion coefficients are selected for anions, cations (essentially Cs) and elements existing largely as neutral species (on average) under the relevant porewater conditions. To define selected parameter sets, a large amount of original experimental data, published in peer-reviewed journal articles and proceedings and in reviewed reports, was evaluated.

4.4.3 Sorption (including exchange of major ions)

Overview

An overview of sorption and ion exchange processes relevant for the buffer is given in Section 3.5.3. Since the composition of the backfill and buffer materials is similar in most respects, the process can be treated in the same fashion.

Handling in the the PSAR

Before saturation: Sorption of radionuclides is neglected before saturation since there is no continuous transport pathway (water) available. The geochemical evolution of the backfill during saturation is not considered in the PSAR.

After saturation: Ion exchange is included in the scenario-specific modelling of the chemical evolution for the thermal phase and the post-thermal long-term phase; see heading "Handling" in the description of process Alterations of accessory minerals, Section 3.5.6.

Failed canister: Sorption is included in the modelling of radionuclide transport for the long-term phase, see heading "Handling" for process 3.6.2. As for the buffer, sorption is treated through element-specific Kd values derived for specific conditions (see Ochs and Talerico (2004) and the **Data report** for the definition of data and associated uncertainties).

4.4.4 Alterations of backfill accessory minerals

Overview

The backfill material consists not only of montmorillonite, but also other accessory minerals as well as accessory minerals. In the repository environment, these can be dissolved and sometimes re-precipitated depending on the prevailing conditions.

Basically, the same chemical processes that occur in the buffer may also act in the backfill (Section 3.5.6).

The main differences are:

1. The temperature in the backfill is much lower and the thermal gradients are small. Dissolution/ precipitation of minerals due to temperature effects is of minor importance in the backfill.
2. The initial composition is different.
3. Both advective and diffusive transport of species may be active in the backfill.

Handling in the PSAR

Before saturation: Geochemical processes will be the same both before and after saturation phases. This is just a matter of water flow and solutes transport. No specific modelling of the geochemical evolution in the backfill for the saturation phase has been done.

Thermal period: The thermal effects on the chemical evolution of the backfill are not included in the PSAR, since the temperature elevation and the thermal gradients are small.

After saturation: The process is included in the scenario-specific modelling of the backfill chemical evolution for the post-thermal long-term phase together with the modelling for thebuffer as described in Section 3.5.6. The model considers advection, diffusion, ion-exchange and mineral dissolution/ precipitation in the backfill compartment. pH in the backfill is buffered by calcite precipitation-dissolution, which in turn is affected by calcium availability due to cation exchange processes. As exchange reactions reach equilibrium with incoming water more easily in the backfill than in the buffer (where the CEC is larger), the excess of calcium is used to precipitate calcite until equilibrium is obtained, decreasing the pH of porewater in the backfill.

Failed canister: In the case of a failed canister, vast amounts of metallic iron, originating from the corroding cast iron canister insert, will be added to the geochemical system. This was not included in the model mentioned above, and will most likely not have an effect on the backfill.

4.4.5 Aqueous speciation and reactions

Overview

This process is in general identical with the corresponding process in the buffer (Section 3.5.4)

Handling in the PSAR

Before saturation: Geochemical processes will be the same before and after saturation. This is just a matter of water flow and solutes transport, something to be considered in other sections.

After saturation: The process is included in the scenario-specific modelling of the backfill chemical evolution for the thermal phase and the post-thermal long-term phase. This is described in Section 4.4.4.

Failed canister: The backfill is assumed to be unaffected geochemically from the canister insert. However, the properties of the backfill are considered in the radionuclide transport calculations.

4.4.6 Gaseous speciation and reactions

Overview

This process is in general identical with the corresponding process in the buffer, see Gaseous speciation and reactions (3.5.5). Both the buffer and backfill unsaturated volumes need to be considered in the assessment of canister corrosion.

4.4.7 Osmosis

Overview

The general principle for this process is the same as for the corresponding buffer process (Section 3.5.7). The absolute effects of osmosis increases with increasing montmorillonite/water ratio, but swelling pressure increases more, and the relative pressure drop is consequently more pronounced at low montmorillonite/water ratios. The tunnel backfill material has to balance the swelling pressure from the buffer to limit the expansion of the buffer into the backfill.

Handling in the PSAR

The effects of the ionic strength of the groundwater on the hydraulic properties of the backfill are handled by direct application of empirical data mainly given in Karnland et al. (2006).

4.4.8 Montmorillonite transformation

Overview

The general principle for this process is the same as for the corresponding buffer process (Section 3.5.8). In principle all possible transformation processes are very temperature dependent. The temperature is significantly lower in the tunnel backfill compared to the buffer, and transformation processes in the backfill is consequently even less probable than in the buffer. One possible exception is pH dependant local alteration in volumes that are in direct contact with concrete, e.g. tunnel plugs or wall reinforcement.

Handling in the PSAR

The alteration of the swelling component in the backfill is treated in the same way as for the buffer (Section 3.5.8). The only difference is the maximum temperature and the amount of material. The process is included in a separate modelling task of between the tunnel plugs and the backfill (Grandia et al. 2010). Since the temperature is low under all conditions, montmorillonite alteration, in the form of illitization, can be neglected in the backfill. It is also assumed that the cement in the repository will be of the "low-pH" type and will have insignificant impact on the properties of the backfill.

4.4.9 Backfill colloid release

Overview

Water uptake by the tunnel backfill material and its resultant swelling is limited by the tunnel walls, and a swelling pressure is developed in the backfill material. Fractures intersecting the tunnel imply that no swelling restrictions are present, and that swelling continues until a thermodynamic equilibrium

is reached without the development of swelling pressure. This free swelling may lead to separation of individual montmorillonite layers, or small groups of mineral layers (dispersion). The same principles are valid for the backfill system as for the buffer (see Section 3.5.11) with the following exceptions:

1. Deposition holes will not be placed in rock volumes with larger fractures or severe groundwater flow. The option to fully avoid such zones may not be present in the placement of deposition tunnels. The tunnel backfill material may thereby be exposed to more adverse conditions than the buffer material both with respect to fracture apertures and flow rates.
2. The tunnel backfill material will have lower content of montmorillonite or other swelling minerals compared to the buffer material. Colloid release leads to replacement of lost montmorillonite by swelling of the remaining montmorillonite, which leads to a successive deterioration of the sealing properties. In principle, high quality bentonite materials will thereby stay relatively homogeneous and the sealing properties will decrease generally but slowly. In contrast, accessory minerals in low quality bentonite materials may serve as a filter and prevent replacement of lost material. This potential filter effect may reduce the loss of montmorillonite, but it may also lead to high local hydraulic conductivity in the depleted part of the backfill. The content and the grain size distribution of the accessory material will determine the extent of such a filter function.

Handling in the PSAR

The handling of the process is the same as for the corresponding process in the buffer (Section 3.5.11). The main difference is that the total mass of backfill is much larger than of the buffer.

4.4.10 Radiation-induced transformations

Overview

Montmorillonite in the backfill can be broken down by γ radiation. The result is a decrease in the montmorillonite concentration. The process can be neglected in the backfill based on the same reasoning as for the buffer (see Section 3.5.13).

Handling in the PSAR

The process is neglected since the dose rate in the tunnel backfill is too low to have any effects (see also Section 3.5.13).

4.4.11 Microbial processes

Overview

Micro-organisms interact with their surroundings, and they commonly have a significant effect on the geochemical record of their environment. From a microbiological perspective, the backfill will constitute an environment with mixed characters from two other well defined environments of the repository concept; the geosphere and the buffer. This backfill environment will, however, have some characteristics that significantly distinguish it from the two other mentioned environments. One is the possible presence of organic material in structural and stray material. Another is the gas/water interface that will develop during the saturation process. Finally, there will be oxygen in the backfill until it has been consumed and reduced by microbes and/or by inorganic oxygen scavengers such as sulphides.

The effects of microbial processes on the chemical stability of the geosphere are thoroughly discussed in the **Geosphere process report**. Similar effects can be obtained in the backfill, but the differences in the content in stray materials and the gas compared to the geosphere may increase the rates of microbial processes during an initial phase.

Microbial processes in the buffer are discussed in Section 3.5.15. Those processes are expected to be limited to an initial phase, after which temperature, radiation, desiccation and the swelling pressure are assumed to deactive the microbes in the buffer (Pedersen et al. 2000a). The radiation, desiccation and the swelling pressure limiting effects on microbial processes in the backfill will be less pronounced

or as good as absent but continued microbial activity may very well be possible. On the other hand, the consequences of microbial activity is rather positive than negative in this part of the repository because of the oxygen reducing and redox-lowering effects caused by most active microorganisms.

A key concern is however the microbial production of sulphide in the backfill. The backfill volume is large and it is therefore difficult to assign mass restrictions on the content of sulphate and organic carbon that are needed to produce sulphide. It is also difficult to ensure that the backfill density is sufficient to supress the process everywhere in the tunnel.

Handling in the PSAR

Mass balance calculations are performed to show how different kinds of residual materials remaining in the repository will contribute to microbial oxygen reduction. It can be assumed that all organic matter will be able to serve as nutrients for microbes. Furthermore, the availability of hydrogen will be decisive for microbial activity in the long term. This means that an increased effect of microbial activity must be expected until all organic matter has been consumed, and subsequently an activity that is controlled by the supply of hydrogen will proceed. This means that oxygen, ferric iron, sulphate and carbon dioxide will be reduced to water, ferrous iron, sulphide and methane, respectively. The scope of these reactions is dependent on mass flows.

In the PSAR it is assumed that microbial sulphide production can persist in the tunnel backfill. The effect on canister corrosion is calculated based on limitation on solubility of sulphide minerals and diffusive transport in the buffer.

4.5 Radionuclide transport processes

4.5.1 Speciation of radionuclides

Overview

See the corresponding buffer process; Section 3.6.1.

Handling in the PSAR

The handling of the process is the same as for the corresponding process in the buffer (see Section 3.6.1). Data and boundary conditions for the backfill will be used.

4.5.2 Transport of radionuclides in the water phase

Overview

See the corresponding buffer process; Section 3.6.2.

Handling in the PSAR

The handling of the process is the same as for the corresponding process in the buffer (see Section 3.6.2). Data and boundary conditions for the backfill will be used.

5 Processes in the tunnel plugs

5.1 Thermal processes

5.1.1 Heat transport

Overview

Tunnel plugs are typically located some 6 m from the outermost canister in each tunnel. The plug volumes are sufficiently small that the temperatures are controlled by the temperature of the surrounding rock, meaning that the plug temperatures can be calculated without account of the heat transport properties of the plug material. Therefore, the process is without significance to the thermal evolution in the plug region.

Handling in the PSAR

Because of the small thermal gradients and the relatively low temperatures in the tunnel plugs there is no specific handling of the heat transport process.

5.1.2 Freezing

Overview

Freezing of the tunnel plugs is of no significance. When freezing due to permafrost growth starts, the repository is closed and saturated and the tunnel plugs have no performance requirement at this stage.

Handling in the PSAR

Process is neglected since there are no long-term performance requirements on the plugs.

5.2 Hydraulic processes

5.2.1 Water uptake and transport under unsaturated conditions

Overview

The function of the bentonite seal is to prevent water from flowing out through the plug, and correspondingly to prevent gas from flowing in. The sealing function of the concrete dome will be less important once the bentonite seal has reached water saturated conditions. The main function of the filter section was originally to drain inflowing water from the backfilled deposition tunnel and to prevent this flow from interfering with the building of the concrete plug. The current design of the tunnel plugs, with a filter section adjacent to the bentonite seal, and the requirement that the plug will be gas tight means that the filter will be water filled at the onset of the operation of the plug. This in turn means that the water saturation of the bentonite seal will be quite well controlled.

The processes involved regarding “water uptake and transport under unsaturated conditions” in the bentonite seal is essentially the same as those in the buffer, which are described in detail in the buffer Section 3.3.1.

Handling in the PSAR

The water saturation of the bentonite seal in the plug has been modelled (Task 12 in Åkesson et al. 2010a). In these models the seal, with a thickness of 0.7 m and located between the concrete plug and the filter, was made of bentonite blocks and pellets in a similar configuration to the backfill. Under the condition that there is good availability of water at the plug, either natural or artificial, then the saturation process is a fairly simple one-dimensional hydration problem. If the pellet filling of the seal were to seal quickly, then the hydration would only occur from one side, and this process would take around twenty years. If, on the other hand, there were a sustained piping through the pellet filling, then the hydration would be two-sided, resulting in a saturation time of around five years.

A full-scale test of the Dome Plug was carried out at the Äspö HRL during 2013 to 2018. The design of this essentially follows the current reference design with a 0.5 think bentonite seal, and did also include a 1 m long backfilled section. The filter section was artificially pressurized with ~4 MPa during ~3 years, and during the dismantling operation it was found that the seal had been completely water saturated at that time (Grahm et al. 2015, Åkesson et al. 2019).

The water uptake in this test and its mechanical evolution were also predicted through numerical modelling prior to the dismantling. The time-scale of hydration was however overestimated by the presented models, approximately with the order of a factor 2–3. The reason for this discrepancy was probably that the hydration problem was complicated in at least three ways in comparison to a simple water-uptake problem: i) the homogenization problem, caused by the pellets-filled slot along the circumference of the block-stack and the deformable filter, which means that the dry density of the seal decreased significantly with time; ii) the high filter pressure, which means that the hydration didn't only follow the diffusion-like suction-driven water uptake, but also as an external pore-pressure-driven saturation front; and iii) the potential circumventing of the hydration problem by supplying water to the seal on the "backside" along the concrete beams.

To define the required plug performance, the maximum allowed cumulative leakage through the plug is considered to be a certain fraction of the available pore volume of the pellet-filled slots in the entire tunnel. A value of 10 % is used as an example in the PSAR. This requirement is however in process of being reformulated. Moreover, although the seal constitutes the main resistance, it will require access to water and time to develop a high flow resistance. During this period the sealing ability will rely on the plug itself (or actually the low transmissivity between the concrete and the rock). These circumstances thus imply a relation between: i) the maximum allowed leakage, ii) the flow resistance of the plug and, iii) the time needed for the seal to become functional.

The analysis of needed sealing abilities for the plug and the bentonite (Åkesson et al. 2010a) shows that an aperture smaller than ~5 μm in the contact zone between the concrete plug and the rock surface is required in order to obtain a sufficiently high flow resistance in the concrete plug/rock interface itself if the entire water pressure gradient is taken by the concrete plug without considering the sealing ability of the clay seal. A larger aperture can nevertheless be acceptable if the hydraulic conductivity of the pellet-filled slot in the clay seal is considered. If this conductivity is lower than approx. 10^{-10} m/s, then there is no need to rely on the plug/rock interface. It is noted that this value is much higher than the hydraulic conductivity at the expected density of the homogenised seal.

5.2.2 Water transport under saturated conditions

Overview

As described in Section 5.2.1, the plug is required to seal for a short period only. The hydro-mechanical evolution of the plug is described in that section. After full water saturation and when the hydrostatic water pressure is reached, the plug has no sealing function and very little water will flow past the plug due to the low hydraulic gradient. The plug will thus be an integrated part of the backfill and will have one very tight section with the bentonite seal and a highly permeable section (the filter) as well as a concrete plug. However, the permeable section are only local and will not influence the overall hydraulic behaviour of the tunnel backfill.

Handling in the PSAR

Due to that there is no demand of the plug after saturation this process will not be handled in the PSAR in any other way than a discussion around a local part of the tunnel with higher hydraulic conductivity.

5.2.3 Gas transport and dissolution

Overview

Gas processes in the plugs are only relevant for the saturation period. For the bentonite part of the plug – this is described in Section 5.2.1 and 3.3.1.

Leakage of air from the main tunnel through the plug to the disposal tunnel could occur if there is a lack of gas tightness in the plug. Gas tightness is defined as the ability of the plug to restrict leakage of a gas phase. It does not involve transport of gases dissolved in water. The plug should be able to restrict gas transport until the main tunnel is water filled. This is important not only to restrict transport of oxygen in to the tunnel, but also to restrict leakage of water vapour out from the disposal tunnel. This is especially important in "dry" deposition tunnels that can be expected to remain unsaturated during the operational period of the repository. This requirement is fulfilled by the current design of the plug. The filter in the tunnel plug will be water filled at the onset of the operation of the plug. The bentonite seal component will thereby be artificially saturated, which means that the plug will be an efficient seal for water vapour. Transport of oxygen will only be possible through diffusion of dissolved gas through the bentonite seal. This will be very limited due to low solubility of oxygen, geometrical restrictions and the relatively short duration of the operation phase.

Transport of hydrogen gas generated from corrosion of steel components in the repository is not an issue for the tunnel plugs.

Handling in the PSAR

The saturation process is treated as a part of the THM description of the plug, see Section 5.2.1.

The tunnel plugs are assumed to the gas tight in the PSAR. However, the consequences of a leaking plug are assessed as a separate case. The assessment such case is presented in SKB (2014).

A gas tightness test was performed within the framework of the Domplu field experiment (Åkesson 2018). This was implemented by draining the water from the filter, by pressurizing the filter with helium gas to 0.4 bar gauge, and by monitoring the gas pressure evolution. A minor gas pressure increased was observed which indicated that a noticeable inflow of water occurred during this measurement. The monitoring was complemented with a sniffer leak search along the entire front surface of the concrete plug. No detectable concentrations were however found. The test therefore verified that the seal was gas tight.

5.2.4 Piping/erosion

Overview

The process of erosion is described in the buffer chapter, Section 3.3.4. Since erosion is mainly a concern for the bentonite seal in the plug, the same description is valid here.

After full saturation and reestablishment of hydrostatic water pressure, the plug is not required to have any sealing function. Any consequences of erosion of the plug itself are thus not important. The plug and bentonite seal are instead required to stop eroding water from the tunnel to pass the plug during the saturation phase. The bentonite seal is expected to prevent leakage. If there are open fractures between the concrete and the rock, and water flows through these fractures due to malfunction of the bentonite seal when the plug is expected to seal, the function of the plug is not fulfilled. Self-sealing of cracks in the plug or the rock will not occur. This is a pessimistic assumption based on that no real proof of sealing of cracks has been obtained (Börgesson et al. 2015).

Handling in the PSAR

Erosion of the bentonite seal is thus not a concern but will rather decrease flow past the plug. The process for the plug will not be separately handled in the PSAR. Possible erosion from the bentonite seal does not influence the overall performance since the seal has no intended function once the operation of the downstream tunnels and rooms are completed and the hydraulic gradients have been restored.

5.3 Mechanical processes

5.3.1 Swelling/mass redistribution

Overview

The plug is a complex composite of different materials. A general description of the plug, its required performance and the hydro-mechanical evolution are given in Section 2.5.1. The backfill will during saturation increase its swelling pressure and compress the drainage material. The bentonite seal will also increase its swelling pressure during saturation and compress the drainage material. The bentonite seal will increase its swelling pressure during saturation and stress the plug. In addition, there will be a hydraulic pressure on the concrete plug. The concrete plug is designed to withstand this pressure so it will only move slightly and improve the contact with the rock in the slot. If the backfill outside the plug consists of crushed rock, which will be the case for the plug facing the central area, there is no pressure on the plug from that side until a water pressure is built up. However, this interaction has two implications that must be considered:

1. If the water pressure outside the plug comes before swelling, (i.e. the central area is water filled before the backfill in the tunnel) and water pressure is developed inside the concrete plug there may be consequences for the plug since it is not designed to take such pressure. This implies that the concrete plug may break and that water may flow backwards through the plug. However, there are probably no negative consequences of this case, but this may need to be investigated.
2. After long time the concrete plug may be degraded and the bentonite from the bentonite seal and the backfill inside the plug may expand and penetrate into the possible open spaces in the plug and further on into the slot between the roof and the crushed rock in the backfill of the central area. In stagnant water, this is not expected to yield problems and can be estimated but if there is water movements in the slot there may be substantial erosion.

The mechanical processes relevant to the bentonite seal are the same as those reported for the buffer; see Section 3.4.1.

Handling in the PSAR

The water saturation evolution and the evolution of the stresses and displacements of the bentonite seal are modelled and reported in Åkesson et al. (2010a, Task 16) as well as the swelling of the backfill and the bentonite seal following the disintegration of the plug (Task 17 and 22).

The bentonite seal of the Domplu experiment tests was designed with the premise that the swelling pressure on the concrete plug should not exceed 2 MPa (Grahm et al. 2015, Åkesson et al. 2019). This is also a requirement in the current reference design. For MX-80 bentonite, such a swelling pressure level can be reached at a dry density level of approximately 1 400 kg/m^3. Bentonite blocks with a relatively low dry density were therefore specially manufactured. The average installed dry density of the bentonite seal in Domplu was 1 560 kg/m^3, and in order to reduce the swelling pressure, a pellets-filled slot behind the filter section was installed and dimensioned to a thickness of 150 mm. In addition, the gravel filling in the filter section was assessed to exhibit a specific compressibility. By taking these compressible components into account, a theoretical final swelling pressure on the Domplu concrete plug was calculated to 2.48 MPa (Grahm et al. 2015), which corresponds to a dry density of ~1 450 kg/m^3. The weighed mean value of the dry density measurements in the seal during the dismantling was found to be 1 342 kg/m^3. This means that design premise of limiting the swelling pressure on the concrete plug to 2 MPa could be fulfilled. The main reason for the difference between the expected and the implemented dry density levels appeared to be that the gravel filling was more compressible than first anticipated.

5.4 Chemical processes

5.4.1 Advective transport of species

Overview

In this context advection refers to transport of any forms of additional matter, e.g. ions, molecules or colloids, with porewater flow. The transport direction is thereby principally from volumes of high water pressure to volumes of lower pressure. The advection is closely related to water flow in the tunnel plug, which is described in Section 5.2.2.

The maximum pressure gradients over the tunnel plug will occur during the installation period when one side of the plug will be pressurised by the hydrostatic pressure and the other side is kept drained. After closure, different inflow rates and volumes in the compartments may lead to a significant gradient. After full water saturation of the compartments, the pressure gradient will be induced by the regional pressure gradients, and comparatively much smaller. Additional causes of small pressure gradients may also be present by e.g. differences in salinity and temperature on the two sides of the plug.

Handling in the PSAR

Since there are no requirements on stability of the plug after saturation of the repository, this process will not be handled in the PSAR in any other respect than as a discussion of the implications of a local part of the tunnel with higher hydraulic conductivity.

5.4.2 Diffusive transport of species

An overview of diffusion processes and phenomena relevant for bentonite is given in Sections 3.5.2. These considerations also apply to the bentonite parts of the tunnel plug.

The heterogeneous pore and crack structure of concrete results in the co-existence of different diffusional pathways through the concrete part of the plug. The greatest effective diffusivity is expected in any cracks or cracks and, in their absence, the larger pores. The granite or silica aggregates in the concrete offers a negligible diffusion pathway, and this is a very significant component of the plug. The diffusion of ionic species is affected by ion–ion electrostatic interactions (e.g. Galíndez and Molinero 2010) and the condition of electroneutrality in the system. Surface–ion interactions can also affect diffusion through porous matrices such as bentonite clay (e.g. Ochs et al. 2001, SKB 2010a) and cement/concrete (e.g. Zhang and Buenfield 1997, Chatterji 2004). Surface–ion effects occur in small pores with negatively charged surfaces, as found in highly alkaline concrete. Anion exclusion occurs when the pore size is so small that the cation-rich electric double layers (EDL) generated by the negatively charged pore surfaces overlap and create a barrier to anionic species. The converse of anion exclusion is enhanced cation diffusion, resulting from the relatively high dissolved cation concentrations generated in the EDL.

The extent of diffusive transport of ionic species is also affected by electro-osmotic effects that may arise from natural telluric currents or induced currents from electrical conductors.

Handling in the PSAR

Diffusion is included in the calculations of alteration of concrete see Section 5.4.4.

The plug is not included in the radionuclide transport calculations. Sorption (including exchange of major ions)

5.4.3 Sorption (including exchange of major ions)

Overview

Sorption processes for the bentonite seal, the processes are the same as those for the buffer described in Section 3.5.5.

In the concrete part of the plug, radionuclides and major ions may undergo a range of interactions with the matrix (hardened cement paste). In comparison, interaction with the aggregate material can often be neglected. Exceptions to this may be sorption of simple cations, especially Cs, to layer silicate minerals contained in the aggregate material derived from crystalline rock.

The interaction of radionuclides and major ions with the cement matrix is probably best described with the term “uptake”. Because the cement matrix consists of several types of mineral phases with different properties, a range of solid-liquid interactions may take place. At the same time, the relative proportion of mineral phases, as well as their properties, is known to change as a function of cement matrix degradation. This process will to some degree depend on cement and groundwater composition, but is in general terms fairly well understood and the cement matrix composition can be modelled fairly well as a function of porewater exchange cycles.

In case of the more crystalline aluminate phases (ettringite/monosulphate, hydrogarnet), solid-liquid interactions may involve ion exchange and surface complexation reactions as well as the formation of classical solid solutions. However, the most relevant solid phases in hydrated cement systems are calcium-silica-hydrates (CSH), which are amorphous, very reactive, and possess a high specific surface area. Interaction of major ions, and in particular of actinides/lanthanides and transition elements, with these mineral phases typically results in some type of incorporation, often in an ill-defined and non-stoichiometric fashion. The latter case may be non- or only partly reversible.

As a result of this complexity, the nature of the uptake process has not yet been established for most radioelements. This is corroborated by the amorphous and reactive nature of cement mineral phases. Further, nearly all cements contain a relatively high inventory of stable isotopes of many potentially relevant radionuclides, which means that isotopic exchange rather than chemical interactions have to be considered in some cases.

On the other hand, a number of systematic uptake studies have become available during the last decade, which allows defining K_d for many relevant elements as a function of conditions within reasonable uncertainty ranges.

No adverse effects on sorption by concrete admixtures are expected. Available cement degradation models further allow tying sorption data developed for one particular cement degradation state to other relevant stages.

Interaction of the solid cement matrix with groundwater influences the overall system composition (and hence sorption of trace elements), but the nature of the respective processes are closer to dissolution/precipitation phenomena than to ion exchange in the classical sense.

Concrete-bentonite interaction occurring at the interface of the two parts of the tunnel plugs may lead to changes in the mineralogy of the respective materials, which will also influence sorption.

Handling in the PSAR

Sorption of radionuclides in tunnel plugs is neglected in the PSAR.

5.4.4 Alteration of concrete

Overview

The plug is expected to maintain its functionality until the repository is closed and the hydrogeological conditions are restored (Malm 2012, Magnusson and Mathern 2015, Posiva SKB 2017). However, alteration of concrete can introduce chemical changes in the porewater affecting the performance of the surrounding backfill, even long after repository closure.

Concrete degradation based on typical Portland cement (OPC) is mainly characterised by a sequential step leaching process, which was already described by Atkinson (1985). The consecutive degradation steps are: 1) an alkaline leachate with a pH > 13 and high concentrations of Na^+ and K^+; 2) the dissolution of portlandite [$Ca(OH)_2(s)$] buffering the pH at a value of approximately 12.5; and 3) decalcification of the calcium silicate hydrates (CSH) continuously decreasing their Ca/Si ratio and with pH < 11. The last step occurs until the full degradation of concrete.

There are other processes that can speed up concrete degradation, among the most relevant being carbonation, sulphate attack and dissolution of minor constituents of concrete. In the case of carbonation, the calcium leaching in combination with carbonate contents from porewater from surrounding materials can lead to the precipitation of calcite at the interface of concrete with surrounding materials. The relevance of this process depends on the concentration of carbonate in the porewater of surrounding materials, being a beneficial process (it can reduce available porosity at the interface). The same is also true for the dissolution of minor constituents from concrete, as an example, dissolution of magnesium bearing phases can result in the precipitation of secondary minerals at the interface, such as brucite or other magnesium silicate hydrates (MSH), also reducing the porosity. A different case is related with sulphate attack; as sulphate from the porewater of surrounding materials can enter the concrete domain and lead to the precipitation of ettringite [$Ca_6Al_2(SO_4)_{12} \cdot 26H_2O$]. Due to the crystal structure of ettringite in can produce mechanical cracks facilitating water circulation and accelerating concrete degradation.

The extent of concrete degradation is a function of the hydraulic properties of the concrete and the surrounding materials and their evolution with time. Therefore, the low permeability of concrete and backfill limits the extent of the degradation process. However, high pH values, as those expected during the first two steps of degradation of OPC-based concrete can affect the chemical stability of backfill material (i.e. increasing the dissolution rate of clay minerals as shown by Bildstein and Claret (2015). For this reason, low-pH cement has been recommended for the use in the concrete plug (Vogt et al. 2009). The mix is characterized by adding a hydraulic binder as silica fume. This addition results in decreasing the Ca/Si ratio, favouring the formation of calcium silicate hydrates (CSH) instead of portlandite. Consequently, the second step of degradation with pH ~ 12.5 related to portlandite dissolution, does not occur and leachates from concrete degradation have lower pH values, decreasing the negative impact on the backfill materials.

In the last 5 years the project granted by European Commission CEBAMA addressed some of the key questions regarding the long-term safety and the use of cement-based materials in nuclear waste disposal applications (Duro et al. 2020). Two of the objectives of the project were: 1) the study of the cement alteration processes and how they may impact the physical properties of the materials, and 2) perform a benchmark of numerical models used to quantify the evolution of cementitious materials under experimental and repository conditions.

Several laboratory experiments of the interaction of low-pH concrete and water interaction where conducted in the frame of the CEBAMA project (Vehmas et al. 2020). The results from these experiments show that most changes occur at the interface (<0.4 mm after 180 days of experimental time) resulting in the decalcification of CSH phases, decreasing the Ca/Si ratio and with pH values below that of equilibrium with portlandite. Other changes depend on composition of contacting water. Thus, waters containing substantial magnesium result in precipitation of brucite or magnesium silicate hydrates (MSH). Precipitation of ettringite was also observed in some cases. Calcite and gypsum were detected in some samples but limited to the interface space. All these processes result in changes in porosity, being the net change depending on water composition. The results were in agreement with a long-term experiment conducted by Mäder et al. (2017) with both low-pH and OPC concrete in Mont Terri underground laboratory.

Idiart el al. (2020) conducted a model benchmark of the concrete – clay interface with the aim of test the different modelling approaches, the relevance of long-term low-pH concrete degradation processes, the durability of the hydraulic and mechanical properties of concrete and the effects on the clay-based materials. The results show that, after 100 000 years of simulation, alteration is restricted to few centimetres in the concrete side from the interface and porosity changes are very small, indicating that degradation is a slow process. Changes in the alteration zone are in agreement with the experimental results (Vehmas et al. 2020) and porewater changes are only predicted near the interface in the clay side with pH<11, maintaining any potential effect on the clay very close to the interface.

Dependencies between process and tunnel plug variables

Table 5-1 shows how the process influences and is influenced by all tunnel plug variables.

Plug geometry: The geometry of the plug affects the process by considering the total mass of concrete and the reactive phases it contains. Therefore, the total pool of these mineral phases will affect the geochemical evolution of the system.

Pore geometry: The solid-to-liquid ratio will affect the degradation of concrete, at higher ratios the degradation will be slower, as a minor mass of minerals dissolved is needed to attain saturation. On the other hand, the dissolution – precipitation of cement mineral phases can modify the pore geometry and the total porosity of the system, and thus, modifying the degradation rate of concrete.

Temperature: Thermodynamic constants of chemical reactions are highly dependent of the temperature. However, temperatures in concrete plug are not expected to vary significantly, and therefore, minimal effects on the geochemical processes are foreseen.

Water content: This variable will affect the dissolution of cement phases as reactions can only take place in wetted surfaces. However, the process only considers full water saturation, as minimal changes are expected to occur until that time.

Table 5-1. Direct dependencies between the process "Alteration of concrete" and the defined tunnel plug variables and a short note on the handling in the PSAR.

Variable	Variable influence on process		Process influence on variable	
	Influence present? (Yes/No) Description	Handling of influence (How/Why not)	Influence present? (Yes/No) Description	Handling of influence (How/Why not)
Plug geometry	Yes	Plug mass considered	The degradation will reduce the mass	Plug mass considered
Pore geometry	Yes	The solid-to-liquid ratio is considered.	Yes. Dissolution – precipitation of solid phases can modify the porosity of the system.	Porosity changes due to dissolution – precipitation reactions is considered.
Temperature	Yes, temperature effect on thermodynamic constants.	Constant temperature assumed	No	
Water content	Yes, Could affect concentrations	Saturated conditions assumed	No	
Gas content	No		No	
Hydrovariables (pressure and flows)	Yes. Effect on reaction rates and transport of chemical components	Included in mass balance	No	
Stress state	No		No	
Plug materials – composition and content	Yes, reactivity with minerals. Cement mineralogy	Included in modelling	Yes, modification of mineral composition. Concrete degradation	Included in modelling
Porewater composition	Yes, Affecting reactivity of system components	Included in modelling	Yes, reaction with minerals results in changes in porewater composition	Included in modelling

Gas content: Gases can form or dissolve through chemical reactions, although their partial pressures are considered in the models, it is not expected that gases can form in the concrete plug.

Hydrovariables (pressure and flows): Transport of water and solutes is a very important variable on the degradation rate of concrete. The faster the solutes are transported away from the system, the faster the dissolution rates occurs, as the saturation state of those minerals being dissolved are maintained

at low values. For the same reason, the precipitation of secondary phases will be inhibited, as the concentrations in porewater won't increase enough to reach saturation. However, if transport of solutes occurs at a slow rate, then dissolution of cement phases will occur at a slower rate, but precipitation of secondary phases is more likely to occur.

Stress state: This variable has no effect on the alteration of concrete process.

Plug materials – composition and content: This is one of the most relevant variables influencing this process. The type and amount of minerals is essential to determine how their dissolution – precipitation behaviour will affect the chemical evolution of the system, modifying both the porewater composition and the minerals present in the system (i.e. newly precipitated minerals and amount of existing minerals).

Porewater composition: The porewater composition will determine which of the minerals in the system will dissolve or precipitate, and thus the dissolution – precipitation of these minerals will modify the chemical composition of porewater.

Boundary conditions

There are no particular boundary conditions to discuss for these processes. The relevant boundary conditions in order to treat the process quantitatively are those of the transport processes that control the solutes transport between the concrete plug, the backfill and the groundwater as adjacent system components, i.e. the boundary conditions of the processes diffusion and advection.

Time perspective

Since cement leaching is mainly a coupled diffusion-reaction phenomenon, the time needed for complete degradation of concrete plugs will be highly dependent on the relative surface area of the concrete where diffusion exchange with backfill porewater can take place. This parameter will be related to the thickness of the plug. However, the porosity and permeability increase due to concrete degradation is not always taken into account which could lead to an overestimate of the calculated degradation times. Modelling results indicate that even after 100 000 years low-pH concrete degradation is minimal and restricted to a zone of few centimetres close to the interface with surrounding materials.

Handling in the PSAR

The concrete plug durability is important as its degradation can result in an increased pH in the near field in the repository. The rate of degradation will impact the geochemical conditions in the contact area with the backfill and potentially also further away from the plug. Therefore, the cement plug durability has to be evaluated by long term reactive transport modelling, accounting for the coupling between dissolution/precipitation of minerals and porosity/diffusivity/hydraulic conductivity changes.

Specific tunnel plug models have to evaluate quantitatively the long term durability of cementitious components of the repository, including the time evolution of the main physical and chemical properties, the time evolution of the hydrochemical conditions close to the cementitious components as a result of the alkaline perturbation produced by cement leaching, and the hydrogeochemical effects produced by the alkaline perturbation on the adjacent barriers.

Handling boundary conditions: The degradation of cementitious components will be highly dependent on the external boundary conditions. On one hand, the rate of external groundwater renewal and the chemistry composition of the external groundwater have a strong influence on the out diffusion of ions from concrete plug: a renewal of the external groundwater by advection would accelerate the degradation of cement. On the other hand, the chemistry of the external groundwater will also influence the processes. For example, high carbonate concentrations in the external groundwater would probably produce calcite precipitation and/or the precipitation of other secondary minerals, which may reduce the porosity and therefore the cement degradation rate.

Handling influences between variables and process: Cement degradation phenomena have a strong coupling between physical and chemical processes. Then, solute transport and geochemical reactions should be coupled in the models to account for relevant processes such as dissolution/precipitation of CSH and porosity changes due to mineral dissolution and precipitation. At the same time, changes in porosity are coupled with solute diffusion and water flow, so numerical models should account for these fundamental relations.

Handling coupling to other processes: Concrete degradation will produce an alkaline perturbation and a leachate plume that could reach the buffer, backfill and geosphere. The performance requirement for the buffer is currently a pH < 11. The purpose of the handling of this process is to demonstrate that this requirement is met. The interaction of the hyperalkaline plume with the external groundwater could trigger mineral dissolution/precipitation processes that could influence the groundwater flow and solute transport properties of the buffer, backfill and geosphere. Coupled reactive transport models should account for these couplings in order to evaluate the magnitude these effects.

Uncertainties

Uncertainties in mechanistic understanding

A main uncertainty is related to the complex solubility behaviour of CSH phases, which has been oversimplified in previous models of cement degradation. Other uncertainties are associated with the long-term evolution of the pore network and the diffusivity in the concrete. The diffusivity depends strongly on the porosity values, and the coupling between the dissolution processes and the resulting microstructural changes are not fully coupled.

Model simplification uncertainty in PSAR

The calculations to evaluate the degradation of the concrete plug can be made using a simplified 2D geometry, where the plug is sandwiched between two sections of bentonite backfill. Furthermore, the solid phases considered is a simplification of the CSH phases that really precipitate. The implications of this are discussed in the modelling report (Grandia et al. 2010).

Input data and data uncertainty in PSAR

The main uncertainties concern the composition of the concrete plug and the thermodynamic stability of calcium-silicate-hydrates. The implications of this are discussed in the modelling report (Grandia et al. 2010).

5.4.5 Aqueous speciation and reactions

Overview

This process is in general identical with the corresponding process in the buffer (Section 3.5.4).

Handling in the PSAR

The process is included in a separate modelling task of the plug (concrete part) degradation. This is further described in Section 5.4.4.

5.4.6 Osmosis

Overview

Flow of a solvent into a solution through a semipermeable membrane is termed osmosis if the driving force is differences in concentration. The concrete may serve as a semipermeable membrane and osmotic flow may take place in the system component. The alkali-binding capacity in the interlayer of the C-S-H phases will be limited and Chlorine will only become ad-sorbed in comparison to the innerlayer structure of smectites where it can become absorbed.

Handling in the PSAR

The magnitude and especially the lack of significant osmotic flow in the tunnel plug make this process less important and will not be considered in the PSAR.

5.4.7 Montmorillonite transformation

Overview

This process is in general identical with the corresponding process in the buffer (3.5.8) for the bentonite part of the plug.

Handling in the PSAR

The process is neglected since no long term performance is expected from the bentonite part in the tunnel plug component.

5.4.8 Montmorillonite colloid release

Overview

This process is in general identical with the corresponding process in the buffer (3.5.11) for the bentonite part of the plug.

Handling in the PSAR

The process is neglected since no long term performance is expected from the bentonite part in the tunnel plug component.

5.4.9 Microbial processes

Overview

Microorganisms interact with their surroundings, and they commonly have a significant effect on the geochemical record of their environment (Madigan et al. 2008). See also Section 3.5.15.

Plasticisers that will be added to the concrete will contain organic polymers of varying compositions, e.g. polycarboxylate polymers. The amounts to be used will be significant. The amount of plasticisers will be 6–7 kg /m^3 concrete. Plasticisers introduce a significant uncertainty, because their composition and solubility, and thereby their availability to microbes, are not well known. In cases where a grouting activity fails and the grout do not solidify properly; large amount of organic carbon may be available for microbial growth in particular on grouted surfaces as concrete additives are designed to sorb strongly onto the cement grains. The availability of organics from grout and in the central area, ramp and shaft on places where groundwater from grouted sites seep through the tunnel walls is thus expected to be very limited

There are two main influences from the structural material variable on microbial processes.

Microbial sulphate reduction during microbial growth on plasticisers will result in sulphide. The sulphide may accumulate as iron sulphide inside the plugs. During the open phase, oxygen will oxidise the sulphide and sulphuric acid can form. Local acid attacks on the concrete may occur. This effect will diminish after backfilling on both sides of the plug, when oxygen is consumed, but it may introduce an issue during the open phase.

Excess amounts of organic material in aquifers will trigger growth of opportunistic microorganisms that will increase in numbers. Several groundwater microorganisms produce complexing agents that very efficiently mobilise trace elements, including many radionuclides (Kalinowski et al. 2004, 2006, Johnsson et al. 2006, Essén et al. 2007, Moll et al. 2008).

Handling in the PSAR

Mass balance calculations are made to show how different kinds of residual materials remaining in the repository will contribute to microbial oxygen reduction. It can be assumed that all organic matter will be able to serve as nutrients for microbes.

5.5 Radionuclide transport processes

5.5.1 Speciation of radionuclides

Overview

See corresponding process description for the buffer, Section 3.6.1.

Handling in the PSAR

This process is indirectly handled through the selection of parameters for radionuclide transport in the backfill. In general, the handling of the process is the same as for the corresponding process in the buffer (see Section 3.6.1.).

5.5.2 Transport of radionuclides in the water phase

Overview

The plug covers a limited volume with tunnel backfill on each side (except the plugs facing the central area). The hydraulic conductivity of a degraded plug may be high and transport of dissolved species may be rapid, but since the geometry is restricted, the plug will not affect the overall transport pattern in the repository.

Handling in the PSAR

The plug is considered to be a part of the tunnel backfill in the radionuclide transport calculations. No specific considerations are done for the plug.

5.5.3 Transport of radionuclides in a gas phase

Overview

For gas transport to occur through concrete, the capillary pressure in the concrete pore system must be exceeded. It can be assumed that even though the concrete has degraded the capillaries will be much smaller than the fractures in the bedrock through which gas can also be transported and thus the concrete will not act as a sink or a transport path for gases.

Handling in the PSAR

The delay of a gaseous release of radionuclides is neglected in the PSAR. The overall process is treated according to Section 3.6.3.

6 Processes in the central area

6.1 Thermal processes

6.1.1 Heat transport

Overview

The thermal conductivity of the repository host rock is in the range 2.0–4.0 W/(m · K) (Back et al. 2007, Sundberg et al. 2008). The thermal conductivity of the crushed rock filling out shafts and ramps in the central area is significantly lower, although there are no parameter values available. In addition, the volume fraction of the central area or, more generally, of the rock between the deposition areas that is occupied by backfilled excavations is very small. These facts together mean that the thermal conditions in backfilled shafts and ramps are controlled and dominated by the temperature evolution of the surrounding rock, and that details in the description of the heat transport within the crushed rock backfill are unimportant.

Handling in the PSAR

There is no specific handling of heat transport in the central area during the thermal phase since the temperature in the central area is not directly related to any type of performance. Results from thermal analyses of the repository rock mass give sufficient information on the temperature in central area.

6.1.2 Freezing

Overview

During periods of cold climate it cannot be excluded that the temperature in the central area will drop to values below 0 °C (**Climate report**). This means that the water in the crushed rock backfill may freeze. This will affect the hydraulic and mechanical properties of the material.

Handling in the PSAR

Due to the small amount of ice lens formation and the limited impact on the hydraulic conductivity on the material in central area, the process can be neglected.

6.2 Hydraulic processes

6.2.1 Water uptake and transport under unsaturated conditions

Overview

Water transport in the crushed rock filled in the central area before saturation is mainly governed by the inflow rate and inflow distribution in the rock. Since the expected hydraulic conductivity of the crushed rock is high, and since there will be an open slot at the roof, the resistance to water inflow into the filling material will be very low. The only relevant processes for the crushed rock are the following:

- Transport of water in liquid phase, which is controlled and driven by
  - a liquid pressure gradient,
  - gravity.
- Compression of air.
- Transport in water of dissolved air.

Handling in the PSAR

For the main tunnels, the transport tunnels and the lower parts of the ramp and the shaft, there is a requirement that the hydraulic conductivity shall not exceed the value of 10^{-8} m/s. For the central area there is no corresponding requirement regarding the **Closure production report**.

The inflow and successive water filling into these parts was modelled as a part of the THM modelling of the buffer, backfill and other system components (Åkesson et al. 2010a). If the inflow rates to the central area would be estimated, e.g. with a large scale DFN model similar to the models adopted for the deposition tunnels (Joyce et al. 2013), then it would be quite simple to calculate the time needed to reach water saturated conditions.

6.2.2 Water transport under saturated conditions

Overview

Water transport under saturated conditions is mainly driven by a water pressure gradient. The process can be described by Darcy's law. The general description of the water transport processes given in the previous section for unsaturated crushed rock is also valid under saturated conditions. In addition, the temperature gradient and salt content gradient may, after full pore pressure equilibrium is established, be an important factor for driving water flow due to the low natural pressure gradient.

Handling in the PSAR

The central area is an isolated part of the repository. However, the hydraulic conductivity can be high and there may be a need to include this feature in the hydrogeological model, at least as a sensitivity study.

6.2.3 Gas transport and dissolution

Overview

Transport of gas in the central area can occur in two phases of the repository evolution:

Water saturation phase

The backfill consisting of crushed rock will be emplaced dry, which means that there is a substantial amount of air that needs to be dissolved and transported away. Also the rock may contain dissolved gas. This was discussed in Section 6.2.1

Gas transport from a defective canister after saturation

Hydrogen gas from the corrosion of the cast iron insert could potentially escape from the repository by transport through the central area, ramp and shaft. The crushed rock backfill could act as a passageway for gas under certain conditions. However, it is not evident that gas from the canister will ever reach these areas.

Handling in the PSAR

The process involving trapped air is only relevant during the saturation phase (see Section 6.2.1).

The escape of corrosion gas from the canister through the crushed backfill is not considered in the PSAR.

6.2.4 Piping/erosion

Overview

The central area, the main tunnels, the transport tunnels and the lower parts of the ramp and the shaft, are all expected to be water-filled through the localized inflow through fractures. No significant pore-pressure build-up is expected in the central area (with high-conductivity crushed rock) until water-saturated conditions have been reached. A minor pressure build-up can however be expected for the tunnels, ramp and shaft due to the hydraulic conductivity requirement for these fillings ($<10^{-8}$ m/s).

Handling in the PSAR

Piping and erosion could lead to a loss or redistribution of fine particles of the crushed rock in the main tunnels, transport tunnels,, ramp and shaft. However, the consequence in the tunnels and ramp is considered not to affect the behaviour since the open slot at the roof will dominate. In the shaft, where no open slot is expected after emplacement and compaction, piping and erosion could change the properties. However, the hydraulic in the crushed rock in the shaft will under all circumstances be higher than in the surrounding rock and the contribution from piping will be negligible.

6.3 Mechanical processes

6.3.1 Swelling/mass redistribution

The crushed rock has no swelling potential so mechanically it will only have a passive role. The interaction with the other parts will be governed by the stiffness and friction angle of the crushed rock. The stresses in the crushed rock are rather low since they are only caused by the self-weight of the material. In the central area the effective vertical stress (= total stress minus porewater pressure) varies from zero at the roof to 50–100 kPa in the floor, depending on the height of the rooms. The horizontal stress is about half the vertical one.

Handling in the PSAR

Most of the mechanical effects related to mass redistribution are so small that they can be ignored in the safety assessment since the requirements on the crushed rock backfill are low.

6.3.2 Liquefaction

Overview

Liquefaction is a process implying that a stiff material (soil) turns into liquid due to an affect with short duration (see e.g. Lambe and Whitman 1969). It may take place in a loose sand when the porewater pressure is increased either due to a vibration that makes the sand particles float in the porewater (since they tend to go into a higher degree of compaction, but the water temporarily prevents it) or due to a strong upward water flow that releases the effective stresses between the particles (quicksand). It may also take place in clay that has been settled in salty water (forming an open structure with a high water ratio). If the salt is partly washed out by fresh water, the clay structure cannot hold the high amount of water at moulding or vibrations, meaning that the structure collapses when exposed to vibrations.

These two types of liquefaction cannot take place in a backfill of crushed rock that has been compacted, since the density is too high. The consequences of liquefaction would anyway be negligible. The only conceivable effect is that a loose rock block in the roof may sink but this effect would be local.

Handling in the PSAR

Since the process cannot occur and the consequences are negligible if it should occur, the process is neglected.

6.4 Chemical Processes

6.4.1 Advective transport of species

Overview

In this context, advection refers to transport of any forms of additional matter, e.g. ions, molecules or colloids, with porewater flow. The transport direction is thereby principally from volumes of high water pressure to volumes of lower pressure. The process leads to redistribution of solutes in the porewater and thus affects the porewater composition. The advection is closely related to water flow in the central area, which is described in Section 6.2.2.

The backfill material in the central area consists of only crushed rock with a fuller distribution. The hydraulic conductivity is thereby relatively high ($> 2 \times 10^{-8}$ m/s). Advective flow will thereby be the dominant transport process in these repository components.

Handling in the PSAR

See Section 6.2.2

6.4.2 Diffusive transport of species

Overview

A basic description of this process is given in Section 3.5.2. However, advection is expected to dominate in the crushed rock of the central area, see 6.4.1.

Handling in the PSAR

The process is neglected, since advective transport will dominate.

6.4.3 Sorption

Overview

Radionuclides and major ions in percolating or porewater of the central area can be bound to the surfaces of the crushed rock material in several ways (see below). These processes are henceforth summarised under the term sorption and can affect the mobility of most radionuclides. The transport of major ions in the crushed rock is also influenced by these processes, which may influence the rate of weathering, see Section 6.4.4. In fresh crushed crystalline rock, the principal (primary or rock-forming) minerals offering surfaces relevant for sorption are micas. In comparison, the other major primary minerals in typical crystalline rock (quartz and feldspars) have a significantly smaller specific surface area and/or a lower concentration of relevant surface sites per unit mass. Upon exposure of the fresh surfaces to water, further surfaces of secondary minerals may be created as a result of weathering, such as clay minerals from feldspars or, under non-reducing conditions, Fe(III)-hydroxides from Fe in the crystal lattice of different primary minerals. Under reducing conditions, Fe(II/III) minerals (magnetite) or Fe(II) phases, such as siderite, may form. In weathered material, sorption will probably be dominated by the secondary minerals. The principle type of surfaces offered by these minerals and the respective possible sorption reactions (surface complexation, ion exchange) are described in Section 3.5.5. Both mica as well as clay minerals are 2:1 layer silicates that consist of octahedral alumina sheets sandwiched between tetrahedral silica sheets, 1:1 clay minerals (kaolinite) may also occur. They differ in terms of layer charge and type of interlayer cation: Micas possess a high layer charge compensated by K+. The interlayer distance is small and the layers are not expandable. The surface area and CEC are therefore smaller than in case of clay minerals. Clay minerals have a lower layer charge, with large hydrated cations (especially Na) occupying the interlayer space. Typically, this renders clay minerals expandable (exceptions are the 1:1 clays and 2:1 clays with a collapsed structure, such as illite), with a large interlayer surface area and higher CEC. Both minerals feature the same two types of distinctly different types of surfaces where two main types of sorption take place (e.g. Sposito 1984, Stumm and Morgan 1996): i) planer siloxane or “layer” surface carrying a permanent charge and ii) variable charge, oxide-type edge surfaces with exposed AlOH and SiOH functional groups. The surfaces of Fe(III)-hydroxides and -oxides are similar to the edge surfaces of clays, but the exposed FeOH-groups typically show a higher affinity for many metal ions and reactive anions than clay edge surface groups (Dzombak and Morel 1990). Further, hydrous forms of these minerals may (partly) re-crystallise over time, which can lead to the (irreversible) incorporation of adsorbed species. Because Fe is a redox-sensitive element, adsorbed species may also undergo redox reactions on these surfaces.

Handling in the PSAR

Sorption in the central area is pessimistically neglected in the transport modelling for the geosphere (see the **Geosphere process report**, Sorption process for the justification).

6.4.4 Alteration of the central area backfill

Overview/general description

The geochemical evolution due to the interaction of groundwater with the crushed rock filling the central area is not expected to be very different than what it is expected from the groundwater interaction with the rock matrix or fracture-filling minerals Geosphere process report, processes: Reactions groundwater/rock matrix and Dissolution/ precipitation of fracture-filling minerals (SKB 2010b). The processes driving the geochemical evolution of these systems are mainly related to the dissolution – precipitation of minerals. Some of these reactions are relatively fast, as dissolution – precipitation of carbonate minerals and other fracture-filling minerals; whereas other reactions occur very slowly, limited kinetic dissolution rates (i.e. dissolution of most granite-forming silicates) and irreversible. All these reactions will control the composition of porewater that potentially can reach the near field of the repository system, especially considering that thr central area may be a preferential pathway for groundwater (see Section 6.2.2).

Dependencies between process and central area variables

Table 6-1 shows how the process influences and is influenced by all central area variables.

Central area geometry: The central area geometry will determine the total mass of minerals able to react with porewater. In addition, these system parts will connect with water conducting fractures as well as with other parts of the repository, thus allowing that evolved porewater from the central area and the ramp and shaft can interact with these other system parts.

Central area pore geometry: The pore geometry in the central area will affect the geochemical behaviour of the system in several ways. First it will determine the solid/water ratio, affecting the reactivity of the system, i.e. more water is able to dissolve more minerals. The pore geometry will also affect the hydraulic conductivity, and therefore, changes in groundwater flow velocity will affect the dissolution – precipitation reactions, especially those reactions kinetically driven. Finally, the pore geometry affects the reactive surface of minerals, as rock fragments will have a larger reactive surface than surrounding rock matrix.

The increase in reactive surface area of minerals and porosity will mainly affect the dissolution kinetic rates of both rock-forming minerals and fracture-filling minerals. As the present-day groundwater at repository depth has been interacting with all these minerals for a long period of time, increasing the surface area of such minerals will have a minor effect on the chemical composition of the groundwater. On the other hand, it is expected that initially, after filling the tunnels and shaft with crushed rock, all the void spaces will be filled with air, leading to an increase in the dissolution rate of those minerals able to oxidise (i.e. pyrite and iron-bearing silicates). Then, the increased mineral surface areas and the larger water-to-solid ratios will help to consume the oxygen faster, thus neutralising the possible effect of having oxidant waters at the repository depth.

Although the dissolution – precipitation of minerals can modify the pore geometry, the high initial total porosity is not expected to change significantly due to this process.

Temperature: Thermodynamic constants of chemical reactions are highly dependent of the temperature. However, temperatures in the central area are not expected to vary significantly, and therefore, minimal effects on the geochemical processes are foreseen.

Water content: Geochemical reactions are only expected to occur once this system part is saturated. Once the system is water saturated the effect of this variable will take place as described for the central area pore geometry variable.

Table 6-1. Direct dependencies between the process "Alteration of the central area backfill" and the defined central area variables and a short note on the handling in SR-Site.

Variable	Variable influence on process		Process influence on variable	
	Influence present? (Yes/No) Description	**Handling of influence (How/Why not)**	**Influence present? (Yes/No) Description**	**Handling of influence (How/Why not)**
Central area geometry	Yes, important from mass-balance point of view, connects to water conducting fractures as well as to other repository parts	Included in modelling/ evaluation (mass-balance)	No	
Central area pore geometry	Yes. Gives solid/liquid ratio Indirectly through hydraulic conductivity	Included in modelling	May be affected by dissolution precipitation	Neglected, since hydraulic conductivity always will remain high
Temperature	Yes, temperature effect on thermodynamic constants and kinetic rates.	Neglected since the temperature variations in the central area will b eminor	No	
Water content	Yes, reactions only take place in the saturated domain.	Neglected, only saturated conditions are considered	No	
Gas content	No, but indirectly through water composition by affecting content of dissolved gases		Potentially, if a gas phase would form	Neglected, since the formation of a gas phase is of no concern
Hydrovariables (pressure and flows)	Yes, determines the turn-around rate of water	Included in modelling	No	
Stress state	No		No	
Central area materials – composition and content	Yes	Included in modelling	Yes	Included in modelling
Central area porewater composition	Yes	Included in modelling	Yes	Included in modelling
Structural and stray materials	Yes	Included in modelling	Yes	Neglected

Gas content: Gases can form or dissolve through chemical reactions, although their partial pressures are considered in the models, it is not expected that gases can form in these system parts. If gases from other system parts reach the central area, then they can dissolve in the relatively large volume of water, thus affecting the dissolution – precipitation of minerals.

Hydrovariables (pressure and flows): The high groundwater flow velocities expected in the central area and shaft will clearly affect the dissolution – precipitation reactions in the system, as porewater will be replaced relatively fast and dissolution can continue as equilibrium will be hardly achieved.

Stress state: This variable has no effect on the geochemical evolution process.

Central area materials – composition and content: This is one of the most relevant variables influencing this process. The type and amount of minerals is essential to determine how their dissolution – precipitation behaviour will affect the chemical evolution of the system, modifying both the porewater composition and the minerals present in the system (i.e. newly precipitated minerals and amount of existing minerals).

Central area porewater composition: The porewater composition will determine which of the minerals in the system will dissolve or precipitate, and thus the dissolution – precipitation of these minerals will modify the chemical composition of porewater. Moreover, changes in surface waters, as infiltration of ice-melting derived water, will very rapidly affect the chemical composition of the porewater, and hence the chemical evolution of the system.

Structural and stray materials: An additional aspect that can affect the geochemical behaviour of the crushed rock backfill is the presence of structural and stray materials. The time-length from the excavation of the repository until the use of excavated material as backfill will be relatively large. In this time frame it is expected that some biological activity take place in the depots where excavated material will be stored. Therefore, a certain amount of organic matter (i.e. dead animals and plants) will be present in the backfill material. Also the presence of other stray material (i.e. rejected metallic components) cannot be disregarded. The presence of such materials in the backfill can contribute to the geochemical evolution of the system, especially considering the likely activity of bacteria. Thus, the presence of organic matter can contribute to maintain the system under reducing conditions via the activity of sulphate-reducing bacteria and/or iron-reducing bacteria, or even, in the case of oxygen intrusion (i.e. ice-melting waters) due to the activity of aerobic bacteria see also Section 6.4.9. In this later case, it is worth noting that due to the larger hydraulic conductivity and porosity (compared to the surrounding rock) this will be a preferential path for surface waters, including ice-melting water during glaciation periods.

Boundary conditions

There are no particular boundary conditions to discuss for these processes. The relevant boundary conditions in order to treat the process quantitatively are those of the transport processes that control the exchange of solutes between the backfill water and the water in the adjacent geosphere and surface waters through the top seal above, i.e. the boundary conditions of the processes diffusion and advection.

Model studies/experimental studies

No specific studies of chemical processes in the crushed rock backfill of central area, ramp and shaft have been done. However, see also the description of the processes: Reactions groundwater/rock matrix and Dissolution/precipitation of fracture-filling minerals in the **Geosphere process report**.

Natural analogues/observations in nature

No specific natural analogues have been investigated concerning the geochemical processes expected in excavated tunnels and backfilled with crushed rock. However, the processes will be equivalent to those occurring in organic matter-bearing aquifers, as gravel aquifers or backfilled abandoned mines where organic matter is present (Postma and Jakobsen 1996, Jakobsen and Postma 1999, Banwart 1999, Hartog et al. 2004, Massmann et al. 2004, Park et al. 2006, Jakobsen and Cold 2007). In these systems, reducing conditions are maintained through different types of bacterial mediated organic matter degradation reactions. The specific type of organic matter degradation depends on the type and amount of organic matter as well as on the dominant electron acceptor in groundwater.

Time perspective

The processes considered are of relevant importance at different timescales. In early stages after repository closure (once the crushed rock backfill is emplaced) the processes involving oxygen consumption from trapped air will be the most relevant. Once the reducing conditions are restored, the water – rock interaction processes will continue for the whole repository life-span. A special case is related to the intrusion of ice-melting derived water and penetration of oxygen to repository depths. In this case, the processes involving oxygen consumption will be constrained to the glaciation – deglaciation timescales.

Handling in the PSAR

The geochemical evolution in the crushed rock backfill of the central area shouldbe evaluated through a reactive transport or mass-balance model, where the processes in this system component are implemented together with transport processes (advection). Two different time periods have to be evaluated, one for the initial times (during the water saturation after backfilling until a water saturation stationary state is reached) and the other considering a water-saturated system and its response to the intrusion of ice-melting water (glaciation – deglaciation timescales).

Initially, the system is assumed to be unsaturated and the pore space filled with air. Thereafter the system gradually saturates with present-day groundwater from the tunnel walls and evolved surface water from upper parts of the system. The evolution of the system has to consider the consumption of dissolved gases in equilibrium with atmosphere conditions (i.e. $pCO_2 = 10^{-3.5}$ bar and $pO_2 = 10^{-0.7}$ bar) and how these dissolved gases affect the dissolution – precipitation of rock-forming and fracture-filling minerals present in the system. Moreover, the effect of organic matter degradation must be considered, first through oxidation reactions involving aerobic bacteria and, once oxygen has been consumed, through reactions involving sulphate-reduction or iron-reduction bacteria. The evolution of the system must be assessed to evaluate the oxygen consumption and to determine the stationary redox state of the system.

The second part of the system evaluation should consider a glaciation – deglaciation time period, where oxygen-rich ice-melting water can intrude the system from the surface. In this case, full saturation can be assumed (i.e. the output conditions from the previous case) and the water-rock reactions consuming oxygen, including organic matter degradation, implemented in the model. This will allow assessing the penetration depth of oxygen and the potential impact on the repository, as well as the redox buffering capacity of the system.

Handling boundary conditions: Two main boundary conditions have to be considered. One is the transport conditions from tunnel walls into the backfilled system and the other is the composition and flow conditions of surface water entering into the system from the surface.

Transport conditions have to be handled according to the process advection. Initial chemical compositions of both groundwater and surface water (including ice-melting derived water) will be based on the hydrogeological modelling, see Section 6.2.2.

Handling influences between variables and process: Groundwater flow and composition are defined as part of the boundary condition as stated above. The volume and porosity of the central area is considered and fracture and matrix minerals are fully included in the modelled system, as well as stray materials. The saturation phase is neglected in the geochemical model, since it is short in duration and will have limited impact.

Handling coupling to other processes: The model here considered only includes the coupling with transport processes as well as with the microbial activity.

Uncertainties

Uncertainties in mechanistic understanding

Some critical uncertainties remain concerning the mechanistic understanding of the processes that control the redox state of the system. These are mainly related to the degradation of organic matter. Although a generic organic matter and mass-balance can be used (CH_2O), the lack of knowledge on the mechanistic degradation of the specific organic matter could introduce a large uncertainty to the system.

In addition, most of the secondary precipitation/dissolution processes that are temperature driven are thermodynamically controlled. Hence, there is no need for a detailed mechanistic understanding. However, some of the silicate transformations are kinetically controlled and their mechanistic understanding in the considered conditions is poor. This is mainly related to the dissolution of rock-forming silicates and their transformation into clay minerals. Although these reactions occur at a very slow rate, their effect on the overall geochemical evolution is not yet clear.

Model simplification uncertainty in PSAR

There are several rock-forming minerals, such as silicates other than silica, which tend to dissolve at a very slow kinetic rate and irreversibly. Other silicates (usually clay minerals) precipitate at similarly slow rates. However, the dissolution-precipitation processes involving these two groups of minerals could affect the pH evolution of the system as well as the chemical composition of the groundwater, thus affecting the chemical long-term evolution of the system.

Modelling of chemical reactions driven by microbial activity generally makes use of kinetic rates for organic matter degradation. The computed rates are generally fast as compared with the timescale of reactions with rock-forming minerals. The results of the modelling are strongly coupled to the microbial processes considered and to the values of the parameters used. The introduced simplifications, such as considering a generic organic matter (i.e. CH_2O), could result in differences with respect to actual rates of oxygen consumption.

Input data and data uncertainty in PSAR

Another source of uncertainty relates to the quantitative estimation of sensitive parameters associated with microbial kinetics, such as growth rate and half saturation constants in the kinetic expressions. Such parameters are both microbe dependent and environment dependent. Usually, parameter values are obtained in laboratory conditions by means of physiological (i.e. growth) in vitro experiments which cannot be fully representative of repository conditions. Results of current in situ microbe investigations, as well as model calibration based on field experimental data could be helpful for the up-scaling of key microbial parameters. Nevertheless, model calculations involving microbial processes, even if they are calibrated against experimental field data, are necessarily of qualitative value.

6.4.5 Alteration of concrete components

Overview/

In the central area, cement-bearing materials can be present as construction concrete and grout can remain in the system after backfilling this system part. The alteration of such materials can affect the system in two different ways: 1) as a consequence of its degradation the porosity can increase, thus creating favourable pathways for groundwater to enter into the system, and 2) the increase of alkalinity due to the interaction of groundwater with these materials can enhance the dissolution rate of smectite (Section 3.5.8 in Buffer chapter), weakening the effectiveness of the bentonite backfill in the deposition tunnels as a hydraulic barrier.

The processes associated to the alteration of concrete components are equivalent to those considered for concrete in the tunnel plug (Section 5.4.4).

Handling in the PSAR

The degradation of the concrete in the central area is assumed to be equivalent with the degradation of the concrete part of the tunnel plug (Section 5.4.4). No separate modelling will be done.

6.4.6 Aqueous speciation and reactions

Overview

This process is in general the same as the corresponding process in the buffer (Section 3.5.4.)

Handling in the PSAR

The process is included in a separate modelling task of the central area geochemical evolution. This is further described in Section 6.4.4.

6.4.7 Osmosis

Overview

The general process is described for the buffer system in Section 3.5.7. In the crushed rock the effect will be insignificant since the material itself will not have a semi-permeable behaviour.

Handling in the PSAR

The process is neglected since osmotic effects will be insignificant in the crushed rock material.

6.4.8 Corrosion of steel components

Overview

Steel in the reinforcements in the central area will not be stable under repository conditions. Corrosion of steel is described in the **Fuel and canister process report**. The main resulting products will be some type of iron-oxide and hydrogen gas. Neither of the corrosion products is assumed to have direct any negative impact on the repository performance.

Handling in the PSAR

The total amount of steel is included in all mass-balance calculations of effects of microbial activity, see Section 6.4.9. The corrosion rate of steel reinforcements will pessimistically be neglected.

6.4.9 Microbial processes

Overview

An overview of potential microbial processes in “non-bentonite” areas are given in Section 5.4.9.

Handling in the PSAR

Microbial degradation of organic carbon and consumption of hydrogen from metal corrosion is considered in the modelling of the geochemical evolution repository. This will be done through a combination of thermodynamic, kinetic and mass balance models/assumption. See also Section 6.4.4.

6.4.10 Colloid release

Overview

Fractures intersecting the central area mean that rigid volumes restrictions are not present everywhere, and that small-sized material may enter the fractures. Separation of individual particles from the introduced material may then take place (dispersion). The behaviour of the particles will be dominated by thermal motion if the particles are small enough i.e. they have colloidal properties. The individual colloidal particles may then be transported away from the tunnels into fractures by diffusion or by groundwater flow in the fractures. The magnitude of the process is governed by the size distribution of the crushed rock. The material can be chosen in such a way that colloid formation may be neglected.

Handling in the PSAR

The process is neglected due to the very small possible effect, also for the unlikely case that all particles of colloidal size are transported away. No credit is taken for the fine particles under any circumstances and the hydraulic conductivity is assumed to be high under all circumstances.

6.4.11 Radiation induced transformation

Overview

The central area is too far away from the canisters to be affected by the g-radiation. The effect of a-radiation from radionuclides from damaged canisters can also be neglected, since the levels will be extremely small (see Section 3.5.13).

Handling in the PSAR

The process is neglected.

6.5 Radionuclide transport processes

6.5.1 Speciation of radionuclides

Overview

See corresponding process description for the buffer, Section 3.6.1.

Handling in the PSAR

This process is indirectly handled through the selection of parameters for radionuclide transport in the rock. In general, the handling of the process is the same as for the corresponding process in the geosphere; see process transport of radionuclides in the water phase in the **Geosphere process report**.

6.5.2 Transport of radionuclides in the water phase

Overview

The central area is represented as a volume with high hydraulic conductivity and high porosity in the geosphere transport model.

Handling in the PSAR

Delay of radionuclides in the central area is pessimistically neglected. See process transport of radionuclides in the water phase in the **Geosphere process report**.

7 Processes in the top seal

7.1 Thermal processes

7.1.1 Heat transport

Overview

At the bottom boundary of the top seal, the rock peak temperature occurs about 1 000 years after deposition, and will be between 5 and 7 °C above the initial temperature at 100 m below ground surface, and correspondingly smaller at shallower depths (Hökmark et al. 2009). The volume of the top seal is small enough for its thermal evolution to be completely controlled by the slow and modest change in the temperature of the surrounding rock mass, regardless of the heat transport properties of the top seal materials. The modest temperature variations cannot influence the variables in any way that impacts on the performance of the top seal. Therefore, the process heat transport in the top seal is not addressed further.

Handling in the PSAR

The process is neglected.

7.1.2 Freezing

Overview

The top seal of the shafts from ground surface down to approx. 50 m depth will be filled with big boulders. The size of the boulders will be in the range of metres. During freezing periods, the water between the boulders will be frozen and the system will have temperatures well below 0 °C. When water undergoes phase change to ice, energy is released (333 J/g) and volume expansion takes place (approximately 9 %). In a porous medium containing water in the pores, water will turn into ice if the temperature is low enough. Not all the water in the pores will freeze at a given temperature. The amount of water in liquid phase is known as unfrozen water. The evidence establishing the existence of a continuous, unfrozen water phase that separates ice from the mineral matrix in porous media like soils is widely accepted (Anderson 1966, Miller 1963, Nersesova and Tsytovich 1965, Williams 1964). The amount of unfrozen water depends on various factors (Anderson and Tice 1972) among which particle mineral composition, specific surface area of particles, temperature, presence of solutes and pressure are the most significant.

In a very coarse-grained material, like boulders, the amount of unfrozen water is negligible due to the very small specific surface in the system and corresponding big voids between particles. In relation to the salt content of the water, the porewater turns into ice at temperatures close to 0 °C. As the unfrozen water content is negligible, this means that all water freezes to ice at the same temperature, i.e. close to 0 °C.

During freezing, water expands. In a system with high hydraulic conductivity, the expansion during freezing will expel water out of the pore system at the same rate as water expands during the ice forming process. Neither volume increase nor stress increase of the system will take place as long as water can be expelled in an open system. No ice lensing with accompanying frost heave will take place, as the unfrozen water content will be negligible and thus no suction will be developed. Frost penetration rates in ground, relevant for frost penetration due to low temperatures at the ground surface, are at most in the range 2–3 m/year.

A freezing ground can be regarded as an open system if the hydraulic conductivity is greater than 10^{-5} m/s (conservative value) for normal freezing rates. A very coarse-grained material like boulders will have a hydraulic conductivity of about 10^{-1} m/s and therefore no frost phenomena will be present. Particles of rock materials will be affected by freezing if fractures are present in the particles before freezing and thawing and the particles stay in a water-saturated environment. Water having penetrated into open fractures and voids in the particles will expand, and if the fractures are small, or if freezing takes place in a direction that closes the entry of the fractures, an open system will not be present in

the particle itself. High pressures can build up thus causing cracking of the particle. The phenomenon is known from nature as frost cracking. The process goes on until solid parts of rocks, without fractures, remain. Particles without cracks will not be affected by freezing. This is also well known from nature.

The boulders used as top seal will thus be affected as they to some extent will have cracks. The material will be successively finer and the end result of the particle size will be dependent on the amount of cracks in the material used. Boulders of granite or similar hard rock will not end up in a smaller material than gravel and stones. If the boulders initially are free of fractures, freezing will not affect the material.

From the level of −370 m up to the level of −50 m, the ramp and shaft are sealed with crushed rock. Freezing-thawing cycles could case the material to settle or grains to crack. However, effects of freezing in this part is assumed to have negligible effect on the performance since the hydraulic conductivity is high already att the beginning.

Handling in the PSAR

Due to the high hydraulic conductivity of the top seal, no stress increase or expansion will take place. The process can therefore be neglected. Particles will be affected and broken into smaller pieces. The final condition will be particles of stone size. This may have an effect on the accessibility to the repository.

7.2 Hydraulic processes

7.2.1 Water uptake and transport under unsaturated conditions

Overview

Water transport in the crushed rock filled in the top before saturation is mainly governed by the inflow rate and inflow distribution in the rock. Since the expected hydraulic conductivity of the crushed rock is very high and since there may be an open slot at the roof in the ramp, since the backfill material has no swelling properties, the resistance to water inflow into the filling material will be very low. The important processes are the same as for the central area (Section 6.2.1).

The hydraulic behaviour depends very much on the grain size distribution and the density of the crushed rock. Since the exact values of hydraulic conductivity are not determined and since there are no demands on the hydraulic conductivity it is assumed that it is so high that the top seal filling material is filled with water at the same rate as it enters from the fractures in the rock and flows downwards until the water comes into contact with the underlying less permeable backfill. Part of the water will then flow into this backfill and part will stay and fill up the top seal. The blasted and crushed rock used for the top seal is expected to have a hydraulic conductivity of 10^{-1} m/s or higher.

Handling in the PSAR

This process is only handled by a rough estimate of the time it may take to fill the top seal with water. It will under all circumstances be a short duration.

7.2.2 Water transport under saturated conditions

Overview

Water transport under saturated conditions is mainly driven by a water pressure gradient. The process can be described by Darcy's law.

Handling in the PSAR

Included in the hydrogeological large scale model as a feature with high hydraulic conductivity (see the **Geosphere process report**).

7.2.3 Gas transport and dissolution

Overview

Gas transport in the top seal is basically the same process as that in the central area, see Section 6.2.3. However, since the conductivity of the material will be high, trapped gas will escape very easily

Handling in the PSAR

The process is neglected and the saturation of the top seal is assumed to be rapid, see also Section 7.2.1.

7.2.4 Piping and erosion

Overview

Water inflow into the top seal will take place mainly through fractures and will contribute to the water-filling of the crushed rock.

Since the hydraulic conductivity of the blasted and crushed rock in the top seal is so high, there will be no resistance to water inflow, not even when the crushed rock is dry. This means that all inflowing water is easily absorbed by the crushed rock and that piping cannot take place. Since there are no fine-grained particles in the filling, no or little erosion will take place.

Handling in the PSAR

Since piping and erosion cannot take place in the top sealing, this process is neglected.

7.3 Mechanical processes

7.3.1 Swelling and mass redistribution

Overview

The crushed rock has no swelling potential so it will mechanically only have passive roles. The interaction with the other parts will be governed by the stiffness, the friction angle and the own weight of the crushed rock.

In the top seal of the ramp the effective vertical stress (= total stress minus porewater pressure) varies from zero at the roof to 50–100 kPa in the floor, depending on the height of the ramp. In the top seal of the shaft, the stresses in the bottom of the top seal can be rather high due to the large depth (200 m), but the friction against the rock walls reduces the stresses significantly (silo effect). The horizontal stress is about half the vertical one.

Handling in the PSAR

Most of the mechanical effects related to mass redistribution are so small that they can be ignored in the safety assessment since the demands on the backfill of the top seal are only to preserve the seal and obstruct human intrusion.

7.4 Chemical Processes

7.4.1 Advective transport of species

Overview

In this context, advection refers to transport of any forms of additional matter, e.g. ions, molecules or colloids, with porewater flow. The transport direction is thereby principally from volumes of high water pressure to volumes of lower pressure. The process leads to redistribution of solutes in the porewater and thus affects the porewater composition. Advection is closely related to water flow in the top seal, which is described in Section 7.2.2.

The backfill material in the top seal consists of moraine, crushed rock and rock-like material. The hydraulic conductivity is not known but can be assumed to be high (~0.1 m/s). Advective flow will thereby be the dominant transport process in this component.

Handling in the PSAR

The top seal is included in the hydrogeological large scale model as a feature with high hydraulic conductivity (see the Geosphere process report). This model provides the evolution of the salinity field, but also data on the transport and mixing of water types.

7.4.2 Diffusive transport of species

Overview

A basic description of this process is given in Section 3.5.2. Because of the hydraulic situation in the top seal, diffusion is of no importance in this system part.

Handling in the PSAR

The process is neglected since advective transport will dominate in the top seal.

7.4.3 Sorption (including exchange of major ions)

Overview

Radionuclides and major ions contained in water in the top seal can be bound to the surfaces of the large rocks in the same way as has already been described for the crushed rock material of the central area, (Section 6.4.3). In a qualitative sense, the sorption processes will be nearly identical to those taking place in crushed rock material, although the proportion of the various types of mineral surfaces is likely to differ somewhat between crushed vs. non-crushed material. Quantitatively, sorption onto large rock blocks will be of comparatively little importance, due to their small specific surface area and the comparatively short contact time of percolating water.

Handling in the PSAR

The process is neglected. (Sorption on the cement minerals provides additional safety).

7.4.4 Alteration of concrete components

Overview

In the top seal, cement-bearing materials can be present as construction concrete, and grout will remain in the system after backfilling this system part. The alteration of such materials can affect the system in two different ways: 1) as a consequence of its degradation the porosity can increase, thus creating favourable pathways for groundwater to enter into the system, and 2) the increase of alkalinity due to the interaction of groundwater with these materials could possibly enhance the dissolution rate of montmorillonite in the buffer and backfill (Section 3.5.8 in the Buffer chapter), weakening the effectiveness of bentonite in buffer and the clay backfill in the deposition tunnels and in the lower part of the ramp and shaft as a hydraulic barrier.

The processes associated to the alteration of concrete components are equivalent to those considered for concrete in the tunnel plug (Section 5.4.4)

Handling in the PSAR

The process is neglected since there is a long distance from concrete structures in the top seal to the clay components in the deposition tunnel backfill and the buffer and the performance requirements on the clay backfill in the ramp and shaft is limited. See also Section 5.4.4.

7.4.5 Aqueous speciation and reactions

Overview

This process is in general the same as the corresponding process in the buffer (Section 3.5.4.)

Handling in the PSAR

No geochemical processes are considered in the top seal because of the distance to, and thus limited impact on, essential repository barriers.

7.4.6 Colloid release

Overview

Fractures intersecting the top seal mean that rigid volumes restrictions are not present everywhere, and that small sized material may enter the fractures. Separation of individual particles from the introduced material may then take place (dispersion).

The behaviour of the particles will be dominated by thermal motion if the particles are small enough i.e. they have colloidal properties. The individual colloidal particles may then be transported away from the deposition hole in fractures by diffusion or by groundwater flow in the fractures.

The process is considered not relevant for the upper part (100 m) of the top seal component, since the coarse gravel material in principle has the same properties as the surrounding rock with respect to colloid release. The lower part of the top seal component (100–200 m below surface) consists of crushed rock with a fuller size distribution. The smallest fractions may in principle form colloids at the groundwater interface.

Handling in the PSAR

This process is neglected in the top seal due to the very small possible effect, also for the unlikely case that all particles of colloidal size are transported away.

7.4.7 Steel corrosion

Overview

Steel in the reinforcements in the top seal will not be stable under repository conditions, see Corrosion of steel in the **Fuel and canister process report**. However, there are no long term performance requirements on the reinforcements and the corrosion products and gases are not expected to have any impact on the other parts of the repository.

Handling in the PSAR

The process is neglected based on the reasoning above.

7.4.8 Microbial processes

Overview

Microbial processes in a crushed rock environment is described in the section about the plug (Section 5.4.9)

Handling in the PSAR

It is not foreseen that microbial processes can interfere with the top seal in a way that will influence the performance of the repository. The process is therefore neglected.

7.5 Radionuclide transport processes

7.5.1 Speciation of radionuclides

Overview

See corresponding process description for the buffer, Section 3.6.1.

Handling in the PSAR

This process is indirectly handled through the selection of parameters for radionuclide transport in the rock. In general, the handling of the process is the same as for the corresponding process in the geosphere; see the process Transport of radionuclides in the water phase in the Geosphere process report.

7.5.2 Transport of radionuclides in the water phase

Overview

The top seal can be considered as a part of the rock with high hydraulic conductivity and a high porosity. If radionuclides would enter the central area the additional transport time to the surface would be rather limited.

Handling in the PSAR

The top seal is considered to be a part of the rock in the radionuclide transport calculations, see the process Transport of radionuclides in the water phase in the **Geosphere process report**.

8 Processes in the bottom plate

8.1 Thermal processes

8.1.1 Heat transport

Overview

The effect of the 20 mm copper plate below the bentonite barrier will be to even out the temperature such that the central parts and the peripheral parts both tend to approach the area average. In addition, there will be a small general increase of the vertical heat flux across the bottom bentonite block, leading to a small reduction of the canister temperature.

Handling in the PSAR

Because of the modest impact on the temperatures in the interior of the deposition hole, there is no specific handling of heat transport in the bottom plate. The copper plate is, however, explicitly included in the thermal near-field models.

8.1.2 Freezing

Overview

Since the current design of the bottom plate only consist of copper, freezing is irrelevant. The process could be removed from this report, but is kept in case the design changes in the future.

Handling in the PSAR

No handling.

8.2 Hydraulic processes

8.2.1 Water uptake and transport under unsaturated conditions

Overview

When water enters the deposition hole, a rather complicated interplay between the bottom plate, the buffer and the rock will start. Since the contact zones between the rock and the copper plate are not tight, water may penetrate and a water pressure may act on the plate.

Since the current design of the bottom plate only consist of copper, water uptake and transport is irrelevant. The process could be removed from this report, but is kept in case the design changes in the future.

Handling in the PSAR

No handling. However, the mechanical interaction between the buffer and the bottom plate is included in Section 3.4.1.

8.2.2 Water transport under saturated conditions

Overview

The bottom plate will restrict movement of water from possible fractures in the bottom of the deposition hole to the buffer. The will be an interface between the copper plate and the rock below. This interface will most like have a higher hydraulic conductivity than the surrounding rock and bentonite and may act as a local preferential pathway if there are fractures connected to it.

Handling in the PSAR

The process is neglected in the PSAR. The effects described above are too local to have any effect on the water transport in the repository.

8.2.3 Piping/erosion

Overview

Piping and erosion will not occur in the bottom plate. Piping of the pellets filling in the buffer (Section 3.3.4) will however have an important role in the hydro-mechanical interaction between the bottom plate and the buffer (Section 3.4.1.).

Handling in the PSAR

None.

8.3 Mechanical processes

8.3.1 Swelling and mass redistribution

Overview

A high water pressure may occur in the surface between the rock and the bottom plate and can be present rather soon after installation of the buffer. Since the contact zone between the rock and the copper plate is not tight, water will penetrate and a water pressure will act on the entire plate. If this water pressure is higher than the own weight of the buffer and the canister, the entire package will lift and be moved upwards. This process is handled in Section 3.4.1.

Handling in the PSAR

No handling. However, the mechanical interaction between the buffer and the bottom plate is included in Section 3.4.1.

8.4 Chemical processes

8.4.1 Advective transport of species

Overview

No advective flow may take place through the copper plate as long as it is intact, and all flow has to take place outside the edge of the plate. There are however an interface between the plate and the rock below where advective transport can take place.

Handling in the PSAR

The process is neglected in the PSAR. The effect described above is too local to have any effect on the transport of species in the repository.

8.4.2 Diffusive transport of species

Overview

Not relevant for a pure copper plate. The process could be removed from this report, but is kept in case the design changes in the future.

Handling in the PSAR

No handling.

8.4.3 Sorption (including exchange of major ions)

Overview

For the actual copper plate (copper metal surface), no sorption reactions are expected to take place and this process is neglected. The process could be removed from this report, but is kept in case the design changes in the future.

Handling in the PSAR

No handling.

8.4.4 Aqueous speciation and reactions

Overview

For the actual copper plate no aqueous reactions n reactions are expected to take place and this process is neglected. The process could be removed from this report, but is kept in case the design changes in the future.

Handling in the PSAR

No handling.

8.4.5 Corrosion of copper

Overview

The copper plate will behave similar to the copper in the canister overpack (see **Fuel and canister process report**, section copper corrosion). The difference is that the copper plate only has bentonite on one side and the other side will be exposed to the rock.

Handling in the PSAR

The copper plate is neglected in the PSAR. It is assumed to have no mass-transfer resistance in the assessment. It could also act as a sink for sulphide that could have corroded the canister. This feature is pessimistically neglected.

8.4.6 Microbial processes

Overview

Microorganisms interact with their surroundings, and they commonly have a significant effect on the geochemical record of their environment. No microbial processes can take place in the copper plate itself. The interface between the plate and the rock may however be a favourable environment for microbial activity.

Handling in the PSAR

The properties of the interface in this respect will be similar to those of fractures in the rock. The handling of the process is described in the **Geosphere process report**.

9 Processes in borehole seals

9.1 Thermal processes

9.1.1 Heat transport

Overview

For borehole seals extending a distance l = 400 m from the repository horizon to the ground surface, the heat flow Q would be less than 0.2 W if the temperature difference DT between the ends of the tube is about 40 °C even if the seals are made of solid 75 mm (A = 0.0044 m^2) diameter copper rods with thermal conductivity λ = 390 W/(m · K). (Q = λ · A · DT/l). In reality it will be much less.

Because of the small heat flow, the temperature disturbances (cooling of rock in the bottom end and heating in the top end) will be very modest and involve very small rock volumes in the immediate vicinity of the tube. In the concrete portions and, in particular, in the bentonite filling not covered by copper tubes, the heat flow is vanishingly small. The temperatures of the borehole seals are almost completely determined by the thermal evolution of the surrounding rock, i.e. practically independent of the heat transport within the seals.

Handling in the PSAR

The evolution of the rock temperature at different positions within and around the repository is calculated in Hökmark et al. (2009). Because of the small thermal gradients and the relatively low temperatures in the borehole seals, there is no specific handling of the heat transport process in the borehole seals.

9.1.2 Freezing

Overview

The overview and general description of the corresponding buffer process, Section 3.2.2, are also valid for the bentonite part of the borehole seals. In contrast to the corresponding buffer process, two new aspects must be considered:

- Freezing will occur in the borehole seals.

  The extension of the frozen uppermost section of the ground during permafrost periods will vary with time and is predicted to have a maximum penetration of approximately 250 m (Hartikainen 2004).

- A temperature gradient is imposed over the bentonite, due to the vertical geometry.

  This temperature gradient, in turn, corresponds to a suction gradient and water may be transported in the bentonite to form ice lenses e.g. at the interfaces between bentonite and concrete.

When bentonite freezes, the swelling pressure will fall to zero in the temperature interval 0 °C > T > T_c. T_c is a density dependent critical temperature. For a saturated density of 2 000 kg/m^3, the critical temperature T_c is < –5 °C. A thermal gradient below 0 °C will thus correspond to a swelling pressure gradient which might cause redistribution of the bentonite.

When the pressure drop occurs, the transport paths in the surrounding rock will be frozen.

Water flow from the induced suction gradient can be estimated by identifying swelling pressure with suction:

$$\nabla\psi = -\nabla P_s = -\frac{\partial P_s}{\partial T}\nabla \qquad (9\text{-}1)$$

where ψ is suction (see Section 3.3.1). The derivative $\frac{\partial P_s}{\partial T}$ has an estimated value of 1 MPa/°C for temperatures below 0 °C (see Section 3.2.2).

A typical geothermal temperature gradient is 0.025 °C/m and using this value together with a value of the hydraulic conductivity of 10^{-13} m/s, the corresponding water flux is 2.5×10^{-13} m/s or approximately 8 μm/y, which is also the estimated ice lens growth.

Table 9-1 summarises how the process influences and is influenced by all borehole seal variables and how these effects are treated in the PSAR.

Table 9-1. Direct dependencies between the process "Freezing" and the defined borehole seal variables and a short note on the handling in the PSAR.

Variable	Variable influence on process		Process influence on variable	
	Influence present? (Yes/No) Description	Handling of influence (How/Why not)	Influence present? (Yes/No) Description	Handling of influence (How/Why not)
Borehole geometry	Yes, determines the thermal boundary conditions	Included in the assessment	No	
Pore geometry	Yes	Included in the assessment	No	
Temperature	Yes	Included in the assessment	No	
Water content	Yes, via freezing point and transport capacity	Included in the assessment	Yes, If freezing takes place redistribution of water	Neglected
Gas content	(Yes)	A gas content would affect the process but the buffer will be completely saturated when freezing	no	
Hydrovariables (pressure and flows)	Yes, freezing induces water transport	Included in the assessment	Yes	Included in the assessment
Stress state	Yes, Influences the freezing point to a small degree	Included in the assessment	Yes. Swelling pressure affected also before ice formation	Included in the assessment
Sealing materials – composition and content	Yes, via the specific surface area	Included in the assessment	No	
Porewater composition	Yes, via the specific surface area and types of counter ions	Neglected, effect assumed to be small	No	
Structural and stray materials	No		No	

Boundary conditions

When freezing of the bentonite in the borehole seals occurs, the water in the surrounding rock and most of the water in the concrete will be in ice form. Hence, transfer of water between rock and bentonite at the same level will be very limited. The slowly varying temperatures of the rock surrounding the seals also constitute a boundary condition.

Model studies/experimental studies

The general temperature response in compacted bentonite has been worked out both theoretically and experimentally in Birgersson et al. (2010). The same report also estimates the water transport capacity in a vertically extended bore hole seal.

Natural analogues/observations in nature

This has not been done yet. However, some knowledge can probably be gathered by studying permafrost areas.

Time perspective

Freezing of borehole seals are relevant during the entire repository lifetime.

Handling in the safety assessment the PSAR

Ice lens formation in the bentonite component in a bore hole seal was evaluated in the main report of SR-Site (SKB 2011). The conclusion was that the effect was negligible. The updated design of the seal with shorter bentonite sections makes ice lens formation even more unlikely (Section 2.9). The effect is therefore neglected in the PSAR.

Uncertainties

Uncertainties in mechanistic understanding

The freezing of soils is a well-known process.

Model simplification uncertainties for the above handling in the PSAR

The reproducibility of the pressure response due to freezing in bentonite is good.

Input data and data uncertainties for the above handling in the PSAR

The key uncertainty is the location and duration of the permafrost front. Other uncertainties are related to the suction gradient and the assumed hydraulic conductivity. How this affects the conclusions about the process is discussed in Birgersson et al. (2010).

9.2 Hydraulic processes

9.2.1 Water uptake and transport under unsaturated conditions

Overview

Water transport in bentonite under unsaturated conditions is a complex process that is dependent on, inter alia, temperature, smectite content, degree of water saturation and water content in the different parts of the bentonite. The most important driving force for water saturation under deep repository conditions is a negative capillary pressure in the pores of the bentonite that leads to water uptake from the surrounding rock. The supply of water from the rock by water transport in fractures and in the rock matrix is also a decisive factor for the temporal evolution of the process.

For the bentonite part of the investigation holes, the process of water uptake and transport under unsaturated conditions is identical with the process described for the buffer (Section 3.3.1).

The sand part of the bore holes can be assumed to be saturated very rapidly.

Handling in the PSAR

The hydration of the previous design of the borehole seals was evaluated in Åkesson et al. (2010a). The results showed that the bentonite part of the seal was hydrated relatively rapid even with the assumption of a low-conductivity rock. This conclusion will not change with the new design. The hydration time of the borehole seal is therefore neglected in the PSAR.

9.2.2 Water transport under saturated conditions

Overview

Water flow in saturated bentonite is a special case of unsaturated flow. The processes involved are the same as for unsaturated conditions, but can vary widely in importance compared with unsaturated conditions.

The most important mechanism under saturated conditions is transport of water in liquid phase, which is driven by a water pressure gradient. This transport process can be described by Darcy's law. The hydraulic conductivity K is a function of the composition of the buffer, the void ratio, e, the ion concentration in the porewater, i_c, and the temperature, T.

The hydraulic conductivity of MX-80 to low-salinity water after complete saturation is approximately 10^{-13} m/s (for a dry density of 1 500 kg/m^3).

Handling in the PSAR

The water flow along the holes can be neglected as long as the bentonite remains its low hydraulic conductivity. This case will thus not be further handled in the PSAR. If there is a risk that a large part of the bentonite will be lost or transformed to obtain other properties, these cases must be handled. Cases with unsealed boreholes are discussed in the **Geosphere process report**.

9.2.3 Gas transport/dissolution

Overview

Gas processes in the borehole seals are only relevant for the saturation period and only for the bentonite part of the seal – this is described in Section 3.3.1

Handling in the PSAR

The process was included in the supporting sensitivity analyses of the saturation phase in SR-Site see Section 9.2.1. The saturation phase is neglected in the PSAR.

9.2.4 Piping and erosion

Overview

As described for the corresponding buffer process (Section 3.3.4), piping and erosion are primarily a problem in the unsaturated stage when water flows between different parts of rock cavities. Since the investigation holes are filled with water from start, erosion will not take place after installation. There are no high axial hydraulic gradients along the hole so there will be no axial water flow that can erode the bentonite. Any large fracture zones that may cause flow along the investigation hole during installation are presupposed to be grouted and sealed. The bentonite sections are also sealed by concrete plugs to even further minimize the risk for piping.

Handling in the PSAR

Since piping and erosion of the bentonite cannot occur in stagnant water, the process is ruled out for the seals in the investigation holes.

9.3 Mechanical processes

9.3.1 Swelling and mass redistribution

Overview

Water is absorbed by both unsaturated and saturated bentonite (that is able to physically expand) and causes swelling. If the bentonite is unable to expand freely, a swelling pressure develops, which locally reaches its peak at full water saturation.

The new Sandwich-concept (Section 2.9.1) implies that the main part of a borehole is filled with a permeable material such as sand or gravel, while strategically positioned bentonite seals are placed in selected borehole sections with good rock quality i.e. there are no water bearing fractures present. The number of sealing sections in a borehole can be decided after a characterization of the borehole so that interaction between water bearing fracture zones at different depths can be minimized. To prevent interaction between the different materials, concrete is positioned a certain length in the transition zones between bentonite and sand. In addition, bridge plugs made of copper are installed to separate different materials (Figure 2-15).

The bentonite in the current Sandwich-concept is tightly confined between concrete plugs and copper expanders. The swelling required here is for the installed bentonite cylinders to expand into the voids between the cylinder and the rock wall.

Model/experimental studies

The homogenization of the bentonite seals was tested by Sandén et al. (2018). The main objectives with the test were to measure and demonstrate the swelling pressure built up and the sealing effect of dense bentonite installed in a rock section. The dry density of the bentonite installed in the simulated borehole section varied between 1 440 kg/m^3 (at the test tube walls) and 1 580 kg/ m^3 (at the central parts).

The registered swelling pressure from the bentonite against the simulated rock wall was around 5 MPa which is well in agreement with the expected 4–6 MPa (Åkesson et al. 2010a).

Handling in the PSAR

No sensitivity studies on the direct performance of the borehole plugs will be performed in PSAR. However, the effect of open boreholes is considered in the geohydrological modelling (Joyce et al. 2010).

9.3.2 Liquefaction

Overview

Liquefaction in bentonite is described in Section 3.4.2.

Handling in the PSAR

Since the process cannot occur, it will not be handled in the PSAR.

9.4 Chemical processes

9.4.1 Advective transport of species

Overview

In this context, advection refers to transport of any forms of additional matter, e.g. ions, molecules or colloids, with porewater flow. The transport direction is thereby principally from volumes of high water pressure to volumes of lower pressure. The process leads to redistribution of solutes in the porewater and thus affects the porewater composition. There are several possible causes of pressure gradients in the borehole seals, e.g. external water pressure, affinity for water in the bentonite and temperature induced volume change of the water. Advection is closely related to water flow in the borehole seals, which is described in Section 9.2.2. Advection may though be different compared to pure water flow due to ion equilibrium effects in the case of ions, and due to filtering by nano-sized pores in the case of colloids.

Advective transport is of importance in the bentonite part of the borehole seals during the saturation period. Under saturated conditions, the transport of solutes in the bentonite porewater is expected to be dominated by diffusion, see Section 9.4.2. Advective flow will probably be significant in the sand parts of the seals and also in the cement parts in the long term perspective due to cement degradation.

Handling in the PSAR

No detailed modelling of advection is required before saturation. Open boreholes will be considered as a variant in the hydrogeological modelling (Joyce et al. 2010).

9.4.2 Diffusive transport of species

An overview of diffusion processes and phenomena as relevant for bentonite and concrete are given in Sections 3.5.2 and 5.4.2, respectively, these considerations also apply to the concrete- and bentonite-parts of the borehole seals. Luna et al. (2006) conclude that the main diffusion parameters (incl. porosity) will not be significantly affected by an alkaline plume. Diffusion in the sand parts can be assumed to be relatively unimportant, since advection is expected to dominate.

Handling in the PSAR

Transport of species with diffusion in the borehole seals is not considered.

9.4.3 Sorption (including exchange of major ions)

Overview/general description

Seals of investigation boreholes consist of bentonite in copper tubes, plus low-pH concrete in the conductive areas. The sorption processes taking place in these systems are the same as in other bentonite and concrete parts of the repository system and are described in Sections 3.5.6 and 5.4.3 respectively. The effects of concrete-bentonite interaction and the behaviour of organic concrete admixtures are described in Section 5.4.4.

Handling in the PSAR

Sorption of radionuclides is neglected both in the concrete, in the sand and the bentonite parts of the borehole seals. No radionuclide transport is assumed to take place in an intact seal. In the case of a defect seal, sorption is pessimistically neglected.

9.4.4 Alteration of concrete

Overview

The pH evolution from the concrete part of the borehole seals will in most respects be identical to the effect from the plugs (Section 5.4.4). Therefore, the results from modelling of the pH evolution in and around the concrete plugs will be used to draw conclusions regarding the pH evolution in and around borehole seals

Handling in the PSAR

The interaction between the bentonite and the concrete in the borehole seals can be described in the same way as the interaction between the tunnel plugs and the backfill (Grandia et al. 2010). The conclusion is that there will be an increase in the pH in the bentonite closest to the concrete, but the duration of the pH pulse and the penetration depth will be small. The cement part of the concrete will degrade with time, but the ballast material will remain. Thereby, the loss of bentonite to the flowing water in the fracture can be assumed to be limited.

9.4.5 Aqueous speciation and reactions

Overview

This process is in general identical with the corresponding process in the buffer (Section 3.5.4).

Handling in the PSAR

The process is included in a separate modelling task of between the tunnel plugs and the backfill (Grandia et al. 2010). The results can be applied to the borehole seals as well.

9.4.6 Alterations of accessory minerals

Overview

The bentonite material consists not only of montmorillonite, but also of accessory minerals. In the system under consideration, these can be dissolved and sometimes re-precipitated depending on the prevailing conditions.

The reactions relevant for the borehole seals are basically the same as those in the buffer (Section 3.5.6). However, there are a few differences in the significance of the processes.

- The temperature is lower and the thermal gradient in the borehole seal is small. Dissolution/ precipitation of minerals due to temperature effects are of minor importance in the seals.
- The total volume of bentonite in a seal is much less than in a deposition hole. Therefore the effects of changes in groundwater chemistry will be much faster.
- The borehole seals are not in direct contact with the deposition holes and changes in the porewater chemistry will not affect the barriers in the repository

The geochemical evolution of the bentonite part of the borehole seal will be equivalent to that of the bentonite buffer (see Section 3.5.6 on alteration of accessory minerals of the buffer system part), and therefore it can be used as analogue.

Handling in the PSAR

As described above, the geochemical evolution in the borehole seals will be of limited importance for the performance of the repository. The process is therefore neglected in the PSAR. (The results from the modelling geochemical evolution in the buffer can be used as an analogue).

9.4.7 Osmosis

Overview

See buffer Section 3.5.7

Osmosis is of importance only in the bentonite component of the borehole seals.

Handling in the PSAR

The salinity of the groundwater will affect the swelling pressure of the bentonite parts of the seals. This will be evaluated in the **Post-closure safety report** in a similar manner to the same process for the buffer, see buffer Section 3.5.7.

9.4.8 Montmorillonite transformation

Overview

Temperature, which is a main factor in montmorillonite transformation in nature, will be relatively low in the montmorillonite parts of the seals and no significant hydrothermal alteration is consequently expected. Possible threats are high pH solutions from cement, which may lead to dissolution of the montmorillonite, see buffer Section 3.5.8. However, the cement is supposed to be of low pH type.

Handling in the PSAR

The stability of the montmorillonite itself and the interaction between low-pH cement and bentonite is handled in the same way as for the buffer, see Section 3.5.8.

9.4.9 Montmorillonite colloid release

Overview

The process is the same as for the buffer (Section 3.5.11).

Handling in the PSAR

In the case of diluted waters, loss of bentonite from the borehole seal cannot be excluded. However, in the new Sandwich-concept the bentonite sections are placed in positions with intact rock and the risk from erosion should therefore be minimised. However, open boreholes will under all circumstances be treated as a case in the hydrogeological modelling.

9.4.10 Microbial processes

Overview

It is not foreseen that microbial processes can interfere with the seals in a way that will influence the performance of the neither the seal nor the repository.

Handling in the PSAR

Microbial processes in the borehole seal is not treated in the PSAR. Sulphate reducing bacteria could potentially affect the copper expanders, but since these have no intended performance after installation, the process can be neglected.

9.5 Radionuclide transport processes

9.5.1 Speciation of radionuclides

Overview

See corresponding process description for the buffer, Section 3.6.1

Handling in the PSAR

This process is indirectly handled through the selection of parameters for radionuclide transport in the rock. In general, the handling of the process is the same as for the corresponding process in the geosphere; see process Transport of radionuclides in the water phase in the **Geosphere process report**.

9.5.2 Transport of radionuclides in the water phase

Overview

If the borehole seals work as intended they do not have to be considered in the radionuclide transport calculations. If not, they are represented as a pipe with high hydraulic conductivity in the geosphere transport model.

Handling in the PSAR

The borehole seals are considered to be a part of the rock in the radionuclide transport calculations. See process Transport of radionuclides in the water phase in the **Geosphere process report**.

References

SKB's (Svensk Kärnbränslehantering AB) publications can be found at www.skb.com/publications. SKBdoc documents will be submitted upon request to document@skb.se, with the exception of internal documents.

References with abbreviated names

Backfill production report, 2022. Produktionsrapport Återfyllning. SKBdoc 1525864 ver 4.0, Svensk Kärnbränslehantering AB. (In Swedish.) (Internal document.)

Buffer production report, 2022. Produktionsrapport Buffert. SKBdoc 1392269 ver 5.0, Svensk Kärnbränslehantering AB. (In Swedish.) (Internal document.)

Canister production report, 2022. Produktionsrapport Kapsel. SKBdoc 1407944 ver 2.0, Svensk Kärnbränslehantering AB. (Internal document.)

Climate report, 2020. Post-closure safety for the final repository for spent nuclear fuel at Forsmark – Climate and climate related issues, PSAR version. SKB TR-20-12, Svensk Kärnbränslehantering AB.

Closure production report, 2022. Produktionsrapport Förslutning. SKBdoc 1387771 ver 3.0, Svensk Kärnbränslehantering AB. (In Swedish.) (Internal document.)

Data report, 2022. Post-closure safety for the final repository for spent nuclear fuel at Forsmark – Data report, PSAR version. SKB TR-21-06, Svensk Kärnbränslehantering AB.

Deposition tunnel plug production report, 2022. Produktionsrapport Valvplugg. SKBdoc 1562518 ver 3.0, Svensk Kärnbränslehantering AB. (In Swedish.) (Internal document.)

FEP report, 2010. FEP report for the safety assessment SR-Site. SKB TR-10-45, Svensk Kärnbränslehantering AB.

FHA report, 2010. Handling of future human actions in the safety assessment SR-Site. SKB TR-10-53, Svensk Kärnbränslehantering AB.

Fuel and canister process report, 2022. Post-closure safety for the final repository for spent nuclear fuel at Forsmark – Fuel and canister process report, PSAR version. SKB TR-21-02, Svensk Kärnbränslehantering AB.

Geosphere process report, 2022. Post-closure safety for the final repository for spent nuclear fuel at Forsmark – Geosphere process report, PSAR version. SKB TR-21-04, Svensk Kärnbränslehantering AB.

Model summary report, 2022. Post-closure safety for the final repository for spent nuclear fuel at Forsmark – Model summary report, PSAR version. SKB TR-21-05, Svensk Kärnbränslehantering AB.

Post-closure safety report, 2022. Post-closure safety for the final repository for spent nuclear fuel at Forsmark – Main report, PSAR version. SKB TR-21-01, Svensk Kärnbränslehantering AB.

Radionuclide transport report, 2022. Post-closure safety for the final repository for spent nuclear fuel at Forsmark – Radionuclide transport report, PSAR version. SKB TR-21-07, Svensk Kärnbränslehantering AB.

Spent fuel report, 2021. Använt kärnbränsle att hantera i KBS-3-systemet. SKBdoc 1380282 ver 3.0, Svensk Kärnbränslehantering AB. (In Swedish.) (Internal document.)

Regular references

Aagard P, Helgeson H C, 1983. Activity/composition relations among silicates in aqueous solution. II, Chemical and thermodynamic consequences of ideal mixing of atoms on homological sites in montmorillonites, illites, and mixed-layer clays. Clay and Clay Minerals 31, 207–217.

Abend S, Lagaly G, 2000. Sol–gel transitions of sodium montmorillonite dispersions. Applied Clay Science 16, 201–227.

Abercrombie H J, Hutcheon I E, Bloch J D, de Caritat P, 1994. Silica activity and the smectite-illite reaction. Geology 22, 539–542.

Ageskog L, Jansson P, 1999. Heat propagation in and around the deep repository. Thermal calculations applied to three hypoithetical sites: Aberg, Beberg and Ceberg. SKB TR-99-02, Svensk Kärnbränslehantering AB.

Alonso E, Gens A, Josa A, 1990. Constitutive model for partially saturated soils. Géotechnique 40, 405–430.

Alonso U, Missana T, García Gutiérrez M, Morejón J, Mingarro M, Fernández A M, 2019. CIEMAT studies within POSKBAR project. Bentonite expansion, sedimentation and erosion in artificial fractures. SKB TR-19-08, Svensk Kärnbränslehantering AB.

Alt-Epping P, Tournassat C, Rasouli P, Steefel C I, Mayer K U, Jenni A, Mäder U, Sengor S S, Fernández R, 2014. Benchmark reactive transport simulations of a column experiment in compacted bentonite with multispecies diffusion and explicit treatment of electrostatic effects. Computational Geosciences 19, 535–550.

Anastácio A S, Aouad A, Sellin P, Fabris J D, Bergaya F, Stucki J W, 2008. Characterization of a redox-modified clay mineral with respect to its suitability as a barrier in radioactive waste confinement. Applied Clay Science 39, 172–179.

Andersland O B, Ladanyi B, 1994. An introduction to frozen ground engineering. New York: Chapman & Hall.

Anderson D M, 1966. Phase composition of frozen montmorillonite-water mixtures from heat capacity measurements. Soil Science Society of America Journal 30, 670–675.

Anderson D M, Tice A R, 1972. Predicting unfrozen water contents in frozen soils from surface area measurements. Highway Research Record 393, 12–18.

Anderson D M, Tice A R, 1973. The unfrozen interfacial phase in frozen soil water systems. In Ecological studies: analysis and synthesis, vol 4. New York: Springer, 107–124.

Angeli M, Soldal M, Skurtveit E, Aker E, 2009. Experimental percolation of supercritical CO_2 through a caprock. Energy Procedia 1, 3351–3358.

Appelo C A J, 2013. A review of porosity and diffusion in bentonite. Posiva Working Report 2013-29, Posiva Oy, Finland.

Appelo C A J, Wersin P, 2007. Multicomponent diffusion modeling in clay systems with application to the diffusion of tritium, iodide and sodium in Opalinus Clay. Environmental Science & Technology 41, 5002–5007.

Arcos D, Bruno J, Benbow S, Takase H, 2000. Behaviour of bentonite accessory minerals during the thermal stage. SKB TR-00-06, Svensk Kärnbränslehantering AB.

Arcos D, Bruno J, Karnland O, 2003. Geochemical model of the granite–bentonite–groundwater interaction at Äspö HRL (LOT experiment). Applied Clay Science 23, 219–228.

Arcos D, Grandia F, Domènech C, 2006. Geochemical evolution of the near field of a KBS-3 repository. SKB TR-06-16, Svensk Kärnbränslehantering AB.

Arcos D, Grandia F, Domènech C, Fernádez A M, Villar M V, Muurinen A, Carlsson T, Sellin P, Hernán P, 2008. Long-term geochemical evolution of the near field repository: insights from reactive transport modelling and experimental evidences. Journal of Contaminant Hydrology 102, 196–209.

Arthur R, Zhou W, 2005. Reactive-transport model of buffer cementation. SKI Report 2005:59, Swedish Nuclear Power Inspectorate.

Atkinson A, 1985. The time dependence of pH within a repository for radioactive waste disposal. AERE Report R-11777, UKAEA.

Back P E, Wrafter J, Sundberg J, Rosén L, 2007. Thermal properties. Site descriptive modelling Forsmark – stage 2.2. SKB R-07-47, Svensk Kärnbränslehantering AB.

Baeyens B, Bradbury M H, 1997. A mechanistic description of Ni and Zn sorption on Na-montmorillonite. Part I: Titration and Sorption Measurements. Journal of Contaminant Hydrology 27, 199–222.

Baeyens B, Bradbury M H, 2004. Cation exchange capacity measurements on illite using the sodium and cesium isotope dilution technique: effects of the index cation, electrolyte concentration and competition: modeling, Clays and Clay Minerals 52, 421–431.

Baker A J, Lever D A, Rees J H, Thorne M C, Tweed C J, Wikramaratna R S, 1997. Nirex 97: An assessment of the post-closure performance of a deep waste repository at Sellafield. Volume 4: The gas pathway. Nirex Report S/97/012, UK Nirex Ltd.

Banwart S A, 1999. Reduction of iron(III) minerals by natural organic matter in groundwater. Geochimica et Cosmochimica Acta 63, 2919–2928.

Bengtsson A, Pedersen K, 2016. Microbial sulphate-reducing activity over load pressure and density in water saturated Boom Clay. Applied Clay Science 132–133, 542–551.

Bengtsson A, Pedersen K, 2017. Microbial sulphide-producing activity in water saturated Wyoming MX-80, Asha and Calcigel bentonites at wet densities from 1500 to 2000 kg m^{-3}. Applied Clay Science 137, 203–212.

Bengtsson A, Edlund J, Hallbeck B, Heed C, Pedersen K, 2015. Microbial sulphide-producing activity in MX-80 bentonite at 1750 and 2000 kg m^{-3} wet density. SKB R-15-05, Svensk Kärnbränslehantering AB.

Bengtsson A, Blom A, Hallbeck B, Heed C, Johansson L, Stahlén J, Pedersen K, 2017a. Microbial sulphide-producing activity in water saturated MX-80, Asha and Calcigel bentonite at wet densities from 1500 to 2000 kg m^{-3}. SKB TR-16-09, Svensk Kärnbränslehantering AB.

Bengtsson A, Blom A, Johansson L, Taborowski T, Eriksson L, Pedersen K, 2017b. Bacterial sulphide-producing activity in water saturated iron-rich Rokle and iron-poor Gaomiaozi bentonite at wet densities from 1750 to 1950 kg m^{-3}. SKB TR-17-05, Svensk Kärnbränslehantering AB.

Bengtsson A, Blom A, Taborowski T, Schippers A, Edlund J, Pedersen K, 2017c. FEBEX-DP: Microbiological report. Arbeitsbericht NAB 16-015, Nagra, Switzerland.

Bergaya F, Theng B K G, Lagaly G (eds), 2006. Handbook of clay science. Amsterdam: Elsevier. (Developments in clay science 1)

Bildstein O, Claret F, 2015. Stability of clay barriers under chemical perturbations. In Tournassat C, Steefel C I, Bourg I C, Bergaya F (eds). Amsterdam: Elsevier. (Developments in clay science 6), 155–188.

Birgersson M, 2017. A general framework for ion equilibrium calculations in compacted bentonite. Geochimica et Cosmochimica Acta 200, 186–200.

Birgersson M, Goudarzi R, 2013. Studies of vapor transport from buffer to tunnel backfill (Sauna effects). SKB R-13-42, Svensk Kärnbränslehantering AB.

Birgersson M, Goudarzi R, 2016. Vapor transport and sealing capacity of buffer slots (“sauna” effects). SKB TR-15-09, Svensk Kärnbränslehantering AB.

Birgersson M, Goudarzi R, 2017. Summary report on “sauna” effects. SKB TR-17-07, Svensk Kärnbränslehantering AB.

Birgersson M, Goudarzi R, 2018. Investigations of gas evolution in an unsaturated KBS-3 repository. SKB TR-18-11, Svensk Kärnbränslehantering AB.

Birgersson M, Karnland O, 2009. Ion equilibrium between montmorillonite interlayer space and an external solution – Consequences for diffusional transport. Geochimica et Cosmochimica Acta 73, 1908–1923.

Birgersson M, Karnland O, 2015. Flow and pressure response in compacted bentonite due to external fluid pressure. SKB TR-14-28, Svensk Kärnbränslehantering AB.

Birgersson M, Karnland O, Nilsson U, 2008. Freezing in saturated bentonite – a thermodynamic approach. Physics and Chemistry of the Earth, Parts A/B/C 33, S527–S530.

Birgersson M, Börgesson L, Hedström M, Karnland O, Nilsson U, 2009. Bentonite erosion. Final report. SKB TR-09-34, Svensk Kärnbränslehantering AB.

Birgersson M, Karnland O, Nilsson U, 2010. Freezing of bentonite. Experimental studies and theoretical considerations. SKB TR-10-40, Svensk Kärnbränslehantering AB.

Birgersson M, Hedström M, Karnland O, 2011. Sol formation ability of Ca/Na-montmorillonite at low ionic strength. Physics and Chemistry of the Earth, Parts A/B/C 36, 1572–1579.

Birgersson M, Hedström M, Karnland O, Sjöland A, 2017. Bentonite buffer: macroscopic performance from nanoscale properties. In Apted M J, Ahm J (eds). Geological repository systems for safe disposal of spent nuclear fuels and radioactive waste. 2nd ed. Woodhead Publishing, 319–364.

Boles J R, Franks S G, 1979. Clay diagenesis in Wilcox sandstones of southwest Texas: implication of smectite diagenesis on sandstone cementation. Journal of Sedimentary Research 49, 55–70.

Bourg I C, Sposito G, Bourg A C M, 2006. Tracer diffusion in compacted, water-saturated bentonite. Clays and Clay Minerals 54, 363–374.

Bradbury M H, Baeyens B, 1997. A mechanistic description of Ni and Zn sorption on Na-montmorillonite. Part II: modelling. Journal of Contaminant Hydrology 27, 223–248.

Bradbury M H, Baeyens B, 1999. Modelling the sorption of Zn and Ni on Ca-montmorillonite. Geochimica et Cosmochimica Acta 63, 325–336.

Bradbury M H, Baeyens B, 2003. Near-field sorption data bases for compacted MX-80 bentonite for performance assessment of a high-level radioactive waste repository in Opalinus clay host rock. Nagra Technical Report NTB 02-18, Nagra, Switzerland.

Bradbury M H, Baeyens B, 2005. Modelling the sorption of Mn(II), Co(II), Ni(II), Zn(II), Cd(II), Eu(III), Am(III), Sn(IV), Th(IV), Np(V) and U(VI) on montmorillonite: Linear free energy relationships and estimates of surface binding constants for some selected heavy metals and actinides. Geochimica et Cosmochimica Acta 69, 875–892.

Bruno J, Arcos D, Duro L, 1999. Processes and features affecting the near field hydrochemistry. Groundwater-bentonite interaction. SKB TR-99-29, Svensk Kärnbränslehantering AB.

Brusewitz A M, 1986. Chemical and physical properties of paleozoic potassium bentonites from Kinnekulle, Sweden. Clays and Clay Minerals 34, 442–454.

Burst J F, 1969. Diagenesis of Gulf Coast clayey sediments and its possible reaction to petroleum migration. AAPG Bulletin 53, 73–93.

Börgesson L, 2019. Loads of the canister caused by uneven swelling pressure from the buffer. SKBdoc 1577755 ver 1.0, Svensk Kärnbränslehantering AB.

Börgesson L, Hernelind J, 2009. Mechanical interaction buffer/backfill. Finite element calculations of the upward swelling of the buffer against both dry and saturated backfill. SKB R-09-42, Svensk Kärnbränslehantering AB.

Börgesson L Hernelind J, 2017. Modelling of the mechanical interaction between the buffer and the backfill in KBS-3V. Modelling results 2015. SKB TR-16-08, Svensk Kärnbränslehantering AB.

Börgesson L, Sandén T, 2006. Piping and erosion in buffer and backfill materials. Current knowledge. SKB R-06-80, Svensk Kärnbränslehantering AB.

Börgesson L, Fredrikson A, Johannesson L-E, 1994. Heat conductivity of buffer materials. SKB TR 94-29, Svensk Kärnbränslehantering AB.

Börgesson L, Johannesson L-E, Sandén T, Hernelind J, 1995. Modelling of the physical behaviour of water saturated clay barriers. Laboratory tests, material models and finite element application. SKB TR 95-20, Svensk Kärnbränslehantering AB.

Börgesson L, Johannesson L-E, Raiko H, 2009. Uneven swelling pressure on the canister simplified load cases derived from uneven wetting, rock contours and buffer density distribution. SKBdoc 1206894 ver 1.0, Svensk Kärnbränslehantering AB.

Börgesson L, Sandén T, Dueck A, Andersson L, Jensen V, Nilsson U, Olsson S, Åkesson M, Kristensson O, Svensson U, 2015. Consequences of water inflow and early water uptake in deposition holes. EVA project. SKB TR-14-22, Svensk Kärnbränslehantering AB.

Börgesson L, Åkesson M, Kristensson O, Dueck A, Hernelind J, 2016. EBS TF – THM modelling. BM 2 – Large scale field tests. SKB TR-13-07, Svensk Kärnbränslehantering AB.

Börgesson L, Hedström M, Birgesson M, Karnland O, 2018. Bentonite swelling into fractures at conditions above the critical coagulation concentration. SKB TR-17-11, Svensk Kärnbränslehantering AB.

Börgesson L, Åkesson M, Hernelind J, 2020a. EBS TF – THM modelling. Homogenisation task. SKB P-18-05, Svensk Kärnbränslehantering AB.

Börgesson L, Hernelind J, Åkesson M, 2020b. Assessment of the formation of a cavity after the loss of bentonite. SKB TR-20-13, Svensk Kärnbränslehantering AB.

Cai M, Kaiser P K, Tasaka Y, Maejima T, Morioka H, Minami M, 2004. Generalized crack initiation and crack damage stress thresholds of brittle rock masses near underground excavations. International Journal of Rock Mechanics & Mining Sciences 41, 833–847.

Carlson L, Karnland O, Oversby V M, Rance A P, Smart N R, Snellman M, Vähänen M, Werme L O, 2007. Experimental studies of the interactions between anaerobically corroding iron and bentonite. Physics and Chemistry of the Earth, Parts A/B/C 32, 334–345.

Chatterji S, 2004. Ionic diffusion through thick matrices of charged particles. Journal of Colloid and Interface Science 269, 186–191.

Cho W J, Lee J O, Chun K S, 1999. The temperature effects on hydraulic conductivity of compacted bentonite. Applied Clay Science 14, 47–58.

CIMNE, 2002. Code Bright. Ver 2.2. User's manual. Departamento Ingenería del Terreno, Cartográfica y Geofísica, Universitat Politècnica de Catalunya, Barcelona.

Claesson J, Probert T, 1996. Temperature field due to time-dependent heat sources in a large rectangular grid. I. Derivation of analytical solution. SKB TR 96-12, Svensk Kärnbränslehantering AB.

Clayton C J, Hay S J, 1994. Gas migration mechanisms from accumulation to surface. Bulletin of the Geological Society of Denmark 41, 12–23.

Colten-Bradley V A, 1987. Role of pressure in smectite dehydration: effects on geopressure and smectite-to-illite transformation. AAPG Bulletin 71, 1414–1427.

Coutoure R A, 1985. Steam rapidly reduces the swelling capacity of bentonite. Nature 318, 50–52.

Cui D, Eriksen T E, 1995. Reversibility of strontium sorption on fracture fillings. In Murakami T, Ewing R C (eds). Scientific basis for nuclear waste management XVIII: symposium held in Kyoto, Japan, 23–27 October 1994. Pittsburgh, PA: Materials Research Society. (Materials Research Society Symposium Proceedings 353), 1045–1052.

Cuss R J, Harrington F J, Noy D J, 2010. Large scale gas injection test (Lasgit) performed at the Äspö Hard Rock Laboratory. Summary report 2008. SKB TR-10-38, Svensk Kärnbränslehantering AB.

Cuss R J, Harrington F J, Tamayo-Mas E, Noy D J, Birchall D J, Sellin P, Nord M, 2022. Large scale gas injection test (Lasgit) performed at the Äspö Hard Rock Laboratory. Final report. SKB TR-22-06, Svensk Kärnbränslehantering AB.

de Groot S R, Mazur P, 1984. Non-equilibrium thermodynamics. New York: Dover.

Degueldre C, Pfeiffer H-R, Alexander W, Wernli B, Bruetsch R, 1996. Colloid properties in granitic groundwater systems. I: Sampling and characterisation. Applied Geochemistry 11, 677–695.

Derjaguin B, Landau L, 1941. Theory of the stability of strongly charged lyophobic soils and of the adhesion of strongly charged particles in solutions of electrolytes. Acta Physicochimica URSS 14, 633–662.

Dixon D, 2019. Review of the T-H-M-C properties of MX-80 bentonite. NWMO-TR-2019-07, Nuclear Waste Management Organization, Canada.

Dixon D A, Graham J, Gray M N, 1999. Hydraulic conductivity of clays in confined tests under low hydraulic gradients. Canadian Geotechnical Journal 36, 815–825.

Domènech C, Arcos D, Bruno J, Karnland O, Muurinen A, 2004. Geochemical model of the granite-bentonite-groundwater at Äspö (LOT experiment). In Oversby V M, Werme L O (eds). Scientific basis for nuclear waste management XXVII: symposium held in Kalmar, Sweden, 15–19 June 2003. Warrendale, PA: Materials Research Society. (Materials Research Society Symposium Proceedings 807), 855–860.

Dong H L, 2012. Clay-microbe interactions andimplications for environmental mitigation. Elements 8, 113–118.

Donnan F G Z, 1911. Theorie der Membrangleichgewichte und Membranpotentiale bei Vorhandensein von mcht dialysierenden Elektrolyten. Ein Beitrag zur physikalisch-chemischen Physiologie. Zeitschrift für Elektrochemie 17, 572–581.

Donohew A T, Horseman S T, Harrington J F, 2000. Gas entry into unconfined clay pastes between the liquid and plastic limits. Chapter 18. In Cotter-Howells J D, Campbell L S, Valsami-Jones E, Batchelder M (eds). Environmental mineralogy: microbial interactions, anthropogenic influences, contaminated land and waste management. London: Mineralogical Society, 369–394.

Dueck A, 2004. Hydro-mechanical properties of a water unsaturated sodium bentonite: laboratory study and theoretical interpretation. PhD thesis. Lund University, Sweden.

Dueck A, 2010. Thermo-mechanical cementation effects in bentonite investigated by unconfined compression tests. SKB TR-10-41, Svensk Kärnbränslehantering AB.

Dueck A, Börgesson L, 2021. Bentonite homogenisation. Three studies based on laboratory test results. SKB P-21-05, Svensk Kärnbränslehantering AB.

Dueck A, Nilsson U, 2010. Thermo-hydro-mechanical properties of MX-80. Results from advanced laboratory tests. SKB TR-10-55, Svensk Kärnbränslehantering AB.

Dueck A, Johannesson L-E, Kristensson O, Olsson S, 2011a. Report on hydro-mechanical and chemical-mineralogical analyses of the bentonite buffer in Canister Retrieval Test. SKB TR-11-07, Svensk Kärnbränslehantering AB.

Dueck A, Goudarzi R, Börgesson L, 2011b. Buffer homogenisation, status report. SKB TR-12-02, Svensk Kärnbränslehantering AB.

Dueck A, Goudarzi R, Börgesson L, 2014. Buffer homogenisation, status report 2. SKB TR-14-25, Svensk Kärnbränslehantering AB.

Dueck A, Goudarzi R, Börgesson L, 2016. Buffer homogenisation, status report 3. SKB TR-16-04, Svensk Kärnbränslehantering AB.

Dueck A, Goudarzi R, Börgesson L, 2018. Buffer homogenisation, status report 4. SKB TR-17-04, Svensk Kärnbränslehantering AB.

Dueck A, Börgesson L, Kristensson O, Malmberg D, Åkesson M, Hernelind J, 2019. Bentonite homogenisation. Laboratory study, model development and modelling of homogenisation processes. SKB TR-19-11, Svensk Kärnbränslehantering AB.

Dueck A, Goudarzi R, Jensen V, Börgesson L, 2022a. Buffer homogenisation – status report 5. SKB TR-21-14, Svensk Kärnbränslehantering AB

Dueck A, Nilsson U, Jensen V, Börgesson L, 2022b. Compressive strength of bentonites. Factors influencing results from unconfined compression tests. SKB TR-21-13, Svensk Kärnbränslehantering AB.

Duro L, Altmaier M, Holt E, Mäder U, Claret F, Grambow B, Idiart A, Valls A, Montoya V, 2020. Contribution of the results of the CEBAMA project to decrease uncertainties in the Safety Case and Performance Assessment of radioactive waste repositories. Applied Geochemistry 112, 104479. doi:10.1016/j.apgeochem.2019.104479

Durrant C B, Begg J D, Kersting A B, Zavarin M, 2018. Cesium sorption reversibility and kinetics on illite, montmorillonite, and kaolinite. Science of the Total Environment 610–611, 511–520.

Dvinskikh S V, Szutkowski K, Furó I, 2009. MRI profiles over very wide concentration ranges: application to swelling of a bentonite clay. Journal of Magnetic Resonance 198, 146–150.

Dzombak D A, Morel F M M, 1990. Surface complexation modelling: hydrous ferric oxide. New York: Wiley.

Eberl D, Hower J, 1976. Kinetics of illite formation. Geological Society of America Bulletin 87, 1326–1330.

Eriksen T E, Jansson M, 1996. Diffusion of I^-, Cs^+ and $Sr2^+$ in compacted bentonite. Anion exclusion and surface diffusion. SKB TR 96-16, Svensk Kärnbränslehantering AB.

Eriksson P, 2019. Development of thermo-hydraulic model for pellet fillings. SKB P-19-12, Svensk Kärnbränslehantering AB.

Eriksson P, 2020. Hållfasthetskrav på återfyllnadsblock för att klara buffertuppsvällning. SKBdoc 1906167 ver 1.0, Svensk Kärnbränslehantering AB. (In Swedish.)

Eriksson P, Hedin A, 2019. Modelling of sulphide fluxes in unsaturated buffer and backfill for a KBS-3 repository. SKBdoc 1696975 ver 2.0, Svensk Kärnbränslehantering AB.

Eriksson S, 2007. Äspö Hard Rock Laboratory. Prototype repository. Analysis of microorganisms, gases, and chemistry in buffer and backfill, 2004–2007. SKB IPR-08-01, Svensk Kärnbränslehantering AB.

Essén S A, Johnsson A, Bylund D, Pedersen K, Lundström U S, 2007. Siderophore production by Pseudomonas stutzeri under aerobic and anaerobic conditions. Applied and Environmental Microbiology, 73, 5857–5864.

Evans D F, Wennerström H, 1999. The colloidal domain: where physics, chemistry, biology, and technology meet. 2nd ed. New York: Wiley-WCH.

Favre F, Tessier D, Abdelmoula M, Génin J M, Gates W P, Boivin P, 2002. Iron reduction and changes in cation exchange capacity in intermittently watterlogged soil. European Journal of Soil Science 53, 175–183.

Fernández A M, Marco J F, Nieto P, León F J, Robredo L M, Clavero M Á, Cardona A I, Fernández S, Svensson D, Sellin P, 2022. Characterization of bentonites from the in situ ABM5 Heater Experiment at Äspö Hard Rock Laboratory, Sweden. Minerals 12, 471.

Fourdrin C, Allard T, Monnet I, Menguy N, Benedetti M, Calas A, 2010. Effect of radiation-induced amorphization on smectite dissolution. Environmental Science & Technology 44, 2509–2514.

Fransson Å, Åkesson M, Andersson L, 2017. Bentonite Rock Interaction Experiment. Characterization of rock and installation, hydration and dismantling of bentonite parcels. SKB R-14-11, Svensk Kärnbränslehantering AB.

Fritz B, Kam M, Tardy Y, 1984. Geochemical simulation of the evolution of granitic rocks and clay minerals submitted to a temperature increase in the vicinity of a repository for spent nuclear fuel. KBS TR 84-10, Svensk Kärnbränslehantering AB.

Fuentes-Cantillana J L, García-Siñeriz J L, 2000. FEBEX: Full-scale engineered barriers experiment for a deep geological repository for high-level radioactive waste in crytalline host rock: Final report. Publicación tecnica 1/2000, ENRESA, Spain.

Galíndez J M, Molinero J, 2010. Assessment of the long-term stability of cementitious barriers of radioactive waste repositories by using digital-image-based microstructure generation and reactive transport modeling. Cement and Concrete Research 40, 1278–1289.

Gaucher E C, Blanc P, Matray J-M, Michau N, 2004. Modeling diffusion of an alkaline plume in a clay barrier. Applied Geochemistry 19, 1505–1515.

Geier J, Thatcher K E, Newson R K, Benbow S J, Dessirier B, 2018. Research on resaturation of bentonite buffer. SSM Report 2018:21, Swedish Radiation Safety Authority.

Gimmi T, Kosakowski G, 2011. How mobile are sorbed cations in clays and clay rocks? Environmental Science & Technology 45, 1443–1449.

Giroud N, Tomonaga Y, Wersin P, Briggs S, King F, Vogt T, Diomidis N, 2018. On the fate of oxygen in a spent fuel emplacement drift in Opalinus Clay. Applied Geochemistry 97, 270–278.

Glaus M A, Frick S, Rossé R, Van Loon L R, 2010. Comparative study of tracer diffusion of HTO, $^{22}Na^{+}$ and $^{36}Cl^{-}$ in compacted kaolinite, illite and montmorillonite. Geochimica et Cosmochimica Acta 74, 1999–2010.

Glaus M A, Birgersson M, Karnland O, Van Loon L, 2013. Seeming steady-state uphill diffusion of $^{22}Na^{+}$ in compacted montmorillonite. Environmental Science & Technology 47, 11522–11527.

Glaus M A, Aertsens A, Appelo C A J, Kupcik T, Maes N, Van Laer L, Van Loon L R, 2015. Cation diffusion in the electrical double layer enhances the mass transfer rates for Sr^{2+}, Co^{2+} and Zn^{2+} in compacted illite. Geochimica et Cosmochimica Acta 165, 376–388.

Goudarzi R, Börgesson L, Röshoff K, Bono N, 2003a. Äspö Hard Rock Laboratory. Canister Retrieval Test. Sensors data report (period 001026–030501). Report No:6. SKB IPR-03-30, Svensk Kärnbränslehantering AB.

Goudarzi R, Åkesson M, Hökmark, 2008. Äspö Hard Rock Laboratory. Temperature Buffer Test. Sensors data report (period 030326–080101). Report No:11. SKB IPR-08-16, Svensk Kärnbränslehantering AB.

Graham C C, Harrington J F, Cuss R J, Sellin P, 2012. Gas migration experiments in bentonite: implications for numerical modelling. Mineralogical Magazine 76, 3279–3292.

Grahm P, Malm R, Eriksson D, 2015. System design and full-scale testing of the Dome Plug for KBS-3V deposition tunnels. Main report. SKB TR-14-23, Svensk Kärnbränslehantering AB.

Grandia F, Galíndez J-M, Molinero J, Arcos D, 2010. Evaluation of low-pH cement degradation in tunnel plugs and bottom plate systems in the frame of SR-Site. SKB TR-10-62, Svensk Kärnbränslehantering AB.

Greene-Kelly R, 1953. Irreversible dehydration of montmorillonite. Part II. Clay Mineral Bulletin 2, 52–56.

Grütter A. von Gunten H.R, Kohler M, Rössler E, 1990. Sorption, desorption and exchange of cesium on glaciofluvial deposits. Radiochimica Acta 50, 177–184.

Gu B X, Wang L M, Minc L D, Ewing R C, 2001. Temperature effects on the radiation stability and ion exchange capacity of smectites. Journal of Nuclear Materials 297, 345–354.

Guldbrand L, Jönsson B, Wennerström H, Linse P, 1984. Electrical doube-layer forces. A Monte Carlo study. Journal of Chemical Physics 80, 2221–2228.

Hallbeck L, Pedersen K, 2008. Characterization of microbial processes in deep aquifers of the Fennoscandian Shield. Applied Geochemistry 23, 1796–1819.

Hansbo S, 1960. Consolidation of clay, with special reference to influence of vertical drains: a study made in connection with full-scale investigations at Skå-Edeby. PhD thesis. Chalmers University of Technology, Sweden.

Harrington J F, Horseman S T, 2003. Gas migration in KBS-3 buffer bentonite. Sensitivity of test parameters to experimental boundary conditions. SKB TR-03-02, Svensk Kärnbränslehantering AB.

Harrington J F, Noy D J, Horseman S T, Birchall J D, Chadwick R A, 2009. Laboratory study of gas and water flow in the Nordland Shale, Sleipner, North Sea. In Grobe M, Pashin J C, Dodge R L (eds). Carbon dioxide sequestration in geological media: state of the science: AAPG. (Studies in Geology 59), 521–543.

Harrington J F, de La Vaissière, Noy D J, Cuss R J, Talandier J, 2012. Gas flow in Callovo-Oxfordian claystone (COx): results from laboratory and field-scale measurements. Mineralogical Magazine 76, 3303–3318.

Hartikainen J, 2004. Estimation of permafrost depth at Forsmark. TKK-RM-04-05. Helsinki University of Technology, Finland.

Hartog N, van Bergen P F, de Leeuw J W, Griffioen J, 2004. Reactivity of organic matter in aquifer sediments: geological and geochemical controls. Geochimica et Cosmochimica Acta 68, 1281–1292.

Haveman S A, Pedersen K, 2002. Distribution of culturable anaerobic microorganisms in Fennoscandian shield groundwater. FEMS Microbiology Ecology 39, 129–137.

Haynes H M, Nixon S, Lloyd J R, Birgersson M 2019. Verification of microbial sulfide-producing activity in Calcigel bentonite at saturated densities of 1750 and 1900 kg m^{-3}. SKB P-19-07, Svensk Kärnbränslehantering AB.

Hedin A, 2004. Integrated near-field evolution model for an KBS-3 repository. SKB R-04-36, Svensk Kärnbränslehantering AB.

Hedström M, Birgersson M, Nilsson U, Karnland O, 2011. Role of cation mixing in the sol formation of Ca/Na-montmorillonite. Physics and Chemistry of the Earth, Parts A/B/C 36, 1564–1571.

Hedström M, Ekvy Hansen E, Nilsson U, 2016. Montmorillonite phase behaviour. Relevance for buffer erosion in dilute groundwater. SKB TR-15-07, Svensk Kärnbränslehantering AB.

Henry C, Boisson J-Y, Bouchet A, Meunier A, 2007. Thermally induced mineral and chemical transformations in calcareous mudstones around a basaltic dyke (Perthus Pass, southern Massif Central, France). Possible implications as a natural analogue of nuclear waste disposal. Clay Minerals 42, 213–231.

Hernelind J, 2010. Modelling and analysis of canister and buffer for earthquake induced rock shear and glacial load. SKB TR-10-34, Svensk Kärnbränslehantering AB.

Hetzel F, Doner H E, 1993. Some colloidal properties of beidellite: comparison with low and high charge montmorillonite. Clays and Clay Minerals 41, 453–460.

Holmboe M, Wold S, Jonsson M, 2010. Colloid diffusion in compacted bentonite: microstructural constraints. Clays and Clay Minerals 58, 532–541.

Holmboe M, Wold S, Jonsson M, 2012. Porosity investigation of compacted bentonite using XRD profile modeling. Journal of Contaminant Hydrology 128, 19–32.

Horseman S T, Harrington J F, Sellin P, 1999. Gas migration in clay barriers. Engineering Geology 54, 139–149.

Hower J, Mowatt T C, 1966. The mineralogy of illites and mixed-layer illite/montmorillonites. American Mineralogist 51, 825–854.

Hower J, Elsinger E V, Hower M E, Perry E A, 1976. Mechanism of burial metamorphism of argillaceous sediment: 1. Mineralogical and chemical evidence. Geological Society of America Bulletin 87, 725–737.

Huang W-H, Chen W-C, 2004. Swelling behavior of a potential buffer material under simulated near field environment. Journal of Nuclear Science and Technology 41, 1271–1279.

Huang W-L, Longo J M, Pevear D R, 1993. An experimentally derived kinetic model for smectite-to-illite conversion and its use as a geothermometer. Clays and Clay Minerals 41, 162–177.

Huertas F, Fuentes-Cantilliana J L, Rivas F, Linares J, Farina P, Jockwer N, Kickmaier W, Martinet M A, Samper J, Alonso E, Elorza F S, 2000. Full scale engineered barriers experiment for a high level radioactive waste in crystalline host rock (FEBEX project): final report. EUR 1914, European Commission.

Huertas F J, Rozalen M L, Garcia-Palma S, Iriarte I, Linares J, 2005. Dissolution kinetics of bentonite under alkaline conditions. In: Michau N (ed). ECOCLAY II: effects of cement on clay barrier performance – phase II. EUR 21921, European Commission.

Hökmark H, Claesson J, 2005. Use of an analytical solution for calculating temperatures in repository host rock. Engineering Geology 81, 353–364.

Hökmark H, Fälth B, 2003. Thermal dimensioning of the deep repository. Influence of canister spacing, canister power, rock thermal properties and nearfield design on the maximum canister surface temperature. SKB TR-03-09, Svensk Kärnbränslehantering AB.

Hökmark H, Karnland O, Pusch R, 1997. A technique for modeling transport/conversion processes applied to smectite-to-illite conversion in HLW buffers. Engineering Geology 47, 367–378.

Hökmark H, Lönnqvist M, Kristensson O, Sundberg J, Hellström G, 2009. Strategy for thermal dimensioning of the final repository for spent nuclear fuel. SKB R-09-04, Svensk Kärnbränslehantering AB.

Hökmark H, Lönnqvist M, Fälth B, 2010. THM-issues in repository rock. Thermal, mechanical, thermo-mechanical and hydro-mechanical evolution of the rock at the Forsmark and Laxemar sites. SKB TR-10-23, Svensk Kärnbränslehantering AB.

Idiart A, Coene E, 2019. Modelling diffusion through compacted bentonite in the BHA vault. Report for the safety evaluation SE-SFL. SKB R-19-10, Svensk Kärnbränslehantering AB.

Idiart A, Pękala M, 2016. Models for diffusion in compacted bentonite. SKB TR-15-06, Svensk Kärnbränslehantering AB.

Idiart A, Laviña M, Kosakowski G, Cochepin B, Meeussen J, Samper J, Mon A, Montoya V, Munier I, Poonoosamy J, Montenegro L, Deissmann G, Rohmen S, Damiani L, Coene E, Naves A, 2020. Reactive transport modelling of a low-pH concrete / clay interface. Applied Geochemistry 115, 104562. doi:10.1016/j.apgeochem.2020.104562

Jakobsen R, Cold L, 2007. Geochemistry at the sulfate reduction–methanogenesis transition zone in an anoxic aquifer – a partial equilibrium interpretation using 2D reactive transport modeling. Geochimica et Cosmochimica Acta 71, 1949–1966.

Jakobsen R, Postma D, 1999. Redox zoning, rates of sulfate reduction and interactions with Fe-reduction and methanogenesis in a shallow sandy aquifer, Rømø, Denmark. Geochimica et Cosmochimica Acta 63, 137–151.

Johannesson L-E, Sandén T, Dueck A, Ohlsson L, 2010. Characterization of a backfill candidate material, IBECO-RWC-BF. Baclo Project – Phase 3. SKB R-10-44, Svensk Kärnbränslehantering AB.

Johannesson L-E, Kristensson O, Åkesson M, Eriksson P, Hedin M, 2014. Tests and simulations of THM processes relevant for the buffer installation. SKB P-14-22, Svensk Kärnbränslehantering AB.

Johnsson A, Arlinger J, Pedersen K, Ödegaard-Jensen A, Albinsson Y, 2006. Solid-aqueous phase partitioning of radionuclides by complexing compounds excreted by subsurface bacteria. Geomicrobiology Journal 23, 621–630.

Joyce S, Simpson T, Hartley L, Applegate D, Hoek J, Jackson P, Swan D, Marsic N, Follin S, 2010. Groundwater flow modelling of periods with temperate climate conditions – Forsmark. SKB R-09-20, Svensk Kärnbränslehantering AB.

Joyce S, Swan D, Harley L, 2013. Calculation of open repository inflows for Forsmark. SKB R-13-21, Svensk Kärnbränslehantering AB.

Judd A G, Sim R H, 1998. Shallow gas migration mechanisms in deep water sediments. In Ardus D A, Hobbs R, Horsnell M, Jardine R, Long D, Sommerville J (eds). Offshore site investigation and foundation behaviour ’98: New Frontiers: proceedings of an International Conference, London, 22–24 September 1998. London: Society of Underwater Technology, 163–174.

Kahn A, 1958. The flocculation of sodium montmorillonite by electrolytes. Journal of Colloid Science 13, 51–60.

Kalinowski B E, Oskarsson A, Albinsson Y, Arlinger J, Ödegaard-Jensen A, Andlid T, Pedersen K, 2004. Microbial leaching of uranium and other trace elements from shale mine tailings at Ranstad. Geoderma 122, 177–194.

Kalinowski B E, Johnsson A, Arlinger J, Pedersen K, Ödegaard-Jensen A, Edberg F, 2006. Microbial mobilization of uranium from shale mine waste. Geomicrobiology Journal 23, 157–164.

Karnland O, 1997. Bentonite swelling pressure in strong NaCl solutions. Correlation between model calculation and experimentally determined data. SKB TR 97-31, Svensk Kärnbränslehantering AB.

Karnland O, Birgersson M, 2006. Montmorillonite stability. With special respect to KBS-3 conditions. SKB TR-06-11, Svensk Kärnbränslehantering AB.

Karnland O, Sandén T, Johannesson L-E, Eriksen T E, Jansson M, Wold S, Pedersen K, Motamedi M, Rosborg B, 2000. Long term test of buffer material. Final report on the pilot parcels. SKB TR-00-22, Svensk Kärnbränslehantering AB.

Karnland O, Muurinen A, Karlsson F, 2005. Bentonite swelling pressure in NaCl solutions – experimentally determined data and model calculations. In Alonso E, Ledesma A (eds). Advances in understanding engineered clay barriers: proceedings of the International Symposium on Large Scale Field Tests in Granite, Sitges, Barcelona, 12–14 November 2003. London: Taylor & Francis Group, 241–256.

Karnland O, Olsson S, Nilsson U, 2006. Mineralogy and sealing properties of various bentonites and smectite-rich clay material. SKB TR-06-30, Svensk Kärnbränslehantering AB.

Karnland O, Olsson S, Nilsson U, Sellin P, 2007. Experimentally determined swelling pressure and geochemical interactions of compacted Wyoming bentonite with highly alkaline solutions. Physics and Chemistry of the Earth, Parts A/B/C 32, 275–286.

Karnland O, Olsson S, Dueck A, Birgersson M, Nilsson U, Hernan-Håkansson T, Pedersen K, Nilsson S, Eriksen T E, Rosborg B, 2009. Long term test of buffer material at the Äspö Hard Rock Laboratory, LOT project. Final report on the A2 test parcel. SKB TR-09-29, Svensk Kärnbränslehantering AB.

Kato H, Muroi M, Yamada N, Ishida H, Sato H, 1995. Estimation of effective diffusivity in compacted bentonite. In Murakami T, Ewing R C (eds). Scientific basis for nuclear waste management XVIII: symposium held in Kyoto, Japan, 23–27 October 1994. Pittsburgh, Pa.: Materials Research Society. (Materials Research Society Symposium Proceedings 353), 277–284.

Kaufhold S, Dohrmann R, Sandén T, Sellin P, Svensson D, 2013. Mineralogical investigations of the alternative buffer material test – I. Alteration of bentonites. Clay Minerals 48, 199–213.

Kaufhold S, Dohrmann R, Götze N, Svensson D, 2017. Characterisation of the second package of the alternative buffer material experiment (ABM) – I. Mineralogical reactions. Clays and Clay Minerals 65, 27–41.

Kaufhold S, Dohrmann R, Ufer K, Svensson D, Sellin P, 2021. Mineralogical analysis of bentonite from the ABM5 Heater Experiment at Äspö Hard Rock Laboratory, Sweden. Minerals 11, 669.

Khaled E M, Stucki J W, 1991. Iron oxidation state effects on cation fixation in smectites. Soil Science Society of America Journal 55, 550–554.

Kim J, Dong H, Seabaugh J, Newell S W, Eberl D D, 2004. Role of microbes in the smectite-to-illite reaction. Science 303, 830–832.

King F, Ahonen L, Taxén C, Vuorinen U, Werme L, 2001. Copper corrosion under expected conditions in a deep geologic repository. SKB TR-01-23, Svensk Kärnbränslehantering AB.

Kjellander R, Marčelja S, 1984. Correlation and image charge effects in electric double layers. Chemical Physical Letters 112, 49–53.

Kjellander R, Marčelja S, Quirk J P, 1988. Attractive double-layer interactions between calcium clay particles. Journal of Colloid and Interface Science 126, 194–211.

Klein C, Hurlbut C S, 1998. Manual of mineralogy. 21st ed. New York: Wiley.

Knutsson S, 1983. On the thermal conductivity and thermal diffusivity of highly compacted bentonite. SKB TR 83-72, Svensk Kärnbränslehantering AB.

Kodama H, 1966. The nature of the component layers in rectorite. American Mineralogist 51, 1035–1055.

Kozaki T, Saito N, Fujishima A, Sato S, Ohashi H, 1998. Activation energy for diffusion of chloride ions in compacted sodium montmorillonite. Journal of Contaminant Hydrology 35, 67–75.

Kristensson O, Hökmark H, 2010. Äspö Hard Rock Laboratory. Prototype Repository. THM modelling of the bentonite buffer. Canister mid-height 1-D radial models, holes #1 and #3. SKB IPR-07-22, Svensk Kärnbränslehantering AB.

Kumpulainen S, Kiviranta L, Korkeakosi P, 2016. Long-term effects of iron heater and Äspö groundwater on smectite clays: Chemical and hydromechanical results from *in situ* alternative buffer material (ABM) test package 2. Clay Minerals 51, 129–144.

Kurosawa S, Yui M, Yoshikawa H, 1997. Experimental study of colloid filtration by compacted bentonite. In Gray W J, Triay I R (eds). Scientific basis for nuclear waste management XX: symposium held in Boston, Massachusetts, 2–6 December 1996. Pittsburgh, Pa.: Materials Research Society. (Materials Research Society Symposium Proceedings 465), 963–970.

Laaksoharju M (ed), 2003. Äspö Hard Rock Laboratory. Status report of the colloid investigation conducted at the Äspö HRL during the years 2000–2003. SKB IPR-03-38, Svensk Kärnbränslehantering AB.

Laaksoharju M, Wold S, 2005. The colloid investigations conducted at the Äspö Hard Rock Laboratory during 2000–2004. SKB TR-05-20, Svensk Kärnbränslehantering AB.

Laaksoharju M, Smellie J, Nilsson A-C, Skårman C, 1995. Groundwater sampling and chemical characterisation of the Laxemar deep borehole KLX02. SKB TR 95-05, Svensk Kärnbränslehantering AB.

Lagaly G, Ziesmer S, 2003. Colloid chemistry of clay minerals: the coagulation of montmorillonite dispersions. Advances in Colloid and Interface Science 100–102, 105–128.

Lambe T W, Whitman R V, 1969. Soil mechanics. New York: Wiley.

Landolt D, Davenport A, Payer J, Shoesmith D, 2009. A review of materials and corrosion issues regarding canisters for disposal of spent fuel and high-level waste in Opalinus Clay. Nagra Technical Report 09-02, Nagra, Switzerland.

Lantenois S, Lanson B, Muller F, Bauer A, Jullien M, Plançon A, 2005. Experimental study of smectite interaction with metal Fe at low temperature: 1. Smectite destabilization. Clays and Clay Minerals 6, 597–612.

Lazo C, Karnland O, Tullborg E-L, Puigdomenech I, 2003. Redox properties of MX-80 and Montigel bentonite-water systems. In Finch R J, Bullen D B (eds). Scientific basis for nuclear waste management XXVI. Warrendale, PA: Materials Research Society. (Materials Research Society Symposium Proceedings 757), paper II8.1.

Le Bell J C, 1978. Colloid chemical aspects of the “confined bentonite concept”. KBS TR 97, Svensk Kärnbränsleförsörjning AB.

Lee J O, Kang I M, Cho W J, 2010. Smectite alteration and its influence on the barrier properties of smectite clay for a repository. Applied Clay Science 47, 99–104.

Leupin O X (ed), Birgersson M, Karnland O, Korkeakoski P, Sellin P, Mäder U, Wersin P, 2014. Montmorillonite stability under near-field conditions. Nagra Technical Report 14-12, Nagra, Switzerland.

Liu L, Moreno L, Neretnieks I, 2009. A dynamic force balance model for colloidal expansion and its DLVO-based application. Langmuir 25, 679–687.

Livi K J T, Senesi G S, Scheinost A C, Sparks D L, 2009. Microscopic examination of nanosized mixed Ni-Al hydroxide surface precipitates on pyrophyllite. Environmental Science & Technology 43, 1299–1304.

Lopez-Fernandez M, Cherkouk A, Vilchez-Vargas R, Jauregui R, Pieper D, Boon N, Sanchez-Castro I, Merroun M L, 2015. Bacterial diversity in bentonites, engineered barrier for deep geological disposal of radioactive wastes. Microbial Ecology 70, 922–935.

Lu N, Reimus P W, Parker G R, Conca J L, Triay I R, 2003. Sorption kinetics and impact of temperature, ionic strength and colloid concentration on the adsorption of plutonium-239 by inorganic colloids. Radiochimica Acta 91, 713–720.

Luna M, Arcos D, Duro L, 2006. Effects of grouting, shotcreting and concrete leachates on backfill geochemistry. SKB R-06-107, Svensk Kärnbränslehantering AB.

Lundgren K, 2004. Final disposal of fuel – electron radiation outside copper canister. SKB TR-04-06, Svensk Kärnbränslehantering AB.

Luterkort D, Johannesson L-E, Eriksson P, 2017. Buffer design and installation method. Installation report. SKB TR-17-06, Svensk Kärnbränslehantering AB.

Lynch F L, 1997. Frio shale mineralogy and the stoichiometry of the smectite-to-illite reaction: the most important reaction in clastic sedimentary diagenesis. Clays and Clay Minerals 45, 618–631.

Lynch L, Reynolds R C, 1985. The stoichiometry of the smectite-illite reaction. In Program with abstracts, 21st Annual Meeting of The Clay Minerals Society, Baton Rouge, Louisiana, 1984.

Maanoja S, Lakaniemi A-M, Lehtinen L, Salminen L, Auvinen H, Kokko M, Palmroth M, Muuri E, Rintala J, 2020. Compacted bentonite as a source of substrates for sulfate-reducing microorganisms in a simulated excavation-damaged zone of a spent nuclear fuel repository. Applied Clay Science 196, 105746. doi:10.1016/j.clay.2020.105746

Madigan M T, Martinko J M, Dunlap P V, Clark D P, 2008. Brock biology of microorganisms. 12th ed. San Francisco, CA: Pearson/Benjamin Cummings.

Madigan M, Martinko J, Stahl D, Clark D, 2012. Brock biology of microorganisms. 13th ed. San Francisco: Pearson Education.

Madina V, Azkarate I, 2004. FEBEX project post-mortem analysis: Corrosion study. Publicación técnica 08/2004, ENRESA, Spain.

Maes N, Bruggeman C, Govaerts J, Martens E, Salah S, Van Gompel M, 2011. A consistent phenomenological model for natural organic matter linked migration of Tc(IV), Cm(III), Np(IV), Pu(III/IV) and Pa(V) in the Boom Clay. Physics and Chemistry of the Earth, Parts A/B/C 36, 1590–1599.

Magnusson J, Mathern A, 2015. System design of Dome plug. Experience of low-pH concrete mix B200. Material properties from laboratory tests and full-scale castings. SKB P-14-26, Svensk Kärnbränslehantering AB.

Malm R, 2012. Low-pH concrete plug for sealing the KBS-3V deposition tunnels. SKB R-11-04, Svensk Kärnbränslehantering AB.

Malmberg D, Kristensson O, 2014. Thermo-hydraulic modelling of the bentonite buffer in deposition hole 6 of the Prototype Repository. In Clays in natural and engineered barriers for radioactive waste confinement. London: Geological Society. (Special Publications 400), 251–263.

Malmberg D, Åkesson M, 2018. Modelling the Interactions between Engineered and Natural Barriers. Task 8 of SKB Task Forces EBS and GWFTS. SKB P-17-03, Svensk Kärnbränslehantering AB.

Marques Fernandes M, Baeyens B, Bradbury M H, 2008. The influence of carbonate complexation on lanthanide sorption on montmorillonite. Radiochimica Acta, 96, 691–697.

Marques Fernandes M, Stumpf T, Baeyens B, Walther C, Bradbury M H, 2010. Spectroscopic identification of ternary Cm-carbonate surface complexes. Environmental Science & Technology 44, 921–927.

Marques Fernandes M, Scheinost A C, Baeyens B, 2016. Sorption of trivalent lanthanides and actinides onto montmorillonite: Macroscopic, thermodynamic and structural evidence for ternary hydroxo and carbonato surface complexes on multiple sorption sites. Water Research 99, 74–82.

Marshall M H M, McKelvie J R, Simpson A J, Simpson M J, 2015. Characterization of natural organic matter in bentonite clays for potential use in deep geological repositories for used nuclear fuel. Applied Geochemistry 54, 43–53.

Masurat P A, 2006. Potential for corrosion in disposal systems for high level radioactive waste by *Meiothermus* and *Desulfovibrio*. PhD thesis. Göteborg University.

Masurat P A, Pedersen K, 2003. Microbial sulphide production in compacted bentonite at the commencement of long-term disposal of high-level radioactive waste. In Oversby V M, Werme L O (eds). Scientific basis for nuclear waste management XXVII: symposium held in Kalmar, Sweden, 15–19 June 2003. Warrendale : Materials Research Society. (Materials Research Society Symposium Proceedings 807)

Masurat P, Eriksson S, Pedersen K, 2010a. Evidence for indigenous sulphate-reducing bacteria in commercial Wyoming bentonite MX-80. Applied Clay Science 47, 51–57.

Masurat P, Eriksson S, Pedersen K, 2010b. Microbial sulphide production in compacted Wyoming MX-80 bentonite under in situ conditions relevant to a repository for high-level radioactive waste. Applied Clay Science 47, 58–64.

Massmann G, Pekdeger A, Merz C, 2004. Redox processes in the Oderbruch polder groundwater flow system in Germany. Applied Geochemistry 19, 863–886.

Melkior T, Gaucher E C, Brouard C, Yahiaoui S, Thoby D, Clinard C, Ferrage E, Guyonnet D, Tournassat C, Coelho D, 2009. Na^+ and HTO diffusion in compacted bentonite: effect of surface chemistry and related texture. Journal of Hydrology 370, 9–20.

Metcalfe R, Moore Y A, 1998. Hydrogeochemical processes accompanying heating of clay-rich sediments and rocks: a review. Technical Report WE/98, British Geological Survey, Keyworth, UK.

Miller R D, 1963. Discussion of "Saturation, phase composition and freezing point depression in a rigid soil model" by Lange and McKim. In Procceedings of the 1st International Conference on Permafrost, Lafayette, Indiana, 11–15 November 1963. Washington D.C.: National Academy of Sciences, 191–192.

Missana T, Adell A, 2000. On the applicability of DLVO theory to the prediction of clay colloids stability. Journal of Colloid and Interface Science 230, 150–156.

Mitchell J K, 1993. Fundamentals of soil behavior. New York: Wiley.

Moll H, Johnsson A, Schäfer M, Pedersen K, Budzikiewicz K, Bernhard G, 2008. Curium(III) complexation with pyoverdins secreted by a groundwater strain of *Pseudomonas fluorescens.* Biometals 21, 219–228.

Moore D M, Reynolds R C, 1989. X-Ray diffraction and the identification and analyses of clay minerals. New York: Oxford University Press.

Moore D M, Reynolds R C, 1997. X-ray diffraction and the identification and analysis of clay minerals. 2nd ed. Oxford: Oxford University Press.

Morel J-P, Marry V, Turq P, Morel-Desrosiers N, 2007. Effect of temperature on the retention of Cs^+ by Na-montmorillonite: microcalorimetric investigation. Journal of Materials Chemistry17, 2812–2817.

Mosser-Ruck R, Cathelineau M, Guillaume D, Charpentier D, Rousset D, Barres O, Michau N, 2010. Effects of temperature, pH, and iron/clay and liquid/clay ratios on experimental conversion of dioctahedral smectite to berthierine, chlorite, vermiculite, or saponite. Clays and Clay Minerals 2, 280–291.

Motamedi M, Karnland O, Pedersen K, 1996. Survival of sulfate reducing bacteria at different water activities in compacted bentonite. FEMS Microbiology Letters 141, 83–87.

Muurinen A, 1994. Diffusion of anions and cations in compacted sodium bentonite. Espoo: Technical Research Centre of Finland. (VTT Publications 168)

Muurinen A, Carlsson T, 2007. Eh and pH in compacted MX-80 bentonite. NF-PRO RTD2, Deliverable 2.2.14, European Commission.

Muurinen A, Carlsson T, 2010. Experiences of pH and Eh measurements in compacted MX-80 bentonite. Applied Clay Science 40, 23–27.

Mäder U, Jenni A, Lerouge C, Gaboreau S, Miyoshi S, Kimura Y, Cloet V, Fukaya M, Claret F, Otake T, Shibata M, Lothenbach B, 2017. 5-year chemico physical evolution of concrete claystone interfaces Mont Terri rock laboratory (Switzerland). Swiss Journal of Geosciences 110, 307–327.

Nakata K, Nagasaki S, Tanaka S, Sakamoto Y, Tanaka T, Ogawa H, 2000. Sorption and desorption kinetics of Np(V) on magnetite and hematite. Radiochimica Acta, 88, 453–458.

NEA, 2012. Thermodynamic sorption modeling in support of radioactive waste disposal safety cases. NEA sorption project Phase III. Paris: OECD/NEA.

Negron A, Ramos S, Blumenfeld A L, Pacheco G, Fripiat J J, 2002. On the structural stability of montmorillonite submitted to heavy γ-irradiation. Clays and Clay Minerals 50, 35–37.

Neretnieks I, Moreno L, 2018. Revisiting bentonite erosion understanding and modelling based on the BELBaR project findings. SKB TR-17-12, Svensk Kärnbränslehantering AB.

Neretnieks I, Liu L, Moreno L, 2009. Mechanisms and models for bentonite erosion. SKB TR-09-35, Svensk Kärnbränslehantering AB.

Neretnieks I, Moreno L, Liu L, 2017. Clay erosion – impact of flocculation and gravitation. SKB TR-16-11, Svensk Kärnbränslehantering AB.

Nersesova Z A, Tsytovich N A, 1965. Unfrozen water in frozen soils. In: Permafrost: Proceedings of the International Conference on Permafrost. Lafayette, Indiana, 11–15 November 1963. Washington: National Academy of Sciences, 230–234.

Neuzil C E, 2000. Osmotic generation of "anomalous" fluid pressures in geological environments. Nature 403, 182–184.

Newman A C D, Brown G, 1987. The chemical constitution of clays. In Newman A C D (ed). Chemistry of clays and clay minerals. Harlow: Longman. (Mineralogical Society monograph 6)

Norris S, 2015. EC FORGE Project: Updated consideration of gas generation and migration in the safety case. In Shaw R P (ed). Gas generation and migration in deep geological radioactive waste repositories. London: Geological Society of London. (Geological Society Special Publication 415), 241–258.

Norrish K, 1954a. Manner of swelling of montmorillonite. Nature 173, 256–257.

Norrish K, 1954b. The swelling of montmorillonite. Discussions of the Faraday Society 18, 120–134.

Ochs M, Talerico C, 2004. SR-Can. Data and uncertainty assessment. Migration parameters for the bentonite buffer in the KBS-3 concept. SKB TR-04-18, Svensk Kärnbränslehantering AB.

Ochs M, Lothenbach B, Wanner H, Sato H, Yui M, 2001. An integrated sorption-diffusion model for the calculation of consistent distribution and diffusion coefficients in compacted bentonite. Journal of Contaminant Hydrology 47, 283–296.

Ochs M, Lothenbach B, Shibata M, Yui M, 2004. Thermodynamic modeling and sensitivity analysis of porewater chemistry in compacted bentonite. Physics and Chemistry of the Earth, Parts A/B/C 29, 129–136.

O'Day P A, Brown G E, Parks G A, 1994. X-ray absorption spectroscopy of cobalt(II) multinuclear surface complexes and surface precipitates on kaolinite. Journal of Colloid and Interface Science 165, 269–289.

Olsson S, Jensen V, Johanesson L-E, Hansen E, Karnland O, Kumpulainen S, Kiviranta L, Svensson D, Hansen S, Lindén J, 2013. Prototype Repository. Hydro-mechanical, chemical and mineralogical characterization of the buffer and tunnel backfill material from the outer section of the Prototype Repository. SKB TR-13-21, Svensk Kärnbränslehantering AB.

Ortiz L, Volckaert G. Mallants D, 2002. Gas generation and migration in Boom Clay, a potential host rock formation for nuclear waste storage. Engineering Geology 64, 287–296.

Park J, Sanford R A, Bethke C M, 2006. Geochemical and microbiological zonation of the Middendorf aquifer, South Carolina. Chemical Geology 230, 88–104.

Pedersen K, 2001. Diversity and activity of microorganisms in deep igneous rock aquifers of the Fennoscandian Shield. In: Fredrickson J K, Fletcher M (eds). Subsurface microbiology and biogeochemistry. Chichester: Wiley, 97–139.

Pedersen K, 2002. Microbial processes in the disposal of high level radioactive waste 500 m underground in Fennoscandian shield rocks. In Keith-Roach M J, Livens F R (eds). Interactions of microorganisms with radionuclides. Amsterdam: Elsevier, 279–311.

Pedersen K, Motamedi M, Karnland O, Sandén T, 2000a. Cultivability of microorganisms introduced into a compacted bentonite clay buffer under high-level radioactive waste repository conditions. Engineering Geology 58, 149–161.

Pedersen K, Motamedi M, Karnland O, Sandén T, 2000b. Mixing and sulphate-reducing activity of bacteria in swelling, compacted bentonite clay under high-level radioactive waste repository conditions. Journal of Applied Microbiology 89, 1038–1047.

Pedersen K, Arlinger J, Hallbeck A, Hallbeck L, Eriksson S, Johansson J, 2008. Numbers, biomass and cultivable diversity of microbial populations relate to depth and borehole specific conditions in groundwater from 3 to 450 m depth in Olkiluoto, Finland. The ISME Journal 2, 760–775.

Pellegrini R, Horseman S, Kemp S, Rochelle C, Boisson J Y, Lombardi S, Bouchet A, Parneix J-C, 1999. Natural analogues of the thermo-hydro-chemical and thermo-hydromechanical response. EUR 19114, European Commission.

Pérez del Villar L, Delgado A, Reyes E, Pelayo M, Fernández-Soler J M, Cózar J S, Tsige M, Quejido A J, 2005. Thermochemically induced transformations in Al-smectites: a Spanish natural analogue of the bentonite barrier behaviour in a radwaste disposal. Applied Geochemistry 20, 2252–2282.

Perronnet M, Jullien M, Villiéras F, Raynal J, Bonnin D, Bruno G, 2008. Evidence of a critical content in Fe(0) on FoCa7 bentonite reactivity at 80 °C. Applied Clay Science 38, 187–202.

Perry E, Hower J, 1970. Burial diagenesis in Gulf Coast pelitic sediments. Clays and Clay Minerals 18, 165–177.

Petsev D N, Starov V M, Ivanov I B, 1993. Concentrated dispersions of charged colloidal particles: sedimentation, ultrafiltration. and diffusion. Colloids and Surfaces A: Physicochemical and Engineering Aspects 81, 65–81.

Philip J R, de Vries D A, 1957. Moisture movement in porous materials under temperature gradients. Transactions of the American Geophysical Union 38, 221–231.

Plötze M, Kahr G, Hermanns Stengele R, 2003. Alteration of clay minerals – gamma-irradiation effects on physicochemical properties. Applied Clay Science 23, 195–202.

Pont A, Idiart A, 2022. Numerical model for the quantification of buffer bentonite mass losses due to expansion, erosion and sedimentation. Posiva SKB Report 13, Posiva Oy, Svensk Kärnbränslehantering AB.

Pont A, Coene E, Idiart A, 2020. Bentonite erosion project. Preliminary study for the numerical simulation of bentonite erosion. SKB P-20-16, Svensk Kärnbränslehantering AB.

Posiva SKB, 2017. Safety functions, performance targets and technical design requirements for a KBS-3V repository. Conclusions and recommendations from a joint SKB and Posiva working group. Posiva SKB Report 01, Posiva Oy, Svensk Kärnbränslehantering AB.

Postma D, Jakobsen R, 1996. Redox zonation: equilibrium constraints on the Fe(III)/SO_4-reduction interface. Geochimica et Cosmochimica Acta 60, 3169–3175.

Potts M, 1994. Desiccation tolerance of prokaryotes. Microbiological Reviews 58, 755–805.

Pusch R, 1977. Influence of cementation on the deformation properties of bentonite/quartz buffer substance. KBS TR 14, Svensk Kärnbränsleförsörjning AB.

Pusch R, 1985. Final report of the Buffer Mass Test – Volume III: Chemical and physical stability of he buffer materials. Stripa Project TR 85-14, Svensk Kärnbränslehantering AB.

Pusch R, Karnland O, 1988. Hydrothermal effects on montmorillonite. A preliminary study. SKB TR 88-15, Svensk Kärnbränslehantering AB.

Pusch R, Madsen F T, 1995. Aspects on the illitization of the Kinnekulle bentonites. Clays and Clay Minerals 43, 261–270.

Pusch R, Ranhagen L, Nilsson K, 1985. Gas migration through Mx-80 bentonite. Nagra NTB 85-36, Nagra, Switzerland.

Pusch R, Karnland O, Lajudie A, Lechelle J, Bouchet A, 1993a. Hydrothermal field test with French candidate clay embedding steel heater in the Stripa mine. SKB TR 93-02, Svensk Kärnbränslehantering AB.

Pusch R, Karnland O, Lajudie A, Decarreau A, 1993b. MX 80 clay exposed to high temperatures and gamma radiation. SKB TR 93-03, Svensk Kärnbränslehantering AB.

Pusch R, Takase H, Benbow S, 1998. Chemical processes causing cementation in heat-affected smectite – the Kinnekulle bentonite. SKB TR-98-25, Svensk Kärnbränslehantering AB.

Pusch R, Drawrite A B, Yong R N, Nakano M, 2010. Stiffening of smectite buffer clay by hydrothermal effects. Engineering Geology 116, 21–31.

Pushkareva R, Kalinichenko E, Lytovchenko A, Pushkarev A, 2002. Irradiation effect on physicochemical properties of clay minerals. Applied Clay Science 21, 117–123.

Puura E, Kirsimäe K, 2010. Impact of the changes in the chemical composition of pore water on chemical and physical stability of natural clays. A review of natural cases and related laboratory experiments and the ideas on natural analogues for bentonite erosion/non-erosion. SKB TR-10-24, Svensk Kärnbränslehantering AB.

Pytte A M, 1982. The kinetics of smectite to illite reaction in contact metamorphic shales. MA thesis. Dartmouth College, Hanover, N. H.

Rabung T, Pierret M C, Bauer A, Geckeis H, Bradbury M H, Baeyens B, 2005. Sorption of Eu(III)/Cm(III) on Ca-montmorillonite and Na-illite. Part 1: Batch sorption and time-resolved laser fluorescence spectroscopy experiments. Geochimica et Cosmochimica Acta 23, 5393–5402.

Reid C, Lunn R, El Mountassir G, Tarantino A, 2015. A mechanism for bentonite buffer erosion in a fracture with a naturally varying aperture. Mineralogical Magazine 79, 1485–1494.

Robinson R A, Stokes R H, 1959. Electrolyte solutions. London: Butterworths.

Romero L, Thompson A, Moreno L, Neretnieks I, Widén H, Boghammar A, 1999. Comp23/ Nuctran user's guide. SKB R-99-64, Svensk Kärnbränslehantering AB.

Sánchez M, Villar M V, Lloret A, Gens A, 2007. Analysis of the expansive clay hydration under low hydraulic gradient. In Schanz T (ed). Experimental unsaturated soil mechanics. Berlin Heidelberg: Springer. (Springer Proceeding in Physics 112), 309–318.

Sandén T, Nilsson U, 2020. Installation, monitoring, dismantling and initial analyses of material from LOT test parcel S2 and A3. Results from field test. SKB TR-20-11, Svensk Kärnbränslehantering AB.

Sandén T, Börgesson L, 2010. Early effects of water inflow into a deposition hole. Laboratory test results. SKB R-10-70, Svensk Kärnbränslehantering AB.

Sandén T, Börgesson L, Dueck A, Goudarzi R, Lönnqvist M, 2008. Deep repository – engineered barrier system. Erosion and sealing processes in tunnel backfill materials investigated in laboratory. SKB R-08-135, Svensk Kärnbränslehantering AB.

Sandén T, Olsson S, Andersson L, Dueck A, Jensen V, Hansen E, Johnsson A, 2014. Investigation of backfill candidate materials. SKB R-13-08, Svensk Kärnbränslehantering AB.

Sandén T, Börgesson L, Nilsson U, Dueck A, 2017. Full scale buffer swelling test at dry backfill conditions in Äspö HRL. In situ test and related laboratory tests. SKB TR-16-07, Svensk Kärnbränslehantering AB.

Sandén T, Nilsson U, Johannesson L-E, Hagman P, Nilsson, G, 2018. Sealing of investigation boreholes. Full scale field test and large-scale laboratory tests. SKB TR-18-18, Svensk Kärnbränslehantering AB.

Sandén T, Kristensson O, Lönnqvist, Börgesson L, Nilsson U, Goudarzi R, 2020. Buffer swelling. Laboratory tests and modelling. SKB TR-20-04, Svensk Kärnbränslehantering AB.

Sander R, 2015. Compilation of Henry's law constants (version 4.0) for water as solvent. Atmospheric Chemistry and Physics 15, 4399–4981.

Sato H, Yui M, Hideki Y, 1995. Diffusion behaviour for Se and Zr in sodium-bentonite. In Murakami T, Ewing R C (eds). Scientific basis for nuclear waste management XVIII: symposium held in Kyoto, Japan, 23–27 October 1994. Pittsburgh, PA: Materials Research Society. (Materials Research Society Symposium Proceedings 353), 269–276.

Savage D, 2012. Prospects for coupled modelling. STUK-TR 13, Radiation and Nuclear Safety Authority, Finland.

Savage D, Noy D J, Mihara M, 2002. Modelling the interaction of bentonite with hyperalkaline fluids. Applied Geochemistry 17, 207–223.

Savage D, Benbow S, Watson C, Takase H, Ono K, Oda C, Honda A, 2010. Natural systems evidence for the alteration of clay under alkaline conditions: an example from Searles Lake, California. Applied Clay Science 47, 72–81.

Schatz T, Akhanoba N, 2016. Buffer erosion in sloped fracture environments. Posiva 2016-13, Posiva Oy, Finland.

Schatz T, Kanerva N, Martikainen J, Sane P, Olin M, Seppälä A, Koskinen K, 2013. Buffer erosion in dilute groundwater. Posiva 2012-44, Posiva Oy, Finland.

Schatz T, Martikainen J, 2010. Laboratory studies on the effect of freezing and thawing exposure on bentonite buffer performance: Closed-system tests. Posiva 2010-06, Posiva Oy, Finland.

Scheidegger A M, Sparks D L, 1996. Kinetcs of the formation and the dissolution of nickel surface precipitates on pyrophyllite. Chemical Geology 132, 157–164.

Scheidegger A M, Lamble G M, Sparks D L, 1997. Spectroscopic evidence for the formation of mixed-cation hydroxide phases upon metal sorption on clays and aluminum oxides. Journal of Colloid and Interface Science 186, 118–128.

Schott J, Acker M, Barkleit A, Brendler V, 2012. The influence of temperature and small organic ligands on the sorption of Eu(III) on Opalinus Clay. Radiochimica Acta 100, 315–324.

Schwyn B, 2003. Sorption values (K_d), effective diffusion coefficients (D_e) and accessible porosities (e) for bentonite used in safety assessment calculations within the Project Opalinus Clay (Entsorgungsnachweis). In Bradbury M H, Baeyens B. Nearfield sorption data bases for compacted MX-80 bentonite for performance assessment of high-level radioactive waste repository in Opalinus Clay host rock. Nagra Technical Report 02-18, Nagra, Switzerland, 125–130.

Schäfers A, Gens A, Rodriguez-Dono A, Baxter S, Tsitsopoulos V, Holton D, Malmberg D, Sawada M, Yafei Q, Ferrari A, Laloui L, Sjöland A, 2020. Increasing understanding and confidence in THM simulations of Engineered Barrier Systems. Environmental Geotechnics 2020 7, 59–71.

Sellin P (ed), Åkesson M, Kristensson O, Malmberg D, Börgesson L, Birgersson M, Dueck A, Karnland O, Hernelind J, 2017. Long re-saturation phase of a final repository. Additional supplementary information. SKB TR-17-15, Svensk Kärnbränslehantering AB.

Sena C, Salas J, Arcos D, 2010a. Aspects of geochemical evolution of the SKB near field in the frame of SR-Site. SKB TR-10-59, Svensk Kärnbränslehantering AB.

Sena C, Salas J, Arcos D, 2010b. Thermo-hydro-geochemical modelling of the bentonite buffer LOT A2 experiment. SKB TR-10-65, Svensk Kärnbränslehantering AB.

Senger R, 2015. Scoping calculations in support of the design of the Fullscale Emplacement experiment at the Mont Terri URL: Evaluation of the effects and gas transport phenomena. Nagra Arbeitsberich 13–98, Nagra, Switzerland.

Shelton A, Sellin P, Missana T, Schäfer T, Červinka R, Koskinen K, 2018. Synthesis report: Colloids and related issues in the long term safety case. SKB TR-17-17, Svensk Kärnbränslehantering AB.

SKB, 1999. SR 97. Processes in the repository evolution. Background report to SR 97. SKB TR-99-07, Svensk Kärnbränslehantering AB.

SKB, 2004. Interim initial state report for the safety assessment SR-Can. SKB R-04-35, Svensk Kärnbränslehantering AB.

SKB, 2008. Site description of Forsmark at completion of the site investigation phase. SDM-Site Forsmark. SKB TR-08-05, Svensk Kärnbränslehantering AB.

SKB, 2009. Underground design Forsmark. Layout D2. SKB R-08-116, Svensk Kärnbränslehantering AB.

SKB, 2010a. Buffer, backfill and closure process report for the safety assessment SR-Site. SKB TR-10-47, Svensk Kärnbränslehantering AB.

SKB, 2010b. Geosphere process report for the safety assessment SR-Site. SKB TR-10-48, Svensk Kärnbränslehantering AB.

SKB, 2011. Long-term safety for the final repository for spent nuclear fuel at Forsmark. Main report of the SR-Site project. SKB TR-11-01, Svensk Kärnbränslehantering AB.

SKB, 2013. Svar till SSM på begäran om komplettering rörande buffert och återfyllning under driften av slutförvarsanläggningen. SKBdoc 1371890 ver 2.0, Svensk Kärnbränslehantering AB.

SKB, 2014. Svar till SSM på begäran om komplettering rörande grundvattenkemi på kort och medellång sikt. SKB 1437441 ver 1.0, Svensk Kärnbränslehantering AB. (In Swedish.)

Skurtveit E, Aker E, Soldal M, Angeli M, Hallberg E, 2010. Influence of micro fractures and fluid pressure on sealing efficiency of caprock: a laboratory study on shale. 10th International Conference on Greenhouse Gas Control Technologies, Amsterdam, 19–23 September 2010.

Smellie J, Karlsson F, 1996. A reappraisal of some Cigar Lake issues of importance to performance assessment. SKB TR 96-08, Svensk Kärnbränslehantering AB.

Soltermann D, Marques Fernandes M, Baeyens B, Dähn R, Joshi P A, Scheinost A C, Gorski C A, 2014a. Fe(II) uptake on natural montmorillonites. I. Macroscopic and spectroscopic characterization. Environmental Science & Technology 48, 8688–8697.

Soltermann D, Marques Fernandes M, Baeyens B, Miehé-Brendlé J, Dähn R, 2014b. Competitive Fe(II)-Zn(II) uptake on a synthetic montmorillonite. Environmental Science & Technology 48, 190–198.

Sposito G, 1981. Trace metals in contaminated waters. Environmental Science & Technology 15, 396–403.

Sposito G, 1984. The surface chemistry of soils. New York: Oxford University Press.

Stetter K O, 1996. Hyperthermophilic procaryotes. FEMS Microbiology Reviews 18, 145–158.

Stroes-Gascoyne S, Pedersen K, Haveman S A, Dekeyser K, Arlinger J, Daumas S, Ekendahl S, Hallbeck L, Hamon C J, Jahromi N, Delaney T-L, 1997. Occurrence and identification of micro-organisms in compacted clay-based buffer material designed for use in a nuclear fuel waste disposal vault. Canadian Journal of Microbiology 43, 1133–1146.

Stucki J W, Low P F, Roth C B, Golden D C, 1984. Effects of oxidation state of octahedral iron on clay swelling. Clays and Clay Minerals 32, 357–362.

Stucki J W, Lee K, Zhang L, Larson R A, 2002. Effects of iron oxidation state on the surface and structural properties of smectites. Pure and Applied Chemistry 74, 2081–2094.

Stumm W, Morgan J J, 1996. Aquatic chemistry: chemical equilibria and rates in natural waters. 3rd ed. New York: Wiley.

Sudheer Kumar R, Podlech C, Grathoff G, Warr L N, Svensson D, 2021. Thermally induced bentonite alterations in the SKB ABM5 Hot Bentonite Experiment. Minerals 11, 1017.

Sundberg J, Wrafter J, Back P-E, Rosén L, 2008. Thermal properties Laxemar. Site descriptive modelling, SDM-Site Laxemar. SKB R-08-61, Svensk Kärnbränslehantering AB.

Svemar C, Johannesson L-E, Grahm P, Svensson D, Kristensson O, Lönnqvist M, Nilsson U, 2016. Prototype Repository. Opening and retrieval of outer section of Prototype Repository at Äspö Hard Rock Laboratory. Summary report. SKB TR-13-22, Svensk Kärnbränslehantering AB.

Svensson D, 2015. The bentonite barrier: swelling properties, redox chemistry and mineral evolution. PhD thesis. Lund University, Sweden.

Svensson D, Dueck A, Nilsson U, Olsson S, Sandén T, Lydmark S, Jägerwall S, Pedersen K, Hansen S, 2011. Alternative buffer material. Status of the ongoing laboratory investigation of reference materials and test package 1. SKB TR-11-06, Svensk Kärnbränslehantering AB.

Svensson D, Lundgren C, Johannesson L-E, Norrfors K, 2017a. Developing strategies for acquisition and control of bentonite for a high level radioactive waste repository. SKB TR-16-14, Svensk Kärnbränslehantering AB.

Svensson D, Lundgren C, Wikberg P, 2017b. Experiments with bentonite and sulphide – results from experiments 2013–2016. SKB P-16-31, Svensk Kärnbränslehantering AB.

Svensson D, Eriksson P, Johannesson L-E, Lundgren C, Bladström T, 2019. Development and testing of methods suitable for quality control of bentonite as KBS-3 buffer and backfill. SKB TR-19-25, Svensk Kärnbränslehantering AB.

Svensson D, Kalinowski B E, Turner S, Dopson M, 2020. Activity of sulphate reducing bacteria in bentonite as a function of water availability. SKB TR-20-08, Svensk Kärnbränslehantering AB.

Svensson P D, Hansen S, 2010a. Intercalation of smectite with liquid ethylene glycol – resolved in time and space by synchrotron X-ray diffraction. Applied Clay Science 48, 358–367.

Svensson P D, Hansen S, 2010b. Freezing and thawing of montmorillonite – a time resolved X-ray diffraction study. Applied Clay Science 49, 127–134.

Svensson P D, Hansen S, 2013a. Redox chemistry in two iron-bentonite field experiments at Äspö hard rock laboratory, Sweden: an XRD and Fe K-edge XANES study. Clays and Clay Minerals 61, 566–579.

Svensson P D, Hansen S, 2013b. Combined salt and temperature impact on montmorillonite hydration. Clays and Clay Minerals 61, 328–341.

Tachi Y, Yotsuji K, 2014. Diffusion and sorption of Cs^+, Na^+, I^- and HTO in compacted sodium montmorillonite as a function of porewater salinity: Integrated sorption and diffusion model. Geochimica et Cosmochimica Acta 132, 75–93.

Tachi Y, Seida Y, Nakazawa N, Yamada K, Yotsuji K, Suyama T, Ochs M, Yui M, 2010. Diffusion of neptunium(V) in compacted montmorillonite: Effect of salinity and carbonate. Radiochimica Acta 98, 711–718.

Tachi Y, Yotsuji K, Suyama T, Ochs M, 2014. Integrated sorption and diffusion model for bentonite. Part 2: porewater chemistry, sorption and diffusion modeling in compacted systems. Journal of Nuclear Science and Technology 51, 1191–1204.

Takahashi H, 2013. Microstructural analysis by X-ray nano-CT and its implications on HDO diffusion in compacted montmorillonite. In Clay characterization from nanoscopic to microscopic resolution. NEA Clay Club Workshop Proceedings, Karlsruhe, Germany, 6–8 September 2011. NEA/RWM/CLAYCLUB(2013)1, OECD/NEA, 151–154.

Tertre E, Castet S, Berger G, Loubet M, Giffaut E, 2006. Surface chemistry of kaolinite and Na-montmorillonite in aqueous electrolyte solutions at 25 and 60 °C: Experimental and modeling study. Geochimica et Cosmochimica Acta 70, 4579–4599.

Tessier D, 1990. Behaviour and microstructure of clay minerals. In De Boodt M, Hayes M H B, Herbillon A (eds). Soil colloids and their associations in aggregates. Plenum Press, 387–415.

Thunvik R, Braester C, 1991. Heat propagation from a radioactive waste repository. SKB 91 reference canister. SKB TR 91-61, Svensk Kärnbränslehantering AB.

Tinnacher R M, Holmboe M, Tournassat C, Bourg I C, Davis J A, 2016. Ion adsorption and diffusion in smectite: molecular, pore, and continuum scale views. Geochimica et Cosmochimica Acta 177, 130–149.

Tissot B, Pelet R, 1971. Nouvelles données sur les mécanismes de genèse et de migration du pétrole: simulation mathématique et application à la prospection. In Proceedings of the 8th World Petroleum Congress, Moscow, 13–18 June 1971. Essex: Elsevier, 35–46.

Tombács E, Szekeres M, 2004. Colloidal behaviour of aqueous montmorillonite suspensions: the specific role of pH in the presence of indifferent electrolytes. Applied Clay Science 27, 75–94.

van Olphen H, 1963. An introduction to clay colloid chemistry. New York: Wiley Interscience.

van Olphen H, 1991. An introduction to clay colloid chemistry: for clay technologists, geologists and soil scientists. 2nd ed. New York: Wiley.

Vehmas T, Montoya V, Alonso MC, Vašíček R, Rastrick E, Gaboreau S, Večerník P, Leivo M, Holt E, Fink N, Mouheb NA, Svoboda J, Read D, Červinka R, Vasconcelos R, Corkhill C, 2020. Characterization of Cebama low-pH reference concrete and assessment o fits alteration with representative waters in radioactive waste repositories. Applied Geochemistry 121, 104703. doi:10.1016/j.apgeochem.2020.104703

Velde B, Vasseur G, 1992. Estimation of the diagenetic smectite to illite transformation in time-temperature space. American Mineralogist 77, 967–976.

Verburg K, Baveye P, 1994. Hysteresis in the binary exchange of cations on 2:1 clay minerals: a critical review. Clays and Clay Minerals 42, 207–220.

Verwey E J W, Overbeek J T G, 1948. Theory of the stability of lyophobic colloids: the interaction of sol particles having an electric double layer. New York: Elsevier.

Vidstrand P, Stigsson M, Åkesson M, Fransson Å, 2017. SKB Task Forces EBS and GWFTS. Modelling the interaction between engineered and natural barriers. A compilation of Task 8 descriptions. SKB P-16-05, Svensk Kärnbränslehantering AB.

Villar M V, Martín P L, Romero F J, Barcala J M, Gutiérrez-Rodrigo V, 2012. Gas transport through bentonite: influence of dry density, water content and boundary conditions. In Skoczylas F, Davy C A, Agostini F, Burlion N (eds). Propriétés de transfert des géomatériaux. Transfert 2012: actes du colloque, Lille, France, 20–22 mars 2012. 379–389.

Villar M V, Iglesias R J, Abós H, Martínez V, de la Rosa C, Manchón M A, 2016. FEBEX-DP on-site analyses report. Nagra Arbeitsbericht NAB 16-12, Nagra, Switzerland.

Villar M V, Iglesias R J, Gutiérrez-Álvarez C, Carbonell B, Campos R, Campos G, Martín P, Castro B, 2018. Thermo-hydro-mechanical postmortem analisis of bentonite performed at CIEMAT. NAB 16-24, Nagra, Switzerland.

Vogels R J M J, Kloprogge J T, Geus J W, 2005. Synthesis and characterization of saponite clays. American Mineralogist 90, 931–944.

Vogt C, Lagerblad B, Wallin K, Baldy F, Jonasson J-E, 2009. Low pH self compacting concrete for deposition tunnel plugs. SKB R-09-07, Svensk Kärnbränslehantering AB.

Wanner H, Wersin P, Sierro N, 1992. Thermodynamic modelling of bentonite-groundwater interaction and implications for near field chemistry in a repository for spent fuel. SKB TR 92-37, Svensk Kärnbränslehantering AB.

Wanner H, Albinsson Y, Wieland E, 1996. A thermodynamic surface model for caesium sorption on bentonite. Fresenius' Journal of Analytical Chemistry 354, 763–769.

Werme L, 1998. Design premises for canister for spent nuclear fuel. SKB TR-98-08, Svensk Kärnbränslehantering AB.

Wersin P, Kober F (eds), 2017. FEBEX-DP Metal corrosion and iron-bentonite interaction studies. Nagra Arbeitsbericht NAB 16-016, Nagra, Switzerland.

Wersin P, Johnson L H, Schwyn B, Berner U, Curti E, 2003. Redox conditions in the near field of a repository for SF/HLW and ILW in Opalinus Clay. Technical Report 02-13, Nagra, Switzerland.

Wersin P, Curti E, Appelo C A J, 2004. Modelling bentonite–water interactions at high solid/liquid ratios: swelling and diffuse double layer effects. Applied Clay Science 26, 249–257.

Wersin P, Kiczka M, Rosch D, 2014a. Safety case for the disposal of spent nuclear fuel at Olkiluoto. Radionuclide solubility limits and migration parameters for the canister and buffer. Posiva 2012-39, Posiva Oy, Finland.

Wersin P, Kiczka M, Rosch D, Ochs M, Trudel D, 2014b. Safety case for the disposal of spent nuclear fuel at olkiluoto. Radionuclide solubility limits and migration parameters for the canister and buffer. Posiva 2012-40, Posiva Oy, Finland.

Wersin P, Kiczka M, Koskinen K, 2016. Porewater chemistry in compacted bentonite: Application to the engineered buffer barrier at the Olkiluoto site. Applied Geochemistry 74, 165–175.

Wikramaratna R S, Goodfield M, Rodwell W R, Nash P J, Agg P J, 1993. A preliminary assessment of gas migration from the copper/steel canister. SKB TR 93-31, Svensk Kärnbränslehantering AB.

Williams P J, 1964. Unfrozen water content of frozen soils and soil moisture suction. Geotechnique 14, 231–246.

Wold S, 2003. On diffusion of organic colloids in compacted bentonite. PhD thesis. Department of Chemistry, Nuclear Chemistry, Royal Institute of Technology, Stockholm. (TRITA-KKE 0302)

Yang G, Neretnieks I, Moreno L, Wold S, 2016. Density functional theory of electrolyte solutions in slit-like nanopores II. Applications to forces and ion exchange. Applied Clay Science 132–133, 561–570.

Yu J-W, Neretnieks I, 1997. Diffusion and sorption properties of radionuclides in compacted bentonite. SKB TR 97-12, Svensk Kärnbränslehantering AB.

Zhang J Z, Buenfeld N R, 1997. Presence and possible implications of a membrane potential in concrete exposed to chloride solution. Cement and Concrete Research 17, 853–859.

Zhang Z Z, Low P F, 1989. Relation between the heat of immersion and the initial water content of Li-, Na-, and K-montmorillonite. Journal of Colloid and Interface Science 133, 461–472.

Zheng L, Samper J, 2008. A coupled THMC model of FEBEX *mock-up* test. Physics and Chemistry of the Earth, Parts A/B/C 33, S486–S498.

Zysset M, 1992. Die protoneninduzierte Auflösung von K-Montmorillonit. PhD thesis. Institute of Inorganic, Analytical and Physical Chemistry, University of Bern, Switzerland.

Åkesson M, 2012. Temperature Buffer Test. Final report. SKB TR-12-04, Svensk Kärnbränslehantering AB

Åkesson M, 2018. Full-scale test of the Dome Plug for KBS-3V deposition tunnels. Gas tightness test. SKB P-17-37, Svensk Kärnbränslehantering AB.

Åkesson M, 2020a. EBS TF – THM modelling. Water transport in pellets-filled slots – modelling of test cases A and C. SKB P-20-19, Svensk Kärnbränslehantering AB.

Åkesson M, 2020b. EBS TF – THM modelling. Water transport in pellets-filled slots – evaluation of model contributions. SKB P-20-18, Svensk Kärnbränslehantering AB.

Åkesson M, Hökmark H, 2007. Mechanical model for unsaturated MX-80. In Schanz T (ed). Theoretical and numerical unsaturated soil mechanics. Berin, Heidelberg: Springer (Springer Proceeding in Physics 113), 3–10.

Åkesson M, Laitinen H, 2022. Gas phase composition during the unsaturated period. Status report June 2022. SKBdoc 1983850 ver 1.0, Svensk Kärnbränslehantering AB.

Åkesson M, Kristensson O, Börgeson L, Dueck A, Hernelind J, 2010a. THM modelling of buffer, backfill and other system components. Critical processes and scenarios. SKB TR-10-11, Svensk Kärnbränslehantering AB.

Åkesson M, Börgesson L, Kristenssson O, 2010b. SR-Site data report. THM modelling of buffer, backfill and other system components. SKB TR-10-44, Svensk Kärnbränslehantering AB.

Åkesson M, Malmberg D, Börgesson L, Hernelind J, Ledesma A, Jacinto A, 2012. Temperature Buffer Test. Final THM modelling. SKB P-12-07, Svensk Kärnbränslehantering AB.

Åkesson M, Sandén T, Goudarzi R, Malmberg D, 2019. Full-scale test of the Dome Plug for KBS-3V deposition tunnels. Monitoring, function tests and analysis of bentonite components. SKB P-18-15, Svensk Kärnbränslehantering AB.

Åkesson M, Goudarzi R, Börgesson L, 2020. EBS TF – THM modelling. Water transport in pellets-filled slots – laboratory tests and task descriptions. SKB P-19-06, Svensk Kärnbränslehantering AB.

Arkitektkopia AB, Bromma, 2022

SKB is responsible for managing spent nuclear fuel and radioactive waste produced by the Swedish nuclear power plants such that man and the environment are protected in the near and distant future.

skb.se